

AIR QUALITY MODELING

Theories, Methodologies,
Computational Techniques, and
Available Databases and Software

Volume II - Advanced Topics

Editor

Paolo Zannetti

Chapter Authors

Domenico Anfossi
Elisa Canepa
David B. Carrington
Judith C. Chow
Giovanna Finzi
Rosa M. González Barras
John S. Irwin

Hope Michelsen
Giuseppe Nunnari
Darrell W. Pepper
Juan L. Pérez
William Physick
Betty K. Pun
Richard O. Richter

Roberto San José
Christian Seigneur
Patrick J. Sheehan
Zbigniew Sorbjan
John G. Watson

Contributors

Gervásio Degrazia
Enrico Ferrero
Mark Hibberd

Peter Hurley
Ashok Luhar
Silvia Trini Castelli

Han van Dop
Paolo Zannetti

AIR QUALITY MODELING

Theories, Methodologies, Computational Techniques,
and Available Databases and Software

Volume II – Advanced Topics

Blank Page

Dedicated to Maryann

Blank Page

AIR QUALITY MODELING
Theories, Methodologies, Computational Techniques,
and Available Databases and Software
Volume II – Advanced Topics

Editor

Paolo Zannetti

Chapter Authors

Domenico Anfossi, Elisa Canepa, David B. Carrington, Judith C. Chow, Giovanna Finzi,
Rosa M. González Barras, John S. Irwin, Hope Michelsen, Giuseppe Nunnari,
Darrell W. Pepper, Juan L. Pérez, William Physick, Betty K. Pun, Richard O. Richter,
Roberto San José, Christian Seigneur, Patrick J. Sheehan, Zbigniew Sorbjan, John G. Watson

Contributors

Gervásio Degrazia, Enrico Ferrero, Mark Hibberd, Peter Hurley,
Ashok Luhar, Silvia Trini Castelli, Han van Dop, Paolo Zannetti

Published by

The EnviroComp Institute
Air & Waste Management Association



Copyright © 2005 EnviroComp Institute and Air & Waste Management Association. All rights reserved.

Notice regarding copyrights: Chapter authors retain copyrights to their original materials. All requests for permission to reproduce chapter material should be directed to the appropriate author(s); all other requests should be directed to the Air & Waste Management Association, One Gateway Center, 3rd Floor, 420 Ft. Duquesne Blvd., Pittsburgh, PA 15222, USA.

ISBN 0-923204-86-5 (CD-ROM)

Printed in the United States of America.

Copies of this CD-ROM may be purchased by visiting The EnviroComp Institute at www.envirocomp.org/aqm or the Air & Waste Management Association's online library at www.awma.org, or by contacting A&WMA directly at 1-800-270-3444 or 1-412-232-3444. Please reference A&WMA Order Code OTHP-25. This book is also available in hard copy format (ISBN 0-923204-85-7) from the A&WMA.

For updates, additional information, and online discussion regarding this book series, please visit www.envirocomp.org/aqm.

Table of Contents – Volume II^{1, 2}

	<u>Preface</u>	<u>xi</u>
	<u>About the Editor</u>	<u>xiii</u>
	<u>About the Publishers</u>	<u>xv</u>
	<u>About the Chapter Authors/Contributors for Volumes I and II</u>	<u>xvii</u>
<u>1</u>	<u>The Problem – Air Pollution</u>	<u>1</u>
<u>2</u>	<u>The Tool – Mathematical Modeling</u>	<u>3</u>
<u>3</u>	<u><i>Emission Modeling</i></u>	<u>5</u>
<u>4</u>	<u>Air Pollution Meteorology</u>	<u>7</u>
<u>5</u>	<u>Meteorological Modeling</u>	<u>9</u>
	<u><i>5A Mesoscale Meteorological Modeling</i></u>	
	<u>5B Large-Eddy Simulations of the Atmospheric Boundary Layer</u>	<u>11</u>
	<u>1 Introduction</u>	<u>11</u>
	<u>2 Theoretical Background</u>	<u>14</u>
	<u>3 The ABL Simulations</u>	<u>35</u>
	<u>4 Final Remarks</u>	<u>74</u>
	<u><i>5C Computational Fluid Dynamics of Microscale Meteorological Flows</i></u>	
<u>6</u>	<u>Plume Rise</u>	<u>83</u>
<u>7</u>	<u>Gaussian Plume Models</u>	<u>85</u>
	<u><i>7A Introduction to Gaussian Plume Models</i></u>	
	<u><i>7B Simulation Algorithms in Gaussian Plume Models</i></u>	
<u>8</u>	<u><i>Gaussian Puff Models</i></u>	<u>87</u>
<u>9</u>	<u><i>Special Applications of Gaussian Models</i></u>	<u>89</u>

¹ Chapters in italics will be provided in subsequent volumes.

² The table of contents of Volume I can be found on [page 635](#) of this book.

<u>10</u>	<u>Eulerian Dispersion Models</u>	<u>91</u>
<u>11</u>	<u>Lagrangian Particle Models</u>	<u>93</u>
1	<u>The Lagrangian Approach</u>	<u>94</u>
2	<u>Lagrangian Stochastic Models (LSM)</u>	<u>95</u>
3	<u>LSM Applications</u>	<u>128</u>
<u>12</u>	<u>Atmospheric Transformations</u>	<u>163</u>
1	<u>Introduction</u>	<u>164</u>
2	<u>Gas-Phase Transformations</u>	<u>165</u>
3	<u>Heterogeneous and Aqueous Processes</u>	<u>172</u>
4	<u>Chemical Transformations Involved in the Formation of Air Toxics</u>	<u>179</u>
5	<u>Chemistry of the Upper Atmosphere: Stratospheric Ozone</u>	<u>183</u>
6	<u>Modeling of Gas-Phase Chemistry</u>	<u>193</u>
7	<u>Modeling of Heterogeneous and Aqueous Processes</u>	<u>199</u>
8	<u>Modeling of Reactive Plumes</u>	<u>207</u>
9	<u>Eulerian Models</u>	<u>212</u>
<u>13</u>	<u>Deposition Phenomena</u>	<u>233</u>
1	<u>Introduction</u>	<u>234</u>
2	<u>Different Deposition Parameterizations</u>	<u>240</u>
3	<u>Examples of Deposition Monitoring Programs</u>	<u>248</u>
4	<u>Examples of Air Quality Models</u>	<u>251</u>
5	<u>Sensitivity Analysis by Using the OPANA Model</u>	<u>257</u>
<u>14</u>	<u>Indoor Air Pollution Modeling</u>	<u>267</u>
1	<u>Introduction</u>	<u>270</u>
2	<u>Fluid Flow Fundamentals</u>	<u>274</u>
3	<u>Contaminant Sources</u>	<u>284</u>
4	<u>Design Criteria</u>	<u>293</u>
5	<u>Simple Modeling Techniques</u>	<u>297</u>
6	<u>Dynamics of Particles and Gases/Vapors</u>	<u>310</u>
7	<u>Numerical Modeling – CFD</u>	<u>322</u>
<u>15</u>	<u>Modeling of Adverse Effects</u>	<u>349</u>
<u>15A</u>	<u>Modeling of Health Risks Associated with Combustion</u>	<u>351</u>
	<u>Facility Emissions</u>	
1	<u>Introduction</u>	<u>351</u>
2	<u>Case Study</u>	<u>354</u>
	<u>15B Odor Modeling</u>	
	<u>15C Visibility Modeling</u>	
	<u>15D Ecological Adverse Effects</u>	
	<u>15E Global Issues</u>	

<u>16</u>	<u>Statistical Modeling</u>	<u>395</u>
<u>16A</u>	<u>Air Quality Forecast and Alarm Systems</u>	<u>397</u>
1	<u>Introduction</u>	<u>398</u>
2	<u>Some Literature Results</u>	<u>401</u>
3	<u>Time Series Modelling</u>	<u>405</u>
4	<u>Building a Model for Air Quality Forecast</u>	<u>419</u>
5	<u>Identification of Statistical Air Quality Models</u>	<u>426</u>
6	<u>An Operational Decision Support System</u>	<u>437</u>
7	<u>Conclusions</u>	<u>445</u>
	<u>Appendix</u>	<u>453</u>
<u>16B</u>	<u>Receptor Models</u>	<u>455</u>
1	<u>Introduction</u>	<u>455</u>
2	<u>Receptor Model Types</u>	<u>457</u>
3	<u>Multivariate Receptor Model Mathematics</u>	<u>465</u>
4	<u>Model Input Measurements</u>	<u>469</u>
5	<u>Receptor Model Assumptions, Performance Measures, and Validation Procedures</u>	<u>482</u>
6	<u>Summary and Conclusions</u>	<u>491</u>
<u>17</u>	<u>Evaluation of Air Pollution Models</u>	<u>503</u>
1	<u>Introduction</u>	<u>503</u>
2	<u>Terminology</u>	<u>504</u>
3	<u>Background</u>	<u>507</u>
4	<u>Framework</u>	<u>510</u>
5	<u>Performance Measures</u>	<u>516</u>
6	<u>Model Evaluation</u>	<u>526</u>
7	<u>Statistical Model Evaluation</u>	<u>528</u>
8	<u>Model Quality Assurance</u>	<u>543</u>
9	<u>Guidelines for Model Evaluation: Towards Harmonization in Model Evaluation Methodology</u>	<u>547</u>
<u>18</u>	<u>A Historical Look at the Development of Regulatory Air Quality Models for the United States Environmental Protection Agency</u>	<u>557</u>
1	<u>Introduction</u>	<u>557</u>
2	<u>Legislative History of Air Pollution Modeling</u>	<u>561</u>
3	<u>Air Quality Models for Individual Industrial Facilities</u>	<u>566</u>
4	<u>The Development of Urban-Scale Long-Term Air Quality Models</u>	<u>575</u>
5	<u>Development of Tropospheric Chemistry Models</u>	<u>579</u>
6	<u>Current Issues and Trends in Model Development</u>	<u>598</u>
<u>19</u>	<u>Case Studies – Air Pollution Modeling at Local, Regional, Continental, and Global Scales</u>	<u>623</u>
<u>20</u>	<u>The Future of Air Pollution Modeling</u>	<u>625</u>
<u>21</u>	<u>Active Groups in Air Pollution Modeling</u>	<u>627</u>
<u>22</u>	<u>Available Software</u>	<u>629</u>

<u>23</u>	<u>Available Databases</u>	<u>631</u>
<u>24</u>	<u><i>Physical Modeling of Air Pollution</i></u>	<u>633</u>
	<u>Table of Contents – Volume I</u>	<u>635</u>
	<u>In Memoriam – Philip M. Roth</u>	<u>639</u>
	<u>Authors’/Contributors’ Index for Volumes I and II</u>	<u>641</u>
	<u>Subject Index for Volumes I and II</u>	<u>643</u>

Preface

This is the second volume in a book series on air quality modeling published by the EnviroComp Institute and the Air & Waste Management Association (A&WMA). The series seeks to provide environmental scientists, engineers, researchers, and students with a comprehensive, organized, and evolving body of information in virtually all aspects of computer simulation of air pollution and related atmospheric phenomena. Each volume in the series expands the scope of our efforts by presenting new chapter topics and updates of material included in previous volumes.

All volumes in this series are available in both a traditional book format and an electronic format (CD-ROM). The electronic version is not a simple digital copy of the printed files, but includes additional material, such as active Internet pointers and computer animations. In addition, the CD-ROM material can be quickly and easily searched by keywords. The book series also has its own Web page, www.envirocomp.org/aqm, which readers are encouraged to visit for additional information.

While Volume I primarily presented introductory material, Volume II focuses on more advanced topics. Together, the two volumes cover a large spectrum of scientific issues, even though some important chapters (e.g., emission modeling and meteorological modeling) will not be addressed until Volume III. Due to the growing interest in global issues, we also expect to include new chapters dealing with continental and global air pollution and global climate change.

I want to express my sincere thanks to the chapter authors for their competence, dedication, and patience in the production of this volume. Thanks are also due to A&WMA Publications Director Andy Knopes for his help and support in the preparation of both volumes. Sincere appreciation is again extended to Scott Cragin who, as with Volume I, provided valuable editorial and organizational assistance throughout the entire book production cycle. Finally, we thank Ms. Ji Ohm for her final review of the chapters and publication assistance.

I hope you will find this new volume on air quality modeling interesting and helpful in your efforts to better understand this complicated issue.

Paolo Zannetti
Fremont, California

Blank Page

About the Editor

Dr. Paolo Zannetti is the President of the EnviroComp Institute and EnviroComp Consulting, Inc. in Fremont, California. He received a Doctoral Degree in Physics from the University of Padova (Italy) and has managed a range of environmental projects throughout his professional career. With a specialization in air pollution and environmental modeling and software, Dr. Zannetti's experience has covered research and development studies, teaching, consulting, modeling software development, project management, editorial activities, and expert testimony. In addition to authoring in 1990 the first comprehensive textbook on this topic (*Air Pollution Modeling — Theories, Computational Methods and Available Software*), Dr. Zannetti has authored more than 200 publications, primarily for peer-reviewed journals and conference proceedings. For more information, visit <http://www.envirocomp.org/html/meetus/zannetti.htm>.

Blank Page

About the Publishers

The EnviroComp Institute

The International Institute of Environmental Sciences and Environmental Computing (EnviroComp) is a nonprofit, Internet-based institute and software laboratory dedicated to the study of environmental sciences and pollution phenomena. Founded in 1996, the EnviroComp Institute also promotes the publication of a unique, new-generation series of environmental books in electronic format. For more information, visit the institute's Web site at <http://www.envirocomp.org>.

The Air & Waste Management Association

The Air & Waste Management Association (AWMA) is a nonprofit, nonpartisan professional organization that provides information, training, and networking opportunities to thousands of environmental professionals around the world. AWMA was founded in 1907 and is headquartered in Pittsburgh, Pennsylvania. For more information, visit the association's Web site at <http://www.awma.org>.

Blank Page

About the Chapter Authors/Contributors for Volumes I and II
([Additional information](#) is provided in the CD-ROM version)

Anfossi

Dr. Domenico Anfossi
CNR - ISAC, Sezione di Torino
Corso Fiume 4
I-10133 - Torino
ITALY

Phone: +39 011 6606376
Phone direct: +39 011 3839826
Fax: +39 011 6600364
Email: anfossi@to.infn.it or d.anfossi@isac.cnr.it
Work site: <http://www.isac.cnr.it>

Builtjes

Dr. Peter J.H. Builtjes
Professor
TNO Environment, Energy and Process Innovation
Department of Environmental Quality
Laan van Westenenk 501
P.O. Box 342
7300 AH Apeldoorn
THE NETHERLANDS

Phone: +31 555493038
Fax: +31 555493252
Email: p.j.h.builtjes@mep.tno.nl

Byun

Dr. Daewon W. Byun
Professor
312 Science & Research Bldg. 1
Geoscience Department
University of Houston
Houston, Texas 77204-5007
USA

Email: dwbyun@math.uh.edu

Canepa

Elisa Canepa, Ph.D.
Atmospheric and Oceanic Physics Group
INFN - Department of Physics
University of Genova
Via Dodecaneso 33
I-16146 Genova
ITALY

Phone: +39 010 353 6354
Fax: +39 010 353 6354
Email: elisa.canepa@fisica.unige.it or
canepae@libero.it

Work site: <http://www.fisica.unige.it/~atmosfe/>
Personal site: <http://www.fisica.unige.it/~canepae/>

Carrington

David B. Carrington, Ph.D.
Los Alamos National Laboratory
CCS-4 Transport Methods
P.O. Box 1663 MS D409
Los Alamos, NM 87545
USA

Phone: (505) 667-3569
Email: dcrrngtn@lanl.gov

Chow

Judith C. Chow, Sc.D.
Department of Atmospheric Sciences
Desert Research Institute
University of Nevada, Reno
2215 Raggio Parkway
Reno, NV 89512
USA

Phone direct: (775) 674-7050
Fax: (775) 674-7009
Email: judy.chow@dri.edu
Work site: <http://www.das.dri.edu/>
Personal site: <http://www.dri.edu/People/judyc/>

Degrazia

Dr. Gervásio A. Degrazia
Universidade Federal de Santa Maria
Departamento de Física
97105900 Santa Maria – RS
BRASIL

Phone: +55 55 2208616

+55 55 2208032

Email: degrazia@ccne.ufsm.br

Eastman

Joseph L. Eastman, Ph.D.
Research Faculty
UMBC/GEST
Hydrological Sciences Branch
NASA/GSFC Code 974
Building 33, Room A322
Greenbelt, MD 20771
USA

Phone: (410) 279-9702

Fax: (301) 614-5808

Email: eastman@hsb.gsfc.nasa.gov or

jleastman@comcast.net

Work site: <http://gest.umbc.edu/directory.html>

Ferrero

Dr. Enrico Ferrero, Ph.D.
Dip. di Scienze e Tecnologie Avanzate
Universita' del Piemonte Orientale "A. Avogadro"
Via Bellini, 25/G
15100 Alessandria
ITALY

Phone: +39 013 136 0151

Fax: +39 013 136 0199

Email: enrico.ferrero@unipmn.it

Work site: <http://dista.unipmn.it/>

Personal site: <http://www.mfn.unipmn.it/~ferrero>

Finzi

Prof. Giovanna Finzi
Dipartimento di Elettronica per l'Automazione
Università degli Studi di Brescia
Via Branze 38, 25123 Brescia
ITALY

Phone: +39 030 371 5459
Fax: +39 030 380014
Email: finzi@ing.unibs.it
Personal site: <http://www.ing.unibs.it/~finzi>

González Barras

Prof. Dr. Rosa M. González Barras
Department of Geophysics and Meteorology
Faculty of Physics, Complutense University of Madrid (UCM)
Ciudad Universitaria
28040 Madrid
SPAIN

Phone: +34 91 394 4513
Fax: +34 91 394 4798
Email: rgbarras@fis.ucm.es
Work site: <http://www.ucm.es/info/Geofis/>

Hibberd

Dr. Mark Hibberd
CSIRO Atmospheric Research
PMB1
Aspendale VIC 3195
AUSTRALIA

Phone: +61 3 9239 4400
Phone direct: +61 3 9239 4545
Fax: +61 3 9239 4444
Email: mark.hibberd@csiro.au
Work site: <http://www.dar.csiro.au>
Personal site: <http://www.dar.csiro.au/profile/hibberd.html>

Hurley

Dr. Peter Hurley
CSIRO Atmospheric Research
PMB1
Aspendale VIC 3195
AUSTRALIA

Phone: +61 3 9239 4400
Phone direct: +61 3 9239 4547
Fax: +61 3 9239 4444
Email: peter.hurley@csiro.au
Work site: <http://www.dar.csiro.au>
Personal site: <http://www.dar.csiro.au/profile/hurley.html>

Irwin

John S. Irwin, CCM
John S. Irwin and Associates
1900 Pony Run Road
Raleigh, NC 27615-7415
USA

Phone: (919) 541-5682
Email: irwin.john@epa.gov or
jsirwinetal@nc.rr.com

Keen

Prof. Cecil S. Keen
Atmospheric Sciences / Geography (c/o Box 2)
Minnesota State University
Mankato, MN 56002-8400
USA

Phone: (507) 389-5169
Fax: (507) 345-1283
Email: cecil.keen@mnsu.edu
Work site: <http://www.mnsu.edu/weather>

Lacser

Avraham Lacser, Ph.D.
Israel Institute for Biological Research (IIBR)
POB 19
NESS ZIONA 74100
ISRAEL

Phone: +972 8 9381488
Fax: +972 8 9401404
Email: lacser@iibr.gov.il
Work site: <http://www.iibr.gov.il>

Lee

Russell Lee
Meteorologist
5806 Prosperity Church Road
Suite A2-128
Charlotte, NC 28269
USA

Phone: (704) 947-8024
Fax: (704) 947-8024
Email: Russell.Lee@RFLee.com
Work site: <http://www.RFLee.com>

Luhar

Dr. Ashok Luhar
CSIRO Atmospheric Research
PMB1
Aspendale VIC 3195
AUSTRALIA

Phone: +61 3 9239 4400
Phone direct: +61 3 9239 4624
Fax: +61 3 9239 4444
Email: ashok.luhar@csiro.au
Work site: <http://www.dar.csiro.au>
Personal site: <http://www.dar.csiro.au/profile/luhar.html>

Lyons

Walter A. Lyons, Ph.D., CCM
FORENSIC METEOROLOGY ASSOCIATES, Inc. (FMA)
46050 Weld County Road 13
Fort Collins, CO 80524
USA

Phone: (800) 854-7219
Fax: (970) 482-8627
Email: walyons@frie.com
Work site: <http://www.forensic-weather.com>

Michelsen

Dr. Hope Michelsen
Combustion Research Facility
Sandia National Labs
P. O. Box 969; MS 9055
Livermore, CA 94551
USA

Phone direct: (925) 294 2335
Fax: (925) 294 2276
Email: hamiche@ca.sandia.gov
Work site: <http://www.ca.sandia.gov/CRF/>

Moon

Dennis A. Moon, Ph.D.
Chief Scientist
WindLogics, Inc.
Itasca Technology Exchange
201 NW 4th St.
Grand Rapids, MN 55744
USA

Phone: (651) 556-4281
Email: dmoon@WindLogics.com
Work site: <http://www.WindLogics.com>

Moussiopoulos

Dr. Eng. Nicolas Moussiopoulos
Professor and Laboratory Director
Laboratory of Heat Transfer and Environmental Engineering
Box 483, Aristotle University
GR-54124 Thessaloniki
GREECE

Phone: +30 2310 996011
Fax: +30 2310 996012
Email: moussio@vergina.eng.auth.gr
Work site: <http://aix.meng.auth.gr/lhtee/>
Personal site: <http://www.envirocomp.org/html/meetus/moussio.htm>

Nelson

Thomas E. Nelson
FMA Research, Inc.
Yucca Ridge Field Station
46050 Weld County Road
Fort Collins, CO 80524
USA

Email: tnelson@frii.com

Nunnari

Prof. Giuseppe Nunnari
Dipartimento di Ingegneria, Elettrica, Elettronica e dei Sistemi
Viale A. Doria, 6
95125 Catania
ITALY

Phone: +39 095 738 2306
Fax: +39 095 330793
Email: gunnari@diees.unict.it
Work sites: <http://www.dees.unict.it/users/gunnari/>
<http://www.diees.unict.it>
Group site: <http://www.scg.dees.unict.it/>

Oettl

Dietmar Oettl
Institute for Internal Combustion Engines and
Thermodynamics
Graz University of Technology
Inffeldgasse 25
A-8010 Graz
AUSTRIA

Phone: +43 316 873 8081
Email: oettl@vkmb.tu-graz.ac.at
Work site: <http://fvkma.tu-graz.ac.at>

Pepper

Dr. Darrell W. Pepper
Professor and Director, NCACM
Department of Mechanical Engineering
University of Nevada Las Vegas
4505 Maryland Parkway
Las Vegas, NV 89154-4027
USA

Phone: (702) 895-1056
Fax: (702) 895-0498
Cell: (702) 528-7213
Email: dwpepper@nscee.edu
Work site: www.unlv.edu/Research_Centers/NCACM

Pérez

Dr. Juan L. Pérez
Environmental Software and Modelling Group
Computer Science School, Technical University of Madrid
(UPM)
Campus de Montegancedo, Boadilla del Monte
28660 Madrid
SPAIN

Phone: +34 91 336 7465
Fax: +34 91 336 7412
Email: jlperez@fi.upm.es
Work site: <http://artico.lma.fi.upm.es>

Physick

Dr. William Physick
CSIRO Atmospheric Research
PMB1
Aspendale VIC 3195
AUSTRALIA

Phone: +61 3 9239 4400
Phone direct: +61 3 9239 4636
Fax: +61 3 9239 4444
Email: bill.physick@csiro.au
Work site: <http://www.dar.csiro.au>
Personal site: <http://www.dar.csiro.au/profile/physick.html>

Pun

Dr. Betty K. Pun
Air Quality Division
Atmospheric and Environmental Research, Inc
2682 Bishop Drive, Suite 120
San Ramon, CA 94583
USA

Phone: (925) 244-7125
Fax: (925) 244 7129
Email: pun@aer.com
Work site: <http://www.aer.com>

Reynolds

Steven D. Reynolds
Envair
12 Palm Avenue
San Rafael, CA 94901
USA

Email: steve@sreynolds.com
Personal site: <http://www.sreynolds.com>

Richter

Dr. Richard O. Richter, P.E.
Exponent, Inc.
320 Goddard, Suite 200
Irvine, CA 92612
USA

Phone: (949) 341-6015
Fax: (949) 341-6059
Email: rrichter@exponent.com
Work site: <http://www.exponent.com>

Roth¹

Philip M. Roth, Ph.D.

San José

Prof. Dr. Roberto San José
Environmental Software and Modelling Group
Computer Science School - Technical University of Madrid
(UPM)
Campus de Montegancedo - Boadilla del Monte
28660 Madrid
SPAIN

Phone: +34 91 336 7465
Fax: +34 91 336 7412
Email: roberto@fi.upm.es
Work site: <http://artico.lma.fi.upm.es>

¹ Deceased. See [page 639](#).

Seigneur

Dr. Christian Seigneur
Air Quality Division
Atmospheric and Environmental Research, Inc.
2862 Bishop Drive, Suite 120
San Ramon, CA 94583
USA

Phone direct: (925) 244-7121
Fax: (925) 244-7129
Email: seigneur@aer.com
Work site: <http://www.aer.com>

Sheehan

Dr. Patrick J. Sheehan
Exponent, Inc.
1970 Broadway, Suite 250
Oakland, CA 94612
USA

Phone: (510) 208-2008
Fax: (510) 208-2039
Email: psheehan@exponent.com
Work site: <http://www.exponent.com>

Sorbjan

Prof. Zbigniew Sorbjan
Department of Physics
Marquette University
Milwaukee, WI 53201
USA

Phone: (414) 288-7458
Fax: (414) 288-3989
Email: sorbjan@mu.edu
Work site: <http://www.mu.edu/~sorbjan>

Thé

Jesse Thé, Ph.D., P.Eng.
Lakes Environmental Software Inc.
306 Milla Court
Waterloo - Ontario - N2L 6N4
CANADA

Phone: (519) 746-5995
Fax: (519) 746-0793
Email: Jesse@WEBLAKES.com
Work site: <http://www.WEBLAKES.com>

Tourlou

Dr. Eng. Paraskevi-Maria Tourlou
Hellenic Ministry of Transport and Communications
Land Transport Safety Directorate
Anastaseos 2 & Tsigante str.
GR-10191 Papagos, Athens
GREECE

Phone: +30 210 6508468 and 2310 996011
Fax: +30 210 6508493 and 2310 996012
Email: evelina@aix.meng.auth.gr
Work site: <http://aix.meng.auth.gr/lhtee/>

Trini Castelli

Dr. Silvia Trini Castelli
CNR - ISAC, Sezione di Torino
Corso Fiume 4
I-10133 - Torino
ITALY

Phone: +39 011 660 6376
Phone direct: +39 011 383 9828
Fax: +39 011 660 0364
Email: S.TriniCastelli@isac.cnr.it
Work site: <http://www.isac.cnr.it>

van Dop

Dr. Han van Dop
Institute for Marine and Atmospheric Research Utrecht
Utrecht University
P.O. Box 80.005
3508 TA Utrecht
THE NETHERLANDS

Phone: +31 30 253 3154
Fax: +31 30 254 3163
Email: h.vandop@phys.uu.nl
Personal site: <http://www.phys.uu.nl/~dop/>

Venkatram

Akula Venkatram, Ph.D.
Professor of Mechanical Engineering
A343 Bourns Hall
Riverside, CA 92521
USA

Phone: (909) 787-2195
Fax: (909) 787-2899
Email: venky@engr.ucr.edu
Personal sites: <http://www.engr.ucr.edu/mechanical/people/venkatram.html>
<http://www.engr.ucr.edu/~venky/>

Watson

John G. Watson, Ph.D.
Department of Atmospheric Sciences
Desert Research Institute
University of Nevada, Reno
2215 Raggio Parkway
Reno, NV 89512
USA

Phone direct: (775) 674-7046
Fax: (775) 674-7009
Email: john.watson@dri.edu
Work Site: <http://www.das.dri.edu/>
Personal site: <http://www.dri.edu/People/johnw/>

Yamartino

Dr. Robert J. Yamartino
191 East Grand Ave. #206
Old Orchard Beach, ME
USA

Email: rjy@maine.rr.com

Zannetti

Dr. Paolo Zannetti, QEP
President, EnviroComp Consulting, Inc. and
The EnviroComp Institute
2298 Ocaso Camino
Fremont, CA 94539
USA

Phone: (510) 490-3438
Fax: (510) 490-3357
Email: zannetti@envirocomp.com
Work site: <http://www.envirocomp.com> and
<http://www.envirocomp.org>
Personal site: <http://www.envirocomp.org/html/meetus/zannetti.htm>

Blank Page

Chapter 1

The Problem – Air Pollution

A chapter dedicated to the topic “The Problem – Air Pollution” was presented in Volume I of this book series.

For additional information, the reader can visit:

- <http://www.lbl.gov/Education/ELSI/pollution-main.html>
A general introduction to outdoor and indoor air pollution
- <http://www.epa.gov/ebtpages/airairpollutants.html>
<http://www.epa.gov/ebtpages/airairpollution.html>
The US EPA sites with detailed descriptions of air pollution issues and the chemicals causing air pollution (browse the listed pointers and the subtopics for additional information)
- <http://www.airquality.co.uk/archive/index.php>
A general introduction to air pollution with specific information about the UK
- <http://www.lanl.gov/orgs/d/d4/aquality/aqlinks.html>
Air quality links to available data, international air pollution issues, online meteorological data, dispersion models, and other useful sites

BRANK
P
e

Chapter 2

The Tool – Mathematical Modeling

A chapter dedicated to the topic “The Tool – Mathematical Modeling” was presented in Volume I of this book series.

For additional information, the reader can visit:

- <http://www.epa.gov/oar/oaqps/modeling.html>
The US EPA site with pointers to EPA-related modeling activities and topics
- <http://www.arb.ca.gov/html/soft.htm#modeling>
Air quality modeling software and some associated documentation
- <http://www.shodor.org/metweb/index.html>
A course introducing the basic concepts of meteorology and air quality necessary to understand meteorological computer models

BRANKLEY
P. 200

Chapter 3

Emission Modeling

A brief introduction to the topic “Emission Modeling” was presented in Volume I of this book series. A full chapter on this topic is expected to be published in Volume III.

For additional information, the reader can visit:

- <http://www.epa.gov/ttn/chief/efpac/index.html>
The Emissions Factors and Policy Applications Center (EFPAC) of the US EPA
- <http://www.epa.gov/otaq/ap42.htm>
The US EPA compilation of air pollutant emission factors for stationary point and area sources, fugitive dust on roadways, paved roads, unpaved road emission, and mobile sources
- <http://www.epa.gov/OMSWWW/models.htm>
The US EPA site describing emission models and inventories

BRANK
P
e

Chapter 4

Air Pollution Meteorology

A chapter dedicated to the topic “Air Pollution Meteorology” was presented in Volume I of this book series.

For additional information, the reader can visit:

- <http://www.shodor.org/metweb/index.html>
A course introducing the basic concepts of meteorology and air quality necessary to understand meteorological computer models
- <http://www.lanl.gov/orgs/rres/maq/>
A site describing meteorology and air quality topics

BRANKEN
P
e

Chapter 5

Meteorological Modeling

A brief introduction to the topic “Meteorological Modeling” was presented in Volume I of this book series. A Chapter on this topic (5B – Large-Eddy Simulations of the Atmospheric Boundary Layer) is included in the following pages. Other chapters are expected to be published in Volume III, according to the following plan:

5A – Mesoscale Meteorological Modeling

5B – Large-Eddy Simulations of the Atmospheric Boundary Layer

5C – Computational Fluid Dynamics of Microscale Meteorological Flows

For additional information, the reader can visit:

- <http://box.mmm.ucar.edu/mm5/>
The site of the PSU/NCAR mesoscale model (known as MM5), which is a limited-area, nonhydrostatic, terrain-following sigma-coordinate model designed to simulate or predict mesoscale atmospheric circulation
- <http://earthtec.vwh.net/download/calmet.pdf>
The user’s guide of the CALMET model, which is a diagnostic 3-dimensional meteorological model, part of the CALPUFF modeling system
<http://www.src.com/calpuff/calpuff1.htm>
- [http://ww2010.atmos.uiuc.edu/\(Gh\)/guides/mtr/home.rxml](http://ww2010.atmos.uiuc.edu/(Gh)/guides/mtr/home.rxml)
Online Meteorology Guide - a collection of web-based instructional modules that use multimedia technology and the dynamic capabilities of the web

- <http://www.fluent.com/solutions/whatefd.htm>
<http://www.cham.co.uk/website/new/cfdintro.htm>
An introduction to Computational Fluid Dynamics (CFD)

Sorbjan, Z. 2005. *Large-Eddy Simulations of the Atmospheric Boundary Layer*. Chapter 5B of *AIR QUALITY MODELING - Theories, Methodologies, Computational Techniques, and Available Databases and Software. Vol. II – Advanced Topics*. (P. Zannetti, Editor). Published by The EnviroComp Institute (www.envirocomp.org) and the Air & Waste Management Association (www.awma.org).

Chapter 5B

Large-Eddy Simulations of the Atmospheric Boundary Layer

Zbigniew Sorbjan

Department of Physics, Marquette University, Milwaukee, WI (USA)
Institute of Meteorology and Water Management, Warsaw (Poland)
sorbjanz@mu.edu

Abstract: In this Chapter, the large-eddy simulation technique is described. The presented material consists of two parts. In the first one, technical issues including filtering, subgrid modeling, and numerical integration, are discussed. In the second part, simulations of typical prototypes of the atmospheric boundary layer are presented, including convective, neutral, stable, and cloud-topped cases.

Key Words: atmospheric boundary layer, cloud-free boundary layer, cloud-topped boundary layer, turbulence, mixing, convection, mixed layers, large-eddy simulations.

1 Introduction

The atmospheric boundary layer (ABL) is an inherently complex and heterogeneous system, which is under permanent transition, enforced by a variety of internal and external factors. Some of its fascinating signatures are revealed on satellite images, showing intricate cloud patterns organized in a coherent fashion (Figure 1).

An understanding of the ABL, its structure and dynamics, is essential for weather prediction and environmental studies. During the last four decades, the fundamental knowledge of boundary layer turbulence has been achieved as a result of extensive experimental effort [e.g., Augstein et al. (1973), Holland and Rasmusson (1973), Brost and Wyngaard (1984 a, b), Brümmer et al. (1985),

Albrecht et al. (1988), Webster and Lucas (1992), Albrecht et al. (1995), LeMone and Grossman (1999), Curry et al. (2000), Kristovich et al. (2000), White et al. (2000), LeMone et al. (2002), and Paulos et al. (2002)]. The experimental work has been supplemented by numerical research, especially "large-eddy simulations" (LES).

In LES, most of the turbulence (i.e., large eddies) is directly resolved from the Navier-Stokes equations, and only the small-scale (subgrid) turbulence is modeled [e.g., Lilly (1967), Nieuwstadt (1990), and Mason (1994)]. Note that we differentiate between two commonly used terms: modeling and simulating. "Modeling" is understood here as approximating, while "simulating" is considered as more realistic and reliable representation of nature, faithful to the essential physics of the flow.

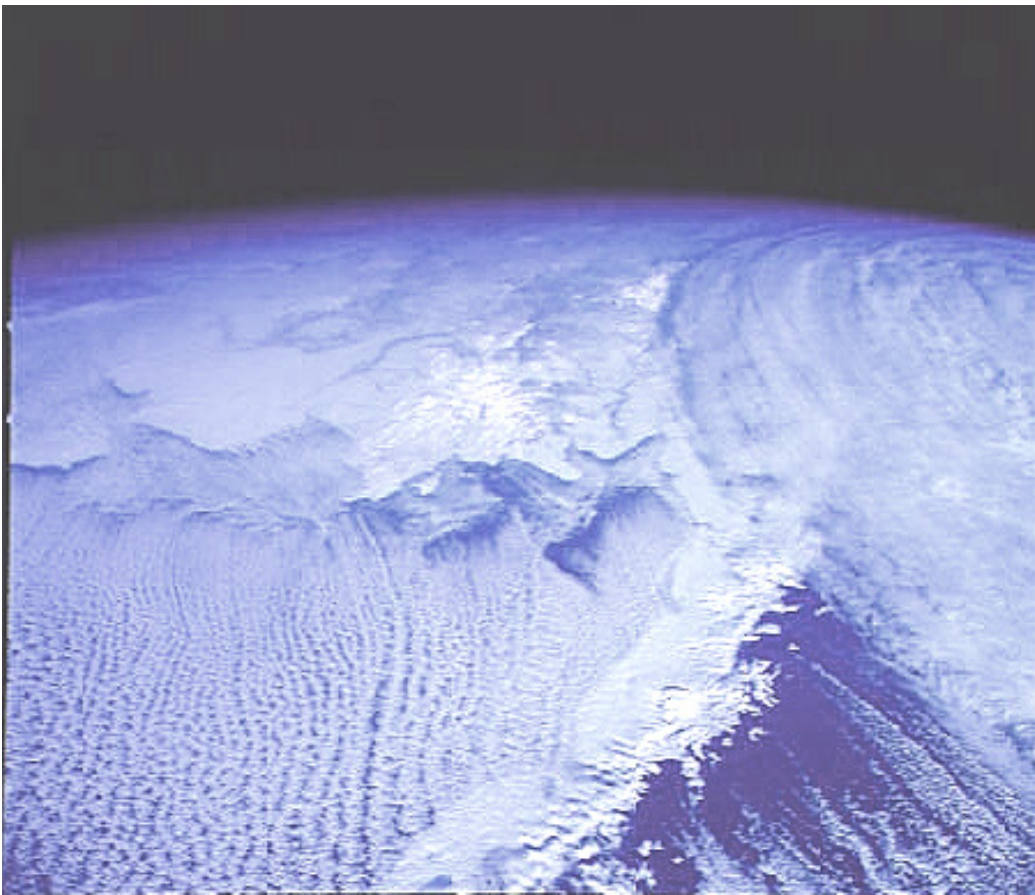


Figure 1. Rolls and cells marked by cumuli clouds during an outbreak of cooler air over a warmer ocean (NASA).

The LES technique was developed by Deardorff (1970; 1972; 1973; 1974 a, b). The early LES focused on the cloud-free, convective boundary layers [e.g., Schemm and Lipps (1976), Moeng (1984, 1986), Schmidt and Schumann (1989), and Mason (1989)]. Effects of shear were considered later by Mason (1992 a),

Moeng and Sullivan (1994), Glendening (1996), Kim et al. (2003), and Sorbjan (2004 a, c)].

The important role of clouds in the dynamics of the atmospheric boundary layer has generated interest in LES of cloud-topped mixed layers. In particular, the boundary layer containing stratus and stratocumulus clouds has attracted extensive consideration [e.g. Deardorff (1976, 1980), Sommeria (1976), Moeng (1986), Schumann and Moeng (1991), Moeng and Schumann (1991), Kogan et al. (1995), Moeng et al. (1996), Lewellen and Lewellen (1996), Shen and Moeng (1993), Khairoutdinov and Kogan (1999), Jian and Cotton (2000), Stevens et al. (1998, 1999, 2001), Siebesma et al. (2003), and Neggers et al. (2002)].

LES of the ABL with cumulus clouds have also been performed. The pioneering study was done by Sommeria (1976) and continued by Cuijpers and Duynkerke (1993), Siebesma et al. (2002), and Brown et al. (2002).

Thereafter, there were also attempts to employ the LES to simulate the stably stratified flows in the ABL. The effort attracted much less attention due to the difficulties in resolving small-scale turbulence. The pioneering simulation of the stably stratified boundary layer was performed by Mason and Derbyshire (1990). The simulation was later repeated with various subgrid models by Brown et al. (1994), Andren (1996), Kosovic and Curry (1999), Cedeval and Street (1999), Saiki et al. (1999), Beare et al. (2004), and Beare and MacVean (2004).

Other ABL simulations included diurnal transitions. The first LES study of the decaying atmospheric convective mixed layer was performed by Nieuwstadt and Brost (1986). The authors analyzed a case of the shearless, clear mixed layer, in which turbulence decayed as a result of a sudden shut-off of the upward surface heat flux. The study of Nieuwstadt and Brost was followed by Sorbjan (1997), who considered a gradual change of the heat flux with time in response to the decreasing sun's elevation. Acevedo and Fitzjarrald (1999, 2001) undertook a LES study in order to understand the effects of moistening close to the earth's surface during the early evening transition.

A few LES studies were conducted on advective transitions. Chlond and Müller (1997) considered horizontal roll vortices in the ABL by using a "very large-eddy" approach applied to a LES-type model with periodic boundary conditions. Within their Lagrangian approach, a LES model "traveled" with the geostrophic wind speed along the wind direction. Another approach was applied by Mayor et al. (2002) who performed a LES study of a cold-air outbreak over Lake Michigan. Schröter and Raasch (2002) performed a high-resolution study of cell broadening during cold air outbreaks.

Diffusion in the clear-sky convective boundary layer was significantly advanced by the numerical simulations and laboratory experiments of Willis and Deardorff (1976, 1978, 1981). Their investigations demonstrated that for elevated sources, the average plume centerline, defined as the mean maximum concentration, descended within a short distance from the source until it reached the ground. In contrast, the average centerline from near surface releases ascended after a short downwind distance. LES of diffusion in the stratocumulus-topped ABL was performed by Sorbjan and Uliasz (1999).

The purpose of this Chapter is to review the theoretical basis of LES, and to present the most typical results. The discussed topics are addressed to air-pollution engineers, who intend to improve their understanding of complex processes controlling diffusion within the atmospheric boundary layer. This Chapter is organized as follows. The LES approach is described in Section 2. A short overview of the governing equations is presented in Section 2.1, followed by brief information on filtering, subgrid modeling, and numerical integration in Sections 2.2 and 2.3. Large-eddy simulations of typical boundary layers regimes are presented in Section 3. The considered cases include the convective, neutral, stable, and cloudy conditions.

2 Theoretical Background

2.1 Basic Equations

The most general set of equations which governs the motion of a compressible, viscous fluid consists of:

- the momentum equations:
$$\frac{du_i}{dt} = -\frac{1}{\rho_o} \frac{\partial p}{\partial x_i} - 2 \varepsilon_{ijk} \Omega_j u_k - g \delta_{i3} - \frac{\partial \sigma_{ij}}{\partial x_j} \quad (1)$$

- the continuity equation:
$$\frac{d\rho}{dt} = -\rho \frac{\partial u_j}{\partial x_j} \quad (2)$$

- the first law of thermodynamics:
$$C_p \frac{dT}{dt} - \frac{1}{\rho} \frac{dp}{dt} = S \quad (3)$$

- and the ideal gas law:
$$p = \rho R_d T \quad (4)$$

where $i, j, k = 1, 2, 3$ (note that repeated indices indicate summation), p , ρ , and T are the static pressure, air density, and the absolute temperature respectively, u_j is the j -component of the velocity, R_d is the gas constant, C_p is the specific heat at constant pressure, g is the gravity acceleration. Moreover, $d/dt = \partial/\partial t + u_j \partial/\partial x_j$ is the total derivative, σ_{ij} is the anisotropic part of the viscous stress tensor,

$\sigma_{ij} = 2\nu S_{ij} + \beta S_{kk} \delta_{ij}$, where ν is the molecular viscosity, δ_{ij} is the Kronecker delta, and $S_{ij} = \frac{1}{2}(\partial u_i / \partial x_j + \partial u_j / \partial x_i)$ is the rate of strain. Since $\sigma_{kk} = 0$, the coefficient β has to be defined as $\beta = -2/3 \nu$. S is the heating/cooling flux involving radiation, phase changes, and diffusion. The diffusion part of S has the form $\partial F_i / \partial x_i$, where the molecular heat flux is described as $F_i = -D \partial T / \partial x_i$, and D is the molecular diffusivity. The term $2\mathcal{E}_{ijk} \Omega_j u_k$ is the Coriolis acceleration, Ω_j is the j -component of the earth's angular velocity, \mathcal{E}_{ijk} is the component of the unit tensor, equal to 1 for even permutations of the indices (i, j, k), -1 for odd permutations, and 0 otherwise. Note that in the coordinate system in which the x-axis is pointing east, the y-axis is pointing north, and the z-axis is pointing vertically, the components of the earth's angular velocity Ω are defined as $\Omega_1 = 0$, $\Omega_2 = \Omega \cos \phi$, $\Omega_3 = \Omega \sin \phi$, where ϕ is the latitude.

The above equations have been developed from the 17th to the 19th centuries by a number of scholars. Among them were: Isaac Newton (1687), who discovered the laws of dynamics, Robert Boyle (1662), Jacques Charles (1787), Joseph Gay-Lussac (1802), Amerigo Avogadro (1813), who contrived the ideal gas equation, Leonhard Euler (1755), who invented the non-viscous flow equations and the continuity equation, Claude-Louis Navier (1827) and Georg Stokes (1845), who developed the viscous flow equations, and Rudolf Clausius (1851), who formulated the first law of thermodynamics.

The set (1)-(4) is often simplified due to the fact that the atmospheric boundary layer is relatively shallow with respect to the depth of the entire atmosphere. Consequently, the density variation with height can be neglected. Following the usual practice in this case, we will consider the atmosphere to be in a state slightly removed from an adiabatic atmosphere at rest. We consider an expansion of the governing parameters into basic state values (denoted by the index "o") and perturbations (denoted by the index "):

$$\begin{aligned}
 p &= p_o + p'' \\
 T &= T_o + T'' \\
 \rho &= \rho_o + \rho'' \\
 u_j &= u_{jo} + u_j'' \quad (i = 1, 2, 3)
 \end{aligned} \tag{5}$$

where:

the basic state pressure: $p_o = \rho_o R_d T_o$

the basic state temperature: $dT_o / dz = -\Gamma_a = -10 \text{ K/km}$

the basic state density:

$$\frac{1}{\rho_o} \frac{\partial p_o}{\partial x_i} = -2 \mathcal{E}_{ijk} \Omega_j G_k \quad (i = 1, 2) \quad (6)$$

$$\frac{1}{\rho_o} \frac{\partial p_o}{\partial x_3} = -g$$

the basic velocity:

$$u_{jo} = 0$$

and G_k are the components of the geostrophic wind. The geostrophic wind is allowed to be a function of height (baroclinicity): $G_k = G_{ko} + T_k z$, where T_k is the thermal wind, and $G_{ko} = G_k(z = 0)$.

For the ideal gas law (4), we will obtain:

$$p'' = p - p_o = R_d (\rho T - \rho_o T_o) = R_d (\rho_o T'' + \rho'' T_o + \rho'' T'') \quad (7)$$

Note that (7) can be rewritten as:

$$p''/p_o = T''/T_o + \rho''/\rho_o + \rho'' T_o''/(\rho_o T_o) \quad (8)$$

which can be simplified as:

$$p''/p_o = T''/T_o + \rho''/\rho_o \quad (9)$$

Note that the order of p'' in (9) can be evaluated as $\rho_o u_j''^2$ (which is equivalent to assuming in the momentum equation that the flow is caused by a pressure gradient: $\partial u_j''^2/\partial x_j = 1/\rho_o \partial p''/\partial x_j$). Consequently,

$$p''/p_o \sim O(u_j''^2/R_d T_o) \sim O(\gamma M^2) \quad (10)$$

where $M = u_j''/c_s$ is the Mach number, $c_s = (\gamma R_d T_o)^{0.5}$ is the adiabatic speed of sound in ideal gas, $\gamma = C_p/C_v$ is equal to 1.4 for dry air, and C_p and C_v are the specific heat coefficients at constant pressure and volume. Assuming that $M \ll 1$, we can neglect the effects of motion-induced pressure changes in (9), which yields:

$$T''/T_o + \rho''/\rho_o = 0 \quad (11)$$

From the definition of the potential temperature $\Theta = T (1000/p)^{R_d/C_p}$, it follows that

$$\frac{d\Theta}{\Theta} = -\frac{dT}{T} - \frac{R_d}{C_p} \frac{dp}{p} \quad (12)$$

and also

$$\frac{\Theta''}{\Theta_o} = \frac{T''}{T_o} - \frac{R_d}{C_p} \frac{p''}{p_o} \quad (13)$$

Using (11) and (13), we arrive at:

$$\frac{\Theta''}{\Theta_o} = -\frac{\rho''}{\rho_o} \quad (14)$$

Based on (12), Equation (3) can be written in terms of the potential temperature

$$\frac{T}{\Theta} \frac{d\Theta}{dt} = S \quad (15)$$

Near the earth's surface ($T/\Theta \sim 1$), so

$$\frac{d\Theta}{dt} = S \quad (16)$$

From Equations (2) and (3), we will get in the adiabatic case ($S = 0$):

$$\begin{aligned} \frac{\partial u_j}{\partial x_j} &= \frac{1}{\rho} \frac{d\rho}{dt} = \\ &= \frac{1}{p} \frac{dp}{dt} - \frac{1}{T} \frac{dT}{dt} = \frac{C_v}{C_p} \frac{d \ln p}{dt} \end{aligned} \quad (17)$$

Based on (6):

$$\begin{aligned} \frac{\partial \ln p}{\partial t} &\sim u_o'' \frac{\partial \ln p}{\partial x} \sim \frac{u_o''}{\rho R_d T_o} \frac{\rho u_o''^2}{L_o} \sim \frac{u_o''^3}{R_d T_o L_o} \\ \frac{\partial \ln p}{\partial x_3} &\sim \frac{g}{R_d T_o} = \frac{1}{H} \end{aligned} \quad (18)$$

where $H = R_d T_o / g \sim 10$ km is the height of the isothermal atmosphere, L_o is the horizontal length scale, and u_o'' is the scale of the horizontal velocity perturbations.

Based on (17) – (18) we will obtain

$$\frac{\partial u_j}{\partial x_j} \sim \frac{u_o''^3}{c_s^3 L_o} + \frac{C_v}{C_p} \frac{w_o''}{H} \quad (19)$$

where w_o'' is the scale of the vertical velocity perturbations. Assuming that all terms of the velocity divergence have a similar magnitude: $u_o''/L_o \sim w_o''/D$, where D is the scale of convective motion, $u_o''^2/c_s^2 \ll 1$, and $D/H \ll 1$, yields:

$$\frac{\partial u_j}{\partial x_j} = \frac{u_o''}{L_o} \left[\frac{u_o''}{c_s^2} + \frac{C_v}{C_p} \frac{D}{H} \right] \sim 0 \quad (20)$$

The result is called the "incompressible approximation".

In the momentum equations, the pressure and gravity terms can be expressed as:

$$-\frac{1}{\rho} \frac{\partial p}{\partial x_i} - g \delta_{ij} = -\frac{1}{\rho_o + \rho''} \frac{\partial (p_o + p'')}{\partial x_i} - g \delta_{ij} \quad (21)$$

Since

$$\frac{1}{\rho_o + \rho''} = \frac{1}{\rho_o} \frac{1}{\left[1 + \frac{\rho''}{\rho_o}\right]} = \frac{1}{\rho_o} \left[1 - \frac{\rho''}{\rho_o} + \dots\right] \approx \frac{1}{\rho_o} \left[1 - \frac{\rho''}{\rho_o}\right] \quad (22)$$

then, based on (6) we have

$$\frac{1}{\rho} \frac{\partial p}{\partial x_i} = -2 \varepsilon_{ijk} \Omega_j G_k + \frac{1}{\rho} \frac{\partial p''}{\partial x_i} \quad (\text{for } i = 1, 2) \quad (23)$$

$$\frac{1}{\rho} \frac{\partial p}{\partial x_3} - g = \quad (24)$$

$$= \frac{1}{\rho_o} \left[1 - \frac{\rho''}{\rho_o}\right] \left[\frac{\partial p_o}{\partial x_3} + \frac{\partial p''}{\partial x_3} \right] - g = \frac{1}{\rho_o} \frac{\partial p''}{\partial x_3} - \frac{\rho''}{\rho_o^2} \frac{\partial p_o}{\partial x_3} =$$

$$= \frac{1}{\rho_o} \frac{\partial p''}{\partial x_3} - \frac{[\Theta - \Theta_o]}{\Theta_o} g$$

where Θ_o is the reference temperature. The result is called the "Boussinesq approximation". It neglects density variations in fluid except when they are coupled with the gravity acceleration.

Applying all of the above-described simplifications, we will rewrite (1)-(4) in the following form:

$$\begin{aligned} \frac{du_i}{dt} &= -\frac{1}{\rho_o} \frac{\partial p''}{\partial x_i} - 2 \varepsilon_{ijk} \Omega_j (u_k - G_k) + \frac{g}{\Theta_o} (\Theta - \Theta_o) \delta_{i3} - \frac{\partial \sigma_{ij}}{\partial x_j} \\ \frac{\partial u_j}{\partial x_j} &= 0 \\ \frac{d\Theta}{dt} &= S \end{aligned} \quad (25)$$

The above system constitutes five equations with five unknowns: u_1, u_2, u_3, Θ and p'' . The system can only be solved numerically (e.g., by a finite difference method). The resulting approach is called the direct numerical simulation (DNS). Its applications are limited to relatively small domain problems, as will be explained below.

2.2 Filtering

Basic flows in the atmospheric boundary layer take on the form of large eddies. Their size is proportional to the flow geometry and characterized by scale L (e.g., the height of the ABL). Large eddies fall apart into smaller and smaller ones due to flow instabilities. This cascade continues until the smallest flow scales are reached. There, the motion is damped out by viscosity and dissipated into heat.

The smallest scale of motion is described by “the Kolmogorov microscale” η . The dimensional analysis predicts that $\eta = \nu^{3/4} / \varepsilon^{1/4}$, where ε is the dissipation rate, and ν is the kinematic viscosity. For $\nu = 10^{-5} \text{ m}^2/\text{s}$ and $\varepsilon = 10^{-3} \text{ m}^2/\text{s}^3$, we obtain $\eta = 10^{-3} \text{ m} = 1 \text{ mm}$. The ratio of both scales, η and L , is $L/\eta = Re^{3/4}$, where $Re = UL/\nu$ is the Reynolds number, and U is a characteristic velocity scale.

The number of grid points needed to numerically resolve all turbulent motions in 3-dimensional space should be at least

$$N \sim (L/\eta)^3 = Re^{9/4} \quad (26)$$

For $U = 10 \text{ m/s}$, $L = 1000 \text{ m}$, $\nu = 10^{-5} \text{ m}^2/\text{s}$, and $Re = 10^9$. Consequently, the required number of grid points in the atmospheric boundary layer is $N \sim 10^{20}$. This number is beyond the capacity of modern computers. Thus, DNS is restricted to flows that are characterized by more modest Reynolds numbers, in the order of 10^2 - 10^3 (which is not very useful in solving the ABL problems).

To resolve this numerical resolution difficulty, the approach called “large-eddy simulation” (LES) was invented. The philosophy behind this technique is that the largest eddies define the flow, and are primarily responsible for all transport processes, such as the exchange of momentum, heat, or contaminants. Large eddies contain most of the energy, do most of the transporting of conserved properties, and vary from flow to flow. The smaller eddies are believed to be more universal (self-similar), less dependent on boundary conditions, and consequently easier to model. Therefore, LES is designed to directly resolve (simulate) the larger scales of motion while approximating (modeling) the smaller ones.

It is important to precisely define the quantities to be computed by LES. This is done by filtering or removing the smallest-scale components from the governing equations (Leonard, 1974). The filtered velocity is defined by:

$$\bar{u}_i(x) = \int_{-\infty}^{\infty} G(x, X) u_i(X) dX \quad (27)$$

where one-dimensional notation is used for convenience (the generalization to three dimensions is straight-forward). $G(x, X)$ is the filter kernel with a compact support (i.e., G is large only when x and X are not far apart).

Filter functions, which have been applied in LES, include "box", Gaussian, and "cut-off" kernels. The box kernels imply simply an average over a rectangular region. It is a natural choice when finite difference or finite volume methods are used to solve the filtered equations:

$$\bar{u}_i(x) = \frac{1}{2\Delta} \int_{x-\Delta}^{x+\Delta} u_i(X) dX \quad (28)$$

Two versions of this filter have been used. In the moving box filter, the average is taken over a region of space surrounding any chosen point. According to this definition, \bar{u}_i is a continuous function of x . A filter, which is an average over a grid volume of a finite difference or finite volume mesh, is tied more closely to the numerical method. According to this definition, \bar{u}_i is a piecewise constant function of x .

Gaussian kernels have the advantage of being smooth and infinitely differentiable in both physical and Fourier space. Cut-off kernels are defined in Fourier space. They eliminate all of the Fourier coefficients, which belong to wave numbers above a particular cutoff. It is natural to use them in conjunction with spectral methods.

When the Navier-Stokes equations are filtered, the following set of equations is obtained:

$$\frac{\partial \bar{u}_i}{\partial t} + \frac{d\bar{u}_i \bar{u}_j}{dx_j} = -\frac{1}{\rho_o} \frac{\partial \bar{p}''}{\partial x_i} - 2 \varepsilon_{ijk} \Omega_j (\bar{u}_k - G_k) + \frac{g}{\Theta_o} (\bar{\Theta} - \Theta_o) \delta_{i3} - \frac{\partial \bar{\sigma}_{ij}}{\partial x_j}$$

$$\frac{\partial \bar{u}_j}{\partial x_j} = 0 \quad (29)$$

$$\frac{\partial \bar{\Theta}}{\partial t} + \frac{\partial \bar{u}_j \bar{\Theta}}{\partial x_j} = \bar{S}$$

Assuming that:

$$\tau_{ij} = \overline{u_i u_j} - \bar{u}_i \bar{u}_j$$

$$H_j = \overline{u_j \Theta} - \bar{u}_j \bar{\Theta} \quad (30)$$

we will obtain:

$$\frac{\partial \bar{u}_i}{\partial t} + \frac{d\bar{u}_i \bar{u}_j}{dx_j} = -\frac{1}{\rho_o} \frac{\partial \bar{p}''}{\partial x_i} - 2 \varepsilon_{ijk} \Omega_j (\bar{u}_k - G_k) - \frac{g}{\Theta_o} (\bar{\Theta} - \Theta_o) \delta_{i3} - \frac{\partial \tau_{ij}}{\partial x_j}$$

$$\frac{\partial \bar{u}_j}{\partial x_j} = 0 \quad (31)$$

$$\frac{\partial \bar{\Theta}}{\partial t} + \frac{\partial \bar{u}_j \bar{\Theta}}{\partial x_j} = -\frac{\partial H_j}{\partial x_j} + \bar{S}$$

Above, it was also assumed that the turbulent terms exceeded the molecular ones: $\partial \tau_{ij} / \partial x_i \gg \partial \bar{\sigma}_{ij} / \partial x_i$ and $\partial H_i / \partial x_i \gg \partial \bar{\mathcal{G}}_i / \partial x_i$.

Note that the same form of equations as (31) would be obtained if the ensemble-averaging were employed, instead of the filtering. One important difference between filtering and ensemble averaging is that the ensemble-averaging operator applied twice yields the originally averaged field, $\overline{\overline{u}_i} = \bar{u}_i$. Generally, this expression is not true for filtering operators. The exception is the cutoff filter for which such equality does hold.

Employing the ensemble-averaging, and then decomposing fields into averaged values and fluctuations (e.g., $u_i = \bar{u}_i + u'_i$ and $\Theta = \bar{\Theta} + \theta'$) yields:

$$\begin{aligned}
\tau_{ij} &= \overline{u_i u_j} - \bar{u}_i \bar{u}_j = \\
&= \overline{(\bar{u}_i + u'_i)(\bar{u}_j + u'_j)} - \overline{(\bar{u}_i + u'_i)(\bar{u}_j + u'_j)} = \overline{u'_i u'_j} \\
H_j &= \overline{u_i \Theta} - \bar{u}_i \bar{\Theta} = \\
&= \overline{(\bar{u}_i + u'_i)(\bar{\Theta}_j + \theta'_j)} - \overline{(\bar{u}_i + u'_i)(\bar{\Theta}_j + \theta'_j)} = \overline{u'_i \theta'_j}
\end{aligned} \tag{32}$$

In the context of the LES, τ_{ij} is called the “subgrid scale Reynolds stress”, and H_j is called the “subgrid scale heat flux”. Note that τ_{ij} and H_j are undefined, and need to be modeled. Subgrid scale (SGS) modeling is the most distinctive feature of the LES, and is the subject of the next section.

2.3 Subgrid-Scale Modeling

The term “subgrid” refers to the filters closely connected to a grid, which is used to discretize the basic flow equations. This approach was used in the earliest LES. Generally, the connection between the utilized filter and grid is not needed (i.e., the nomenclature is more restrictive than necessary).

As mentioned before, the smallest scale motions are involved in the viscous dissipation of kinetic energy. In a large-eddy simulation, this role must be taken over by the subgrid scales. The parameterization of the subgrid terms must comply with this requirement. The simplest choice for such parameterization is (note the similarity to the molecular fluxes):

$$\begin{aligned}
\tau_{ij} &= -2k_m \left(\bar{S}_{ij} - \frac{1}{3} \bar{S}_{kk} \delta_{ij} \right) + \frac{2}{3} E \delta_{ij} \\
H_j &= -k_h \frac{\partial \bar{\Theta}}{\partial x_j}
\end{aligned} \tag{33}$$

where k_m and k_h are the eddy viscosity and diffusivity, $E = \frac{1}{2} \overline{u_k u_k}$ is the subgrid turbulent kinetic energy, and $\bar{S}_{ij} = \frac{1}{2} (\partial \bar{u}_i / \partial x_j + \partial \bar{u}_j / \partial x_i)$ is the averaged rate of strain. Equation (33a) is valid in both incompressible ($\bar{S}_{kk} = 0$) and compressible cases.

The system (31) is usually rewritten in the form:

$$\begin{aligned}
\frac{\partial \bar{u}_i}{\partial t} + \frac{d \bar{u}_i \bar{u}_j}{dx_j} &= -\frac{\partial \pi}{\partial x_i} - 2 \varepsilon_{ijk} \Omega_j (\bar{u}_k - G_k) + \frac{g}{\Theta_o} (\bar{\Theta} - \Theta_o) \delta_{i3} - \frac{\partial T_{ij}}{\partial x_j} \\
\frac{\partial \bar{u}_j}{\partial x_j} &= 0 \\
\frac{\partial \bar{\Theta}}{\partial t} + \frac{\partial \bar{u}_j \bar{\Theta}}{\partial x_j} &= -\frac{\partial H_j}{\partial x_j} + \bar{S}
\end{aligned} \tag{34}$$

where

$$\begin{aligned}
\pi &= \frac{\bar{p}''}{\rho_o} + \frac{2}{3} E \\
T_{ij} &= -2k_m (\bar{S}_{ij} - \frac{1}{3} \bar{S}_{kk} \delta_{ij}) \\
H_j &= -k_h \frac{\partial \bar{\Theta}}{\partial x_j}
\end{aligned} \tag{35}$$

Note that the turbulent kinetic energy, E , is included in the pressure term π .

In the above system, the coefficients k_m and k_h remain undefined. In order to evaluate them, we will consider closure models based on the subgrid turbulent kinetic energy (TKE). The TKE equation can be obtained (from equation 34a) in the following form (Sorbjan, 1989):

$$\frac{\partial E}{\partial t} + \frac{\partial \bar{u}_j E}{\partial x_j} = -T_{ij} \bar{S}_{ij} + \beta H_3 - \frac{\partial \Pi_j}{\partial x_j} - \varepsilon \tag{36}$$

where $\Pi_j = \overline{u_j(u_k u_k / 2 + p)} - \bar{u}_j \overline{(u_k u_k / 2 + p)}$, $H_3 = \overline{u_3 \Theta} - \bar{u}_3 \bar{\Theta}$, and $\beta = g/T_o$ is the buoyancy parameter. The first two terms on the right-hand side of (36) are the production term due to shear and the local buoyancy, respectively. The third term is turbulent transport, and the last term is viscous dissipation, ε .

Let us consider the first subgrid model based on (36). As stated before, the dissipation rate is given by definition of the Kolmogorov microscale η :

$$\varepsilon = \frac{v^3}{\eta^4} \tag{37}$$

where ν is the kinematic viscosity. By analogy, we shall assume that the net rate of energy transfer out of the filtered flow field (large eddies) is given by

$$\varepsilon_f = \frac{k_m^3}{\Delta_f^4} \quad (38)$$

where Δ_f is the filter width, which also is the length scale of the smallest eddies of the filtered flow field. Assuming in (38) that the dissipation is balanced by the shear production, $\varepsilon_f = -T_{ij} \bar{S}_{ij}$, and $T_{ij} = -2k_m \bar{S}_{ij}$, we have:

$$\varepsilon_f = k_m^3 \Delta_f^{-4} = 2 k_m \bar{S}_{ij} \bar{S}_{ij} \quad (39)$$

The resulting Smagorinsky's model (1963) is of the form:

$$k_m = (C_s \Delta)^2 (2 \bar{S}_{ij} \bar{S}_{ij})^{1/2} \quad (40)$$

where C_s is the constant of proportionality between Δ_f and the grid size Δ , $\Delta_f = C_s \Delta$, and $\Delta = (\Delta x \Delta y \Delta z)^{1/3}$.

For Smagorinsky's model, the net rate of the transfer of energy out of the filtered flow ε_f is clearly positive. It has been generally agreed that on the average, the energy is transferred from large scales to small scales ("forward scatter"). The reverse energy flow ("backscatter") from the small scales to the large ones, associated with random fluctuations of the subgrid-scale stresses, can also occur intermittently. In Smagorinsky-type models, ε is always positive. Therefore, these models are absolutely dissipative (i.e., they cannot predict backscatter).

A more complex closure model is based on the assumption that the eddy viscosity and diffusivity coefficients, k_m and k_b , are functions of the subgrid turbulent kinetic energy, E , and the length scale, Δ :

$$k_m = C_m \Delta \sqrt{E} \quad (41)$$

$$k_b = k_m / Pr$$

where C_m is a universal constant, Pr is the Prandtl number, and E is calculated from the TKE equation (36), in which the dissipation rate and the turbulent transport term can be parameterized as (Deardorff, 1980):

$$\varepsilon = C_\varepsilon \frac{E^{3/2}}{\lambda} \quad (42)$$

$$\Pi_i = -2k_m \frac{\partial E}{\partial x_i}$$

where λ is the mixing length. The functions Pr , λ , as well as parameters C_m and C_ε need to be specified to close the subgrid model.

Both approaches described above (equations 40 and 41) have several problems. They do not predict the correct asymptotic behavior near a solid boundary, and do not allow for the SGS energy backscatter to the resolved scales. To overcome these hurdles, other models, like non-linear models (Kosovic, B and J. Curry, 1999), similarity models (Bardina et al., 1980), dynamic models (Germano et al., 1992, and Lilly, 1992), and mixed models can be proposed.

2.4 Thermodynamic Formulation

In case when water vapor is present in the atmosphere, the potential temperature Θ in (34) is replaced by the virtual potential temperature Θ_v , defined as:

$$\Theta_v = \Theta (1 + 0.61 q_v) \quad (43)$$

where q_v is the water vapor content (i.e., the specific humidity equal to the mass of water vapor in a volume of air, or the mixing ratio, which is the mass of water vapor in a unit mass of air). Note that Θ_v can be interpreted as the temperature of the dry air, which has the same density as the moist air under consideration.

When the phase changes occur, water vapor, as well as liquid water, is present in the air. As a result the virtual potential temperature has the form:

$$\Theta_v = \theta (1 + 0.61 q_v - q_L) \quad (44)$$

where q_L is the liquid water specific humidity (mass of water in a volume of air). Presence of moisture enhances the buoyancy, while liquid water increases the density of a parcel.

To diagnose the potential temperature θ from Θ_v in (44), two additional equations are required for q_v and q_L :

$$\begin{aligned} \frac{\partial \bar{q}_v}{\partial t} + \frac{\partial \bar{u}_j \bar{q}_v}{\partial x_j} &= -\frac{\partial Q_{vj}}{\partial x_j} - e \\ \frac{\partial \bar{q}_L}{\partial t} + \frac{\partial \bar{u}_j \bar{q}_L}{\partial x_j} &= -\frac{\partial Q_{Lj}}{\partial x_j} + e \end{aligned} \quad (45)$$

where Q_{vj} and Q_{Lj} are the turbulent fluxes, e is the evaporation/condensation rate (we assume that no form of precipitation is present). The evaporation/condensation rates in (45) can be eliminated by adding both equations, which yields:

$$\frac{\partial \bar{q}_T}{\partial t} + \frac{\partial \bar{u}_j \bar{q}_T}{\partial x_j} = -\frac{\partial Q_{Tj}}{\partial x_j} \quad (46)$$

where $q_T = q_v + q_L$ is the total water specific humidity, and Q_{Tj} is the total water content turbulent flux.

When phase changes take place in the atmosphere, it is convenient to consider the liquid water potential temperature θ_L as a prognostic variable. The temperature θ_L can be expressed in a linearized version, defined by Betts (1973):

$$\Theta_L = \Theta - (L/C_p) q_L \quad (47)$$

where L is the latent heat of vaporization, C_p is the specific heat of dry air at constant pressure, and Θ is the potential temperature. The liquid water potential temperature and the total water specific humidity are conserved in moist adiabatic process (for no-drizzle case). The temperature θ_L reduces to the dry potential temperature in the absence of liquid water. Based on this definition, the equation for the liquid water potential temperature can be obtained from (34c) and (45b) in the form:

$$\frac{\partial \bar{\Theta}_L}{\partial t} + \frac{\partial \bar{u}_j \bar{\Theta}_L}{\partial x_j} = -\frac{\partial H_{Lj}}{\partial x_j} + \bar{S} \quad (48)$$

As a result of the described modifications, the following system of equations can be obtained:

$$\begin{aligned} \frac{\partial \bar{u}_i}{\partial t} + \frac{\partial \bar{u}_i \bar{u}_j}{\partial x_j} &= -\frac{\partial \pi}{\partial x_i} - 2 \varepsilon_{ijk} \Omega_j (\bar{u}_k - G_k) + \frac{g}{\Theta_o} (\bar{\Theta}_v - \bar{\Theta}_o) \delta_{i3} - \frac{\partial T_{ij}}{\partial x_j} \\ \frac{\partial \bar{\Theta}_L}{\partial t} + \frac{\partial \bar{u}_j \bar{\Theta}_L}{\partial x_j} &= -\frac{\partial H_{Lj}}{\partial x_j} + \bar{S} \\ \frac{\partial \bar{q}_T}{\partial t} + \frac{\partial \bar{u}_j \bar{q}_T}{\partial x_j} &= -\frac{\partial Q_{Tj}}{\partial x_j} \end{aligned} \quad (49)$$

$$\frac{\partial E}{\partial t} + \frac{\partial \bar{u}_j E}{\partial x_j} = -T_{ij} \bar{S}_{ij} + \beta H_v - \frac{\partial \Pi_j}{\partial x_j} - \varepsilon$$

$$\frac{\partial \bar{u}_j}{\partial x_j} = 0$$

where $H_v = \overline{u_3 \Theta_v} - \overline{u_3} \overline{\Theta_v} = -k_h \frac{\partial \overline{\Theta_v}}{\partial x_3}$, $H_{Lj} = -k_h \frac{\partial \overline{\Theta_L}}{\partial x_j}$, $Q_{Tj} = -k_h \frac{\partial \overline{q_T}}{\partial x_j}$, and in addition (33), (40), and (41) also apply.

The subgrid buoyancy term in the TKE equation has to be evaluated in terms of the new model variables Θ_L and q_T . For this purpose, we have to consider two cases, unsaturated and saturated.

In the unsaturated case, when $q_L = 0$, $q_v = q_T$, and $\Theta_L = \Theta$. Based on the definition of the virtual temperature (44), we have (Cuijpers and Duynkerke, 1993):

$$\overline{w' \theta_v'} = (1 + 0.61 q_T) \overline{w' \theta_L'} + 0.61 \Theta \overline{w' q_T'} \quad (50)$$

where the ensemble averaging notation (32) is applied for simplicity, and the new (meteorological) notation is being used: $u_1 = u$, $u_2 = v$, and $u_3 = w$.

In the saturated case, $q_T = q_s + q_L$ and $q_v = q_s$, so:

$$\overline{w' \theta_v'} = (1 + 1.61 q_s - q_T) \overline{w' \theta'} + \Theta (1.61 \overline{w' q_s'} - \overline{w' q_T'}) \quad (51)$$

where q_s is the saturation specific humidity. The flux of $\overline{w' q_s'}$ can be evaluated as:

$$\overline{w' q_s'} = \overline{w' \frac{dq_s}{dT}} \theta' = 0.622 \frac{L}{R_d T} q_s \frac{\overline{w' \theta'}}{\Theta} \quad (52)$$

where the Clausius-Clayperon equation, $\frac{dq_s}{dT} = 0.622 \frac{L}{R_d T} q_s$, is used. Taking (47) into consideration and $q_T = q_s + q_L$, we have:

$$\overline{w' \theta'} = \overline{w' \theta_L'} + \frac{\Theta}{T} \overline{w' q_L'} = \overline{w' \theta_L'} + \frac{\Theta}{T} \frac{L}{C_p} (\overline{w' q_L'} - \overline{w' q_s'}) \quad (53)$$

Inserting (52) and (53) into (51), we obtain:

$$\overline{w'\theta'_v} = \frac{1-q_T+1.61q_s\left(1+0.622\frac{L}{R_dT}\right)}{1+0.622\frac{L}{R_dT}\frac{L}{C_pT}q_s} \overline{w'\theta'_L} + \Theta \overline{w'q'_T} \left\{ \frac{L}{C_pT} \frac{1-q_T+1.61q_s\left(1+\frac{0.622L}{R_dT}\right)}{1+0.622\frac{L}{R_dT}\frac{L}{C_pT}q_s} - 1 \right\} \quad (54)$$

For the calculation of the subgrid-scale buoyancy terms $\beta \overline{w'\theta'_v}$ [Equations (50), or (54)], as a function of the liquid water potential temperature flux $\beta \overline{w'\theta'_L}$ and the total water specific humidity flux $\beta \overline{w'q'_L}$, it has to be determined whether the grid box is saturated or unsaturated. This is usually done by applying the procedure described in Sommeria and Deardorff (1977). In the procedure, it is assumed that the grid box is unsaturated as long as the total water specific humidity q_T is below its saturation value, while it is fully saturated when q_T exceeds it.

The source term, S , on the right hand side of the temperature equations includes divergences (d/dz) of the longwave upwelling and downwelling radiation fluxes (F^\downarrow, F^\uparrow), and also of the shortwave upwelling and downwelling fluxes (S^\downarrow, S^\uparrow). Radiative cooling/warming, expressed by these fluxes, can significantly influence turbulence when clouds or fog are present in the ABL.

Typical distribution of the radiative fluxes in the stratus-topped boundary layer is shown in Figure 2. Longwave cooling at the cloud top exists due to the different radiative properties of water vapor and water. Water vapor cannot emit longwave radiation, while water droplets emit as black-body emitters at all longwave frequencies. This leads to a sharp change in the downward flux across the cloud top. The downward longwave flux, F^\downarrow , above the cloud is smaller than the flux in the cloud layer. On the other hand, the upward flux F^\uparrow remains quite uniform with height, with only a slight change at the cloud base, due to the slight difference in temperature.

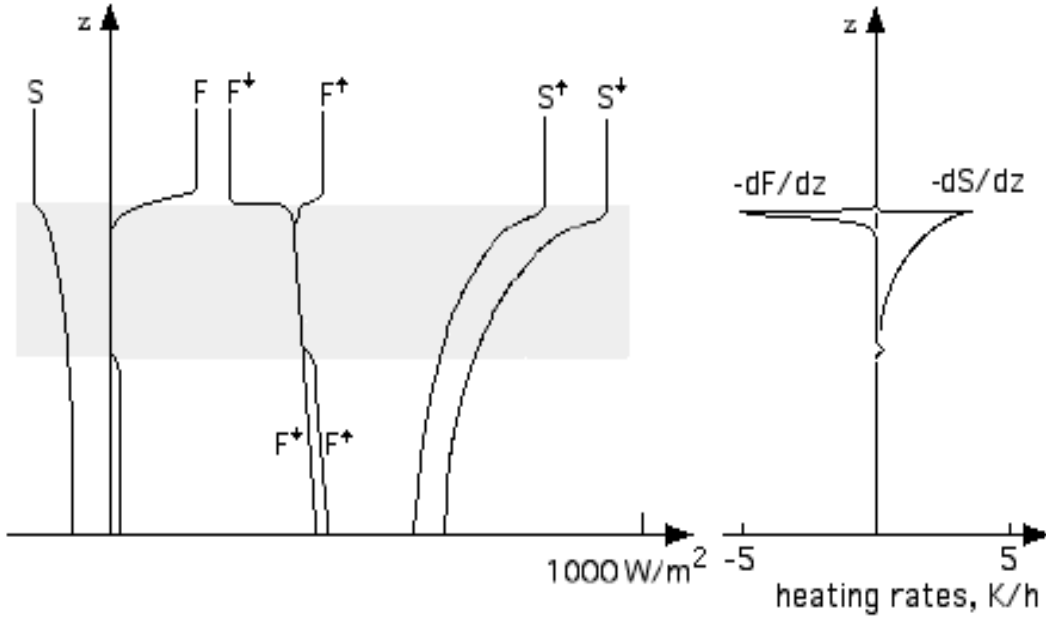


Figure 2. Typical distribution of radiative fluxes in the stratus topped ABL: longwave and shortwave fluxes (upwelling and downwelling fluxes are marked by arrows), net fluxes F and S , and the corresponding heating/cooling rates. The cloud layer is shaded.

The net flux $F = F^\downarrow - F^\uparrow$ sharply increases with height at the cloud top. The resulting flux divergence leads to a strong cooling (about several K/hour) over a very thin layer (of about 50 m) at the cloud top (a typical clear-air longwave radiation cooling is about 1-2 K/day). Note that the net solar flux $S = S^\downarrow - S^\uparrow$ inside the cloud is more uniformly distributed. The shortwave heating is smaller than the longwave cooling, and it is distributed over a thicker layer within a cloud.

Radiation can be modeled in different ways. In the simplest approach, radiation is parameterized as the sum of two components: a clear sky radiative cooling component, typically taken to be -2 K/day everywhere below the inversion, and a cloud-associated "Beer's law". In the latter, long-wavelength radiative cooling is assumed to be proportional to the liquid-water content and exponentially attenuated. The resulting radiative flux F is (Moeng, 2000):

$$F(x, y, z) = F_i \exp[-\rho_o K_a \int_z^\infty q_L(x, y, Z) dZ] \quad (55)$$

where F_i is the longwave radiation flux above the cloud, ρ_o is the reference density, K_a is the longwave absorption coefficient, and q_L is the local liquid water mixing ratio. In a more complex approach, the method of Toon et al. (1989), or the SBDART model (Santa Barbara DISTORT Atmospheric Radiative Transfer, Ricchiazzi et al. 1998) can be applied.

2.5 Numerical Scheme

Typically for discretisation of the LES governing equations, a staggered grid (Arakawa's grid C) is used. In this arrangement, the velocity components are defined on the sides of a rectangular grid volume, while scalars (i.e. the pressure, temperature, specific humidity, subgrid TKE, and exchange coefficients) are defined in the center. The vertical velocity is defined at the bottom and at the top of the grid volume, and the components of the stress tensor T as shown in Figure 3.

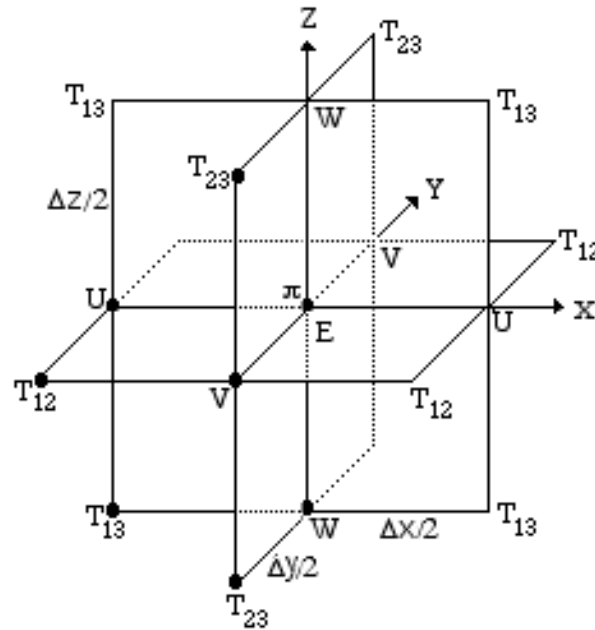


Figure 3. A view of a grid cell centered at a grid point (i, j, k) . The variables with indices (i, j, k) are indicated by darkened circles. Note that the velocity components are defined on the sides of a rectangular grid volume, while scalars (i.e. pressure, subgrid TKE, temperature, the specific humidity, and the exchange coefficients) are defined in the center.

The governing differential equations are transformed into finite difference ones, with the advection terms written in flux form. The monotone scheme developed by Beets and Koren (1996) is often applied. The diffusion terms are expressed by using a second-order, spatial central difference scheme. The Coriolis terms are averaged over four points in order to center them at the respective point under consideration. Although this presents no problems, it does mean that total kinetic energy may not be conserved quite as accurately as in the absence of these terms (Deardorff, 1973).

In time-dependent numerical simulations, it is necessary to start with the initial conditions being as realistic as possible, especially for mean wind and temperature structures. Random initial perturbations of substantial amplitude have to be superimposed upon the mean fields of temperature and vertical velocity.

Time-advancement is often executed by using the fourth-order Runge-Kutta method, which is stable and accurate. It can be explained, noting that each LES prognostic equation can be written in the form:

$$\frac{\partial \Phi}{\partial t} = F \quad (56)$$

where Φ is any prognostic variable (i.e., u , v , w , Θ , q , and E). During each time step, the 3-stage numerical scheme is applied for each equation:

$$\begin{aligned} \Phi^{(1)} &= \Phi^{(m)} + \Delta t_1 (C_{11} F^{(m)} + C_{21} F^{(m-1)}) \\ \Phi^{(2)} &= \Phi^{(1)} + \Delta t_2 (C_{12} F^{(1)} + C_{22} F^{(m)}) \\ \Phi^{(m+1)} &= \Phi^{(2)} + \Delta t_3 (C_{13} F^{(2)} + C_{23} F^{(1)}) \end{aligned} \quad (57)$$

where m and $m+1$ are moments of time. The coefficients in (57) are defined as follows: $C_{11} = 8/15$, $C_{12} = 5/12$, $C_{13} = 3/4$, $C_{21} = 0$, $C_{22} = -17/60$, and $C_{23} = -5/12$. At each stage the most current values of Φ are used in the functional evaluation. The time steps Δt_1 , Δt_2 , and Δt_3 are calculated at each stage from the Courant-Friedrichs-Levy condition (1928):

$$n = \Delta t_i \max_j (|u_j| / \Delta x_j) \quad (58)$$

where n is a Courant-Friedrichs-Levy number, assumed to be 0.20, and $i = 1, 2, 3$. The total time step is $\Delta t = \Delta t_1 + \Delta t_2 + \Delta t_3$.

The Courant-Friedrichs-Levy condition can be alleviated by allowing the coordinate system to translate downstream with the approximate speed U_i of the average flow. Consequently, translating variables can be introduced: $x_{i(g)} = x_i - U_i t$ and $u_{i(g)} = u_i - U_i$. In such a Galilean transformation, it must be remembered that the translation speed needs to be taken into account when formulating the lower boundary condition on the stress and the heat flux (with $u_i = u_{i(g)} + U_i$), and also with respect to the Coriolis terms, which are transformed as: $f(u_i - G_i) = f(u_{i(g)} + U_i - G_i)$, where G_i is the component of the geostrophic wind and f is the Coriolis parameter.

At the lower boundary, the vertical velocity w is set to zero. It is also assumed that $\partial E / \partial z = 0$ for the TKE. For horizontal velocities, one resorts to the Monin-Obuhkov similarity. This is because profiles near the surface are strongly curved. This curvature cannot be resolved within the first grid cell. This means that a relation is specified between the surface stress and the horizontal velocity in the first grid cell. Furthermore, it is assumed that the velocity and stress are parallel. Surface similarity is then used to obtain the surface temperature, T , from the temperature calculated in the center of the first grid cell.

With respect to the upper boundary conditions, it is assumed: $\partial u/\partial z = \partial v/\partial z = w = T_{13} = T_{23} = \partial E/\partial z = H_3 = 0$. The temperature gradient at the top of the calculation domain is set equal to the gradient Γ , which is prescribed in the initial conditions as the temperature gradient above the boundary layer. The horizontal boundary conditions are assumed to be periodic (Figure 4).

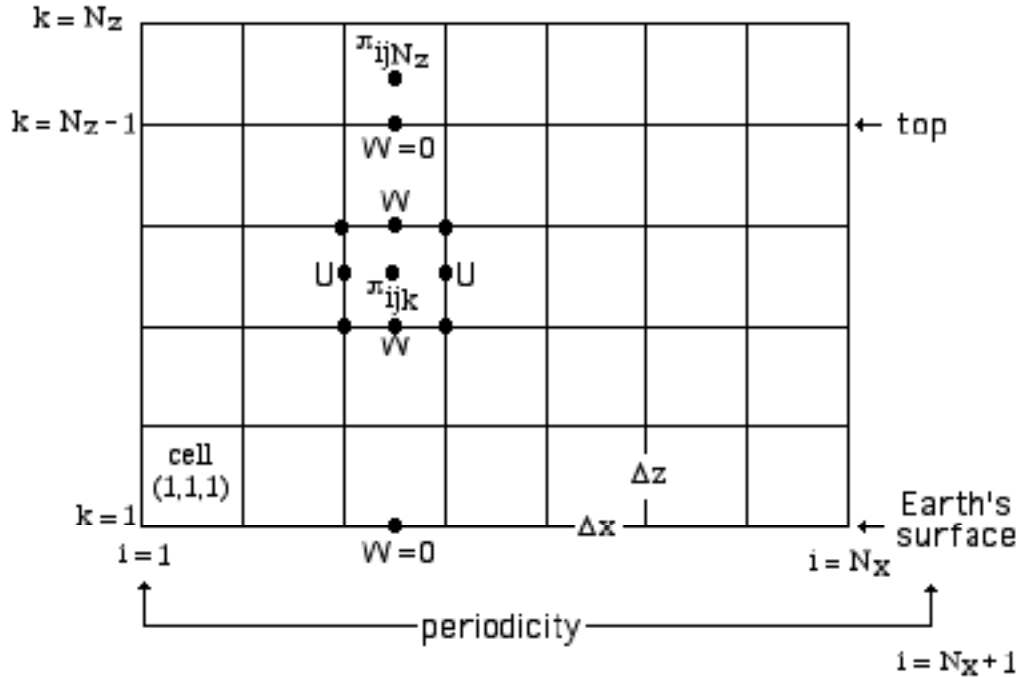


Figure 4. The side view of the mesh. At the lower boundary (the earth's surface), and at the level $k = N_z - 1$ (top level of the model), the vertical velocity w is set to zero. Values in cells located above the top level are calculated based on boundary conditions.

To avoid reflecting gravity waves from the top of the domain, a damping layer is used. The role of the damping layer is to dissipate gravity waves before they can reflect back into the boundary layer. This is accomplished by adding a relaxation term in the form $r(\Phi - \Phi_0)$ to the equations of motion in the upper part of the domain, where Φ is a prognostic parameter and Φ_0 is its value near the top of the domain. The relaxation term dampens fluctuations at time scales larger than a prescribed relaxation time scale $\tau = 1/r$. The relaxation parameter is a function of height:

$$r(z) = r_o \{1 - \cos [\pi (z - z_b)/(z_T - z_b)]\}^2/2 \quad (59)$$

where r_o is a given relaxation constant (order of 0.01 s^{-1}), z_T and z_b indicate the top of the computational domain and the bottom of the damping layer respectively.

Often, there is need to consider a large-scale vertical motion, referred to as subsidence W . Subsidence can be included by adding source terms representing

the downward advection (e.g., $-W \partial \Theta / \partial z$). These terms are relatively small and should be included only in the thermodynamic equations for temperature and humidity (and other scalars), where they can be important in maintaining long-term balances. In the boundary layer, the subsidence velocity can be assumed to be given by $W = -D z$, where D is the large-scale divergence. Above the ABL, $W = -D z_i$.

To find pressure, one might consider Equation (56), written only for velocity components, u , v , and w . The functions F should be expressed in a form in which the pressure terms are singled out:

$$\begin{aligned} F_u &= f_u - \partial \pi / \partial x \\ F_v &= f_v - \partial \pi / \partial y \\ F_w &= f_w - \partial \pi / \partial z \end{aligned} \quad (60)$$

Based on (57) and (60), we will obtain for the first partial time step:

$$\begin{aligned} u^{(1)} &= D_u^{(m)} - C_{11} \Delta t_1 \partial \pi / \partial x \\ v^{(1)} &= D_v^{(m)} - C_{11} \Delta t_1 \partial \pi / \partial y \\ w^{(1)} &= D_w^{(m)} - C_{11} \Delta t_1 \partial \pi / \partial z \end{aligned} \quad (61)$$

where

$$\begin{aligned} D_u^{(m)} &= u^{(m)} + \Delta t_1 (C_{11} f_u^{(m)} + C_{21} F_u^{(m-1)}) \\ D_v^{(m)} &= v^{(m)} + \Delta t_1 (C_{11} f_v^{(m)} + C_{21} F_v^{(m-1)}) \\ D_w^{(m)} &= w^{(m)} + \Delta t_1 (C_{11} f_w^{(m)} + C_{21} F_w^{(m-1)}) \end{aligned} \quad (62)$$

Note that analogous expressions are obtained for the sequential partial time steps,

The continuity equation can be written in the finite differences form:

$$\delta_x u^{(1)} + \delta_y v^{(1)} + \delta_z w^{(1)} = 0 \quad (63)$$

where

$$\begin{aligned} \delta_x u^{(1)} &= (u^{(1)}_{i+1,j,k} - u^{(1)}_{i,j,k}) / \Delta x \\ \delta_y v^{(1)} &= (v^{(1)}_{i,j+1,k} - v^{(1)}_{i,j,k}) / \Delta y \\ \delta_z w^{(1)} &= (w^{(1)}_{i,j,k+1} - w^{(1)}_{i,j,k}) / \Delta z \end{aligned} \quad (64)$$

and the indices, i , j , and k refer to a cell number (see Figure 4). Substituting (61) into (63) yields the pressure equation:

$$\delta_{xx} \pi_{i,j,k} + \delta_{yy} \pi_{i,j,k} + \delta_{zz} \pi_{i,j,k} = G_{i,j,k} \quad (65)$$

where

$$\delta_{xx} \pi_{i,j,k} = (\pi_{i+1,j,k} - 2 \pi_{i,j,k} + \pi_{i-1,j,k}) / \Delta x^2$$

$$\delta_{yy} \pi_{i,j,k} = (\pi_{i,j+1,k} - 2 \pi_{i,j,k} + \pi_{i,j-1,k}) / \Delta y^2$$

$$\delta_{zz} \pi_{i,j,k} = (\pi_{i,j,k+1} - 2 \pi_{i,j,k} + \pi_{i,j,k-1}) / \Delta z^2$$

$$G_{i,j,k} = [\delta_x D_u^{(m)} + \delta_y D_v^{(m)} + \delta_z D_w^{(m)}] / (C_{11} \Delta t_1)$$

for $i = 1, \dots, N_x$, $j = 1, \dots, N_y$, $k = 1, \dots, N_z - 1$, and the operators δ_x , δ_y , and δ_z defined as in (64). Employing (61)-(64), and assuming the vertical velocity $w_{i,j,1} = w_{i,j,N_z-1} = 0$, yields the vertical boundary conditions for pressure:

$$(\pi_{i,j,2} - \pi_{i,j,1}) / \Delta z^2 = R_{i,j,1} - L_1 \quad \text{for } k = 1 \quad (66)$$

$$-(\pi_{i,j,N_z} - \pi_{i,j,N_z-1}) / \Delta z^2 = R_{i,j,N_z-1} + L_{N_z-1} \quad \text{for } k = N_z - 1$$

where

$$L_k = (\pi_{i+1,j,k} - 2 \pi_{i,j,k} + \pi_{i-1,j,k}) / \Delta x^2 + (\pi_{i,j+1,k} - 2 \pi_{i,j,k} + \pi_{i,j-1,k}) / \Delta y^2$$

$$R_{i,j,1} = (\delta_x D_u^{(m)}_{i,j,1} + \delta_x D_v^{(m)}_{i,j,1} + D_w^{(m)}_{i,j,2}) / (C_{11} \Delta t_1)$$

$$R_{i,j,N_z-1} = (\delta_x D_u^{(m)}_{i,j,N_z-1} + \delta_x D_v^{(m)}_{i,j,N_z-1} - D_w^{(m)}_{i,j,N_z-1}) / (C_{11} \Delta t_1)$$

Because of the assumed periodic boundary conditions, we will express the variables in (65)-(66) in a spectral form:

$$\pi_{ijk} = \sum_{m=0}^{N_x-1} \sum_{n=0}^{N_y-1} p(m, n, k) \exp[2\Pi I (\frac{im}{N_x} + \frac{jn}{N_y})] \quad (67)$$

$$G_{ijk} = \sum_{m=0}^{N_x-1} \sum_{n=0}^{N_y-1} g(m, n, k) \exp[2\Pi I (\frac{im}{N_x} + \frac{jn}{N_y})]$$

where $\Pi = 3.14\dots$, $I = \sqrt{-1}$. After the substitution of (67) into (65), we will have:

$$p(m, n, k+1) - [1 + S(m, n)] p(m, n, k) + p(m, n, k-1) = g(m, n, k) \Delta z^2 \quad (68)$$

where $S(m,n) = 4 \frac{\Delta z^2}{\Delta x^2} \sin^2\left(\frac{\Pi m}{N_x}\right) + 4 \frac{\Delta z^2}{\Delta y^2} \sin^2\left(\frac{\Pi n}{N_y}\right)$. Analogous equations for the boundary conditions can be obtained. The term $g(m,n,k)$ can be calculated based on G_{ijk} using the fast Fourier transformation (FFT) subroutine.

Note that (68) constitutes a tri-diagonal system of algebraic equations, which can be solved by employing the factorization method. It is worth mentioning that the case $m = n = 0$ has to be treated separately [i.e., $p(0, 0, k)$ has to be set to an arbitrary constant (e.g., zero)] because the pressure is calculated with an accuracy to a constant. Based on $p(m, n, k)$, the pressure π can be calculated by using the reverse FFT subroutine.

Finally, it should be mentioned that the solutions of the governing LES equations are obtained in a form of fields, which are variable in space and time. Therefore, LES results are usually presented as horizontal and time averaged parameters, defined as

$$\langle u_i \rangle = \frac{1}{L_x L_y T} \int_0^{t_0+T} \int_0^{L_x} \int_0^{L_y} u_i(x, y, z, t) dx dy dt \quad (69)$$

where L_x and L_y define the horizontal domain of a simulation, and T is the time averaging period. Consequently, any LES parameter can be expressed as a mean value and a fluctuation, for example:

$$\begin{aligned} u_i(x, y, z, t) &= \langle u_i \rangle(z) + u_i'(x, y, z, t) \\ \Theta(x, y, z, t) &= \langle \Theta \rangle(z) + \Theta'(x, y, z, t) \end{aligned} \quad (70)$$

Note that any total flux

$$H_{total} = \langle \Theta' u_i' \rangle + \langle H_i \rangle \quad (71)$$

consists of the resolvable flux $\langle \Theta' u_i' \rangle$, which is derived from a LES simulation using (69)-(70), and a subgrid flux $\langle H_i \rangle$, which is obtained by averaging of subgrid fluxes (modeled within a LES).

3 The ABL Simulations

Flow in the boundary layer over land is primarily controlled by the diurnal cycle of the earth's surface energy budget. During the day, a portion of the energy gained at the earth's surface is transferred to the atmosphere as a sensible heat flux, and also used in the evaporation process. This transfer can generate vertical

motions called convection. At night, convection stops and turbulence in the cloud-free ABL can only be generated by wind shear and radiative cooling.

The structure of the ABL is usually classified into four characteristic types: convective, neutral, stable, and cloud-topped. These four prototypes of the ABL have been intensively studied during the last several decades. The LES technique has been especially helpful in this respect. Examples of such simulations are presented below.

3.1 The Convective ABL

3.1.1 Free Convection

Free-convection refers to calm (no mean wind) conditions, controlled only by the strength of the surface heat flux. It is numerically the simplest to achieve because the horizontal domain can be relatively small, while a simulation is relatively short. The boundary conditions during such simulations usually remain unchanged. Consequently, the obtained results are equivalent to the ABL around the solar noon, when all fluxes are approximately constant within a period of about two hours.

Forcing applied at two surfaces, limiting the convective atmospheric boundary layer, the underlying one (where convection is originated), and the upper one (where it is constrained), causes the convective ABL to have a multilayer structure. It consists of the surface layer near the earth's surface, the mixed layer above it, and the interfacial layer next to the free atmosphere (see Chapter 4 in volume I of this book series). The convective surface layer is characterized by a sharp decrease in the potential temperature with height. In the mixed layer, the temperature gradient decreases to zero. In the interfacial layer, there is a sharp increase in the potential temperature with height (as shown in Figure 7a).

Convection in the shearless mixed layer (its animation can be found at the web site: <http://www.mmm.ucar.edu/asr96/sullivan1.html>) is organized in a form of characteristic cell patterns, depicted in Figure 5. Regions of slowly sinking air are surrounded by the areas with updrafts (shaded areas in the figure). Downdrafts cover more than half the area of the horizontal plane over the bulk of the mixed layer depth. Such organization of convection is responsible for non-Gaussian behavior of convective diffusion [Deardorff (1972); Willis and Deardorff (1976, 1978, 1981)]. For elevated sources, the average plume centerline, defined as the mean maximum concentration, descends within a short distance from the source until it reaches the ground. In contrast, the average centerline from near surface releases ascends after a short downwind distance.

Experiments performed by Deardorff (1970) showed that the characteristic of turbulence in the mixed layer can be expressed in terms of similarity scales in the form:

$$\begin{aligned}
 w^* &= (\beta z_i H_o)^{1/3} && \text{for vertical velocity} \\
 \Theta^* &= H_o/w^* && \text{for temperature} \\
 q^* &= Q_o/w^* && \text{for a passive scalar} \\
 z_i &&& \text{for height} \\
 \tau^* &= w^*/z_i && \text{for time}
 \end{aligned} \tag{72}$$

where H_o and Q_o are the surface (virtual) potential temperature and scalar fluxes (of water vapor, CO_2 , O_3 , etc.), $\beta = g/T_o$ is the buoyancy parameter, and z_i is the depth of the mixed layer, traditionally defined as a level at which the heat flux H_o is most negative.

Since there is only one height scale, one temperature scale, and one humidity scale in (72), dimensionless statistics of turbulence in the ABL are expected to be unique functions of a single non-dimensional parameter z/z_i . However, observations show (Sorbján, 1991) that in the upper portion of the mixed layer, a substantial scatter of dimensionless quantities exists, especially for statistics of scalars (temperature, humidity, and concentration of passive scalars). This indicates that the set of scales in equation (72) is incomplete.

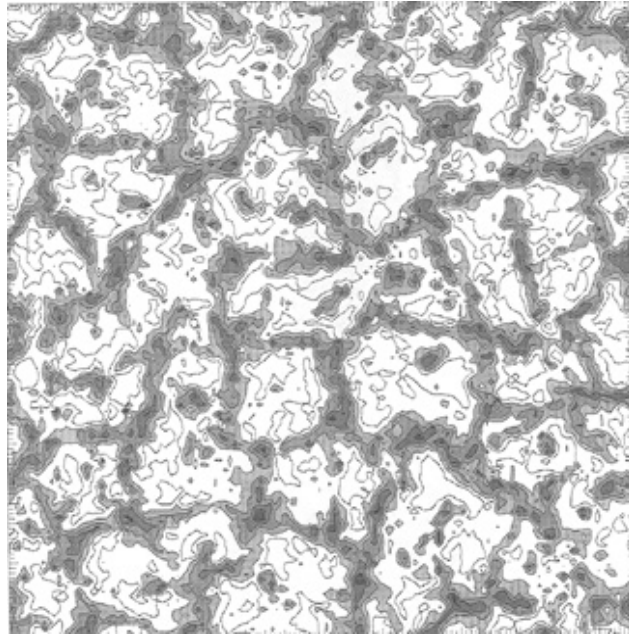


Figure 5. Horizontal cross-section of the LES generated vertical velocity field at $z/z_i = 0.3$ during free convection. Shaded areas indicate updrafts.

The described scatter can be related to a strong sensitivity of statistical moments at the top of the mixed layer to values of the potential temperature gradient γ_i in

the interfacial layer (Sorbjan, 1996 a, b). For example, the (negative) ratio of the heat fluxes at the top and bottom of the mixed layer ($-H_i/H_o$) increases when γ_i increases, and decreases when γ_i decreases to zero. This indicates that γ_i should be treated as an independent scaling parameter for temperature. Analogously, scalar gradients, g_i , at the top of the mixed layer should be treated as additional scaling parameters for other scalars.

The temperature gradient γ_i changes from case to case due to advective transformations, and also during morning transitions from stable to convective conditions. Depending on the intensity of nocturnal cooling, γ_i in the capping inversion, above the evolving morning mixed layer, occurs in a broad range of values, from circa 0.001 K m^{-1} to 0.1 K m^{-1} . Also, the scalar gradient, g_i , varies strongly depending on the content of a scalar q in the mixed layer and in the free atmosphere.

The inclusion of scalar gradients, γ_i and g_i , as governing parameters introduces alternate similarity scales valid in the interfacial layer (Sorbjan, 2004a):

$$\begin{aligned}
 S_w &= w^* && \text{for vertical velocity} \\
 S_\theta &= \gamma_i w^* / N_i && \text{for temperature} \\
 S_q &= g_i w^* / N_i && \text{for humidity (or other scalar)} \\
 S_h &= w^* / N_i && \text{for height} \\
 S_t &= 1 / N_i && \text{for time}
 \end{aligned} \tag{73}$$

where $N_i = [\beta\gamma_i]^{0.5}$ is the Brunt-Väisälä frequency in the interfacial layer. Temperature scale, S_θ , is dependent on the surface heat flux (through w^*) and the temperature gradient, γ_i . The passive scalar scale, S_q , depends on the surface heat flux, the temperature gradient γ_i , and also on the scalar gradient g_i .

To further discuss the free-convective case, let us consider the results of two LES (referred to as A and B), which employed a mesh of $64 \times 64 \times 60$ grid points (Sorbjan, 2004b). The grid increments were $\Delta x = \Delta y = 40 \text{ m}$, and $\Delta z = 30 \text{ m}$. The initial mixed layer was 600 m deep with a uniform potential temperature of 299 K. The interfacial layer was initially 150 m thick. In run A, the initial temperature gradient γ_i in the interfacial layer was equal to 0.01 K m^{-1} , while in run B, it was 0.1 K m^{-1} . In the free-atmosphere, the temperature gradient was assumed to be $\Gamma = 0.003 \text{ K m}^{-1}$. The surface heat flux H_o was assumed to equal 0.075 K m s^{-1} . The simulation time was 26529.4 s in run A and 28459.1 s in run B (i.e., 5000 total time steps).

Figure 6 shows the time history of the mixed layer depth z_i (defined as the height where the heat flux is most negative) and the surface temperature T_o . The curves

representing T_o are alike during both simulations, showing a 3K-increase of the surface temperature. The curves representing z_i diverge in their steepness and smoothness. This indicates that the structure of turbulence at the bottom of the mixed layer in both runs is comparable (because the value of the surface heat flux in both runs is the same), and it differs at the top (because the values of γ_i in both runs are different).

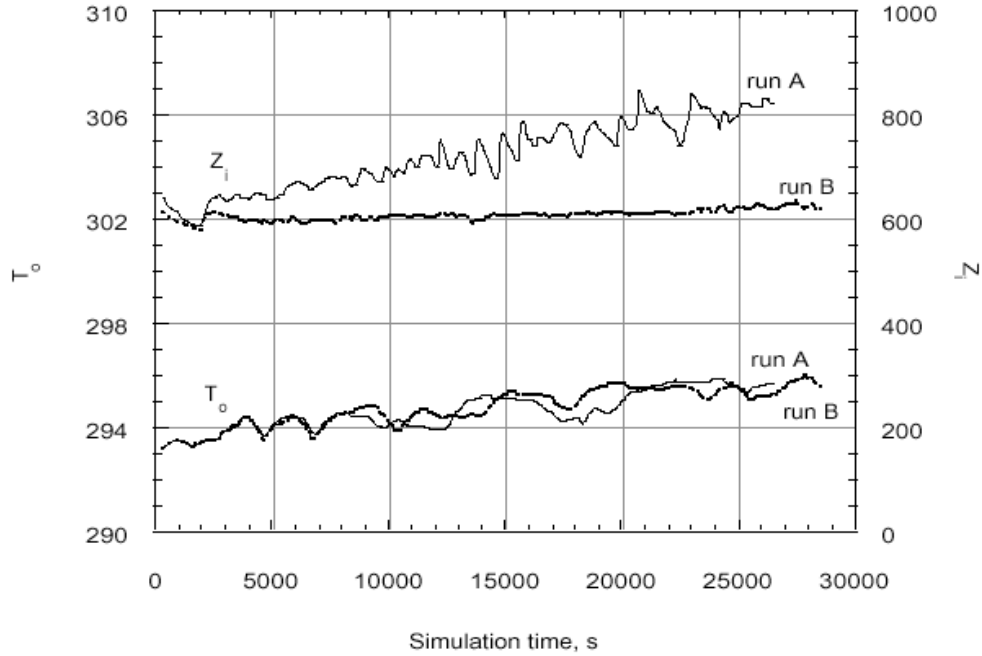
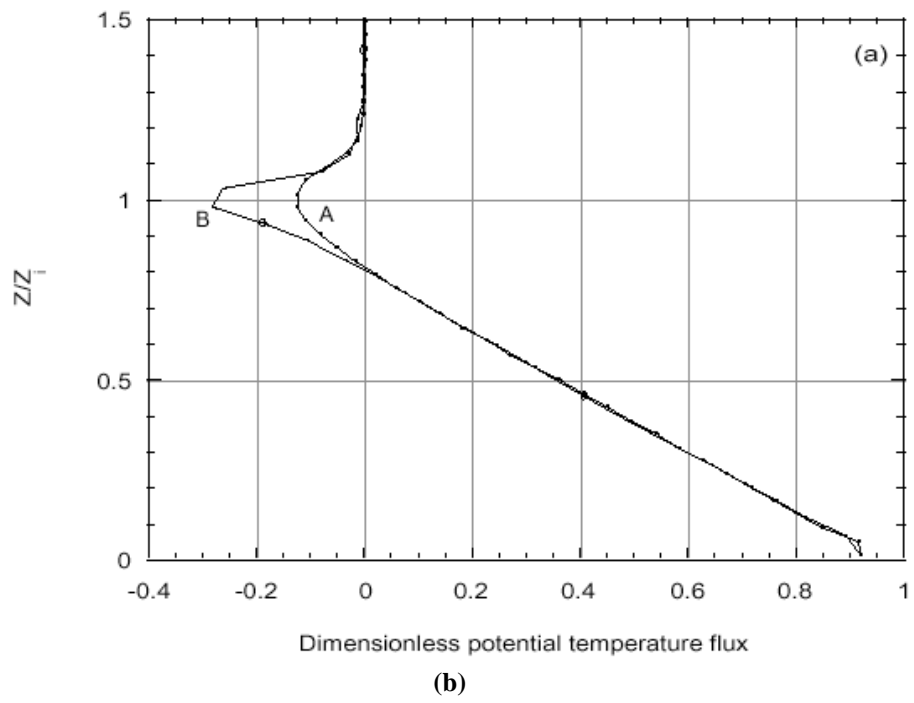
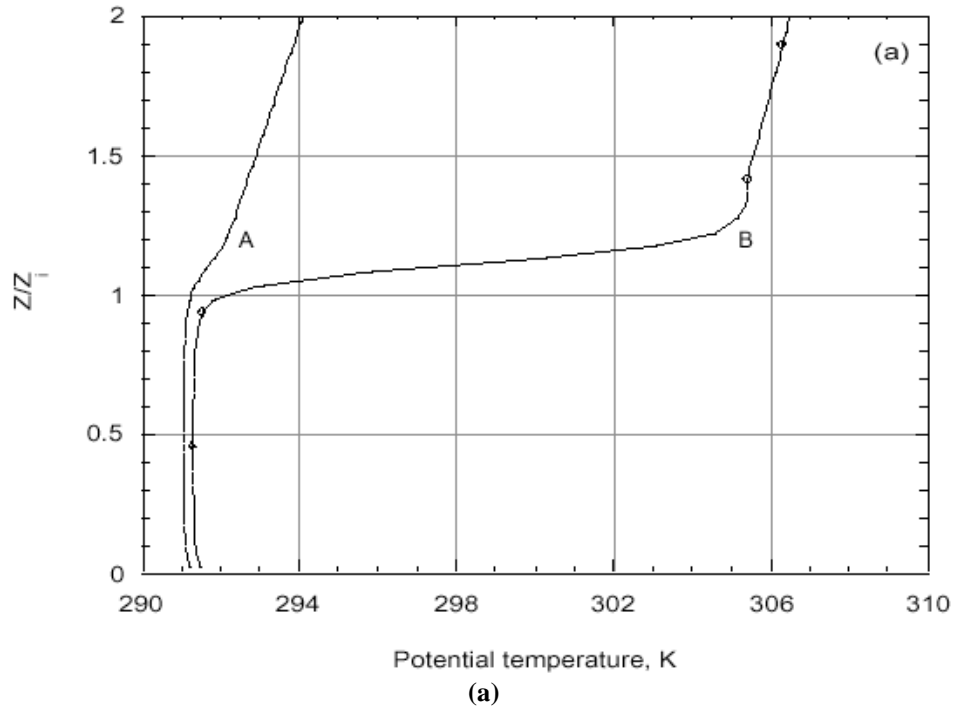


Figure 6. Time history of the averaged height of the mixed layer z_i , and the surface temperature T_o , obtained in free-convective runs A and B.

Figure 7 depicts profiles of the potential temperature θ , its dimensionless flux, and variance. In run A, the dimensionless heat flux at the top of the mixed layer is $H_i/H_o = -0.15$, while in Run B, it is about -0.3 . There is a substantial difference in the values of the temperature variances, $\sigma_\theta^2/\theta_*^2$, at the top of the mixed layer in both runs. In run A, the peak dimensionless variance is about 8, while it is about 40 in run B.



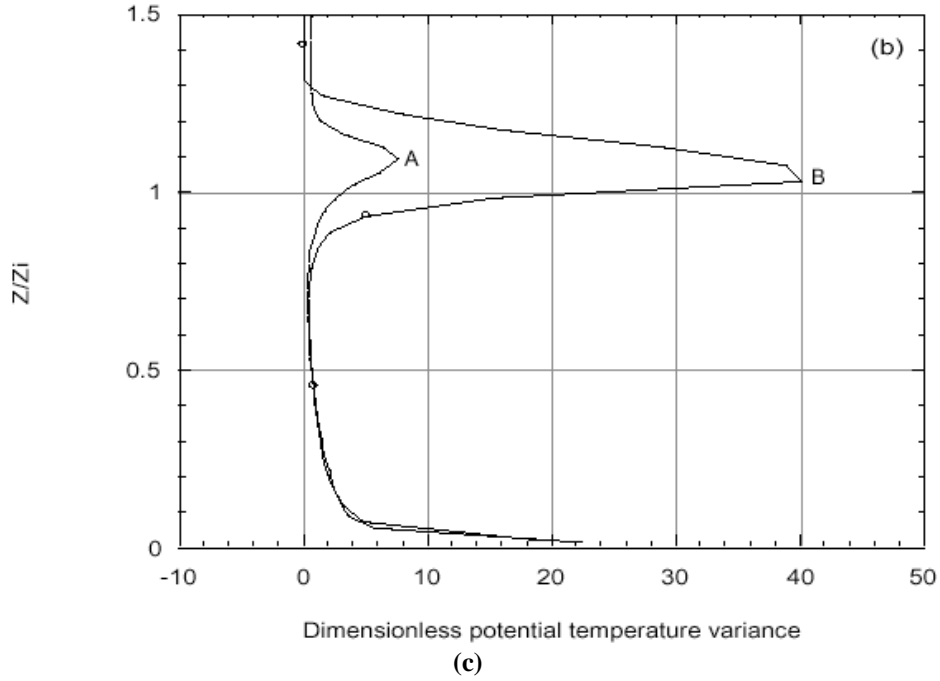


Figure 7. Vertical profiles of: (a) potential temperature, (b) its dimensionless flux, (c) its dimensionless variance in free-convective runs A and B. Diamonds are used to mark run B. The convective scaling (72) is applied.

Profiles of dimensionless velocity variances are shown in Figure 8. There are relatively small differences between profiles of the velocity variances σ_u^2/w_*^2 and σ_w^2/w_*^2 in runs A and B. The values of the horizontal velocity variances in the mixed layer increase slightly when γ_i increases, and the values of the vertical velocity variances decrease. For the purpose of the mixed layer parameterizations, the influence of γ_i on the velocity statistics could be neglected.

The characteristic (e.g., peak) values of the second moments at the top of the mixed layer can be related to the interfacial scales (2) in the following way (Sorbján, 2004 a, b):

$$\begin{aligned}
 H_i &= -c_H S_w S_\theta \\
 Q_i &= -c_Q S_w S_q \\
 \sigma_{\theta i}^2 &= c_\theta S_\theta^2 \\
 \sigma_{q i}^2 &= c_q S_q^2 \\
 C_{\theta q i} &= c_{\theta q} S_\theta S_q
 \end{aligned} \tag{74}$$

where the index "i" refers to the interfacial layer, $C_{\theta q}$ is the temperature-humidity covariance, and the minus in the first two expressions is added in order to stress that the fluxes and gradients are inversely proportional. The parameters c_H , c_Q , c_θ , c_q , and $c_{\theta q}$ are anticipated to be constant.

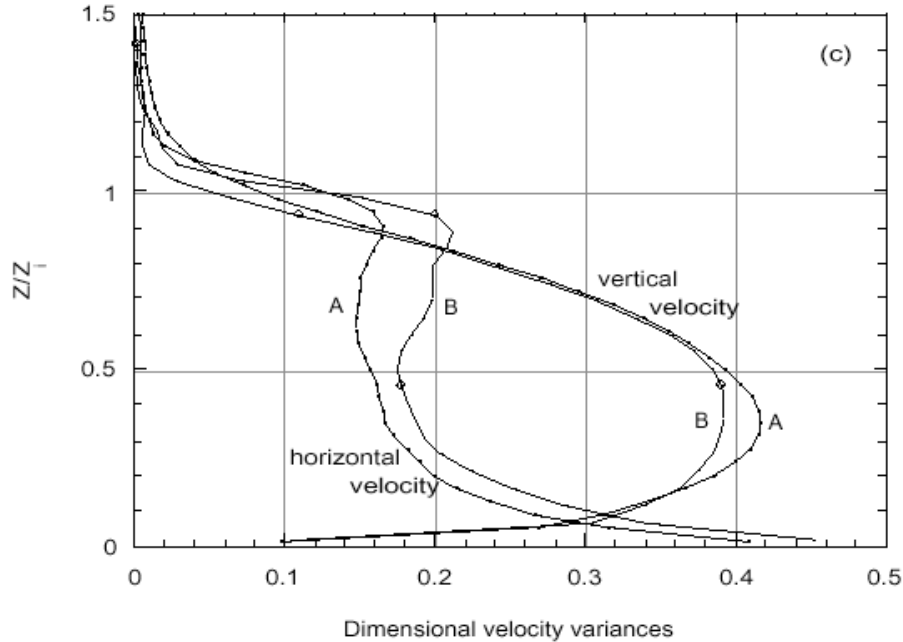


Figure 8. Vertical profiles of dimensionless horizontal σ_u^2/w_*^2 and vertical σ_w^2/w_*^2 velocity variances, obtained in runs A and B. Diamonds are used to mark run B.

The comparison of values given by Equation (74a) with the LES results is shown in Figure 9. In the Figure, the values obtained from Lilly's (1969) classical expression for the entrainment heat flux ($H_i = -\Delta\Theta dz_i/dt$, where $\Delta\Theta$ is the temperature jump at the top of the mixed layer) are also depicted. The expression was originally obtained for the stratocumulus-topped ABL, with a sharp temperature jump $\Delta\Theta$ in an infinitesimally thin interfacial layer. It has been commonly used in cloud-free conditions, even though the underlying assumptions regarding the infinitesimal depth of the interfacial layer are not valid in this case. The expression (74a) seems to be a better approximation of the obtained LES results for larger heat flux ratios, and therefore could be treated as an alternative to Lilly's equation for the cloud-free case.

Based on (74), statistical moments of scalars during free-convection can be expressed in terms of two semi-empirical similarity functions F_m and F_i of the dimensionless height z/z_i (Sorbjan, 2004 a, b):

$$M = S_m F_m(z/z_i) + S_i F_i(z/z_i) \quad (75)$$

where M is a statistical moment, S_m is a combination of the mixed layer scales (72), S_i is a combination of the interfacial scales (73), and F_m and F_i are arbitrary, best-fit functions of a dimensionless argument z/z_i .

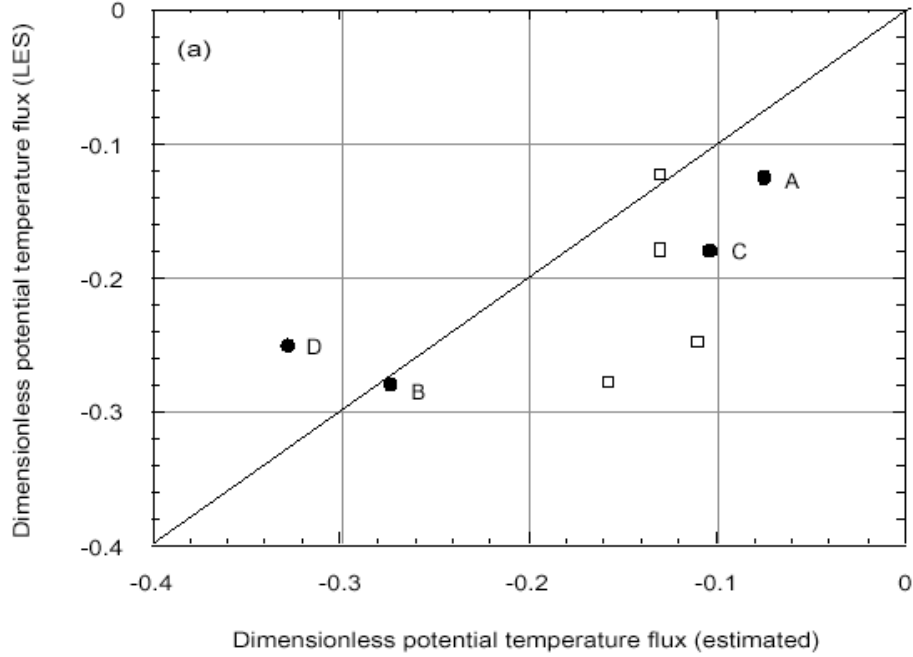


Figure 9. Comparison of the simulated (LES) and estimated from Equation 74a values of the temperature flux ratio H_i/H_0 (dark circles). The squares indicate the values calculated based on Lilly's (1969) expression $H_i = \Delta\Theta dz_i/dt$.

For example, in the case of the heat flux and humidity fluxes, Equation 75 takes the following linear form in the mixed layer (for $z/z_i < 1$):

$$\begin{aligned} H &= w_* \Theta_* (1 - z/z_i) - c_H S_w S_\theta z/z_i \\ Q &= w_* q_* (1 - z/z_i) - c_Q S_w S_q z/z_i \end{aligned} \quad (76)$$

For the variances and covariances, the following expressions could be proposed:

$$\begin{aligned} \sigma_\theta^2 &= c_1 \Theta_*^2 \frac{(1 - z/z_i)}{(z/z_i)^{2/3}} + c_\theta S_\theta^2 \frac{(z/z_i)^9}{(2.05 - z/z_i)^8} \\ \sigma_q^2 &= c_2 q_*^2 \frac{(1 - z/z_i)^8}{(z/z_i)^{2/3}} + c_q S_q^2 \left[\frac{(z/z_i)^3}{(2.2 - z/z_i)^5} + c_s \right] \\ C_{\theta q} &= c_3 \Theta_* q_* \frac{(1 - z/z_i)}{(z/z_i)^{2/3}} + c_{\theta q} S_\theta S_q \frac{(z/z_i)^8}{(2.2 - z/z_i)^8} \end{aligned} \quad (77)$$

and also

$$\frac{d\Theta}{dz} = -\frac{\Theta_*}{z_i} \frac{(1-z/z_i)^4}{(z/z_i)^{4/3}} + \frac{S_\theta}{S_h} \frac{(z/z_i)^9}{(2.23-z/z_i)^9} \quad (78)$$

$$\frac{dq}{dz} = -\frac{q_*}{z_i} \frac{(1-z/z_i)^4}{(z/z_i)^{4/3}} + \frac{S_q}{S_h} \frac{(z/z_i)^9}{(2.23-z/z_i)^9}$$

where c_H , c_Q , c_1 , c_2 , c_3 , c_θ , c_q , $c_{\theta q}$ are empirical constants, and all the expressions are valid below the level at which a moment has its peak (roughly, $z/z_i < 1.1$). For small z , Equation 77 coincides with the Monin-Obukhov similarity predictions.

3.1.2 Forced Convection

During forced convection, turbulence is controlled not only by the strength of the surface heat flux, but also by wind shear. The presence of a sufficiently strong wind breaks the free-convective cells (Figure 5) and replaces them with horizontal rolls, depicted in Figure 10. The forced-convection case is numerically more difficult to achieve because the horizontal domain needs to be larger (several times larger than z_i), while a simulation must be longer (in terms of time steps) than in the free-convective case.

Let us consider six LES runs of the forced convection case, with a mesh of $64 \times 64 \times 60$ grid points, and the grid increments $\Delta x = \Delta y = 40$ m and $\Delta z = 30$ m (Sorbjan, 2004c). All the runs have been obtained for three values of the geostrophic wind G , and for two values of the temperature gradient γ_i in the interfacial layer. The performed runs hereafter are referred to as W05, W10, W15, S05, S10, and S15. The letter "W" indicates runs, for which the initial temperature inversion strength γ_i was relatively weak and equal to 0.01 K m^{-1} . The letter "S" denotes runs with stronger temperature gradients in the interfacial layer, equal to 0.1 K m^{-1} . The numbers 05, 10 and 15 express the assumed values of the geostrophic wind in m s^{-1} . The simulation time was 30460.3 s in run W05 and 14109.6 s in run W15 (10,000 total time steps).

Figures 11 a-b shows the resulting profiles of the potential temperature and wind velocity components. Two families of temperature profiles are depicted in Figure 11a, one with a small temperature jump in the interfacial layer (runs W05, W10 and W15), and the other with a large one (runs S05, S10 and S15). There are three families of u-component velocity (Figure 11b) associated with the values of the geostrophic wind, 5, 10 and 15 m s^{-1} .

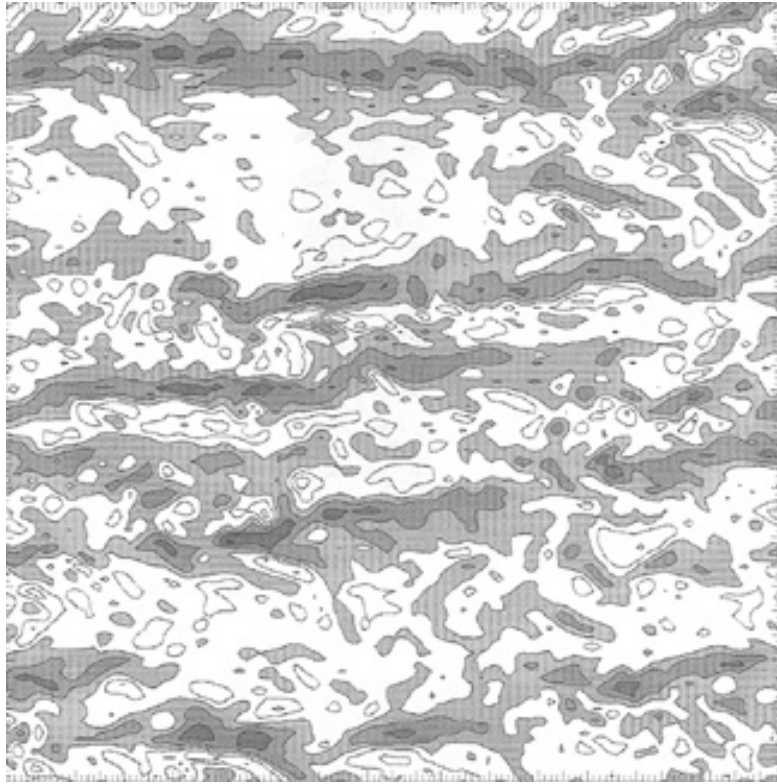
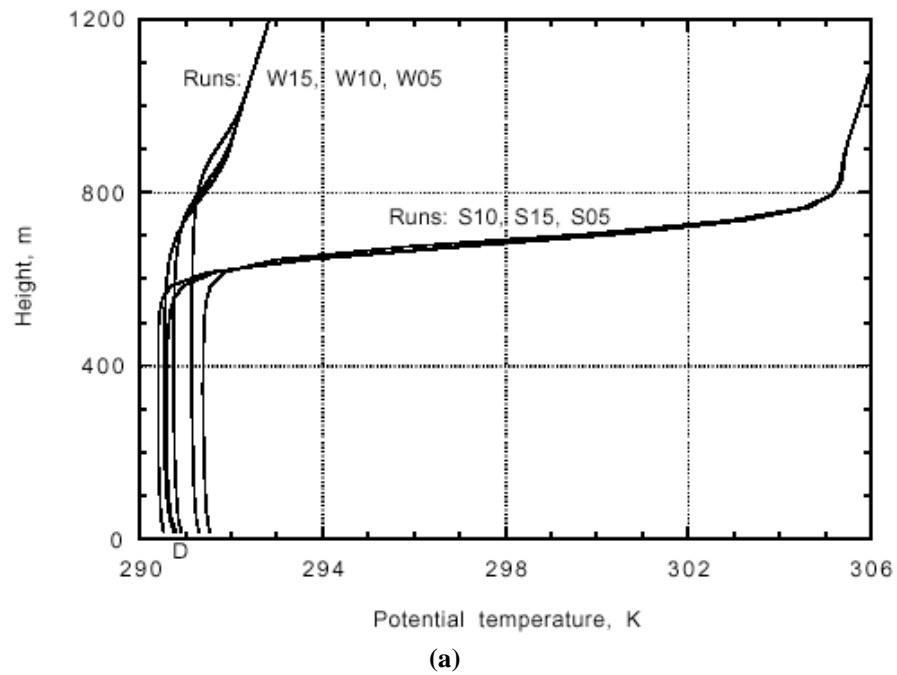


Figure 10. Horizontal cross-section of the LES generated vertical velocity field at $z/z_i = 0.3$ during forced convection. Shaded areas indicate updrafts.



(a)

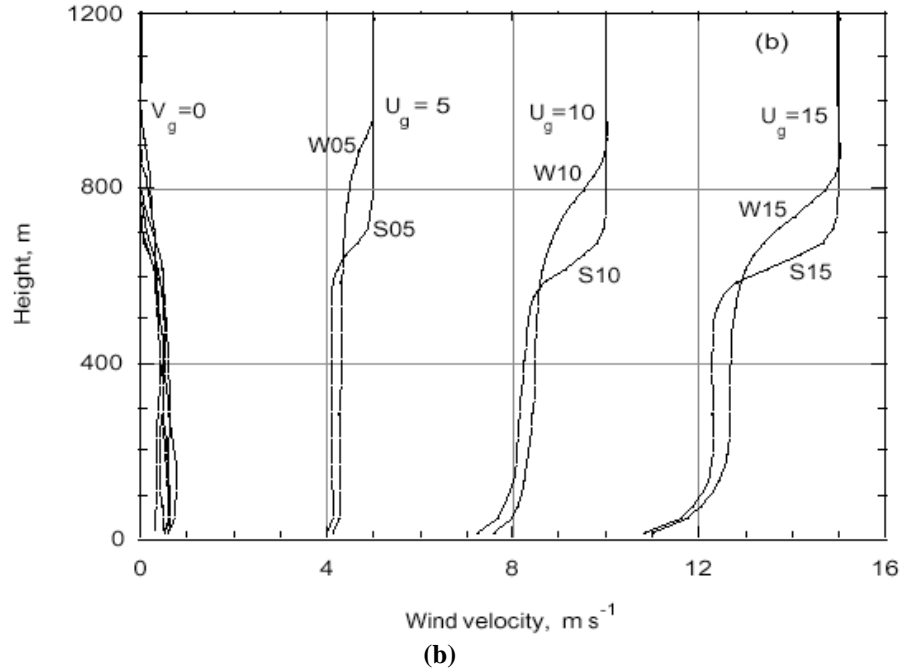


Figure 11. Vertical profiles of: (a) potential temperature, (b) wind velocity components during forced-convective LES runs W05, S05, W10,S10, W15 and S15.

In Figures 12 a-b, the second moments of the potential temperature are shown. Figure 3a indicates that the negative peak values of heat flux H_i increase with the strength of the capping inversion γ_i and with the value of the geostrophic wind G . The same conclusion applies to the temperature variance $\sigma_{\theta_i}^2$ in Figure 13b (note spurious consequences of a sharp temperature gradient in run S15). The dependence of $\sigma_{\theta_i}^2$ on the temperature gradient γ_i is much stronger than on the geostrophic shear.

The second moments of the horizontal and vertical velocity are shown in Figures 13 a-b. The mixed layer values of the horizontal velocity variances σ_u^2/w_*^2 increase when the geostrophic wind increases and seem to be independent of γ_i . The values of the vertical velocity variances $\sigma_{w_i}^2/w_*^2$ at the top of the mixed layer increase when both γ_i and G increase (note spurious consequences of a sharp velocity gradients near the earth's surface).

When wind shear is present, Equation (75) is not valid, because statistics of turbulence at the top of the mixed layer are dependent not only on the temperature gradient γ_i , but also on velocity gradients $s_{xi} = du/dz|_i$ and $s_{yi} = dv/dz|_i$ in the interfacial layer, or equivalently on the interfacial Richardson number (Sorbjan, 2004 a, c):

$$\text{Ri} = \frac{\beta \gamma_i}{s_{x_i}^2 + s_{y_i}^2} \quad (79)$$

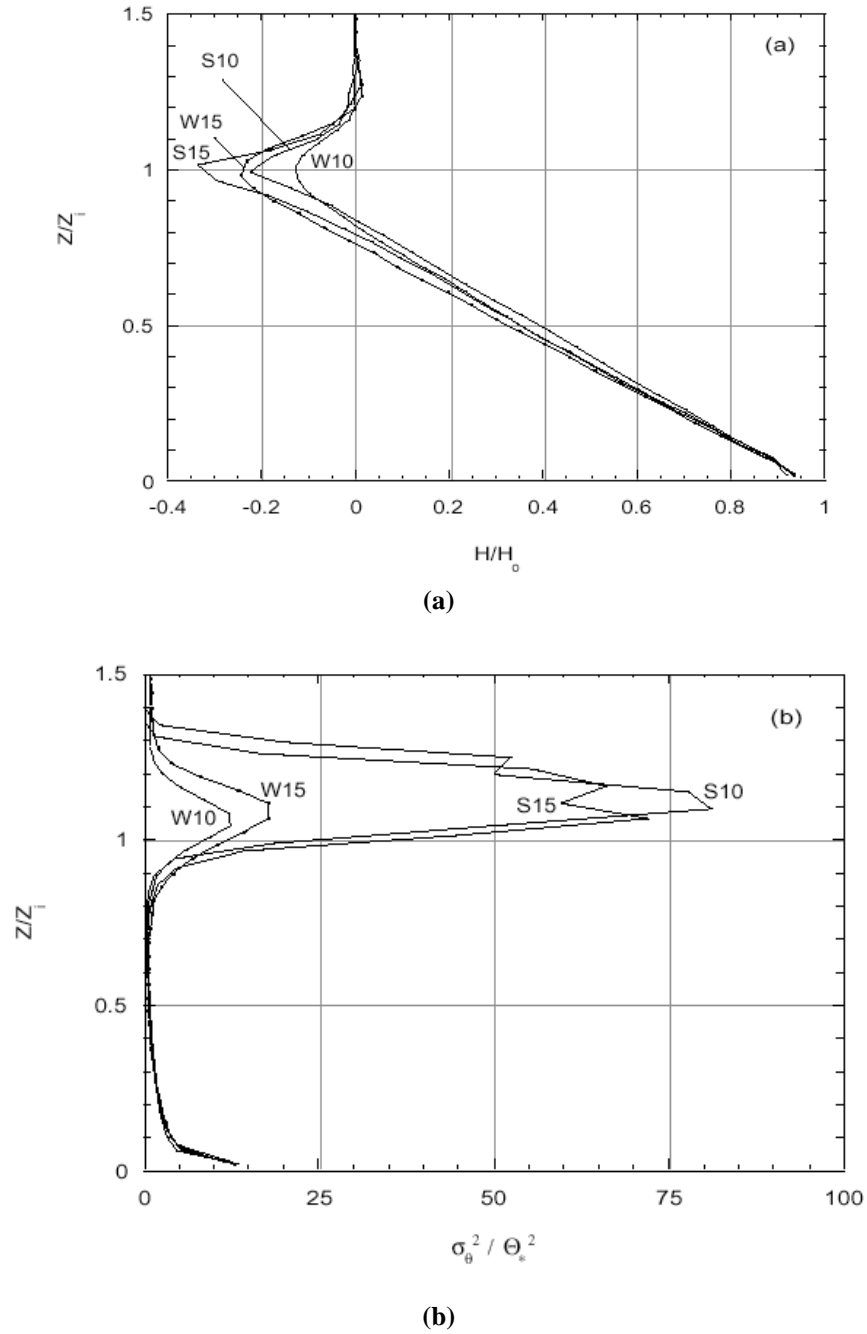


Figure 12. Vertical profiles of: (a) potential temperature flux H/H_0 , (b) potential temperature variance $\sigma_\theta^2 / \Theta_*^2$, obtained in runs W10, W15, S10, and S15.

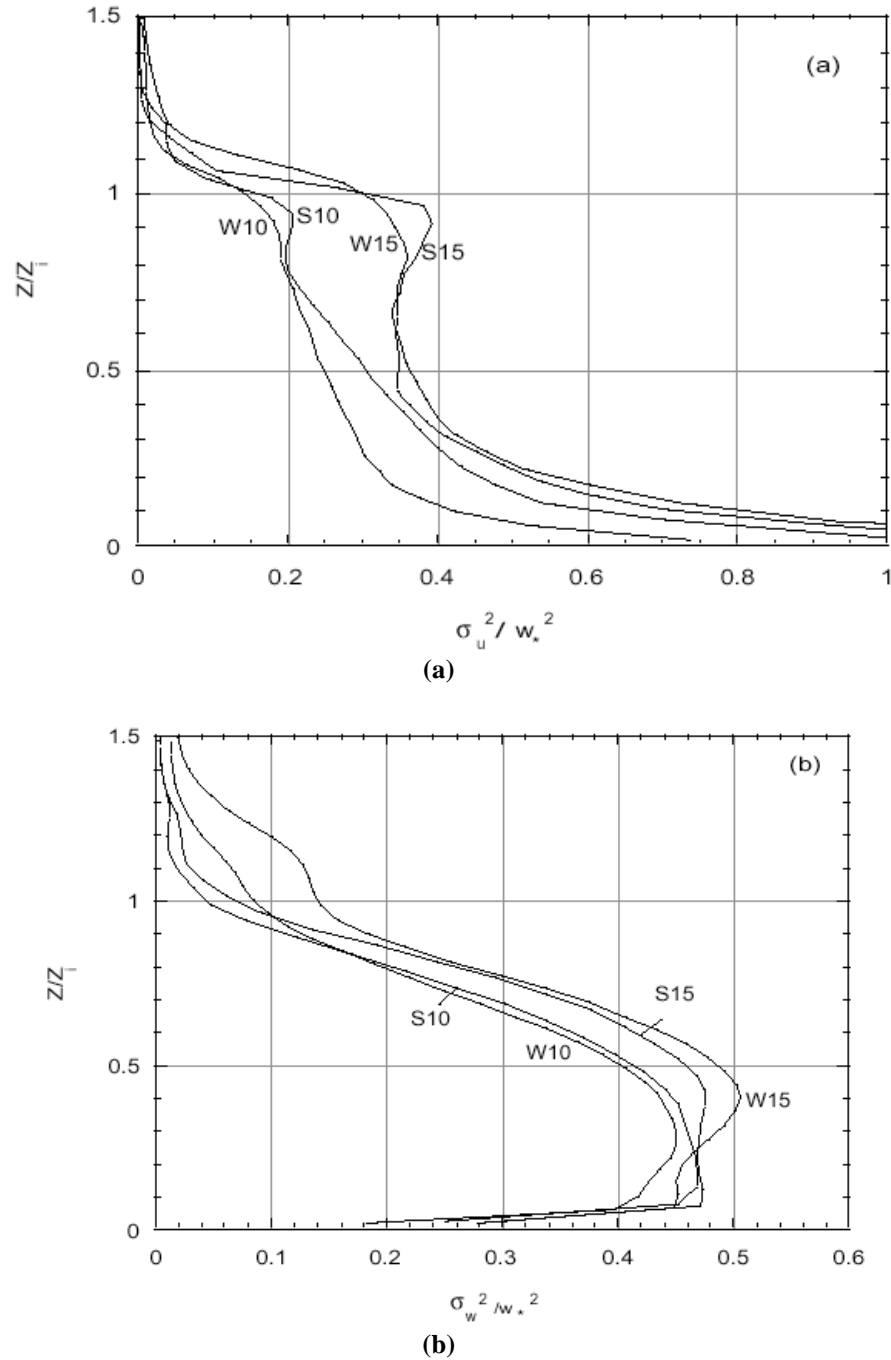


Figure 13. Vertical horizontal σ_u^2/w_*^2 and vertical σ_w^2/w_*^2 velocity variances, obtained in runs W10, W15, S10, and S15.

Characteristic values of statistical moments at the top of the mixed layer, scaled by the interfacial scales S , are not expected to be constant as in the free-convection case, but they should be functions of the interfacial Richardson number (Sorbjan, 2004 a, c):

$$\begin{aligned}
H_i / (S_w S_\theta) &= -c_H (1 + c_r / Ri) / (1 + 1 / Ri)^{1/2} \\
Q_i / (S_w S_q) &= -c_Q (1 + c_r / Ri) / (1 + 1 / Ri)^{1/2} \\
\sigma_{\theta_i}^2 / S_\theta^2 &= c_\theta (1 + c_r / Ri) / (1 + 1 / Ri) \\
\sigma_{q_i}^2 / S_q^2 &= c_q (1 + c_r / Ri) / (1 + 1 / Ri) \\
C_{\theta q_i} / (S_\theta S_q) &= c_{\theta q} (1 + c_r / Ri) / (1 + 1 / Ri) \\
\sigma_{w_i}^2 / S_w^2 &= c_w (1 + c_r / Ri)
\end{aligned} \tag{80}$$

In analogy to (75), statistical moments in the sheared ABL (above the surface layer) can also be represented as a sum of two similarity functions F_m and F_i , multiplied by similarity scales (72) and (73):

$$M = S_m F_m(z/z_i) + S_i F_i(z/z_i, 1/Ri) \tag{81}$$

where the function F_i , in this case, depends on the dimensionless height z/z_i , and also on the interfacial Richardson number Ri . We will assume that $F_i(z/z_i, 1/Ri) = F_1(z/z_i) F_2(1/Ri)$, and $F_2(1/Ri) \rightarrow 1$ when $1/Ri \rightarrow 0$. As a result, (81) coincides with (75) in the shearless case. Equation (81) is valid only above the surface layer since the dependence on z/L is neglected, where $L = -u_*^3 / (\kappa \beta H_\theta)$ is the Monin-Obukhov length, u_* is the friction velocity, and κ is the von Karman constant.

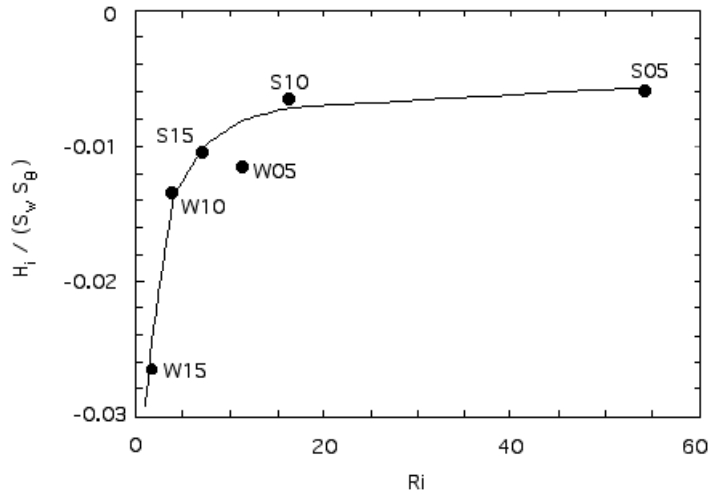


Figure 14. The dimensionless heat flux $H_i / (S_w S_\theta)$ obtained from the LES (dark circles) as a function of the interfacial dynamic Richardson number Ri . Equation 80a is represented by a curve. The LES run names are indicated next to each point.

Figure 14 shows values (points) of the dimensionless entrainment heat flux $H_i / (S_w S_\theta)$ obtained from the LES, as a function of the interfacial dynamic

Richardson number Ri . The run names are indicated next to each point. The curve and the points agree quite well. As expected, the negative values of the dimensionless entrainment heat flux increase when Ri decreases, and decrease when Ri increases.

Figure 15 depicts the values of the dimensionless vertical velocity variance σ_{wi}^2/S_w^2 at the top of the mixed layer (points), obtained from the LES. In the figure, the estimated dimensionless peak variance, based on Equation 7d, is represented by a curve. The curve and the points agree quite well. The obtained results show that σ_{wi}^2/S_w^2 strongly increases when Ri decreases, and decreases when Ri increases.

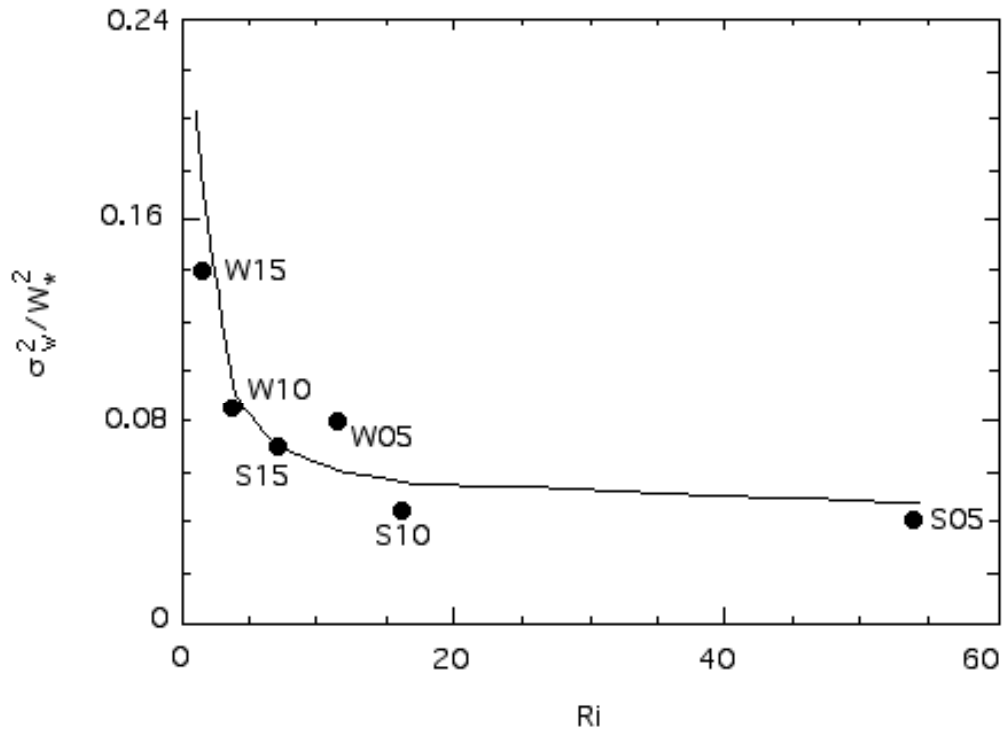


Figure 15. The dimensionless variance σ_{wi}^2/S_w^2 obtained from the LES model (dark circles) as a function of the interfacial dynamic Richardson number Ri . Equation 80a is represented by a curve. The LES run names are indicated next to each point.

Based on (80)-(81), the following expressions could be proposed Sorbjan (2004c):

$$\begin{aligned}
H &= w_* \Theta_* (1 - z/z_i) - c_H S_w S_\theta \frac{(1 + c_{rH}/Ri)}{(1 + 1/Ri)^{0.5}} z/z_i \\
Q &= w_* q_* (1 - z/z_i) - c_Q S_w S_q \frac{(1 + c_{rQ}/Ri)}{(1 + 1/Ri)^{0.5}} z/z_i \\
\sigma_\theta^2 &= c_1 \Theta_*^2 \frac{(1 - z/z_i)}{(z/z_i)^{2/3}} + c_\theta S_\theta^2 \frac{(1 + c_r/Ri)}{(1 + 1/Ri)} \frac{(z/z_i)^9}{(2.05 - z/z_i)^8} \\
\sigma_q^2 &= c_2 q_*^2 \frac{(1 - z/z_i)^8}{(z/z_i)^{2/3}} + c_q S_q^2 \frac{(1 + c_r/Ri)}{(1 + 1/Ri)} \left[\frac{(z/z_i)^3}{(2.2 - z/z_i)^5} + c_s \right] \\
C_{\alpha_q} &= c_3 \Theta_* q_* \frac{(1 - z/z_i)}{(z/z_i)^{2/3}} + c_{\alpha_q} S_\theta S_q \frac{(1 + c_r/Ri)}{(1 + 1/Ri)} \frac{(z/z_i)^8}{(2.2 - z/z_i)^8} \\
\sigma_w^2 &= 1.4 c_3 (1 - z/z_i)^{4/3} (z/z_i)^{2/3} + c_w S_w^2 (1 + c_r/Ri) (z/z_i)^{1/2} (1.1 - z/z_i)^{1/3}
\end{aligned} \tag{82}$$

and also:

$$\begin{aligned}
\frac{d\Theta}{dz} &= -\frac{\Theta_*}{z_i} \frac{(1 - z/z_i)^4}{(z/z_i)^{4/3}} + \frac{S_\theta}{S_h} \frac{(z/z_i)^9}{(2.23 - z/z_i)^9} \\
\frac{dq}{dz} &= -\frac{q_*}{z_i} \frac{(1 - z/z_i)^4}{(z/z_i)^{4/3}} + \frac{S_q}{S_h} \frac{(z/z_i)^9}{(2.23 - z/z_i)^9}
\end{aligned} \tag{83}$$

The above expressions are valid for $S_\theta > 0$, below the level at which a moment has its peak (roughly, $z/z_i < 1.1$). When $1/Ri \rightarrow 0$, the free-convection profiles (77)-(78) are obtained. The constants in (82) should be evaluated based on available atmospheric observations.

3.2 Neutral ABL

By definition, the neutral boundary layer is characterized by a constant with height potential temperature, and a zero turbulent heat flux. The neutral ABL is often referred to as the Ekman layer, after V.V. Ekman, who first solved (in 1905) simplified equations of the atmospheric motion for this case, governed by a balance of the Coriolis, pressure gradient, and friction forces.

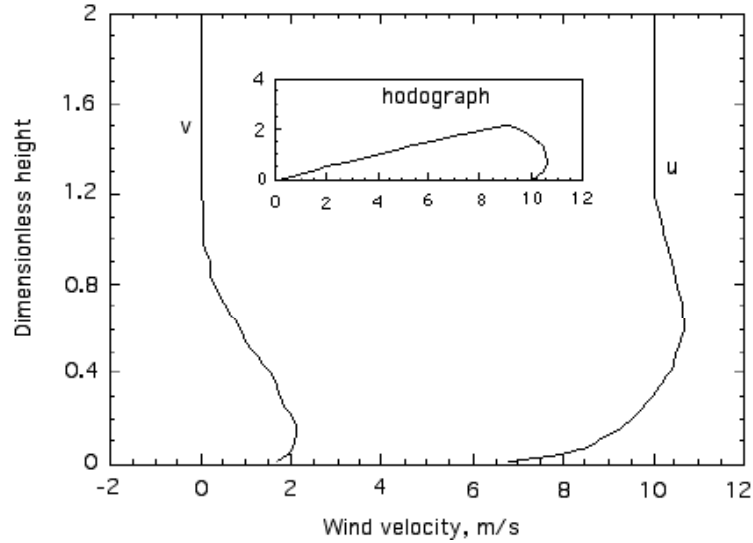
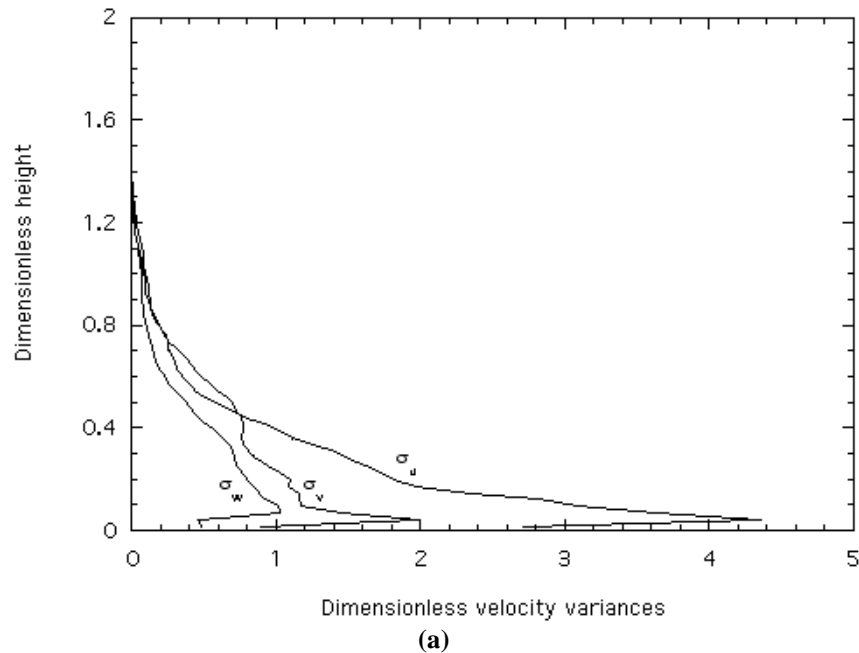


Figure 16. Vertical profiles of wind velocity components u and v from a simulation of a neutral ABL. The wind velocity hodograph is also shown.

In practice, the neutral boundary layer can exist only over marine surfaces when the ocean surface and the air flowing above it have nearly the same temperature. Over land, the neutral ABL is practically absent (note that diurnal transitions do not produce a zero heat flux in the entire ABL, but only in the surface layer and only for a very brief period of time).



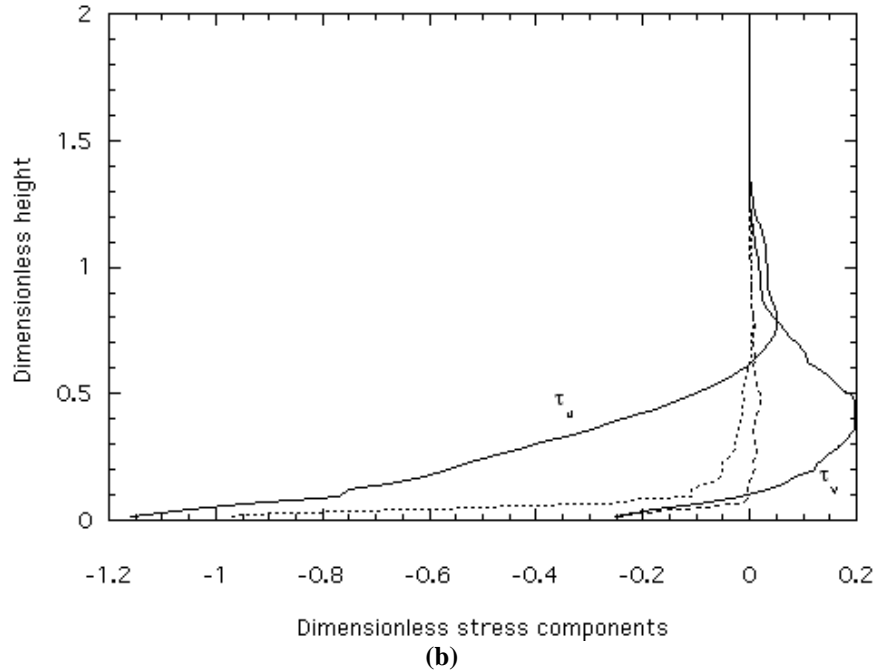


Figure 17. Vertical profiles from a simulation of a neutral ABL (a) Variances of three components of wind velocity, scaled by u_*^2 , (b) components of stress vector (the subgrid fluxes marked by dotted lines).

The physics of the neutral case is not very complex. Turbulence is generated only by wind shear. There is no entrainment unless the stable interfacial layer is assumed at the top. Numerically, the case requires a relatively long integration time to achieve steady conditions, but the horizontal domain does not need to be substantial. The case has not generated much interest and only a few simulations of the neutral ABL have been simulated (Mason and Thompson, 1987 and Andren et al., 1994).

As an example of the neutral case, let us consider the results of a LES, with a mesh of $16 \times 16 \times 80$ grid points, and the grid increments $\Delta x = \Delta y = 50$ m and $\Delta z = 40$ m. The simulation was performed for 135,118.8 s (i.e., 25,000 time steps), with the geostrophic wind $G = 10$ m/s, the Coriolis parameter $f = 0.0001$ s⁻¹, and the roughness parameter $z_o = 0.01$ m. The potential temperature was assumed constant in the entire domain. Therefore, there was no entrainment generated by wind. The resulting friction velocity was $u_* = \sqrt{\tau_o / \rho} = 0.3708$ m s⁻¹ (where τ_o is the surface stress, and ρ the air density). The Ekman height scale $L_E = \kappa u_* / f = 2832$ m (where κ is the von Karman constant). The results of the simulation are depicted in Figures 16 and 17. The vertical axes in the figures are scaled by L_E .

Figure 16 shows the vertical profiles of the wind components, as well as the resulting wind hodograph. The cross-isobar angle of about 30° is obtained. The velocity variances, depicted in Figure 17a, decrease with height. Figure 17b presents the total and subgrid contributions to the stress vector components.

3.3 Stable ABL

The stable ABL is usually observed at night over land, or over cold marine surfaces, when the heat flux is negative and turbulence is generated mainly by wind shear. The stable case is difficult to simulate, because the grid spacing must be small (a few meters), and the simulation time long. Stronger cooling rates at the surface require a higher grid resolution. If grid spacing is too coarse, a simulation can produce a spurious laminarization of the flow. There have been only a few reported stable ABL simulations (Mason and Derbyshire, 1990, Brown et al., 1994, Andren, 1996, Galmarini et al., 1998, Kosovich and Curry, 2000, Saiki et al. 2000, Beare et al., 2004, and Beare and MacVean, 2004).

In stable conditions, turbulence is local and suppressed by stratification effects. Based on this premise, Nieuwstadt (1984) introduced the local similarity scaling in this case:

$$\begin{aligned}
 U_*(z) &= [\tau(z)/\rho]^{1/2} && \text{for velocity} \\
 g_*(z) &= -\frac{H(z)}{U_*(z)} && \text{for temperature} \quad (84) \\
 \Lambda_*(z) &= -\frac{U_*^2(z)}{\kappa \beta g_*(z)} && \text{for height}
 \end{aligned}$$

where $H(z)$, and $\tau(z)/\rho$ are turbulent fluxes of heat and momentum. The above scales are analogous to the Monin-Obukhov scaling in the surface layer. As in the surface layer, it could be expected that statistical moments that are non-dimensionalized by local scales are constant (Sorbjan, 1986).

For $z/h < 1$, it can be assumed that $\tau/\rho(z) = u_*^2(1 - z/h)^{\alpha_1}$ and $H(z) = H_o(1 - z/h)^{\alpha_2}$, where h is the depth of the stable layer, u_* is the friction velocity, H_o is the surface value of the heat flux, and α_1 and α_2 are empirical parameters that are case (radiative conditions) dependent. Once they are determined, all turbulent statistics of the flow may be predicted, assuming their proportionality to the local scales. For example, during the 1973 Minnesota experiment, it was found that $\alpha_1 = 2$ and $\alpha_2 = 3$ (Sorbjan, 1986). Nieuwstadt (1984) found $\alpha_1 = 3/2$ and $\alpha_2 = 1$ based on data collected from the Cobauw tower. Note that $\alpha_2 = 1$ indicates quazi-stationary conditions with uniformly constant cooling of the ABL.

As an example of a stable ABL simulation, let us consider a run with a mesh of 64 x 64 x 64 points and with grid increments $\Delta x = \Delta y = \Delta z = 6$ m. The initial potential temperature was equal to 265 K in the first 100-m layer, and decreases by 1K/100 m above it. The surface cooling, assumed as 0.25K/h, was applied for 9 hours. The geostrophic wind was $G = 8$ m/s, the Coriolis parameter $f = 1.39 \times$

10^{-4} s^{-1} , and the roughness parameter $z_0 = 0.1 \text{ m}$. The resulting friction velocity is $u_* = 0.29 \text{ m/s}$. The described setup is similar to the case considered by Beare et al. (2004). The LES results, obtained after 1-hour averaging, are presented in Figures 18-21.

Figure 18 displays the profile of the potential temperature. During the simulation, the surface temperature decreases by about 2 degrees. This cooling rate decreases with height, and is nil at the level of about 250 m. As expected, the temperature profile has a negative curvature, except near the underlying surface and at the top the boundary layer.

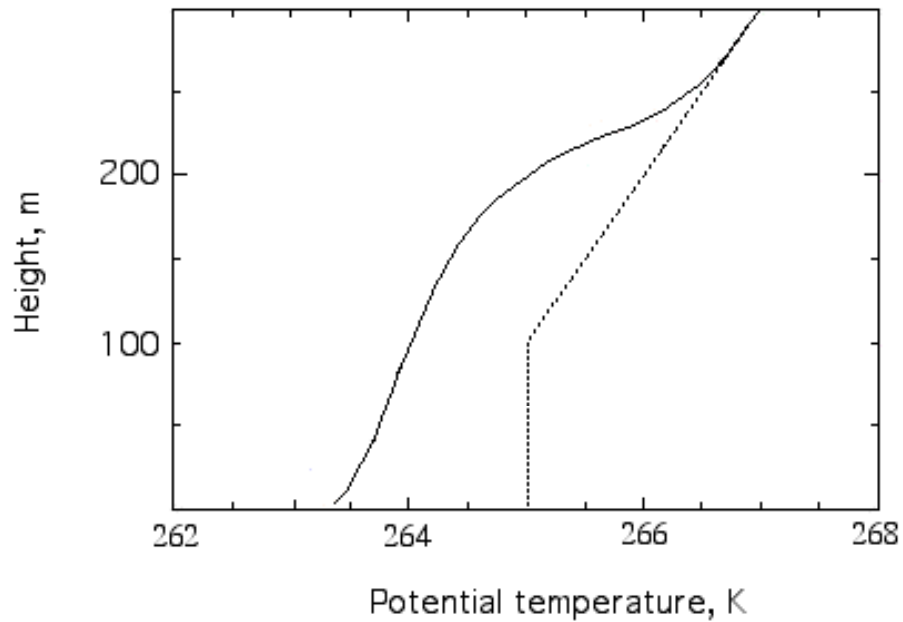


Figure 18. The initial (dotted line) and final profiles of the potential temperature obtained from a LES of a stable ABL.

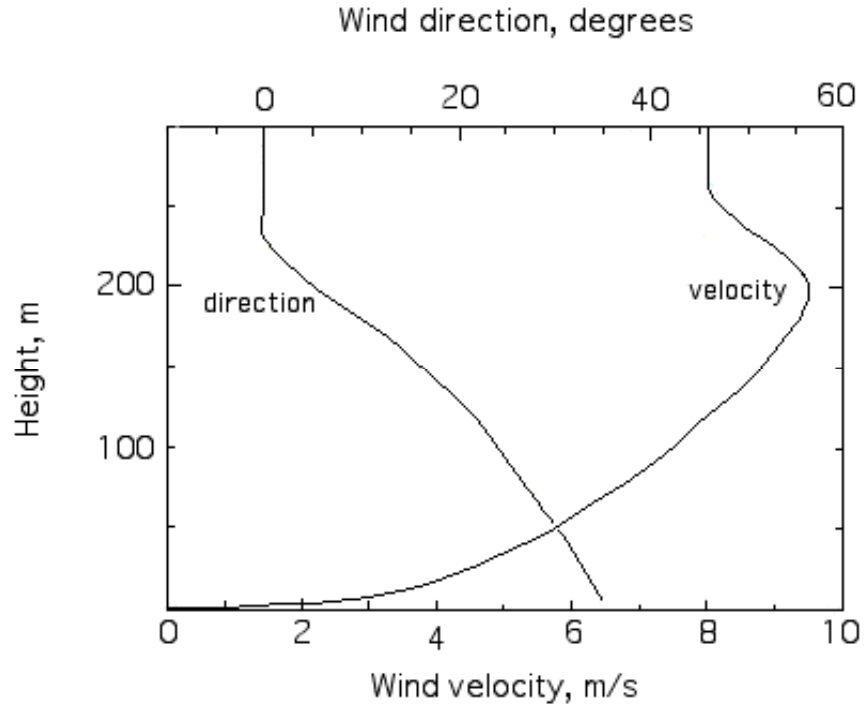


Figure 19. Vertical profiles of wind velocity and direction obtained from a LES simulation of a stable ABL.

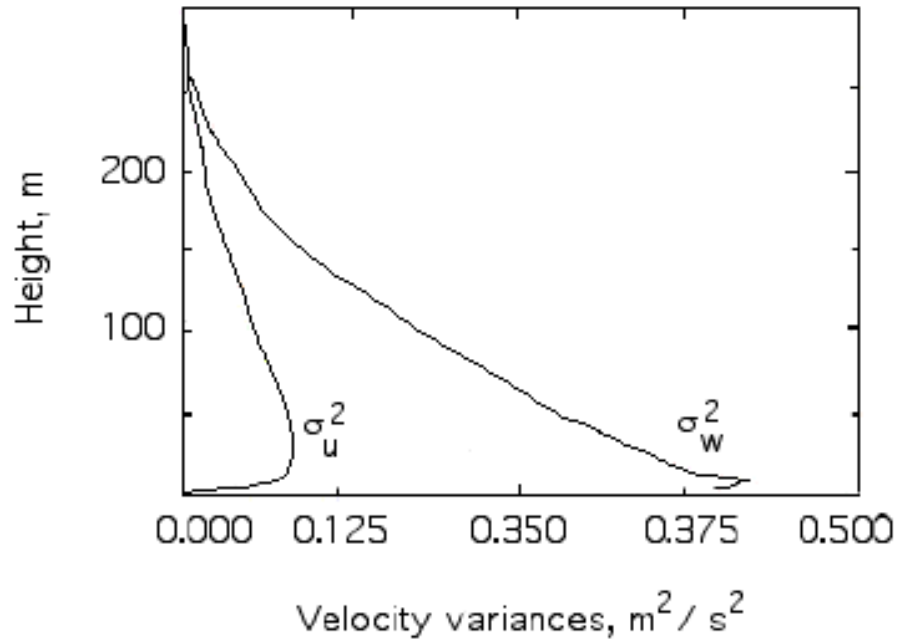


Figure 20. Vertical profiles of the velocity variances obtained from a simulation of a stable ABL.

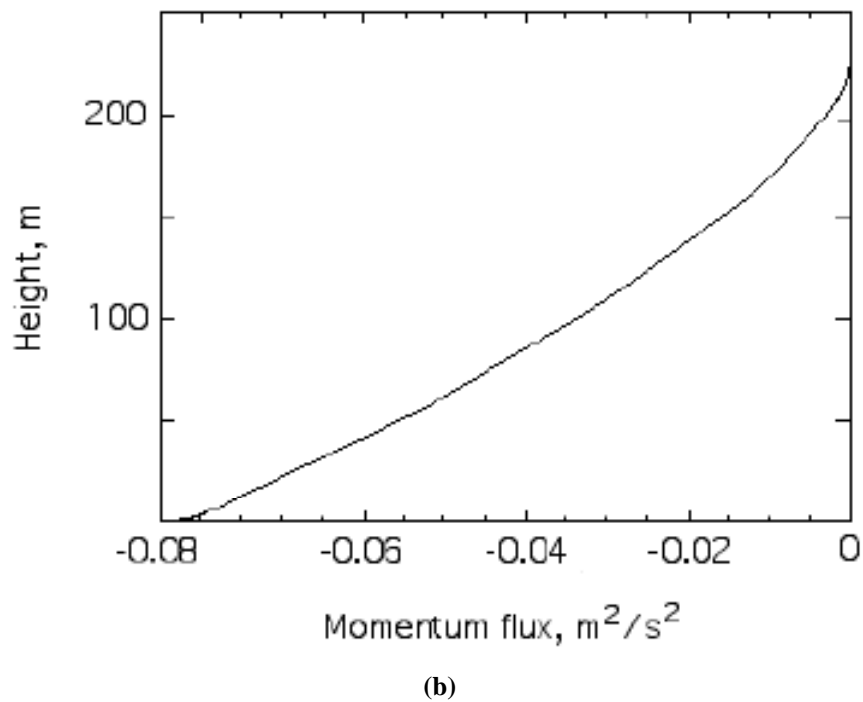
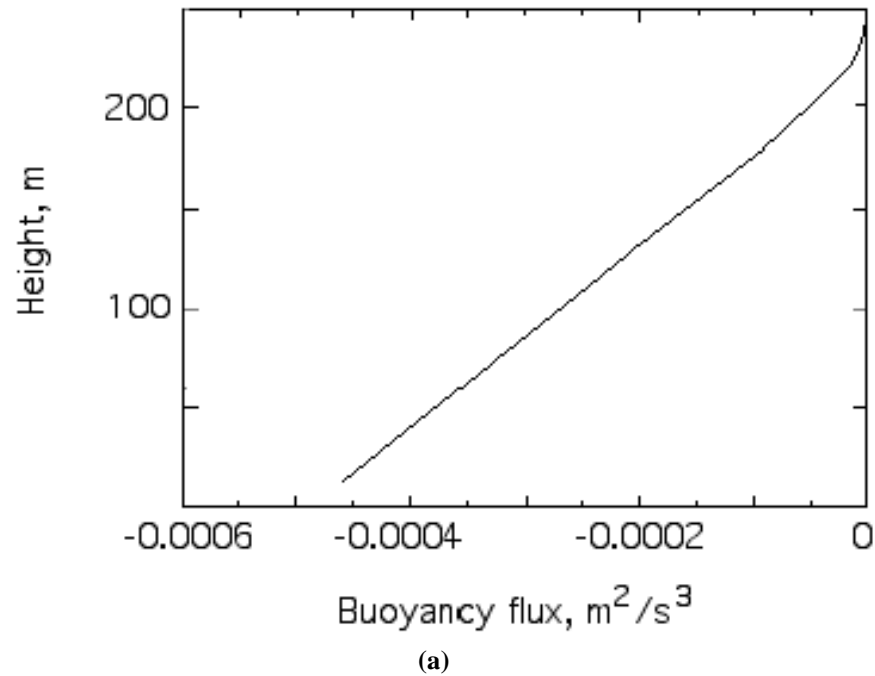


Figure 21. Vertical profiles of buoyancy and momentum fluxes obtained from a simulation of a stable ABL.

The convex (i.e., $\partial^2\Theta/\partial z^2 < 0$) curvature is caused by turbulent cooling ($\partial\Theta/\partial t < 0$). Note that turbulent warming (morning transition) causes the potential temperature curvature near the surface to be positive (concave since $\partial\Theta/\partial t$ and

$\partial^2 \Theta / \partial z^2 > 0$). Any departure from such profiles can be an indication of radiative and/or advective cooling or warming, or of a lack of continuous turbulence.

Vertical profiles of the wind velocity and the wind direction are shown in Figure 19. A super-geostrophic wind of about 9.5 m/s is present near the top of the ABL. It can be identified as "low-level jet-stream" – a typical phenomenon in stable conditions. The cross-isobar angle is about 40°.

The velocity variances are depicted in Figure 20. They decrease with height and arrive at zero values at about $z = 250$ m. A nearly linear profile of the heat flux in Figure 21a indicates that quasi-stationary conditions have been reached with uniformly constant cooling of the ABL. The stress in Figure 21b can be described by $\alpha_l = 3/2$.

3.4 Cloud-Topped ABL

Cloudiness is the most characteristic feature of the Earth when viewed from space. Satellite photographs often show intriguing cloudy patterns, which can be qualified as hexagonal cells with vertical axes, opened (no clouds in the center of each cell, only at the edges), or closed (clouds in the center of each cell, openings at the edges), with diameters from a few to tens of kilometers (Figure 22), and also opened or closed horizontal roll vortices, with horizontal axes (Figure 1). Agee (1987) identified six types of the ABL events, which occur over both oceanic and continental surfaces. The specified types include "cold-air outbreaks", controlled by surface heating and moistening, "cloud-topped boundary layers", driven by radiative cooling and warming, as well as "continental circulations", affected by surface sensible and latent heat fluxes. The boundary layer clouds include stratus, stratocumulus, and shallow cumulus. By definition, their lifting condensation level is below the top of the mixed layer.



Figure 22. Convective cells with vertical axes: opened (no clouds in the center of each cell, only at the edges), and closed (clouds in the center of each cell, openings at the edges), viewed from a space shuttle (NASA).

Stratus and stratocumulus can collectively be called "stratiform clouds". They have some common microphysical characteristics and formation mechanisms. A favorable condition for their occurrence is a large-scale subsidence. Due to radiative and evaporative cooling, the depth of the capping interfacial layer is very thin, and the temperature jump in this layer is quite large. Fractional cloudiness of stratus and stratocumulus clouds is about 100%. The stratiform clouds form over both, continental and marine locations.

Cumulus clouds are formed by the local ascent of humid buoyant air parcels. They are frequently referred to as fair-weather cumulus, cumulus humilis, or non-precipitating cumulus clouds, and occur over all regions of lands and ice-free global ocean with high frequency in the tropics. Their fractional cloudiness reaches up to about 30%. Cumulus convection intensifies the vertical transport of

heat, moisture, and momentum, and deepens the ABL. Cumuli clouds are important in the venting of air pollutants.

Examples of large-eddy simulations with stratiform and cumuliform clouds are presented below.

3.4.1 Stratiform-Clouds Topped ABL

Stratus and stratocumulus clouds have a strong impact on the dynamics of the ABL. Their presence introduces additional buoyancy sources and sinks, which are absent in the previously discussed convection cases. As a result, the cloud-topped ABL is more difficult to simulate than its cloud-free counterpart.

Physical processes in a cloud-topped boundary layer are schematically depicted in Figure 23. The sketch in the figure is a reminder of a medieval clock, whose mechanism is propelled by a gravity force (such a 13th century clock is still operational in a cathedral church in Gdansk, Poland). The operation of the cloud-topped ABL is "somewhat" similar.

The main factor which drives downward motion and turbulence within the stratiform-topped ABL is longwave radiative cooling at the cloud top. Turbulence generates entrainment. Entrainment brings warm inversion air into the cloud. The warm air mixes with radiatively cooled cloud air. The mixed air is less heavy, which reduces the efficiency of radiative cooling in driving turbulence. Weaker turbulence reduces entrainment (negative feedback).

On the other hand, entrainment brings warm and dry air, which causes the mixed air to be unsaturated. The resulting evaporative cooling enhances turbulence and produces stronger entrainment (positive feedback). The evaporative cooling may lead to an instability process, in which parcels cool even more, sink, and break up a solid cloud deck.

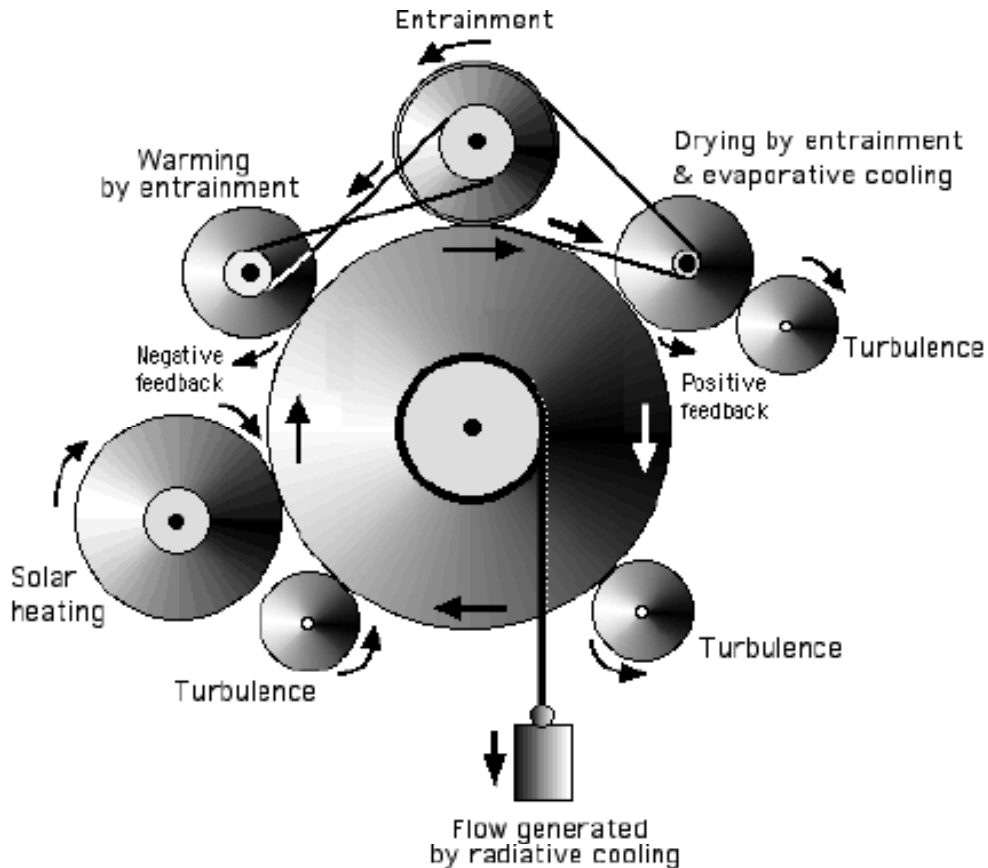


Figure 23. Schematic of turbulence generation within a stratocumulus cloud.

Influence of solar radiation comes from the solar absorption inside the cloud layer. Solar heating is more uniformly distributed through the layer (Figure 2). Near the cloud top, the solar heating can offset radiative cooling in generating turbulence. Inside the cloud, the solar heating can "burn" it. Together, these two effects can control a diurnal cycle of marine stratocumulus clouds even though the ocean surface temperature remains the same. Thus, the clouds thin (or disappear) in the daytime, and thicken at night.

When the whole cloud layer is warmed by solar heating, the cloud layer may become warmer than the subcloud layer. The resulting formation of a thin stably stratified layer at the cloud base can "decouple" the cloud layer from the underlying surface, and cutoff the moisture supply from the surface into the cloud layer. In addition, cooling introduced by the evaporation of drizzle can cool the sub-cloud layer, and consequently further stabilize the interface between the cloud and its sub-cloud layer. This leads to a rapid thinning of the cloud layer during the daytime, and also has an important influence on the radiative balance at the Earth's surface.

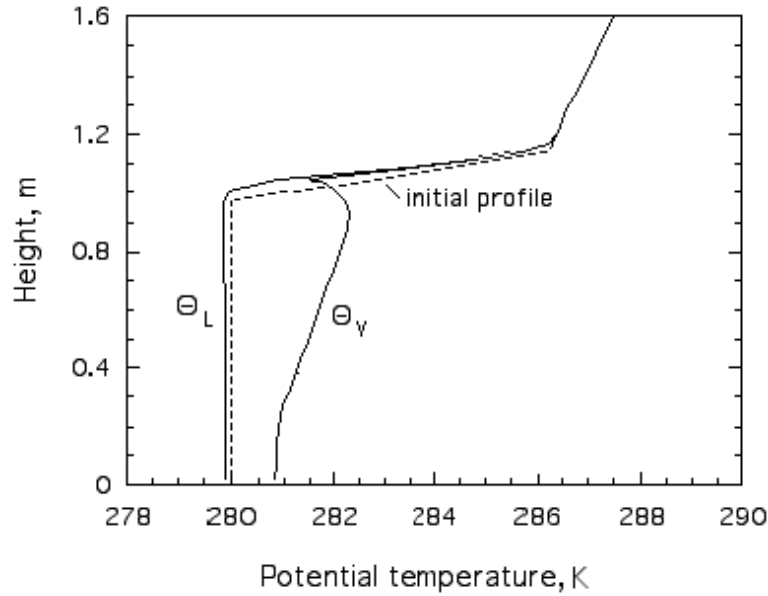
A multilayer structure of the cloud-topped ABL causes universal scaling not to exist for this case. However, the use of some form of mixed layer scaling can be at least partly successful (Nichols, 1989). The mixed layer scales are of the form:

$$\begin{aligned}
 W_* &= (\beta B_v z_c)^{1/3} && \text{for vertical velocity} \\
 T_{v*} &= \frac{B_v}{W_*} && \text{for temperature} \\
 q_{T*} &= \frac{Q_T}{W_*} && \text{for total water specific humidity}
 \end{aligned} \tag{85}$$

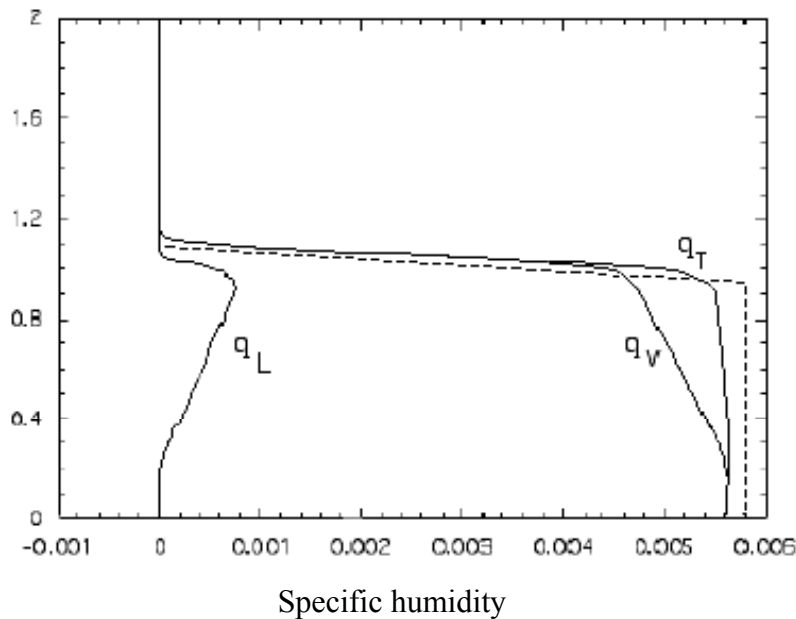
where $B_v = 2.5 / z_c \int_0^{z_c} H_v(z) dz$, Q_T is the total water specific humidity flux at the earth's surface, z_c is the top of the cloud layer, and β is the buoyancy parameter. Note that the above scales coincide with (72) in the cloud-free case (when $H_i/H_0 = -0.2$ is assumed).

In order to further discuss the cloud-topped case, let us consider the results of a LES, with a mesh of 32 x 32 x 60 grid points, and the grid increments $\Delta x = \Delta y = 60$ m and $\Delta z = 30$ m (a quite coarse resolution!). The simulation was performed for 15,136.7 s (i.e., 1200 total time steps) in shearless conditions. The initial mixed layer was 700 m deep with a uniform potential temperature of 280 K. The interfacial layer was initially 100 m deep. The initial temperature gradient γ_i in the interfacial layer was equal to 0.06 K m^{-1} . In the free-atmosphere, the temperature gradient was $\Gamma = 0.004 \text{ K m}^{-1}$. The surface turbulent heat flux H_0 was assumed to be nil. The surface humidity flux Q_0 was 0.00001. The results of the simulation are presented in Figures 24-29.

Figure 24a shows the vertical profiles of the liquid water potential temperature Θ_L and the virtual potential temperature Θ_v . The specific humidity profiles, q_v , q_L , and q_T , are depicted in Figure 24b. The liquid water potential temperature, Θ_L , and the total specific humidity, q_T , are conserved in a moist adiabatic process. Therefore, these quantities are well-mixed within the ABL. The virtual potential temperature Θ_v is not well mixed. The initial profiles of temperature and humidity are also shown in the figures. The liquid water potential temperature slightly decreases with time as a result of radiative cooling. The total mixing ratio slightly decreases with time due to the growth of the mixed layer.



(a)



(b)

Figure 24. Vertical profiles of: (a) liquid water potential temperature Θ_L , virtual potential temperature Θ_V , (b) specific humidity q_v , liquid water specific humidity q_L , and total water specific humidity q_T , obtained in a simulation of a stratocumulus-topped ABL. Initial temperature and humidity profiles are marked by dotted lines.

The vertical profiles of the liquid water potential temperature flux H_L , the radiative flux F , and their sum $R = H_L + F$ are depicted in Figure 25. Note that

integrating the equation for the horizontally averaged liquid water potential temperature $\partial\Theta_L/\partial t = -\partial R/\partial z$, yields:

$$R(z) = R(0) - \int_0^z \frac{\partial Q_L}{\partial t} dz \quad (86)$$

As mentioned above, $\partial\Theta_L/\partial t = \text{const} < 0$ in the initial mixed layer. As a result, the flux R in Figure 25 is approximately a linear and increasing function of height. Near the top of the mixed layer, $\partial\Theta_L/\partial t < 0$, and R increases non-linearly until it reaches its value R_i at the top of the cloud layer. The resulting turbulent heat flux H_L is the difference between the total flux R and the radiative flux F . In the lower part of the mixed layer, $F = 0$ and $H_L = R$. At the top of the cloud layer, H_L rapidly decreases with height, and reaches its negative minimum.

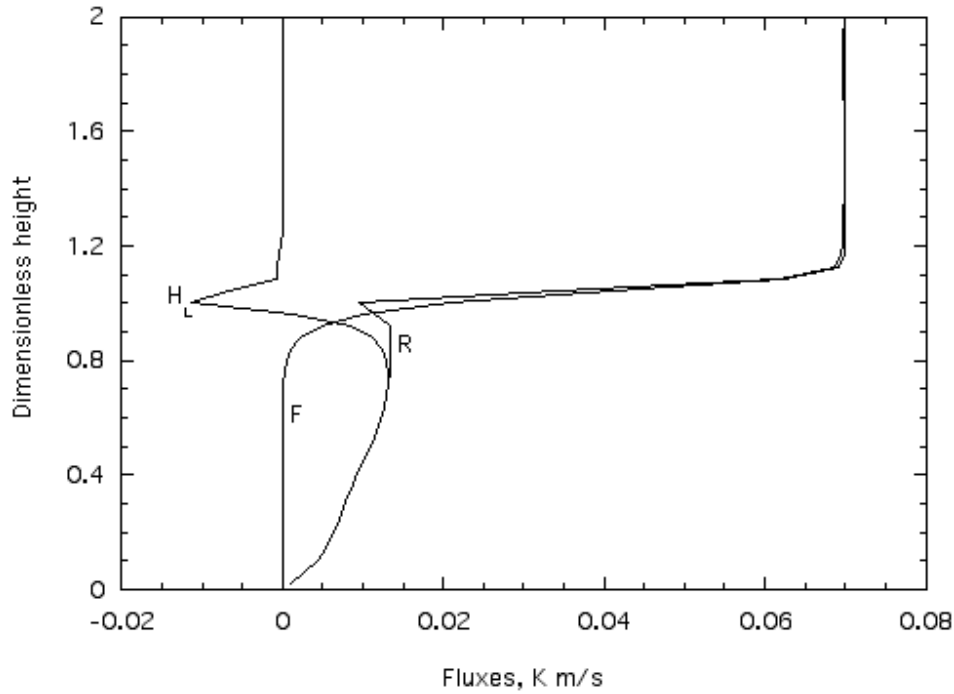


Figure 25. Liquid water potential temperature flux H_L , net radiative flux F , and their sum $R = H_L + F$, obtained in a simulation of a stratocumulus-topped ABL.

Analogous arguments can be applied to the total water specific humidity flux in Figure 26. Its equation: $\partial q_T/\partial t = -\partial Q_T/\partial z$ indicates that because $\partial q_T/\partial t < 0$, then the turbulent flux $Q(z)$ is an increasing function of height in the mixed layer. Above the mixed layer, $\partial q_T/\partial t > 0$, the turbulent flux $Q(z)$ decreases to zero.

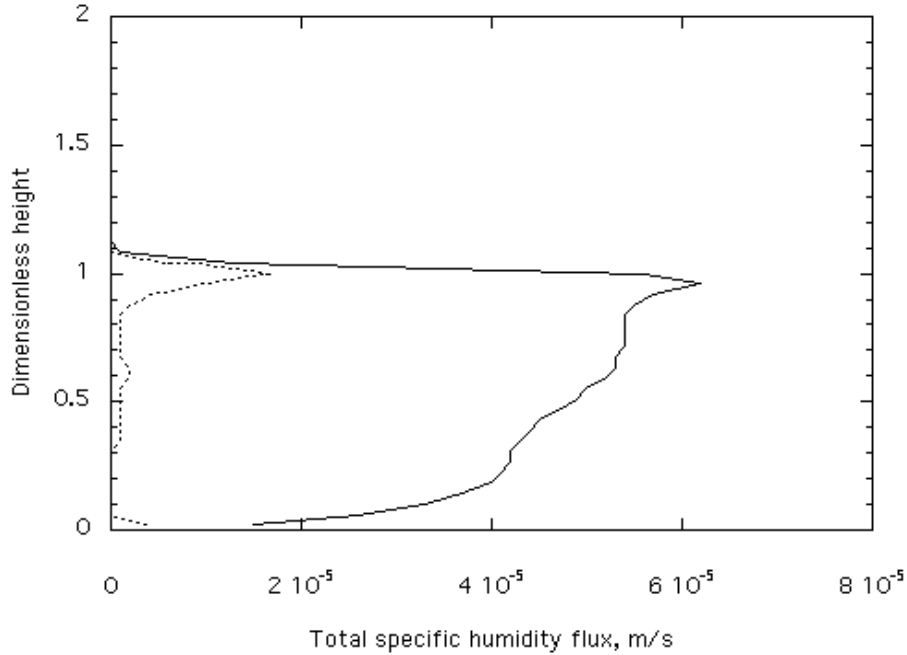


Figure 26. Total water specific humidity flux, obtained in a simulation of a stratocumulus-topped ABL. The subgrid flux is indicated by the dotted line.

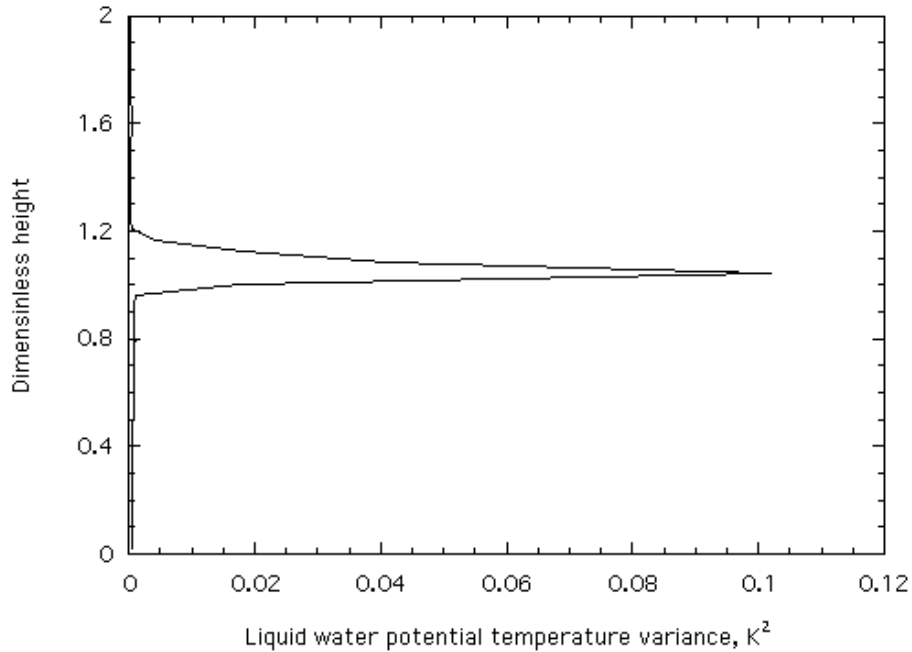


Figure 27. Variance of the liquid water potential temperature from LES of a stratocumulus-topped ABL.

The vertical profile of the liquid water potential temperature variance $\sigma_{\theta_L}^2$ is shown in Figure 27. The variance is nearly zero in the mixed layer and in the free atmosphere. At the top of the cloud layer, the variances has a sharp peak. The total water specific humidity variance $\sigma_{q_T}^2$ (not shown) has a very similar profile.

Profiles of the velocity variances are presented in Figure 28. Their vertical distribution is somewhat similar to the free-convective case in Figure 8, even though the mechanisms triggering convection in both cases are different. As mentioned before, in the free-convective case, convection is generated by the heating of the underlying surface, while in the cloud-capped case, it is generated by radiative cooling. The horizontal variances σ_u^2 and σ_v^2 in Figure 28 sharply decrease with height in the surface layer, and are nearly constant in the mixed layer. The vertical velocity variance σ_w^2 has a maximum in the mixed layer. The maximum is located higher than in the clear-sky case in Figure 8.

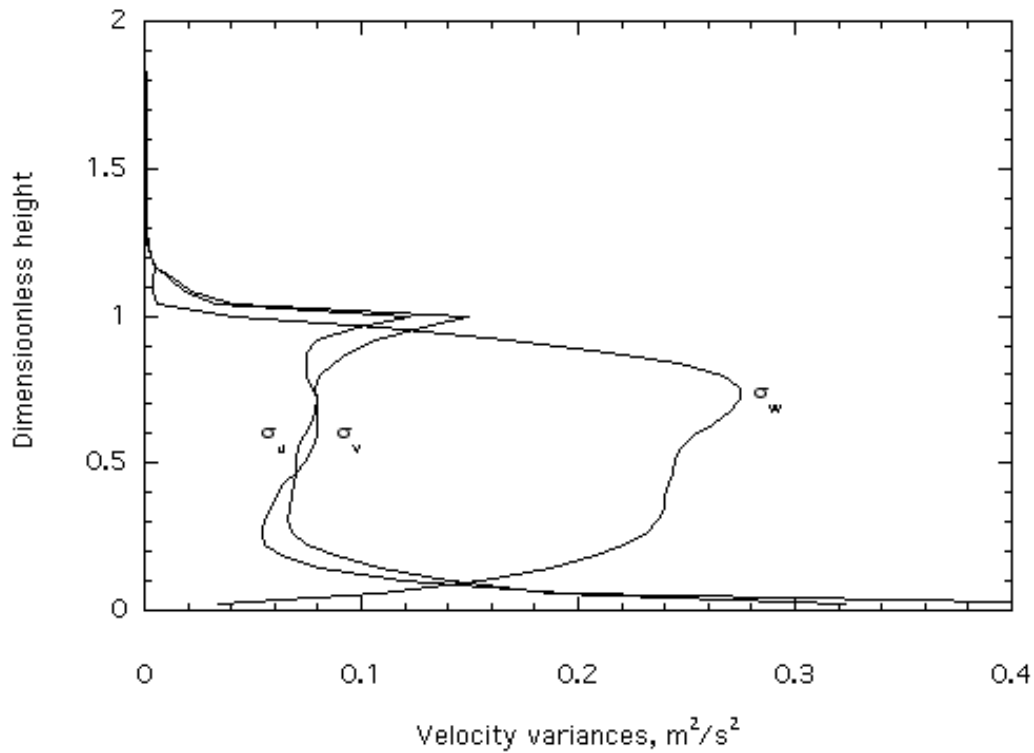


Figure 28. Vertical profiles of the velocity variances from a simulation of a stratocumulus-topped ABL.

The vertical velocity skewness S_w is shown in Figure 29. The values of S_w are negative near the surface and positive in the cloud layer. The negative skewness below the cloud base is due to stronger narrow downdrafts surrounded by larger areas of weaker updrafts. On the other hand, a positive skewness in the cloud layer indicates stronger narrow updrafts surrounded by larger areas of weaker downdrafts. It also implies that downdrafts cover more than half the area of the horizontal plane.

Further analysis indicates that in the lower part of the cloud layer and in the sub-cloud layer, the liquid water potential temperature Θ_L in updrafts is slightly higher than in the vicinity. On the other hand, Θ_L in downdrafts is slightly lower. This picture is different at the top of the cloud layer, where turbulence generates

entrainment. Entrainment brings warm and dry inversion air into the cloud. This air mixes with radiatively cooled cloud air. As a result, Θ_L in the sinking air is slightly higher than its vicinity, and the rising air is slightly lower.

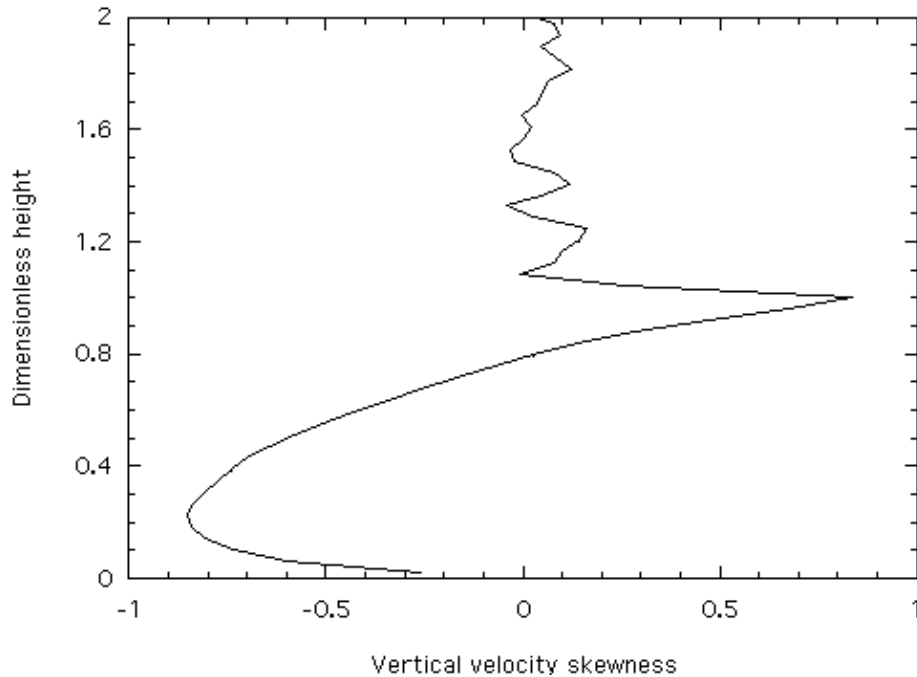


Figure 29. The vertical velocity skewness from a simulation of a stratocumulus-topped ABL.

3.4.2 Cumulus-Topped ABL

The structure of the cumulus-capped convective boundary layer is controlled by various processes including subsidence, latent heat, radiative cooling, temperature advection, and surface warming. Due to subsidence, warm and dry air is being brought down in the free atmosphere. By entrainment of this air, the ABL gets warmer and drier. Advective cooling and moistening intensifies this process. The drying causes evaporation and upward flux of moisture from the surface. The latent heat, released during the formation of clouds, enhances the buoyancy of updrafts and the production of turbulence in clouds. Presence of clouds modifies the radiative fluxes.

The cumulus convection often takes on the form of open cells and rolls. The cell patterns are clearly visible in Figure 1. The roll structures can be seen in Figure 30 as cloud streets. As mentioned in Section 3.1, wind shear is the main factor responsible for the appearance of these coherent structures in convective conditions. Animations of the cumulus-topped ABL can be found at the web site: <http://www.knmi.nl/~siebesma/gcss/animations/3D.html>.

Let us consider the results of two cumulus simulations. The first simulation was performed under windless conditions, and hereafter will be referred to as F – free

convection. The second one characterizes convection with the presence of wind, and hereafter will be referred to as S – sheared convection. In both simulations, a mesh of 32 x 32 x 75 grid points was employed. The grid increments were $\Delta x = \Delta y = 50$ m and $\Delta z = 40$ m in the first run, and $\Delta x = \Delta y = 100$ m and $\Delta z = 40$ m in the second one.

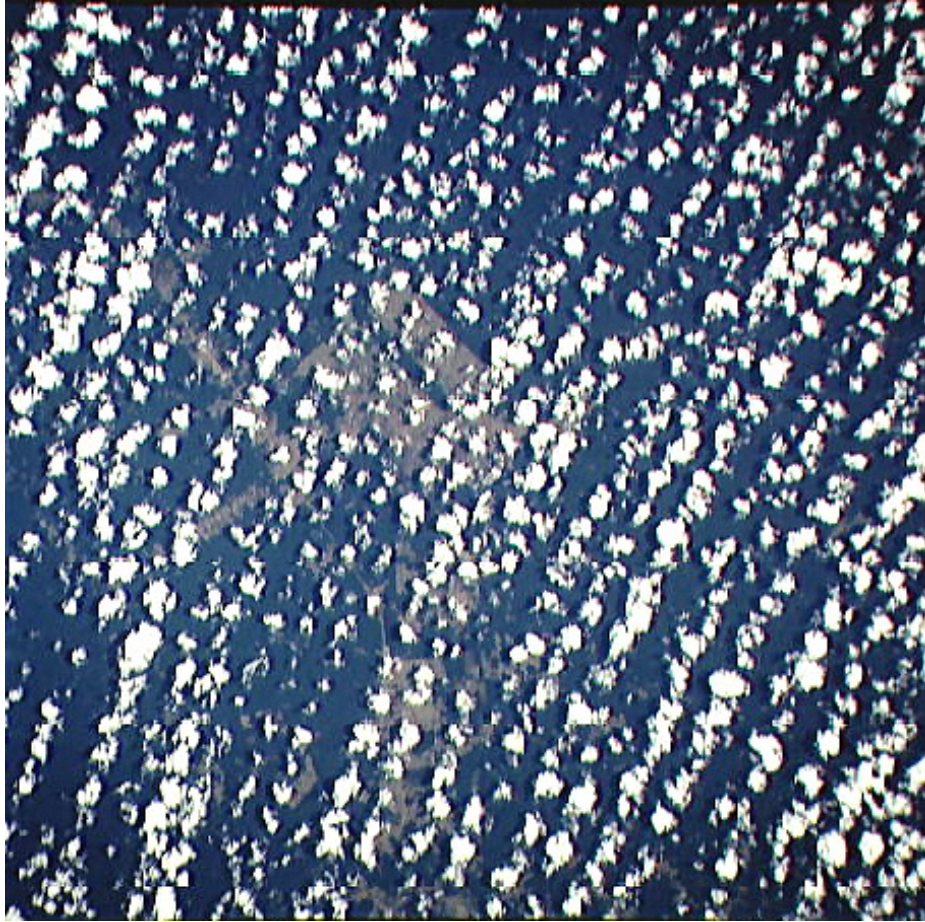


Figure 30. Convective rolls marked by cumulus clouds (NASA).

The initial mixed layer was 520 m deep, with a uniform potential temperature of 298.5 K. Initially, no clouds were present. Therefore, the initial liquid water potential temperature and the potential temperature were equal. Above the mixed layer, the temperature gradient was 3.85 K/km up to 1480 m, then 11.15 K/km up to 2000 m, and 3.65 K/km above 2000 m. Initially, the specific humidity at the surface was 0.017. It decreased with height to 0.0163 at the level of 520 m, again to 0.0107 at 1480 m, then went further down to 0.0042 at 2000 m. Finally, it decreased to zero at the top of the vertical domain.

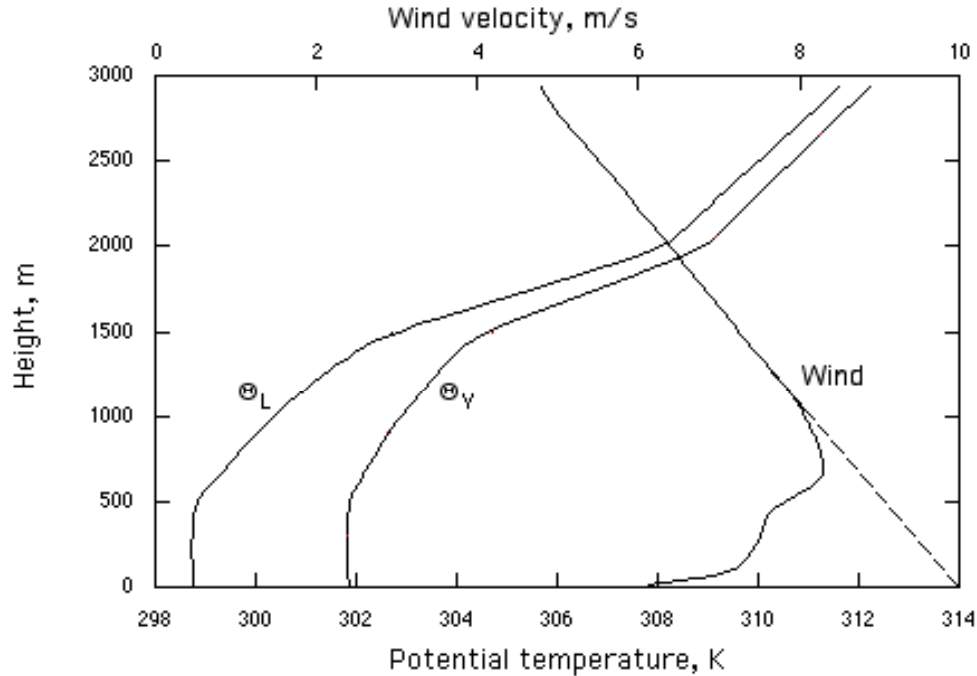


Figure 31. Vertical profiles of the liquid water potential temperature Θ_L , the virtual potential temperature Θ_v , and the wind velocity (in run S), obtained from large-eddy simulations of shearless and sheared cumulus convection. Note that the same temperature profiles were obtained in both simulations. The geostrophic wind is marked by a dotted line.

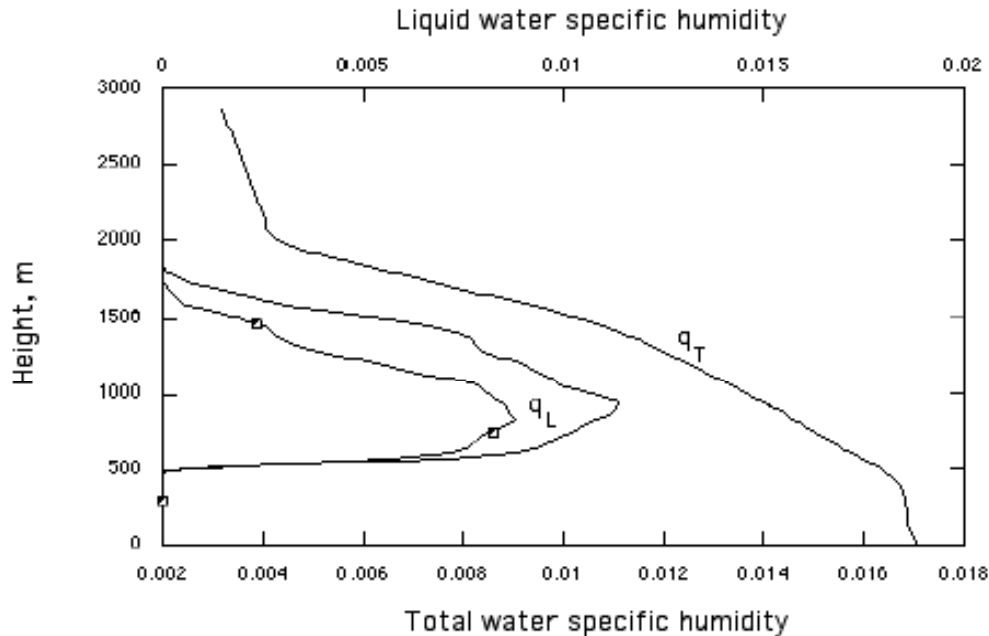


Figure 32. Vertical profiles of the total water specific humidity q_T (the same in both runs), the liquid water specific humidity q_L , obtained from large-eddy simulations of shearless and sheared (marked by squares) cumulus convection.

The LES was initialized assuming that the surface heat flux H_o equals to 0.008 K m s^{-1} , and the humidity flux $Q_o = 0.000052$. In run S, the geostrophic wind was 10 m/s at the surface, and its u-component increased linearly with height by a rate of 0.0018 s^{-1} (negative shear case, Sorbjan, 2004a). The roughness parameter was $z_o = 0.012 \text{ m}$ and the Coriolis parameter $f = 0.0000376 \text{ s}^{-1}$. The absorber at the top of the domain was $10 \text{ grid points deep}$, and the relaxation constant $r_o = 0.01 \text{ s}^{-1}$.

A large-scale subsidence (applied to q_T , Θ_L , u , and v) was assumed to decrease linearly with height from zero at the surface to -0.0065 m/s at $z = 1500 \text{ m}$, and then linearly decrease to zero at 2100 m . The prescribed radiative cooling was $2.315 \times 10^{-5} \text{ K/s}$ below 1500 m , and then it decreased linearly to zero at $z = 2500 \text{ m}$, and remained zero above. The advective drying of q_T was $-1.2 \times 10^{-8} \text{ s}^{-1}$ in the first 300 m above the surface, it decreased to zero at 500 m , and stayed nil above. The simulation time was $21,608 \text{ s}$ in run F and $22,591 \text{ s}$ in run S (i.e., 3000 total time steps). Statistics were obtained during the last 1000 time steps. The described setup is similar to the BOMEX case, considered by Siebesma et al. (2002).

The resulting profiles of temperature in both cases and wind velocity in run S are shown in Figure 31. The simulation conditions were defined in such a way that the radiative cooling approximately balanced the vertical gradient of the heat flux. As a result, the potential temperature does not change much during both simulations. The virtual potential temperature in the mixed layer is larger than the potential temperature, due to the presence of water vapor. There is clearly a two-layer structure of convection in both presented cases. The lower layer (mixed layer) is governed by the surface heat flux generated convection. The temperature and wind velocity profiles in the mixed layer are similar to those described in Section 3.1. The mixed layer values are nearly constant with height, and sharply increase above 500 m .

Vertical profiles of the total water specific humidity q_T and the liquid water specific humidity q_L are shown in Figure 32. The initial conditions were defined in such a way that the advective drying approximately balanced the moistening by the surface flux. Consequently, the total water specific humidity changes little during the simulations. The cloud layer is defined by the liquid water specific humidity, and is confined approximately between 500 m and 1750 m . The total water specific humidity q_T is nearly constant with height in the mixed layer, and sharply decreases above 500 m .

Profiles of the buoyancy flux βH_v and the liquid water potential temperature flux H_L are depicted in Figures 33 a-b. The buoyancy flux in Figures 33a decreases linearly up to the cloud base, where it reaches a negative peak of about 20% of the surface flux. This indicates that the entrainment processes in the subcloud mixed layer are similar to those described in Section 3.1. In the cloud layer, there is a positive buoyancy flux due to positive buoyant updrafts in the cloud layer.

The liquid water potential temperature flux H_L in Figure 33b linearly decreases to a minimum value in the cloud layer. Above this level, H_L rapidly decreases to zero.

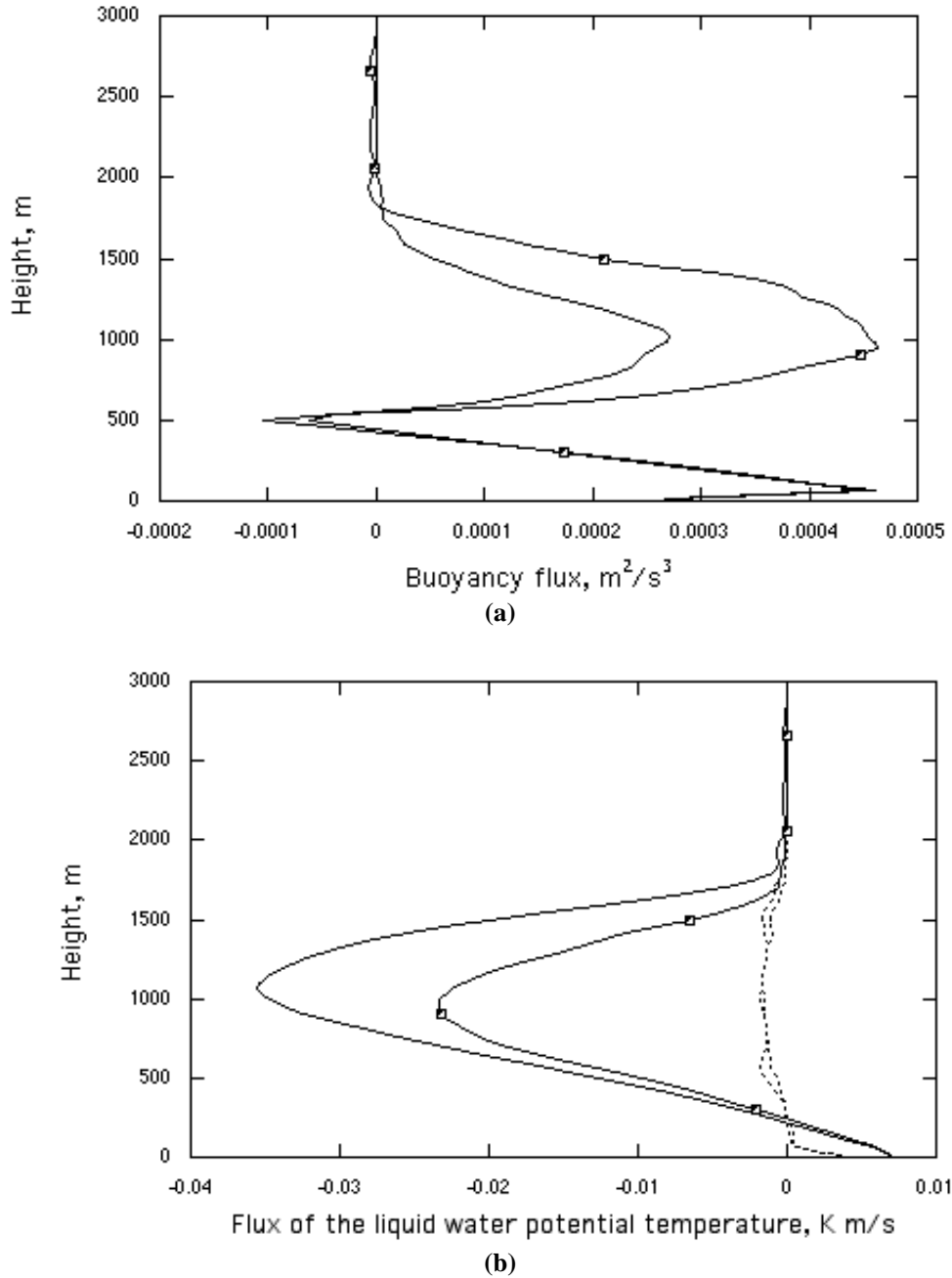


Figure 33. Vertical profiles of: (a) the buoyancy flux, and (b) the flux of the liquid water potential temperature, obtained from large-eddy simulations of shearless and sheared (marked by squares) cumulus convection. Subgrid fluxes are indicated by dotted lines.

In order to understand this behavior, it is useful to inspect Equation (54) together with Figure 34 (which shows the total water specific humidity flux Q_T).

Consequently, it can be concluded that in the cloud layer, the flux H_L is dominated by a negative flux Q_T . The total water specific humidity flux Q_T in Figure 34 is nearly constant with height in the mixed layer in run F. It slightly decreases with height in run S. This is due to the fact that the total water specific humidity is nearly constant in time. The total water specific humidity fluxes Q_T reach their peaks in the cloud layer, and decrease to zero at its top.

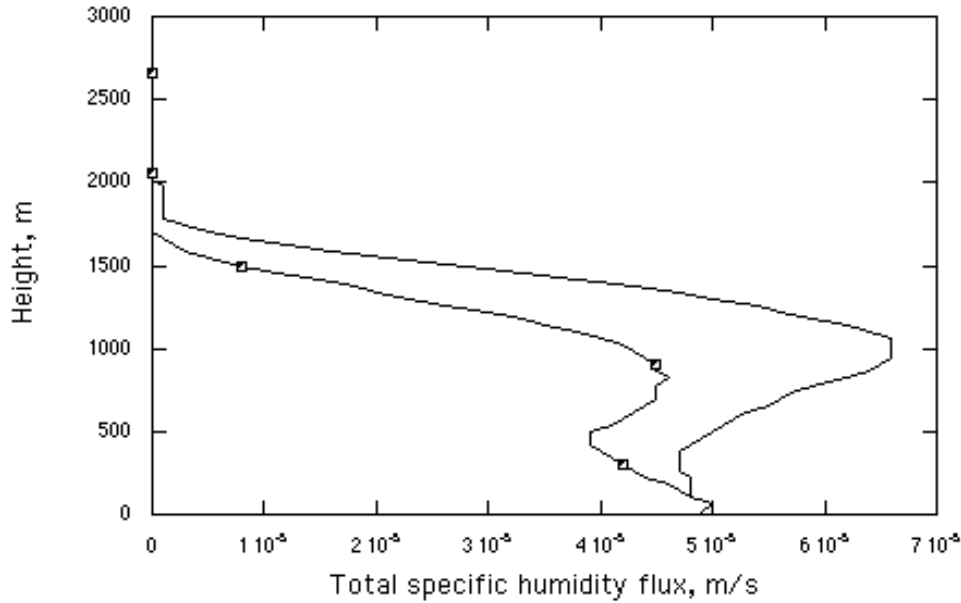


Figure 34. A vertical profile of the total water specific humidity flux obtained from large-eddy simulations of shearless and sheared (marked by squares) cumulus convection.

Further analysis indicates that the temperature excesses θ'_L in updrafts (not shown) are positive in the lower half of the subcloud mixed layer, and negative above. In downdrafts, the temperature excesses θ'_L are negative in the lower half of the subcloud mixed layer, and positive above. As a result, the flux of the liquid water potential temperature in Figure 33b is negative above 250 m level.

The vertical velocities in updrafts are positive and relatively larger, while the vertical velocities in downdrafts are negative and relatively smaller. Consequently, the area covered by updrafts must be smaller than the area covered by downdrafts. The resulting vertical velocity skewness (not shown) is positive. It increases from zero at the earth's surface to about 2.5-3 in the cloud layer, and decreases to zero above it.

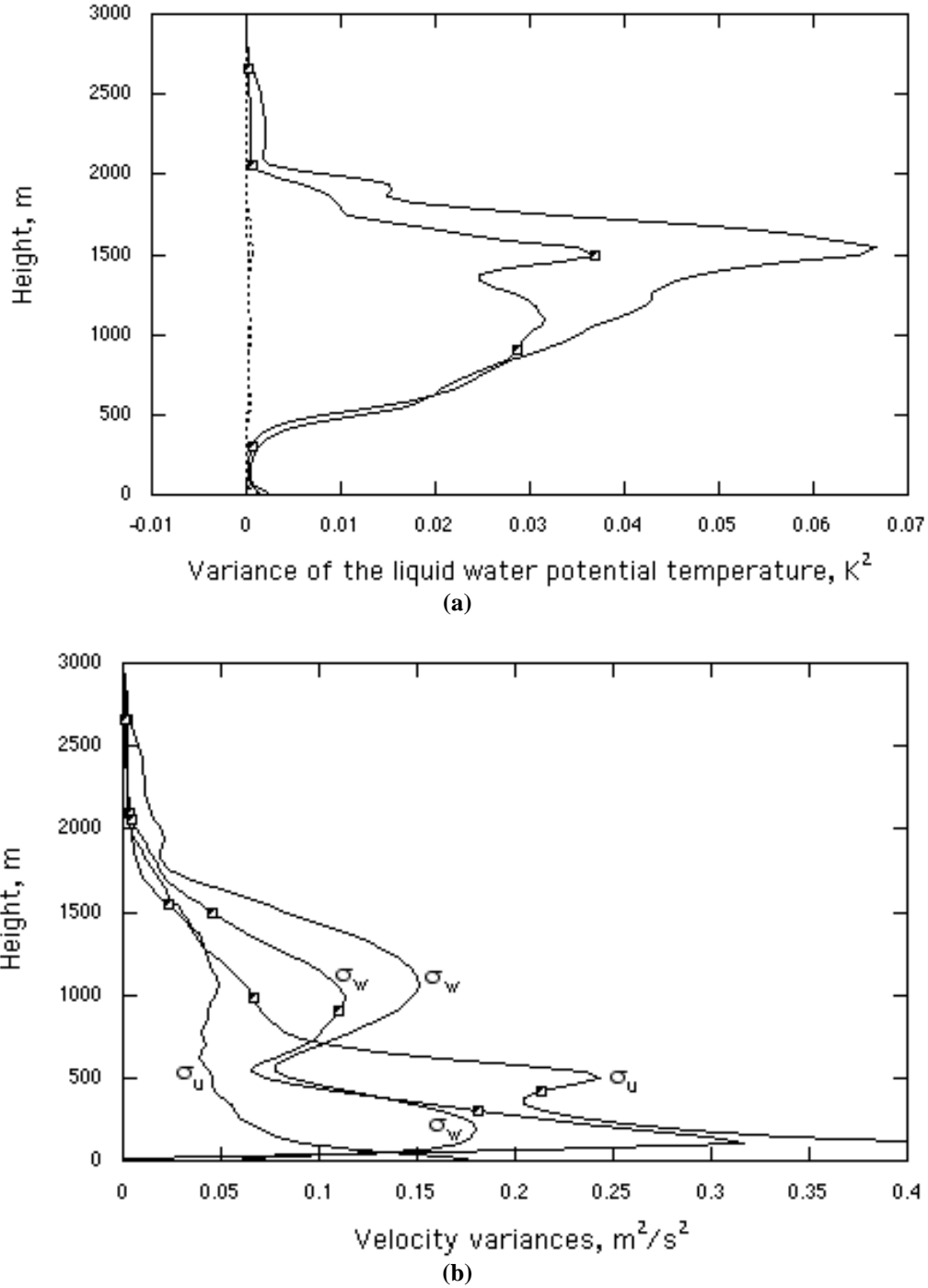


Figure 35. Vertical profiles of: (a) the variance of the liquid water potential temperature, (the subgrid contributions are marked by dotted lines), and (b) the wind velocity variances, obtained from large-eddy simulations of shearless and sheared (marked by squares) cumulus convection.

Variances of the liquid water potential temperature $\sigma_{\theta L}^2$ and the wind velocity components, σ_u^2 , σ_v^2 , and σ_w^2 , are presented in Figure 35. The figure indicates a two-layer structure of the cloud-topped ABL in both runs. In the subcloud mixed

layer, the temperature and velocity variances are very similar to their counterparts in the cloud-free convective mixed layer, described in Section 3.1. The temperature variance sharply increases with height at the top of the 500 m mixed layer. It continues increasing above the mixed layer, and has a peak near the top of the cloud layer. The vertical velocity σ_w^2 has one peak in the mixed layer (like in the cloud-free case), and a second peak in the cloud layer.

4 Final Remarks

The test large-eddy simulations, presented in this Chapter, were performed for the sake of demonstrating the LES technique using some arbitrarily governing parameters. For this reason, they have not been compared with available atmospheric observations. Comparison of LES with atmospheric data constitutes an independent subject, which is out of the scope of this Chapter. To obtain more information on this issue, the reader is referred to the following sources: Schumann and Moeng (1991), Nieuwstadt et al. (1992), Cuijpers and Duynkerke (1993), Shen and Moeng (1993), Khairoutdinov and Kogan (1999), Kosovic and Curry (1999), and Neggers et al. (2002).

As demonstrated above, the main benefit of using the LES approach is in its ability to generate various flow regimes, test theories, evaluate, refine, and develop parameterizations of the ABL. Within LES, it is quite easy to isolate a particular physical process of interest to study its structure, dynamics, and impact on the ABL. Large-eddy simulations allow one to visualize the 3D spatial and temporal evolution of turbulence. All these advantages have led to several important breakthroughs, which have changed views on the ABL turbulence and diffusion. In this respect, one could mention about the development of convective scaling, discovery of the mixed-layer entrainment processes, analysis of cloud-topped convection, and understanding of convective diffusion.

Inter-comparisons initiated in the early 1990s have provided confidence that LES is generally a useful source of information on the ABL. Such inter-comparisons included cellular, shearless convection [Nieuwstadt et al. (1992)], stratocumulus convection based on FIRE case of July 7, 1987 [Moeng, et al. (1996) and Bechtold et al. (1996)], smoke-topped convection [Bretherton et al. (1999)], the drizzling stratocumulus convection, based on ASTEX (Lagrangian-1) case [Duynkerke (1997)], cumulus sheared convection, based on ATEX data [Stevens et al. (2001)], and on BOMEX data [Siebesma et al. (2003)], the cumulus diurnal transition [Brown et al. (2002), ARM data], and a stable boundary layer [Beare et al. (2004)].

In spite of increasing reliance on LES as a research tool, there is still considerable uncertainty concerning the fidelity of large-eddy simulations. Several LES studies have shown substantial variations in predictions of some important statistics. For example, in the smoke cloud case, entrainment rates differed by up to a factor of

two (Bretherton et al., 1999). In simulations of trade-wind cumuli, the stratiform cloud fraction and the variance of total-water mixing ratio were found to be highly sensitive to the choice of numerics, resolution, and subgrid parameterization (Stevens et al., 2001).

The presented Chapter focused on atmospheric turbulence and omitted a discussion of diffusion simulations. Readers interested in this specific topic are referred to the papers of Nieuwstadt and de Valk (1987), Haren and Nieuwstadt (1989), Schumann (1989), Mason (1992b), Sykes and Henn (1992), Nieuwstadt and Meeder (1997), Weil et al. (1997), and Nieuwstadt (1998).

Acknowledgements

Some of the results presented in this Chapter were obtained during research supported by the National Science Foundation, grant no. ATM-0400590.

References

- Acevedo, O. and D.R. Fitzjarrald, 1999. Observational and numerical study of turbulence during early evening transition. 13th Symposium on Boundary Layers and Turbulence, 10-15 January, 1999, Dallas, Texas.
- Acevedo, O. and D.R. Fitzjarrald, 2001. The early evening surface-layer transition: temporal and spatial variability. *J. Atmos. Sci.*, 58: 2650-2667.
- Agee, E.M., 1987. Mesoscale cellular convection over the oceans. *Dyn. Atmos. and Oceans.*, 10: 317-341.
- Albrecht, B.A., C.S. Bretherton, D. Johnson, W. H. Scubert, and S. Frish, 1995. The Atlantic stratocumulus transition experiment, ASTEX, *Bull. Amer. Meteorol. Soc.*, 76, 6: 889-904.
- Albrecht, B.A., D.A. Randal, S. Nichols, 1988. Observations of marine stratocumulus clouds during FIRE, *Bull. Amer. Meteorol. Soc.*, 69, 6: 618-626.
- Andren, A., 1996. The structure of stably stratified atmospheric boundary layers: a large-eddy simulation study. *Q. J. Roy. Met. Soc.*, 121: 961-985.
- Andren, A., A. Brown, J. Graf, P. J. Mason, C-H. Moeng, F. T. M. Nieuwstadt, and U. Schumann, 1994. Large-eddy simulation of a neutrally-stratified boundary layer: a comparison of four computer codes. *Q.J.R. Meteorol. Soc.*, 120: 1457-1484.
- Augstein, E., H. Riehl, F. Ostapoff, V. Wagner, 1973. Mass and energy transport in an undisturbed Atlantic trade-wind flow. *Mon. Weath. Rev.*, 101, 2: 101-111.
- Ball, F.K., 1960. Control of the inversion height by surface heating. *Quart. J. Roy. Meteor. Soc.*, 86: 483-494.
- Bardina, J., J. H. Ferziger, W. C. Reynolds, 1980. Improved subgrid scale models for large eddy simulations. *AIAA Paper 80-1357*.
- Beare, R. J., and 16 co-authors, 2004. An intercomparison of large-eddy simulations of the stable boundary layer. Submitted to *Boundary-Layer Meteorology*.

- Beare, R. J., and M.K. Macvean, 2004. Resolution sensitivity and scaling of large-eddy simulations of the stable boundary layer. *Boundary-Layer Meteorology*, 112, 257-281.
- Bechtold, P., S. K. Krueger, W. S. Lewellen, E. van Meijgaard, C. H. Moeng, D. A. Randall, A. van Ulden, and S. Wang., 1996. Modeling a Stratocumulus-topped PBL: Intercomparison among different one-dimensional codes and with large eddy simulation. *Bull. Amer. Meteorol. Soc.*, 77. 9: 2033-2042.
- Beets, C and B. Koren 1996. Large-eddy simulation with accurate implicit subgrid-scale diffusion. Dept. of Numerical Mathematics Rep. NM-R9601. Stichting Mathematisch Centrum, Utrecht, Netherlands, 24 pp.
- Betts, A.K., 1973. Non-precipitating cumulus convection and its parameterization. *Quart. J. Roy. Meteor. Soc.*, 99: 178-196.
- Bretherton, C. S., M. K. MacVean, P. Bechtold, A. Chlond, W.R. Cotton, J. Cuxart, H. Cuijpers, M. Khairoutdinov, B. Kosovic, D. Lewellen, C.H. Moeng, B. Stevens, R. I. Sykes, and M. C. Wyant, 1999. An intercomparison of radiatively-driven entrainment and turbulence in a smoke cloud, as simulated by different numerical models. *Q. J. R. Meteor. Soc.*, 125: 391-423.
- Brost R. A. and J. C. Wyngaard, 1984a. Marine stratocumulus layers: Part I. *J. Atmos. Sci.*, 39: 800-817.
- Brost R. A. and J. C. Wyngaard, 1984b. Marine stratocumulus layers: Part II. *J. Atmos. Sci.*, 39: 818-836.
- Brown, A., S.H. Derbyshire, and P.J. Mason, 1994. Large-eddy simulation of the stable atmospheric boundary layers with a revised stochastic subgrid model. *Q.J. Roy. Met. Soc.*, 120: 1485-1512.
- Brown, A., R. T. Cederwall, A. Chlond, P. G. Duynkerke, J. C. Golaz, M. Khairoutdinov, D. C. Lewellen, A. P. Lock, M. K. McVean, C.-H. Moeng, R. A. Neggers, A. P. Siebesma, and B. Stevens, 2002. Large-eddy simulation of diurnal cycle of shallow convection over land. *Q.J.R. Meteorol. Soc.*, 128: 1075-1093.
- Brümmer, B. S., S. Bakan, and H. Hinzpeter, 1985. KONTUR: Observations of clouds streets and open cellular structures. *Dyn. Atmos. Oceans*, 9: 281-294.
- Cedeval, R. and R. L. Street, 1999. Turbulence modification in the evolving stable boundary layer: a large eddy simulation. *13th Symp. on Boundary Layers and Turbulence*, Dallas Texas, AMS January, 1999.
- Chlond A. and G. Muller, 1997. Very large-eddy modelling of convective structures during cold-air outbreaks. *Colloquium on Clear and Cloudy boundary Layers*, Amsterdam, 26-29 August, 1997.
- Cuijpers J. W. M., and P. G. Duynkerke, 1993. Large-eddy simulation of trade wind cumulus clouds. *J. Atmos. Sci.*, 50: 3894-3908.
- Curry, J. A., P. Hobbs, M. King, D. Randall, P. Minnis, et al., 2000. FIRE Arctic Cloud Experiment. *Bull. Amer. Meteorol. Soc.*, 81: 5 -29.
- Deardorff, J. W., 1970. Preliminary results from numerical integration of the unstable planetary boundary layers. *J. Atmos. Sci.*, 27: 1209-1211.

- Deardorff, J. W., 1972. Numerical integration of neutral and unstable planetary boundary layers. *J. Atmos. Sci.*, 29: 91-115.
- Deardorff, J. W., 1973. Three-dimensional numerical modeling of the planetary boundary layers. In *Workshop on Micrometeorology*, D. A. Haugen, Ed., Amer. Meteor. Soc., 271-311.
- Deardorff, J. W., 1974a. Three-dimensional numerical study of the height and mean structure of a heated planetary boundary layer. *Bound.-Layer Meteor.*, 7: 81-106.
- Deardorff, J. W., 1974b. Three-dimensional numerical study of turbulence in an entraining mixed layer. *Bound.-Layer Meteor.*, 7: 199-226.
- Deardorff, J. W., 1976. On the entrainment rate of a stratocumulus-topped mixed layer. *Quart. J. Roy. Meteor. Soc.*, 102: 563-582.
- Deardorff, J. W., 1980. Stratus-capped mixed layers derived from a three-dimensional model. *Bound.-Layer Meteor.*, 18: 495-527.
- Duynkerke, P. G., P. J. Jonker, A. Chlond, M. C. Van Zanten, J. Cuxart, P. Clark, E. Sanchez, G. Martin, G. Lenderink, J. Teixeira, 1997. Intercomparison of three- and one-dimensional model simulations and aircraft observations of stratocumulus. *Bound. Layer Meteorol.*, 92: 453-487.
- Galmarini, S, C. Beeds, P. G. Duynkerke, and J. V.-G. de Arellano, 1998. Stable nocturnal boundary layers: a comparison of one-dimensional and large-eddy simulation models. *Bound. Layer Meteorol.*, 88: 181-210.
- Germano, M. U., Piomell, P. Moin, 1992. A dynamic subgrid-scale eddy diffusivity model. *Phys. Fluids A3* (7): 1760-1765.
- Glendening, J. W., 1996. Linear eddy features under strong shear conditions. *J. Atmos. Sci.*, 53: 3430-3449.
- Haren, L. van and F. T. M. Nieuwstadt, 1989. The behaviour of passive and buoyant plumes in a convective boundary layer, as simulated with large-eddy simulation model. *J. Applied Meteor.*, 28: 818-832.
- Henn D. S. and R. I. Sykes 1992. Large-eddy simulation of dispersion in the convective boundary layer. *Atmos. Envir.*, 26A: 3145-3159.
- Holland J. Z. and E. M., Rasmusson, 1973. Measurements of the atmospheric mass, energy, and momentum budgets over 500-kilometer square of tropical ocean. *Month. Weath. Rev.*, 101,1: 44-55.
- Jian, H. and W. R. Cotton, 2000. Large-eddy simulation of shallow cumulus convection during BOMEX: sensitivity to microphysics and radiation. *J. Atmos. Sci.*, 57: 582-594.
- Mason P. J. and D. J. Thompson, 1987. Large-eddy simulation of the neutral-static-stability planetary boundary layer. *Q.J.R. Meteorol. Soc.*, 113: 413-443.
- Mason P. J. and S.H. Derbyshire, 1990. Large-eddy simulation of the stably-stratified atmospheric boundary layer. *Bound.-Layer Meteor.*, 53: 117-162.
- Mayor, S. D., P. R. Spalart, G. J. Tripoli, 2002. Application of a perturbation recycling method in the large-eddy simulation of a mesoscale convective internal boundary layer. *J. Atmos. Sci.*, 59: 2385-2395.

- Khairoutdinov, M. and J. Kogan, 1999. A large eddy simulation model with explicit microphysics: validation against aircraft observations of a stratocumulus-topped boundary layer. *J. Atmos. Sci.*, 56: 2115-2131.
- Kim, S.-W., S.-U. Park, and C.-H. Moeng, 2003. Entrainment processes in the convective boundary layer with varying wind shear. *Bound.-layer. Meteor.*, 108: 221-245.
- Kogan, Y. L., M. P. Khairoutdinov, D. K. Lilly, Z. N. Kogan, Q. Liu, 1995. Modeling of stratocumulus cloud layers in a large eddy simulation model with explicit microphysics. *J. Atmos. Sci.*, 52: 2923-2940.
- Kosovic, B and J. Curry, 1999. Large-eddy simulation of a quasi-steady stably-stratified atmospheric boundary layer. *13th Symp. on Boundary Layers and Turbulence*. Dallas, Texas, AMS.
- Kristovich, D., G. Yang, J. Verline, P. J. Sousonis, P. Mourad, D. Lenschow, R. M. Rauber, M. K. Ramamurthy, B. F. Jewett, K. Beard, E. Cutrim, P. J. DeMott, E. W. Eloranta, M. R. Hjermfeld, S. M. Kreidenweis, J. Martin, J. Moore, H. T. Ochs, D. C. Rogers, J. Scala, G. Tripoli, J. Young., 2000. The lake-induced convection experiment and the snowband dynamics project. *Bull. Amer. Meteorol. Soc.*, 127: 519-542.
- LeMone, M. A. and R. L., Grossman, 1999. Evolution of potential temperature and moisture during the morning: CASES-97. *13th Symp. on Boundary Layers and Turbulence*, Dallas Texas, January, 1999, AMS.
- LeMone, M. A. R, Grossman, R. T. McMillen, K. Liou, S. C. Ou, S. McKeen, W. Angevine, K. Ikeda, and F. Chen: Cases-97, 2002. Late-morning warming and moistening of the convective boundary layer over Walnut River watershed. *Bound.-layer. Meteor.*, 104: 1-52.
- Leonard, A, 1974. On energy cascade in large eddy simulations of turbulent fluid flows. *Adv. in Geophysics*, 18A: 237-248.
- Lewellen, D. C., and W. S. Lewellen, 1996. Influence of Bowen ratio on boundary layer cloud structure. *J. Atmos. Sci.*, 53: 175-187.
- Lilly, D. K., 1967. The representation of small-scale turbulence in numerical simulation experiments. In: *Proc. IBM Sci. Comp. Symp. on Envir. Sci.* Nov., 14-16, 1966. T. J. Watson Res. Center. Yorktown Hills, N.Y., IBM Form 320-1951, pp. 195-210.
- Lilly, D. K., 1968. Models of Cloud-Topped Mixed Layers under Strong Inversion. *Quart. J. Roy. Meteor. Soc.*, 94: 292-309.
- Lilly, D.K., 1992. A proposed modification of the Germano subgrid-scale closure method. *Phys. Fluids A*. 633-635.
- Mason, P. J., and D. J. Thompson, 1987. Large-eddy simulations of the neutral-static-stability planetary boundary layer. *Quarterly J. Royal Meteorology Society*. Vol. 113, pp. 413-444.
- Mason, P. J., 1989. Large-eddy simulation of the convective atmospheric boundary layer. *J. Atmos. Sci.*, 46: 1492-1516.
- Mason P. J., and S. H. Derbyshire, 1990. Large-eddy simulation of the stably-stratified atmospheric boundary layer. *Boundary-Layer Meteorology*, 53: 17-162.
- Mason, P.J., 1992a. Large-eddy simulation of dispersion in convective boundary layer with wind shear. *Atmospheric Environment*, 26, 9, 1551-1571.

- Mason P. J., 1992b. Large-eddy simulation of dispersion from an elevated point source in the convective boundary layer. *Atmos. Envir.*, 26A: 1561-1572.
- Mason, P. J., 1994. Large-eddy simulation: A critical review of the technique. *Quart. J. Roy. Meteor. Soc.*, 120, 1-26.
- Moeng, C.-H. 1984. A large-eddy simulation for the study of planetary boundary layer turbulence. *J. Atmos. Sci.*, 41: 2052-2062.
- Moeng, C.-H., 1986. Large-eddy simulation of a stratus-topped boundary Part I: Structure and budgets. *J. Atmos. Sci.*, 43: 2886-2900.
- Moeng C.-H. and U. Schumann, 1991. Composite structure of plumes in stratus-topped boundary layers. *J. Atmos. Sci.*, 48: 2280-2291.
- Moeng, C. H. and P. P. Sullivan, 1994. 'A Comparison of Shear and Buoyancy Driven Planetary Boundary Layer Flows'. *J. Atmos. Sci.*, 51: 999-1022.
- Moeng, C.-H., W. R. Cotton, C. Bretherton, A. Chlond, M. Khairoutidinov, S. Krueger, W. S. Lewellen, M. K. MacVean, J. R. M. Pasquier, H. A. Rand, A. P. Siebesma, B. Sievers, and R. I. Sykes, 1996. Simulation of a stratocumulus-topped planetary boundary layer: Intercomparison among Different numerical codes. *Bull. Amer. Meteor. Soc.*, 77: 261-278.
- Moeng, C.-H., 2000. Entrainment rate, cloud fraction, and liquid water path of PBL stratocumulus clouds. *J. Atmos. Sci.*, 57: 3627-3643.
- Neggers, R. A., P. G. Dunkerke, and S. M. Rodts, 2002. Shallow cumulus convection: a validation of large-eddy simulation against aircraft and Landsat observations. *15th Symp. on Boundary Layers and Turbulence*. July, Wageningen, The Netherlands, AMS.
- Nichols, S., 1989. The structure of radiatively driven convection in stratocumulus. *Quart. J. Roy. Met. Soc.*, 115: 487-511.
- Nieuwstadt, F. T. M., 1984. The turbulent structure of the stable, nocturnal boundary layer. *J. Atmos. Sci.*, 44: 2202-2216.
- Nieuwstadt, F. T. M. and R. A. Brost, 1986. The decay of convective turbulence. *J. Atmos. Sci.*, 43: 532-546.
- Nieuwstadt, F. T. M. and J. P. J. M. de Valk, 1989. A Large-eddy simulation and non-buoyant plume dispersion in the atmospheric boundary layer. *Atmos. Envir.*, 21, 12: 2573-2587.
- Nieuwstadt, F. T. M., 1990. Direct and large-eddy simulation of free convection. *Proc. 9th Interna. Heat Transfer Conference*, Jerusalem 19-24 August 1990. Amer. Soc. Mech. Eng., Vol 1: 37-47.
- Nieuwstadt, F. T. M., P. J. Mason, C. H. Moeng, and U. Schumann, 1992. Large-eddy simulation of convective boundary-layer: A comparison of four computer codes. *Turbulent Shear Flows 8*, (Durst H. et al., Eds), Springer-Verlag, pp. 343-367.
- Nieuwstadt, F. T. M. and J.P. Meeder, 1997: Large-eddy simulation of air pollution dispersion: a review. *New Tools in Turbulence Modeling. Les Houches School*, May 21-31 1996, (Eds: O. Metais and J.O. Ferziger), Springer-Berlin, pp. 265-279.
- Nieuwstadt, F. T. M., 1998. Review of Diffusion processes in the convective boundary layer. In: *Buoyant convection in Geophysical flows*, E.J. Plae (ed.): pp. 371-399.

- Paulos, G. S., W. Blumen, D. C. Fritts, J. K. Lundquist, J. Sun, S. P. Burns, C. Nappo, R. Banta, R. Newsome, J. Cuxart, E. Terradellas, B. Basley, and M. Jensen, 2002. Cases-99: A comprehensive investigation of the stable nocturnal boundary layer, *Bull. Amer. Meteorol. Soc.*, April, 576-581.
- Ricchazzi, P, S. Yang, C. Gautier, and D. Sowle, 1998. A research and teaching software tool for plane-parallel radiative transfer in the earth's atmosphere. *Bull. Amer. Meteorol. Soc.*, 79, 10: 2101-2114.
- Saiki, E. M., C. H. Moeng and P. P. Sullivan, 1999. Large-eddy simulation of the stably stratified planetary boundary layer. *13th Symp. on Boundary Layers and Turbulence*. Dallas, Texas, AMS.
- Schemm, C. E., and F. B. Lipps, 1976. Some results from a simplified three-dimensional numerical model of atmospheric turbulence. *J. Atmos. Sci.*, 33: 1021-1041.
- Shen, S. and C.-H. Moeng, 1993. Comparison of a computer-simulated stratus-topped boundary layer with aircraft observations. *Bound.-layer. Meteor.*, 65: 29-53.
- Schmidt, H. and Schumann, U. 1989. Coherent structures of the convective boundary layer derived from large-eddy simulations. *J. Fluid Mech.*, 200: 511-562.
- Schröter, M. and S. Raasch, 2002. Broadening of convective cells during cold air outbreaks: a high resolution study using a parallelized LES model. *15th Symp. on Boundary Layers and Turbulence*. July, Wageningen, The Netherlands, AMS.
- Schumann, U, 1989. Large-eddy simulation of turbulent diffusion with chemical reactions in the convective boundary layer. *Atmos. Envir.*, 23: 1713-1727.
- Schumann, U. and Moeng C.-H. 1991. Plume fluxes in clear and cloudy convective boundary layers. *J. Atmos. Sci.*, 48: 2280-2291.
- Siebesma, A. P., C. Bretherton, A. Brown, A. Chlond, J. Cuxart, P. Duynkerke, H. Jiang, M. Khairoutdinov, D. Lewellen, C. H. Moeng, E. Sanchez, B. Stevens, D. E. Stevens, 2003. A large-eddy simulation intercomparison study of shallow cumulus convection. *J. Atmos. Sci.*, 60: 1201-1219.
- Sommeria, G., 1976. Three-dimensional simulation of turbulent processes in an undisturbed trade wind boundary layer. *J. Atmos. Sci.*, 33: 216-241.
- Sommeria, G., and J. W. Deardorff, 1977. subgrid-scale condensation in models of nonprecipitating clouds. *J. Atmos. Sci.*, 34: 344-355.
- Sorbjan, Z., 1986. On similarity in the atmospheric boundary layer. *Bound.-Layer Meteor.*, 34: 377-397.
- Sorbjan, Z, 1989. *Structure of the atmospheric boundary layer*. Prentice Hall, 316 pp.
- Sorbjan, Z, 1991. Evaluation of local similarity functions in the convective boundary layer. *J. Appl. Meteor.*, 30: 1565-1583.
- Sorbjan, Z., 1995. Toward evaluation of heat fluxes in the convective boundary layer. *J. Appl. Meteor.*, 34: 1092-1098.
- Sorbjan, Z., 1996a. Numerical study of penetrative and "solid-lid" non-penetrative convective boundary layers. *J. Atmos. Sci.*, 53: 101-112.

- Sorbjan, Z., 1996b. Effects caused by varying strength of the capping inversion based on a large-eddy simulation of the shear-free convective boundary layer. *J. Atmos. Sci.*, 53: 2015-2024.
- Sorbjan, Z., 1997. Decay of convective turbulence revisited. *Bound.-Layer Meteor.*, 82: 501-515.
- Sorbjan, Z. and M. Uliasz, 1999. Large-eddy simulation of atmospheric dispersion in the nocturnal cloud-topped atmospheric boundary layer. *13th Symp. on Boundary Layers and Turbulence*, Dallas Texas, January, 1999.
- Sorbjan Z., 2001. An evaluation of local similarity on the top of the mixed layer based on large-eddy simulations. *Boundary-Layer Meteorology*, 101: 183-207.
- Sorbjan Z., 2004a. Large-eddy simulation of the baroclinic boundary layer. *Boundary-Layer Meteorology*, 112: 57-80.
- Sorbjan Z., 2004b. Statistics of scalar fields in the atmospheric boundary layer based on large-eddy simulations. Part 1: Free convection. Accepted to *Boundary-Layer Meteorology*.
- Sorbjan Z., 2004c. Statistics of scalar fields in the atmospheric boundary layer based on large-eddy simulations. Part 2: Forced convection. Submitted to *Boundary-Layer Meteorology*.
- Stevens, B., W. Cotton, G. Feingold, C. and H. Moeng, 1998. Large eddy simulations of strongly precipitating, shallow, stratocumulus-topped boundary layers. *J. Atmos. Sci.*, 55: 3616-3638.
- Stevens, B., C. H. Moeng, and P. P. Sullivan, 1999. Large-eddy simulations of radiatively driven convection: sensitivities to the representation of small scales. *J. Atmos. Sci.*, 56: 3963-3984.
- Stevens, B. A. S. Ackerman, B. A. Albrecht, A. R. Brown, A. Chlond, J. Cuxart, P. G. Duynkerke, D. C. Lewellen, M. K. MacVean, R. A. Neggers, E. Sanchez, A. P. Siebesma, and D. E. Stevens, 2001. Simulation of trade wind cumuli under a strong inversion. *J. Atmos. Sci.*, 58: 1870-1891.
- Sykes R. I., and D.S. Henn, 1988. A large-eddy simulation of turbulent sheared convection. *J. Atmos. Env.*, 26A: 3145-3159.
- Sykes R. I., and D.S. Henn, 1992. A large-eddy simulation of dispersion in the convective boundary layer. *J. Atmos. Sci.*, 46: 1106-1118.
- Toon, O. B., C. P. McKay, T. P. Ackerman, and K. Santhanam, 1989. Rapid calculations of radiative heating rates and photodissociation rates in inhomogeneous multiple-scattering atmospheres. *J. Geophys. Res. Atmos.*, 94, (D13): 16287-16301.
- Webster P. J., and R. Lucas, 1992. Toga COARE: the coupled ocean-atmosphere response experiment. *Bull. Amer. Meteorol. Soc.*, 73, 9: 1377-1416.
- Weil, J. C., P. P Sullivan and C.-H. Moeng, 1997. Lagrangian modeling of dispersion in the convective boundary layer using LES velocity fields. Preprint Vol. 12 *Symp. on Boundary layers and Turbulence*, Vancouver, Canada, pp. 108-109.
- White, A. B., R. J. Zamora, K. J. Olszyna, C. A. Russell, B. D. Templeman, J. W. Bao, 2000. Observations and numerical study of the morning transition: a case study from SOS-99. *13th Symp. on Boundary Layers and Turbulence*. Dallas, Texas, AMS.
- Willis, G. E. and J. W. Deardorff, 1976. A laboratory study of dispersion from an elevated source in a convective mixed layer. *Atmos. Environ.*, 12: 1305-1313.

Willis, G. E. and J. W. Deardorff, 1978. A laboratory study of diffusion into a convective planetary boundary layer. *Quart. J. R. Meteorol. Soc.*, 105: 109-117.

Willis, G. E. and J. W. Deardorff, 1981. A laboratory study of dispersion from a source in the middle of the convective mixed layer. *Atmos. Environ.*, 12: 1305-1313.

Wyngaard, J. C., and R. A. Brost, 1984. Top-down and bottom-up diffusion of a scalar in the convective boundary layer. *J. Atmos. Sci.*, 41: 102-112.

Chapter 6

Plume Rise

A chapter dedicated to the topic “Plume Rise” was presented in Volume I of this book series.

For additional information, the reader can visit:

- <http://www.lakes-environmental.com/aermodvol1/652.html>
A summary of basic plume rise formulations
- <http://www.cwrw.utexas.edu/gis/gishydro03/Classroom/trmproj/Nopmongcol/report.htm>
A plume rise model for forest fires

BRANK
P
e

Chapter 7

Gaussian Plume Models

A chapter dedicated to the topic “7A - Introduction to Gaussian Plume Models” was presented in Volume I of this book series. Other chapters are expected to be published in Volume III, according to the following plan:

7A – Introduction to Gaussian Plume Models

7B – Simulation Algorithms in Gaussian Plume Models

For additional information, the reader can visit:

- <http://www.epa.gov/scram001/userg/regmod/isc3v2.pdf>
Description of model algorithms of the Industrial Source Complex (ISC3) dispersion models
- http://www.epa.gov/scram001/7thconf/aermod/aermod_mfd.pdf
Description of model algorithms of the AERMOD modeling system, which consists of two pre-processors and the dispersion model: 1) the AERMIC meteorological preprocessor (AERMET) provides AERMOD with the meteorological information it needs to characterize the PBL; 2) The AERMIC terrain pre-processor (AERMAP) both characterizes the terrain, and generates receptor grids for the dispersion model (AERMOD)

BRANK P 2000

Chapter 8

Gaussian Puff Models

A brief introduction to the topic “Gaussian Puff Models” was presented in Volume I of this book series. A full chapter on this topic is expected to be published in Volume III.

For additional information, the reader can visit:

- <http://earthtec.vwh.net/download/calpuff.pdf>
A user’s guide to the CALPUFF dispersion model, which is part of the CALPUFF modeling system: <http://www.src.com/calpuff/calpuff1.htm>

BRANK P. 2000

Chapter 9

Special Applications of Gaussian Models

A brief introduction to the topic “Special Applications of Gaussian Models” was presented in Volume I of this book series. A full chapter on this topic is expected to be published in Volume III.

For additional information, the reader can visit

- <http://www.epa.gov/scram001/tt22.htm#rec>
A US EPA site where some models developed for special applications are listed

BRANK
P
e

Chapter 10

Eulerian Dispersion Models

A chapter dedicated to the topic “Eulerian Dispersion Models” was presented in Volume I of this book series.

For additional information, the reader can visit:

- <http://www.epa.gov/asmdnerl/CMAQ/index.html>
The US EPA site describing the Models-3 project. Models-3 and Community Multi-scale Air Quality (CMAQ) software in combination form a powerful third generation air quality modeling and assessment system that enables users to execute air quality simulation models for their specific problem domain and visualize the results
<http://www.ntis.gov/products/bestsellers/cpn8867.asp?loc=4-2-0>
- <http://www.ce.gatech.edu/~todman/24itm.pdf#search='air%20pollution%20grid%20models'>
A research paper on adaptive grids in air pollution modeling
- <http://parallel.bas.bg/~ceco/ps/boro02pap.pdf#search='air%20pollution%20grid%20models'>
A research paper on “Flexible Two-Level Parallel Implementations of a Large Air Pollution Model” that also describes The Danish Eulerian Model (DEM)

BRANK P 2000

Anfossi, D. and W. Physick 2005. *Lagrangian Particle Models*. Chapter 11 of *AIR QUALITY MODELING – Theories, Methodologies, Computational Techniques, and Available Databases and Software. Vol. II – Advanced Topics* (P. Zannetti, Editor). Published by The EnviroComp Institute (<http://www.envirocomp.org/>) and the Air & Waste Management Association (<http://www.awma.org/>).

Chapter 11

Lagrangian Particle Models

Domenico Anfossi ⁽¹⁾ and William Physick ⁽²⁾

⁽¹⁾ CNR - Istituto di Scienze dell'Atmosfera e del Clima, Torino (Italy)
anfossi@to.infn.it

⁽²⁾ CSIRO Atmospheric Research, Aspendale VIC (Australia)
bill.physick@csiro.au

Contributors:

Gervásio Degrazia ⁽¹⁾, Enrico Ferrero ⁽²⁾⁽³⁾, Mark Hibberd ⁽⁴⁾, Peter Hurley ⁽⁴⁾, Ashok Luhar ⁽⁴⁾, Silvia Trini Castelli ⁽²⁾⁽³⁾, Han van Dop ⁽⁵⁾

⁽¹⁾ Universidade Federal de Santa Maria, Departamento de Física, Santa Maria, RS (Brazil)

degrazia@ccne.ufsm.br

⁽²⁾ Dipartimento di Scienze e Tecnologie Avanzate, Università del Piemonte Orientale "A. Avogadro", Alessandria (Italy)

ferrero@unipmn.it, trini@to.infn.it

⁽³⁾ CNR - Istituto di Scienze dell'Atmosfera e del Clima, Torino (Italy)

ferrero@unipmn.it, trini@to.infn.it

⁽⁴⁾ CSIRO Atmospheric Research, Aspendale VIC (Australia)

mark.hibberd@csiro.au, peter.hurley@csiro.au, ashok.luhar@csiro.au

⁽⁵⁾ Institute for Marine and Atmospheric Research, Utrecht (The Netherlands)

h.vandop@phys.uu.nl

Abstract: Lagrangian particle dispersion models are being increasingly used to simulate air pollution dispersion at different spatial and temporal scales and in various stability conditions. In this Chapter, a review of the present state of the art of Lagrangian stochastic models for the description of airborne dispersion in the Planetary Boundary Layer is presented. These models are based on the generalised Langevin equation. Their theoretical basis and relevant implementation aspects are reviewed, and examples of main applications are discussed.

Key Words: Lagrangian air pollution modelling, Langevin equation, stochastic models, mesoscale dispersion, footprint analysis, long-range transport.

1 The Lagrangian Approach (W. Physick, D. Anfossi)

Basically two kinds of models are available to numerically simulate air pollution dispersion: Eulerian models and Lagrangian models. The main difference between the Eulerian and Lagrangian view is that the Eulerian reference system is fixed (with respect to the earth) while the Lagrangian reference system follows the instantaneous fluid velocity.

In a Lagrangian stochastic model (LSM), also called Lagrangian Particle or Random Walk model, the motion of air masses or particles passively following the flow is studied. To simulate the presence of turbulent eddies, particle velocities are subject to a random forcing. Consequently, these models are of stochastic type. The fictitious particles (computer-particles), which represent pollutant gases or aerosols, are considered small enough to follow the motion of smallest eddies and, at the same time, big enough to contain a large number of molecules. Each particle is moved at each time step by transport due to mean wind and diffusion, related to the turbulent wind velocity fluctuations.

In the single particle models considered here, the trajectory of each particle represents an individual statistical realisation in a turbulent flow characterised by certain initial conditions and physical constraints. Thus the motion of any particle is independent of the other particles, and consequently the concentration field must be interpreted as an ensemble average. The basic relationship for an instantaneous source located at x_0 (Csanady, 1973) is:

$$C(x, t) = Q P(x, t | x_0, t_0) \quad (1)$$

where C is the concentration at time t and location x , Q is the emitted mass at time $t = 0$ and $P(x, t | x_0, t_0)$ is the probability that a particle that was at x_0 at time t_0 arrives at x at time t . To compute $P(x, t | x_0, t_0)$ it is necessary to release a large number of particles, to follow their trajectories and to calculate how many of them arrive in a small volume surrounding x at time t . It is worth noting that particles move in the computational domain without any grid, using as input the values of the first two or three (sometimes four) moments of the probability density distribution (PDF) of wind velocity at the location of the particle. This input information comes either from measurements or from parameterisations

appropriate to the actual stability conditions (unstable, neutral, stable), to the type of site (flat or complex terrain, coast, etc.), and to the time and space scales considered.

This review covers various aspects of LSM derivation and applications. In Section 2, we describe the theoretical basis of LSMs (Langevin equation, Fokker-Planck equation, PDFs, turbulence parameterisation) and present the related technical information (i.e., link with meteorological models, boundary conditions, concentration calculation). Particular topics that can be covered within the framework of LSMs (plume rise, reactive chemistry and the prediction of higher order concentration moments) are also included. Section 3 deals with the application of LSMs under various conditions.

2 Lagrangian Stochastic Models (LSMs)

2.1 Historical Development (D. Anfossi)

LSMs are mainly based on the generalised Langevin equation for particle velocity. LSMs are based on the Langevin equation for particle position also exist, but do not have wide use and we do not discuss them in the present review. Before describing this equation and discussing its details, it may be worthwhile to briefly recall the historical milestones of its derivation (Gardiner, 1990; Rodean, 1996; Anfossi, 2000). The first one was the 1905 Einstein paper on the explanation of Brownian motion. In this paper the concept of stochastic modelling of natural phenomena was introduced for the first time. The main result was that the root-mean-square value of the displacement of the substance particles contained in the flow, under the assumption that successive displacements are independent from the previous ones, is proportional to the square root of the time as diffusion proceeds. Three years later in 1908, Langevin proposed an alternate method to explain the Brownian motion. His method was based on the derivation of an equation, named after him, in which it is assumed that two forces act on each particle: a deterministic one representing the viscous drag and a stochastic one accounting for the random impacts of the other molecules of the liquid. The original Langevin equation reads:

$$\frac{dv}{dt} = -\beta v + \lambda \mu(t) \quad (2)$$

where v is the velocity, t is the time, μ is a random function, and β and λ are two constants. Obviously, in later applications to atmospheric turbulent dispersion, the two terms on the r.h.s. of equation (2) represent the friction force exerted by the flow on the particle (the deterministic term) and the accelerations caused by pressure fluctuations (the stochastic term).

Equation (2) was the first example of a stochastic differential equation. A complete and rigorous treatment of such class of equations was not available until the 1950s. In particular, when manipulating stochastic equations, it should be noted that $[\mu(t)]^2$ is of the order dt and so cannot be neglected in comparison with dt . Consequently, the usual "function of a function" derivation rule must be substituted by Ito's formula that prescribes that the derivative of a stochastic function of velocity and position $f(x, u)$ is:

$$d[f(x, u)] = \left(u \frac{\partial f}{\partial x} + a \frac{\partial f}{\partial u} + b \frac{\partial^2 f}{\partial u^2} \right) dt + b \frac{\partial f}{\partial u} d\mu \quad (3)$$

where a and b are functions of x and u .

The Langevin equation is a Lagrangian equation. Its corresponding Eulerian equation is the Fokker-Planck equation derived in the years 1915-1917. The diffusion equation written by Einstein in his 1905 derivation is a special case of the Fokker-Planck equation. Taylor (1921) considered correlated particle displacements and obtained the fundamental results that the mean-square value of the displacement is proportional to the time elapsed from the emission in the first phase of the diffusion process and is proportional to the square root of time for longer times, thus recovering, in this second limit, the Einstein result. Obukhov (1959) first proposed that the evolution of the motion of an air particle in the atmosphere be described as a Markov process. Smith (1968) assumed that the Lagrangian turbulent fluctuation of a given parcel velocity at time $t + \tau$, $v'(t + \tau)$, is related to the same quantity at time t , $v'(t)$, according to the following relationship:

$$v'(t + \tau) = v'(t)R(\tau) + v''(t) \quad (4)$$

in which $R(\tau)$ is the autocorrelation coefficient at time lag τ and $v''(t)$ is a random velocity fluctuation, assumed independent of $v'(t)$. Both Equations (2) and (4) assume stationary and homogeneous turbulence. It is interesting to point out the relation between these two equations. The second one can be considered either the finite difference form of the first one (Sawford, 1985; Gifford, 1982), or it can be obtained by integrating the first one with respect to time (Legg and Raupach, 1982). On the other hand, Equation (2) can be derived from Equation (4) by combining the latter with its Taylor series expansion and dropping higher order terms (Gaffen et al., 1987; Durbin and Petterson Reif, 2001).

Hanna (1979) showed, by direct comparison with atmospheric Eulerian and Lagrangian turbulence data, that Equation (4) is approximately valid, and therefore applicable, in the planetary boundary layer (PBL).

Since the 1970s, many pioneering papers (e.g., Reid, 1979; Zannetti, 1981, 1984; Ley, 1982; Davis, 1983) have appeared in the literature aimed at simulating

atmospheric turbulent dispersion by means of the Langevin equation, written as follows:

$$dv' = -\frac{v'}{T_L} dt + \sigma_v \left(\frac{2}{T_L} \right)^{\frac{1}{2}} d\mu \quad (5)$$

or in its finite difference form (Equation 4), where T_L is the Lagrangian time scale and σ_v is the velocity standard deviation. Zannetti (1981, 1984), in particular, proposed the first model that considered all the correlations among the three wind components.

However, it became immediately clear that Equation (5) could not be applied in non-homogeneous turbulence, because it leads to accumulation of particles in the regions where σ_v is small. This is an important point since vertical turbulence conditions in the PBL are never homogeneous. In neutral stability, turbulence is non-homogeneous but, generally, Gaussian. In convective conditions turbulence is neither homogeneous nor Gaussian. This problem was examined by, among others, Wilson et al. (1981), Legg and Raupach (1982) and Sawford (1985), who attributed the accumulation to a mean drift velocity induced by the gradient in vertical velocity variance. A proposed drift term correction to the r.h.s. of equation (5) for the vertical component generally had the following expression: $1/2 \left(1 + w'^2 / \sigma_w^2 \right) \partial \sigma_w^2 / \partial z dt$. This was used with success, for instance, by Brusasca et al. (1989). Since then particular attention has been paid to dispersion in convective conditions in the literature. In these conditions, the vertical velocity PDF is not Gaussian due to the presence of updrafts and downdrafts, and, as a consequence, it is necessary to take into account at least the third order moment of the vertical velocity fluctuations. With relation to this problem, important contributions were given by the basic papers of Baerentsen and Berkowicz (1984), Thomson (1984), van Dop et al. (1985), and De Baas et al. (1986) introducing the treatment of updrafts and downdrafts, and consequently of skewed PDFs, into the Langevin equation, thus obtaining realistic and physically correct simulations of dispersion in convective conditions (see Section 2.2). The test database, widely used by the international community, was due to Willis and Deardorff (1976, 1978, 1981) who performed very skilful and comprehensive water tank tracer dispersion experiments.

The conclusive paper, at least for the moment, defined by Rodean (1996) as a "classical landmark paper", was due to Thomson (1987). He demonstrated that by using the "well-mixed condition" (particles that are initially uniformly distributed in space, must remain so and they have the same velocity distribution as the fluid) as the criterion for selecting the correct model for the diffusion of scalars in a turbulent flow, the atmospheric dispersion of pollutants can be successfully simulated with LSMs based on a generalised form of the Langevin equation. This form is capable of representing skewed inhomogeneous non-stationary conditions, without adding any "ad hoc" drift correction term, and incorporates an exact

formulation of non-Gaussian turbulence. Also, unlike in previous versions of the Langevin equation, it is not necessary to incorporate the skewness of the convective boundary layer (CBL) in the random term, which remains Gaussian.

2.2 Theory (E. Ferrero)

LSMs are based on the Langevin equation that describes the temporal evolution of the velocity of pollutant particles in a turbulent field. The solution of the Langevin equation is a continuous stochastic Markov process. In fact, particle position and velocity, in a turbulent flow, can be considered a bivariate Markov process in the range of the turbulent energy spectrum between the Kolmogorov time scale τ_n (approximately equal to the correlation time of the accelerations) and the velocity correlation Lagrangian time scale T_L .

The Langevin equation for the turbulent velocity can be written as follows:

$$du_i(t) = a_i(\vec{x}, \vec{u}, t) \cdot dt + b_{i,j}(\vec{x}, \vec{u}, t) \cdot dW_j \quad (6)$$

and is coupled to the equation for the position $x(t)$:

$$dx_i(t) = u_i(t) \cdot dt \quad (7)$$

where $d\vec{W}$ is an incremental Wiener process that is Gaussian with zero mean and variance of:

$$\langle dW_i(t) \cdot dW_j(t') \rangle = \delta_{ij} \delta(t - t') \cdot dt \cdot dt'$$

where the notation $\langle \rangle$ represents an ensemble average.

The term $b_{i,j}(\vec{x}, \vec{u}, t) \cdot$ can be derived from the Kolmogorov theory of local isotropy in the inertial sub-range (Monin and Yaglom, 1975). This theory is based on similarity relations valid in a particular interval of the turbulence spectrum. The energy is transferred from the larger vortices to the smaller ones, the smallest scales of the atmospheric turbulence, where it is dissipated by the viscosity. Inside this energetic cascade, there is a part of the spectrum where the vortices are sufficiently small so that they are not affected by the anisotropy induced from the larger vortices and are not dissipated as heat. This part of the turbulent spectrum is called the inertial sub-range. This interval coincides with the interval of temporal scales in which the turbulent velocities can be considered a Markov process.

By defining the structure function of the Lagrangian velocities, in one dimension, as:

$$D = \langle (u_i(t) - u_i(t + dt))^2 \rangle = \langle du_i(t)^2 \rangle \quad (8)$$

then (if $\tau_n \leq dt \leq T_L$), the following relationship can be considered:

$$D = C_0 \cdot \varepsilon \cdot dt$$

where ε is the dissipation rate of turbulent kinetic energy and C_0 is a universal constant.

Substituting $du_i(t)$, as given by the Langevin equation in (8), averaging and considering only the terms of the order of dt , leads to:

$$D = \langle du_i^2 \rangle = b_{ij}^2 \cdot \langle dW_i^2 \rangle = b_{ij}^2 dt = \delta_{ij} C_0 \cdot \varepsilon \cdot dt$$

and

$$b_{ij} = \delta_{ij} \sqrt{C_0 \cdot \varepsilon} \quad (9)$$

An Eulerian description of a continuous Markov process is available through the Fokker-Planck equation. If the position and turbulent velocity can be considered a continuous stochastic Markov process, the Fokker-Planck equation can be used to

calculate the coefficient \vec{a} of the Langevin equation for any given probability density function (PDF) (Gardiner, 1990).

$$\begin{aligned} \frac{\partial P(\vec{x}, \vec{u}, t)}{\partial t} + \frac{\partial}{\partial x_i} \left(u_i(\vec{x}, t) \cdot P(\vec{x}, \vec{u}, t) \right) = \\ - \frac{\partial}{\partial u_i} \left(a_i(\vec{x}, \vec{u}) \cdot P(\vec{x}, \vec{u}, t) \right) + \frac{1}{2} \cdot \frac{\partial^2}{\partial u_i \partial u_j} \left(b_{ij}^2(\vec{x}) \cdot P(\vec{x}, \vec{u}, t) \right) \end{aligned}$$

where $P(\vec{x}, \vec{u}, t)$ is the Eulerian PDF of the particles.

In the stationary case, $P(\vec{x}, \vec{u}, t)$ does not depend on time and the Fokker-Planck equation reduces to:

$$\begin{aligned} \frac{\partial}{\partial x_i} \left(u_i \left(\vec{x} \right) \cdot P \left(\vec{x}, \vec{u} \right) \right) = \\ - \frac{\partial}{\partial u_i} \left(a_i \left(\vec{x}, \vec{u} \right) \cdot P \left(\vec{x}, \vec{u} \right) \right) + \frac{1}{2} \cdot \frac{\partial^2}{\partial u_i \partial u_j} \left(b_{ij}^2 \left(\vec{x} \right) \cdot P \left(\vec{x}, \vec{u} \right) \right) \end{aligned} \quad (10)$$

where b_{ij} is given by (9).

Following Thomson (1987), it can be stated that a LSM satisfies the well-mixed condition (if the particles are initially well-mixed in the fluid, they will remain so), if $P \left(\vec{x}, \vec{u} \right)$ is equal to the Eulerian *atmospheric* PDF. This is a necessary and sufficient condition. In other words all moments of $P \left(\vec{x}, \vec{u} \right)$ must equal the measured or parameterised moments.

In one dimension, the Fokker-Planck equation can be solved and the term $a(x, u)$ calculated, for a given PDF, as follows (Thomson, 1987):

$$a(x, u) = \frac{1}{P(x, u)} \cdot \left(\frac{C_0 \varepsilon}{2} \cdot \frac{\partial P(x, u)}{\partial u} + \phi(x, u) \right) \quad (11)$$

where

$$\phi(x, u) = - \frac{\partial}{\partial x} \cdot \int_{-\infty}^u u \cdot P(x, u) \cdot du \quad (12)$$

and

$$\phi \rightarrow 0 \quad \text{per} \quad |u| \rightarrow \infty$$

In addition (Hinze, 1975; Tennekes, 1982; Rodean, 1994; Luhar and Britter, 1989; Weil, 1990; Reynolds, 1998),

$$\frac{C_0 \varepsilon}{2} = \frac{\sigma^2}{T_L} \quad (13)$$

LSMs usually are one-dimensional models solving one or two and, in some cases, three Langevin equations, one for each Cartesian direction. The extension to a fully three dimensional model was addressed by Sawford and Guest (1988), Sawford (1993) and Borgas and Sawford (1994). It can be demonstrated that a unique solution for the Fokker-Planck equation, in the three-dimensional case, exists only for homogeneous, isotropic turbulence (Borgas and Sawford, 1994).

The non-uniqueness of the 2D and 3D solution is related to the first term on the right side of (10), as this equation can be satisfied by any vector obtained through adding a rotational vector, in \vec{u} space, to \vec{a} P (Sawford, 1993; Rotach et al., 1996).

Concerning the value of the basic constant C_0 , different values can be found in the literature, mainly ranging from about 2 to 4 (Luhar and Britter, 1989; Hurley and Physick, 1991, 1993; Physick et al., 1994; Tassone et al., 1994; Rotach et al., 1996; Degrazia and Anfossi, 1998). Sawford (1991) showed that C_0 is a function of the Reynolds number based on the Eulerian Taylor microscale, Re_λ . C_0 reaches an asymptotic value, $C_0 = 7$, for growing Re_λ . The variability in the value of this constant was discussed by Du (1997), who suggested that it can be related to the method used for estimating C_0 and proposed the value 3.0 ± 0.5 for using in Lagrangian Stochastic models in neutral conditions. Reynolds (1998) demonstrated that the value 5.0 ± 0.5 gives satisfactory results in simulating a wind tunnel boundary layer and suggested that one-dimensional Lagrangian stochastic models are inconsistent with the supposed universality of C_0 . Anfossi et al. (2000), by analysing turbulence observations made in the surface layer, under unstable conditions by a sonic anemometer, found $C_0 = 4.3$ for the crosswind and vertical turbulent velocity components and $C_0 = 3.2$ for the longitudinal one. According to these authors, the partitioning of C_0 in different spatial components is a consequence of the directional dependence of the Eulerian correlation functions due to the local isotropy in the inertial sub-range.

Stohl and Thomson (1999) stressed the effects of the density variation in the boundary layer and proposed a density correction term. They also demonstrated that this term influences the surface concentration.

The theory of this section is applicable to one-particle models, and these have been widely tested and applied to many different situations characterised by non-homogeneous turbulence and different stability conditions (see section 2.10). However, it should be stressed that a one-particle model is only able to describe the absolute dispersion and to predict the mean concentration fields. When one is interested in the relative dispersion and mean-square concentration field, a two-particle model should be developed and applied (Durbin, 1980), although recently one-particle Lagrangian models have been used in conjunction with the meandering plume approach of Gifford (1959) to determine higher order concentration fluctuation statistics for practical applications (Section 20). In the two-particle case, the assumption of Markovian and continuous process should be made jointly for the positions and velocities of the particles pair (Thomson, 1990; Sawford, 1993; Borgas and Sawford, 1994). An important advantage of the two-particle model is the ability to include second order chemical reaction (Crone et al. 1999). Unfortunately, in the case of the two-particle model, a unique solution of the Fokker-Planck equation does not exist even in isotropic turbulence in the fully three-dimensional case (Sawford, 1993).

A hybrid LSM, referred to as the PARTPUFF (Hurley, 1994), was designed to save computer time for high horizontal-resolution simulations. This model employs the LSM approach in the vertical direction, and a Gaussian puff approach in the horizontal directions. This method allows a particle/puff to influence more than one horizontal grid-point, enabling a reduction in the number of particles needed in a simulation. A related approach in which puffs and particles are combined is described by De Haan and Rotach (1998).

2.3 Choice of Eulerian PDF (E. Ferrero, D. Anfossi, M. Hibberd)

The main input of physical data to LSMs is through the PDF of Eulerian turbulent velocities (see Equation [10]), the form of which depends on the prevailing turbulence characteristics. If this PDF is Gaussian, it can be fully described by the mean and standard deviation, otherwise higher order moments are also needed. For actual atmospheric PDFs, their non-Gaussian form can usually be described sufficiently and accurately by adding moments up to third or fourth order.

Since most LSM applications concern vertical dispersion in the convective boundary layer (CBL), we will mainly focus on this kind of dispersion. In convective conditions the vertical velocity PDF is asymmetric and, as a consequence, to correctly describe dispersion, it is necessary to prescribe an analytical expression for the PDF based on the measured higher order moments of Eulerian vertical velocity fluctuations.

In this section we present PDFs that are most commonly used in LSMs: Gaussian, bi-Gaussian and Gram-Charlier. The various closure schemes used with the bi-Gaussian PDF form are described. Advantages of analytical solutions and approaches other than closure (such as using a quadratic form for the acceleration term in the stochastic equation) are discussed.

2.3.1 Gaussian PDF

In homogeneous turbulence the PDF of velocity fluctuations is assumed to be Gaussian. This assumption may also be made for inhomogeneous Gaussian turbulence, which, for example, is a good first approximation for the neutral PBL. This choice implies that the generalised Langevin equation (see Equation [6]) in inhomogeneous conditions, without the Reynolds stress terms, reduces to the following form for each component (Rodean, 1996):

$$du_i = -\frac{u_i}{T_{Li}} dt + \frac{1}{2} \left[1 + \left(\frac{u_i}{\sigma_{u_i}} \right)^2 \right] \frac{\partial \sigma_{u_i}^2}{\partial x_i} dt + \sigma_{u_i} \left(\frac{2}{T_{Li}} \right)^{\frac{1}{2}} d\mu \quad (14)$$

This equation was first proposed by Wilson et al. (1983) and rigorously derived by Thomson (1987). Inhomogeneous turbulence equation (14) further reduces to:

$$du_i = -\frac{u_i}{T_{Li}} dt + \sigma_{ui} \left(\frac{2}{T_{Li}} \right)^{\frac{1}{2}} d\mu \quad (15)$$

This equation is identical to Equation (5).

2.3.2 Bi-Gaussian PDF

Pearson (1894) was the first to suggest the use of linear combinations of normal distributions for fitting observed frequency distributions having a non-Gaussian shape, for example

$$P(w, z) = A \cdot P_A(w_A, \sigma_A) + B \cdot P_B(w_B, \sigma_B) \quad (16)$$

where $A + B = 1$, $A > 0$, $B > 0$ and P_A and P_B are Gaussian PDFs with means w_A and w_B , and standard deviations σ_A and σ_B .

Baerentsen and Berkowicz (1984) first introduced this PDF into LSMs, where the Gaussian PDFs have the form

$$P_A = \left[(2\pi)^{1/2} \sigma_A \right]^{-1} \exp \left[- (w - w_A)^2 / (2\sigma_A^2) \right] \quad (17)$$

and similarly for P_B . (Note that there is a potential for confusion when using equations given in the literature because some authors use absolute values of the means in the PDF expressions rather than their assigned values.) The values of the parameters (A , B ; w_A , w_B ; σ_A , σ_B) are obtained from the definition of the moments of the distribution:

$$\overline{w^n} = A \cdot \int_{-\infty}^{+\infty} w^n \cdot P_A(w, z) \cdot dw + B \cdot \int_{-\infty}^{+\infty} w^n \cdot P_B(w, z) \cdot dw \quad (18)$$

where $\overline{w^n}$ are the measured or parameterised moments of the atmospheric PDF. In principle, the six unknowns can be determined by solving the zeroth to fifth order moment equations. However, the absence of data for the highest moments makes it more practical to use just the first few moments and to make some closure assumption. Writing out Equation (18) for the first four moments leads to the following system of equations:

$$A + B = 1$$

$$Aw_A + Bw_B = \overline{w} = 0$$

$$A(w_A^2 + \sigma_A^2) + B(w_B^2 + \sigma_B^2) = \overline{w^2} \quad (19)$$

$$A(w_A^3 + 3w_A\sigma_A^2) + B(w_B^3 + 3w_B\sigma_B^2) = \overline{w^3}$$

$$A(w_A^4 + 6w_A^2\sigma_A^2 + 3\sigma_A^4) + B(w_B^4 + 6w_B^2\sigma_B^2 + 3\sigma_B^4) = \overline{w^4}$$

Baerentsen and Berkowicz (1984) considered the first three moments and used the closure assumption

$$\sigma_A = |w_A| \quad \sigma_B = |w_B| \quad (20)$$

to solve for the parameters:

$$w_B = \frac{\overline{w^3} - \sqrt{(\overline{w^3})^2 + 8 \cdot (\overline{w^2})^3}}{4 \cdot \overline{w^2}}, \quad w_A = -\overline{w^2} / 2w_B,$$

$$A = \frac{w_B}{w_B - w_A}, \quad B = 1 - A \quad (21)$$

This system of equations has probably been the most widely employed of the closures described here, although some of the other closures give better results. Using the closure in Equation (20) with equation (16) for the PDF in the Fokker-Planck equation (Equations [10] and [12]), Luhar and Britter (1989) obtained an explicit expression for Φ . The general expression for Φ in their model is:

$$\begin{aligned} \phi = & AP_A \left[\frac{\sigma_A^2}{A} \frac{\partial A}{\partial z} + \frac{\partial \sigma_A}{\partial z} \left(\sigma_A + \frac{w(w - w_A)}{\sigma_A} \right) + w \frac{\partial w_A}{\partial z} \right] + \\ & \frac{1}{2} \frac{\partial(Aw_A)}{\partial z} \left[1 - \operatorname{erf} \left(\frac{w - w_A}{\sqrt{2}\sigma_A} \right) \right] + \\ & BP_B \left[\frac{\sigma_B^2}{B} \frac{\partial B}{\partial z} + \frac{\partial \sigma_B}{\partial z} \left(\sigma_B + \frac{w(w - w_B)}{\sigma_B} \right) + w \frac{\partial w_B}{\partial z} \right] + \\ & \frac{1}{2} \frac{\partial(Bw_B)}{\partial z} \left[1 - \operatorname{erf} \left(\frac{w - w_B}{\sqrt{2}\sigma_B} \right) \right] \end{aligned} \quad (22)$$

where $\operatorname{erf}(z)$, the error function, is defined as:

$$\operatorname{erf}(z) = \frac{2}{\sqrt{\pi}} \cdot \int_0^z \exp(-s) \cdot ds$$

and any closure assumption can be substituted in Equation (22).

Weil (1990) generalised the Baerentsen and Berkowicz (1984) closure assumption to:

$$\sigma_A = R|w_A| \quad \text{and} \quad \sigma_B = R|w_B|, \quad (23)$$

and obtained solutions:

$$w_A = \frac{1}{2} \sqrt{\overline{w^2}} \left[\alpha S + \left(\alpha^2 S^2 + \frac{4}{\beta} \right)^{\frac{1}{2}} \right], \quad w_B = \frac{1}{2} \sqrt{\overline{w^2}} \left[\alpha S - \left(\alpha^2 S^2 + \frac{4}{\beta} \right)^{\frac{1}{2}} \right] \quad (24)$$

where:

$$S = \frac{\overline{w^3}}{\left(\overline{w^2}\right)^{\frac{3}{2}}}, \quad \alpha = \frac{1 + R^2}{1 + 3R^2} \quad \text{and} \quad \beta = 1 + R^2$$

S is the skewness. Weil used a value of $R = 3/2$. The Eulerian PDF generated using this closure assumption has been found to lead to good agreement with point source dispersion results in the CBL and is recommended over the Baerentsen and Berkowicz (1984) form (Luhar et al., 1996).

Du et al. (1994) considered all four moments listed in Equations (19) with $A = 0.4$ and assumed the Gaussian value of 3 for the kurtosis $K \left(= \overline{w^4} / \overline{w^2}^2 \right)$:

$$\overline{w^4} = 3(\overline{w^2}) \quad (25)$$

They obtained

$$w_A = (\overline{w^3})^{1/3}, \quad w_B = -\frac{2}{3}(\overline{w^3})^{1/3} \quad (26)$$

$$\sigma_A = \left[\overline{w^2} - 0.280(\overline{w^3})^{2/3} \right]^{1/2}, \quad \sigma_B = \left[\overline{w^2} - 0.927(\overline{w^3})^{2/3} \right]^{1/2}$$

Equations (26) yield real solutions for $S \leq 1.12$.

Another closure for the bi-Gaussian PDF that includes up to the fourth moment was proposed by Anfossi et al. (1996). They suggested two different closures without assuming any a priori value for $\overline{w^4}$. The first closure assumed $\sigma_A = \sigma_B = \sigma$ and the second closure set $A = B = 1/2$. Both PDFs had restrictions on the range of skewness S and kurtosis K to ensure real solutions were obtained. A comparison among different closures performed by Ferrero et al. (1998b) in CBL dispersion showed that these closures perform as well as the one by Du et al. (1994) but generally less well than the one by Baerentsen and Berkowicz (1984) and the Gram Charlier method (described below).

The closure assumptions considered so far are not well behaved as the skewness approaches zero, i.e., they do not collapse to a simple Gaussian PDF. In order to overcome this problem, Luhar et al. (1996) proposed a more generalised form of Weil's (1990) closure, based on the skewness value S :

$$w_A = m \sigma_A, \quad w_B = -m \sigma_B, \quad m = (2/3)S^{1/3} \quad (27)$$

This has the correct property that the bi-Gaussian PDF collapses to a Gaussian PDF in the zero skewness limit and so can be used to investigate the influence of skewness on dispersion in the CBL. It gives the following values for the parameters

$$\sigma_A = \sqrt{\overline{w^2}} \left[\frac{B}{A(1+m^2)} \right]^{1/2}, \quad \sigma_B = \sqrt{\overline{w^2}} \left[\frac{B}{B(1+m^2)} \right]^{1/2} \quad (28)$$

$$A = \frac{1}{2} \left[1 - \left(\frac{r}{4+r} \right)^{1/2} \right], \quad B = 1 - A,$$

where

$$r = \left[(1 + m^2)^3 S^2 \right] / \left[(3 + m^2)^2 m^2 \right]$$

and the kurtosis is given by

$$K = (1 + r)(3 + 6m^2 + m^4) / (1 + m^2)^2$$

Luhar et al. (1996) reported that the 2/3 constant in Equation (27) was chosen to best match the observed values for the higher moments of $S = 0.8$ and $K = 3.9$ in most of the CBL. Comparison with laboratory experiments of Hibberd and Sawford (1994) showed that this closure produced similar CBL dispersion results to those obtained with the Weil (1990) closure, and better than those of Baerentsen and Berkowicz (1984) and Du et al. (1994).

The model of Rotach et al. (1996) has also the property that it has a skewed PDF for convective conditions and is “well behaved” in the Gaussian limit. As an additional advantage it is more than one-dimensional (i.e., it includes the effect of velocity covariances).

Wilson and Flesch (1993) warn of the risk of numerical underflows/overflows with all these models when evaluating the tails of the exponential distributions; use of double precision and sufficiently small timesteps is recommended.

2.3.3 Gram-Charlier PDF

Most of the closures described so far are based on the idea that A and B in Equation (14) may be associated with the fractions of the area occupied by updrafts and downdrafts, w_A and w_B with the mean updraft and downdraft velocities, and σ_A and σ_B with the corresponding variances of the vertical velocity fluctuations. However, De Baas et al. (1986) and Anfossi et al. (1996) note that all these PDFs are just mathematical approximations. It is not necessary that the parameters in the model be directly related to physical quantities. In all cases, it is just the moments of the PDFs that are derived from experimental data.

An alternative form of the PDF proposed by Anfossi et al. (1996) and Ferrero and Anfossi (1998a, b) on the basis of these considerations is the Gram-Charlier PDF. This PDF, truncated to fourth order (GC4), has the following form (Kendall and Stuart, 1977):

$$P(x, z) = \frac{e^{-x^2/2}}{\sqrt{2\pi}} (1 + C_3 H_3 + C_4 H_4) \quad (29)$$

where H_3 and H_4 are Hermite polynomials and C_3 and C_4 are their coefficients, whose expressions are:

$$\begin{aligned} H_3 &= x^3 - 3x & H_4 &= x^4 - 6x^2 + 3 \\ C_3 &= \overline{\mu^3}/6 & C_4 &= (\overline{\mu^4} - 3)/24 \end{aligned} \quad (30)$$

and $\overline{\mu^3}, \overline{\mu^4}$ are the standardised moments of w and $x = w/\sigma_w$. Solving Equation (12) in which P is given by Equation (29), the following expressions are found:

$$\Phi = \frac{1}{2} \frac{\partial \sigma_w^2}{\partial z} \frac{e^{-\frac{x^2}{2}}}{\sqrt{2\pi}} \left[1 - C_4 + x^2(1 + C_4) - 2C_3x^3 - 5C_4x^4 + C_3x^5 + C_4x^6 \right] \quad (31)$$

and

$$a = \sigma_w \frac{\frac{1}{T_{Lw}}(T_1) + \frac{\partial \sigma_w}{\partial z}(T_2)}{T_3} \quad (32)$$

where

$$\begin{aligned} T_1 &= -3C_3 - x(15C_4 + 1) + 6C_3x^2 + 10C_4x^3 - C_3x^4 - C_4x^5 \\ T_2 &= 1 - C_4 + x^2(1 + C_4) - 2C_3x^3 - 5C_4x^4 + C_3x^5 + C_4x^6 \\ T_3 &= 1 + 3C_4 - 3C_3x - 6C_4x^2 + C_3x^3 + C_4x^4 \end{aligned} \quad (33)$$

We note that a Gram-Charlier distribution truncated to third order (GC3) can be derived from Equations (33) simply by setting $C_4 = 0$. If C_3 is also set to zero, Equation (29) reduces to the Gaussian PDF. Thus, this PDF also has the correct property of collapsing to a Gaussian PDF when the skewness is equal to zero.

Gram-Charlier series expansions, though showing good correspondence to experiments (e.g., Frenkiel and Klebanoff, 1967; Antonia and Atkinson, 1973; Durst et al., 1992; Anfossi et al., 1996) can exhibit small negative probabilities in the tails of the distribution (Frenkiel and Klebanoff, 1967; Flesch and Wilson, 1992; Du et al., 1994; Anfossi et al., 1996). Numerical experiments (Ferrero and Anfossi, 1998b) showed that discarding these non-physical probabilities is inconsequential in practical applications because these unrealistic velocities occur so rarely.

Advantages of the Gram-Charlier (GC) PDFs are their computational efficiency and the ability to include information on the Eulerian moments directly. The GC form also provides greater flexibility in choosing the shape of the PDF to match observations. It has been shown to give good results both in the atmospheric surface layer (Anfossi et al., 1996) and for all stabilities in PBL dispersion (Ferrero and Anfossi, 1998b; Tinarelli et al., 2000).

An alternative way of using the GC PDF was proposed by Tassone et al. (1994). They assumed that the variance of the Gaussian distribution included in the GC PDF (see equation 29) is proportional to, rather than equal to, the second moment of vertical velocity distribution (included in the Hermite polynomials): $\sigma_w^2 = f(z) \overline{w^2}$, where the value of f is determined empirically. By comparing this closure to the Willis and Deardorff (1981) water tank experiments, Vinter Falk (1998) found that the position and size of the ground level concentration peak were well predicted but the right side (positive velocities) of the PDF could present a pronounced non-physical dive in the plume centreline.

2.3.4 Quadratic Form for the Acceleration Term

Franzese et al. (1999) adopted a different approach and assumed that the deterministic acceleration term in the stochastic differential equation can be parameterised as a quadratic function of velocity:

$$a(w, z) = \alpha(z)w^2 + \beta(z)w + \gamma(z) \quad (34)$$

The coefficients are assumed to be height dependent. Their values are determined from the first four moments of the Eulerian velocities with integration of the Fokker-Planck equation.

The main advantage of this approach is its computational efficiency. Tests showed that model run times were reduced to a quarter of those for the Luhar and Britter (1989) model. A further advantage is that moments up to fourth order can be used without any predefined form for the PDF. However, the skewness cannot exceed a value of about 0.6, otherwise the model does not produce a vertically well-mixed concentration distribution at large times. This is probably due to the inadequacy of the first few moments for fully describing the physical PDF (Borgas, pers. comm.). In fact, all the methods discussed in this section are approximations to physical PDFs and may fail to properly describe dispersion in particular circumstances.

2.4 Turbulence Parameterisation (G. Degrazia)

A turbulence parameterisation is an approximation to nature in the sense that we are putting in physical models an approximated relation that in principle can be used as a surrogate for the natural true unknown term. The reliability of each model strongly depends on the way turbulent parameters are calculated and related to the current understanding of the PBL. Most of the turbulence

parameterisations used in advanced dispersion models are based on PBL similarity theories (Hanna, 1982; Stull, 1988; Holtslag and Moeng, 1991; Kaimal and Finnigan, 1994; Sun, 1993; Rodean, 1994).

Through classical statistical diffusion theory (Batchelor, 1949), it is possible to relate turbulent parameters (wind velocity standard deviations σ_i ($i = u, v, w$) and Lagrangian decorrelation time scales T_{Li}) to spectral distribution of turbulent kinetic energy (TKE). Following this approach, Hanna (1982) and Degrazia et al. (2000) developed expressions for the Lagrangian decorrelation time scales based on the peak wavelength of the turbulent velocity spectra. These two parameterisations that can be used in Lagrangian stochastic dispersion models are presented here. Parameterisations for the third order moments for the vertical velocity (w^3) and the dissipation rate (ε) are also presented.

2.4.1 Hanna's Parameterisation

Based on analyses of field experiments (Hanna, 1968; Kaimal et al., 1976, 1982; Caughey, 1979; Hanna, 1981), theoretical considerations (Panofsky et al., 1977; Irwin, 1979a) and second-order closure model (Wyngaard et al., 1974), Hanna (1982) proposed the following parameterisations:

in the unstable case:

for $\frac{z}{z_i} < 0.03$

$$\sigma_u = \sigma_v = (u_*)_o \left[12 + \frac{1}{2} \frac{z_i}{|L|} \right]^{1/3} \quad (35)$$

$$\sigma_w = 0.96 w_* \left(3 \frac{z}{z_i} - \frac{L}{z_i} \right)^{1/3} \quad (36)$$

for $0.03 < \frac{z}{z_i} < 0.4$

$$\sigma_w = w_* \min \left\{ 0.96 \left(3 \frac{z}{z_i} - \frac{L}{z_i} \right)^{1/3}, 0.763 \left(\frac{z}{z_i} \right)^{0.175} \right\} \quad (37)$$

for $0.4 < \frac{z}{z_i} < 0.96$

$$\sigma_w = 0.722 w_* \left(1 - \frac{z}{z_i} \right)^{0.207} \quad (38)$$

for $0.96 < \frac{z}{z_i} < 1$

$$\sigma_w = 0.37w_* \quad (39)$$

$$T_{Lu} = T_{Lv} = 0.15 \frac{z_i}{\sigma_u} \quad (40)$$

$$T_{Lw} = 0.1 \frac{z}{\sigma_w} \frac{l}{0.55 + 0.38 \left[\frac{(z - z_0)}{L} \right]} \quad \frac{z}{z_i} < 0.1 \quad \text{and} \quad -\frac{(z - z_0)}{L} < 1 \quad (41)$$

$$T_{Lw} = 0.59 \frac{z}{\sigma_w} \quad \frac{z}{z_i} < 0.1 \quad \text{and} \quad -\frac{(z - z_0)}{L} > 1 \quad (42)$$

$$T_{Lw} = 0.15 \frac{z_i}{\sigma_w} \left[1 - \exp\left(-\frac{5z}{z_i}\right) \right] \quad \frac{z}{z_i} > 0.1 \quad (43)$$

in the stable case:

$$\sigma_u = 2(u_*)_0 \left(1 - \frac{z}{h} \right) \quad \text{and} \quad \sigma_w = \sigma_v = 1.3(u_*)_0 \left(1 - \frac{z}{h} \right) \quad (44)$$

$$T_{Lu} = 0.15 \frac{h}{\sigma_u} \left(\frac{z}{h} \right)^{0.5} ; T_{Lv} = 0.07 \frac{h}{\sigma_v} \left(\frac{z}{h} \right)^{0.5} \quad \text{and} \quad T_{Lw} = 0.10 \frac{h}{\sigma_w} \left(\frac{z}{h} \right)^{0.8} \quad (45)$$

and in the neutral case:

$$\sigma_u = 2(u_*)_0 \exp\left(-\frac{3f_c z}{(u_*)_0}\right) \quad \text{and} \quad \sigma_w = \sigma_v = 1.3(u_*)_0 \exp\left(-\frac{2f_c z}{(u_*)_0}\right) \quad (46)$$

$$T_{Lu} = T_{Lv} = T_{Lw} = \frac{0.5 \frac{z}{\sigma_w}}{1 + 15 \frac{f_c z}{(u_*)_0}} \quad (47)$$

where $(u_*)_0$ is the surface friction velocity; z_i is the Convective Boundary Layer (CBL) height; z is the height above the surface; L is the Monin-Obukhov length; w_* is the convective velocity scale; z_0 is the aerodynamic roughness; h is the

height of the turbulent stable boundary layer and f_c is the Coriolis parameter ($f_c = 10^{-4} s^{-1}$ in mid-latitudes).

2.4.2 Degrazia et al. Parameterisation

Degrazia et al. (2000) parameterisation is based on Taylor's statistical diffusion theory, in which the shear buoyancy PBL spectra are modelled by means of a linear combination of the convective and mechanical turbulent energy. In this parameterisation, the buoyant and mechanical wind turbulent velocity variances ($\sigma_{ib}^2, \sigma_{is}^2$) are given by the following expressions:

$$\sigma_{ib}^2 = \int_0^{\infty} S_{ib}^E(n) dn = \frac{1.06 c_i \psi_{\varepsilon}^{2/3} w_*^2 \left(\frac{z}{z_i} \right)^{2/3}}{\left[(f_m^*)_i^c \right]^{2/3}} \quad (48)$$

and

$$\sigma_{is}^2 = \int_0^{\infty} S_{is}^E(n) dn = \frac{2.32 c_i \phi_{\varepsilon}^{2/3} u_*^2}{\left[(f_m^*)_i^{n+s} \right]^{2/3}} \quad (49)$$

On the other hand, the Lagrangian decorrelation time scale assumes the following expression:

$$T_{Li} = \frac{l_i}{\sigma_i} = \frac{z}{\sqrt{c_i}} \left\{ \frac{0.14 \left(\frac{-\bar{L}}{z_i} \frac{z_i}{-L} \right)^{1/2}}{\left[(f_m^*)_i^c \right]^{2/3} w_* \left(\psi_{\varepsilon} \frac{z}{z_i} \right)^{1/3}} + \frac{0.059}{\left[(f_m^*)_i^{n+s} \right]^{2/3} \left(\phi_{\varepsilon}^{n+s} \right)^{1/3} u_*} \right\} \quad (50)$$

where $-\bar{L}/z_i$ is an average stability parameter for the convective PBL, in which a typical value $-\bar{L}/z_i = 0.01$ will be used and $c_i = \alpha_i (0.5 \pm 0.05) (2\pi\kappa)^{-2/3}$ with $\kappa = 0.4$ and $\alpha_i = 1, 4/3, 4/3$ for u, v and w components, respectively (Sorbjan, 1989).

To construct the wind velocity variances and Lagrangian decorrelation time scales from Equations (48), (49) and (50) for PBL Lagrangian dispersion models, it is necessary to have expressions for $w_*, u_*, \psi_{\varepsilon}, \phi_{\varepsilon}^{n+s}, (f_m^*)_i^c$ and $(f_m^*)_i^{n+s}$.

For a convective PBL, $(\psi_\varepsilon)^{2/3} \approx 0.75$ (Wilson, 1997), $w_* = (u_*)_0(-z_i/\kappa L)^{1/3}$ and, recalling that $(f_m^*)_i^c = z/(\lambda_m)_i$ and that $(\lambda_m)_i$ is the peak wavelength of the turbulent velocity spectra, $(f_m^*)_i^c$ expressions for $i = u, v, w$ can be derived. According to Kaimal et al. (1976), Caughey (1982) and Degrazia and Anfossi (1998)

$$(\lambda_m)_u = (\lambda_m)_v = 1.5z_i \text{ and } (\lambda_m)_w = 1.8z_i \left[1 - \exp\left(-4\frac{z}{z_i}\right) - 0.0003 \exp\left(8\frac{z}{z_i}\right) \right] \quad (51)$$

so that

$$(f_m^*)_i^c = z/(B_i z_i) \quad (52)$$

$$\text{with } B_u = B_v = 1.5 \text{ and } B_w = 1.8 \left[1 - \exp\left(-\frac{4z}{z_i}\right) - 0.0003 \exp\left(\frac{8z}{z_i}\right) \right] \quad (53)$$

For a neutral or stable PBL ϕ_ε^{n+s} can be written (Sorbjan, 1989) as $\phi_\varepsilon^{n+s} = \phi_\varepsilon^n (1 + 3.7z/\Lambda)$, where $\phi_\varepsilon^n = 1.25$ and $\Lambda = L(1 - z/h)^{(1.5\alpha_1 - \alpha_2)}$ is the local Monin-Obukhov length. For a shear dominated stable boundary layer, $\alpha_1 = 1.5$ and $\alpha_2 = 1.0$. Furthermore, for a neutral or stable PBL, $u_*^2 = (u_*^2)_0(1 - z/h)^{\alpha_1}$ in which $\alpha_1 = 1.7$ for the neutral case (Wyngaard et al., 1974). Then, following Stull (1988) and Sorbjan (1989), and by considering $(u_*)_0/G = 0.03$ (Hanna, 1982) it follows that:

$$(f_m^*)_i^{n+s} = (f_m)_{is}^n \left(1 + 0.03a_i \frac{f_c z}{(u_*)_0} + 3.7 \frac{z}{\Lambda} \right) \quad (54)$$

where $(f_m)_{is}^n$ is the frequency of the spectral peak in the surface for neutral conditions, G is the geostrophic wind speed and $f_c = 10^{-4} s^{-1}$ is the Coriolis parameter. According to Sorbjan (1989), $(f_m)_{us}^n = 0.045$, $(f_m)_{vs}^n = 0.16$ and $(f_m)_{ws}^n = 0.33$. Furthermore, $a_w = 500$ (Hanna, 1968; Hanna, 1981) as a consequence of the Blackadar mixing length hypothesis (i.e., the asymptotic length scale $l_\infty \approx G/f_c$ is limited by a constant value, equal for all the components), we found $a_u = 3889$ and $a_v = 1094$.

2.4.3 Formulas for $\overline{w^3}$ in the CBL

In a CBL with non-divergent horizontal flow, the vertical velocity has a zero mean value but a strongly negative mode (the most frequent value of the vertical velocity). This indicates that within the CBL (except in shallow layers near the ground and in the capping inversion base), the probability density of the vertical velocity fluctuations has a positive skewness. In the present subsection we present four expressions for the vertical profile of the third moment of the vertical velocity in a CBL, suggested by Rotach et al. (1996), Weil (1990), Luhar and Britter (1989) and De Baas et al. (1986), respectively. These formulations for the third moment of the vertical wind velocity fluctuations are the following:

i) Rotach et al. (1996)

$$\frac{\overline{w^3}}{w_*^3} = 1.3 \left(\frac{z}{z_i} \right) \left(1 - \frac{z}{z_i} \right)^2 \quad (55)$$

ii) De Baas et al. (1986)

$$\frac{\overline{w^3}}{w_*^3} = 1.4 \left(\frac{z}{z_i} \right) \exp \left(-2.5 \frac{z}{z_i} \right) \quad (56)$$

iii) Luhar and Britter (1989)

$$\frac{\overline{w^3}}{w_*^3} = 0.8 \left(\frac{\overline{w^2}}{w_*^2} \right)^{3/2} \quad (57)$$

iv) Weil (1990)

$$\frac{\overline{w^3}}{w_*^3} = 0.84 \left(\frac{z}{z_i} \right) \left(1 - \frac{z}{z_i} \right) \quad (58)$$

2.4.4 Formulas for ε

Many expressions for the dissipation rate ε can be found in the literature. Among them the following are reported.

In convective conditions (Weil, 1994):

$$\frac{\varepsilon z_i}{w_*^3} = 0.85 - 1.25 \frac{z}{z_i} \quad \frac{z}{z_i} < 0.4 \quad (59)$$

$$\frac{\varepsilon z_i}{w_*^3} = 0.49 - 0.36 \frac{z_i}{z} \quad \frac{z_i}{z} \geq 0.4 \quad (60)$$

In stable conditions, PBL is generally rather shallow and consequently can be modelled with near surface layer scaling (Kerschgens et al., 2000). According to Kaimal and Finnigan (1994) ε can be estimated by

$$\varepsilon = \frac{u_*^3}{\kappa z} \left(1 + 5 \frac{z_i}{L} \right) \quad (61)$$

Alternatively, ε can be obtained by equation (13).

2.4.5 Additional Parameterisations

One problem with the use of LSMs for real situations is that the technique is computationally expensive, although this is becoming less of a problem with the availability of faster computers. This problem was overcome to a large extent by Hurley and Physick (1993a, b), by using a homogeneous, skewed form of the Langevin equation and associated turbulence parameterisations,

$$\sigma_{u,v,w} = 0.6w_*, \quad T_{Lu,Lv,Lw} = 0.6z_i / w_* \quad (62)$$

that agrees with observations in the middle 80% of the CBL. This approach reduced the number of terms to be calculated in the Langevin equation and enabled a much larger timestep to be used. By comparing results to the Willis and Deardorff (1976, 1978, 1980, 1983, 1987) and Deardorff and Willis (1982) experiments, they showed this simplified model could reproduce the important aspects of the experiments for CBL dispersion, and plume rise and entrainment, while decreasing the computational expense by an order of magnitude.

More recently, Nasstrom and Ermak (1999a, b) developed a model for dispersion in skewed homogeneous turbulent flow using a form of the Langevin equation that has a linear (in velocity) deterministic acceleration term and a non-Gaussian process for the random acceleration term. This model contrasts with that of Hurley and Physick, which incorporated a non-linear deterministic term and a Gaussian random term, following the findings of Thomson (1987). Although both models are able to accurately simulate the (w, z) phase space trajectory of a particle, the

advantage of the Nasstrom and Ermak model is that it is able to use a time step that is four times larger than that of the non-linear-Gaussian model.

The problem of reducing the computer time, maintaining the physical correctness (i.e., the well mixed condition) was also dealt with by Tinarelli et al. (2000), who adopted a variable time step Δt . For a correct numerical integration of the Langevin equations, the time step must be a small fraction of the smaller Lagrangian time scales (τ_x, τ_y, τ_z). The latter attain small values near the boundaries of the atmospheric boundary layer (ABL) and much larger values in the main part of the ABL. Thus using a constant, and therefore very small, time step leads to unnecessarily long computer times. Following a suggestion of Wilson and Flesch (1993), these authors introduced three “vertical inhomogeneity time scales” defined as follows:

$$\tau_f(x, y, z) = \left(\frac{\sigma_w}{f} \frac{\partial f}{\partial z} \right)^{-1} \quad (63)$$

where f , in turn, is $\overline{w^2}$, $\overline{w^3}$ and the three Lagrangian time scales τ_i . They also chose Δt as a small fraction ($1/5, 1/10$) of the minimum time scale among τ_x, τ_y, τ_z and the three τ_f .

In the following Section, the wider range of turbulence parameterisations available to an LSM when linked to a meteorological model is discussed.

2.5 Link with Meteorological Models (W.L. Physick, S. Trini Castelli)

To assess the physics of transport and diffusion of pollutants, it is necessary to provide a description of the meteorological processes in the atmosphere, where the main parameters associated with dispersion problems are the mean wind field, turbulence, surface-layer parameters and the height of the atmospheric boundary layer. In the case of LSMs, the mean wind transport of marked particles can be derived from observations or from diagnostic and prognostic meteorological models. The turbulence fields for the diffusion can be obtained by combining similarity theory with empirical parameterizations (Section 2.4) or can be transferred directly from a meteorological model when that model's turbulence is predicted using a turbulent kinetic energy scheme.

In section 2.2, it was shown that the correct general form of the Langevin equation is

$$dw' = a dt + (C_0 \varepsilon)^{1/2} dW \quad (64)$$

where a_i is a function of moments of the turbulent velocity distribution and ε is the eddy dissipation rate. In Gaussian turbulence, only the second-order moment

(the variance) is needed, whereas for non-Gaussian turbulence (e.g. convective boundary layer turbulence) the third and sometimes fourth-order moments must be specified (see Section 2.3). Here we discuss how these variables are obtained when a LSM is linked to a meteorological model.

When a *diagnostic* wind model (discussed in Chapter 5) or wind observations provide the meteorology for a LSM, the mean winds are used to transport particles, but the necessary turbulence parameters (dissipation rate and moments) must be specified in the LSM using formulations such as those discussed in Section 2.4. These schemes are written in terms of Lagrangian de-correlation timescale T_{Li} rather than the eddy dissipation rate, but for the vertical component, the two variables are often linked via the relation

$$T_{Lw} = \frac{2\sigma_w^2}{C_0\varepsilon} \quad (65)$$

(see equation 13). Meteorological parameters needed by formulations such as those of Hanna and Degrazia et al. in the previous Section include z_i , L , w^* , z_0 , and u^* . These are difficult to estimate if only wind data are available, but methods such as those proposed by van Ulden and Holtslag (1985) can be used to estimate these parameters from routinely available meteorological measurements.

When the winds from a *prognostic* meteorological model are used to drive a LSM, then a meteorological pre-processor prepares these parameter values from the output of the prognostic model. This way there is consistency between the winds and turbulence parameters used in the LSM. For example, in the RMS modelling system, the meteorological model RAMS (Pielke et al., 1992) and the Lagrangian stochastic particle model SPRAY (Tinarelli et al., 1994, Tinarelli et al., 2000) interface through the pre-processing code MIRS (Trini Castelli and Anfossi, 1997, Trini Castelli, 2000). MIRS processes the meteorological fields produced by RAMS (or alternatively, data fields derived from observations or diagnostic models) and prepares the meteorological file as input to SPRAY.

Pre-processors can offer a number of options to calculate the atmospheric boundary layer parameters, especially the height of the boundary layer. Several approaches for estimating the latter in convective conditions are proposed in the literature. For instance, MIRS includes the Gryning and Batchvarova (1990) simplified model and its complete version, Batchvarova and Gryning (1991), the gradient Richardson number profile method, where the ABL inversion layer is identified by the height where Ri overtakes a critical value Ri_c (Maryon and Buckland, 1994, McNider and Pielke, 1981), and the diffusion coefficient profile method. The latter detects the inversion layer height by considering discontinuities in the diffusion coefficient profile and is limited to diurnal simulation. In particular meteorological conditions a constant ABL height can sometimes be assumed over the entire domain (e.g. Kalthoff et al., 1998). The Deardoff (1974) boundary layer height is often employed for neutral conditions while the stable boundary layer height is usually estimated by the Zilitinkevich

(1972) formulation. Estimation of a boundary layer height in stable conditions is often difficult, and this can be avoided by using an expression for σ_w involving the local Richardson number (McNider et al., 1988).

However a value for z_i is only needed when schemes such as those of Hanna or Degrazia et al. are employed in a LSM to describe the turbulence, or to define the upper boundary of the diffusive volume, permeable or impermeable, in the LSM. When a prognostic meteorological model with a turbulent kinetic energy (TKE) boundary-layer scheme provides the fields for a LSM, the dissipation rate and moments needed by Equation (64) can be calculated from the meteorological model's TKE fields. Using TKE profiles avoid further parameterisation (meaning 'simplification') of the ABL structure, although some TKE schemes do not predict ε , necessitating a parameterisation in terms of the TKE. A disadvantage can occur at nighttime when TKE values, and hence variances, can be so low that an arbitrary lower limit needs to be set in order to simulate realistic diffusion. An evaluation of ten TKE schemes, including tracer experiments was carried out by Hurley (1997), while examples of coupled meteorological and Lagrangian stochastic models using TKE boundary-layer formulations can be found in Yamada (1985), Tremback et al. (1993), Uliasz (1994), Hurley (1999) and Ferrero et al. (2000a). The latter two use third- and fourth-order moments for the convective boundary layer.

Two different approaches to interface the meteorological and the dispersion model are used: *online* when the particle model is run at the same time as the meteorological model; and *offline*, when the particle model is run from the stored output (usually at hourly intervals) of a meteorological simulation carried out previously. The *online* approach has the advantage of proposing an integrated modelling system and of providing a contemporary run-time meteorological and dispersive scenario. This way, the dispersion model results are able to affect the meteorology (e.g., aerosol levels can affect radiation calculations). In the case of the *offline* approach, the advantage is the independence of the two models and the consequent flexibility, so that different configurations for the dispersion description can be set and tested without having to re-run the meteorology each time. A disadvantage of running a dispersion model offline is that it is possible to introduce large errors in the trajectories of particles in regions of rapidly changing winds, such as coastal areas. The vast majority of air quality models, including those referred to in this section, are run in offline mode, apart from the model TAPM (Hurley, 1999; Hurley et al., 2001), which uses an integrated approach that also allows for specification of the emissions as a function of the meteorology.

2.6 Boundary Conditions (W.L. Physick)

At the lateral and upper boundaries of a two- or three-dimensional LSM, particles are usually allowed to pass out of the modelling domain and are no longer tracked. However at the lower boundary, and in those models where the upper boundary is considered to be rigid (e.g., a model of the convective boundary layer, CBL), a condition is needed for a particle impinging on a boundary. A more

complex condition is necessary when deposition is being simulated and particles are specified to lose a fraction of their mass at the rigid boundaries (see section 2.9). A further situation addressed in this sub-section is the correct formulation to allow exchange of particles across an interface with a discontinuity in turbulence properties.

2.6.1 Upper and Lower Boundary Conditions

The mathematical boundary condition on turbulent vertical velocity that is commonly applied at the upper and lower boundaries of a LSM is that of perfect reflection, i.e., a particle impinging on a boundary leaves the boundary in the opposite direction but at the same speed. This condition is appropriate for Gaussian turbulence or skewed inhomogeneous turbulence (where the Lagrangian time scale is normally very small near the boundaries), but if used for skewed homogeneous turbulence, it will lead to an accumulation or deficit of particles at the boundaries. Modifications of the perfect reflection condition for non-zero skewness by Weil (1990) and Hurley and Physick (1993a) were shown by Thomson and Montgomery (1994) (TM) to provide acceptable solutions for small values of the Lagrangian time-scale τ , but the departure from a uniformly-mixed profile became greater as τ increased. Considering now only the lower boundary, TM proposed that a correct boundary condition is

$$\int_{w_r}^{\infty} w P_E(w, z_b) dw = \int_{-\infty}^{w_i} w P_E(w, z_b) dw \quad (66)$$

where w_r is the reflected velocity, w_i is the incident velocity and P_E is the assumed vertical velocity distribution of particles at the boundary z_b (a corresponding equation can be derived for the upper boundary). The basis of this equation was their assertion that the relevant quantity to be considered is the PDF of the velocities of particles which leave z_b during a fixed time interval, rather than just the PDF of particles leaving the boundary at a particular time t , $P_E(w, z_b) / \int_0^{\infty} P_E(w, z_b) dw$ ($w \geq 0$), as used by Weil (1990). The former PDF is $w P_E(w, z_b) / \int_0^{\infty} w P_E(w, z_b) dw$ ($w \geq 0$) since more of the faster-moving particles will leave $z = z_b$ in a given time interval.

Knowing the incident velocity w_i of a particle, equation (66) is used to obtain w_r . When P_E is the commonly-used bi-Gaussian expression for skewed convective turbulence (equations 16 and 17), the solution to equation (66) consists of numerical integrals and error functions and is obtained for each particle from prepared look-up tables (TM). The time-consuming nature of this process in a three-dimensional Lagrangian stochastic model has been addressed by Anfossi et al. (1997) who proposed two approximate analytical solutions to equation (66).

The first one made use of a Taylor series expansion and still involved error functions, but the second one involved a regression curve between w_i and w_r as a function of skewness and $w_i/(\overline{w^2})^{1/2}$. Curve coefficients were obtained from many “exact” (look-up table) solutions to Equation (66) over a range of variance and skewness values. Although both solutions of Anfossi et al. satisfy the well-mixed condition and do not appreciably depart from the correct or “exact” solution, the regression method uses considerably less computing resources and seems a suitable approach to applying boundary conditions in three-dimensional particle models. Note that although Anfossi et al. used the Baerentsen and Berkowicz (1984) closure (see section 2.3), their solutions can be modified for other closure schemes.

While the above formulation of the boundary condition is based on a positive correlation between the incident and reflected speeds, Nasstrom and Ermak (1999b) developed and tested a formulation in which reflected speed is negatively correlated with the incident speed. This originated from observation of near-surface convective circulation patterns in which air in the core of a downdraft region penetrates deep into the surface layer and, rather than moving back up immediately, spreads away from its centre along the surface, while moving horizontally toward convergence zones that feed the updrafts in the mixed layer. Application of this boundary condition in simulations of the Willis and Deardorff (1976, 1978, 1981) convective tank experiments clearly showed its superiority over the positively-correlated condition.

2.6.2 An Interface Condition

The problem of random-walk modelling of diffusion across an infinitesimally-thin interface at which the turbulence statistics change discontinuously has been addressed by Thomson et al. (1997). They argued that if the Lagrangian time scale τ on which particles forget their velocity is much larger than the time particles spent within the interface, then particle trajectories in (z,w) -space within the interface are deterministic and do not cross each other. As a result, the trajectories will generally take the form illustrated in Figure 1(a), although cut-off circulations (Figure 1(b)) and other configurations are possible.

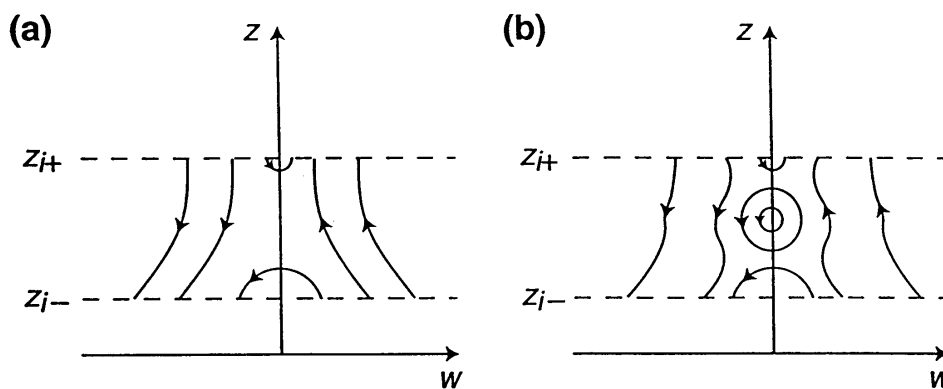


Figure 1. Illustration of some possible flows in (z, w) -space [From Thomson et al. (1997)].

By using the fact that the flux between two streamlines in (z,w) -space must be conserved, and considering a particle entering the interface (lower and upper boundaries z_{i-} and z_{i+}) from below with incident velocity w_i , they showed that its velocity w at a height z within the interface can be obtained from

$$\int_w^\infty w p_a(z, w) dw = \int_{w_i}^\infty w p_a(z_{i-}, w) dw \quad (67)$$

where p_a is the density of well-mixed tracer particles. Equation (67) is equally applicable if $w < 0$. From here on, the integrals will be denoted by F , e.g. the left-hand side of equation (67) is $F_w^\infty(z)$. If $F_0^\infty(z) < F_{w_i}^\infty(z_{i-})$ at any height in the interface then the particle will be reflected, i.e. the particle will be reflected if w_i is less than the critical value w_c which is defined for the CBL case of $F_0^\infty(z)$ decreasing monotonically within the interface by

$$F_{w_c}^\infty(z_{i-}) = F_0^\infty(z_{i+}) \quad (68)$$

Otherwise, the particle will be transmitted. The reflection and transmission velocities w_r and w_t are given by

$$F_{w_r}^\infty(z_{i-}) = F_{w_i}^\infty(z_{i-}) \quad (w_r < 0) \quad (69)$$

and

$$F_{w_t}^\infty(z_{i+}) = F_{w_i}^\infty(z_{i-}) \quad (w_t > 0) \quad (70)$$

Similar relations can be derived for particles entering the interface from above. Note that particles approaching the interface from the side of weaker turbulence (above in the CBL case) are always transmitted. When implementing the interface condition in a random walk model, the particle velocity should be changed at the instant the particle reaches the interface, with $z(t + \Delta t)$ being calculated in a way that accounts for the change in velocity during the time step.

2.7 Concentration Calculations Using Particle Models (W.L. Physick)

Particle models are a set of algorithms for the generation of realistic trajectories of imaginary, fictitious particles that simulate atmospheric motion. Each particle can be tagged by a mass of pollutant that can be either constant or time-varying to allow loss of mass due to ground deposition and chemical decay phenomena. If the emission rate of a pollutant is $Q \text{ g s}^{-1}$ and the release rate of particles is $N \text{ s}^{-1}$, then the mass of each particle is $Q/N \text{ g}$. This way, the spatial distribution of particle mass in the computational domain allows the calculation of a three-dimensional mass concentration field, under certain computational assumptions.

For example, the most straightforward assumption is the superimposition in the computational domain of a three-dimensional concentration grid, with spacing (Δx , Δy , Δz). As one particle in the sampling domain represents a concentration of

$$C = Q/(N\Delta x\Delta y\Delta z), \quad (71)$$

the concentrations are computed simply by counting the number of particles in each grid cell and accumulating their masses. If concentrations need to be computed only at “receptor” points (e.g., at a ground level), receptor cells can be defined around these points and particles counted only inside those cells. A rigorous concentration calculation, however, should not just add up the particle mass in a given cell at a given time. In fact, the contribution of each particle mass should be weighted by the total time the particle spends inside the cell during each time step (Lamb, 1979), although in reality this is rarely done.

It is important that sufficient particles are released per time step to give meaningful concentrations. One way to address this problem is to calculate N according to the desired accuracy of the predicted ground-level concentrations. If this accuracy is denoted by e , then C must be less than e . This relation is used to calculate the minimum value of N in the following manner.

$$N = Q/(e\Delta x\Delta y\Delta z) \quad (72)$$

A three-dimensional mesoscale LSM is often run in two modes; *near-source* mode to determine the maximum ground level concentration (GLC), which usually occurs within 5 km of a stack in convective conditions, and *far-field* mode to examine the dispersion many kilometres from the stack. Experiments have shown (Physick et al., 1994b) that a sampling box of 1000 x 1000 x 25 m is adequate to calculate GLCs at distances further than 5 km from the source, but that it is necessary to reduce the box size to 250 x 250 x 25 m to obtain realistic GLCs closer in.

One of the great advantages of Monte-Carlo particle models is their “grid-free” characteristics, which allow higher time and space resolution than other simulation techniques. In this respect, grid-free concentration calculations (i.e. calculations that do not require the definition of cells) to maintain this important feature of the model is appealing. “Kernel” methods (Gingold and Monaghan, 1982) allow grid-free concentration calculations that are smooth and efficient. Kernel methods for air quality modelling are discussed by Lorimer (1986). A general form of kernel density estimator is

$$c(\mathbf{r}, t) = \frac{A(\mathbf{r})}{l^3} \sum_{i=1}^n m_i W(\mathbf{r}_i - \mathbf{r}, l) \quad (73)$$

where c is the concentration in \mathbf{r} at time t ; l is the time-dependent resolution bandwidth (or smoothing length); m_i is the pollutant mass of each particle i ; W is the smoothing kernel, which is a function of l and the distance $\mathbf{r}_i - \mathbf{r}$ of each particle i from the receptor point. $A(\mathbf{r})$ is a correction term for concentration computation at locations \mathbf{r} close to the boundary of the computational domain D , where

$$A(\mathbf{r}) = \frac{l^3}{\int_D W(\mathbf{r}' - \mathbf{r}, l) d\mathbf{r}'} \quad (74)$$

which, for an infinite domain D , reduces to $A(\mathbf{r}) = 1$ everywhere.

Several kernel functions W are available in the literature, and a discussion of the optimal choice of kernel for different situations is given by de Haan (1999). The most common is the Gaussian kernel, in which

$$\mathbf{d}_i = \mathbf{r}_i - \mathbf{r} \quad (75)$$

and

$$W(\mathbf{d}_i, l) = \frac{1}{(2\pi)^{3/2}} \exp\left(-\frac{1}{2} \frac{|\mathbf{d}_i|^2}{l^2}\right) \quad (76)$$

The choice of l is critical. This term should not be kept constant as done in many applications, but it should change in relation to a natural length scale. In general, l should be particle dependent and should be related to the mean interparticle separation around \mathbf{r} . Only particles with $|\mathbf{d}_i| < l$ give substantial contribution to c (Lorimer, 1986). If l is too small, the spatial distribution of the concentration c is “jagged” with a series of local maxima at each \mathbf{r}_i ; if l is too large, c becomes overly smooth.

Using a Gaussian kernel, the particle model becomes very similar to the puff models described in Chapter 8. It is important to note that for a puff model, l is substituted by σ_x , σ_y , and σ_z (i.e., the standard deviations of the spatial concentration distributions of each puff), and these values are related to the physics of atmospheric diffusion, while, in the kernel method, l should be related only to the density of the particles around \mathbf{r} . However, Yamada and Bunker (1988) use a kernel density estimator for their RAPTAD particle model, which in reality makes it a puff model, in which each particle i is associated with time-growing σ_{xi} , σ_{yi} and σ_{zi} values that are estimated based on the homogeneous diffusion theory by Taylor (1921).

2.8 Buoyancy Phenomena Simulation (H. van Dop)

The concept of the random walk has some attractive features also for plume rise formulations. Zannetti (1984) and Cogan (1985) (see Chapter 6) pioneered Lagrangian models for buoyant dispersion, however, on a somewhat ad-hoc basis. Also in section 4.4 of chapter 6 in Volume I of this book series, a more fundamental formulation of buoyant tracers is presented.

Two major aspects distinguish buoyant and passive dispersion:

- (i) buoyant fluid particles “create” their own turbulent field in an environment with its own turbulent characteristics, and
- (ii) the exchange processes between the plume particles and the (turbulent) environment is an essential element in the dynamics.

The buoyant plume is an envelope, which contains a mixture of ambient and (most of the) originally released, buoyant fluid. Some of the original buoyant fluid may be taken away from the plume and become so remote that it is no longer considered to be part of it. On the other hand, the volume of the plume expands due to turbulent intrusions of ambient air resulting in an increasing ambient fraction and consequently, a gradual loss of plume buoyancy.

A Lagrangian plume particle can be defined as a small entity, which possesses the mean characteristics (velocity, temperature) of the plume. Stochastic fluctuations, directly related to the turbulent intensity within the plume, determine the rate of growth of the plume width and are superimposed on the mean characteristics. Ultimately the plume (particle) dynamics must converge to the environmental dynamics. An important difference, however, between temperature and velocity is that for velocity changes (by pressure forces), no mass exchange is required, whereas (turbulent) temperature changes require the exchange of (particle) mass and environmental mass, thus in conflict with the (conventional) idea of Lagrangian particles moving with conserved properties in a turbulent flow.

In section 4.4 of chapter 6 in Volume I of this book series, we formulated the dynamic equations for such a particle. It should be noted that this concept, where a plume is thought to consist of a superposition of many independent trajectories of plume particles disregards all kinds of non-linear processes within the infrastructure of the plume. Their dynamic effects are thus ignored.

According to inertial sub-range theory we expect the following relationship between the temperature dissipation function, ε_θ , and the structure function, D_θ :

$$D_\theta \equiv \overline{[\Theta(t) - \Theta(t + \tau)]^2} = \varepsilon_\theta \tau$$

We further expect that the autocorrelation of Θ is exponential, and consequently, its spectrum behaves as ω^{-2} . This enables the dynamic description of temperature to be suitably formulated in a Lagrangian framework as a Langevin equation:

$$d\Theta = -\frac{\Theta - \Theta_a}{T_p} dt + \varepsilon_B^{1/2} d\omega_B(t),$$

since it guarantees the above properties. As we saw in section 4.4 of chapter 6 in Volume I of this book series, the Lagrangian formulation explains the basic features of plume motion in complex environments.

2.9 Reactive Chemistry (P. Hurley)

A theoretical approach to the inclusion of reactive chemistry in a Lagrangian framework has, as yet, not been dealt with in a satisfactory way. This is true of all Lagrangian approaches (Plume, Puff and Particle models). In LSMs, many independent particles are tracked, along with information on position and incremental mass of a pollutant. First-order reactions, where there is a single species, can be represented fairly simply in a Lagrangian approach, by exponentially decaying particle mass. Higher-order reactions, where there are more than one species, cannot be handled by changing individual particle mass because of the non-linear nature of the chemical reactions.

For atmospheric applications, a hybrid Lagrangian/Eulerian approach is, so far, the only way of incorporating chemical reactions into Lagrangian air pollution models. For example, in the model of Chock and Winkler (1994a, b), a Eulerian Grid Model (EGM) incorporating a 10 reaction photochemical scheme is solved for pollutant advection and diffusion using the LSM, while chemistry is solved for using the EGM. Similarly, in the Lagrangian Atmospheric Dispersion Model (LADM) of Physick et al. (1994b), the LSM was extended to incorporate a simple, semi-empirical photochemistry scheme called the Integrated Empirical Rate (IER) method. LADM used a LSM approach to solve for advection and diffusion, and a local Eulerian approach to solve for the chemistry. These hybrid approaches use a method to convert between particle mass and total concentration as follows. At each timestep, for each particle, summed particle mass in a volume (either fixed grid or moving local grid) is converted to total concentration for each species, and then the chemical reactions are performed in this volume to determine the new concentrations. These new concentrations are then converted back to individual particle mass using a mass weighted approach that uses the change in concentration and the previous (before reaction) particle mass. This approach has the advantage that both advection and diffusion for each species is solved for using the LSM approach, which is more accurate for advection and better represents diffusion close to point sources compared to the Eulerian approach, but has the disadvantage that conversion of concentration to particle mass is computationally expensive.

An alternative hybrid approach is used in The Air Pollution Model (TAPM) of Hurley (1999). In TAPM, an EGM incorporating the Generic Reaction Set (GRS) photochemical scheme, optionally includes a LSM for user-selected point sources. The approach taken in this model is that the LSM solves advection and diffusion for pollutant species emitted from selected point sources without

chemical transformation, and the EGM is run side-by-side to include advection and diffusion by non-LSM sources and to compute the chemical reactions using total concentration (LSM + EGM). This approach avoids the need to convert between particle mass and concentration for use in the chemical reactions, thus saving computer resources. Note that this approach can allow the EGM concentration to be negative. For example, in the case when all emissions are represented by the LSM, then losses resulting from chemical reactions can result in negative concentration in the EGM, but positive total (LSM + EGM) concentration.

Of course, a preferred approach would be to include chemical reactions directly in the Lagrangian framework, but from a theoretical viewpoint, it is not clear how this can be achieved at the moment.

2.10 Predicting Higher-Order Concentration Moments (A. Luhar)

One-particle Lagrangian stochastic models have been successful in capturing the essential features of mean tracer dispersion in the atmospheric boundary layer, and are now used routinely in larger-scale modelling systems for air quality management and impact assessment studies. However, since these models assume that each tracer particle has an independent motion, they can only predict the ensemble-mean concentration field. They cannot provide any information about the higher order concentration fluctuation statistics (e.g., the variance), which is required when addressing topics such as “peak-to-mean” concentration ratios, odour estimates, uncertainty in air quality models, and accidental release of toxic and flammable gases.

The two-particle Lagrangian stochastic approach (see also Section 2.2) in which two particles are released simultaneously with their motions correlated, can provide information on the variance of the concentration distribution, but developments in this area have so far been restricted to (idealised) homogeneous, isotropic turbulence in studies of the fundamental aspects of relative diffusion (e.g., Thomson, 1990; Borgas and Sawford, 1994). An extension of this approach to inhomogeneous flows in the atmospheric boundary layer is difficult, largely because of the mathematical complexities generated by the turbulence characteristics, and the extensive input requirements (e.g., the field of two-point Eulerian velocity statistics) which, at present, can only be obtained from high-resolution turbulence models.

Recently, one-particle Lagrangian models have been used in conjunction with the meandering plume approach of Gifford (1959) to determine higher order concentration fluctuation statistics for practical applications (Weil, 1994; de Haan and Rotach, 1998; Luhar et al., 2000). The original analytical model of Gifford assumes that the total (or absolute) dispersion can be split into two independent (Gaussian) parts—the meandering part and the relative-diffusion part—with the production of the fluctuations caused solely by the meandering of the ensemble-mean instantaneous plume. The spread of the mean instantaneous plume is prescribed according to the relative diffusion theory. This model has been

particularly successful for predictions close to the source where meandering is the primary mechanism responsible for generating fluctuations, but it ignores the in-plume fluctuations that dominate the overall fluctuation statistics in the far field.

In the skewed meandering plume model of Luhar et al. (2000) developed for the convective boundary layer, the relative diffusion is parameterised, and a one-particle Lagrangian model is used to determine the meander trajectory distribution of the instantaneous plume. The in-plume fluctuations in the model are accounted for via a gamma probability density function (PDF) based on the work of Yee and Wilson (2000). The use of the one-particle Lagrangian approach for the meander trajectory calculation accounts for the flow inhomogeneity. The model of Luhar et al. (2000) is an improvement over other models based on the meandering plume concept (Weil, 1994; de Haan and Rotach, 1998), and can be applied to skewed as well as Gaussian turbulent flows.

In the meandering plume approach, the movement of the centroid of the instantaneous plume is described in a fixed (or absolute) coordinate system relative to the source while the concentration distribution within the instantaneous plume is specified in a relative (or local) coordinate system whose origin is located at the centroid of the instantaneous plume. All model concentration statistics are calculated in the fixed coordinate system. If one assumes that the plume meanders in the lateral (i.e., crosswind) direction (y) is statistically independent of that in the vertical direction (z), the n th moment of concentration at location (y, z) at travel time t is given as (Luhar et al., 2000):

$$\begin{aligned} \overline{c^n}(t, y, z) &= \frac{1}{\lambda^n} \frac{\Gamma(n + \lambda)}{\Gamma(\lambda)} \frac{1}{(\sqrt{2\pi}\sigma_{yr})^n} \frac{\sigma_{yr}}{(n\sigma_{ym}^2 + \sigma_{yr}^2)^{1/2}} \\ &\times \exp\left[-\frac{ny^2}{2(n\sigma_{ym}^2 + \sigma_{yr}^2)}\right] \int_0^h (\overline{c_{zr}})^n(z, z_m, t) p_{zm}(z_m, t) dz_m \end{aligned}$$

where $\lambda = 1/i_{cr}^2$, i_{cr} is the concentration fluctuation intensity in the relative coordinate system, $\Gamma(\lambda)$ is the gamma function, σ_{yr} and σ_{ym} are the relative and meander spreads, respectively. In the lateral direction, h is the boundary-layer height, $\overline{c_{zr}}$ is the mean vertical concentration distribution in the relative frame (which is taken to be skewed in the CBL), p_{zm} is the meander PDF in the vertical which is calculated numerically using a one-particle Lagrangian model. The above equation assumes that the lateral meander and relative components are Gaussian. It reduces to the concentration moment equation of Yee and Wilson (2000) if the vertical components are also assumed to be Gaussian, and further to Gifford's moment equation if the in-plume concentration fluctuations within the relative plume are neglected (i.e., $i_{cr} \rightarrow 0$, $\lambda \rightarrow \infty$).

An animation of the output of the above skewed meandering plume model can be viewed at <http://www.dar.csiro.au/pollution/Meander/index.html>.

3 LSM Applications

3.1 Simulation of Dispersion in Convective Conditions, Including Fumigation (P. Hurley)

LSMs have been used to model dispersion from passive point sources in both fully developed convective boundary layers (CBL) and for fumigation into growing CBL, including thermal internal boundary layers (TIBL). Results from these models have been compared to data, including laboratory experiments relevant to the CBL, laboratory experiments of fumigation and CBL entrainment, and field experiments. The demonstrated ability of LSMs to model both near- and far-source GLCs associated with emissions from elevated sources, especially in convective conditions, has led to them being applied to assessments of the impact of existing and proposed power stations, smelters, etc. (Noonan et al., 1994; Physick et al., 1995).

Early applications of the LSM approach within a mesoscale meteorological model (e.g., McNider, 1981) suffered from the lack of a theoretical basis for the Langevin equation when applied to the inhomogeneous, skewed turbulence of the CBL (see also Section 2.1). Although simulations looked qualitatively reasonable, the Gaussian, homogeneous form of the traditional Langevin equation, even with the drift correction term of Legg and Raupach (1982), resulted in particle accumulation in regions of lower turbulence (e.g., near the boundaries of the CBL). The development of a form of the Langevin equation for Gaussian, inhomogeneous turbulence by Wilson et al. (1981) and Thomson (1984), allowed LSMs to be formulated in a way that alleviated this problem for Gaussian turbulence. Non-Gaussian or skewed turbulence, as present in the CBL, was usually included in LSMs through the random forcing term in the Langevin equation. For example, this approach was used by Baerentsen and Berkowicz (1984), De Baas et al. (1986) and Sawford and Guest (1987), and results from these models were compared to the laboratory experiments of Willis and Deardorff (1976, 1978, 1981). As described in Section 2.2, theoretical developments by Thomson (1987) allowed the use of a form of the Langevin equation that could handle skewed, inhomogeneous turbulence. This new theory allowed the skewed nature of the CBL to be more correctly incorporated into the non-random terms of the Langevin equation in a way that satisfied the well-mixed criteria, while leaving the random terms Gaussian. It was applied to model the laboratory experiments of Willis and Deardorff (1976, 1978, 1981) independently by Sawford (personal communication, 1989) and Luhar and Britter (1989).

Various closure schemes for PDFs under CBL conditions were discussed in section 2.3 of chapter 6 in Volume I of this book series, but the evaluation by Luhar et al. (1996) identified important differences between the schemes, with implications for modelling fumigation. The largest differences between closures occurred for the case where the source height was near the top of the CBL (which is relevant to fumigation). It is not only the peak ground level concentration value

that is strongly influenced by the choice of closure scheme, but also the distance downwind at which the plume first reaches the ground. For this source height, the laboratory data against which the schemes were evaluated showed no distinguishable peak, a characteristic that was reproduced by two of the four closures, and was also observed for low entrainment rates in direct measurements of fumigation in further tank experiments by Hibberd and Luhar (1996). These laboratory fumigation experiments were designed to determine the influence of entrainment rate on concentration levels for a wider range of growth rates than previously examined by Deardorff and Willis (1982).

Comparison of LSM predictions to CBL and fumigation field data include those of Brusasca et al. (1989) for Karlsruhe, Rotach et al. (1996) for Copenhagen, Ferrero et al. (1995) for Copenhagen, and Luhar and Sawford (1995) for Nanticoke. Generally, simulations compared well to the data and to predictions from simpler models. LSMs should also be compared to datasets gathered in convective conditions in complex terrain, as this is potentially where they will have advantages over Gaussian plume or puff Lagrangian models, as discussed in Section 3.5. More comparisons with field data are needed, and should be done with LSMs for the above-mentioned datasets, as well as for other available CBL datasets such as CONDORS (Eberhard et al., 1988) and Kincaid (Hanna and Paine, 1989) for the CBL, and Kwinana for coastal fumigation (Sawford et al., 1998).

3.2 Simulation of Dispersion in Stable Conditions (E. Ferrero)

As an example of application of a LSM to a real case in stable conditions, simulation results from the Lillestrøm (Norway) experiment (Gronskei, 1990; Olesen, 1998) are presented. The data set includes the measurements of tracer released from a 36 m mast. The campaign took place in an almost flat, residential area during winter with the sun at very low angles above the horizon. The ground was snow-covered, the temperature was around minus 20°C and rather strong stable conditions prevailed, with low or near calm wind conditions (Olesen, 1995). The comparison is made in terms of crosswind integrated concentrations (CY) and arcwise maximum (ARCMAX/Q), normalised by the emission rate Q , and the standard deviation of the crosswind concentration distribution (SIGY).

The Lillestrøm experiment was simulated with LSMs by Ferrero et al. (1996), Ries et al. (1997) and Rotach (1998). Ferrero et al. (1996) used, as input for the model, the measured data and the Hanna (1982) turbulence parameterisation (Section 2.4); for the horizontal Lagrangian time scales, they imposed a constant value equal to 300 s and the boundary layer height was computed from:

$$z_i = 0.25 \frac{u_*}{f}$$

The results were satisfactory as far as SIGY was concerned, while the results about ARCMAX/Q and CY/Q were less accurate. It was also found that the model underestimated the concentrations on the first arc in some runs.

Ries et al. (1997) applied three LSMs to simulate the Lillestrom data set. Each model was initialized with the same pre-processor and wind standard deviations but with different Lagrangian time scale parameterisations. Despite this being the

only difference, simulation results were significantly different, confirming the great importance of a correct choice of the time scales in LSMs (Ferrero and Anfossi, 1998).

Rotach (2001) applied a Lagrangian particle dispersion model to this data set distinguishing the urban cases, in which the roughness sub-layer is considered, from non-urban cases in which it is neglected. He suggested that in the urban atmosphere the surface layer is not close to the ground, but it is superposed to the roughness sub-layer whose extension is $3 h_b$, where h_b is the average building height. The results obtained are comparable with those of Ferrero et al. (1996) except for SIGY, which is predicted less accurately.

It should be mentioned that the Lillestrøm data set has some problems when models based on similarity theory for the turbulence description are used (Gryning, 1999). However, this data set was here introduced because, to our knowledge, there are no other published examples of LSM simulation of dispersion exercises carried out in stable conditions.

3.3 Simulation of Dispersion in Neutral Conditions (E. Ferrero)

A useful representation of the real atmospheric flow in neutral conditions can be obtained in a wind tunnel. The initial and boundary conditions in the experiments carried out in such a facility can be controlled and accurately reproduced. For these reasons, these kinds of experiments are good tests for model evaluation. An example is the wind tunnel EPA-RUSVAL tracer experiment (Khurshudyan et al., 1990) which involved a neutral flow on a 2-D valley with an aspect ratio $a/H = 8$. Measurements were taken of the turbulence parameters and the 3D concentration field. Ferrero et al. (1999) simulated this experiment using a complete 3-D model system (RMS, see also Section 2.5) based on the mesoscale model RAMS (Pielke et al.), the interface code MIRS (Trini Castelli and Anfossi, 1997; Trini Castelli, 2000) and the LSM SPRAY (Tinarelli et al., 2000). The simulated cases consisted of a source placed near the bottom of the valley. They implemented in RAMS two new turbulence models (E-l and E- ϵ), providing, through the code MIRS, the input for the dispersion model SPRAY. They found an improvement in the model results using the turbulent quantities directly calculated from the output of the turbulence model instead of using the Hanna (1982) parameterisations based on the surface layer theory.

In a previous work (Tinarelli et al., 1994) the same team applied an old version of SPRAY to a similar experiment carried out in the same wind tunnel (Khurshudyan et al., 1981) simulating a neutral flow over a gentle hill. The three-dimensional mean flow field was provided by a mass-consistent model and the turbulence quantities were parameterised. The results were satisfactory.

The validation of a LSM coupled to a mass-consistent model against data measured in a wind tunnel was presented by Duran et al. (1998). They simulated the dispersion of radionuclides released from a reactor building of two nuclear power plants, the first one over flat terrain and the second over hilly terrain. The

turbulence characteristics were modified in order to take into account the wake region generated by the building.

3.4 Simulation of Dispersion in Urban Conditions (E. Ferrero)

As an example of application of a LSM to a case of urban (stable and unstable) boundary layer, the Indianapolis experiment (TRC, 1986) is presented. This data set includes many buoyant tracer releases in an urban area in different stability conditions. The emission point is an 84 m stack and measurements of ground level concentrations are available on arcs at distances between 0.25 and 12 km from the source. Meteorological data are given at different locations in urban, suburban and rural areas in the surface layer and some quantities have also been measured at a height of 94 m at the top of a building. Vertical profiles of wind velocity and temperature were gathered from minisondes and acoustic sounders. The model comparison is made in terms of cross wind-integrated concentrations (CY), standard deviation of the crosswind concentration distribution (SIGY), arcwise maximum (ARCMAX) and azimuth of the maximum (AZMAX).

Both daytime and nighttime releases were simulated by Ferrero et al. (1998 and 1999) using a LSM. The input of the model was prescribed by both measured quantities and parameterisations (De Baas et al., 1986; Hanna, 1982) or similarity relationships. The model evaluation results for the daytime cases demonstrate that SIGY and AZMAX agree with the corresponding measured quantities while CY and ARCMAX are overestimated. In the simulations of the nighttime cases, the authors imposed a neutral parameterization in the case of $|L| > 100$ (where L is the Monin-Obukhov length), in order to take into account the additional mixing due to the presence of the urban boundary layer, as also stressed by Hanna et al. (2001), obtaining better results than using stable parameterization.

The influence of a strong plume rise was stressed by Rotach (1998), who simulated the Indianapolis experiment with a LSM. He observed that plume rise reduces the effects of the roughness sub-layer concept introduced in his model and seems to be responsible for deficiencies in the simulations of the concentrations close to the source.

As another example, the Copenhagen tracer experiment can be considered. In particular, we refer to the following papers: Rotach and de Haan (1997), de Haan and Rotach (1998), Rotach (1999) and Rotach (2001). In Rotach and de Haan (1997), it is stressed that, in the urban boundary layer, a roughness sub-layer covers the lower part of the surface layer wherein surface layer scaling cannot be valid, owing to the presence of roughness elements and the resulting disturbances of the flow. If a roughness sub-layer is included by modifying the turbulence and flow structure in the lowest metres of the domain according to observed (urban) roughness sub-layer characteristics, it is shown that the model performance is considerably improved. In de Haan and Rotach (1998) the Copenhagen data set is used to validate the Puff-Particle Model, which is based on a particle model. All the statistics considered in the comparison show that this model is able to reproduce the tracer observations.

Satisfactory results in simulating these experiments were also obtained by Ferrero et al. (1995) using their LSM.

3.5 Simulation of Dispersion in Low Wind Speed Conditions (D. Anfossi)

Dispersion in low wind speed and stable conditions is governed by meandering (low frequency horizontal wind oscillations), weak, layered and intermittent turbulence, air stagnation and gravity waves (Mahrt, 1999; Gryning, 1999). These characteristics give rise to highly non-stationary and inhomogeneous diffusion conditions. Even if the stability reduces the vertical dispersion, meandering disperses the plume over rather wide angular sectors. Thus, in particular, the resulting ground level concentration is generally much lower than that predicted by standard Gaussian plume models (Sagendorf and Dickson, 1974; Wilson et al., 1976). As a consequence, different types of models should be used. Among these, the LSM has proved to be a reliable modelling tool (e.g., Brusasca et al., 1992; Ries et al., 1996; Oettl et al., 2001).

Brusasca et al. (1992) proposed an “ad hoc” algorithm to account for the meandering in their LSM LAMBDA (Brusasca et al., 1989). This algorithm is based on the Gifford fluctuating plume model (1960). By defining σ_i ($i = u, v$) as the measured hourly averaged horizontal wind standard deviation, σ_i^T part is due to the turbulence and σ_i^M the remaining part due to the meandering, this last is computed as:

$$\sigma_v^M = \sqrt{(\sigma_v)^2 - (\sigma_v^T)^2} \quad (77)$$

The total sampling time (1 h) was split into N (= 20) sub-periods of 3 min. Then, series of wind vectors were randomly picked in such a way as to obtain a close approximation of the observed hourly values of mean wind speed, mean wind direction and standard deviation. The model was tested against the Idaho National Engineering Laboratory (INEL) tracer data set (Sagendorf and Dickson, 1974). Three experiments characterised by plume spread of 48°, 138° and 360°, respectively, at an arc of 200 m from the source, were chosen. The model reproduced the observed ground level concentrations with a reasonable degree of confidence.

Oettl et al. (2001) based their LSM on the analysis of the wind velocity Eulerian autocorrelation functions $R_i(\tau)$ computed over one year of sonic anemometer observations. The resulting $R_i(\tau)$ for the horizontal components of the wind vector showed a negative loop, attributed to the meandering. Their model uses a time-step PDF with uniform distribution (Wang and Stock, 1992). This means that random time-steps and a negative intercorrelation parameter $\rho_{u,v}$ for the horizontal wind components (to account for the observed $R_{u,v}(\tau)$ characteristics) are used. Mean time-intervals $\overline{\Delta t_h}$ are calculated from:

$$\overline{\Delta t_h} = 3 \cdot T_{Lu,Lv} \cdot \left(\frac{1 - \rho_{u,v}}{2 + \rho_{u,v}} \right) \quad (78)$$

where $T_{Lu,Lv}$ are the Lagrangian decorrelation time scales and the PDF has the following expression:

$$f(\overline{\Delta t_h}) = \begin{cases} \frac{1}{2 \cdot \overline{\Delta t_h}} & \text{for } \Delta t_h \leq 2 \cdot \overline{\Delta t_h} \\ 0 & \text{for } \Delta t_h > 2 \cdot \overline{\Delta t_h} \end{cases} \quad (79)$$

The result is an enhanced dispersion in low wind situations. Since the model reduces to the Langevin equation for $\rho_{u,v} = 0.9$, it can be used for all wind speeds simply by adjusting the intercorrelation parameter. This model was applied to the same INEL dispersion data (all the tests were simulated) and showed reasonable agreement.

3.6 Transport and Dispersion at the Mesoscale (W.L. Physick)

As well as showing skill in predicting near-source maximum GLCs from point sources, LSMs are particularly useful for applying to dispersion of pollutants by sea breezes and in complex terrain. It is not only the good agreement shown with observed concentrations that is impressive, but also the insight into the dispersion processes that is available through both static and animation plots of particle positions.

3.6.1 Sea Breeze Dispersion

Using a three-dimensional meteorological model (RAMS) and a LSM (LPDM), Lyons et al. (1995) discussed the importance for dispersion modelling of accounting for vertical motion. They showed that emissions from shoreline sources can be transported vertically out of the sea breeze inflow layer at the front, as illustrated in Figure 2, and back over the water at higher levels. Using the same models for the same region (Lake Michigan), Eastman et al. (1995) estimated that about 70% of emissions undergo at least one recirculation out over the lake and then back towards the shore. They also ran a Gaussian-plume model (ISC), which is unable to represent vertical motion or recirculation, and showed that surface concentrations derived from the two models differed significantly in structure and magnitude.

When offshore flow in coastal regions advects morning emissions out to sea, they are often returned in the sea breeze inflow during the afternoon. This different type of recirculation (in the horizontal plane) is the primary mechanism responsible for elevated ozone readings in all of Australia's major coastal cities. A coupled meteorological and Lagrangian stochastic model (LADM) has been used successfully in these cities to understand the important processes involved (Physick, 1996). Similarly, recirculation of SO₂ has been observed and modelled with a LSM for Israel by Robinson et al. (1992).

Sea breezes are not just confined to near the coast, but can travel to at least 200 km inland. Buckley and Kurzeja (1997) observed that the sea breeze penetrates to the Savannah River Site (SRS, 150 km inland) from the eastern coast of the United States on about 15% of all nights. Using RAMS and the stochastic model LPDM, Buckley and Kurzeja were able to investigate the sea breeze dispersion of emissions from the SRS, concluding that vertical, horizontal and temporal wind shear, and vertical motion were the dominant factors in the plume dispersion. None of these effects are contained in the surface meteorological files used to run the simpler Gaussian models. In a study done to investigate the effect of SO₂ emissions from coastal regions on National Park Service management areas in Southern Florida (80 km inland), Segal et al. (1988) used RAMS and LPDM, finding that the complexity of the dispersion patterns which can occur for such a large travel distance necessitate a realistic assessment of mesoscale dispersion in coastal regimes.

Kerr et al. (2001 a, b) applied the modelling system RMS (see Section 2.5) to investigate the effects of a typical breeze regime on dispersion in coastal complex terrain. The inhalable particulate matter emitted by Fertilizer Plants located at Cubatão (Brazil) was simulated. Cubatão is an industrial city placed on the flat terrain between the escarpment of *Serra do Mar* sierra (700 to 1000 m high) and the Atlantic Ocean. For a typical daytime circulation, the sea breeze may be blocked by the mountain escarpment (see Figure 3) or overcome the mountain ridge and penetrate deep inland (see Figure 4). Thus, on many occasions, the Cubatão emission may reach São Paulo (44 km inland). For a typical nighttime circulation, the katabatic winds and land breeze transport the particulate matter

over the shoreline plains (see Figure 5) where many towns (700,000 inhabitants) are located.

3.6.2 Dispersion in Complex Terrain

LSMs have been used in a number of simulations of the ASCOT (Atmospheric Studies in COMplex Terrain) tracer data sets. Luhar and Rao (1993) coupled their LSM to a 2D-katabatic flow model to simulate the tracer concentration data obtained over a nearly two-dimensional slope in the Anderson Creek Valley, California. Magnitude predictions were good at nearly all sample sites, but observed concentrations decreased more slowly with time than the predicted ones, most likely due to pooling of the drainage air in the valley basin, causing flow stagnation and emphasising the need for a three-dimensional meteorological field, modelled or analysed.

Tracer concentrations from the 1991 ASCOT Colorado Front Range nocturnal experiment (near the Rocky Flats Plant) were modelled well with a LSM by Luhar and Rao (1994), using winds and turbulence parameters derived from analyses of the observed meteorological data. Their diagnostic approach can be compared to the prognostic approach of Poulos and Bossert (1995) and Fast (1995) who used three-dimensional meteorological models (Fast also used four-dimensional data assimilation) and LSMs to simulate the same period. The time- and space-varying nature of the drainage flow in this challenging region is illustrated by Figure 6 (Fast, 1995), which shows the hourly-averaged concentration and streamlines at two different times. Fast (1995) compared his results, and those from Poulos and Bossert (1995), to the results from air quality models coupled to several diagnostic models and concluded that the latter predict more accurate maximum concentrations. He suggests that this may be due to the stable turbulence parameterisations in the mesoscale prognostic models (rather than the mean wind field) as these directly affect the way diffusion is treated in the LSMs.

Studies involving LSMs in complex terrain under daytime conditions include the Swiss Alps tracer experiments (Anfossi et al., 1998) and the evaluation of emissions from coastal power stations in Australia (Noonan et al., 1994) and Spain (Hernandez et al., 1995).

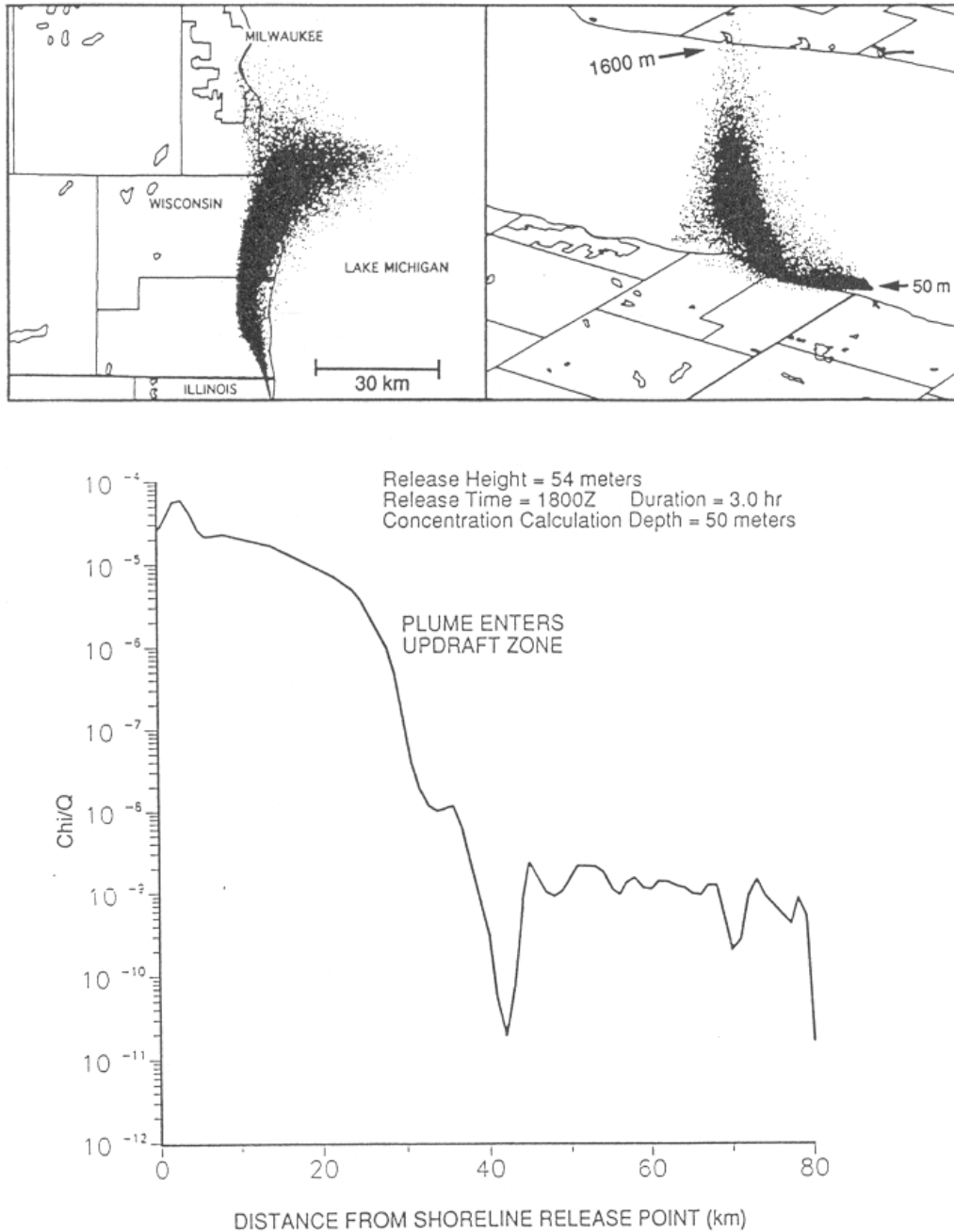


Figure 2. (a) (Top left) Plan view of a simulated plume released from a 50m high shoreline source into a weak lake breeze along the Lake Michigan shoreline; (b) (Top right) Perspective view of the plume from the southwest showing large quantities of the plume being translocated vertically as high as 1600 m due to the strong upward motions in the lake-breeze frontal zone; (c) (Bottom) Modelled normalised surface-layer concentrations at the centreline of the plume demonstrating a dramatic decrease as the plume intersects the lake breeze frontal updrafts.

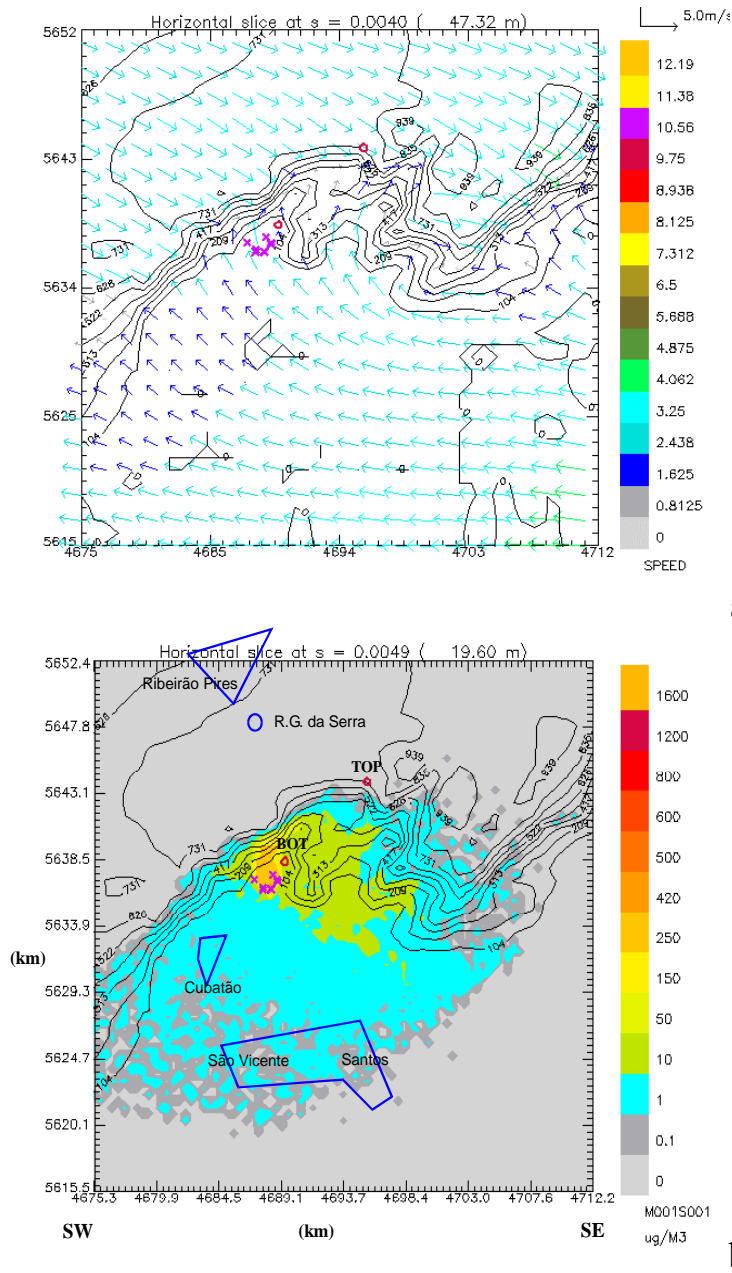
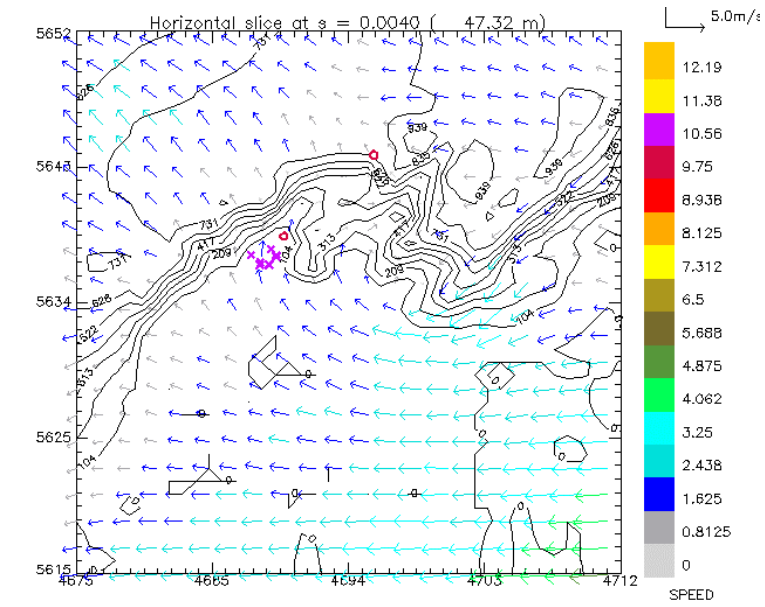
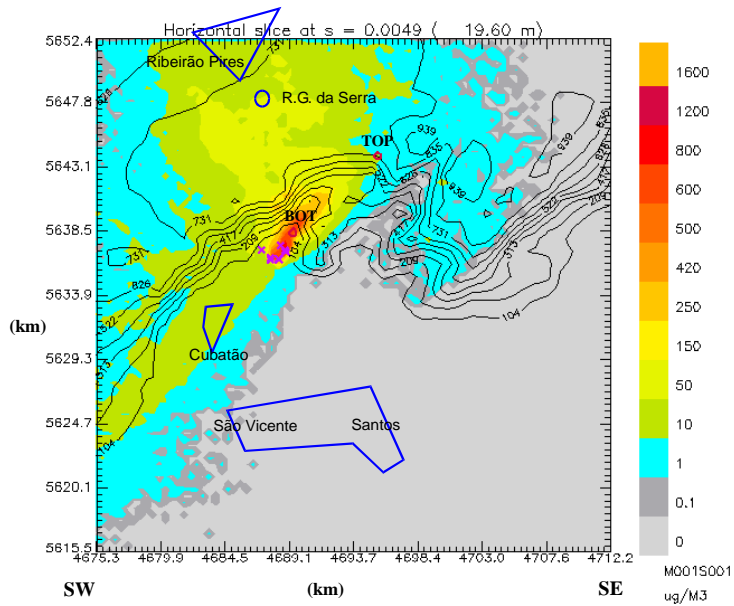


Figure 3. Typical daytime situation with blocked sea breeze. (a) wind field at 47 m a.g.l. computed by RAMS, the colour scale refers to the wind speed intensity in ms^{-1} ; (b) concentration field at ground level, computed by SPRAY, the colour scale refers to concentration amounts in μgm^{-3} .



a



b

Figure 4. As in Figure 3 but for typical daytime situation with sea breeze overcoming the mountain barrier.

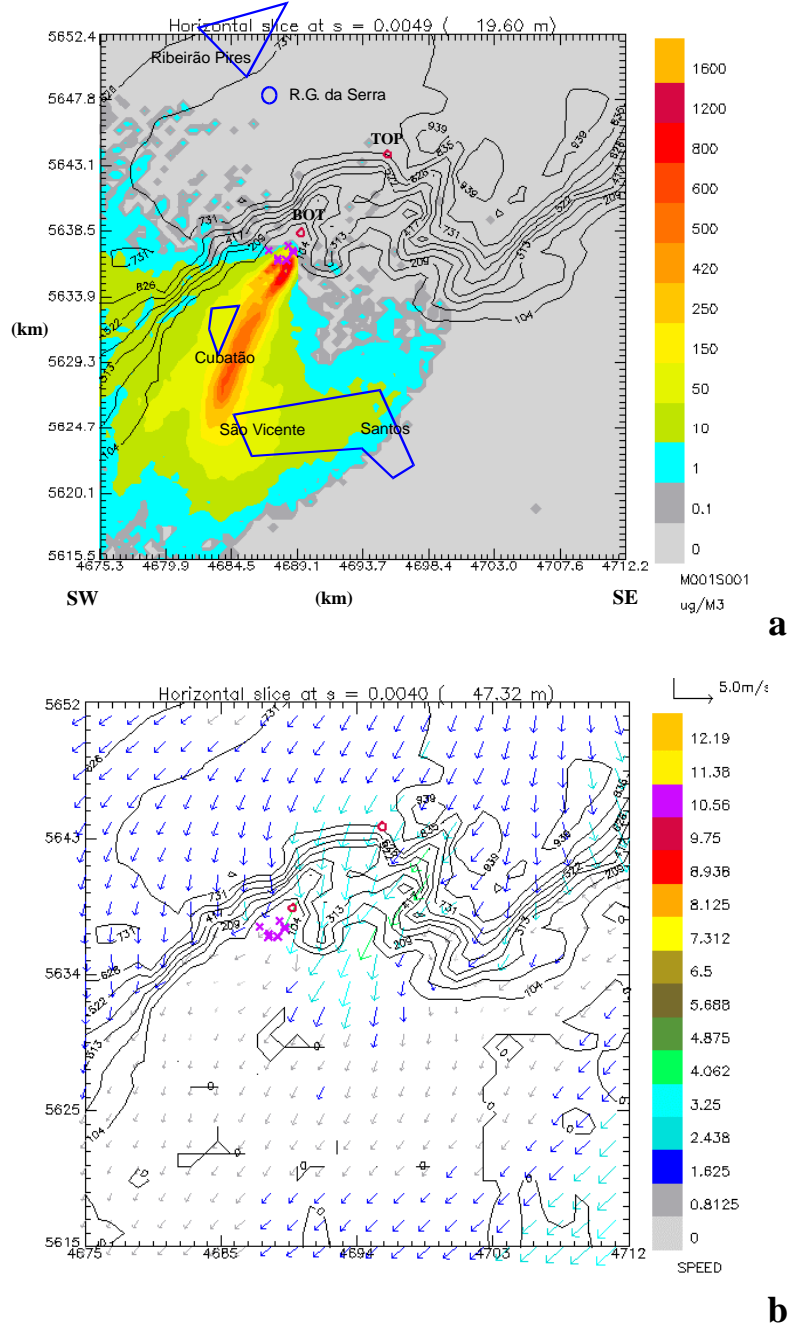


Figure 5. As in Figure 3 but for typical night-time situation with land breeze.

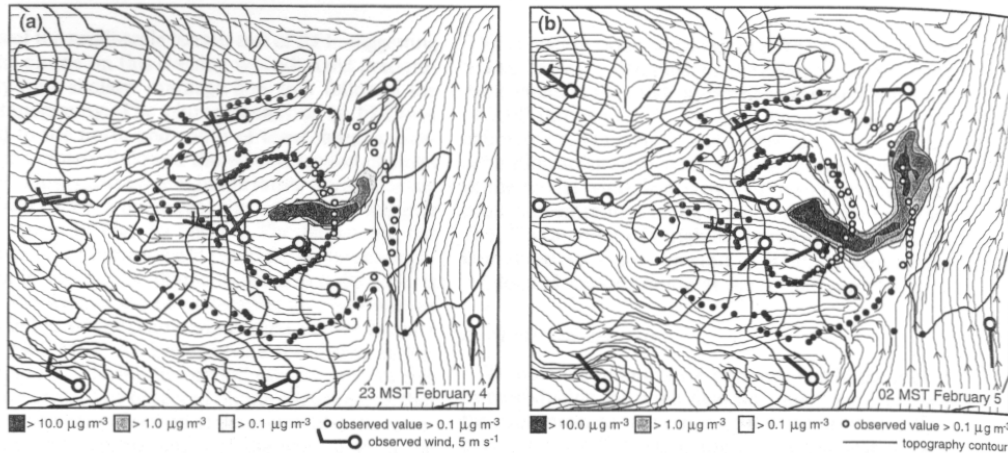


Figure 6. Wind field (streamlines) 26 m AGL at: (a) 2300 MST, 4 February 1991 with hourly-averaged surface concentration between 2300 and 0000 MST; and (b) 0200 MST 5 February 1991 with hourly-averaged surface concentration between 0200 and 0300 MST [From Fast (1995)].

3.6.3 Animation of LSM Simulation

An [animation](#) of a three-dimensional simulation in coastal complex terrain showing particle dispersion and contours of ground-level concentrations from two point sources can be viewed in the CD-ROM version of the book. A frame of the animation is shown in Figure 7. The simulation using the model TAPM (Hurley, 1999; Hurley et al., 2001) begins at midnight and continues for 24 hours (the time on the top left-hand corner shows days, hours and minutes). Terrain is shaded according to elevation, and sea areas are coloured blue. Emissions released at a height of 100 m from the two coastal sources are transported offshore by the prevailing synoptic wind and return over land early afternoon in the sea breeze. Towards the end of the simulation, they are channelled to the northwest along a valley. Particles at all heights are displayed and this is why particles are moving in different directions at any one time. For example, low-level particles can be seen moving inland in the sea breeze, while others at higher levels are moving offshore in the synoptic wind, enhanced by the return flow of the sea-breeze circulation. Note that many more particles are used to calculate the concentrations than are used to visualise the dispersion.

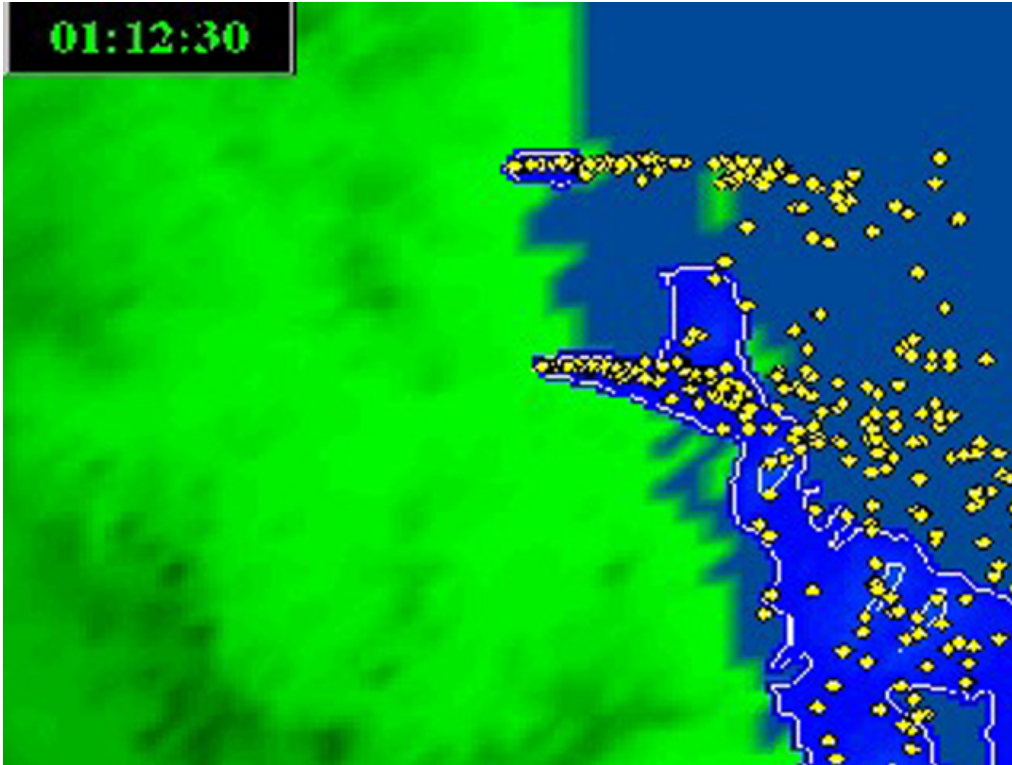


Figure 7. A frame from the animated dispersion of emissions from point sources using a prognostic three-dimensional air quality model TAPM. (The [animation](#) is provided in the CD-ROM version of this book.)

3.7 Long-Range Transport (S. Trini Castelli)

International frontiers are disregarded by pollutants dispersing through the atmosphere. The Chernobyl accident at the end of April 1986 abruptly reminded the modelling community of the importance of improving the reliability of models for long-range transport. The main limitation to this kind of study was the lack of experimental data against which to perform the model validation, and of a common protocol for the evaluation of the results. An important step in developing this framework was the ATMES (Atmospheric Transport Model Evaluation Study) Project, where a quality-controlled database of the measurements collected for the case of the Chernobyl accident was assembled and made available. The results of this study were affected by the uncertainties in the source term and by the heterogeneity of the observed data, due to the accidental conditions of the release. To overcome these deficiencies, in 1992 the field experimental campaign ETEX (European Tracer EXperiment) was carried out. Tracer releases under controlled conditions and systematic monitoring enabled model validation and intercomparison studies, even for the case of emergency response. A common evaluation protocol was also set up. In this section, ATMES and ETEX studies are described and the results obtained by the Lagrangian particle models are summarised and briefly discussed. For identification, classification and description of the other participating models, refer to the relative official literature cited in the sub-sections.

3.7.1 The ATMES Project

The ATMES Project was initiated in November 1986 by a collaboration of IAEA (International Atomic Energy Agency) and WMO (World Meteorological Office), while CEC (Commission of European Community) joined the initiative in 1987 through the JRC (Joint Research Centre). The purpose of ATMES was to review and to intercompare pollutant dispersion models for the atmosphere in order to identify the most promising approaches for the modelling of the long-range transport of radionuclides and to provide guidance for future work. The area considered for the exercise, from 10°W to 40°E and 35°N to 70°N, included most of the European measuring stations for which radiological data were available.

The data set supplied for the exercise contained:

- the estimated source term for the Chernobyl plant (51° 17'N, 30° 15'E) consisting of release data in TBq/day for I¹³¹ and Cs¹³⁷, together with an estimate of the effective height of the initial plume centre-of-mass
- ECMWF meteorological data (wind components, temperature and relative humidity on pressure levels, wind at 10 m height, surface pressure, temperature at 2 m height, total cloud cover) consisting of analyses (for the period between 25 April 12:00 to 10 May 18:00 UTC, with 6 hours time interval and 1.125 degrees resolution, on the area from 81°W to 40.5°E and from 29.25° to North pole) and of forecasts (between 25 April 12:00 to 30 April 12:00)
- KNMI precipitation data from 25 April to 14 May
- list of the locations of the measuring stations, referring to I¹³¹ and Cs¹³⁷ air concentration and Cs¹³⁷ daily deposition

The model results, in terms of air concentrations of I¹³¹ and Cs¹³⁷, Cs¹³⁷ wet and cumulative deposition were requested for a period of 14 days. A large number of modellers, 21, participated in the exercise, so that a statistical methodology was adopted to perform the model intercomparison (Klug et al., 1992). The ranking was performed separately for each data set according to several statistical parameters, like bias, Pearson correlation coefficient, NMSE (Normalised Mean Square Error), Standard Deviation, FA2 and FA5 (Fraction of calculated values within a factor of 2 and 5), FOEX (Factor of Exceedance, that is an absolute overestimation), FMT (Figure of Merit in Time), FMS (Figure of Merit in Space) and Kolmogorov-Smirnov test. The criteria adopted for the ranking was to give equal importance to the different statistical parameters, so that an equal weight was associated with each of them in summing up to obtain a total score.

The seven Lagrangian particle models that participated in the intercomparison are listed in Table 1. To single out the quality of their performances among the other models, Table 2 lists the five models providing the best results for the different data sets.

Table 1. List of the Lagrangian particle models in ATMES.

ATMES Model Number	Model Name	Organisation
4	ADPIC	LLNL (Lawrence Livermore Laboratory, USA)
5	APOLLO	ENEA-DISP (Committee for Research and Development of Nuclear and Alternative energies, I)
8	SPEEDI	JAERI (Japan Atomic Energy Research Institute, J)
9		JMRI (Japan Meteorological Research Institute, J)
11	JMA-GTTM	JMA (Japan Meteorological Agency, J)
18		IAG (Institute of Applied Geophysics, USSR)
20	NAME	MO (Meteorological Office, UK)

Table 2. ATMES statistical ranking for the data subsets: first five models
E = Eulerian, L = Lagrangian puff, LP = Lagrangian Particle.

Sample Size	I ¹³¹ air concentration 700	Cs ¹³⁷ air concentration 700	Cs ¹³⁷ daily deposition 140	Cs ¹³⁷ cumulate d deposition 95	I ¹³¹ forecasted wind field 35	Cs ¹³⁷ forecasted wind field 35
RANK	Model Number and Type					
I	5 (LP)	7 (E)	3 (L)	4 (LP)	2 (E)	10 (E)
II	18 (LP)	5 (LP)	18 (LP)	21 (L)	17 (L)	7 (E)
III	7 (E)	15 (L)	15 (L)	8 (LP) 15 (L)	5 (LP)	2 (E)
IV	17* (L)	19 (L)	4 (LP)	10 (E)	10 (E)	5 (LP)
V	21 (E)	10 (E)	5 (LP)	17 (L)	8 (LP)	15 (L) 17 (L)

*model no. 17 is a Lagrangian segmented-plume model

In Table 3, the ranks corresponding to the total score of the five best models are reported for both the analysed and forecast meteorological input fields. This ranking has been obtained by summing up the partial scores of the models from the different data subsets. Three models did not supply full information about the depositions. The results obtained using the forecasts were provided by ten models.

Table 3. ATMES statistical ranking for the total data: first five models
E = Eulerian, L = Lagrangian puff, LP = Lagrangian Particle.

RANK	Analysis Meteo Input	Forecast Meteo Input
Model Number and Type		
I	5 (LP)	2 (E)
II	4 (LP) 15 (L)	10 (E)
III	17 (L)	7 (E)
IV	18 (LP)	5 (LP)
V	7 (E)	17 (L)

No systematic trend in model performances was evident, with Eulerian and Lagrangian models attaining the same average ranking, and there was no evidence of a correlation between the complexity of the models and improved results. The outcomes of the analysis of the results showed that the cloud trajectories were generally well predicted when using the analysed wind field, while the deterioration of performances when using the forecasted fields was related to the strong dependency of the result quality on the meteorological input data. Improvement in space and time resolution and in the quality of the meteorological and precipitation data was recommended. From Table 3, it can be seen that a good quality contribution was given by the Lagrangian particle models using the analysed fields. In regards to the model sensitivity to simulation parameters, the necessity of improving the description of the boundary layer structure, including the interaction of the pollutant cloud with it, and of the deposition parameters was recognised.

Considering the uncertainty and lack of information of the Chernobyl case, the final recommendation of the conclusive ATMES workshop in 1991 was that "... a controlled release experiment in Europe be launched by releasing from a given location a tracer which can be detected at very large distance" (Klug et al., 1992).

3.7.2 The ETEX Project

The ETEX Project too was sponsored by EC, WMO and IAEA and was aimed at evaluating the ability of meteorological services and research institutions to predict in real time the atmospheric dispersion of inert pollutants over large distances (Nodop, 1997). Two tracer releases were carried out on 23 October and 14 November 1994, for a release period of nearly 12 hours. An ETEX modelling phase was performed in parallel with the experiment. The source was set in Monterfil (2°W, 48° 3'N, 90 m ASL, France) and the sampling domain almost

covered from 43° to 60°N and 2° to 25°E. When the release started, the 28 modellers, previously alerted, were notified of the starting time, source location and emission rate. The models were run in real-time to predict the evolution of the tracer cloud and the predictions were sent to the statistical evaluation team as available. In Table 4, the Lagrangian particle models participating in the real-time phase in ETEX are listed.

Table 4. List of the Lagrangian particle models in ETEX real-time phase.

ETEX real-time Model Name	Organisation
LPDM	DWD (German Weather Service, D)
APOLLO	ANPA (National Agency for Environment, I)
ADPIC	LLNL (Lawrence Livermore Laboratory, USA)
WSPEEDI	JAERI (Japan Atomic Energy Research Institute, J)
NAME II	MetOff (Meteorological Office, UK)
SNAP	NMI (Norwegian Meteorological Institute, N)
LPDM	SRS (Westinghouse Savannah River Laboratory, USA)
STADIUM	TYPHOON (RU)
	KMI (Royal Institute of Meteorology, B)
TRADOS	FMI (Finnish Meteorological Institute, Fi)

For ETEX, statistical measures used in the ATMES case were augmented by the Geometrical Mean Bias (MG) and the Geometric Mean Variance (VG). The statistical analysis of results from the first release showed that a group of models were able to forecast in real time the cloud position and its horizontal extent up to a period of 48 hours, although the forecast worsened for later times. The concentration evolution at the stations was not always correctly reproduced (not even by the best models). A group of 6 models showed excellent performances, 8 models had few excellent and some average performances, and 4 models had intermediate results. In the second experiment, the presence of the ground level tracer cloud was limited to 24 hours after the release and the number of non-zero measurements restricted the statistics to few parameters. None of the participating models were able to simulate correctly the ground level concentrations, neither spatially nor as time evolution. The general model trend was to greatly over-predict the concentrations.

From the analysis of ETEX real-time results, it was not possible to attribute the differences between measurements and predictions specifically to the meteorological or the dispersion phases. Also in order to relate the differences in observed and calculated concentrations to the dispersion simulation, the ATMES II modelling exercise was launched almost two years after the ETEX campaign (Mosca et al., 1998; Girardi et al., 1998). The exercise was open to all the long-range modellers, and participants were required to calculate the concentration field of the ETEX first tracer experiment using a common meteorological input data set, corresponding to the ECMWF analysis for the ETEX period, but also models using non-ECMWF data were considered. The total number of models

participating in ATMES II was 49, 35 of them using ECMWF analyses (coded from 101 to 135) and 14 using non-ECMWF data (coded from 201 to 214). In Table 5, the Lagrangian particle models participating in ATMES II are listed.

Table 5. List of the Lagrangian particle models in ATMES II.

ATMES II Model Number	Model Name	Organisation
101	FLEXPART	IMP (Univ. Wien, Institute of Meteorology and Physics, A)
106	LPDM	DWD (German Weather Service, D)
107	LPDM	DWD (German Weather Service, D)
112	DIFPAR	EDF (French Electricity, F)
113	APOLLO	ANPA (National Agency for Environment, I)
114	MILORD	ICGF/CNR (National Research Council, I)
115	WSPEEDI	JAERI (Japan Atomic Energy Research Institute, J)
116	MRI-LTM	MRI (Meteorological research Institute, J)
118	MATHEW/ ADPIC	FOA (Defence Research Establishment, S)
119	NAME	MetOff (Meteorological Office, UK)
131	SNAP	DNMI (Norwegian Meteorological Institute, N)
132	LPDM	SRS (Westinghouse Savannah River Laboratory, USA)
203	LPDM	DWD (German Weather Service, D)
207	MRI-LTM	MRI (Meteorological research Institute, J)
209	NAME	MetOff (Meteorological Office, UK)
210	NAME	MetOff (Meteorological Office, UK)
213	SNAP	DNMI (Norwegian Meteorological Institute, N)

The statistical analysis of the results was performed on the same parameters as for the ETEX real-time phase and divided into three stages: a *time analysis*, considering concentrations at a fixed location for the whole duration of the episode; a *space analysis*, considering concentrations at a fixed time all over the domain; and a *global analysis*, where all the concentration values at any time and location are considered. In Table 6 the ranking of models based on the global analysis is reported, giving to each statistical index the same weight as in the statistics performed for ATMES and ETEX projects. The rank is given for the different groups separately and then for the total of the models. In the second column the first ten models in the statistical ranking for the group ECMWF (35 models) are listed. In the third column, there are the first five models for the non-ECMWF data models (14) and in the fourth column the first ten models over the total of models (49) are ranked.

As an overall result, a general substantial improvement in ATMES II over those from ETEX real-time phase was found. This was expected on account of the

better resolution of the meteorological fields used and the elapsed time between the two exercises during which improvement in models and tunings of key parameters were possible.

Considering that the participating Lagrangian particle models were 17 out of 49 and that in the ranking of the total models, eight of them are in the first ten, a good performance of this kind of models can be recognised in long-range dispersion modelling.

Table 6. ATMES II exercise: statistical ranking E = Eulerian, L = Lagrangian, LP = Lagrangian Particle, sL = semi-Lagrangian.

RANK	ECMWF Meteo Input Models	Non-ECMWF Meteo Input Models	All Models
Model Number and Type			
I	107 (LP)	209 (LP)	107 (LP)
II	111 (sL)	210 (LP)	111 (sL)
III	131 (LP)	208 (E)	209 (LP)
IV	115 (LP)	203 (LP)	203 (LP)
V	114 (LP)	213 (LP)	114 (LP)
VI	127 (E-L)		210 (LP)
VII	101 (LP)		131 (LP)
VIII	112 (LP)		208 (E)
IX	128 (E)		115 (LP)
X	134 (L)		101 (LP)

3.8 Footprint Analysis of Scalar Fluxes (A. Luhar)

Any surface source, located at $(x', y', 0)$, can potentially contribute to the vertical flux F (e.g., with units of $\text{g m}^{-2} \text{s}^{-1}$) of a scalar measured downwind at point (x, y, z_m) . The term footprint, f , is defined as the contribution per unit surface flux of each unit element of the upwind surface area to the measured vertical flux (Horst and Weil, 1992)

$$F(x, y, z_m) = \int_{-\infty}^{\infty} \int_{-\infty}^x Q_o(x', y', 0) f(x - x', y - y', z_m) dx' dy' \quad (80)$$

where Q_o is the surface emission flux ($\text{g m}^{-2} \text{s}^{-1}$) of an area-source element located at (x', y') upwind of the measurement location. Equation (80) implies that the

measured scalar flux is the integral of the contributions from all elements of upwind surface emissions, whereas the footprint (m^2) is the relative weight given to each elemental source. In general, for a given location, f is a function of only the turbulent flow field that governs transport and diffusion.

Footprint estimation is useful for the identification of the sources of greenhouse gases, such as water vapour and methane that contribute to measured fluxes, and for assessing the relative importance of these sources. For many cases involving surface inhomogeneities, such as changes in surface roughness or moisture (e.g., transition from a relatively smooth arid area to an irrigated crop), footprint analysis can provide an estimate of the key “height-to-fetch” ratio that determines the optimum sitting of instruments for flux measurements. It can also facilitate the interpretation of airborne flux measurements in relation to tower data.

Footprint analysis can often be performed in two dimensions when the source area is of large extent in the crosswind direction with respect to the flux measurement position. For such cases, Equation (80) can be written as

$$F(x, z_m) = \int_{-\infty}^x Q_o(x', 0) f_2(x - x', z_m) dx' \quad (81)$$

where f_2 (m^{-1}) is the two-dimensional footprint. In a region with nearly uniform surface conditions, Q_o can be assumed to be independent of x' .

Equation (81) suggests that the footprint f_2 is the vertical flux F_L ($\text{g m}^{-2} \text{s}^{-1}$) at the measurement point (x, z_m) due to a continuous line source of unit strength located upwind at $(x', 0)$. Thus

$$f_2(x - x', z_m) = \frac{1}{Q_o} \frac{dF(x, z_m)}{dx'} = \frac{F_L(x, z_m)}{q} \quad (82)$$

where q is the line source strength ($\text{g m}^{-1} \text{s}^{-1}$). Figure 8 presents a schematic diagram of the footprint of upwind sources that contribute to the flux measured at (x, z_m) .

Analytical methods have been used to predict flux footprints using analytical solutions to the diffusion equation for horizontally homogeneous surface layers (e.g., Schuepp et al., 1990; Horst and Weil, 1992; Haenel and Grünhage, 1999). However, these methods are not valid when the surface-layer similarity is no longer applicable; for example, above the surface layer (relevant to aircraft data), within plant canopies, or when measuring fluxes from surfaces of limited extent (fetch), such as small lakes or irrigated fields within arid lands, so that the effects of the flow inhomogeneity are important. Under such conditions, Lagrangian stochastic dispersion models prove valuable in predicting the footprint. They are also useful for testing and improving footprint predictions obtained from the analytical solutions. Stochastic models have been used in the past for footprint predictions in the surface layer (Leclerc and Thurtell, 1990; Horst and Weil, 1992), in the convective boundary layer (Wilson and Swaters, 1991), for a step

change in the surface roughness and moisture (Luhar and Rao, 1993), and within and over forest canopies (Baldocchi, 1997). Experimental evaluation of analytical and Lagrangian footprint models has been reported by Finn et al. (1996).

When the turbulent flow is horizontally homogeneous, the footprint f_2 at a given height depends only on the separation between the flux measurement point and the elemental source. However, when the flow is horizontally inhomogeneous, it depends on their actual locations. In the former case, footprints due to a single line source, calculated at several locations downwind of the source, can be used to derive the footprint at a particular location due to a number of line sources located upwind. For this purpose, particles are released at the surface from a crosswind line source of unit emission flux. Particle numbers and corresponding vertical velocities are computed at a number of heights and downwind distances, and are then used to determine the average vertical flux at these locations. This vertical flux is equal to the footprint f_2 (Equation [82]). However, in the horizontally inhomogeneous flow case, one may not use this procedure; the footprints are calculated by placing a number of line sources upwind of the measurement point (e.g., Luhar and Rao, 1993). The Lagrangian stochastic models mentioned above are generally run in forward mode to determine the footprint. That is, particles are released at the source position, and the position and velocity distribution of particles reaching the receptor position is calculated. Flesch et al. (1995) and Flesch (1996) use a backward Lagrangian stochastic technique for footprint calculations, which is potentially more efficient and flexible than the forward Lagrangian stochastic technique. In the backward technique, particles are released at the receptor position and tracked backwards to determine their distribution at the ground to identify the sources contributing to fluxes at the receptor. However, this technique is only approximately valid when the flow is horizontally inhomogeneous.

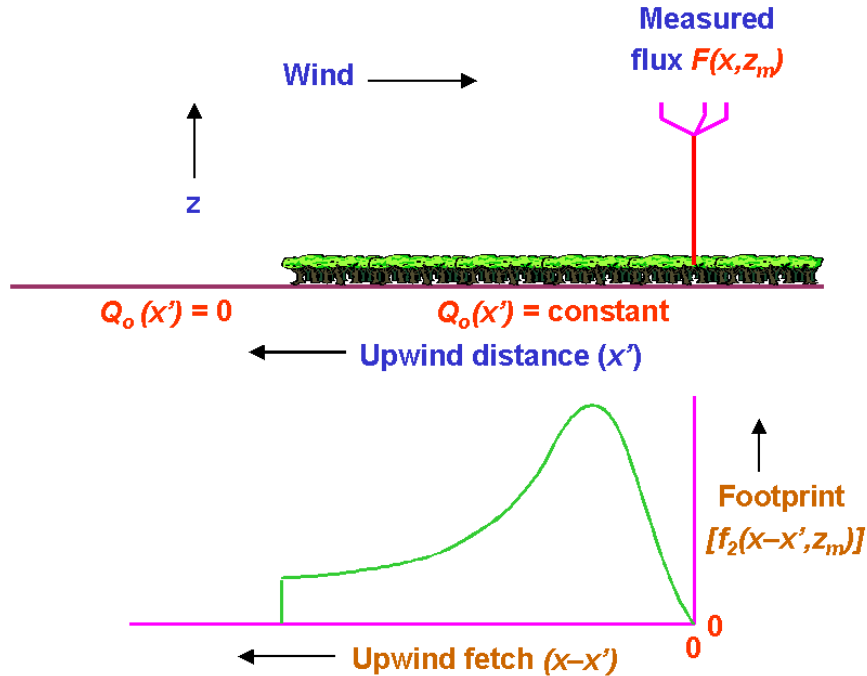


Figure 8. Schematic diagram showing the footprint of upwind sources for the flux measurements made at point (x, z_m) over a surface with simple inhomogeneity.

References

- Anfossi, D., Ferrero, E., Sacchetti, D. and S. Trini Castelli (1996). Comparison among empirical probability density functions of the vertical velocity in the surface layer based on higher order correlations. *Boundary Layer Meteorology*, **82**, 193-218.
- Anfossi, D., Ferrero, E., Tinarelli, G., and Alessandrini, S. (1997) A simplified version of the correct boundary conditions for skewed turbulence in Lagrangian particle models. *Atmospheric Environment*, **31**:301-308.
- Anfossi, D., Desiato, F., Tinarelli, G., Brusasca, G., Ferrero, E. and Sacchetti D. (1998). TRANSALP 1989 experimental campaign –II. Simulation of a tracer experiment with Lagrangian particle models. *Atmospheric Environment*, **32**, 1157-1166.
- Anfossi, D., G. Degrazia, E. Ferrero, S.E. Gryning, M.G. Morselli and S. Trini Castelli (2000). Estimation of the Lagrangian structure function constant C_0 from surface layer wind data, *Boundary Layer Meteorology*, **95**: 249-270.
- Anfossi, D. (2000) Short Review of Lagrangian Stochastic Models for the Simulation of the Atmospheric Pollutant Dispersion. *Hybrid Methods in Engineering*, **2**, 261-279.
- Antonia, R.A. and Atkinson, J.D. (1973). High-order moments of Reynolds shear stress fluctuations in a turbulent boundary layer, *J. Fluid Mech.*, **58**, part 3, 581-593.

- Baerentsen, J.H. and Berkowicz, R. (1984). Monte-Carlo simulation of plume diffusion in the convective boundary layer, *Atmospheric Environment*, **18**, 701-712.
- Baldocchi, D., (1997). Flux footprints within and above forest canopies. *Boundary-Layer Meteorology* **85**, 273-292.
- Batchvarova, E. and Gryning, S.E. (1991). Applied model for the growth of the daytime mixed layer. *Boundary Layer Meteorology*, **56**, 261-274.
- Batchelor, G.K. (1949). Diffusion in a field of homogeneous turbulence, I: Eulerian analysis. *Aust. J. Sci. Res.*, **2**, 437-450.
- Borgas, M. S. and Sawford, B. L., (1994). A family of stochastic models for two-particle dispersion in isotropic homogeneous stationary turbulence. *Journal of Fluid Mechanics* **279**, 69-99.
- Brusasca, G., G. Tinarelli and D. Anfossi (1989). Comparison between the results of a Monte Carlo atmospheric diffusion model and tracer experiments. *Atmospheric Environment*, **23**, 1263 - 1280.
- Brusasca, G., G. Tinarelli, and D. Anfossi, (1992). Particle model simulation of diffusion in low wind speed stable conditions. *Atmospheric Environment*, **4**, 707-723.
- Buckley, R.L. and Kurzeja, R.J. (1997). An observational and numerical study of the nocturnal sea breeze. Part II: chemical transport. *J. Appl. Meteorol.*, **36**, 1599-1619.
- Caughey, S.J. (1982). Observed characteristics of the atmospheric boundary layer, Atmospheric turbulence and air pollution modelling, F.T.M. Nieuwstadt and H. van Dop, eds., Reidel, Dordrecht, 107-158.
- Chock, P. and S. Winkler (1994a). A particle grid air quality modelling approach. 1. The dispersion aspect, *Journal of Geophysical Research*, **99**, 1019-1031.
- Chock, P. and S. Winkler (1994b). A particle grid air quality modelling approach. 2. Coupling with chemistry, *Journal of Geophysical Research*, **99**, 1033-1041.
- Cogan, J.L. (1985). Monte Carlo simulation of a buoyant dispersion. *Atmospheric Environment*, **19**, 867-878.
- Crone, G.C., Dinar, N., van Dop, H. and Verver, G.H.L. (1999). A Lagrangian approach for modelling turbulent transport and chemistry, *Atmospheric Environment*, **33** (29), pp. 4919-4934.
- Csanady, G.T. (1973). *Turbulent diffusion in the environment*. Reidel.
- Davis, P.A. (1983). Markov chain simulations of vertical dispersion from elevated sources into the neutral planetary boundary layer. *Boundary-Layer Meteorology*, **25**, 355-376.
- Deardorff, J.W. (1974). Three-dimensional numerical study of the height and mean structure of a heated planetary boundary layer. *Boundary Layer Meteorology*, **7**, 81-106.
- Deardorff, J. and G. Willis (1982). Ground-level concentrations due to fumigation into an entraining mixed layer, *Atmospheric Environment*, **16**, 1159-1170.
- De Baas, H.F., H. van Dop, and F.T.M. Nieuwstadt, (1986). An application of the Langevin equation for inhomogeneous conditions to dispersion in a convective boundary layer. *Quart. J. Roy. Meteor. Soc.*, **112**, 165-180.

- Degrazia, G.A. and Anfossi, D. (1998). Estimation of the Kolmogorov constant C_0 from classical statistical diffusion theory, *Atmospheric Environment*, **32**, 3611-3614.
- Degrazia, G., Anfossi, D., Carvalho, J.C., Mangia, C., Tirabassi, T., Campos Velho, and H.F. (2000). Turbulence parameterisation for PBL dispersion models in all stability conditions. *Atmospheric Environment*, **34**, 3575-3583.
- de Haan, P. (1999). On the use of density kernels for concentration estimations within particle and puff dispersion models. *Atmospheric Environment*, **33**, 2007-2021.
- de Haan, P., and Rotach, M. W., (1998). A novel approach to atmospheric dispersion modelling: the puff-particle model. *Quarterly Journal of the Royal Meteorological Society*, **124**, 2771–2792.
- Du (1997). Universality of the Lagrangian velocity structure function constant (C_0) across different kinds of turbulence. *Boundary Layer Meteorology*, **83**, 207-219.
- Du, S., Wilson, J.D. and Yee, E. (1994). Probability density functions for velocity in the convective boundary layer and implied trajectory models, *Atmospheric Environment*, **28**, 1211-1217.
- Duran, J., L. Romer, T. Duranova and M. Stubna (1998). A Lagrangian statistical (Monte-Carlo) atmospheric dispersion model validation on the results of wind tunnel experiments 5th Conference on Harmonization within ADM for regulatory purposes 18-21 May, Rodos, Greece.
- Durbin, P.A., 1980, A stochastic model of two-particle dispersion and concentration fluctuations in homogeneous turbulence, *J. Fluid Mech.*, **100**, 2, 279-302.
- Durbin, P.A. and Petterson Reif, A. (2001). Statistical theory and modeling for turbulent flows. John Wiley and Sons, 285 pp.
- Durst, F., Jovanovic, J. and Johansson, T.G., (1992). On the statistical properties of truncated Gram-Charlier series expansions in turbulent wall-bounded flows. *Phys. Fluids*, **A 4**, 118-126.
- Eastman, J.L., Pielke, R.A. and Lyons, W.A. (1995). Comparison of lake-breeze model simulations with tracer data. *J. Appl. Meteorol.*, **34**, 1398-1418.
- Eberhard, W.L., Moninger, W.R. and G.A. Briggs (1988). Plume dispersion in the convective boundary layer. Part I: CONDORS field experiment and example measurements. *J. Appl. Meteorol.*, **27**, 599-616.
- Fast, J.D. (1995). Mesoscale modeling and four-dimensional data assimilation in areas of highly complex terrain. *J. Appl. Meteorol.*, **34**, 2762-2782.
- Ferrero, E., D. Anfossi, G. Brusasca and G. Tinarelli (1995). Lagrangian particle model (LAMBDA): evaluation against tracer data, *Int. J. Environment and Pollution*, **5**, 360-374.
- Ferrero, E. and Anfossi D. (1998a). Sensitivity analysis of Lagrangian Stochastic models for CBL with different PDF's and turbulence parameterizations. Air Pollution Modelling and its Applications XII, S.E. Gryning and N. Chaumerliac eds., Plenum Press, New York, **22**, 673-680.
- Ferrero, E. and Anfossi, D. (1998b). Comparison of PDFs, closures schemes and turbulence parameterizations in Lagrangian Stochastic Models. *Int. J. Environment and Pollution*, **9**, 384-410.
- Ferrero, E., Anfossi, D., Tinarelli, G. and Trini Castelli, S. (2000b). Lagrangian particle simulation of an EPA wind tunnel tracer experiment in a schematic two-dimensional valley. *Air Pollution Modelling and its Applications XIV*, S.E. Gryning and F.A. Schiermeier Eds., Plenum Press, New York.

- Ferrero, E., D. Anfossi, G. Tinarelli and M. Tamiazzo, (2000a). Intercomparison of Lagrangian stochastic models based on two different PDFs., *Int. J. Environment and Pollution*, **14**, 225-234.
- Ferrero, E., Anfossi, D. and Tinarelli, G. (2001). Simulations of Atmospheric Dispersion in Urban Stable Boundary Layer, *Int. J. Environment and Pollution*, **16**, 1-6.
- Finn, D., Lamb, B., Leclerc, M. Y. and Horst, T. W. (1996). Experimental evaluation of analytical and Lagrangian surface-layer flux footprint models. *Boundary Layer Meteorology*, **80**, 283-308.
- Flesch, T.K., Wilson, D.J. and Yee, E. (1995). Backward-Time Lagrangian Stochastic Dispersion Models and their Application to estimate Gaseous Emissions, *J Appl. Meteorol.*, **34**, 1320-1332.
- Flesch, T. K., (1996). The footprint for flux measurements, from backward Lagrangian stochastic models. *Boundary Layer Meteorology*, **78**, 399-404.
- Franzese, P., A. Luhar and M. Borgas (1999). An efficient Lagrangian stochastic model of vertical dispersion in the convective boundary layer, *Atmospheric Environment*, **33**, 2337-2345.
- Frenkiel, F.N. and Klebanoff P.S., (1967). Higher order correlations in a turbulent field. *Phys. Fluids*, **10**, 507-520
- Gaffen, D.J., Benocci C. and Olivari D. (1987) Numerical modeling of buoyancy dominated dispersal using a Lagrangian approach. *Atmospheric Environment*, **21**, 1285-1293.
- Gardiner, C.W. (1990). *Handbook of stochastic methods*. Springer Verlag.
- Gifford, F. A., (1959). Statistical properties of a fluctuating plume dispersion model. *Advances in Geophysics*, **6**, 117-137.
- Gifford, F.A. (1960). Peak to average concentration ratios according to a fluctuating plume dispersion model. *Int. J. Air Pollut.*, **3**, 253-260.
- Gifford, F.A. (1982). Horizontal diffusion in the atmosphere: a Lagrangian-dynamical theory, *Atmospheric Environment*, **16**, 505-512.
- Gingold, R.A., and J.J. Monaghan (1982). Kernel estimates as a basis for general particle methods in hydrodynamics. *J. Computational Phys.*, **46**:429-453.
- Girardi, F., Graziani, G., van Velzen, D., Galmarini, S., Mosca, S., Bianconi, R., Bellasio, R., Klug, W. and Fraser, G. (1998). The European Tracer Experiment. EUR 18143 EN.
- Gronski, K.E. (1990). Variation in dispersion conditions with height over urban areas – Results of dual tracer experiments. *Proceedings from the Symposium on Turbulence and atmospheric Diffusion*, April 30 – May 2, Roskilde, Denmark, American Meteorological society, Boston, MA (USA).
- Gryning, S.E. and Batchvarova, E. (1990). Simple model of the daytime boundary layer height. *Ninth Symposium on turbulence and Diffusion*. American Meteorological Society, 379.
- Gryning, S.E. (1999). Some aspects of atmospheric dispersion in the stratified atmospheric boundary layer over homogeneous terrain. *Boundary-Layer Met.*, **90**, 479-494.
- Haenel, H.-D. and L. Grünhage (1999). Footprint analysis: a closed analytical solution based on height-dependent profiles of wind speed and eddy viscosity. *Boundary Layer Meteorology*, **93**, 395-409.

- Hanna, S.R. (1968). A method of estimating vertical eddy transport in the planetary boundary layer using characteristics of the vertical velocity spectrum. *J. Atmos. Sci.*, **25**, 1026.
- Hanna, S.R. (1979). Some statistics of Lagrangian and Eulerian wind fluctuations. *J. Appl. Met.*, **18**, 518-525.
- Hanna, S.R. (1981). Lagrangian and Eulerian time-scale in the daytime boundary layer. *J. Appl. Meteorol.*, **20**, 242-249.
- Hanna, S.R. (1982). Applications in air pollution modelling, Atmospheric Turbulence and Air Pollution Modelling, F.T.M. Nieuwstadt and H. Van Dop eds., Reidel, Dordrecht.
- Hanna, S. and R. Paine (1989). Hybrid plume dispersion model development and evaluation, *Atmospheric Environment*, **27A**, 1491-1508.
- Hanna, R.S., Bitter, E.R. and Franzese, P., (2001) The effect of roughness obstacles on flow and dispersion at industrial and urban sites, *Report AIChE CCPS Project 132*.
- Hernandez, J.F., Cremades, L. and Baldasano, J.M. (1995). Dispersion modelling of a tall stack plume in the Spanish Mediterranean coast by a particle model. *Atmospheric Environment*, **29**, 1331-1341.
- Hibberd, M. and B. Sawford (1994). A saline laboratory model of the planetary convective boundary layer, *Boundary Layer Meteorology*, **67**, 229-250.
- Hibberd, M. and A. Luhar (1996). A laboratory study and improved PDF model of fumigation into a growing convective boundary layer, *Atmospheric Environment*, **30**, 3633-3649.
- Hinze, J.O. (1975). *Turbulence*. Mc Graw Hill, 790 pp.
- Holtslag, A.A. and Moeng, C.H. (1991). Eddy diffusivity and countergradient transport in the convective boundary layer. *J. Atmos. Sci.*, **48**, 1690-1698.
- Horst, T. W. and J.C. Weil (1992). Footprint estimation for scalar flux measurements in the atmospheric surface layer. *Boundary Layer Meteorology*, **59**, 279-296.
- Hurley, P. (1994). PARTPUFF – A Lagrangian particle/puff approach for plume dispersion modelling applications, *J. App. Meteorology*, **33**, 285-294.
- Hurley, P.J. and Physick, W.L. (1991). A Lagrangian particle model of fumigation by breakdown of the nocturnal inversion. *Atmospheric Environment*, **25A**, 1313-1325.
- Hurley, P. and W. Physick (1993a). A skewed, homogeneous Lagrangian particle model for convective conditions, *Atmospheric Environment*, **27A**, 619-624.
- Hurley, P. and W. Physick (1993b). Lagrangian particle modelling of buoyant point sources – plume rise and entrainment in convective conditions, *Atmospheric Environment*, **27A**, 1579-1584.
- Hurley, P. (1997). An evaluation of several turbulence schemes for the prediction of mean and turbulent fields in complex terrain. *Boundary Layer Meteorology*, **83**, 43-73.
- Hurley, P. (1999). The Air Pollution Model (TAPM) Version 1: Technical Description and Examples. CSIRO Atmospheric Research Technical Paper No. 43.
- Hurley, P., Blockley, A., and Rayner, K. (2001). Verification of a prognostic meteorological and air pollution model for year-long predictions in the Kwinana region of Western Australia. *Atmospheric Environment*, **35** (10): 1871-1880.

Irwin, J.S. (1979a). Estimating plume dispersion – a recommended generalized scheme. Preprints Fourth Symposium on Turbulence, Diffusion and Air Pollution. Am. Meteorol. Soc., 45 Beacon Street, Boston Mass. 02108, 62-69.

Kaimal, J.C., Wyngaard, J.C., Haugen, D.A., Cote', O.R., Izumi, Y., Caughey, S.J. and Readings, C.J. (1976). Turbulence structure in the convective boundary layer. *J. Atmos. Sci.*, **33**, 2152-2169.

Kaimal, J.C.R., Eversole, D., Lenschow, D.H., Stankov, B.B., Kahn, P.H. and Businger, J.A. (1982). Spectral characteristics of the convective boundary layer over uneven terrain. *J. Atmos. Sci.*, **39**, 1098-1114.

Kaimal, J.C. and Finnigan, J.J. (1994) Atmospheric boundary layer flows, Oxford University Press, 289 pp.

Kalthoff, N., Binder, H.J., Kossman, M., Vöggtlin, R., Corsmeier, U., Fiedler, F. and Schlager, H. (1998). Temporal evolution and spatial variation of the boundary layer over complex terrain, *Atmospheric Environment*, **32**, 1179-1194.

Kendall, M. and Stuart, A. (1977) *The advanced theory of statistics*, MacMillan, New York.

Kerschgens, M.J, Nolle, C. and Martens, R. (2000) Comments on turbulence parameters for the calculation of dispersion in the atmospheric boundary layer. *Meteorologische Zeitschrift*, **9**, 155-163.

Kerr, A.F.S, Anfossi, D., Carvalho, Jonas C. and Trini Castelli, S. (2001a). A Dispersion Study of the Aerosol Emitted by Fertilizer Plants in the Region of Serra do Mar Sierra, Cubatão, Brazil, *Int. J. Environment and Pollution*, **16**, 251-263.

Kerr, A., Anfossi, D., Trini Castelli, S. and Nascimento, S.A. (2001b) Investigation of inhalable aerosol dispersion at Cubatão by means of a modelling system for complex terrain. *Hybrid Methods in Engineering*, **2**, 389-407.

Khurshudyan, L.H., Snyder, W.H. and Nekrasov, I.V., (1981). Flow and dispersion of Pollutants within Two-Dimensional Hills, EPA REPORT No. -6000/4-81/067.

Khurshudyan, L.H., Snyder, W.H., Nekrasov, I.V., Lawson, R.E., Thompson, R.S and Schiermeier, F.A., (1990). Flow and Dispersion of Pollutants within Two-Dimensional Valleys, *Summary Report on Joint Soviet-American Study*, EPA REPORT No. 600/3-90/025

Klug, W., Graziani, G., Grippa, G., Pierce, D. and Tassone, C., Eds. (1992). Evaluation of Long Range atmospheric Transport Models using Environmental radioactivity Data from the Chernobyl Accident. The ATMES Report. EUR 14147 EN.

Klug, W. (2000). What did we learn from the ETEX Experiment? *Proceedings of the Millennium NATO/CCMS International Technical Meeting on Air Pollution Modelling and its Application*, Boulder (Colorado, USA) 15-19 May 2000, AMS Ed., 256-268.

Lamb, R.G., H. Hogo, and L.E. Reid (1979) A Lagrangian approach to modelling air pollution dispersion: Development and testing in the vicinity of a roadway. EPA Research Report EPA-600/4-79-023.

Leclerc, M. Y. and G.W. Thurtell (1990) Footprint prediction of scalar fluxes using a Markovian analysis. *Boundary Layer Meteorology*, **52**, 247–258.

Legg, B.J. and Raupach, M.R. (1982) Markov-chain simulations of particle diffusion in inhomogeneous flows: the mean drift velocity induced by a gradient in Eulerian velocity variance. *Boundary Layer Meteorology*, **24**, 3-13.

- Ley, A.J. (1982). A random walk simulation of two dimensional turbulent diffusion in the neutral surface layer. *Atmospheric Environment*, **16**, 2799-2808.
- Lorimer, G.S. (1986). The kernel method for air quality modelling: I. Mathematical foundation. *Atmospheric Environment*, **20**:1447-1452.
- Luhar, A.K., and Britter R.E. (1989). A random walk model for dispersion in inhomogeneous turbulence in a convective boundary layer. *Atmospheric Environment*, **23**, 1191-1924.
- Luhar, A.K. and Rao, K.S. (1993). Random-walk model studies of the transport and diffusion of pollutants in katabatic flows. *Boundary Layer Meteorology*, **66**, 395-412.
- Luhar, A.K. and Rao, K.S. (1994). Lagrangian stochastic dispersion model simulations of tracer data in nocturnal flows over complex terrain. *Atmospheric Environment*, **21**, 3417-3431.
- Luhar, A. and B. Sawford (1995). Lagrangian stochastic modelling of the coastal fumigation phenomenon, *J. Appl. Meteorol.*, **34**, 2259-2277.
- Luhar, A., M. Hibberd, and P. Hurley (1996). Comparison of Closure Schemes used to Specify the Velocity PDF in Lagrangian Stochastic Dispersion Models for Convective Conditions, *Atmospheric Environment*, **30**, 1407-1418.
- Luhar, A. K., Hibberd, M. F. and Borgas, M. S., (2000). A skewed meandering plume model for concentration statistics in the convective boundary layer. *Atmospheric Environment*, **34**, 3599-3616.
- Lyons, W.A., Pielke, R.A., Tremback, C.J., Walko, R.L., Moon, D.A. and Keen, C.S. (1995). Modeling impacts of mesoscale vertical motions upon coastal zone air pollution dispersion. *Atmospheric Environment*, **29**, 283-301.
- Mahrt, L. (1999). Stratified atmospheric boundary layers. *Boundary Layer Meteorology*, **90**, 375-396.
- Maryon, R.H. and Buckland, A.T. (1994). Diffusion in a Lagrangian multiple particle model: a sensitivity study. *Atmospheric Environment*, **28**, No. 12, 2019-2038.
- McNider, R. (1981). Investigation of the impact of topographic circulations on the transport and dispersion of air pollutants, PhD Dissertation, Department of Environmental Sciences, University of Virginia, Charlottesville.
- McNider, R.T. and Pielke, R.A. (1981). Diurnal boundary-layer development over sloping terrain. *J. Atmos. Sci.*, **38**, 2198-2212.
- McNider, R.T., Moran, M.D. and R.A. Pielke (1988). Influence of diurnal and inertial boundary-layer oscillations on long-range dispersion. *Atmospheric Environment*, **22**, 2445-2462.
- Monin, A.S. and Yaglom, A.M., (1965). *Statistical fluid mechanics: mechanics of turbulence*. Vol.1, MIT Press, p.225.
- Mosca, S., Bianconi, R., Bellasio, R., Graziani, G. and Klug, W. (1998). ATMES II – Evaluation of Long-range Dispersion Models using data of the 1st ETEX release. EUR 17756 EN.
- Nasstrom, J.S. and D.L. Ermak (1999a). A homogeneous Langevin equation model, Part I: simulation of particle trajectories in turbulence with a skewed velocity distribution. *Boundary-Layer Meteorol.*, **92**, 343-369.

Nasstrom, J.S. and D.L. Ermak (1999b). A homogeneous Langevin equation model, Part II: simulation of dispersion in the convective boundary layer. *Boundary-Layer Meteorol.*, **92**, 371-405.

Nodop, K, Ed (1997). ETEX Symposium on Long-Range Atmospheric Transport, Model Verification and Emergency Response. *Proceedings of the ETEX Symposium*, Wien (Austria), 13-16 May 1997, EUR 17346 EN.

Noonan, J.A., Physick, W.L., Carras, J. and D. Williams, (1994). Dispersion modelling and observations from elevated sources in coastal terrain, pp 533-540. *Air Pollution Modelling and its Application X*, Edited by S-V. Gryning and M.M. Millan, Plenum Press, New York.

Obukhov, (1959). Description of turbulence in terms of Lagrangian variables. *Adv. Geophys.*, **6**, 113-116.

Oettl, D., R. A. Almbauer, and P. J. Sturm, (2001). A new method to estimate diffusion in stable, low wind conditions. *J. of Appl. Meteor.*, **40**, 259-268.

Olesen, H.R. (1995). Datasets and protocol for model validation *Int. J. Environment and Pollution*, **5**, N. 4-6, 693-701.

Olesen, H. (1998). Tools for model validation. In: S.E. Gryning and N. Chaumerliac, eds., *Air pollution modelling and its applications, XII*, Plenum Press, New York, 665-672.

Panofsky, H.A., Tennekes, H., Lenschow, D.H. and Wyngaard, J.C. (1977). The characteristics of turbulent velocity components in the surface layer under convective conditions. *Boundary Layer Meteorology*, **11**, 335-361.

Pearson, K. (1894). Contributions to the mathematical theory of evolution, *Philosophical Transactions of the Royal Society of London*, **185 - Part I**, 71-110.

Physick, W.L., Noonan, J.A., Manins, P.C, Hurley, P.J. and H. Malfroy (1994a). Application of coupled prognostic windfield and Lagrangian dispersion codes for air quality purposes in a region of coastal terrain. *Air Pollution Modelling and its Applications IX*, H. Van Dop and G. Kallos, eds., Plenum Press, New York.

Physick, W.L., J.A. Noonan, J.L. McGregor, P.J. Hurley, D.J. Abbs and P.C. Manins (1994b). LADM: A Lagrangian Atmospheric Dispersion Model. *CSIRO Division of Atmospheric Research Technical Report No. 24*, 146 pp.

Physick, W.L., Hurley, P.J. and P.C. Manins, (1995). Environmental impact assessment of industrial development at Gladstone, Australia. *Int. J. Environment and Pollution*, **5**, 548-556.

Physick, W.L. (1996). Photochemical smog studies in Australian cities, *Urban Air Pollution, Vol.2*, H. Power and N. Moussiopoulos, Eds., Computational Mechanics Publications, Southampton, Boston, pp. 141-184.

Pielke, R.A., Cotton, W.R., Walko, R.L., Tremback, C.J., Lyons, W.A., Grasso, L.D., Nicholls, M.E., Moran, M.D., Wesley, D.A., Lee, T.J. and Copeland, J.H., (1992). A Comprehensive Meteorological Modeling System -RAMS. *Meteorology and Atmospheric Physics*, **49**, 69-91.

Poulos, G.S. and Bossert, J.E. (1995). An observational and prognostic numerical investigation of complex terrain dispersion. *J. Appl. Meteorol.*, **34**, 650-669.

Reid, J.D (1979). Markov chain simulations of vertical dispersion in the neutral surface layer for surface and elevated releases. *Boundary Layer Meteorology*, **16**, 3-22

- Reynolds, A.M., 1998, Comments on the Universality of the Lagrangian velocity structure function constant (C_0) across different kinds of turbulence, *Boundary-Layer Meteorology*, **89**, 161-170.
- Ries, R., Heil, O. and Wichmann-Fiebig, M. (1997). Intercomparison of Lagrangian dispersion models and validation with Lillestrøm data *Int. J. Environment and Pollution*, **8**, 3-6.
- Robinson, J., Mahre, Y. and E.Wakshal. (1992). The effects of mesoscale circulation on the dispersion of pollutants (SO_2) in the eastern Mediterranean, southern coastal plain of Israel. *Atmospheric Environment*, **26B**, 271-277.
- Rodean, H.C. (1994). Notes on the Langevin model for turbulent diffusion of “marked” particles. Techn. Report UCRL-ID-115869, Lawrence Livermore National Laboratory, 122 pp.
- Rodean, H.C. (1996). Stochastic Lagrangian models of turbulent diffusion. Meteorological Monographs, 26, Amer. Met. Soc., Boston, USA.
- Rotach, M. (1998). Urban simulation of the Lillestrøm and Indianapolis data sets 5th Conference on Harmonization within ADM for regulatory purposes 18-21 May, Rodos, Greece.
- Rotach, M., S. Gryning and C. Tassone (1996). A two-dimensional Lagrangian stochastic dispersion model for daytime conditions, *Q. J. R. Meteorol. Soc.*, **122**, 367-389.
- Rotach, M.W and de Haan, P., 1997, On the Urban Aspect of the Copenhagen Data Set, *Int. J. Environment and Pollution*, **8**, Nos. 3-6, 279-286.
- Rotach, M.W., 1999, On the Influence of the Urban Roughness Sublayer on Turbulence and Dispersion, *Atmospheric Environment*, **33**, 4001–4008.
- Rotach, M.W., 2001, Simulation of urban-scale dispersion using a Lagrangian stochastic dispersion model, *Boundary-Layer Meteorology*, **99**, 379-410.
- Sagendorf, J. F., and C. R. Dickson, (1974). Diffusion Under Low Windspeed, Inversion Conditions. *NOAA Technical Memorandum ERL ARL-52, National Oceanic and Atmospheric Administration*, Air resources laboratory 1750 Foote Drive, Idaho Falls, Idaho 83402, 89 pp.
- Sawford, B.L. (1985). Lagrangian simulation of concentration mean and fluctuation fields. *J. Clim. Appl. Met.*, **16**, 3-22.
- Sawford, B. and F. Guest (1987). Lagrangian stochastic analysis of flux-gradient relationships in the convective boundary layer, *J. Atmos. Sci.*, **44**, 1152-1165.
- Sawford, B.L. and Guest, F.M., (1988). Uniqueness and universality of Lagrangian stochastic models of turbulent dispersion, *8th Symposium on Turbulence and Diffusion*, San Diego, CA, A.M.S., 96-99.
- Sawford, B.L. (1991). Reynolds number effects in Lagrangian stochastic models of turbulent dispersion. *Phys. Fluids*, **A3**, 1577-1566.
- Sawford, B.L. (1993). Recent developments in the Lagrangian stochastic theory of turbulent dispersion. *Boundary Layer Meteorology*, **62**, 197-215.
- Sawford, B.L. and Borgas, M.S. (1994). On the continuity of stochastic models for the Lagrangian velocity in turbulence. *Physica D*, **76**, 297-311.

Sawford, B., A. Luhar, J. Hacker, S. Young, I.-H. Yoon, J. Noonan, J. Carras, D. Williams and K. Rayner (1998). The Kwinana coastal fumigation study: I-Program overview, experimental design and selected results, *Boundary Layer Meteorology*, **89**, 359-384.

Schuepp, P. H., Leclerc, M. Y., MacPherson, J. I. and R.L. Desjardins (1990). Footprint prediction of scalar fluxes from analytical solutions of the diffusion equation. *Boundary Layer Meteorology*, **50**, 355-373.

Segal, M., Pielke, R.A., Arritt, R.W., Moran, M.D., Yu, C-H and Henderson, D. (1988). Application of a mesoscale atmospheric dispersion modeling system to the estimation of SO₂ concentrations from major elevated sources in southern Florida. *Atmospheric Environment*, **22**, 1319-1334.

Smith, F.B. (1968). Conditional particle motion in a homogeneous turbulent field. *Atmospheric Environment*, **2**, 491-508.

Sorbjan, Z. (1989). Structure of the atmospheric boundary layer. Prentice Hall, New Jersey, 317 pp.

Stohl, A. and Thomson, D.J., 1999. A density correction for Lagrangian particle dispersion models. *Boundary-Layer Meteorology* **90**, 155-167.

Stull, R.B. (1988). An introduction to Boundary Layer Meteorology, Kluwer Academic Publishers, Boston, 666 pp.

Sun, W.Y. (1993). Numerical simulation of a planetary boundary layer. Part I: Cloud-free case. *Beitr. Phys. Atmos.*, **66**, 3-16.

Tassone, C., Gryning, S.E. and Rotach, M., (1994). A random walk model for atmospheric dispersion in the daytime boundary layer. In: *Air Pollution Modeling and Its Application X*, S.E.Gryning and Millan M. Millan editors, Plenum Press, 243-251.

Taylor, G.I. (1921). Diffusion by continuous movements. Proc. London Math. Soc., Ser. 2, **20**, 196-211.

Tennekes, H. (1982). Similarity relations, scaling laws and spectral dynamics In: Atmospheric turbulence and air pollution modelling (edited by F.T.M. Nieuwstadt and H. van Dop), Reidel, Dordrecht, 37-68.

Thomson, D.J. (1984). Random walk modelling of diffusion in inhomogeneous turbulence. *Quart. J. Roy. Meteor. Soc.*, **110**, 1107-1120.

Thomson, D.J. (1987). Criteria for the selection of stochastic models of particle trajectories in turbulent flows. *J. Fluid Mech.*, **180**, 529-556.

Thomson, D.J. (1990). A stochastic model for the motion of particle pairs in isotropic high-Reynolds-number turbulence and its application to the problem of concentration variance. *J. Fluid Mech.*, **210**, 113-153.

Thomson, D.J., and Montgomery, M.R., (1994). Reflection boundary conditions for random walk models of dispersion in non-Gaussian turbulence. *Atmospheric Environment*, **28**:1981-1987.

Thomson, D.J., Physick, W.L., and Maryon, R.H., (1997). Treatment of interfaces in random walk dispersion models. *J. Appl. Meteor.*, **36**(9), 1284-1295.

- Tinarelli, G., Anfossi, D., Brusasca, G., Ferrero, E., Giostra, U., Morselli, M.G., Moussafir, J., Tampieri, F. and Trombetti, F. (1994). Lagrangian particle simulation of tracer dispersion in the lee of a schematic two-dimensional hill. *J. Appl. Meteor.*, **33**, No. 6, 744-756.
- Tinarelli, G., Anfossi, D., Bider, M., Ferrero, E. and Trini Castelli, S. (2000). A new high performance version of the Lagrangian particle dispersion model SPRAY, some case studies. *Air Pollution Modeling and its Application XIII*, Gryning, S.E. and Batchvarova, E., Eds.
- TRC (1986). Urban Power Plant plume studies. *EPRI Report EA-5468*, EPRI, 3412 Hillview Ave., Palo Alto, Ca 94304.
- Tremback, C.J., Lyons, W.A., Thorson, W.P. and Walko, R.L. (1993). An emergency response and local weather forecasting software system. *Air Pollution and its Application X*, 423-429.
- Trini Castelli, S. and Anfossi, D. (1997). Intercomparison of 3D turbulence parameterisations for dispersion models in complex terrain derived from a circulation model, *Il Nuovo Cimento*, **20 C**, 3, 287-313.
- Trini Castelli, S. (2000). MIRS: a turbulence parameterisation model interfacing RAMS and SPRAY in a transport and diffusion modelling system. *Int. Rep. ICGF/CNR* No 412/2000.
- Uliasz, M. (1994). Lagrangian particle dispersion modelling. In: *Environmental Modeling, Vol II*, Computational Mechanics Publications, Southampton.
- van Dop, H., Nieuwstadt, F.T.M. and Hunt, J.C.R. (1985). Random walk models for particle displacements in inhomogeneous unsteady turbulent flows, *Phys. Fluids*, **28**, 1639-1653.
- van Dop, H. and Nodop, K. Guest, Eds. (1998). ETEX, a European Tracer Experiment. *Atmospheric Environment*, Vol. 32, no. 24, December 1998, 4089-4378. (S.-E. Gryning and M. M. Millan), Plenum Press, New York, pp.315–323.
- van Ulden, A.P. and Holtslag, A.A.M. (1985). Estimation of atmospheric boundary layer parameters for diffusion applications. *J. Clim. And Appl. Meteorol.*, **24**, 1196-1207.
- Vinter Falk, A.K. (1998). Footprint analysis from random walk models for atmospheric dispersion. Ph.D. Thesis, Technical University of Denmark, Dept of Mathematics, 98 pp.
- Wang, L.-P., and D.E. Stock, (1992). Stochastic Trajectory Models for Turbulent Diffusion: Monte-Carlo Process versus Markov Chains. *Atmospheric Environment*, **9**, 1599-1607.
- Weil, J.C. (1990). A diagnosis of the asymmetry in top-down and bottom-up diffusion using a Lagrangian stochastic model, *J. Atmos. Sci.*, **47**, 501-515.
- Weil, J. C., (1994). A hybrid Lagrangian dispersion model for elevated sources in the convective boundary layer. *Atmospheric Environment* **28**, 3433–3448.
- Willis, G.E. and J. Deardorf (1976). A laboratory model of diffusion into the convective planetary boundary layer. *Quart.J.Roy. Meteorol. Soc.*, **102**, 427-445.
- Willis, G.E. and J. Deardorf (1978). A laboratory study of dispersion from an elevated source within a modeled convective planetary boundary layer. *Atmospheric Environment*, **12**, 1305-1311.
- Willis, G.E. and J. Deardorf (1981). A laboratory study of dispersion from a source in the middle of the convective mixed boundary layer. *Atmospheric Environment*, **15**, 109-117.
- Willis, G. and J. Deardorff (1983). On plume rise within a convective boundary layer, *Atmospheric Environment*, **17**, 2435-2447.

- Willis, G. and J. Deardorff (1987). Buoyant plume dispersion and entrainment in and above a laboratory mixed layer, *Atmospheric Environment*, **21**, 1725-1735.
- Wilson, K.D. (1997). A three-dimensional correlation/spectral model for turbulent velocities in a convective boundary layer. *Boundary Layer Meteorology*, **85**, 35-52.
- Wilson, R. B., Start, G.E., Dickson, C. R. and Ricks, N.R. (1976). Diffusion under low wind speed conditions near Oak Ridge, Tennessee. NOAA Technical Memorandum, ERL ARL-61.
- Wilson, J., G. Thurtell, and G. Kidd (1981). Numerical simulation of particle trajectories in inhomogeneous turbulence, II: systems with variable turbulent velocity scale, *Boundary Layer Meteorology*, **21**, 423-441.
- Wilson, J.D., Legg, B.J. and Thomson, D.J. (1983). Calculation of particle trajectories in the presence of a gradient in turbulent-velocity variance. *Boundary Layer Meteorology*, **27**, 163-169.
- Wilson, J. D. and G.E. Swaters (1991). The source area influencing a measurement in the planetary boundary layer: the “footprint” and the “distribution of contact distance”. *Boundary Layer Meteorology*, **55**, 25-46.
- Wilson, J.D. and Flesch, T.K. (1993). Flow boundaries in random-flight dispersion models: enforcing the well-mixed condition. *J. Appl. Meteor.*, **32**, 1695-1707.
- Wilson, J.D., Thurtell, G.W. and Kidd, G.E. (1981). Numerical simulation of particle trajectories in inhomogeneous turbulence Part II: Systems with variable turbulence velocity scale. *Boundary Layer Meteorology*, **21**, 423-441.
- Wyngaard, J.C., Cote, O.R. and Rao, K.S. (1974). Modelling of the atmospheric boundary layer, *Adv. in Geophys.*, **18A**, Academic Press, 193-212.
- Yamada, T. (1985). Numerical simulations of the night 2 data of the 1980 ASCOT experiments in the California Geysers area. *Archiv. for Meteorol., Geophys. and Bioclim.*, **34**, 223-247.
- Yamada, T., and S.S. Bunker (1988). Development of a nested grid, second moment turbulence closure model and application to the 1982 ASCOT Brush Creek data simulation. *J. Appl. Meteor.*, **27**:562-578.
- Yee, E. and Wilson, D. J., (2000). A comparison of the detailed structure in dispersing tracer plumes measured in grid-generated turbulence with a meandering plume model incorporating internal fluctuations. *Boundary Layer Meteorology*, **94**, 253-296.
- Zannetti, P. (1981). An improved puff algorithm for plume dispersion simulation. *J. Appl. Meteor.*, **20**, 1023-1211.
- Zannetti, P. (1984). New Monte Carlo scheme for simulating Lagrangian particle diffusion with wind shear effects. *Appl. Math. Modeling*, **8**, 188-192.
- Zannetti, P. (1990). *Air pollution modeling. Theories, Computational Methods and Available Software*. Van Nostrand Reinhold, New York.
- Zilitinkevich, S.S. (1972). On the determination of the height of the Ekman boundary layer. *Boundary Layer Meteorology*, **3**, 141-145.

BRANK P 2009

Pun, B.K. et al. 2005. *Atmospheric Transformations*. Chapter 12 of *AIR QUALITY MODELING – Theories, Methodologies, Computational Techniques, and Available Databases and Software. Vol. II – Advanced Topics* (P. Zannetti, Editor). Published by The EnviroComp Institute (<http://www.envirocomp.org/>) and the Air & Waste Management Association (<http://www.awma.org/>).

Chapter 12

Atmospheric Transformations

Betty K. Pun ⁽¹⁾, Christian Seigneur ⁽²⁾ and Hope Michelsen ⁽³⁾

⁽¹⁾ *Atmospheric and Environmental Research, Inc., San Ramon, CA (USA)*
pun@aer.com

⁽²⁾ *Atmospheric and Environmental Research, Inc., San Ramon, CA (USA)*
seigneur@aer.com

⁽³⁾ *Sandia National Laboratories, Livermore, CA (USA)*
hamiche@ca.sandia.gov

Abstract: A typical air quality model tracks the transport and transformation of chemicals in the atmosphere. Transport refers to physical movement (dispersion, emissions, and deposition) of pollutants. Atmospheric transformations encompass both physical and chemical changes of chemicals in the atmosphere. In this chapter, we provide a review of the fundamentals of gas phase chemical reactions, phase transitions, aqueous phase reactions, and an overview of the key processes involved in the formation of ozone, particulate matter, hazardous air pollutants, and halogen chemistry. Modeling air quality entails the mathematical representation of the atmospheric transformations and the numerical solution of the algebraic equations and ordinary differential equations, which are developed in this chapter. The modeling of chemical transformations is discussed, starting with plume models and the gas-phase chemistry at different stages of the plume. We then describe several Eulerian models and their atmospheric mechanisms, including the Carbon Bond Mechanism (CBM)-IV, the Statewide Air Pollution Research Center mechanisms, the Regional Acid Deposition Model mechanism version 2, etc. The modeling of particulate matter and droplets requires a mathematical description of the aqueous-phase and heterogeneous chemistry. Modules that describe the gas/particle partitioning of inorganic species and organic species are discussed. The distribution of the semi-volatile products of gas-phase, aqueous, and heterogeneous reactions onto particles depends on the representation of the particle size distribution. In one-atmosphere approach, a single model would suffice if it included a comprehensive chemical mechanism containing all gas-phase, heterogeneous, and aqueous-phase reactions for all air pollutants of concern and a phase transition module describing all relevant dynamic processes for different types of particles. In practice, chemical mechanisms have been developed to describe the chemical transformation processes for different air pollutants. Therefore, in addition to models describing ozone and particulate matter (PM), specific models exist for hazardous air pollutants and other models describe the stratosphere. To complete the overview of available models for chemical transformations, plume-in-grid type models that combine plume chemistry with urban/regional chemistry are discussed.

Key Words: secondary air pollutants, urban ozone, particulate matter, stratospheric ozone, hazardous air pollutants, thermodynamics, atmospheric chemistry, radicals, heterogeneous and aqueous reactions, chemical mechanisms, kinetics, chemical transport models, plume-in-grid.

1 Introduction

The atmosphere can be viewed as a reactor of sorts, where anthropogenic and biogenic emissions undergo long- and short-range transport processes, chemical reactions, and phase transitions to produce the pollution problems that affect human health and ecological welfare. The role of atmospheric chemistry is particularly important in the following air pollution issues:

1. Tropospheric ozone (O₃) and photochemical smog
2. Fine particulate matter (PM), which also causes regional haze and visibility degradation
3. Global climate change
4. Acid deposition
5. Hazardous air pollutants
6. Stratospheric O₃ depletion

These problems range in geographical scales. Tropospheric O₃ and photochemical smog may be of urban to regional scale, and sometimes involve long range transport, e.g., up the East Coast of the United States or intercontinental transport from Asia to America (Berntsen et al., 1999; Jacob et al., 1999; Wilkening et al., 2000) or from America to Europe (Hogue, 2001). Fine PM¹ of aerodynamic diameter less than 2.5 μm (PM_{2.5}) is an urban pollutant implicated in increased incidences of cardiovascular and pulmonary illness (Health Effects Institute, 2001). On a regional scale, the same small particles contribute to haze and visibility reduction in pristine areas. Acid deposition is typically a regional problem involving acidic gases and PM. PM may also have a substantial influence in the Earth's climate via its effect on the global radiation budget and as cloud condensation nuclei. Toxic air pollutants, including transition metals and persistent organic pollutants, may have local, urban, regional, and global impacts. Halogen-containing compounds are the culprits for stratospheric ozone depletion, which is a global problem.

This chapter provides an overview of the atmospheric transformation processes that are relevant for the air pollution problems at hand. Sections 2 to 5 present the scientific fundamentals. Section 2 introduces gas-phase chemical reactions that are responsible for the formation of O₃ and other pollutants that constitute photochemical smog. In Section 3, we introduce heterogeneous processes, which involve either phase transition or chemical reactions in a liquid phase. Sections 4 and 5 are devoted to the discussions of air toxics and halogen chemistry, respectively. For more details, the readers can refer to any of a number of

¹ The term "fine PM" refers to PM_{2.5} in the United States but to PM₁₀ in Europe. We adopt the United States convention in this chapter.

atmospheric chemistry textbooks, including Finlayson-Pitts and Pitts (2000), Seinfeld and Pandis (1998), Wayne (1991), and Warneck (1988). Mathematical representation and current models for urban-regional air pollution are discussed in Sections 6 to 9. Section 6 focuses on the modeling of gas-phase processes. The mathematical techniques for heterogeneous and aqueous processes are discussed in Section 6. In Section 8 we will discuss plume models. We finish Section 8 with plume-in-grid models, which provide more detailed treatment of atmospheric dispersion of large point sources than Eulerian models, and include relevant chemistry for plumes with higher concentrations than the conditions treated in Eulerian models. In Section 9, we start with the Eulerian models that describe the atmospheric chemistry and transport processes. Additional details of air quality models can be found in Jacobson (1999) and Seinfeld and Pandis (1998) and a number of reviews that are mentioned in the text. Available modeling resources on the World Wide Web include the Community Modeling and Analysis System website (www.cmascenter.org).

2 Gas-Phase Transformations

Atmospheric reactions frequently involve free radicals. Free radicals are reactive species with unpaired electrons in their outer shells. A typical oxidant in the lower atmosphere is the hydroxyl radical (OH). In a hydroxyl radical, the oxygen atom has a total of 7 electrons on its outermost shell (Figure 1), which needs 8 to fill. Therefore, the OH radical has a tendency to snatch hydrogen atoms from other molecules to form a stable water molecule (all outer shells filled).

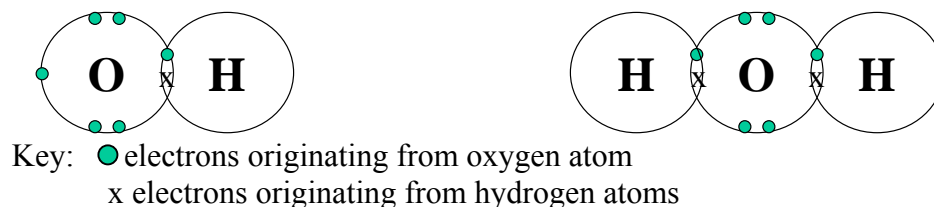


Figure 1. Electronic structures of hydroxyl radical and water molecule.

The molecule that lost a hydrogen atom becomes a free radical. Hence, free radical reactions typically generate free radicals in a chain of reactions. These reactions are terminated when two free radicals combine to form a stable molecule.

2.1 Chemistry of Nitrogen and Oxygen Species

So how do free radicals come about? Typically the formation of free radicals involves breaking a bond (a pair of electrons shared by two atoms) in a stable molecule to form two radicals with unpaired electrons. Solar radiation usually provides the burst of energy required for breaking up a bond. Many stable

molecules absorb photons with specific wavelengths or energy content. If the absorbed energy is large enough (larger than the strength of the bond holding the molecule together), the molecule may break apart and form radicals. This type of reaction is called photolysis in atmospheric chemistry. An example is the photolysis of nitrogen dioxide (NO_2)



In the above reaction, $h\nu$ denotes a photon that is absorbed by NO_2 . NO_2 absorbs over the entire range of UV and visible radiation in the solar spectrum (wavelengths of 300-700 nm). The dissociation of NO_2 forms a nitric oxide (NO) and an oxygen atom. NO is a radical that is stabilized through a process called resonance, meaning that the unpaired electron is delocalized and can be associated with either the N atom or the O atom. The O atom typically reacts with an oxygen molecule (O_2) in the lower troposphere in a combination reaction:



In this reaction, M denotes a third body (typically nitrogen (N_2) or O_2 gas) that serves to remove the excess energy released in the combination of O with O_2 . The resulting molecule is O_3 , which is the key component of photochemical smog. O_3 is chemically reactive, although it is not considered a free radical. The reaction between O_3 and NO is fast



At night, when the photolytic Reaction 1 stops due to the lack of sunlight, Reaction 3 controls the concentrations of O_3 , NO , and NO_2 . As Reaction 3 goes to completion, either O_3 or NO will be depleted, and the more abundant compound will coexist with NO_2 . During the day, Reactions 1, 2, and 3 would be in a photostationary state in an atmosphere that contains only nitrogen and oxygen species. Under photostationary state conditions, the relative concentrations of O_2 , O_3 , NO , and NO_2 would remain constant as the cycle of reactions churns around. (We will discuss the concept of photostationary state some more when we talk about reaction kinetics in Section 6.) However, the stationary state of Reactions 1, 2, and 3 is modified by the presence of hydrogen and carbonaceous species.

2.2 Carbon and Hydrogen Perturbation of N-O Chemistry

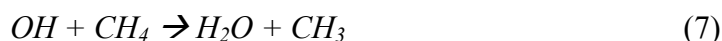
The photostationary state established by Reactions 1, 2, and 3 is perturbed by the presence of OH and carbonaceous species (e.g., CO, methane) even in remote locations. OH originates from the photolysis of O_3



$O(^1D)$ is an oxygen atom in an excited electronic state. It has sufficient energy to break up a water molecule. Two OH radicals are formed in this reaction.



OH is considered the main oxidant in the lower atmosphere. For example, it reacts with carbon monoxide and methane; both are quite ubiquitous in the atmosphere.



Both H and CH_3 , the simplest alkyl group, are very reactive radicals that combine with O_2 in the lower atmosphere to form the hydroperoxyl and methylperoxyl radicals:



When NO is present in the atmosphere, the main reactions for the peroxy radicals are



Therefore, the peroxy radicals do the work for O_3 in Reaction 3. Since NO_2 photolyzes and eventually leads to the formation of O_3 (Reactions 1 and 2), its formation without consuming O_3 allows more O_3 to exist in an environment with a source of peroxy radicals than in an oxygen-nitrogen atmosphere. In Reaction 10, OH is regenerated, and can initiate another cycle of reactions. In Reaction 11, the methoxyl radical product can continue the chain of reactions.

2.3 Complex Organics and Smog Formation

We continue with the reactions of the methoxyl radical, which is the simplest of all alkoxy radicals. The methoxyl radical reacts with O_2 and forms HO_2 and formaldehyde (HCHO).

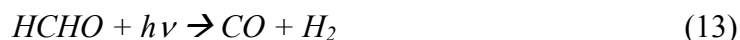


More complex alkoxy radicals can also decompose into alkyl radicals and carbonyl compounds (aldehydes and ketones), or undergo isomerization to generate an alkyl radical with a hydroxy functional group. For these reactions,

the readers may refer to detailed discussions found in Atkinson (1997). We are going to focus on the simpler reactions for illustrative purposes. Of the products of Reaction 12, the fate of HO₂ has been discussed. What happens to the HCHO?

HCHO is the simplest homologue of aldehydes (RCHO). Aldehydes and other carbonyls, i.e., compounds containing the double-bonded carbon-oxygen moiety (C=O) are products of the atmospheric oxidation of many aliphatic hydrocarbons, such as alkanes, alkenes, and alcohols.

Formaldehyde and other simple carbonyls may undergo photolysis. For example,



Reaction 13 produces stable products, while Reaction 14 leads to the formation of two new radicals. Reaction 14 is an example of an “initiation” reaction in the terminology of radical reactions. All aldehydes also react with OH, e.g.,



Like its unsubstituted counterpart, CH₃, HCO quickly reacts with O₂



However, the larger members of the acyl radical family combine with O₂



Here, the (O) notation represents a carbonyl bond. This acyl peroxy radical may undergo an analogous reaction to Reaction 11, or it may also react with NO₂ in a combination reaction



The product of this reaction is a peroxy acetyl nitrate, or PAN. The net effect of Reaction 18a is the removal of a radical, and this reaction can therefore be considered a “termination” reaction. However, this radical removal is not permanent, as PAN can dissociate back into the reactants



An example of a more permanent termination product is nitric acid (HNO₃)



In environments where NO_x is not abundant, organic radicals may react with HO_2 in another termination reaction, e.g.,



Without these termination reactions, alkyl radicals, such as that formed in Reaction 11, will continue generating carbonyls and more radicals. The cycle of reactions HO_2/OH and RO_2/RO converts NO to NO_2 , which then photolyzes to produce O_3 . These reaction cycles are depicted in Figure 2. Hence, the presence of organic compounds enhances the formation of O_3 via the reactions of organic radicals with NO_x .

We have used simple alkanes and aldehydes to illustrate the atmospheric radical chain reactions involving volatile organic compounds (VOC) that are responsible for the formation of smog. In addition to alkanes and aldehydes, other classes of VOC, such as alkenes and aromatic compounds, also participate in smog-producing reactions. Alkenes can be of anthropogenic and biogenic origins, and are typically quite reactive towards OH , O_3 , and NO_3 . Aromatic compounds react typically with OH ; certain ones also react with NO_3 . However, the current understanding of aromatic chemistry is incomplete, so that many of the secondary products remain unidentified. Nonetheless, both classes of compounds are of interest as precursors to secondary organic aerosols, as discussed in Section 2.4.

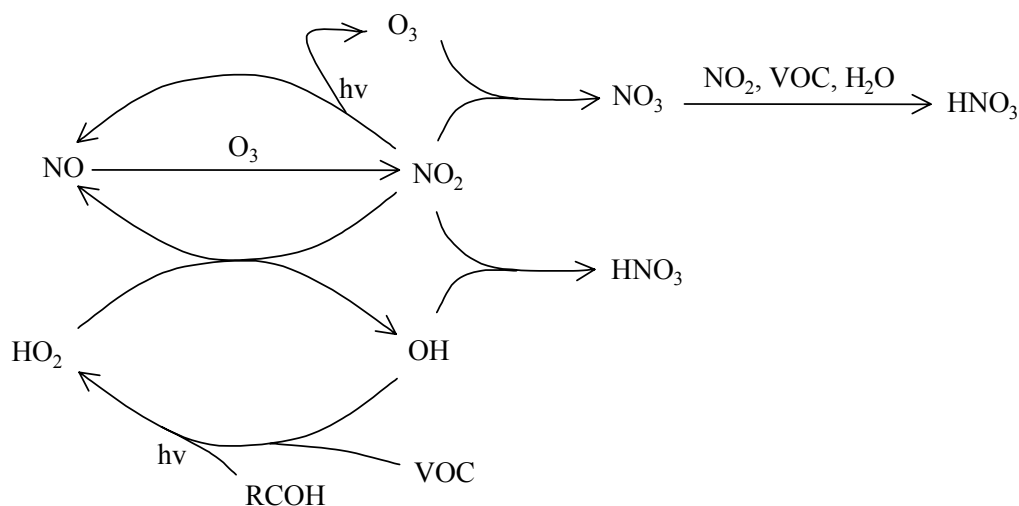


Figure 2. Major chemical cycles involved in the gas-phase production of secondary pollutants, O_3 and HNO_3 (Source: Pun et al., 2001; reprinted with permission of A&WMA).

2.4 Gas-Phase Formation of Condensable Compounds

Organic compounds with certain properties may partition out of the gas phase and into particles. Typically, the affinity for the gas phase is reflected in a compound's saturation vapor pressure - the higher the saturation vapor pressure, the more likely a compound will stay in the gas phase, and vice versa. The presence of functional groups decreases the saturation vapor pressure of a compound. Because functional groups also tend to be more polar than hydrocarbons, functional groups may also increase the water solubility of an organic compound. Solubility and vapor pressure are two parameters that govern the affinity of a compound towards aqueous or organic liquid (or in some cases, solid) phases that are likely to be present in atmospheric particles. Many organic compounds, especially those containing functional groups, have been identified in atmospheric particles. Table 1 lists some of these compounds.

Table 1. Organic compounds in atmospheric particles (source: Saxena and Hildemann, 1996; Schauer and Cass, 1999).

Saxena and Hildemann, 1996	Schauer and Cass, 1999
C10-C34 n-alkanes	Alkanes
C9-C30 n-alkanoic and n-alkenoic acids & their esters	n-alkanoic acids
C10-C35 n-alkanols	n-alkenoic acids
C9, C14 aldehydes	Dicarboxylic acids
Dehydroabietic and other diterpenoid acids and retene	Syringol and substituted syringols
Phthalic and other aromatic polycarboxylic acids & their esters	Aromatic acids
Polycyclic aromatic hydrocarbons (PAH)	PAH
Polycyclic aromatic ketones and quinones	Guaiacols and substituted guaiacols
Cholesterol and other steroids	Substituted phenols
1,2-dimethoxy-4-nitro-benzene and other aromatic N-containing compounds	Resin acids
Lignans	Sugars
Cellulose	

Some compounds listed in Table 1 are emitted directly, either as semi-volatile gases or as particles. In fact, many of the compounds listed in Table 1 are so unique to particular sources that they can be used as tracers to establish the presence or even the fractional contribution of particular sources to particles in an area. Compounds with functional groups can also be formed in the atmosphere. As we have seen in Section 2.3, gas-phase chemical reactions of volatile organic compounds can result in the formation of products that contain functional groups.

These products include aldehydes, ketones, carboxylic acids, alcohols, and nitrates.

Compounds with multiple functional groups are of interest because they can dissolve in aqueous particles that are quite ubiquitous in the lower troposphere. Pun et al. (2000) have investigated the formation of multifunctional compounds from volatile precursors. They concluded that many simple hydrocarbons may act as precursors to very complex organic products, especially via several generations of intermediates. Table 2 shows several classes of multifunctional compounds that may be present in the particulate phase and their possible precursors. These precursor-product relationships were determined based on known gas-phase reactions of which those described in the earlier sections of this chapter are a subset.

Table 2. Multi-functional compounds and likely precursors (source: Pun et al., 2000).

Compounds	Precursors	Intermediates
Dicarboxylic Acids	Diene	Unsat. Monocarboxylic Acid
	Diene	Unsat. Monocarboxylic Acid Unsat. Aldehyde
Dicarboxylic Acids	(ω)-Oxo-Monocarboxylic Acid	See ketoacid entries
α , β Dicarbonyls	Aromatic Compounds	
Dicarbonyls	(a) Cycloalkene / (b) Cycloalkane	
	(a) Alkane / (b) Alkene / (c) Alcohol	Ketone
	Diene	Unsaturated Carbonyl*
	(a) Alkane / (b) Alkene / (c) Unsaturated alcohol / (d) Polyol	Hydroxy Ketone
Ketoacids	Cycloalkene	
	Alkene	Carboxylic Acid
	(a) Alkane / (b) Alkene / (c) Alcohol	Carboxylic Acid, aldehyde
	Diene	Unsaturated Carboxylic Acid
	Diene	Unsaturated Carboxylic Acid, Unsaturated Aldehyde
	Hydroxyacid (see below for secondary formation)	
	Diene	Unsaturated Carbonyl
	Dicarbonyl (Ketoaldehyde) (see above for secondary formation)	
Polyols, e.g. Polyhydroxycarbonyls (Secondary poly-hydroxy compounds also contain carbonyl groups)	Alkane (branched)	
Polyhydroxycarbonyls	Alkene (especially α , β -dihydroxy product) (or) Unsaturated alcohol	

	Branched alcohol	
	Polyol	
Multifunctional compounds # Hydroxycarboxylic Acids	Hydroxy-Alkene	
	Diene	Hydroxy-oxo-alkene
	(a) Alkane / (b) Alkene / (c) Unsat. Alcohol / (d) Branched alcohol / (e) Diol	Hydroxyaldehyde see analogous polyhydroxycarbonyl entries
Hydroxycarboxylic Acids	Diene	Hydroxy-oxo-alkene
Hydroxy-oxo-carboxylic Acids	Diene	Unsat. Carboxylic Acid
	Diene	Unsat. Carboxylic Acid, Unsat. Aldehyde
	Alkene	Carboxylic Acid
Hydroxy-oxo-carboxylic Acids	(a) Alkane / (b) Alkene / (c) Alcohol	Carboxylic Acid, Aldehyde
Nitrophenols	Aromatic compounds	(Phenol)

* Unsaturated carbonyl compounds may be emitted from vegetation.

Multifunctional compounds with acidic / basic and carbonyl groups

3 Heterogeneous and Aqueous Processes

Whereas gas-phase chemistry plays an important role in air pollution problems, the roles of heterogeneous and aqueous processes are also vital in the production of PM_{2.5}, regional haze/visibility degradation, and acid deposition. These processes include phase transition, a physical process, and heterogeneous and aqueous chemical reactions. In this section, we focus primarily on secondary pollutants, nitrate, sulfate, and secondary organic aerosol (SOA), but also note that some of the gas/particle conversion processes are also relevant for primary semi-volatile species.

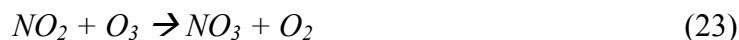
3.1 Gas/Particle Conversion of Inorganic Species

Key inorganic species that convert between gas and particulate phases include sulfuric acid/sulfate, nitric acid/nitrate, hydrochloric acid/chloride, ammonia/ammonium, carbon dioxide/carbonate, and, most definitely, vapor/particulate water. Other non-volatile ions that affect the conversion of these species include sodium, calcium, magnesium, and potassium.

Sulfuric acid (H₂SO₄) and nitric acid (HNO₃) are formed in the atmosphere from emissions of sulfur dioxide (SO₂) and nitrogen oxides (NO_x). In the gas phase, sulfur trioxide (SO₃), which hydrolyzes to form H₂SO₄, is formed in a reaction of SO₂ with OH:



Nitric acid can be formed when NO_2 is oxidized in the atmosphere by OH or O_3 :



Reaction 22 takes place during the day because the concentration of OH drops quickly after sunset. On the other hand, NO_3 tends to photolyze during the day, and the pathway involving NO_3 as an intermediate (24, 25) takes place primarily at night. In addition to the above reactions, HNO_3 is also formed when NO_3 radical abstract hydrogen atoms from hydrocarbons in reactions similar to those discussed in Section 2.2 for the OH radical. There are also two heterogeneous reactions that convert NO_3 or N_2O_5 to HNO_3 . These reactions will be discussed in detail in Section 3.4.

Of the other species that participate in gas/particle conversion, chloride is typically emitted as sea salt particles (as sodium chloride), NH_3 is emitted in gaseous form, and carbonate is emitted in solid form as soil dust with potassium, calcium, and magnesium.

Atmospheric compounds sometimes exist in several states simultaneously. For example, under some conditions, molecular ammonia can exist in the gas phase and the aqueous phase. At the same time, it can be present as ammonium ion. Typically, a species will move from a medium with higher concentration to a medium with lower concentration. Here, concentration may be viewed as the driving force to move from one phase to the other. In the language of thermodynamics, fugacity or activity is used to define this driving force. Any system will progress towards a state of equilibrium between different phases, where the driving force to move from one phase to another is equilibrated between different phases. Some systems may take a long time to reach equilibrium while others reach it almost instantaneously.

The concentrations of the gas-phase and particulate-phase species involved in a thermodynamic equilibrium are typically governed by an equilibrium partition constant. We will explain later how to model equilibria mathematically. We simply note at this point that many species can be in equilibrium with one another simultaneously. For example, in the ammonium/nitrate/sulfate system, the equilibrium relationships that are satisfied are listed in Table 3. Further discussion of the gas/particle (gas/liquid) partitioning process is provided in the aqueous chemistry section (Section 3.3). We will explain the mathematical formulation in greater detail in Section 6. Some of these relationships are between the gas phase and the particle/droplet phase. Other equilibria are

between different aqueous molecules and ions, such as sulfate/bisulfate or aqueous ammonia/ammonium, or between solid species and ions. These equilibrium relationships are functions of temperature, pressure, and relative humidity. For example, higher temperatures favor the gaseous state over the solid or liquid states. Relative humidity governs the amount of water in aqueous particles or droplets, and hence affects aqueous-phase concentrations.

Table 3. Equilibrium relationships in the ammonium/nitrate/sulfate system (source: Nenes et al., 1998).

Reaction	Expression	Equilibrium constant at 298K	Units
$HSO_4^-(aq) \leftrightarrow H^+(aq) + SO_4^{2-}(aq)$	$\frac{[H^+][SO_4^{2-}]\gamma_{H^+}\gamma_{SO_4^{2-}}}{[HSO_4^-]\gamma_{HSO_4^-}}$	0.01015	Mol kg ⁻¹
$NH_{3(g)} \leftrightarrow NH_{3(aq)}$	$\frac{[NH_3]\gamma_{NH_3}}{P_{NH_3}}$	57.64	Mol kg ⁻¹ atm ⁻¹
$NH_{3(aq)} + H_2O_{(aq)} \leftrightarrow NH_4^+(aq) + OH^-(aq)$	$\frac{[NH_4^+][OH^-]\gamma_{NH_4^+}\gamma_{OH^-}}{[NH_{3(aq)}]a_w\gamma_{NH_3}}$	1.805 x 10 ⁻⁵	Mol kg ⁻¹
$HNO_{3(g)} \leftrightarrow H^+(aq) + NO_3^-(aq)$	$\frac{[H^+][NO_3^-]\gamma_{H^+}\gamma_{NO_3^-}}{P_{HNO_3}}$	2.511 x 10 ⁶	Mol ² kg ⁻² atm ⁻¹
$H_2O_{(aq)} \leftrightarrow H^+(aq) + OH^-(aq)$	$\frac{[H^+][OH^-]\gamma_{H^+}\gamma_{OH^-}}{a_w}$	1.01 x 10 ⁻¹⁴	Mol ² kg ⁻²
$(NH_4)_2SO_{4(s)} \leftrightarrow 2NH_4^+(aq) + SO_4^{2-}(aq)$	$[NH_4^+]^2[SO_4^{2-}]\gamma_{NH_4^+}^2\gamma_{SO_4^{2-}}$	1.817	Mol ³ kg ⁻³
$(NH_4)NO_{3(s)} \leftrightarrow NH_{3(g)} + HNO_{3(g)}$	$P_{NH_3}P_{HNO_3}$	5.746 x 10 ⁻¹⁷	Atm ²
$(NH_4)HSO_{4(s)} \leftrightarrow NH_4^+(aq) + HSO_4^-(aq)$	$[NH_4^+][HSO_4^-]\gamma_{NH_4^+}\gamma_{HSO_4^-}$	1.383	Mol ² kg ⁻²
$(NH_4)_3H(SO_4)_2(s) \leftrightarrow 3NH_4^+(aq) + HSO_4^-(aq) + SO_4^{2-}(aq)$	$[NH_4^+]^3[HSO_4^-][SO_4^{2-}]\gamma_{NH_4^+}^3\gamma_{HSO_4^-}\gamma_{SO_4^{2-}}$	29.72	Mol ⁵ kg ⁻⁵

3.2 Gas/Particle Conversion Process of Organic Species (Condensation)

The understanding of gas/particle partition of organic compounds is still in its infancy compared to that of the inorganic compounds. Organic aerosols consist of hundreds of compounds, including many that have not been identified. Some of these compounds may be primary, i.e., non-volatile compounds emitted as

particles or semi-volatile compounds that may be emitted as gases. Others may be secondary, i.e., condensable products formed from the oxidation of volatile compounds, as discussed in Section 2.4. Gas/particle partition has been studied for some individual compounds that have been identified in atmospheric organic particles. However, for complex systems, such as the formation of secondary organic aerosol (SOA) from the oxidation of VOC, the current understanding is based largely on empirical data, typically derived from environmental chambers.

Several theories have been presented in the literature for the equilibrium partition of organic compounds between gases and particles: dissolution, saturation, absorption, adsorption, etc. Soluble species like formic acid, acetic acid, and formaldehyde enter the particulate phase through dissolution into particles or into fog/cloud droplets. However, dissolution as a gas/particle conversion pathway has typically only been studied for systems with few components (Jacobson, 1999 and references therein). The formation of SOA when the gas-phase concentration reaches saturation is determined by the saturation vapor pressure at the given temperature. The saturation vapor pressure is the concentration in the gas phase that is in equilibrium with the pure liquid of the condensing species. The implicit assumption is that the particle contains a liquid phase of the pure liquid. A less stringent assumption, that the particle contains a liquid mixture, gives rise to several absorption theories. Because “like dissolves like”, organic vapors are assumed to be absorbed into a liquid mixture of organic compounds in many absorption theories.

In addition to absorption, adsorption onto organic particles was shown to be a key mechanism through which semi-volatile organic compounds partition into the particle phase (Dachs and Eisenreich, 2000). A gas-phase compound adsorbs onto a particle’s surface, which is different from absorptive partition, in which the gas-phase compounds enter the bulk phase of the particle.

3.3 Aqueous Chemistry

Clouds and fogs can play an important role in the chemistry of atmospheric species, as some reactions taking place in the aqueous phase are sufficiently fast in altering the chemical composition of the atmosphere significantly. Before aqueous reactions can occur, some reactants and products need to be transferred from the gas phase into the droplet phase and vice versa. This gas/particle transfer involves the dissolution of gas-phase species or the evaporation of aqueous species. In Section 2.1, we discussed the relevant gas/particle equilibria. Table 4 presents gas/liquid equilibria for selected atmospheric species active in aqueous chemistry. In addition to the partition between the gas and particle/droplet phase, ionization is also a common process that takes place in both particles and droplets. Table 5 summarizes the ionic dissociation equilibria of SO_2 (H_2SO_3), H_2SO_4 , HNO_3 , NH_3 (NH_4OH), CO_2 (H_2CO_3), and H_2O . In Section 6.2, we will discuss the mathematical formulations of the partition of

chemical species between the gas phase and the droplet phase, and address the ionic balance within the droplets and the calculation of pH.

In theory, aqueous chemical transformations can take place within aqueous particles. However, their liquid water content is not sufficient to lead to significant amounts of chemical conversion (Saxena and Seigneur, 1987; Meng and Seinfeld, 1994). Therefore, we focus here on the chemical transformations taking place in cloud and fog droplets. We will review the chemical transformations of sulfur, nitrogen, organic species, and oxygen species.

3.3.1 Sulfur Species

Cloud and fog droplets act as chemical reactors for the conversion of SO₂ to sulfate. The three major reactions are the oxidation of SO₂ by H₂O₂, O₃ and O₂. The latter reaction must be catalyzed by Fe³⁺ or Mn²⁺ to proceed at a significant rate. Other oxidants such as dichloride ions (Cl₂⁻), organic peroxides, free radicals and NO₂ may also contribute to SO₂ oxidation under special conditions.

The H₂O₂ reaction involves several mechanistic steps. This reaction is relatively insensitive to the acidity, which is measured by the pH (-log₁₀ [H⁺]) of a droplet, in the range of pH encountered in the fog and cloud droplets of the lower atmosphere. Therefore, H₂O₂ represents a key oxidant for SO₂ in a lot of tropospheric environments.

The reaction of SO₂ with O₃ is a strong function of pH. Since its rate decreases with decreasing pH, this reaction is self-limiting (the sulfate formed during the reaction leads to a lower pH). This reaction is most important at pH values above 4.

The reaction of SO₂ with O₂ must be catalyzed by trace metals (Fe³⁺ and Mn²⁺) to proceed at a significant rate. The rates of the reactions differ for various pH ranges. In addition, the kinetics depend on the ionic strength of the solution and the presence of organic compounds. Moreover, there is synergism if both trace metals are present.

3.3.2 Nitrogen Species

Nitrate formation is also enhanced by the presence of cloud and fog droplets. The two major reactions are the hydrolysis of N₂O₅ to two molecules of HNO₃ and the conversion of the NO₃ radical to the NO₃⁻ ion. These reactions are very fast in solution and their kinetics can be assumed to be limited by the gas/droplet mass transfer step. For N₂O₅ and NO₃ gas-phase molecules that reach a droplet, the probabilities that they will be scavenged by a droplet are in the range of 0.01 to 1.0 for N₂O₅ and 10⁻⁴ to 10⁻² for NO₃ (Jacob, 2000). Therefore, nitrate formation will proceed at a significant rate when N₂O₅ and NO₃ are present, i.e., primarily during nighttime.

Other reactions also lead to nitrate formation in the aqueous phase. For example, NO_2 undergoes a disproportionation reaction to form HNO_2 and HNO_3 . However, NO_2 has a low solubility and this reaction is not a major pathway for nitrate formation.

3.3.3 Organic Species

Organic species that contain polar functional groups and have low to moderate molecular weights can dissolve in cloud and fog droplets. Such species include aldehydes, acids and organic nitrate species. Some of those species may interfere with sulfur chemistry (i.e., formation of hydromethanesulfonic acid or HMSA). Also, some organic chemical reactions may take place in solution. For example, Aumont et al. (2000) considered that VOC could be oxidized in droplets by OH radicals. Aldehydes could be converted to carboxylic acids, secondary alcohols to ketones and primary alcohols to carboxylic acids via aldehydes. Such oxidation reactions can lead to the formation of organic compounds that are more conducive to condensation than the original compounds, thereby leading to secondary organic aerosol formation.

3.3.4 Oxidant Species

Radicals such as OH and HO_2 can be scavenged by droplets. Jacob (2000) estimated that the probability for HO_2 scavenging was in the range of 0.1 to 1.0. In droplets, HO_2 radicals can combine to form H_2O_2 . As discussed above, H_2O_2 is a major oxidant for sulfate formation.

The scavenging of radicals by droplets also has a profound effect on oxidant formation. As their gas-phase concentrations decrease due to scavenging by droplets, the photochemical formation of O_3 and OH will decrease. The effect of clouds on oxidant formation was first identified by Seigneur and Saxena (1985) and has been studied by several others since (e.g., Monod and Carlier, 1999; Jacob, 2000). In addition to the scavenging of radicals by droplets, the solubility of organic species, such as aldehydes, that are key precursors of radicals in the gas phase also affect O_3 chemistry.

Table 4. Gas/liquid equilibria of selected species (Jacobson, 1999; Seinfeld and Pandis, 1998).

Gas/liquid equilibrium	Henry's law coefficient at 25° C (M/atm)
$\text{SO}_2(\text{g}) \leftrightarrow \text{SO}_2(\text{aq})$	1.22
$\text{HNO}_3(\text{g}) \leftrightarrow \text{HNO}_3(\text{aq})$	2.10×10^5
$\text{H}_2\text{SO}_4(\text{g}) \leftrightarrow \text{H}_2\text{SO}_4(\text{aq})$	∞
$\text{NH}_3(\text{g}) \leftrightarrow \text{NH}_3(\text{aq})$	5.76×10^1
$\text{CO}_2(\text{g}) \leftrightarrow \text{CO}_2(\text{aq})$	3.41×10^{-2}
$\text{O}_3(\text{g}) \leftrightarrow \text{O}_3(\text{aq})$	1.13×10^{-2}
$\text{NO}(\text{g}) \leftrightarrow \text{NO}(\text{aq})$	1.9×10^{-3}
$\text{NO}_2(\text{g}) \leftrightarrow \text{NO}_2(\text{aq})$	1.00×10^{-2}
$\text{H}_2\text{O}_2(\text{g}) \leftrightarrow \text{H}_2\text{O}_2(\text{aq})$	7.45×10^4

Table 5. Dissociation equilibria of selected species (Jacobson, 1999).

Equilibrium reactions	Equilibrium coefficient at 25° C (M)
$\text{H}_2\text{SO}_3 (\text{aq}) \leftrightarrow \text{HSO}_3^- + \text{H}^+$	1.71×10^{-2}
$\text{HSO}_3^- \leftrightarrow \text{SO}_3^{2-} + \text{H}^+$	5.99×10^{-8}
$\text{H}_2\text{SO}_4 (\text{aq}) \leftrightarrow \text{HSO}_4^- + \text{H}^+$	1.00×10^3
$\text{HSO}_4^- \leftrightarrow \text{SO}_4^{2-} + \text{H}^+$	1.02×10^{-2}
$\text{NH}_4\text{OH} (\text{aq}) \leftrightarrow \text{NH}_4^+ + \text{OH}^-$	1.81×10^{-5}
$\text{H}_2\text{CO}_3 (\text{aq}) \leftrightarrow \text{HCO}_3^- + \text{H}^+$	4.30×10^{-7}
$\text{HCO}_3^- \leftrightarrow \text{CO}_3^{2-} + \text{H}^+$	4.68×10^{-11}
$\text{H}_2\text{O} (\text{l}) \leftrightarrow \text{H}^+ + \text{OH}^-$	1.01×10^{-14}

3.4 Heterogeneous Chemistry

Heterogeneous chemistry refers to chemical reactions that involve two phases. These reactions may take place on the surface of particles, or in the bulk phase of liquid particles. The role of heterogeneous chemistry on the air pollution problems of concern is well studied in a few cases, including the role of polar stratospheric clouds described in Section 5.3. However, much is still unknown.

Several studies have been published (Dentener et al., 1996, Jacob, 2000) that compile current information on heterogeneous reactions and on their impacts on tropospheric pollutants. These reactions include the hydrolysis of N_2O_5 (g), the hydrolysis of NO_2 and NO_3 , and conversion of HO_2 to H_2O_2 (which may also be catalyzed by transition metal ions). In addition, there are proposed reactions for O_3 loss on soot surface and in cycles involving bromine and chlorine radicals. Reactions on mineral aerosols and windblown dust may affect the conversion of SO_2 to sulfate. In some regions of the world, dust concentrations can be high enough to affect the formation of oxidants and acids, (e.g., in Japan or southern Europe). Dentener et al. found in their model simulations that heterogeneous reactions may decrease tropospheric O_3 by up to 10% because of their effect on radical balance.

3.5 Aerosol Dynamics

Aerosol dynamics refer to processes governing the formation, growth and shrinkage of particles as a function of time. Figure 3 depicts the major processes that contribute to such changes in a particle population. New particles are formed from vapor when *nucleation* takes place. Nucleation involves a phase transition from the gas phase to the particle phase and increases the number of particles, as well as the total particle mass. Typically, new particles formed by nucleation are “ultra fine,” in the diameter range of 1 to 10 nm diameter. Homogeneous nucleation occurs when a pure component particle is formed, for example, when the vapor phase is saturated. Heterogeneous nucleation occurs when gaseous molecules of different identities nucleate. Molecules in the gas phase can also *condense* onto an existing particle, increasing its size (but not the total number of

particles). Therefore, nucleation and condensation compete as a gas reaches its saturation vapor pressure. If the concentration of existing particles is high, condensation onto existing particles will prevail. Nucleation is only important in cases where the existing particle concentration is relatively low, and/or the rate of formation of condensing molecules is very high (Wexler et al., 1994). *Evaporation* is the reverse process of condensation, when a particle shrinks. Condensation and evaporation processes control the formation of secondary PM relevant for air quality. Equilibrium between the particulate phase and the gas phase occurs at the surface of the particle. The effect of particle size on equilibrium can also be taken into account to refine the treatment of gas/particle conversion at the surface. This so-called Kelvin effect limits the condensation of gases on particles as the particle size decreases. In addition, the mass transfer of molecules between the bulk phase of the gas and the surface of the particle must also be taken into account, especially for larger particles, where the kinetic transfer may actually limit the rate of condensation and evaporation. Finally, when two particles collide, they may stick to one another and *coagulate* to form a bigger particle, decreasing the total number of particles. Coagulation rates increase as the concentrations of particles increase. At PM concentrations typical of urban and regional atmospheres, coagulation is typically slow enough relative to the other processes affecting the particle size distribution that coagulation can be neglected (Seigneur and Barnes, 1986; Wexler et al., 1994).

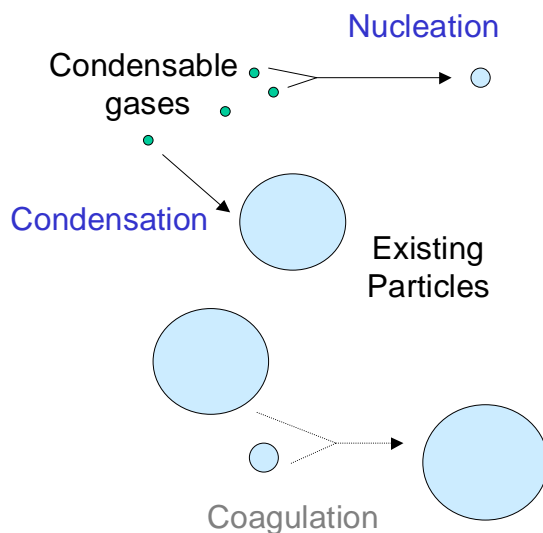


Figure 3. Processes that change the size of a particle.

4 Chemical Transformations Involved in the Formation of Air Toxics

Toxic compounds include a myriad of organic and inorganic compounds that are typically regulated in terms of their potential risk to the human population or wildlife rather than in terms of their ambient concentrations. Organic toxic

compounds include volatile organic compounds (VOC) such as benzene, 1,3-butadiene, and formaldehyde and semi-volatile organic compounds (SVOC) such as polychlorinated dibenzo-p-dioxins and polychlorinated dibenzofurans (PCDD/F), polychlorinated biphenyls (PCB), polycyclic aromatic hydrocarbons (PAH), and several pesticides, herbicides and fungicides. Inorganic toxic compounds include metals that can reside primarily in the particulate phase (e.g., arsenic, lead, chromium) or the gas phase (e.g., mercury, selenium), inorganic gases such as chlorine (Cl_2), hydrochloric acid (HCl) and hydrofluoric acid (HF) and radionuclides such as radon. We will discuss below the atmospheric chemistry of some of these toxic compounds. Radionuclides are not discussed here.

4.1 Inorganic Toxic Compounds

4.1.1 Trace Metals

The toxicity of most trace metals is not a function of their chemical speciation and, consequently, their chemical transformations are generally not relevant. Two major exceptions are chromium (Cr) and mercury (Hg). Cr exists in two valence states in the atmosphere: hexavalent, Cr(VI), and trivalent, Cr(III). Cr(VI) is considered to be carcinogenic whereas Cr(III) is not (IRIS, 2001). It is, therefore, essential to assess the valence of Cr in the atmosphere. Hg also exists in two valence states in the atmosphere: elemental, Hg(0), and divalent (or oxidized), Hg(II). In addition, Hg(II) can be present as gaseous species such as HgCl_2 , as particulate species such as HgO or HgS, or as gaseous species adsorbed to atmospheric particulate matter. These various Hg species have different atmospheric lifetimes ranging from a few hours to about one year (Schroeder and Munthe, 1998). Therefore, it is necessary to take into account the transformations among these Hg species to properly simulate their atmospheric behavior including the relevant source-receptor relationships.

Figure 4 depicts the atmospheric chemistry of Cr (Seigneur and Constantinou, 1995). Chemical transformations between Cr(VI) and Cr(III) take place in aqueous particles or cloud/fog droplets. Cr(VI) can be reduced to Cr(III) by several chemicals including trivalent arsenic, divalent iron, vanadium and sulfur dioxide. Cr(III) can be oxidized to Cr(VI) by reactions with trivalent or tetravalent manganese. Computer simulations that have been conducted for a wide range of plausible atmospheric conditions suggest that typical conditions favor the reduction of Cr(VI) to Cr(III). Only under some extreme conditions could Cr(III) be oxidized to Cr(VI).

Figure 5 depicts the atmospheric transformations of Hg (Lin and Pehkonen, 1999; Ryaboshapko et al., 2001). The oxidation of Hg(0) to Hg(II) can occur both in the gas phase and the aqueous phase (i.e., cloud or fog droplets). However, except for the aqueous oxidation of Hg(0) by dissolved Cl_2 in marine environments, those reactions are relatively slow on average (half-life of a few months).

Reductions of Hg(II) can take place in the aqueous phase by reaction with dissolved SO₂ and HO₂ radicals. Current kinetic data suggest that the latter reaction is considerably faster and consequently dominates the conversion of Hg(II) to Hg(0) in clouds and fog during daytime. At night, oxidation of Hg(0) by Cl₂ (which can reach concentrations on the order of 100 ppt over sea water) will dominate in marine environments. Adsorption of Hg(II) to soot and other atmospheric particulate matter within droplets may inhibit Hg(II) reaction and, therefore, decrease the overall reduction rate of Hg(II) to Hg(0). At this point, it is not clear what fraction of Hg(II) gets adsorbed to particulate matter (experimental data of Seigneur et al., 1998, suggest values in the range of 9 to 55%) and to what extent their adsorption is reversible or irreversible.

4.1.2 Inorganic Gases

Non-metallic inorganic gases listed as air toxics by the U.S. Environmental Protection Agency (EPA) and the State of California include carbon disulfide (CS₂), molecular chlorine (Cl₂), hydrogen chloride (HCl), hydrogen fluoride (HF) and phosphine (PH₃). Among those, Cl₂ is very reactive and will photolyze in the presence of sunlight. The atmospheric chemistry of Cl₂ and HCl is tied to the global chlorine cycle, which includes reactions related to sea salt (Graedel and Keene, 1995; Spicer et al., 1998).

4.2 Organic Toxic Compounds

4.2.1 Volatile Organic Compounds

A myriad of VOC is listed as air toxics by the EPA, the State of California and other regulatory agencies. The toxic VOC that are considered to contribute the most to cancer risk in urban locations include benzene, 1,3-butadiene, formaldehyde, and acetaldehyde. These compounds exhibit a wide range of atmospheric chemical behavior. The reactivity of benzene is quite low (atmospheric lifetime of a few days). On the other hand, 1,3-butadiene is fairly reactive (atmospheric lifetime of about a few hours in a polluted urban environment) and the two aldehydes are primary as well as secondary and are quite reactive (atmospheric lifetimes of a few hours in a polluted urban environment). The reactive species are involved in O₃ formation as discussed in Section 2. Therefore, the assessment of such air toxics requires a full treatment of VOC atmospheric chemistry.

4.2.2 Semi-Volatile Organic Compounds

Several SVOC are listed as air toxics, including PCDD/F, PCB, PAH, and several pesticides, herbicides and fungicides. All organic compounds that contain H atoms react with OH radicals in the atmosphere. Organic compounds that contain double and triple bonds, and certain nitrogen-containing compounds react with NO₃ and O₃. In addition, organosulfur compounds and phenolic compounds react with NO₃ (Atkinson, 1994, 1996, 2000). However, the atmospheric lifetime of

most SVOC is typically on the order of a few days and they are, therefore, subject to long-range transport. The reactivity of SVOC tends to decrease with increasing number of halogen atoms. The partitioning of SVOC between the gas phase and the particulate phase also affects their reactivity. It is generally assumed that the particulate fraction is non-reactive, however, experimental evidence is currently insufficient to assess whether this is actually the case. Some SVOC may also be subject to photolysis, however, experimental data are typically not available to quantify their photolytic rates (Franklin et al., 2000).

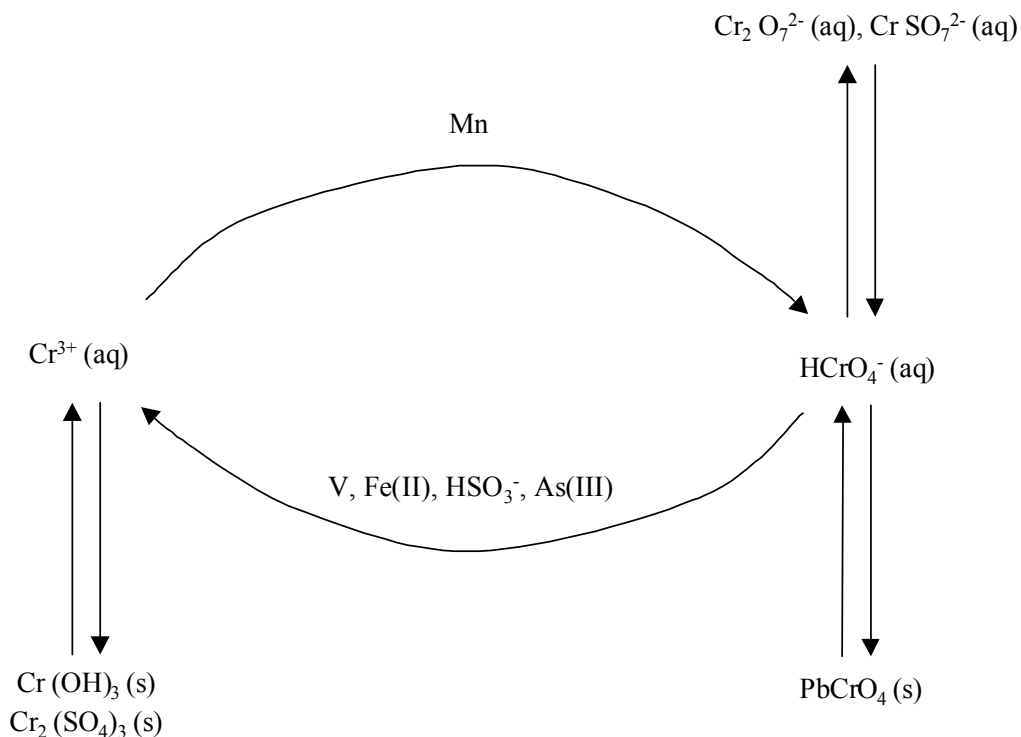


Figure 4. Condensed description of the atmospheric chemistry of chromium (Seigneur and Constantinou, 1995). (Reprinted with permission from ACS).

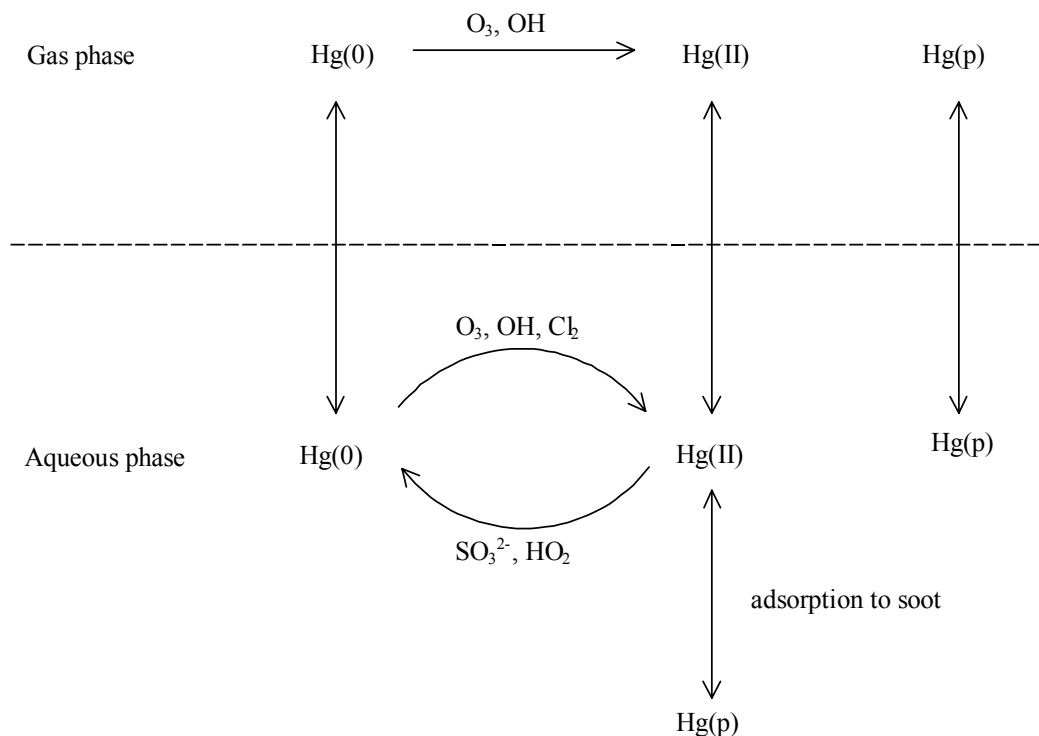


Figure 5. Condensed description of the atmospheric chemistry of mercury (after Ryaboshapko et al., 2001). (Reprinted with permission from ACS).

5 Chemistry of the Upper Atmosphere: Stratospheric Ozone

5.1 Ozone Abundance and Distribution

One of the most pressing, long-standing, and extensively studied global atmospheric issues is the gradual decline in stratospheric ozone (O₃). This decline is particularly noticeable in the lower stratosphere. Although the photochemistry and the meteorology that control the abundance and distribution of stratospheric O₃ have been investigated in great detail over the past several decades, the observations are not always well reproduced by 2-D and 3-D atmospheric models.

O₃ is produced in the stratosphere predominantly via a 2-step process initiated by the UV photolysis of molecular oxygen (Chapman, 1930),



Contrasting these reactions with Reactions 1 and 2 in the troposphere, O₃ is produced the same way, but the source of the oxygen atom is different. NO_x is not abundant in the stratosphere and energy-rich photons needed to dissociate O₂

are not as available in the lower atmosphere. In the stratosphere, O_3 is destroyed by photolysis and oxygen atom recombination (among a number of other mechanisms discussed below),



Reactions 27 and 28 lead to rapid inter-conversion between odd-oxygen species O and O_3 , whereas Reactions 26 and 29 generally control the net production rates of odd oxygen, and thus O_3 , throughout the stratosphere. The vertical distribution of O_3 shown in Figure 6 is largely maintained by this set of reactions, known as the Chapman mechanism.

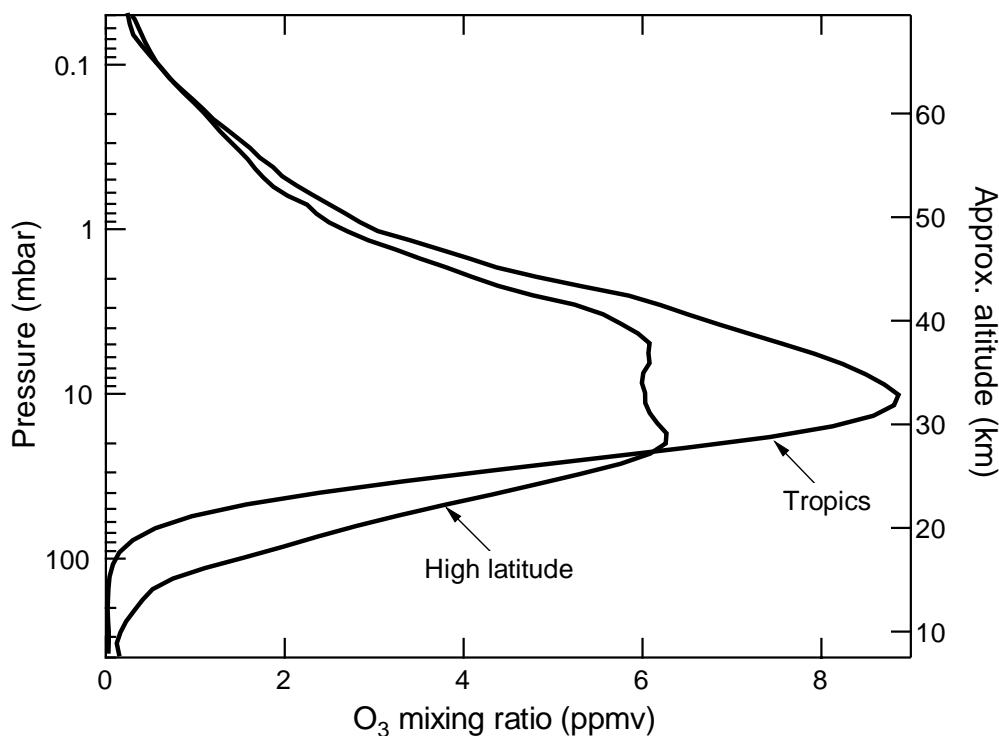


Figure 6. Vertical distribution of stratospheric O_3 at low and high latitudes. O_3 volume mixing ratios are shown as a function of pressure. The approximate altitude is shown for reference. Data were recorded at high southern latitudes and in the tropics by the space-shuttle-borne Atmospheric Trace Molecule Spectrometer (ATMOS) in November 1994.

Below ~ 30 km the photolysis rate of O_2 increases approximately exponentially with increasing altitude (DeMore et al., 1997), which is responsible for the steep gradient in O_3 abundance with altitude in the lower stratosphere. In the middle and upper stratosphere, O_2 photolysis is less altitude dependent, and the O_3 abundance decreases with altitude as temperature (and hence the rate constant of

Reaction 29) increases while pressure (and thus the rate of Reaction 27) continues to decrease.

This simple set of reactions, however, does not fully explain the spatial distribution of O₃ in the stratosphere. In the lower stratosphere, where the instantaneous photochemical lifetime of odd oxygen is in the range of months to years, the O₃ distribution is strongly influenced by transport processes (e.g., Brasseur and Solomon, 1986). For instance, although solar exposure and thus production rates of O₃ are highest in the tropical middle stratosphere, column abundances of O₃ are higher at higher latitudes where the peak in the vertical distribution shifts to lower altitudes. The primary large-scale stratospheric circulation pattern responsible for this redistribution of O₃ is referred to as Brewer-Dobson circulation and is characterized by average upward flow at low latitudes and outward and downward flow at higher latitudes (Dobson, 1929).

5.2 Ozone Depletion via Gas-Phase Chemistry

In addition to the dynamics and chemical mechanisms described above, there are a large number of other processes that influence O₃ abundance and distribution. O₃ can be destroyed, for example, via gas-phase catalytic cycles involving free radical oxides of hydrogen (H, OH, and HO₂) (Bates and Nicolet, 1950; Crutzen, 1971; Johnston, 1971), nitrogen (NO and NO₂) (Crutzen, 1971; Johnston, 1971), chlorine (Cl, ClO, ClO₂) (Molina and Rowland, 1974; Stolarski and Cicerone, 1974), and bromine (Br, BrO) (Wofsy et al., 1975). Iodine oxide radicals may also destroy O₃, but the stratospheric abundance of iodine is too low to have a significant effect on O₃ abundance (Solomon et al., 1994). These cycles can be described by the general form



where X represents H, OH, NO, Cl, or Br. There are additional important cycles that involve more than one radical family, e.g. (McElroy et al., 1986),



One of the more notorious O₃ loss mechanisms is an analog of the above cycle involving the ClO dimer (Molina and Molina, 1987), i.e.,



Model calculations indicate that Reactions 32 to 35 are responsible for 10-30% and Reactions 36 to 39 for ~70% of the O₃ loss observed in the Antarctic lower stratospheric polar vortex during austral spring, i.e., the “ozone hole” (Jones et al., 1989; McElroy and Salawitch, 1989; Solomon et al., 1990).

In the non-polar lower stratosphere, cycles involving OH and HO₂ (HO_x) are estimated to account for 30-50% and cycles involving NO and NO₂ (NO_x) for 20-40% of net O₃ destruction (McElroy, 1982; McElroy and Salawitch, 1989). At altitudes above 21 km, stratospheric O₃ loss is predominantly attributable to cycles involving NO_x (Prather et al., 1984; McElroy and Salawitch, 1989). The contribution of chlorine radicals to O₃ depletion is also significant and increases with increasing altitude up to ~40 km (Prather et al., 1984; McElroy and Salawitch, 1989).

The influence of these reactions on middle stratospheric O₃ is particularly obvious in air masses that have been confined to high latitudes for a couple of weeks or more. When air masses are caught in anticyclone regions, O₃ mixing ratios have been observed to decrease by 20-30% at altitudes between 25 and 40 km (Manney et al., 1995). These “pockets” of low O₃ air have been attributed predominantly to O₃ destruction via cycles involving NO_x under conditions characterized by low O₃ production rates (Nair et al., 1998).

A cycle similar to those that occur in the stratosphere has been implicated in frequent episodic depletion of O₃ in the upper troposphere and in the marine boundary layer. This cycle involves HO_x species and CO, i.e.,



In order for this mechanism to be effective for tropospheric O₃ destruction, NO_x concentrations must be low, which limits the production of O₃ associated with NO_x chemistry coupled with hydrocarbon oxidation (Kley et al., 1996), as discussed in Section 2.

5.3 Role of Heterogeneous Chemistry in Ozone Destruction

Reactions mediated by aerosol and cloud particles have a large effect on lower stratospheric O₃ abundance. One such reaction is the hydrolysis of N₂O₅ to form HNO₃,

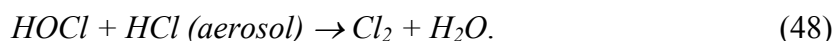
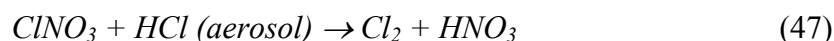


which plays a substantial role in limiting O₃ loss via NO_x chemistry (Cadle et al., 1975). N₂O₅ is produced at night by the following set of reactions



Although N₂O₅ is not directly involved in O₃ depletion, it can be rapidly converted to NO_x by photolysis or thermal decomposition. Nitric acid is much more stable than N₂O₅, and is thus a longer-lived reservoir for reactive nitrogen.

HCl and ClNO₃ act similarly as reservoirs for reactive chlorine and account for the majority of the inorganic chlorine budget under most conditions in the stratosphere. HCl is more photochemically stable than ClNO₃, and its abundance exceeds that of ClNO₃ under steady-state conditions at temperatures greater than 198 K, as shown in Figure 7. At lower temperatures, however, these species react rapidly on surfaces of sulfuric acid aerosols and polar stratospheric clouds (PSCs) to form molecular chlorine, i.e.,



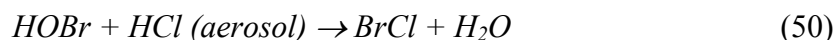
As shown in Figure 8, the rates of these reactions increase exponentially with decreasing temperature (Sander et al., 2000), but temperatures low enough to initiate this process are generally only attained within the polar vortex during the Antarctic and Arctic winters. In the polar spring, Cl₂ is photolyzed to produce atomic chlorine, which participates in catalytic cycles involving Reactions 32 to 39, thereby leading to rapid O₃ loss (McElroy et al., 1986; Solomon et al., 1986). If temperatures are low enough, nearly all of the available inorganic chlorine within the vortex is converted from HCl and ClNO₃ into reactive radicals, and the vortex is described as “fully activated” (see Figure 9).

The impact of aerosols and PSCs on polar O₃ is compounded by the ability of PSCs to sequester HNO₃. These particles can grow large enough to undergo sedimentation from the stratosphere, leaving the polar vortex denitrified and

possibly dehydrated (Toon et al., 1986). Denitrification reduces the rate at which ClO recombines with NO₂ to regenerate the less destructive reservoir species ClNO₃ (McElroy et al., 1986). If denitrification is complete, the rate of the springtime recovery of the vortex is controlled by the rate of HCl production from the reaction of atomic chlorine with methane. This route to recovery is also taken if the vortex is depleted in O₃, in which case Reaction 32 is too slow to generate ClO for the production of ClNO₃ by recombination with NO₂ (see Figure 9). When O₃ is only moderately depleted, and the vortex is not significantly denitrified, active chlorine preferentially recovers into ClNO₃ as the vortex warms. This scenario is common in the Arctic. Under O₃-depleted and/or denitrified conditions, active chlorine is converted into HCl almost exclusively. These conditions are common in the Antarctic (Michelsen et al., 1999).

Temperatures low enough to promote Reactions 46 to 48 may be reached in the lowest part of the stratosphere near the tropopause, but inorganic chlorine concentrations are usually too low to have a significant impact on O₃ abundances in these regions. Reactions 46 to 48 may promote non-polar O₃ loss at temperatures higher than 200 K when stratospheric aerosol abundances are elevated. For example, in response to injection of volcanic sulfur following a major eruption (Hofmann and Solomon, 1989), the elevated concentrations of aerosols may be at least partially responsible for the observed loss of mid-latitude O₃ in the wake of major volcanic activity.

The corresponding reactions involving bromine species,



have rate constants orders of magnitude larger than those of Reactions 46 to 48 at temperatures higher than ~198 K (see Figure 7; Sander et al., 2000). Low abundances of bromine in the stratosphere (currently ~1.5% of the abundance of chlorine), however, limit the contribution of these reactions to non-polar lower stratospheric O₃ loss. In the troposphere, where bromine concentrations can be high, Reactions 49 to 50 are important and have been implicated in the nearly complete depletion of O₃ in the Arctic boundary layer during spring (Fan and Jacob, 1992).

Despite extensive studies of aerosol-mediated chemistry, heterogeneous processes are not understood well to explain previous responses of lower stratospheric inorganic chlorine partitioning to elevated aerosol loading (Webster et al., 2000), and thus to predict the atmospheric response to future volcanic eruptions. These reactions are very likely to be sensitive to aerosol composition. Stratospheric aerosols have been observed to contain soot, crustal and meteoritic components, such as iron, sodium, magnesium, and calcium, in addition to sulfuric acid, nitric acid, and water (Sheridan et al., 1994; Cziczko et al., 2001). Detailed studies of the

influence of these contaminants on stratospheric aerosol-mediated chemistry have yet to be performed. Similar deficiencies exist in the understanding of the effect of phase on aerosol chemistry. Sulfuric acid aerosols may undergo transitions to several metastable phases under stratospheric conditions (Zhang et al., 1993), and a survey of rates of heterogeneous reactions for these phases has not been performed.

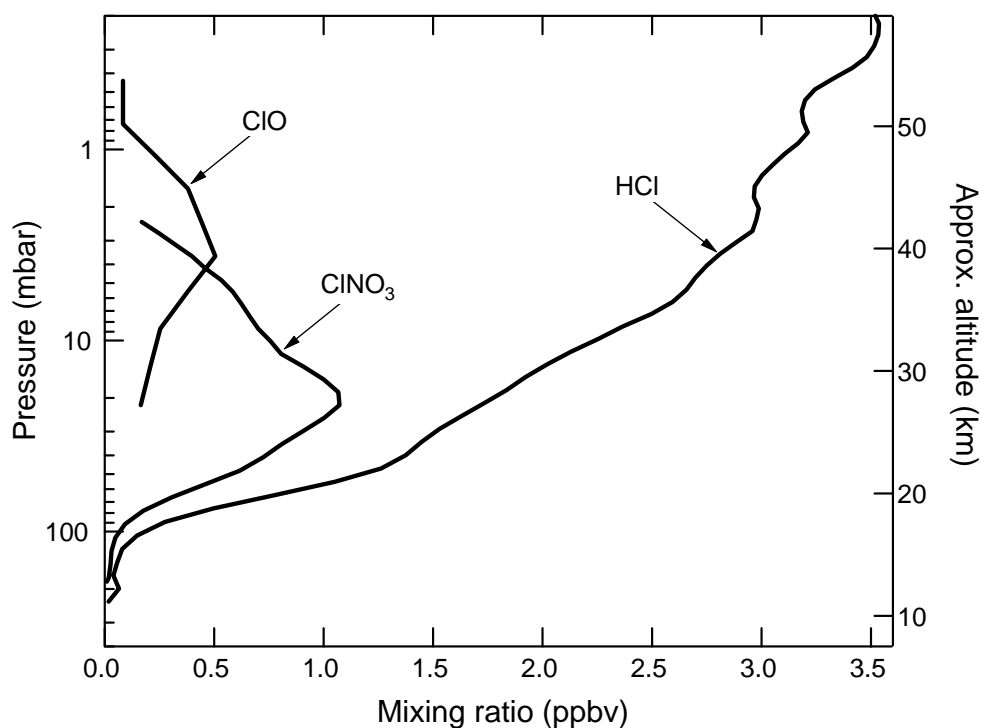


Figure 7. Vertical distributions of inorganic chlorine species. Volume mixing ratios of HCl, ClONO₂, and ClO are shown as a function of pressure. Data were recorded at northern mid-latitudes by ATMOS (HCl, ClONO₂) and the Millimeter-wave Atmospheric Sounder, MAS, (ClO) in November 1994.

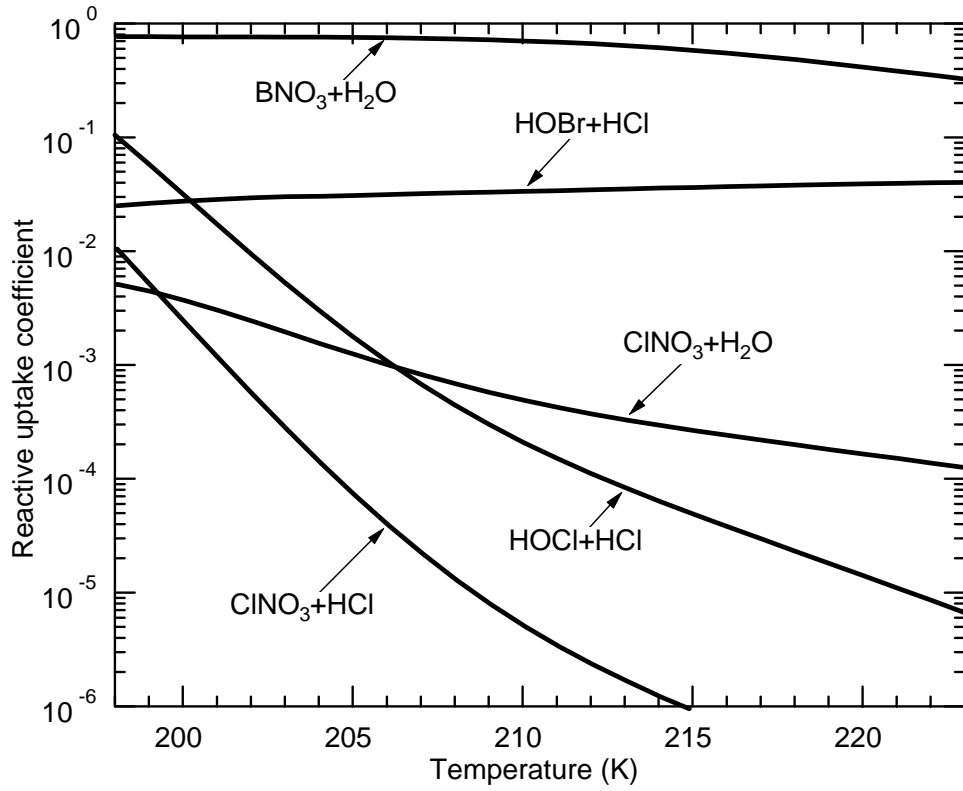


Figure 8. Temperature dependence of the reactive uptake coefficients for atmospherically important aerosol-mediated reactions. Reactive uptake coefficients (γ) for Reactions 46-50 as a function of temperature (Sander et al., 2000).

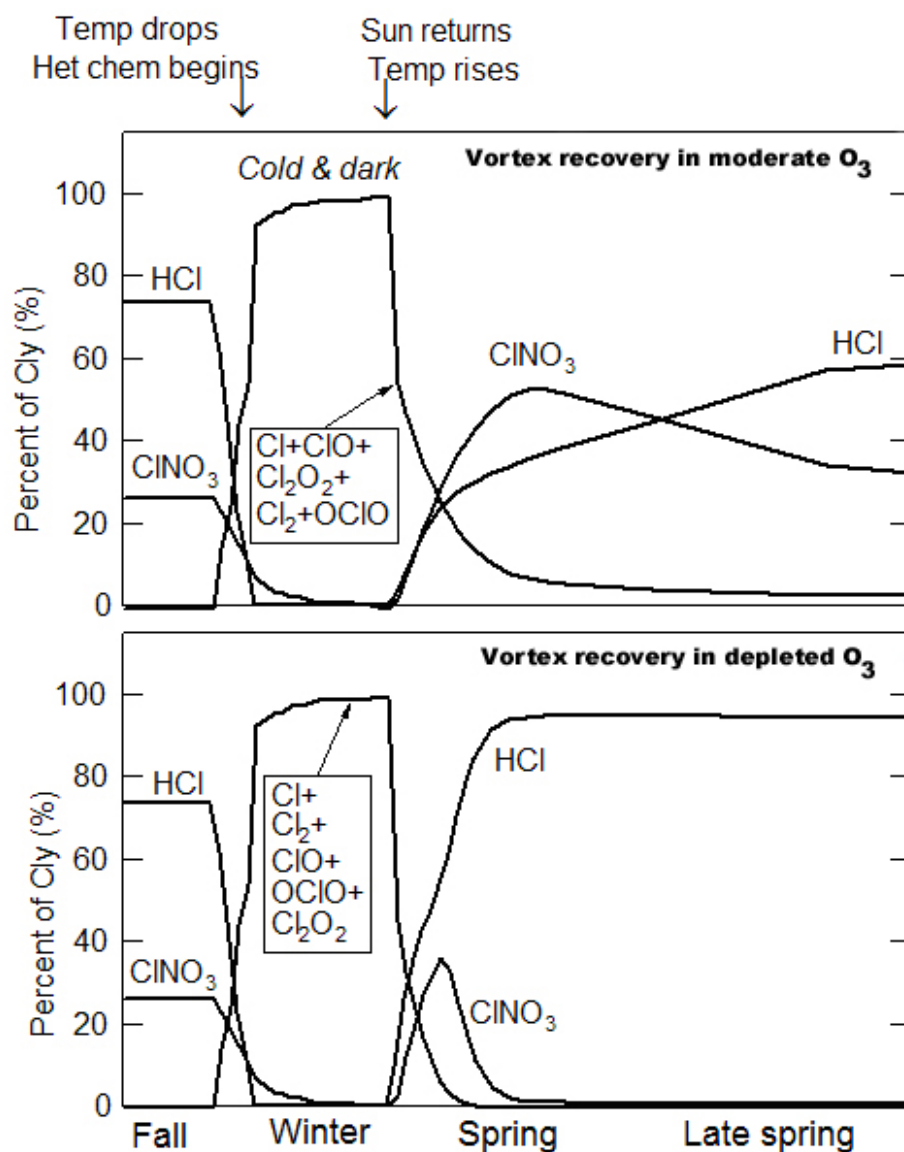


Figure 9. Evolution of the partitioning between inorganic chlorine species in the winter/springtime polar vortices. The partitioning of inorganic chlorine during the activation and recovery of the polar vortex is calculated for conditions under which O_3 is nearly completely depleted in the spring (representative of the Antarctic vortex) and only moderately depleted in the spring (more representative of the Arctic vortex). Modified from Michelsen et al. (2000) with permission from the American Geophysical Union.

5.4 Trends in Ozone and Radical Precursors

Stratospheric O_3 has been decreasing steadily for the past several decades at all extra-tropical latitudes (WMO/UNEP, 1999; Solomon, 1999; Staehelin et al., 2001 and references therein). Mid-latitude column amounts have decreased at a rate of

2-4%/decade since 1970. This decline is largest in the lower stratosphere (5-7%/decade at 15-20 km) and upper stratosphere (~7%/decade at 40 km), and is less significant in the middle stratosphere.

These trends are predominantly attributable to the increase in stratospheric abundances of chlorine and bromine. The main source of stratospheric chlorine is anthropogenic emissions of stable halogenated organic compounds, i.e., chlorofluorocarbons (CFCs) and hydrochlorofluorocarbons (HCFCs) that are not photochemically destroyed in the troposphere. Anthropogenic sources of bromine include halons and methyl bromide, although natural sources constitute a large fraction (~25%) of stratospheric abundances (Wamsley et al., 1998). These species are lofted from the troposphere into the stratosphere, where they are photolyzed to produce chlorine and bromine radicals (Molina and Rowland, 1974; Prather et al., 1984). The Montreal Protocol, originally adopted in 1987, restricts production and use of CFCs, HCFCs, halons, and methyl bromide. As a result tropospheric abundances of most of these gases have ceased to increase. Total inorganic chlorine levels in the stratosphere reached a maximum in the late 1990s and are expected to decline over the next 100 years (WMO/UNEP, 1999; Solomon, 1999; Staehelin et al., 2001). Stratospheric bromine continues to increase, but its abundance is currently only 1.5% that of chlorine. Based on projections of future levels of stratospheric chlorine and bromine, and given no increases in other O₃-destroying radical precursors, O₃ is expected to recover to 1980 levels in 50-100 years (WMO/UNEP, 1999).

The major source of NO_x in the stratosphere is the oxidation of N₂O by O(¹D) (Crutzen, 1971; Nevison et al., 1999). The only significant source of stratospheric N₂O is injection from the troposphere, where abundances have been increasing steadily at a rate of ~0.7 ppb/yr over the past 2-3 decades (WMO/UNEP, 1999). This trend, when extrapolated to the year 2010, is predicted to decrease middle stratospheric O₃ by at least 10% (0.5% decrease in the column amount) from present conditions (Nevison et al., 1999).

Stratospheric HO_x is predominantly generated by the reaction of H₂O with O(¹D). The main sources of stratospheric H₂O are injection from the troposphere and oxidation of CH₄. The atmospheric burden of CH₄ has increased substantially over the past 200 years (Etheridge et al., 1998), and recent studies have shown that H₂O entering the stratosphere from the troposphere is also increasing. Both trends lead to increases in stratospheric humidity. Although increasing CH₄ to levels estimated for 2010 is predicted to lead to an increase in O₃ abundance throughout the stratosphere, increases in H₂O are calculated to cause a decrease in O₃ that is more substantial than the increase caused by the trend in CH₄ (Nevison et al., 1999). Projected increases in stratospheric humidity are predicted to delay the recovery of stratospheric O₃ by 10-30 years (Dvortsov and Solomon, 2001; Shindell, 2001). In addition, rates of aerosol-mediated reactions increase with increasing water vapor mixing ratios, which may have a significant effect on polar O₃ loss.

Temperatures are currently declining throughout most of the stratosphere. The mid-latitude lower stratosphere is cooling at an annual average rate of ~ 0.8 K/decade, and the middle and upper stratosphere are cooling at an average rate of 1-2 K/decade. The winter/springtime lower stratospheric polar vortices are cooling at $\sim 3-4$ K/decade (WMO/UNEP, 1999). The cooling trend in the lower stratosphere is primarily attributable to the downward trend in lower stratospheric O_3 abundances. Increased tropospheric greenhouse gas concentrations are at least partially responsible for the trends observed in the middle and upper stratosphere (WMO/UNEP, 1999). Trends in stratospheric humidity may also contribute to decreasing stratospheric temperatures (Dvortsov and Solomon, 2001). These trends in temperature are predicted to enhance O_3 loss and significantly decrease the rate of recovery of stratospheric O_3 , particularly in the polar vortices (WMO/UNEP, 1999).

6 Modeling of Gas-Phase Chemistry

6.1 Gas-Phase Mechanisms for Ozone Formation

A chemical mechanism consists of a list of chemical reactions, like those discussed in Sections 2 through 5, with rate constants to indicate the kinetic characteristics of each reaction. The reaction rate constant, k , is most commonly a function of temperature, and may be written in the following Arrhenius form:

$$k = A \cdot \exp\left(\frac{-E_a}{RT}\right) \quad (51)$$

where E_a is the activation energy, R is the universal gas constant, and T is the temperature. Two other types of reactions are included in atmospheric gas-phase mechanisms, photolysis and combination reactions. A photolysis reaction involves only one reactant, which absorbs light at some wavelengths. For a compound that absorbs light between λ_1 and λ_2 , the photolysis rate constant (j) is derived as follows:

$$j = \int_{\lambda_1}^{\lambda_2} \sigma(\lambda, T) \phi(\lambda, T) I(\lambda) d\lambda \quad (52)$$

where σ is the absorption cross-section and ϕ is the quantum yield of the reaction, the probability of forming the products of interest per photon absorbed. Both σ and ϕ are properties of the light-absorbing compound and are functions of wavelength and temperature. $I(\lambda)$ is the actinic flux, which is the number of photons at a given wavelength λ . The photolysis rate constant is calculated in most applications as a discrete sum.

When two species combine to form a more stable product, some energy is typically released due to the formation of a chemical bond. Therefore, the presence of a third body facilitates this type of reaction by removing the extra energy, which otherwise may destabilize the newly formed molecule. Because of the importance of the third body stabilization effect, many combination reactions are pressure dependent.

In theory, a master mechanism may be devised that can be used to represent all the chemical reactions in the atmosphere. In practice, however, chemical mechanisms are devised to be just comprehensive enough to include all relevant processes in a particular setting. For example, the reaction of methane may not be included in many urban- to regional-scale chemical mechanisms, but can be important in global scale simulations. Similarly, radicals such as ClO (see Section 5) can be critical to the removal of stratospheric O₃, but are hardly of sufficient concentration to be of concern in the urban atmosphere. For simulating urban to regional O₃ production, chemical mechanisms are devised to represent the pertinent radical chemistry of oxygen, nitrogen, hydrogen, as well as carbonaceous compounds. However, because hundreds or thousands of VOC may be present in the ambient atmosphere, it is impractical to represent each VOC explicitly. Furthermore, the data (e.g., mechanistic and kinetic information) to support detailed mechanisms currently do not exist for many VOC. Four main strategies are currently employed to represent VOC mixtures:

- Surrogate species
- Lumped molecule
- Morphecule
- Lumped structure

In the surrogate species approach, a few VOC are represented explicitly. An entire VOC class may be represented by one of these surrogates and is assumed to react in a similar manner. This approach is especially useful in such cases as monoterpenes, where there are many compounds in the class but only a few (e.g., α -pinene, β -pinene, limonene) have been studied in detail. In the lumped molecule approach, similar compounds (e.g., long-chain alkanes) are grouped together and the reactions of the lumped molecule are devised to represent some average of all the compounds present. A new approach is to use morphecules to represent the organic mixture in the chemical solver. Each morphecule is composed of several allomorphs with different carbon numbers and reaction rates. The composition and property of each morphecule can change with time. The lumped structure approach takes into account the fact that VOC are made up of alkyl chains and functional groups. Modeled groups are chosen to represent the reactions of an alkyl group or a double bond or an aldehyde functional group, etc.

6.2 Formulating Chemical Kinetics as a Mathematical Problem

How do we turn all the mechanistic descriptions of the reactants and products and the reaction rate constants into a mathematical model that can be solved to predict the concentrations of reactants and products? Let's take a generic example:



where R_i are the reactants, P_j are the products, and α_i and β_j are the corresponding stoichiometric coefficients. In this case, the rate of the reaction is the product of the rate constant k_1 multiplied by the concentrations of the reactants, raised to the power of the stoichiometric coefficients:

$$r_1 = k_1 \prod_i [R_i]^{\alpha_i} \quad (54)$$

For each reactant, the rate of change in its concentration due to this reaction is

$$\frac{d[R_i]}{dt} = -\alpha_i r_1 \quad (55)$$

and for each product, the rate of change in its concentration is

$$\frac{d[P_i]}{dt} = \beta_i r_1 \quad (56)$$

Note that the concentrations of the reactants decrease (negative rate of change) and the concentrations of the products increase (positive rate of change). If there is a series of N reactions, the change in concentrations of a compound, which may be a reactant in some reactions and products in other reactions, is calculated as follows:

$$\frac{d[C_i]}{dt} = \sum_{k=1}^N a_{ik} r_k \quad (57)$$

where a_{ik} is the stoichiometric coefficient of compound i in reaction k . If compound i is a reactant in reaction k , $a_{ik} < 0$; if compound i is a product, $a_{ik} > 0$.

This equation is an ordinary differential equation (ODE), since the left hand side is a rate of change or a derivative in time. For each compound in the system, an ODE can be formulated. Therefore, the solution to the chemical kinetics involves the simultaneous solution to a set of ODEs, because the rates of reactions are algebraic functions of concentrations of several species. Initial conditions need to be specified for solving a set of ODEs for concentrations as a function of time.

Let us look at a special example of three reactions:



There are four species involved in these three reactions. Their rates of change are:

$$\frac{d[NO]}{dt} = j_1[NO_2] - k_3[NO][O_3] \quad (61)$$

$$\frac{d[NO_2]}{dt} = -j_1[NO_2] + k_3[NO][O_3] \quad (62)$$

$$\frac{d[O_3]}{dt} = k_2[O][O_2] - k_3[NO][O_3] \quad (63)$$

$$\frac{d[O]}{dt} = j_1[NO_2] - k_2[O][O_2] \quad (64)$$

The radical (oxygen atom) is much more reactive than the other three. Since it reacts faster, the radical has a much shorter lifetime than the molecules. The concentration of the radical changes very quickly according to those of the other species in the system. Therefore, at any instant, the radical can be assumed to be in a pseudo steady state, where $\frac{d[O]}{dt} = 0$, and [O] can be solved algebraically in terms of the instantaneous concentrations of the stable species:

$$[O] = \frac{j_1[NO_2]}{k_2[O_2]} \quad (65)$$

The pseudo steady state assumption is sometimes used in three-dimensional modeling to facilitate the solution of the system of ODEs.

By substituting Equation 65 into the system of ODEs (Equations 61 to 64), we can see that the rates of change of NO and O₃ are exactly equal in magnitude and opposite in direction to that of NO₂. Therefore, the concentrations of NO, O₃, and NO₂ will reach a steady state, called the photostationary state, where

$$[O_3] = \frac{j_1[NO_2]}{k_3[NO]} \quad (66)$$

6.3 Solvers for ODEs

The solution of the atmospheric chemical kinetic equations is a difficult task because the system of ODEs is stiff (i.e., the half-lives of the various species spans several orders of magnitude). The most accurate numerical algorithms for stiff ODEs are based on Gear's method (Gear, 1971). It is, however, computationally demanding and not suitable for large 3-D systems in its original formulation. Numerical algorithms that provide good balance for speed and accuracy for solving stiff ODEs in 3-D systems have been developed and several reviews are available on the subject (e.g., Odman et al., 1992; Dabdub and Seinfeld, 1995; Mathur et al., 1998; Jacobson, 1999).

6.4 Lagrangian/EKMA Results

6.4.1 Eulerian and Lagrangian Implementations

Photochemical schemes, such as those presented above, are used to calculate the dynamics of all photochemical species in each computational cell at each time step. In Eulerian photochemical models (e.g., McRae et al., 1982b; Tesche et al., 1984; Carmichael et al., 1986; Ackermann et al., 1998; EPA, 1999; Jacobson, 2001a; Griffin et al., 2002), the K-theory is used to simulate atmospheric diffusion and a three-dimensional grid is superimposed to cover the entire computational domain. In the Lagrangian photochemical models, columns or walls of cells are advected according to the main wind, in a way that allows the incorporation of the emissions encountered along their trajectory. Lagrangian models also use K-theory to calculate vertical and (when available) horizontal diffusion.

The main advantage of Lagrangian models versus Eulerian ones is computational speed, which can be one to two orders of magnitude faster because of the smaller number of grid cells used in Lagrangian models versus Eulerian models². Lagrangian models, however, provide concentration outputs along trajectories and, therefore, their outputs are difficult to compare with concentration measurements at fixed locations. Eulerian models are described later in this chapter.

6.4.2 The EKMA Technique

A proper elaboration of the outputs of Lagrangian photochemical models allows the use of a simple method, the so-called EKMA (Empirical

² The new generation of Unix workstations and PCs, however, has sharply decreased computer costs.

Kinetic Modeling Approach) technique (Dodge, 1977) to evaluate the importance of both NMHC and NO_x (and their ratio) in formulating O_3 control strategies. An example of EKMA isopleths is presented in Figure 10, in which point A illustrates a city that is characterized by an NMHC: NO_x ratio of 8:1 and a "design" value (defined as the second highest hourly O_3 measured concentration) of O_3 of 0.28 ppm. The isopleths allow the definition of different strategies to meet a certain ozone air quality standard. For example, if no change in ambient NO_x is expected and the future goal for the design value of ozone is 0.12 ppm, then the control strategy requires a progress from point A to point B in Figure 10, i.e., a reduction of NMHC by approximately 67 percent.

As seen in the example above, the EKMA method establishes, graphically, a relationship between the concentrations of ozone "precursors" (NO_x and NMHC) and the design value of ozone. Note the non-linearities in Figure 10:

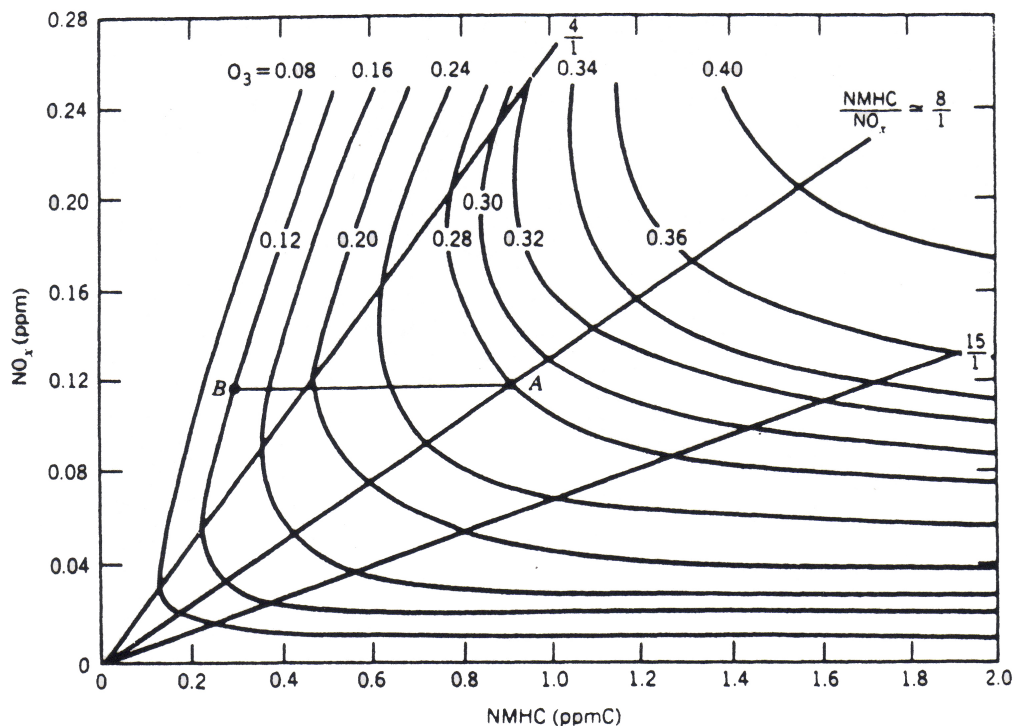


Figure 10. Ozone isopleths used in the EKMA approach (from Dodge, 1977, as presented by Finlayson-Pitts and Pitts, 1986).

EKMA isopleths should be used with caution, since they represent an oversimplified empirical description of complex nonlinear phenomena. Depending on the position of A, different emission reductions of NMHC and/or NO_x can cause both decrease and *increase* of O_3 . For example, for high NMHC-to- NO_x ratios, O_3 does not vary with NHMC controls, while for low NMHC-to- NO_x ratios, NO_x controls can actually *increase* O_3 . Generic isopleths in Figure 10 are

based on a series of chemical, meteorological, geographical, background and emission assumptions. A computer program, the OZIPM-2 package (Gipson, 1984) allows the generation of city-specific isopleths under conditions defined by the user.

7 Modeling of Heterogeneous and Aqueous Processes

7.1 Mathematical Modeling of Aerosol Formation

In the ambient atmosphere, particles are present in different sizes, shapes, phases, colors (light extinction properties), and composition. Each particle undergoes the processes described in Section 3.5. Therefore, one way to formulate a model would be to “follow” the development of individual particles. This is a rather cumbersome way to construct a model. Therefore, mathematical models generally follow a population of particles, which is characterized by its size distribution. This size distribution function can be expressed as number, surface area, or mass of particles in a given particle size (e.g., diameter). The area under the size distribution curve for each size range represents the number, surface area, or mass of particles in that range. Using $n(v,t)$ to represent the continuous particle number distribution as a function of volume and time, the *general aerosol dynamics equation* is formulated as follows:

$$\begin{aligned} \frac{\partial n(v,t)}{\partial t} = & \frac{1}{2} \int_0^v K(v-\tilde{v}, \tilde{v}) n(v-\tilde{v}, t) n(\tilde{v}, t) d\tilde{v} \\ & - n(v,t) \int_{v_0}^{\infty} K(v, \tilde{v}) n(v, t) n(\tilde{v}, t) d\tilde{v} \\ & - \frac{\partial}{\partial v} [I(v)n(v,t)] + J_0(v)\delta(v-v_0) \\ & (+ S(v,t)) \end{aligned} \quad (67)$$

The general dynamics equation is an integral differential equation. The first two terms on the right hand side represent coagulation, where K is the coagulation coefficient as a function of the sizes of the coagulating particles. The third term represents condensation, where

$$I(v) = \Delta v(p_k - e_k) \quad (68)$$

In Equation 68, $I(v)$ is the rate of change of the volume of a particle of size v ; Δv is the volume associated with a monomer; p_k is the frequency (s^{-1}) with which a monomer collides with a k -mer, i.e., condensation, such that the rate of condensation is defined by the product of p_k and number concentration in the particular size range; and e_k is the frequency of monomer evaporation. These processes occur at the surface of the particles, and the mass transfer of the condensing monomers from the bulk gas phase is not taken into account in the

general dynamic equation for aerosols. The fourth term in the general dynamics equation represents nucleation, at size v_0 . The last term is needed in the presence of a source, $S(v,t)$.

In practice, the range of sizes is frequently divided into a number of bins or sections. The number, surface area, or mass of particles in each section then characterizes the aerosol size distribution. This discrete representation of the particle size distribution is called the *sectional* approach. Alternately, the particle size distribution can be approximated by a series of functions characterizing different modes, e.g., lognormal distributions, and this approach is referred to as the *modal* approach.

In the simulation of particles in 3-D models, nucleation, condensation/evaporation, and coagulation need to be modeled in conjunction with kinetic mass transfer from the bulk gas phase to the particle surface. In 3-D models, a number of computational techniques are used to facilitate the numerical simulation of particles. For example, the operator splitting approach is used to solve each term in Equation 67 sequentially. Since coagulation can typically be ignored in urban and regional atmospheres, we will focus on nucleation and condensation/evaporation in the following discussion.

7.2 Nucleation

Among the inorganic compounds of concern, sulfuric acid (H_2SO_4) has a very low vapor pressure and will preferentially reside in the particulate phase. In fact, H_2SO_4 is one of the most important nucleating species. A review of algorithms used in air quality models to predict the absolute rate of nucleation has shown that such algorithms are highly uncertain (Zhang et al., 1999). An alternative approach consists in calculating the relative rates of new particle formation and condensation (McMurry and Friedlander, 1979), and to use the new particle formation rate as a boundary condition at the lower end of the particle size distribution rather than through a detailed mechanistic representation. However, one should note that our understanding of the formation of new particles is still incomplete. Woo et al. (2001) measured the formation of new particles in various ultrafine size ranges depending on the atmospheric conditions. Formation of new particles in the 3-10 nm range is believed to be associated with the nucleation of H_2SO_4 , H_2O and ammonia (NH_3) molecules (McMurry et al., 2000). However, the sources of the new particles formed in the 10-30 nm and 30-45 nm ranges are currently unknown.

Although some organic compounds are known to form new particles, e.g., products from monoterpenes (e.g., Hoffmann et al., 1998; Yu et al., 1999), the nucleation of organic compounds is not currently included in common 3-D models.

7.3 Equilibrium Partitioning of Inorganic Species

Several approaches have been used to simulate the thermodynamic equilibrium of inorganic species between the gas and particulate phases. Note that the same equilibrium relationships are used in the modeling of both aqueous particles and droplets.

7.3.1 Gas/Aqueous Partitioning

Chemical species that are soluble will partition between the gas phase and the aqueous phase. In the case of dissolution, their partitioning involves mass transfer from the bulk gas phase to the surface of the liquid droplets, thermodynamic equilibrium at the surface of the droplet (or particle) between the gas phase and the liquid phase, and mass transfer from the droplet surface to the bulk aqueous phase. The probability that a molecule that encounters the droplet surface will stick to it should also be taken into account; it is represented by the mass accommodation coefficient, α , with values ranging from 0 to 1. In the case of volatilization, these processes take place in reverse order.

The characteristic time for gas-phase diffusion is less than 10^{-2} s. The characteristic time for reaching equilibrium at the gas/droplet interface is less than 1 s for soluble gases that have an accommodation coefficient above 0.1. Characteristic times for diffusion within the droplet range from about 0.01 s for a typical cloud droplet (i.e., radius of 10 μm) to 100 s for a typical raindrop (i.e., radius of 1 mm). Therefore, mass transfer will generally not be rate limiting compared to most aqueous-phase reactions (half-lives on the order of minutes) of interest except for raindrops where aqueous-phase diffusion may become the rate-limiting step.

Thermodynamic equilibrium at the surface of the droplet can be represented by Henry's law for atmospheric trace species since their low concentrations lead to dilute solutions. The gas-phase concentrations, C_g , and the aqueous-phase concentrations, C_a , are thus related as follows.

$$H = \gamma C_a / C_g \quad (69)$$

where H is the Henry's law coefficient (in M/atm) and γ is the activity coefficient of the species in solution. The activity coefficient represents the fact that the droplet is not an ideal solution; it tends toward a value of unity as the solution becomes more dilute. For compounds that are not very soluble, the Henry's law constant can be estimated by the ratio of the saturation vapor pressure to the solubility - both quantities may be measured experimentally or estimated using group contribution methods.

If the liquid water content of the droplet is L (in g/m^3), then the mass balance over the gas and aqueous phases can be expressed as follows.

$$C_T = C_g \times 10^{-6} \times P / RT + C_a \times L / \rho \quad (70)$$

where C_T is the total concentration (gas-phase and aqueous-phase) in moles per m^3 of air, C_g is in ppm, C_a is in moles per liter of water (M), ρ is the density of the droplet in g/L, R is the gas constant ($8.2056 \times 10^{-5} m^3 \text{ atm K}^{-1} \text{ mol}^{-1}$), T is the temperature (K) and P is the pressure (atm). Expressing C_a as a function of C_g with Equation 69 provides the gas-phase concentration as a function of C_T .

$$C_g = \frac{C_T}{10^{-6} \frac{P}{RT} + \frac{LH}{\gamma\rho}} \quad (71)$$

Similarly, the aqueous-phase concentration can be expressed as a function of the total concentration.

$$C_a = \frac{C_T}{10^{-6} \frac{\gamma P}{HRT} + \frac{L}{\rho}} \quad (72)$$

Thus, the amount of a soluble species present in cloud and fog droplets is a function of its solubility (via its Henry's law coefficient, H) and the liquid water content (L).

For a dilute solution, $\gamma = 1$, $\rho = 10^3 \text{ g/L}$. At the surface, $P = 1 \text{ atm}$, and the fraction of the chemical species mass present in the aqueous phase, f_a , is as follows.

$$f_a = \frac{C_a L}{C_T} = \frac{1}{\frac{10^{-6}}{HRTL} + 10^{-3}} \quad (73)$$

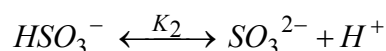
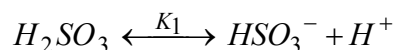
The Henry's law coefficient is a function of temperature (solubility typically increases with decreasing temperature). Values of Henry's law coefficients of major atmospheric species are available, for example, in Seinfeld and Pandis (1998), Jacobson (1999) and Finlayson-Pitts and Pitts (2000). Table 4 presents gas/liquid equilibria for selected atmospheric species.

According to Equation 73, chemical species with a Henry's law coefficient less than 400 M atm^{-1} will have less than 1% of their mass in the aqueous phase for a liquid water content of 1 g/m^3 at 298 K. Such species include O_3 , NO and NO_2 . The Henry's law coefficient of SO_2 is also less than 400 M atm^{-1} . However, SO_2 will dissociate in solution and it is, therefore, necessary to consider its effective

Henry's law coefficient that will include not only $SO_{2(aq)}$ but also its dissociation ions as discussed below.

7.3.2 Ionic Equilibria

Within an aqueous solution, some chemical species may dissociate into ionic forms. For example, the dissociation of $SO_{2(aq)}$ (hydrated as H_2SO_3) is represented as follows.



where

$$K_1 = \frac{\gamma_{HSO_3^{2-}} [HSO_3^-] \gamma_{H^+} [H^+]}{\gamma_{H_2SO_3} [H_2SO_3]} \quad (74)$$

$$K_2 = \frac{\gamma_{SO_3^{2-}} [SO_3^{2-}] \gamma_{H^+} [H^+]}{\gamma_{HSO_3^-} [HSO_3^-]} \quad (75)$$

In a cloud or fog droplet, the solution is generally sufficiently dilute that the activity coefficients $\left(\gamma_{H^+}, \gamma_{H_2SO_3}, \gamma_{HSO_3^-}, \text{ and } \gamma_{SO_3^{2-}} \right)$ can be assumed to be equal to one. The same is not always true for particles. Thus, the concentrations of HSO_3^- and SO_3^{2-} can be expressed as a function of $SO_{2(aq)}$ and the total concentration of dissolved SO_2 (including its ions), $[S(IV)]$ is as follows:

$$[S(IV)] = [SO_2(aq)] \left(1 + \frac{K_1}{[H^+]} + \frac{K_1 K_2}{[H^+]^2} \right) \quad (76)$$

We can then define the effective Henry's law coefficient as the ratio of the total dissolved SO_2 concentration to the SO_2 gas-phase concentration. It is related to the standard Henry's law coefficient as follows:

$$H_{SO_2,e} = H_{SO_2} \left(1 + \frac{K_1}{[H^+]} + \frac{K_1 K_2}{[H^+]^2} \right) \quad (77)$$

Table 5 summarizes the ionic dissociation equilibria of SO_2 (H_2SO_3), H_2SO_4 , HNO_3 , NH_3 (NH_4OH), CO_2 (H_2CO_3) and H_2O . The effective Henry's law

coefficient of SO₂ at a pH of 4.5 is equal to 622 M atm⁻¹; therefore, more than 1% of SO₂ will be present in the cloud droplet for a liquid water content of 1 g/m³.

The droplet must remain electrically neutral, that is, the positive charges of the cations must balance the negative charges of the anions. For a droplet that contains only H₂O and dissolved CO₂, the electroneutrality equation is expressed as follows.

$$[H^+] = [HCO_3^-] + 2[CO_3^{2-}] + [OH^-] \quad (78)$$

where bracket signs denote concentrations. For a CO₂ gas-phase concentration of 360 ppm, the droplet pH is 5.6. For a droplet that contains H₂O, SO₂, H₂SO₄, HNO₃, NH₃ and CO₂, this electroneutrality equation is expressed as follows.

$$[NH_4^+] + [H^+] = [HSO_3^-] + 2[SO_3^{2-}] + [HSO_4^-] + 2[SO_4^{2-}] + [NO_3^-] \\ + [HCO_3^-] + 2[CO_3^{2-}] + [OH^-] \quad (79)$$

The concentrations of the anions and cations of the dissolved species can be expressed in terms of the total concentrations of the dissolved species (using Equation 71) and [H⁺] must be solved numerically via iterative techniques. Techniques frequently used include the Newton bisection method (Press et al., 1997) and others described in the next section. If one assumes that the pH is in the range of 3 to 5 (a typical range of values for most atmospheric conditions), some assumptions can be made that allow the simplification of the system to a quadratic equation for [H⁺] that can be solved analytically.

7.3.3 Solving Inorganic Thermodynamic Equilibria

Depending on the identities of reactants and products, the dimension of the equilibrium coefficient (K_{eq}) change. One should note that when a solid phase is involved, its activity is always assumed to be one. Several approaches are used to solve the thermodynamic equilibrium relationships. The most comprehensive approach consists in minimizing the Gibbs free energy of the multiphase system. In minimizing the Gibbs free energy, one is able to find the most stable state; this approach is, however, computationally prohibitive for explicit incorporation into most 3-D air quality models (an alternative is to parameterize the results of pre-existing simulations and retrieve the desired values from a look-up table when running the air quality model).

A more common approach used in air quality models is to solve the system of equations describing the multiphase equilibria (see Table 3 for an example). The derivation of the equilibrium relationship from the minimization of Gibbs free energy (i.e., finding the most stable state of a system), can be found in many thermodynamics textbooks and is not discussed here.

The above principles are applicable for both aqueous particles and droplets. For any system of species, many equilibrium relationships are satisfied (see Table 3). Therefore, mathematically a system of equilibrium equations needs to be solved simultaneously. As discussed in the previous section, the system of inorganic equations may be simplified algebraically into one equation in $[H^+]$. However, iterative procedures are still required to solve the equations and solving the full set of equations can still be computationally demanding. Therefore, simplifications are often made to break down the entire solution domain into subdomains that can be characterized by specific chemical regimes. In each regime, certain species may be dominant so that the less important species can be neglected without introducing significant errors into the solution. Thus, the number of equilibrium equations is reduced and the solution is obtained more rapidly.

Clearly, the number of chemical species treated in the inorganic aerosol model affects the complexity of the thermodynamic equilibrium calculations. All models treat sulfate, nitrate, ammonium and water. Some models also treat sodium and chloride to represent sea salt. Finally, the most comprehensive models also treat crustal species, i.e., magnesium, calcium, potassium and carbonate (see Zhang et al., 2000 for a comprehensive review of inorganic equilibrium modules).

7.4 Equilibrium Partitioning of Organic Species

For organic species, the first models assumed that condensable organic compounds had very low vapor pressure and consequently partition totally into the particulate phase. This is the so-called “fixed yield” approach. Later, the fixed yield model was improved to represent the saturation of organic compounds in the gas phase, and partition only the portion above saturation into the particulate phase. The saturation model was superseded by several different formulations in recent years. These include absorption, adsorption, and dissolution, as discussed in Section 3.2. One absorption formulation by Pankow (1994a, b) is used in several newer models. For compound i , the partition constant is determined as

$$K_{p,i} = \frac{A_i/TSP}{G_i} = \frac{760RTf_{om}}{10^6 \gamma_{om,i} p_{L,i}^0 MW_{om}} \quad (80)$$

where A_i is the concentration of compound i in the particulate phase (in $\mu\text{g}/\text{m}^3$ air), TSP is the total suspended particulate matter (in $\mu\text{g}/\text{m}^3$ air), G_i is the gas-phase concentration (in $\mu\text{g}/\text{m}^3$ air), R is the universal gas constant ($8.2 \times 10^{-5} \text{ m}^3 \text{ atm mol}^{-1} \text{ K}^{-1}$), T is temperature in K, f_{om} is the weight fraction of the particles that comprise the absorbing organic material phase, $p_{L,i}^0$ (torr) is the saturation vapor pressure of compound i in liquid form (sub-cooled, if necessary), $\gamma_{om,i}$ is the activity coefficient of i in mole fraction scale in the liquid phase, and MW_{om} is the

average molecular weight in the liquid phase. More recently, it has been suggested that the octanol/air partition coefficient may be used instead of $p_{L,i}^0$ as the correlating variable for the particle/air partition coefficient (Pankow, 1998) as follows:

$$K_{p,i} = K_{oa} \frac{\gamma_{oct,i}}{\gamma_{om,i}} \frac{MW_{oct} f_{om}}{10^{12} MW_{OM} \rho_{oct}} \quad (81)$$

where K_{oa} is the octanol/air partition coefficient, $\gamma_{oct,i}$ is the activity coefficient of compound i in octanol, MW_{oct} is the molecular weight of octanol, and ρ_{oct} is the density (kg m^{-3}) of octanol.

The adsorption partition constant in this case takes the following form (Pankow, 1994a,b):

$$K_{p,u} = \frac{N_s a_{tsp} T e^{(Q_l - Q_v)/RT}}{1600 p_{L,i}^0} \quad (82)$$

where N_s is the number of adsorption sites per cm^2 , a_{tsp} is the surface area of the particles ($\text{m}^2 \text{g}^{-1}$), Q_l and Q_v are the enthalpies of desorption and volatilization (kJ mol^{-1}), and R is the universal gas constant in SI units ($8.3 \times 10^{-3} \text{ kJ K}^{-1} \text{ mol}^{-1}$).

Dissolution is formulated using a regular equilibrium relationship (similar to the ammonia-ammonium equilibrium in Table 3, second row).

7.5 Treatment of Aqueous Chemistry and Multiphase Chemistry in Models

The kinetics of the oxidation of S(IV) to S(VI) by H_2O_2 is as follows (S(VI) refers to H_2SO_4 and its ions).

$$\frac{d[S(VI)]}{dt} = k_1 [H^+] [H_2O_2] [S(IV)] \quad (83)$$

where k_1 is in the range of 7.2×10^7 to $9.6 \times 10^7 \text{ M}^{-2}\text{s}^{-1}$ (Lee et al., 1986; Lind et al., 1987). At $\text{pH} = 4.5$ and for a gas-phase H_2O_2 concentration of 1 ppb, the reaction of SO_2 with H_2O_2 is fairly rapid with a half-life of 7 s. The solubility of SO_2 is nearly inversely proportional to the concentration of H^+ (for pH above 2; see ionic equilibria above); therefore, the rate of S(VI) formation via this reaction is nearly independent of pH . Concentrations of H_2O_2 are typically on the order of a few ppb during summer months and less than 0.1 ppb during winter months in mid latitudes. However, concentrations of 1 ppb have been measured during winter in Texas, for example, as air masses from subtropical regions are transported northward (Seigneur et al., 2000).

The kinetic rate expression for the SO₂-O₃ reaction is as follows.

$$\frac{d[S(VI)]}{dt} = (k_2 [H_2SO_3] + k_3 [HSO_3^-] + k_4 [SO_3^{2-}]) [O_3] \quad (84)$$

where $k_2 = 2.4 \times 10^4 \text{ M}^{-1} \text{ s}^{-1}$, $k_3 = 3.7 \times 10^5 \text{ M}^{-1} \text{ s}^{-1}$ and $k_4 = 1.5 \times 10^9 \text{ M}^{-1} \text{ s}^{-1}$ (Hoffmann, 1986). For an O₃ gas-phase concentration of 60 ppb and a droplet pH of 4.5, the half-life of this reaction is 46 min. As the reaction proceeds, the pH of the droplet will decrease because of S(VI) formation. The distribution of S(IV) aqueous species will shift from SO₃²⁻ toward HSO₃⁻ (see ionic equilibria above) and the reaction rate will decrease. Therefore, this reaction is self-limiting.

For a pH value around 4, the following expression is recommended for the SO₂-O₂ oxidation reaction catalyzed by Fe³⁺.

$$\frac{d[S(VI)]}{dt} = k_5 [Fe^{3+}]^2 [S(IV)] \quad (85)$$

where $k_5 = 10^9 \text{ M}^{-2} \text{ s}^{-1}$. This reaction is also a strong function of pH. Martin (1994) provides rate expressions for this catalyzed reaction. It is most important for pH values above 5 and it is self-limiting. For example, for a concentration of 0.1 μM for Fe³⁺ and a pH of 4.5, the half-life of this reaction is 19 hours. For a pH in the range of 5 to 6, the half-life is only 12 min.

Aqueous phase chemical kinetics, like its gas-phase counterpart, involve a stiff system of ordinary differential equations. Techniques to solve stiff ODES have been discussed in Section 6.3.

8 Modeling of Reactive Plumes

8.1 Chemistry of Plumes

Plumes that contain high concentrations of NO_x (e.g., coal-fired power plant plumes) have a chemistry that differs significantly from that of the ambient background because the plume chemistry is initially VOC-sensitive and radical-limited. Therefore, the rates of formation of secondary acids such as HNO₃ and H₂SO₄ are slow as observed in power plant plumes (Richards et al., 1981; Gillani et al., 1998) and reproduced in computer simulations (Seigneur, 1982; Hudischewskyj and Seigneur, 1989; Karamchandani et al., 1998). As the plume becomes more dilute, the NO_x plume concentrations will approach the NO_x concentrations of the ambient background atmosphere. Plume chemistry will then depend on whether oxidant formation in the background atmosphere is NO_x- or VOC-sensitive.

We can distinguish three stages in plume chemistry, as summarized in Figure 12. The number of reactions needed to properly describe the plume chemistry increases from one stage to the next and also differs between daytime and nighttime. Karamchandani et al. (1998) described the chemistry of each stage. We summarize those chemical mechanisms below.

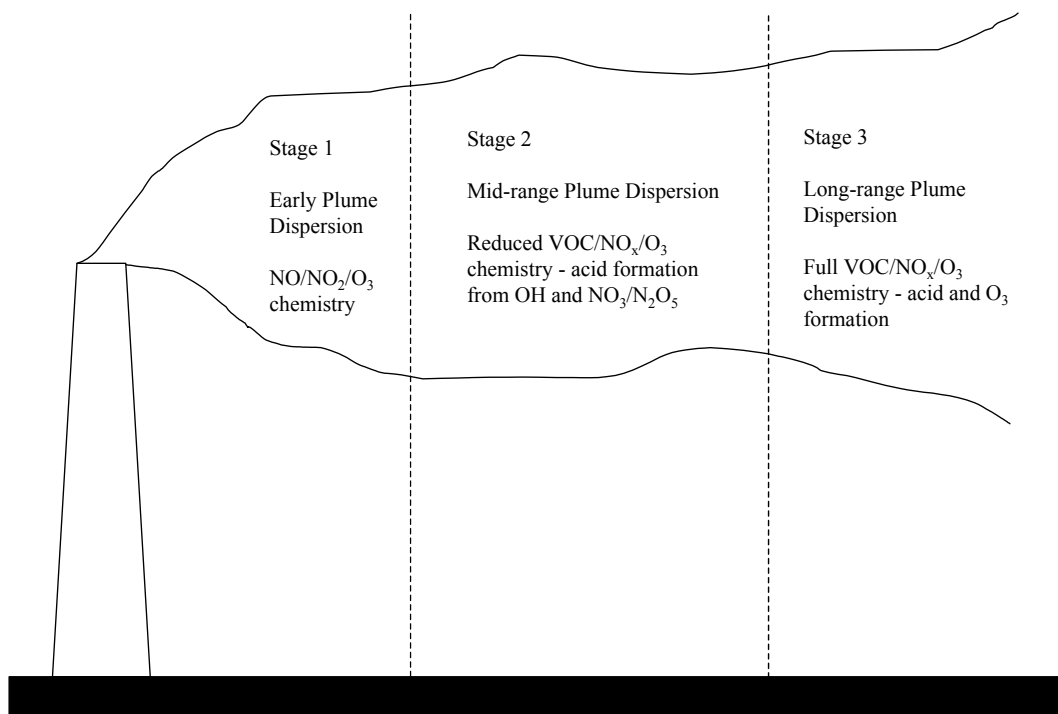


Figure 12. Schematic description of the evolution of plume chemistry with dispersion (source: Karamchandani et al., 1998; reprinted with permission from ACS).

8.1.1 Stage 1 Chemistry

Daytime.

Stage 1 corresponds to the conditions during the early stages of plume dispersion, when NO concentrations are high. During the day, the dominant reactions in this stage include four reactions among five species. This reaction set consists of the three reactions of the photostationary state between NO , NO_2 and O_3 and the termolecular oxidation of NO by O_2 . This latter reaction is important very near the stack where NO concentrations are very high (i.e., above about 1 ppm). At NO concentrations of about 1 ppm, the rate of destruction of NO by O_2 is about 1%/hr. Further downwind, the oxidation of NO by O_2 becomes negligible, because its rate is proportional to the square of the NO concentration and, therefore, decreases rapidly.

Nighttime.

At night, the photolysis of NO_2 does not take place and only the oxidation reactions of NO by O_2 and O_3 need to be taken into account. Therefore, NO gets depleted and converted irreversibly to NO_2 .

8.1.2 Stage 2 Chemistry*Daytime.*

In Stage 2, the mid-range plume dispersion stage, reactions that form the radicals that lead to the formation of HNO_3 and H_2SO_4 must be considered. These radicals also lead to some ozone formation. However, at this stage, NO_x concentrations in the plume are significantly larger than VOC concentrations, so that O_3 concentrations within the plume are still lower than in the background air. Stage 2 daytime chemistry can be represented by the following set of reactions:

- (1) The three photostationary state reactions among NO , NO_2 and O_3 . Note that the termolecular oxidation of NO by oxygen can be neglected in Stage 2 once plume NO concentrations are low enough.
- (2) Photolytic reactions of O_3 , aldehydes, HNO_2 , and H_2O_2 and the two reactions of $\text{O}(^1\text{D})$ that lead to the formation of free radicals and, directly or indirectly, formation of OH and HO_2 radicals.
- (3) Reactions corresponding to PAN chemistry and the production of radicals through PAN thermal decomposition. In the presence of high NO concentrations, PAN can be an important source of radicals.
- (4) The reaction of NO with HO_2 to form NO_2 and OH , thereby converting HO_2 radicals to OH radicals, and oxidizing NO to NO_2 without O_3 consumption.
- (5) The oxidation of NO , NO_2 and SO_2 to HNO_2 , HNO_3 and H_2SO_4 , respectively.

The differences between the daytime Stage 1 and Stage 2 mechanisms reside, therefore, in the fact that the chemistry of OH radicals is included in the Stage 2 mechanism, thereby allowing for secondary acid formation.

At this point of plume chemistry, reactions leading to O_3 formation are not important. This is apparent when comparing the rates of the oxidation reaction of NO to NO_2 by O_3 and HO_2 . O_3 formation takes place when the latter reaction proceeds at a non-negligible rate, thereby producing NO_2 (which by photolysis leads to O_3 formation) without consuming O_3 . In Stage 2, the ratio of the relative rates of the reactions of NO with O_3 and NO with HO_2 at the plume centerline is typically greater than 100. Therefore, in Stage 2, the reaction of NO with HO_2 is essential because it converts HO_2 to OH , but not because of its role in the conversion of NO to NO_2 .

It is interesting to note that the reactions of VOC with OH contribute significantly to the consumption of OH radicals in the plume (the consumption of OH by VOC is commensurate with the reactions leading to secondary acid formation). Therefore, it may seem like VOC reactions with OH should be important. However, this is not the case because the VOC/OH reactions lead to HO₂ radicals, which are rapidly converted back to OH radicals by reaction with NO. This conversion occurs without significantly affecting the NO/NO₂/O₃ concentrations since these concentrations are primarily governed in Stage 2 by the photostationary state reactions, as discussed above. Moreover, the oxidation of VOC in the plume is sufficiently slower than in the background atmosphere, that it can be neglected without significantly affecting the VOC concentrations.

Nighttime.

At night, the photolysis reactions can be neglected. However, additional reactions are required to represent the formation of NO₃ radicals and N₂O₅, and the formation of nitric acid by hydrolysis of N₂O₅. The set of reactions for Stage 2 for nighttime consists of reactions that can be grouped according to the following major categories:

- (1) The oxidation of NO by O₃ to form NO₂.
- (2) The reactions that determine NO₃ radical concentrations, i.e., reactions of NO₂ with O₃ to form NO₃, reactions of NO₃ with NO and NO₂, subsequent formation of N₂O₅ via the latter reaction, and decomposition of N₂O₅ into its precursors.
- (3) The formation of HNO₃ through N₂O₅ hydrolysis.
- (4) The reactions of nocturnal PAN chemistry that lead to OH formation by reaction of NO with peroxy radicals.
- (5) The formation of HNO₂, HNO₃, and H₂SO₄ by reaction of NO, NO₂ and SO₂, respectively, with OH.
- (6) The radical chain termination reactions for regions of the plume where all NO has been consumed by reaction with O₃.

The differences between daytime and nighttime chemistry during Stage 2 can be summarized as follows:

- (1) The lack of NO₂ photolysis at night leads to titration of NO and O₃, which will result in zero NO concentrations at the edges of the plume, and, possibly, zero O₃ concentrations at the plume core, particularly near the stack.
- (2) The chemistry of NO₃ is important at night (NO₃ radicals are photolyzed rapidly during the day) and can lead to significant HNO₃ formation.
- (3) In cases where background PAN concentrations are high (i.e., several ppb), its thermal decomposition in the presence of high NO concentrations leads to significant OH concentrations that are generated through reaction of NO with peroxy radicals (i.e., CH₃COO₂, CH₃O₂, and HO₂). Consequently, HNO₂, HNO₃ and H₂SO₄ formation will take place by OH oxidation of NO, NO₂ and SO₂, respectively. However, the OH

concentrations are lower during nighttime than daytime, since the photolytic reactions that generate radicals do not occur at night.

8.1.3 Stage 3 Chemistry

For dispersion of the plume at long distances where mixing with the background air has become significant, the chemistry of VOC oxidation becomes important. To simulate plume chemistry in Stage 3, a full chemical mechanism must be used.

At that point, plume chemistry will depend on whether the background atmosphere is VOC- or NO_x -sensitive for oxidant formation. If the background is NO_x -sensitive, the plume will display higher oxidant concentrations than the ambient background due to its greater NO_x concentrations; consequently, the formation of secondary acids (H_2SO_4 and HNO_3) will also occur at a faster rate in the plume than in the background. Then, as the plume becomes more dilute, plume chemistry will switch from a VOC-sensitive regime to a NO_x -sensitive regime, i.e., the rates of formation of HNO_3 and H_2SO_4 will decrease sharply and peroxides such as H_2O_2 will start forming in significant amounts in the plume. This behavior has been described via computer simulations (Karamchandani and Seigneur, 1999) as well as observed in data collected by aircraft at different downwind distances within plumes (Gillani et al., 1998). On the other hand, if the background atmosphere is VOC-sensitive for oxidant formation, the plume chemistry will tend to approach the background chemistry asymptotically and the rates of formation of H_2SO_4 and HNO_3 in the plume will approach those of the background as the plume becomes more dilute.

The explicit formulation of a chemical kinetic mechanism for these various stages of plume chemistry has been developed by Karamchandani et al. (1998) along with specific criteria based on plume and background concentrations of key species to identify the boundaries between the various stages in plume chemistry.

8.2 Gaussian Plume Models with Linear Chemistry

As described in Chapter 7A of Volume I, many plume dispersion models assume Gaussian profiles for the crosswind plume concentrations. Several of those plume models have been augmented with a simple treatment of atmospheric chemistry using first-order (i.e., linear) rate expressions. An example of such plume chemistry representation is the Mesopuff chemistry option in CALPUFF (Scire et al., 1990). As was discussed above, plume chemistry is a highly non-linear dynamic system since the VOC/ NO_x ratio changes drastically as the plume becomes diluted into the background atmosphere. Therefore, plume models that use linear chemistry provide an incorrect description of plume chemistry and are unlikely to accurately simulate the concentrations of secondary pollutants such as H_2SO_4 and HNO_3 in the plume. Such models should, therefore, be used only for screening purposes.

8.3 Reactive Plume/Puff Models

Several models have been developed that combine some advanced treatment of atmospheric chemistry with a plume dispersion/transport model. Two major approaches have been used to represent plume dispersion/transport. One approach uses Lagrangian trajectories of plume cross-sections, implicitly involving the slender plume approximation. Another approach uses a population of puffs to represent the plume via their ensemble aggregation. Plume chemistry has been combined with both approaches.

Examples of reactive plume models that are based on plume cross-sections include the Reactive Plume Model (RPM) (Stewart and Liu, 1981), PLMSTAR (Hudischewskyj and Seigneur, 1989), the Panache Réactif en Atmosphère avec Dépôts (PARADE) (Joos and Seigneur, 1994), the Reactive & Optics Model of Emissions (ROME) (Seigneur et al., 1997), and the plume module of the 3-D Models-3/CMAQ modeling system (Gillani and Godowitch, 1999). All these models contain a full chemical kinetic mechanism such as CBM-IV with, in some cases, additional reactions and processes to represent secondary aerosol formation. Evaluation of model simulation results against atmospheric data collected by aircraft in plumes have shown that such reactive plume models can capture the major features of plume dispersion and chemistry, although their performance is typically severely limited by the availability of representative meteorological data (e.g., Hudischewskyj and Seigneur, 1989; Gabruck et al., 1999).

Some of the major weaknesses of plume cross-section models include their inaptitude at properly representing the effect of wind shear on plume dispersion and simulating overlapping plumes. Such limitations can be removed by using a puff modeling approach. SCIPUFF (Sykes et al., 1993; Sykes and Henn, 1995) is an example of a puff model that represents plume transport and dispersion by means of a population of puffs that expand as atmospheric turbulence dilutes their material according to the local micrometeorological characteristics. Wind shear and puff overlap are treated within SCIPUFF and more realistic representations of plume dynamics can be obtained compared to plume cross-section models. SCIPUFF has been augmented with plume chemistry and the resulting model, SCICHEM, has been evaluated against plume data (Karamchandani et al., 2000). In addition, the effect of turbulence on chemical kinetics can be simulated explicitly. This effect is more pronounced near the stack. Also, puff chemistry can be simulated in SCICHEM using the staged chemistry approach described above, in order to minimize computations.

9 Eulerian Models

Eulerian models can be used to simulate the evolution of O₃ and PM in a 3-D gridded domain. Eulerian dispersion models are described in some detail in

Chapter 10 of Volume I. In addition to dispersion and transport, which are related to the meteorological aspect of air pollution modeling, the other components for an Eulerian model include emissions (Chapter 3), chemistry (this chapter), gas/particle partitioning (this chapter), and wet and dry deposition (Chapter 13). Many Eulerian models are currently used in research and regulatory arenas. For urban to regional air quality simulations, we will list models that simulate both O₃ and PM, because PM models have the capability to simulate O₃. We will focus on the components or atmospheric transformations in these models.

9.1 Eulerian Ozone and PM Models

Table 6 lists sixteen 3-D air quality models that have been used for simulating PM in the lower troposphere. Details of twelve of these models can be found in a comprehensive review by Seigneur and Karamchandani (2001). The PM capabilities of CHIMERE, CAMx, AURAMs, and EMEP were developed since 2001, and readers will need to refer to their websites/publications for additional information. CHIMERE was developed by French organizations and is applied for air quality research, management and forecasting. CAMx is an urban/regional model that has been applied primarily in the U.S. but also in Europe. AURAMS is a new model developed by Environment Canada that is designed to treat O₃ formation, PM and acid deposition. EMEP is an Eulerian model for acid deposition and O₃ that has been upgraded to treat PM by incorporating the multicomponent monodisperse model (MULTIMONO) developed at the University of Helsinki (Pirojola and Kulmala, 2000). Another air quality model for O₃, UAM-V, is currently being upgraded for PM, but no documentation is available as of 2004 beyond the design of UAM-VPM.

Table 6. 3-D air quality models for O₃ and PM in the lower troposphere.

Model	Institution	References
CHIMERE	Ecole Polytechnique, INERIS, Université de Paris, Laboratoire d'aérodologie de Toulouse	Schmidt et al., 2001; Bessagnet et al., 2004
CIT model	California Institute of Technology (Caltech)	McRae et al. (1982); McRae and Seinfeld (1983); Harley et al. (1993); Meng et al. (1998); Griffin et al. (2002)
European Acid Deposition Model (EURAD)	Ford Research Center, Germany	Hass et al., 1991, 1993, 1995, 1997; Liu et al., 1997; Langman and Graf, 1997; Ackermann et al., 1998.
Gas, Aerosol, Transport, and Radiation model (GATOR)	University of California at Los Angeles. Stanford University	Jacobson et al. (1996); Jacobson (1997b; 1997c; 2001a; 2001b); Lu et al. (1997a; 1997b).
Long Term Ozone Simulation Model (LOTOS)	TNO	Documentation in preparation

Model	Institution	References
Mesoscale Non-Hydrostatic Chemistry model (Meso-NH-C)	Centre National de Recherches Météorologiques (CNRM) and the Laboratoire d'Aérodologie.	http://www.aero.obs-mip.fr/mesonh
Models-3 Community Multiscale Air Quality modeling system (Models-3/CMAQ)	U.S. EPA Office of Research & Development (ORD) Alternative versions have been developed by Atmospheric and Environmental Research, Inc. (AER) and the National Research Council of Canada	EPA, 1999; Zhang et al., 2004 www.cmascenter.org
Regional Modeling System for Aerosols and Deposition (REMSAD)	Systems Applications International (ICF-Consulting) for the U.S. EPA Office of Air Quality Planning and Standards (OAQPS)	ICF Kaiser/SAI (1999); Wayland (1999); www.remsad.com
SARMAP Air Quality Model (SAQM) with aerosols (SAQM-AERO)	State University of New York at Albany and modified for PM by the Caltech, Sonoma Technology, Inc. and others for the California Air Resources Board (CARB)	Chang et al. (1996); Dabdub et al. (1997).
Sulfur Transport Eulerian Model (STEM) Version III	University of Iowa	Zhang (1994); Carmichael et al. (1998); Song and Carmichael (1999).
Urban Airshed Model (UAM) version IV with aerosols (UAM-AERO) (UAM-IV as host air quality model)	Caltech, Sonoma Technology, Inc. and others for the California South Coast Air Quality Management District (SCAQMD) and the CARB	Lurmann et al. (1997).
UAM-AERO for long-term simulations (UAM-AERO-LT) (UAM-AERO as base model)	Sonoma Technology, Inc. for SCAQMD	Lurmann (2000).
Urban and Regional Multiscale model (URM)	Carnegie-Mellon University and the Georgia Institute of Technology	Odman and Russel, 1991b, Kumar et al. (1994); Kumar and Russell (1996a; 1996b)
CAMx	Environ International Corporation	www.camx.com
EMEP	European Monitoring and Evaluation Programme	www.emep.int/common_publications.html
AURAMS	Environment Canada	Bouchet et al. (2004)

Gas-phase chemistry. The major chemical kinetic mechanisms that are currently in use include the following:

- Carbon-Bond Mechanism IV (CBM-IV)
- The GATOR derivative of the extended CBM version
- Statewide Air Pollution Research Center mechanism (SAPRC), versions 90, 93, 97 or 99
- Regional Acid Deposition Model mechanism version 2 (RADM2)
- Regional Atmospheric Chemistry Mechanism (RACM)
- Caltech Atmospheric Chemistry Mechanism (CACM)
- Regional Lumped Atmospheric Chemical Scheme (ReLACS)
- Micro CB4

Note that a given air quality model may provide the option to use several mechanisms.

CBM-IV is based on functional groups. It includes various versions that differ in their treatment of isoprene chemistry and radical termination reactions. The most recent version (e.g., available in Models-3/CMAQ, version 2001) includes 93 reactions and 36 species. CBM-IV is also used in URM, LOTOS, SAQM-AERO, UAM-AERO, and UAM-AERO-LT. As mentioned above, the GATOR mechanism is based on the CBM formulation.

RADM2, SAPRC, RACM and CACM are based on fixed surrogate molecules for organic compounds. RACM is an updated version of RADM2. SAPRC is updated regularly and the version number corresponds to the year of the update. CACM is based primarily on RACM.

RADM2 includes 158 reactions with 57 species, and it is used in EURAD and Models-3/CMAQ. Various version of SAPRC are used in URM, STEM-III, SAQM-AERO and UAM-AERO; SAPRC99 (<http://www.cert.ucr.edu/~carter>) for 3-D models includes 214 reactions among 78 species. Note that as a stand-alone mechanism (box model mode), SAPRC is flexible and the user is allowed to define the number of organic species and reactions. RACM is used in STEM-III; it includes 237 reactions with 77 species. CACM is used in CIT and Models-3/CMAQ; it includes 361 reactions among 189 species (including the explicit formation of condensable organic compounds). ReLACS was developed by condensing RACM; it is used in Meso-NH-C and includes 128 reactions among 37 species.

The micro CB4 mechanism is used in REMSAD. It includes 60 reactions with a very simplified treatment of VOC chemistry using only three VOC precursors in its original formulation.

Except for CACM, all the chemical kinetic mechanisms presented here were developed for O₃ formation. Therefore, the treatment of SOA formation requires the addition of additional reactions and species.

Solvers for gas-phase chemistry. Several numerical schemes are currently used in 3-D models to solve stiff ODE systems. The major ones include Young and Boris (used in URM, Models-3/CMAQ and CIT), SMVGEAR (used in GATOR and Models-3/CMAQ), the QSSA algorithm (used in Models-3/CMAQ, EURAD, Meso-NH-C and SAQM-AERO) and the implicit-explicit hybrid (IEH) method (SAQM-AERO, UAM-AERO). Other techniques used in some of the 3-D models include the Eulerian backwards-iterative solvers used in Models-CMAQ (mechanism-specific), the column pivot method used in REMSAD, and a sparse-matrix implicit solver used in STEM-III. Some models such as Models-3/CMAQ and Meso-NH-C offer a selection of several numerical schemes. Among those solvers, SMVGEAR is the most accurate; it is however computationally more demanding although it is efficient on parallel machines. The other solvers make compromises between speed and accuracy. Our own testing of Young and Boris, QSSA and IEH suggested that Young and Boris provided the best compromise between speed and accuracy. Test results may vary however depending on the tests selected.

Aqueous and heterogeneous chemistry. The chemical kinetic mechanisms used to simulate the aqueous chemistry range from simplistic mechanisms with only one reaction (oxidation of SO_2 by H_2O_2 in REMSAD) or two reactions (oxidation of SO_2 by H_2O_2 and O_3 in Meso-NH-C) to detailed mechanisms such as the Carnegie-Mellon University (CMU) mechanism with 99 reactions, 34 equilibria and 46 species. The CMU mechanism has been incorporated into Models-3/CMAQ and a version of UAM-AERO. Other mechanisms include the Reactive Scavenging Module (RSM) mechanism used in URM that includes two reactions for the oxidation of SO_2 to sulfate, the GATOR mechanism with 64 reactions and 74 species, the mechanism of Walcek and Taylor (1986) used in EURAD and Models-3/CMAQ that includes five reactions for the oxidation of SO_2 to sulfate, and the mechanism of Möller and Mauersberger (1995) available as an option in EURAD, that includes 66 reactions among 37 species. Some models (UAM-AERO, UAM-AERO-LT and an option in REMSAD) treat aqueous-phase chemistry by arbitrarily increasing the rate of SO_2 and NO_x oxidation to sulfate and nitrate, respectively. Such parameterizations are not recommended because they fail to properly represent the nonlinear relationships between precursors and oxidation products.

Heterogeneous processes include reactions at the surface of cloud droplets and particles. The major reactions taking place at the surface of cloud droplets include the hydrolysis of N_2O_5 to HNO_3 , the oxidation of NO_3 to NO_3^- and the scavenging of HO_2 to form H_2O_2 . These reactions may also occur at the surface of aqueous aerosols with, in addition, the disproportionation of NO_2 to HNO_3 and HNO_2 . Heterogeneous reactions at the surface of cloud droplets are generally treated as part of the bulk aqueous chemistry. Some mechanisms may, however, fail to include one of the reactions assuming that it is treated as part of the gas-phase/heterogeneous chemistry. For example, the CMU mechanism does not include the N_2O_5 hydrolysis reaction. It is, therefore, important to check that

these reactions are included in the model, either in the gas-phase or aqueous-phase mechanism.

Except for STEM-III and a recent version of Models-3/CMAQ, heterogeneous reactions at the surface of particles are not treated in the air quality models reviewed here. Such reactions may affect the formation of O₃, H₂SO₄, and HNO₃ in the presence of high concentrations of particles. For example, a simulation with heterogeneous reactions on particles showed 10% less O₃ production in the Los Angeles basin than the simulation without heterogeneous reactions.

Gas/particle partitioning of inorganic species. The partitioning of inorganic species between the gas phase and the particulate phase is governed by (1) mass transfer from the bulk gas-phase to the surface of the particle and (2) thermodynamic equilibrium of chemical species between the gas and particulate phases and within the particle. Detailed treatment of mass transfer is used only in two models, CIT and GATOR (a version of Models-3/CMAQ also includes this option but it has not been used). Some models use a hybrid approach that combines some full equilibrium assumptions with some size-distributed condensation process (e.g., UAM-AERO, Models-3/CMAQ). All the other models assume full equilibrium between the gas phase and the particulate phase.

The treatment of thermodynamic equilibrium is performed with a few major modules, most of which were reviewed by Zhang et al. (2000). These modules include the following:

- MARS-A: it uses simplifying assumptions for the sulfate/nitrate/ammonium/water system
- ISORROPIA: it uses simplifying assumptions for the same species as MARS-A with, in addition, sodium chloride (representing sea salt)
- SEQUILIB: it treats the same species as ISORROPIA but is not as accurate
- SCAPE2: it includes the same species as ISORROPIA with, in addition, potassium, magnesium, calcium and carbonate (representing soil dust)
- EQUISOLV II: it treats the same species as SCAPE2 but uses a different numerical solution procedure

MARS-A is used in Models-3/CMAQ, EURAD and LOTOS; it is also being incorporated into REMSAD, and Meso-NH-C uses a similar module. ISORROPIA is used in URM, UAM-AERO and Models-3/CMAQ. SEQUILIB was originally used in UAM-AERO and is still used in SAQM-AERO. SCAPE2 is used in CIT, STEM III and Models-3/CMAQ. EQUISOLV II is used in GATOR.

In addition, some models use parameterizations that are either based on simplifying assumptions or derived from a look-up table developed with a thermodynamic equilibrium model. Such parameterizations are used in REMSAD (as an option) and UAM-AERO-LT.

Gas/particle partitioning of organic species. The treatment of the partitioning of organic species between the gas phase and the particulate phase has evolved considerably over the past few years and the algorithms used in the various air quality models tend to reflect the time of their development. The major approaches to treating gas/particle partitioning for organic species can be summarized as follows:

- All condensable organic compounds are assumed to be in the particulate phase
- The partitioning is derived from experimental data (e.g., smog chamber experiments of Odum et al. (1996, 1997) and Griffin et al. (1999)) and is based on absorption into an organic particulate phase.
- The partitioning is based on Henry's law equilibrium for soluble organic compounds.
- The partitioning is derived from first principles and includes (1) absorption into an organic particulate phase and (2) dissolution into aqueous particles, e.g., MADRID (Pun et al., 2000, 2002).

The first approach is used in URM, STEM-III, REMSAD, SAQM-AERO, an early version of UAM-AERO, and, for some species, in GATOR. Note that REMSAD treats SOA as a fraction of the emitted VOC (i.e., there is currently no explicit treatment of SOA formation in the atmosphere; however, this is currently being revised).

The empirical partitioning approach based on absorption into an organic phase is used in Models-3/CMAQ, Meso-NH-C, UAM-AERO and UAM-AERO-LT. The solubility approach is used for some species in GATOR. The more comprehensive approach that includes both absorption into an organic phase and dissolution into aqueous particles is used in CIT and Models-3/CMAQ. EURAD and LOTOS do not treat organic aerosols.

Particle size distribution. The treatment of the particle size distribution in an air quality model falls into one of three categories:

- treatment of fine and/or coarse particles only
- treatment of the particle size distribution with a modal representation
- treatment of the particle size distribution with a sectional representation that includes more than two sections

Models that use the simple treatment of only fine and coarse particles include REMSAD and UAM-AERO-LT. Note that models that use a sectional representation (see below) can be applied with two size sections representing fine and coarse particles, respectively.

Models that use a modal representation include Models-3/CMAQ, EURAD, LOTOS, Meso-NH-C and STEM-III. Models-3/CMAQ and STEM-III treat both fine and coarse particles whereas EURAD, LOTOS and Meso-NH-C treat only fine particles.

Models that use a sectional representation with more than two size sections include URM, GATOR, SAQM-AERO, UAM-AERO, Models-3/CMAQ and CIT.

The models that use only one or two size sections only treat gas/particle partitioning but do not treat particle growth/shrinkage, coagulation and nucleation since the two sections can be assumed to be independent of each other.

Models that use a modal representation treat particle growth/shrinkage, coagulation and nucleation. However, they do not treat the kinetic mass transfer between the bulk gas phase and the particle surface.

Models that use a detailed sectional representation treat particle growth/shrinkage, may treat nucleation as a boundary condition for the lowest size section, and treat, in some cases, mass transfer (CIT and GATOR), except for GATOR, which does not treat coagulation.

9.2 Models for Toxic Air Pollutants

A comparison of five distinct Hg chemistry models developed in North America and Europe using the same data set for initialization has demonstrated that despite a common core of processes for Hg transformation processes, significant discrepancies still remain among the various existing models (Ryaboshapko et al., 2001). For example, maximum aqueous Hg(II) concentrations simulated by the five models during a 48-hour simulation ranged from 55 to 148 ng/l and minimum concentrations ranged from 20 to 110 ng/l. Although all those concentrations commensurate with available atmospheric data (e.g., Ebinghaus and Slemr, 2000), the variability among the models points out that significant uncertainties remain in our understanding of the atmospheric chemistry of Hg.

9.3 Stratospheric Models

A list of 10 two-dimensional models that contributed to the last World Meteorological Organization (WMO) ozone assessment is provided in Table 7. Seven 3-D models under development for assessment are also included.

Table 7. Two- and three-dimensional models for assessing stratospheric ozone.

2-D Model	Institution	Reference
AER	AER	Weisenstein et al. (1998)
CAM	Univ. of Cambridge, UK	Bekki, and Pyle (1994)
CSIRO	Commonwealth Scientific and Industrial Research Organization, Telecommunications and Industrial Physics, Australia	Randeniya et al. (1997)
GSFC	Goddard Space Flight Center	Jackman et al. (1996)
LLNL	Lawrence Livermore National Laboratory	Kinnison et al. (1994):

2-D Model	Institution	Reference
MPIC	Max-Planck-Institut für Chemie, Germany	Groos, et al. (1998):
OSLO	Univ. of Oslo, Norway	Zerefos et al. (1997)
RIVM	National Institute of Public Health and the Environment, Netherlands	Law and Pyle (1993)
SUNY-SPB	State Univ. of NY at Stony Brook and Russian State Hydrometeorological Institute, St. Petersburg, Russia	Smyshlyaev and Yudin (1995)
UNIVAQ	Univ. of L'Aquila, Italy	Pitari et al. (1993)
3-D Model		
UNIVAQ	Univ. of L'Aquila, Italy	Pitari et al. (1992)
GISS	Goddard Institute of Space Studies	Rind et al. (1998)
EMERAUDE	Meteo-France Centre National de Recherches Meteorologiques	Mahfouf et al. (1993)
Arpege/REPROBUS (ARPROBUS)	Meteo-France Centre National de Recherches Meteorologiques	Deque and Piedelievre (1995)
ECHAM3/CHEM European Centre		Steil et al. (1998)
UKMO Mechanistic	UK Met Office	Austin et al. (1992)
UKMO Chemistry-Climate	UK Met Office	Austin et al. (1997)

9.4 Plume-in-Grid Modeling

Three-dimensional (3-D) modeling of air quality is typically based on a gridded representation of the atmosphere where atmospheric variables such as chemical concentrations are assumed to be uniform within each grid cell. Such a grid-based approach necessarily averages emissions within the volume of the grid cell where they are released. This averaging process may be appropriate for sources that are more or less uniformly distributed at the spatial resolution of the grid system. However, it may lead to significant errors for sources that have a spatial dimension much smaller than that of the grid system. For example, stack emissions lead to plumes that initially have a dimension of tens of meters, whereas the grid cell horizontal size is typically several kilometers in urban applications up to about 100 km in regional applications. This artificial dilution of stack emissions leads to (1) lower concentrations of plume material, (2) unrealistic concentrations upwind of the stack, (3) incorrect chemical reaction rates due to the misrepresentation of the plume chemical concentrations and turbulent diffusion, and (4) incorrect representation of the transport of the emitted chemicals. The errors associated with the grid-averaging of stack emissions can be eliminated by using a subgrid-scale representation of stack plumes that is imbedded in the 3-D grid system of the air quality model.

The first subgrid-scale treatment of plumes in 3-D air quality models was the Plume Airshed Reactive Interacting System (PARIS) developed by Seigneur et al.

(1983). Other treatments of subgrid-scale effects have been developed over the years (e.g., Gillani et al., 1986; Sillman et al., 1990; Morris et al., 1991; Kumar et al., 1996; Myers et al., 1996; Gillani and Godowitch, 1999). All these models treat the plume at a subgrid-scale, thereby eliminating some of the errors associated with the 3-D grid representation. However, they fail to represent the complex dispersion processes associated with the plume mixing into the background air because the plume dimensions are represented by simple geometric functions (columns, grids, ellipses, or Gaussian distributions). As discussed above, physical phenomena such as the effect of wind shear on plume dispersion, the effect of plume overlaps (e.g., under conditions of reversal flow or merging of adjacent plumes), and the effect of atmospheric turbulence on chemical kinetics are not (or poorly) represented by such models.

As described above, SCICHEM is a reactive plume model that combines an advanced treatment of plume dynamics with comprehensive atmospheric chemistry. SCICHEM is, therefore, ideally suited to simulate the subgrid-scale processes associated with the plumes of large point sources. SCICHEM has been incorporated into the 3-D Models-3/CMAQ modeling system. Its application to two distinct areas in the eastern United States (Nashville/western Tennessee and the Northeast) suggests that the treatment of large point sources such as coal-fire power plants with an advanced plume-in-grid module leads to small but non-negligible effects on O₃ concentrations and large effects on HNO₃ concentrations (and, therefore, also possibly on H₂SO₄ concentrations). For both O₃ and HNO₃, lower concentrations were simulated when the plume-in-grid treatment was used (Karamchandani et al., 2002).

References

- Ackermann, I.J., H. Hass, M. Memmesheimer, A. Ebel, F.S. Binkowski and U. Shankar, 1998. Modal aerosol dynamics model for Europe: Development and first applications, *Atmos. Environ.* (32): 2981-2999.
- Ames, J., T.C. Myers, L.E. Reid, D.C. Whitney, S.H. Golding, S.R. Hayes, and S.D. Reynolds. 1985a. *SAI Airshed Model Operations Manual. Vol. I: User's Manual. U.S. EPA Publication EPA-600/8-85-007b. U.S. Environmental Protection Agency, Research Triangle Park, North Carolina.* (NTIS No. PB 85-191567)
- Ames, J., S.R. Hayes, T.C. Myers, and D.C. Whitney. 1985b. *SAI Airshed Model Operations Manuals. Vol. II: Systems Manual. EPA Publication EPA-600/8-85-007b. U.S. Environmental Agency, Research Triangle Park, North Carolina.*
- Atkinson, R, 1997. Gas-phase tropospheric chemistry of volatile organic compounds: 1. Alkanes and alkenes. *J. Phys. Chem. Ref. Data* (26): 215-290.
- Austin, J., N. Butchart, and K. Shine, 1992. Possibility of an Arctic ozone hole in a doubled-CO₂ climate. *Nature* (360): 221-225.
- Austin, J., N. Butchart, and R.S. Swinbank, 1997. Sensitivity of ozone and temperature to vertical resolution in a GCM with coupled stratospheric chemistry. *Q.J.R. Meteor. Soc.* (123): 1405-1431.

- Bates, D. R., and M. Nicolet, 1950. The photochemistry of atmospheric water vapor. *J. Geophys. Res.* (55):301-327.
- Bekki, S., and J.A. Pyle, 1994. A two-dimensional modeling study of the volcanic eruption of Mount Pinatubo. *J. Geophys. Res.* (99):18,861-18,869.
- Berntsen, T.J., S. Karlsdottir and D.A. Jaffe, 1999. Influence of Asian emissions on the composition of air reaching northwestern United States, *Geophys. Res. Lett.* (26): 2171-2174.
- Bessagnet, B., A. Hodzic, R. Vautard, M. Beekmann, S. Cheinet, C. Honoré, C. Lioussé and Laurence Rouil, 2004. Aerosol modeling with CHIMERE – preliminary evaluation at the continental scale, *Atmos. Environ.*, (38): 2803-2817.
- Brasseur, G., and S. Solomon, 1986. *Aeronomy of the Middle Atmosphere*. Dordrecht: D. Reidel.
- Boucher, V.S., M.D. Moran, L.P. Crevier, A.P. Dastoor, S. Gong, P.A. Makar, S. Menard, B. Pabla, L. Zhang, 2004. Wintertime and summertime evaluation of the regional PM air quality model AURAMS. In *air Pollution Modelling and Its Application XVI*, C. Borrego and S. Incecik, Editors, Kluwer/Plenum Publishers, New York, 97-104.
- Cadle, R. D., P. Crutzen, and D. Ehhalt, 1975. Heterogeneous chemical reactions in the stratosphere. *J. Geophys. Res.* (80): 3381-3385.
- Carmichael, G.R., L.K. Peters, and T. Kitada. 1986. A second generation model for regional scale transport/chemistry/deposition. *Atmos. Environ.*, (20):173-188.
- Carmichael, G.R., I. Uno, M.J. Phadnis, Y. Zhang and Y. Sunwoo, 1998. Tropospheric ozone production and transport in the springtime in east Asia, *J. Geophys. Res.*, (103): 10649-10671.
- Chang, J.S., S. Jin, Y. Li, M. Beauharnois, K-H. Chang, H-O. Huang, C-H. Lu, G. Wojcik, S. Tanrikulu and J. DaMassa, 1996. The SARMAP Air Quality Model. Part 1 of SAQM *Final Report*. California Air Resources Board, Sacramento, California.
- Chapman, S., 1930. On ozone and atomic oxygen in the upper atmosphere. *Philos. Mag.* (10):369-383.
- Crutzen, P. J., 1971. Ozone production rates in an oxygen-hydrogen-nitrogen oxide atmosphere. *J. Geophys. Res.* (76):7311-7327.
- Cziczo, D. J., D. S. Thompson, and D. M. Murphy, 2001. Ablation, flux, and atmospheric implications of meteors inferred from stratospheric aerosol. *Science* (291):1772-1775.
- Dabdub, D. and J.H. Seinfeld, 1995. Extrapolation techniques used in the solution of stiff ODEs associated with chemical kinetics of air quality models, *Atmos. Environ.* (29): 403-410.
- Dabdub, D., L.L. DeHaan, N. Kumar, F. Lurmann and J.H. Seinfeld, 1997. Computationally efficient acid deposition model for California, *Draft Report*, California Air Resources Board, Sacramento, California.
- Dachs, J. and S.J. Eisenrich, 2000. Adsorption onto aerosol soot carbon dominates gas-particle partitioning of polycyclic aromatic hydrocarbons, *Environ. Sci. Technol.* (34): 3690-3697.
- DeMore, W. B., S. P. Sander, D. M. Golden, R. F. Hampson, M. J. Kurylo, C. J. Howard, A. R. Ravishankara, C. E. Kolb, and M. J. Molina, 1997. *Chemical Kinetics and Photochemical Data for Use in Stratospheric Modeling, Evaluation number 12*. JPL Publication 97-4, Pasadena, California.

Dentener, F.J., G.R. Carmichael, Y. Zhang, J. Lelieveld, P.J. Crutzen, 1996. Role of mineral aerosol as reactive surface in the global troposphere, *J. Geophys. Res.* (101): 22869-22889.

Deque, M., and J.P. Piedelievre, 1995. High resolution climate simulation over Europe. *Clim. Dyn.* (11): 321-339.

Dobson, G. M. B., 1929. Measurements of the amount of ozone in the Earth's atmosphere and its relation to other geophysical conditions. *Proc. R. Soc. London, Ser. A* (122):456-486.

Dodge, M. C. 1977. Combined use of modeling techniques and smog chamber data to derive ozone-precursor relationships. Proceedings, *International Conference on Photochemical Oxidant Pollution and Its Control*, Vol. II, edited by B. Dimitriades, U.S. Environmental Protection Agency Document EPA-600/3-77-001b, pp. 881-889.

Dvortsov, V. L., and S. Solomon, 2001. Response of the stratospheric temperatures and ozone to past and future increases in stratospheric humidity. *J. Geophys. Res.* (106): 7505-7514.

Ebinghaus, R. and F. Slemr, 2000. Aircraft measurements of atmospheric mercury over southern and eastern Germany, *Atmos. Environ.* (34): 895-903.

EPA, 1999. Science Algorithms of the EPA Models-3 Community Multiscale Air Quality (CMAQ) Modeling System, EPA/600/R-99/030, Office of Research and Development, U.S. Environmental Protection Agency, Washington, D.C.

Etheridge, D. M., L. P. Steele, R. J. Francey, and R. L. Langenfelds, 1998. Atmospheric methane between 1000 A.D. and present: Evidence of anthropogenic emissions and climate variability. *J. Geophys. Res.* (103):15,979-15,993.

Fan, S.-M., and D. J. Jacob, 1992. Surface ozone depletion in Arctic spring sustained by bromine reactions on aerosols. *Nature* (359):522-524.

Finlayson-Pitts, B.J., and J.N. Pitts, Jr. 1986. *Atmospheric Chemistry: Fundamental and Experimental Techniques*. New York: John Wiley.

Finlayson-Pitts, B.J. and J.N. Pitts, 2000. *Chemistry of the Upper and Lower Atmosphere*. Academic Press, San Diego, CA.

Franklin, J., R. Atkinson, P.H. Howard, J.J. Orlando, C. Seigneur, T.J. Wallington, C. Zetzsch. 2000. Chapter 2: Quantitative determination of persistence in air, pp. 7-62, in *Persistence and Long-range Transport of Organic Chemicals in the Environment*, G. Klecka et al., eds., Society for Environmental Toxicology and Chemistry, Pensacola, FL.

Gabruck, R.S., R.I. Sykes, C. Seigneur, P. Pai, P. Gillespie, R.W. Bergstrom, P. Saxena, 1999. Evaluation of the reactive and optics model of emissions (ROME), *Atmos. Environ.* (33): 383-399.

Gear, C.W., 1971. *Numerical Initial Value Problems in Ordinary Differential Equations*, Prentice-Hall, Englewood Cliffs, New Jersey.

Gillani, N.V., J.F. Meagher, R.J. Valente, R.E. Imhoff, R.L. Tanner, M. Luria, 1998. Relative production of ozone and nitrates in urban and rural power plant plumes 1. Composite results based on data from 10 field measurement days, *J. Geophys. Res.* (103): 22593-22615.

Gillani, N.V. and J.M. Godowitch, 1999. Plume-in-grid treatment of major point source emissions, Chapter 9 in Byun and Ching, EPA, 1999, *op. cit.*

- Gipson, G.L. 1984. *User's manual for OZIPM-2: Ozone isopleth plotting with optional mechanisms/Version 2. U.S. Environmental Protection Agency Document EPA-450/4-84-024, Office of Air Quality Planning and Standards, Monitoring and Data Analysis Division, Research Triangle Park, North Carolina.*
- Graedel, T.E. and W.C. Keene, 1995. Tropospheric budget of reactive chlorine, *Global Biogeochem. Cycles* (9): 47-77.
- Griffin, R.J., D.R. Cocker III, R.C. Flagan and J.H. Seinfeld, 1999. Organic aerosol formation from the oxidation of biogenic hydrocarbons, *J. Geophys. Res.* (104) 3555-3567.
- Griffin, R.J., D. Dabdub, M.J. Kleeman, M.P. Fraser, G.R. Cass and J.H. Seinfeld, 2002. Secondary organic aerosol: III. Urban/regional scale model of size- and composition-resolved aerosols, *J. Geophys. Res.* (107): 101029/2001JD000544.
- Groos, J.-U., C. Bruhl, and T. Peter, 1998. Impact of aircraft emissions on tropospheric and stratospheric ozone: Part I, Chemistry and 2-D model results. *Atmos. Environ.* (32) 3173-3184.
- Harley, R.A., A.G. Russell, A.G., G.J. McRae, G.R. Cass and J.H. Seinfeld, 1993. Photochemical modeling of the Southern California Air Quality Study, *Environ. Sci. Technol.* (27): 378-388.
- Hass, H., R.J. Jakobs, M. Memmesheimer, A. Ebel and J.S. Chang, 1991. Simulation of a wet deposition case in Europe using the European acid deposition model (EURAD), *Air Pollution Modeling and Its Application VIII*, H. van Dop and D.G. Steyn, eds., 205-213, Plenum Press, New York.
- Hass, H., A. Ebel, H. Feldmann, H.J. Jakobs and M. Memmesheimer, 1993. Evaluation studies with a regional chemical transport model (EURAD) using air quality data from the EMEP monitoring network, *Atmos. Environ.* (27A): 867-887.
- Hass, H., M. Memmesheimer, H. Jakobs and A. Ebel, 1995. Analysis of ozone and precursor budget over Europe as simulated by the Regional Air Quality Model EURAD, in *Regional Photochemical Measurement and Modeling Studies*, A.J. Ranzieri & P.A. Solomon, eds., 934-943, Air & Waste Management Association, Pittsburgh, Pennsylvania.
- Hass, H., P.J.H. Builtjes, D. Simpson and R. Stern, 1997. Comparison of model results obtained with several European regional air quality models, *Atmos. Environ.* (31): 3259-3279.
- Health Effects Institute, 2001. *Airborne particles and health: HEI epidemiologic evidence:* www.healtheffects.org.
- Hofmann, D. J., and S. Solomon, 1989. Ozone destruction through heterogeneous chemistry following the eruption of El Chichón. *J. Geophys. Res.* (94): 5029-5041.
- Hoffmann, T., R. Bandur, U. Marggraf, M. Linscheid, 1998. Molecular composition of organic aerosols formed in the α -pinene/O₃ reaction: implications for new particle formation processes, *J. Geophys. Res.* (103): 25569-25578.
- Hogue, C., 2001. Blowing in the wind, *Chem. Eng. News*, June 25, 2001, pp. 30-31.
- Hudischewskyj, A.B. and C. Seigneur, 1989. Mathematical modeling of chemistry and physics of aerosols in plumes, *Environ. Sci. Technol.* (23): 413-421.
- ICF Kaiser/SAI, 1999. Sensitivity Studies with the REMSAD Modeling System, *Draft Report SYSAPP-99/05 to U.S. Environmental Protection Agency, Office of Air Quality Planning and Standards*, Research Triangle Park, North Carolina.

IRIS, 2001. *U.S. EPA Integrated Risk Information System (IRIS)* <http://www.epa.gov/iris>.

Jackman, C.H., E.L. Fleming, S. Chandra, D.B. Considine, and J.E. Rosenfield, 1996. Past, present, and future modeled ozone trends with comparisons to observed trends. *J Geophys. Res.* (101): 28,753-28,767.

Jacob, D.J., J.A. Logan and P. Murti, 1999. Effects of rising Asian emissions on surface ozone in the United States, *Geophys. Res. Lett.*, (26): 2175-2178.

Jacob, D.J., 2000. Heterogeneous chemistry and tropospheric ozone, 2000. *Atmos. Environ.* (34): 2131-2159.

Jacobson, M.Z., R. Lu, R.P. Turco and O.B. Toon, 1996. Development and application of a new air pollution modeling system, Part I: gas phase simulations, *Atmos. Environ.* (30): 1939-1963.

Jacobson, M.Z., 1997b. Development and application of a new air pollution modeling system – II. Aerosol module structure and design, *Atmos. Environ.* (31): 131-144.

Jacobson, M.Z., 1997c. Development and application of a new air pollution modeling system, Part III: Aerosol-phase simulations, *Atmos. Environ.* (31): 587-608.

Jacobson, M.Z., 1999. *Fundamentals of Atmospheric Modeling*, Cambridge University Press, Cambridge, United Kingdom.

Jacobson, M.Z., 2001a. GATOR-GCMM: A global- through urban-scale air pollution and weather forecast model. 1. Model design and treatment of subgrid soil, vegetation, roads, rooftops, water, sea ice, and snow, *J. Geophys. Res.* (106): 5385-5401.

Jacobson, M.Z., 2001b. Strong radiative heating due to the mixing state of black carbon in atmospheric aerosols, *Nature* (409): 695-697.

Johnston, H., 1971. Reduction of stratospheric ozone by nitrogen oxide catalysts from supersonic transport exhaust. *Science* (173):517-522.

Jones, R. L., J. Austin, D. S. McKenna, J. G. Anderson, D. W. Fahey, C. B. Farmer, L. E. Heidt, K. K. Kelly, D. M. Murphy, M. H. Proffitt, A. F. Tuck, and J. F. Vedder, 1989. Lagrangian photochemical modeling studies of the 1987 Antarctic spring vortex 1. Comparison with AAOE observations. *J. Geophys. Res.* (94):11,529-11,558.

Joos, E. and C. Seigneur, 1994. Application of a reactive plume model to a case study of pollutant oxidation and acid deposition, *Adv. Environ. Sci. Technol.* (28), Environmental Oxidants, J.O. Nriagu and M.S. Simmons, eds., pp. 137-158. John Wiley & Sons, Inc. New York, NY.

Karamchandani, P., A. Koo, C. Seigneur, 1998. A reduced gas-phase kinetic mechanism for atmospheric plume chemistry, *Environ. Sci. Technol.* (32): 1709-1720.

Karamchandani, P. and C. Seigneur, 1999. Simulation of sulfate and nitrate chemistry in power plant plumes, *J. Air Waste Manage. Assoc.* (49): PM-175-181.

Karamchandani, P., L. Santos, I. Sykes, Y. Zhang, C. Tonne, C. Seigneur, 2000. Development and evaluation of a state-of-the-science reactive plume model, *Environ. Sci. Technol.* (34): 870-880.

Karamchandani, P. C. Seigneur, Y. Zhang, 2001. Review of air quality models for acid deposition. *U.S. Environmental Protection Agency*, Washington, D.C.

- Karamchandani, P., C. Seigneur, K. Vijayaraghavan and S.-Y. Wu, 2002. Development and application of a state-of-the-science plume-in-grid model, *J. Geophys. Res.* (107): 4403-4415.
- Kinnison, D.E., K.E. Grant, P.S. Connell, D.A. Rotman, and D.J. Wuebbles, 1994. The chemical and radiative effects of the Mt. Pinatubo eruption. *J. Geophys. Res.* (99): 25,705-25,731.
- Kley, D., P.J. Crutzen, H.G.J. Smit, H. Vömel, S.J. Oltmans, H. Grassl, and V. Ramanathan, 1996. Observations of near-zero ozone concentrations over the convective Pacific: Effects of air chemistry. *Science* (274):230-233.
- Kumar, N. and A.G. Russell, 1996a. Development of a computationally efficient, reactive subgrid-scale plume model and the impact in the northeastern United States using increasing levels of chemical detail, *J. Geophys. Res.* (101): 16737-16744.
- Kumar, N., M.T. Odman and A.G. Russell, 1994. Multiscale air quality modeling: application to southern California, *J. Geophys. Res.* (99): 5385-5397.
- Kumar, N. and A.G. Russell, 1996b. Comparing prognostic and diagnostic meteorological fields and their impacts on photochemical air quality modeling, *Atmos. Environ.*, (30): 1989-2010.
- Langmann, B. and H-F. Graf, 1997. The chemistry of the polluted atmosphere over Europe: simulations and sensitivity studies with a regional chemistry-transport model, *Atmos. Environ.* (31): 3239-3257.
- Law, K.S., and J.A. Pyle, 1993. Modeling trace gas budgets in the troposphere: 1, Ozone and odd nitrogen. *J. Geophys. Res.* (98): 18,377-18,400.
- Lin, C.J. and S.O. Pehkonen, 1999. The chemistry of atmospheric mercury: A review. *Atmos. Environ.* (33): 2067-2080.
- Liu, X., G. Mauersberger and D. Möller, 1997. The effects of cloud processes on the tropospheric photochemistry: An improvement of the EURAD model with a coupled gaseous and aqueous chemical mechanism, *Atmos. Environ.* (31): 3119-3135.
- Lu, R., R.P. Turco and M.Z. Jacobson, 1997a. An integrated air pollution modeling system for urban and regional scales: 1. Structure and performance, *J. Geophys. Res.* (102): 6063-6079.
- Lu, R., R.P. Turco and M.Z. Jacobson, 1997b. An integrated air pollution modeling system for urban and regional scales: 2. Simulations for SCAQS 1987, *J. Geophys. Res.*, (102): 6081-6098.
- Lurmann, F.W., D.A. Godden, and H.M. Collins. 1985. *User's guide to the PLMSTAR air quality simulation model. Environmental Research & Technology Document M-2206-100*, Newbury Park, California.
- Lurmann, F.W., A.S. Wexler, S.N. Pandis, S. Musarra, N. Kumar and J.H. Seinfeld, 1997. Modeling urban and regional aerosols: II. Application to California's south coast air basin, *Atmos. Environ.* (31): 2695-2715.
- Lurmann, F.W., 2000. Simplification of the UAMAERO Model for Seasonal and Annual Modeling: The UAMAERO-LT Model, *Final Report, South Coast Air Quality Management District*, Diamond Bar, California.
- Mahfouf, J.F., D. Cariolle, J.-F. Royer, J.-F. Geleyn, and B. Timbal, 1993. Response of the Meteo-France climate model to changes in CO₂ and sea surface temperature. *Clim. Dyn.* (9): 345-362.

- Manney, G.L., L. Froidevaux, J.W. Waters, R.W. Zurek, J.C. Gille, J. B. Kumer, J. L. Mergenthaler, A. E. Roche, A. O'Neill, and R. Swinbank, 1995. Formation of low-ozone pockets in the middle stratospheric anticyclone during winter. *J. Geophys. Res.* (100):13,939-13,950.
- Mathur, R., J.O. Yound, K.L. Schere and G.L. Gipson, 1998. A comparison of numerical techniques for solution of atmospheric kinetic equations, *Atmos. Environ.* (32): 1535-1553.
- McElroy, M.B., R.J. Salawitch, S.C. Wofsy, and J.A. Logan, 1986. Reduction of Antarctic ozone due to synergistic interactions of chlorine and bromine. *Nature* (321):759-762.
- McElroy, M.B., and R.J. Salawitch, 1989. Changing composition of the global stratosphere. *Science* (243):763-770.
- McMurry, P.H. and S.K. Friedlander, 1979. New particle formation in the presence of an aerosol, *Atmos. Environ.* (13): 1635-1651.
- McMurry, P.H., K.S. Woo, R. Weber, D.R. Chen and D.Y.H. Pui, 2000. Size distribution of 3 to 10 nm in atmospheric particles: implications for nucleation mechanisms, *Phil. Trans. Royal Soc. London* (A358): 2625-2642.
- McRae, G.J., W.R. Goodin and J.H. Seinfeld, 1982b. Development of a second generation mathematical model for urban air pollution. I. Model formulation, *Atmos. Environ.* (16): 679-696.
- McRae, G.J. and J.H. Seinfeld, 1983. Development of a second generation mathematical model for urban air pollution. II. Evaluation of model performance, *Atmos. Environ.* (17): 501-522.
- Meng, Z., D. Dabdub and J.H. Seinfeld, 1998. Size-resolved and chemically resolved model of atmospheric aerosol dynamics, *J. Geophys. Res.* (103): 3419-3435.
- Molina, M.J., and F.S. Rowland, 1974. Stratospheric sink for chlorofluoromethanes: Chlorine atom-catalyzed destruction of ozone. *Nature* (249):810-812.
- Molina, M.J., and L.T. Molina, 1987. Production of Cl₂O₂ from the self-reaction of the ClO radical. *J. Phys. Chem.* (91):433-436.
- Möller, D. and G. Mauersberger, 1995. An aqueous phase reaction mechanism. In *Clouds: Models and Mechanisms*.
- Monod, A. and P. Carlier, 1999. Impact of clouds on tropospheric ozone budget: Direct effect of multiphase photochemistry of soluble organic compounds, *Atmos. Environ.* (33): 4431-4446.
- Nair, H., M. Allen, L. Froidevaux, and R. W. Zurek, 1998. Localized rapid ozone loss in the northern winter stratosphere: An analysis of UARS observations. *J. Geophys. Res.* (103):1555-1571.
- Nenes, A., S.N. Pandis, C. Pilinis, 1998. ISORROPIA: A new thermodynamic equilibrium model for multiphase multicomponent inorganic aerosols, *Aquatic Chem.* (4): 123-152.
- Nevison, C.D., S. Solomon, and R.S. Gao, 1999. Buffering interactions in the modeled response of stratospheric O₃ to increased NO_x and HO_x. *J. Geophys. Res.* (104):3741-3754.
- Odman, M.T. and A.G. Russell, 1991b. Multiscale modeling of pollutant transport and chemistry, *J. Geophys. Res.* (96): 7363-7370.
- Odman, M.T., N. Kumar and A.G. Russell, 1992. A comparison of fast chemical kinetic solvers for air quality modeling, *Atmos. Environ.* (26): 1783-1789.

- Odum, J.R., T. Hoffman, F. Bowman, D. Collins, R.C. Flagan and J.H. Seinfeld, 1996. Gas/particle partitioning and secondary organic aerosol yields, *Environ. Sci. Technol.* (30): 2580-2585.
- Odum, J.R., T.P.W. Jungkamp, R.J. Griffin, H.J.L. Forstner, R.C. Flagan and J.H. Seinfeld, 1997. Aromatics, reformulated gasoline, and atmospheric organic aerosol formation, *Environ. Sci. Technol.*, (31): 1890-1897.
- Pankow, J.F., 1994a. An absorption model of gas/particle partitioning of organic compounds in the atmosphere, *Atmos. Environ.* (28): 185-188.
- Pankow, J.F., 1994b. An absorption model of gas/aerosol partitioning involved in the formation of secondary organic aerosol, *Atmos. Environ.* (28): 189-193.
- Pankow, J.F., 1998. Further discussion of the octanol/air partition coefficient K_{oa} as a correlating parameter for gas/particle partitioning coefficients, *Atmos. Environ.* (32): 1493-1497.
- Pirjola, L. and M. Kulmala, 2000. Aerosol dynamical model MULTIMONO, *Boreal Environ. Res.* (5): 361-374.
- Pitari, G., S. Palermo, G. Visconti, and R.G. Prinn, 1992. Ozone response to a CO₂ doubling: Results from a stratospheric circulation model with heterogeneous chemistry. *J. Geophys. Res.* (97): 5953-5962.
- Pitari, G., V. Rizi, L. Ricciardulli, and G. Visconit, 1993. High-speed civil transport impact: The role of sulfate, nitric acid trihydrate, and ice aerosols studied with a two-dimensional model including aerosol physics. *J. Geophys. Res.* (98): 23,141-23,164.
- Prather, M. J., M. B. McElroy, and S. C. Wofsy, 1984. Reductions in ozone at high concentrations of stratospheric halogens. *Nature* (312): 227-231.
- Press, W.H., S.A. Teukolsky, W.T. Vetterling, B.P. Flannery, 1997. *Numerical Recipes in C, 2nd Edition*. Cambridge University Press, London, U.K.
- Pun, B.K., C. Seigneur, D. Grosjean, P. Saxena, 2000. Gas-phase formation of water-soluble organic compounds in the atmosphere: a retrosynthetic analysis, *J. Atmos. Chem.* (35): 199-233.
- Pun, B.K., M. Liedner, C. Seigneur, 2001. Conceptual Model for Regional Haze in the Upper Midwest. Proceedings, *Regional Haze and Global Radiation Balance – Aerosol Measurements and Models: Closure, Reconciliation and Evaluation*, Bend, OR, October 2-5, 2001.
- Pun, B.K., R.J. Griffin, C. Seigneur and J.H. Seinfeld, 2002. Secondary organic aerosol: II. Thermodynamic model for gas/particle partitioning of molecular constituents, *J. Geophys. Res.*, (107): 4333-4347.
- Randeniya, L.K., P.F. Vohralik, I.C. Plumb and K.R. Ryan, 1997. Heterogeneous BrONO₂ hydrolysis: Effect on NO₂ columns and ozone at high latitudes in summer. *J. Geophys. Res.*, (102): 23,543-23,557.
- Richards, L.W., J.A. Anderson, D.L. Blumenthal, A. Brandt, J.A. McDonald, N. Waters, E.S. Macias, P.S. Bhardwaja, 1981. The chemistry, aerosol physics and optical properties of a western coal-fired power plant plume, *Atmos. Environ.* (15): 2111-2131.
- Rind, D., D. Shindell, P. Lonergan, and N.K. Balachandran, 1998. Climate change and the middle atmosphere: Part III, The doubled CO₂ climate revisited. *J. Clim.*, (11): 876-894.

Ryaboshapko, A., I.Ilyin, R. Bullock, R. Binghaus, K. Lohman, J. Munthe, G. Petersen, C. Seigneur, I. Wangberg, 2001. Intercomparison study of numerical models for long-range atmospheric transport of mercury. *Technical Report 2/2001, Cooperative Programme for Monitoring and Evaluation of the Long-range Transmission of Air Pollutants in Europe, Meteorological Synthesizing Center – East Moscow, Russia.*

Sander, S. P., R. R. Friedl, W. B. DeMore, D. M. Golden, M. J. Kurylo, R. F. Hampson, R. E. Huie, G. K. Moortgat, A. R. Ravishankara, C. E. Kolb, and M. J. Molina, 2000. *Chemical Kinetics and Photochemical Data for Use in Stratospheric Modeling, Evaluation number 13.* JPL Publication 00-3, Pasadena, California.

Saxena, P. and L.M. Hildemann, 1996. Water-soluble organics in atmospheric particles: a critical review of the literature and application of thermodynamics to identify candidate compounds, *J. Atmos. Chem.* (24): 57-109.

Scire, J.S., D.G. Strimaitis, R.J. Yamartino, 1990. *Model formulation and user's guide for the CALPUFF dispersion model*, Earth Tech Concord MA.

Schroeder, W.H. and J. Munthe, 1998. Atmospheric mercury: An overview, *Atmos. Environ.* (32): 809-822.

Schmidt, H., C. Derognat, R. Vautard and M. Beekmann, 2001. A comparison of simulated and observed ozone mixing ratios for the summer of 1998 in Western Europe, *Atmos. Environ.* (35): 6277-6297.

Seigneur, C., 1982. A model of sulfate aerosol dynamics in atmospheric plumes, *Atmos. Environ.* (16): 2207-2228.

Seigneur, C., T.W. Tesche, P.M. Roth, M.-K. Liu. 1983. On the treatment of point source emissions in urban air quality modeling. *Atmos. Environ.*, (17):1655-1676.

Seigneur, C. and H.M. Barnes, 1986. Technical considerations in regional aerosol modeling, in *Air Pollution Modeling and Its Applications, Vol. 5*, C. De Wispelaere, F.A. Schiermeier and N.V. Gillani, eds., pp. 343-369, Plenum Press, New York.

Seigneur, C. 1987. Computer simulation of air pollution chemistry. *Environ. Software*, (2):116.

Seigneur, C. and E. Constantinou, 1995. Chemical kinetic mechanism for atmospheric chromium, *Environ. Sci. Technol.* (29): 223-231.

Seigneur, C., X.A. Wu, E. Constantinou, P. Gillespie, R.W. Bergstrom, I. Sykes, A. Venkatram, P. Karamchandani, 1997. Formulation of a second-generation reactive plume and visibility model, *J. Air Waste Manage. Assoc.* (47): 176-184.

Seigneur, C., H. Abeck, G. Chia, M. Reinhard, N. Bloom, E. Prestbo, and P. Saxena, 1998. Mercury adsorption to elemental carbon (soot) particles and atmospheric particulate matter, *Atmos. Environ.* (32): 2649-2657.

Seigneur, C., P. Pai, I. Tombach, C. McDade, P. Saxena, P. Mueller. 2000. Modeling of potential power plant plume impacts on Dallas Fort Worth visibility, *J. Air Waste Manage. Assoc.* (50): 835-848.

Seigneur, C. and P. Karamchandani, 2001. Review of the State of the Science for Modeling Atmospheric Particulate Matter, *report for Renault*, Guyancourt, France.

Seinfeld J.H. and S.N. Pandis, 1998. *Atmospheric chemistry and Physics*. John Wiley and Sons, New York, NY.

Sheridan, P.J., C.A. Brock, and J.C. Wilson, 1994. Aerosol particles in the upper troposphere and lower stratosphere: Elemental composition and morphology of individual particles in northern midlatitudes. *Geophys. Res. Lett.* (21): 2587-2590.

Shindell, D.T., 2001. Climate and ozone response to increased stratospheric water vapor. *Geophys. Res. Lett.* (28): 1551-1554.

Smyshlyaev, S.P., and V.A. Yudin, 1995. Numerical simulation of the aviation release impact on the ozone layer. *Izv. Atmos. Oceanic Phys.* (31): 116-125.

Solomon, S., R.R. Garcia, F.S. Rowland, and D.J. Wuebbles, 1986. On the depletion of Antarctic ozone. *Nature* (321): 755-758.

Solomon, S., R.W. Sanders, and H.L. Miller, Jr., 1990. Visible and near-ultraviolet spectroscopy at McMurdo Station, Antarctica 7. OCIO diurnal photochemistry and implications for ozone destruction. *J. Geophys. Res.*, (95):13,807-13,817.

Solomon, S., R.R. Garcia, and A.R. Ravishankara, 1994. On the role of iodine in ozone depletion. *J. Geophys. Res.*, (99):20,491-20,499.

Solomon, S., 1999. Stratospheric ozone depletion: A review of concepts and history. *Rev. Geophys.*, (37): 275-316.

Song, C.H. and G.R. Carmichael, 1999. A modeling investigation on tropospheric aerosols over East Asia: I. Model description, *J. Geophys. Res.*, submitted.

Spicer, C.W., E.G. Chapman, B.J. Finlayson-Pitts, R.A. Plastridge, J.M. Hubbe, J.D. Fast, C.M. Berkowitz, 1998. Unexpectedly high concentrations of molecular chlorine in coastal air, *Nature* (394): 353-3656.

Staelin, J., N. R.P. Harris, C. Appenzeller, and J. Eberhard, 2001. Ozone trends: A review. *Rev. Geophys.* (39):231-290.

Steil, B., M. Demeris, C. Bruhl, P.J. Crutzen, V. Grewe, M. Ponater, and R. Sausser, 1998. Development of a chemistry module for GCMs: First results of a multi-annual integration. *Ann. Geophys.* (16): 205-228.

Stewart, D.A., M.K. Liu, 1981. Development and application of a reactive plume model. *Atmos. Environ.* (15): 2377-2393.

Stolarski, R.S., and R.J. Cicerone, 1974. Stratospheric chlorine: A possible sink for ozone. *Can. J. Chem.* (52): 1610-1615.

Sykes, R.I., S.F. Parker, D.S. Henn, W.S. Lewellen, 1993. Numerical simulation of ANATEX tracer data using a turbulence closure model for long-range dispersion, *J. Appli. Met.* (32): 929-947.

Sykes, R.I. and D.S. Henn, 1995. Representation of velocity gradient effects in a Gaussian puff model, *J. Appli. Met.* (34): 2715-2737.

Tesche, T.W., C. Seigneur, W.R. Oliver, and J.L. Haney 1984. Modeling ozone control strategies in Los Angeles. *J. Environ. Eng.*, (110): 208-225.

Toon, O.B., P. Hamill, R.P. Turco, and J. Pinto, 1986. Condensation of HNO₃ and HCl in the winter polar stratosphere. *Geophys. Res. Lett.* (13):1284-1287.

Wamsley, P.R., et al., 1998. Distribution of halon-1211 in the upper troposphere and lower stratosphere and the 1994 total bromine budget. *J. Geophys. Res.* (103):1513-1526.

Warneck, P., 1988. *Chemistry of the natural atmosphere*, Academic Press, San Diego, CA.

Wayland, R.J., 1999. REMSAD – 1990 Base Case Simulation: Model Performance Evaluation – Annual Average Statistics, U.S. Environmental Protection Agency, Office of Air Quality Planning and Standards (OAQPS), Research Triangle Park, North Carolina.

Wayne, R.P., 1991. *Chemistry of the atmospheres, 2nd edition*, Clarendon Press, Oxford, U.K.

Webster, C.R., H.A. Michelsen, M.R. Gunson, J.J. Margitan, J.M. Russell III, G.C. Toon, and W.A. Traub, 2000. Response of lower stratospheric HCl/Cly to volcanic aerosol: Observations from aircraft, balloon, space shuttle, and satellite instruments. *J. Geophys. Res.* (105): 11,711-11,719.

Weisenstein, D.K., M.K.W. Ko, E.G. Dyominov, G. Pitari, L. Ricciardulli, G. Visconti, and S. Bekki, 1998. The effects of sulfur emissions from HSCT aircraft: A 2-D model intercomparison. *J. Geophys. Res.*, (103): 1527-1547.

Wexler, A.S., F.W. Lurmann and J.H. Seinfeld, 1994. Modeling urban and regional aerosols, I. Model development, *Atmos. Environ.* (28): 531-546.

Wilkening, K.E., L.A. Barrie, and M. Engle, 2000. Trans-Pacific air pollution. *Science* (290): 65-67.

Wofsy, S.C., M.B. McElroy, and Y.L. Yung, 1975. The chemistry of atmospheric bromine. *Geophys. Res. Lett.* (2): 215-218.

Woo, K.S., D.R. Chen, D.Y.H. Pui and P.H. McMurry, 2001. Measurement of Atlanta aerosol size distributions: observations of ultrafine particle events, *Aerosol Sci. Technol.* (34): 75-87.

World Meteorological Organization/United Nations Environmental Programme (WMO/UNEP). 1999. *Scientific assessment of ozone depletion: 1998.*, Global Ozone Research and Monitoring Project, Report 44, Geneva, Chapters 1, 4, 5, 11, 12.

Yu, J. R.J. Griffin, D.R. Cocker III, R.C. Flagan, J.H. Seinfeld, 1999. Observation of gaseous and particulate products of monoterpene oxidation in forest atmospheres. *Geophys. Res. Lett.* (26): 1145-1148.

Zannetti, P. 1990. *Air Pollution Modeling*. Van Nostrand Reinhold, New York, NY.

Zerefos, C.S., K. Tourpali, B.R. Bojkov, D.S. Balis, B. Rognerud, and I.S.A. Isaksen, 1997. Solar activity-total column ozone relationships, observations and model studies with heterogeneous chemistry, *J. Geophys. Res.* (102):1561-1569.

Zhang, R., P.J. Wooldridge, J.P. D. Abbatt, and M.J. Molina, 1993. Physical chemistry of the H₂SO₄/H₂O binary system at low temperatures: Stratospheric implications. *J. Phys. Chem.* (91): 433-436.

Zhang, Y., 1994. *The chemical role of mineral aerosols in the troposphere in east Asia*, Ph.D. thesis, Department of Chemical and Biochemical Engineering, University of Iowa, Iowa City, Iowa.

Zhang, Y., C. Seigneur, J.H. Seinfeld, M.Z. Jacobson and F. Binkowski, 1999. A comparative review of algorithms used in air quality models, *Aerosol Sci. Technol.* (31): 487-514.

Zhang, Y., C. Seigneur, J.H. Seinfeld, M. Jacobson, S.L. Clegg and F.S. Binkowski, 2000. A comparative review of inorganic aerosol thermodynamic equilibrium modules: Similarities, differences, and their likely causes, *Atmos. Environ.* (34): 117-137.

Zhang, Y., B. Pun, K. Vijayaraghavan, S.-Y. Wu, C. Seigneur, S. Pandis, M. Jacobson, A. Nenes and J.H. Seinfeld, 2004, Development and application of the Model of Aerosol Dynamics, Reaction, Ionization and Dissolution, *J. Geophys. Res.* (109): D01202, doi:10.1029/2003JD003501.

San José, R. et al. 2005. *Deposition Phenomena*. Chapter 13 of *AIR QUALITY MODELING - Theories, Methodologies, Computational Techniques, and Available Databases and Software. Vol. II – Advanced Topics* (P. Zannetti, Editor). Published by The EnviroComp Institute (<http://www.envirocomp.org/>) and the Air & Waste Management Association (<http://www.awma.org/>).

Chapter 13

Deposition Phenomena

Roberto San José ⁽¹⁾, Juan L. Pérez ⁽¹⁾ and Rosa M. González Barras ⁽²⁾

⁽¹⁾ *Environmental Software and Modelling Group, Computer Science School, Technical University of Madrid, Madrid (Spain)*

roberto@fi.upm.es

jlperetz@fi.upm.es

⁽²⁾ *Department of Meteorology and Geophysics, Complutense University of Madrid, Madrid (Spain)*

rgbarras@fis.ucm.es

Abstract: Deposition phenomena are one of the most important processes occurring in the atmosphere. Deposition phenomena include the exchange of pollutants between the atmosphere and the surface of the earth. This exchange process can be parameterized and modeled by simulating the turbulence characteristics of the atmospheric flow. These turbulence characteristics require specific parameterization procedures to take very different and complex environments such as canopy, water, forest, etc. into account. Deposition phenomena are essential processes in atmospheric modeling since they account for all the pollution removal while the atmospheric dispersion and transport are taking place. A correct modeling is needed to address issues such as the “critical load” concept or “surface damage” quantification. In this chapter we will focus on the current approach to describe deposition processes and the modeling techniques needed to simulate, with atmospheric transport models, the boundary conditions at the surface of the earth.

Key Words: deposition, air quality modeling, surface fluxes, Monin-Obukhov theory, constant flux layer, aerodynamic resistance, canopy resistance, bulk resistance, compensation point.

1 Introduction

The term deposition refers to the transfer of airborne materials (both gaseous and particles) to the surface of the earth (including soil, water and vegetation) by wet and dry removal processes. However, deposition is very difficult to parameterize because the deposition rate of a certain chemical compound depends on boundary layer meteorology, land use data (different kinds of vegetation, water, soil, etc.), the characteristics of the compound (e.g., whether it is in gaseous or in particulate form, or both) and precipitation rate. Deposition is also a strong time varying function with annual changes due to meteorological conditions and vegetation variation (diurnal variation of stomata). Furthermore, there is a stochastic variation due to precipitation.

In this section we will provide a general overview of the art of deposition modeling and in particular, the deposition parameterization into the air quality models that are used today by the research communities and the operational branches in the administration of air quality management in different cities in the world. However, the subject of deposition is much wider; it includes the different deposition monitoring networks that exist in different countries. These deposition-monitoring networks are composed by a series of monitoring stations that measure the air concentrations of different pollutants (gaseous, wet deposition and particulate matter - sedimentation). The measurements are used to validate the different deposition parameterization approaches in order to improve the different deposition models.

Deposition processes are key elements of air quality modelling since an excess or defect on deposition calculations will lead to an incorrect air quality modeling simulation of pollutant concentrations.

The structure of this chapter will be described by the following sections: 1. - Introduction describes the importance of the deposition processes and the basic concepts; 2. - Mathematical formulation into air quality models, which will describe how the deposition processes are incorporated into the mesoscale air quality models (3rd generation); 3. - Different deposition parameterizations, which will describe the different deposition models or approaches, and the current lack of information in many of these areas; 4. - Examples of deposition monitoring programs, which will provide information on different deposition monitoring station networks; 5. - Examples of air quality models, which will describe several important continental and mesoscale air quality models, and how these models deal with the deposition problem; 6. - A special contribution from the author's air quality model on the sensitivity analysis of deposition parameterization on the air concentrations will describe the impact on air concentrations in Madrid, Spain region by using the OPANA model (Operational Atmospheric Numerical pollution model for urban and regional Areas).

1.1 Acid Deposition

“Acid deposition (familiarily "acid rain") is an important issue of public policy in which atmospheric processes play a key role”. This statement from the American Meteorological Society addresses the present state of knowledge and uncertainty about atmospheric aspects of the acid deposition phenomenon in the context of prospective legislation and regulatory action to decrease acid deposition.

Substances are measured for acidity or alkalinity using a scale called “pH”. An acidic compound has a pH value of less than 7 while pure water has a pH of 7.0. The lower a substance's pH, the more acidic it is. Normal rain is slightly acidic because carbon dioxide dissolves into it, and as a result has a pH of about 5.5.

Acid deposition consists of delivery of acidic substances (mainly sulphur and nitrogen oxides), acids and salts through the atmosphere to the earth's surface. These compounds (principally the oxides) are introduced into the atmosphere as by-products of combustion and industrial activity at rates that greatly exceed natural emission rates in industrialised areas such as the American Northeast. Acid deposition also includes contributions from natural sources and deposition of other acidic compounds, but these contributions are relatively minor. Deposition processes include delivery of material to the earth's surface by precipitation processes ("wet deposition") and by direct uptake processes at the earth's surface involving turbulent mixing or settling of gases and particles followed by absorption, adsorption, adhesion, or impaction ("dry deposition"). The direct impact of acidic cloud or fog droplets on vegetation or other surfaces also contributes to acid deposition. Acid deposition is widely held to be responsible for substantial deleterious effects on aquatic ecosystems and, perhaps in conjunction with other factors such as surface level ozone, on forests. Acid deposition along with other pollutants may also influence yields of certain cultivated crops and contribute to deterioration of structural and ornamental materials. In addition, human health may be affected as a result of acid deposition. In viewing its possible economic, ecological, and aesthetic consequences, acid deposition is a phenomenon of widespread concern. This concern is reflected in pending legislation and regulation to reduce acid deposition by controlling emissions of sulphur and/or nitrogen oxides.

Extensive information is available from networks that have monitored wet acid deposition for several years, and in some cases up to a decade or more. In eastern North America, wet acid deposition represented by acid rain is found to be 3 to 10 times greater than values measured in remote locations. On the other hand, dry deposition of gases or particles to surfaces such as vegetation or soil cannot be directly monitored by existing techniques and therefore must be inferred from concentrations of the airborne species with measurements of pertinent meteorological variables and knowledge of surface properties. Because of the difficulties of these air-surface exchange measurements, they have been recently made only at a few stations, and the size of the database is not comparable to that of wet deposition. However, it can be stated that annual dry deposition mass of

SO₂ and NO₂ is substantial and tends to increase in importance relative to wet deposition near the source regions.

The atmosphere is both the pathway by which acid deposition materials travel from sources to places (where they are deposited) and the medium in which air pollutants (mostly combustion products) are transformed into acidic compounds. Meteorological concerns include:

1. Processes of transport and diffusion of surface-derived materials of all kinds
2. Chemical reactions among airborne substances
3. Processes whereby materials are transferred from the atmosphere to surface elements, including vegetation, soils, water bodies and structures

A goal of meteorological research is to provide knowledge that can be used to help shape emission control scenarios that will maximize reduction in acid deposition at a minimum cost to the society. The acid deposition issue is one of several interconnected impacts of man's activities upon the atmospheric/oceanic/biosphere environment. Research directed at acid deposition mechanisms and related control strategies should, when possible, also consider interactions with other issues like control of tropospheric ozone, reduction of greenhouse gas emissions, and mitigation of climatic change stresses.

In order to organize knowledge in a more logical way, scientists have constructed atmospheric transport models, which can be applied to the development of strategies to reduce acid deposition in a particular geographic region through a two-step process:

1. Illustrate how acid deposition at a given location is derived from contributions of nearby and distant emission sources (i.e., the source–receptor relationship)
2. Use this information to predict deposition at this location when emission strengths are changed

However, the source–receptor relations are difficult to establish because acid deposition at any given location is the summation of pollution from numerous upwind sources. Mixing within the atmosphere makes it difficult to distinguish the relative impact of local versus distant sources. Developing an improved understanding of source–receptor relationships requires research into the pertinent meteorological, physical and chemical processes. This research includes laboratory studies of chemical and physical processes, field studies examining transport and transformation of acidic and related substances, and studies of long-range transport using tracer compounds. Then regional-scale numerical models (extending over 1,000 kilometers or more) can be constructed to describe the overall transport and deposition. A variety of regional scale models have been developed in recent years and they are currently undergoing field evaluation. These models offer the promise of improved understanding of regional scale source–receptor relationships in the near future. Although current information on

source–receptor relations for acid deposition is uncertain, much pertinent descriptive and qualitative information is known.

The currently available information is adequate for interpretative evaluation of the changes in deposition patterns expected to result from regional changes in the patterns of the primary emissions. Also, the principles of atmospheric transport and diffusion are well established. The knowledge of atmospheric chemistry is expanding very rapidly; however, it is possible that some reactions important in acid deposition are yet to be identified. Sulphur and nitrogen compounds of concern are inevitably removed from the atmosphere by deposition to the earth's surface. Consequently, reductions in primary emissions will generally result in similar reductions in acid deposition taken as a whole over all receptor locations. However, this is complicated by seasonal and short-term differences in the transport ability of the atmosphere; the scales of transport range from hundreds to thousands of kilometers. Studies involving elemental tracers characteristic of particular regions or of unique events have established this transport on the thousand-kilometer scale.

Consideration of material accumulation is also useful in understanding the larger picture. Comparison of annual wet deposition of sulphur and nitrogen in eastern North America with emissions indicate that about one-third of the emitted material is deposited in precipitation. Comparable amounts are thought to be dry-deposited and the remaining third is thought to be deposited in the western Atlantic Ocean. This information can assist in policy formulation and development of strategies in controlling acid deposition. In particular, the large distance scales require that any approach to the control of acid deposition be regional in scope and not merely local.

Qualitatively, the processes of atmospheric transport, transformation, and deposition are well understood. In recognizing the difficulties involved in construction, execution, and evaluation of numerical models that emulate these processes in a quantitative manner, it is likely that considerable uncertainties in source–receptor relations for acid deposition will remain for some time. However, currently available analytical methods are only adequate for interpretative evaluation of the broad changes in deposition that is expected to result from regional changes in emission patterns.

Acid deposition is primarily attributable to sulphur and nitrogen oxides emissions produced during combustion processes. This deposition extends hundreds to thousands of kilometers from emission sources. It is thus very difficult to identify and quantify the specific source of acid deposition at a given receptor. Gaining a better knowledge of source–receptor relations for acid deposition is the objective of much ongoing research and monitoring. Although policy decisions regarding acid deposition will for some time be made on the basis of incomplete knowledge of source–receptor relations, preliminary decisions can be made today using our present understanding. Disregarding near-term policy decisions, it is essential that research and monitoring continue at a peak level. The American

Meteorological Society emphasizes the seriousness with which it views both the importance and the scientific uncertainties associated with this environmental issue.

1.2 The Control of Atmospheric Deposition

The pollutant control of atmospheric deposition is achievable by controlling the anthropogenic sources that release those pollutants into the atmosphere. No best management practices (BMPs) have been designed specifically to control atmospheric deposition. Storm water runoff BMPs are available for both industrial sites and urban areas. Of course, any management practice that is used to mitigate pollutants in stormwater runoff from watersheds should also target the nutrients and metals that are deposited from the atmosphere. The following is a discussion of natural and anthropogenic sources of atmospheric pollutant deposition and the types of water resources affected by it. It will be followed by a brief outline of the regulatory programs that target the control of atmospheric pollutant sources. This information should provide a starting point for further efforts to control this increasingly important pollutant source.

The deposition of atmospheric nitrogen and metals may impact surface water. Both metals and nitrogen in the atmosphere are derived from natural and anthropogenic sources. Natural sources of metals include volcanic activity, forest fires, windblown dust, vegetation, and sea spray. The primary anthropogenic metal source is the smelting of ores (Salomons and Forstner, 1984). Other anthropogenic sources include stack and fugitive dust (dust that escapes emission controls). Historically, the deposition of lead (Pb) caused the greatest concern for human health. Lead became a problem starting in the 1920s; unleaded gasoline was used only after the invention of the catalytic converter in the mid 1970s since lead deactivates the catalyst. The introduction of unleaded gasoline has reduced the lead levels in the atmosphere to well below the standards outlined in the Clean Air Act. Mercury and other hazardous metals that are produced during industrial processes are strictly controlled at the source under provisions of the Clean Air Act. Thus, metal deposition should not be a significant problem in watersheds of the United States.

On the other hand, atmospheric nitrogen is derived from many elusive sources, many of which are not regulated under the Clean Air Act. Moreover, nitrogen levels appear to be increasing continuously in the atmosphere. Studies indicate that atmospheric deposition of nitrogen poses great risk for the eutrophication of surface water. Thus, the following discussion will focus primarily on the formation and survival of nitrogen in the atmosphere.

The predominant natural source of nitrogen is the microbial decomposition of organic matter in soil and water. Microorganisms release ammonia (NH₃) to the atmosphere during the breakdown of amino acids (Oke, 1978; Smith, 1990). Less pronounced natural sources include the release of organic nitrogen in the form of amino acids and urea from the activity of organisms (Paerl, 1993) and nitrogen

fixation by lightning (Smith, 1990). Predominant anthropogenic atmospheric nitrogen sources include:

1. Emissions of nitrogen oxides (NO_x) from the combustion of fossil fuels
2. Ammonia (NH_3) and ammonium (NH_4^+) emissions from fertilizer and explosive manufacturing plants
3. Volatilization of ammonia-based fertilizer from agricultural fields (Oke, 1978; Lippman, 1989; Paerl, 1993)

Most anthropogenic nitrogen is emitted during the combustion of fossil fuels. Approximately 220 million tons of nitrogen is emitted each year from fossil fuel combustion (Schlesinger, 1991). Fossil fuel-burning power plants and large industries emit 53% of the yearly nitrogen emissions in the United States. Mobile sources (such as cars, trucks, and buses) account for 38% of the total emissions (Puckett, 1994). Under high temperatures and pressure, nitrogen and oxygen in the fuel and air combine to form the relatively harmless nitric oxide (NO) gas. Once in the atmosphere, nitric oxide is oxidized to nitrogen dioxide (NO_2), an irritating gas. Nitric oxide and NO_2 may also be converted to a series of other oxidized species, including HNO_3 , HNO_2 , HO_2NO_2 , NO_3 , N_2O_5 , and organic nitrates (Oke, 1978; Lippman, 1989). The production and application of fertilizers comprise a much smaller, albeit significant, pool of anthropogenic nitrogen emissions. Of approximately 88 million tons of nitrogen fertilizer applied to terrestrial global ecosystems each year, 8 million tons escape to the atmosphere as NH_3 , NH_4^+ , or NO_x ($\text{NO} + \text{NO}_2$) (Hinrichsen, 1986; Schlesinger, 1991). Once emitted into the atmosphere, nitrogen may be deposited locally or may travel great distances before deposition. Many industrial and urban centers of the central U.S. emit nitrogen that is not only deposited locally downwind, but also as far away as the east coast of the U.S. (Paerl, 1993). More than 3.2 million tons of atmospheric nitrogen is deposited on the United States' watersheds each year.

In addition, a sizeable amount of atmospheric nitrogen is deposited in the Atlantic Ocean. Galloway (1990) suggests that 18% to 27% of the total NO_x emitted over the eastern U.S. is advected and deposited over the Atlantic Ocean. Atmospheric nitrogen may be deposited in dry or wet form. Dry deposition involves the settling of particulates over time with gravity. Wet deposition occurs when particulates and aerosols are removed from the atmosphere by a precipitation event (Paerl, 1993). Wet deposition accounts for the majority of nitrogen removed from the atmosphere (Paerl et al., 1990). Deposition of nitrogen (wet and dry) occurs over land and water. The terrestrial ecosystem will incorporate the wet and dry-deposited nitrogen as a nutrient source whenever possible. Between 30% and 60% of the nitrogen deposited on land is thought to be absorbed by the ecosystem.

The degree to which a watershed can retain nitrogen is a function of the soil characteristics, the topography, the underlying geology, the amount and the type of surface vegetation, and the degree of impervious cover (Paerl, 1993). Inevitably, a significant amount of deposited nitrogen will be transported during a

precipitation event into a freshwater system via overland or subsurface flow. Usually freshwater systems are phosphorus-limited and will not use the excess nitrogen. Thus, most of the nitrogen will be delivered to estuarine systems. Recent studies indicate that atmospheric nitrogen accounts for a large portion of the allochthonous (derived from outside the water body) nitrogen in estuaries and coastal oceans. A study by Paerl (1993) indicates that some estuaries in the east coast of the United States may receive between 30% and 40% of the outside nitrogen from the atmosphere while coastal oceans may receive up to 50% from the atmosphere. Estimates from other areas of the eastern seaboard are strikingly similar. Actual percentages in each area vary depending on the location, hydrologic regimes, and human activities. Atmospheric nitrogen and metal deposition regulatory control is the responsibility of local air quality officials and facility managers. Lead and nitrogen are classified as criteria air pollutants, and are governed by National Ambient Air Quality Standards (NAAQS). States must create and implement plans that will permit "air quality areas" to meet the standards for the criteria air pollutants. Areas not meeting the standards are classified as "non-attainment areas" and are subject to further regulation and potential grant withholding (Vandenberg, 1994). Hazardous metals (other than lead) are governed under the National Emission Standards for Hazardous Air Pollutants (NESHAP). NESHAPs are set for individual source types. Every facility governed by NESHAPs is monitored and regulated individually (Vandenberg, 1994). Local air quality officials should be contacted with any questions concerning emissions from facilities in that vicinity.

2 Different Deposition Parameterizations

In this section we will refer to different deposition parameterizations that are used on different air quality models.

Deposition parameterization used in EMEP model (Cooperative programme for monitoring and evaluation of the long range transmission of air pollution in Europe)

Gaseous exchange (POP parameterization)

1. Atmosphere/soil gaseous exchange

The gaseous exchange of pollutants is parameterized using the resistance analogy (Jacobs and van Pul, 1996), as seen in Figure 1.

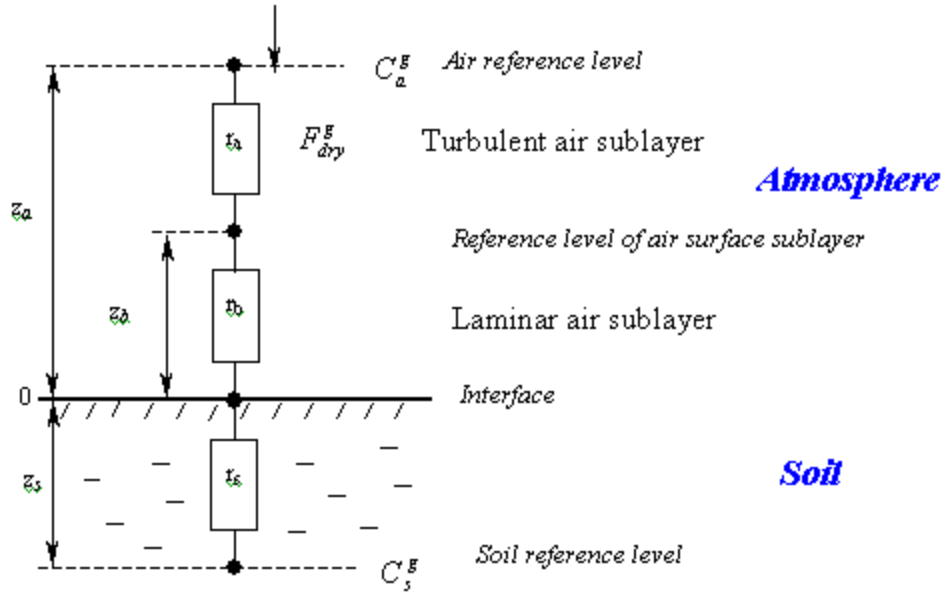


Figure 1. The resistance analogy of the gaseous exchange of pollutants (Jacobs and van Pul, 1996).

The gaseous flux of POP from the atmosphere into soil is driven by the difference between the atmospheric gas concentration at the air reference level C_a^g at height $z_a=50$ m and the soil gas-phase concentration at the soil reference level at depth $z_s=2.5$ mm C_s^g :

$$F_{dry}^g = \frac{C_a^g - C_s^g}{r_a + r_b + r_s} \quad (1)$$

A pollutant, in the transport from the air reference level to the soil reference level, overcomes the following resistances: the turbulent air sublayer resistance r_a , s/cm; the resistance to the transport through the turbulent air sublayer (from z_a to z_b); the laminar surface air sublayer resistance r_b , s/cm; the resistance to the transport through the laminar surface air sublayer to the interface (from z_b to 0); the surface soil resistance r_s , s/cm; and the resistance to the transport through surface soil interface to the soil reference level (from 0 to z_s).

2. Atmosphere/sea gaseous exchange

The boundary condition on the interface between air and sea is derived on the basis of the "two films" model. The gaseous flux from air to sea F_{dry}^g (ng/m²/s) is determined by:

$$F_{dry}^g = \alpha_1 (C_a^g / K_H - C_w^d) ((1 - \alpha_2) D_\mu / \delta + \alpha_2 K_H \dot{h}_f) \quad (2)$$

where:

- C_a^g - gaseous POP concentration at the air reference level, ng/m³
- C_w^d - dissolved POP concentration in the upper mixed layer of seawater, ng/m³
- K_H - dimensionless Henry's law constant
- α_1 - sea surface area increase coefficient, where
 $\alpha_1 = 1.75 - 0.75 \cdot \exp(-0.18 \cdot W_{10})$
- α_2 - coefficient of sea surface area covered with the foam, where
 $\alpha_2 = 1 - \exp(-0.01 \cdot W_{10})$
- δ - molecular layer depth near the water surface, mm, where
 $\delta(W_{10}) = 4 \cdot 10^{-5} \exp(-0.15 \cdot W_{10})$
- $\alpha_1, \alpha_2, \delta$ - functions of wind velocity at 10 m height W_{10} (Sergeev et al., 1979)
- D_μ - coefficient of POP molecular diffusion in water, m²/s
- $\dot{h}_f = 0.008$ - rate of the foam layer decrease on the sea surface, m/s

For internal seas, the gaseous flux, F_{dry}^g (ng/s), is calculated the same way as for soil:

$$F_{dry}^g = \frac{C_a^g / K_H - C_w^d}{r_a + r_b} \quad (3)$$

3. Atmosphere/vegetation gaseous exchange

The gaseous flux of POP from the atmosphere onto the vegetation is affected by the difference between air gas concentration at the reference level C_a^g and the gas concentration at the surface of leaves C_v / K_{va} .

$$F_{dry}^g = k a_v (C_a^g - C_v / K_{va}) \quad (4)$$

where:

- k - mass transfer coefficient, m/s
- a_v - specific surface area of vegetation, m⁻¹
- C_v - volume concentration in vegetation, ng/m³
- K_{va} - bioconcentration factor (BCF)

The bio-concentration factor is determined by the following formula: $K_{va} = m K_{OA}^n$ where K_{OA} is the coefficient of partitioning between octanol and air, and m and n are presented in Table 1.

Table 1. m and n values for grass and forest.

	Grass (Thomas et al., 1998)	Forest (Hortsmann and McLachan, 1998)	
		Coniferous	Deciduous
m	22.91	38	14
n	0.445	0.69	0.76

Example of AOT values (accumulated ozone hourly concentrations above 40 ppb) over Europe for Ozone as a result of EMEP model applications with this deposition approach can be seen in Figure 2.

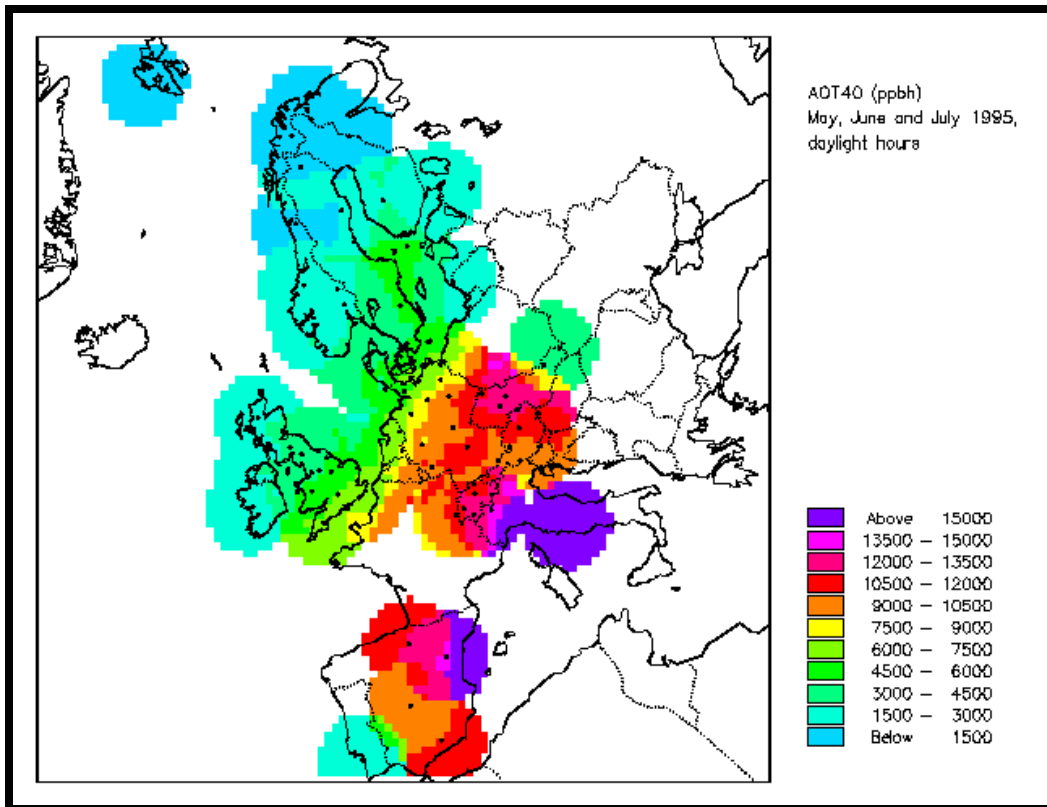


Figure 2. AOT values over Europe for Ozone.

2.1 Dry Deposition of the Particulate Phase

Dry deposition flux of the particulate phase F_{dry}^P (ng/m²/s) is a product of dry deposition velocity V_d (m/s) by particle air concentration C^P (ng/m³) taken at the air reference level $z_a = 50$ (m):

$$F_{dry}^P = V_d \cdot C^P \quad (5)$$

Dry deposition velocity from the reference level z_a is calculated from:

$$V_d = \left(r_a + V_d^{surf^{-1}} \right)^{-1} \quad (6)$$

where:

- r_a - aerodynamic resistance for turbulent transport of a pollutant from z_1 to z_2 , s/m
- z_b - height of the surface layer, m
- V_d^{surf} - surface dry deposition velocity from the surface layer height z_2

which is calculated for sea, soil and forest separately.

Velocity of dry deposition over sea (V_d^{sea} , $z_b = 10$ m), cm/s, is:

$$V_d^{sea} = (A_{sea} u_*^2 + B_{sea}) \quad (7)$$

(regression formula obtained by Pekar (1996) from Lindfors et al. (1991) data.

Velocity of dry deposition over soil (V_d^{land} , $z_b = 1$ m, $z_0 \leq 100$ mm), cm/s:

$$V_d^{land} = (A_{soil} u_*^2 + B_{soil}) \cdot z_0^{C_{mm}} \quad (8)$$

where:

- u_* - friction velocity, m/s
- A, B, C - constants depending on effective diameters of particle-carriers of POP in question
- z_0 - surface roughness, mm (regression formula obtained by Pekar [1996] from Sehmel [1980] data)

Velocity of dry deposition to a forest (V_d^{forest} , $z_b = 20$ m), (adapted from Ruijgrok et al. [1997] data by Erdman [Tsyro & Erdman, 2000]), m/s:

$$V_d^{forest} = E \cdot \frac{u_*^2}{u_k} \quad (9)$$

where $E = a u_*^\beta (1 + g)$ is the total collection efficiency for particles within canopy (it is assumed that relative humidity is 80% on average) and a , β , g are experimental coefficients for each pollutant.

Wind speed at forest height u_h (m/s) is calculated by formula:

$$u_k = \frac{u_*}{k} \left[\ln \left(\frac{z_b - d_0}{z_0} \right) - \psi_m \left(\frac{z_b - d_0}{L} \right) + \psi_m \left(\frac{z_0}{L} \right) \right] \quad (10)$$

where:

- $k = 0.4$ – Karman constant
- $d_0 = 15$ m – zero-plane displacement
- $z_0 = 2$ m – roughness length
- L – Monin-Obukhov parameter
- $\psi_m(\zeta)$ – universal correction function for the atmospheric stability for momentum

2.2 Wet Deposition of the Gaseous and Particle Bound Phase

To define the gaseous phase scavenging with precipitation, equilibrium between the gaseous phase in air and the dissolved phase in precipitation is assumed:

$$C_w^d = W_g C_a^g \quad (11)$$

where:

- C_w^d - dissolved phase concentration in precipitation water, ng/m³
- C_a^g - gaseous phase concentration in air, ng/m³
- $W_g = 1/K_H$ - dimensionless washout ratio for gaseous phase
- K_H - dimensionless Henry's law coefficient

For the description of the particle bound phase scavenging with precipitation, the washout ratio is used:

$$C_w^s = W_p C_a^p \quad (12)$$

where:

- C_a^p - particle bound phase concentration in air, ng/m³
- C_w^s - suspended phase concentration in precipitation water, ng/m³
- W_p - dimensionless washout ratio for the particulate phase

The flux of wet deposition for the gaseous or particulate phase F_w (ng/m²/s) can be calculated by:

$$F_{wet} = h_p \cdot C_w \quad (13)$$

where:

- h_p - precipitation intensity, m/s
- C_w - dissolved or particulate phase concentration in precipitation water, ng/m³

2.3 Dry and Wet Deposition for Pb and Cd

A flux of aerosol dry deposition carrying heavy metals is defined by expression:

$$F(x, y, z = z_0, t) = V_d(x, y, t) \cdot C(x, y, z_1, t) \quad (14)$$

where:

- z_1 - the first calculation level along the vertical
- $z_1 = 50$ m
- V_d – variable over space and time (the deposition velocity on the surface different for different metals)

According to Sehmel (1980) data, the range of variation for V_d is three orders of magnitude. When particles cross the laminar sublayer, two maximum regimes of deposition occur: 1 - for coarse particles - gravitational settling is decreasing with particles size decrease; 2 - for fine particles - deposition due to Brownian diffusion is decreasing with particle size increase. Thus, for particles of intermediate size, minimum deposition should occur. This phenomenon is observed for particles within the range 0.1-1.0 μm . These particles have rather small velocities, thousandth or hundredth fractions of 1 cm/s. Evidently, these particles should dominate in the long-range transport. According to Midford and Davidson (1985) data, maximum spectrum of aerosols with Pb and Cd is accounted for this size range. Median aerodynamic diameters for Pb and Cd equal to 0.55 μm and 0.84 μm respectively. When deposition process was parameterized, we ignored the spectrum using MMD as “effective” particle size. Besides particle sizes, the deposition efficiency is influenced by meteorological conditions and surface properties, and great difference between deposition velocities on land or sea are observed. The parameterization of dry deposition velocity on a dry surface was made on the basis of Sehmel (1980) results, where

similar calculations are given for V_d for a number of surfaces (z_0) and a set of turbulence states (u_*). For the assumption of “effective” sizes, dependences V_d (z_0) for individual u_* were derived. In the double logarithmic scale, they are represented by a family of parallel straight lines that allow the use of the following approximations:

$$V_d^{land}(Pb) = (0.02u_*^2 + 0.01) \cdot (z_0/10^{-3})^{0.33} \quad (15)$$

$$V_d^{land}(Cd) = (0.04u_*^2 + 0.02) \cdot (z_0/10^{-3})^{0.30} \quad (16)$$

where: V_d^{land} [cm/s] is the velocity of dry deposition over land.

Results obtained with the model of Lindfors et al. (1991), which is a modified model of Williams (1982), were used for the parameterization of deposition on the sea surface. Using the resistance analogy method, two layers are considered: turbulent and quasilaminar. In the quasilaminar layer, fluxes are considered on both smooth and broken surface with sea spray that allows considering the washout and coagulation with spray droplets. Using the results of this work, we derived the following approximations for deposition velocities on the marine surface for Pb and Cd:

$$V_d^{sea}(Pb) = 0.15 \cdot u_*^2 + 0.013 \quad (17)$$

$$V_d^{sea}(Cd) = 0.15 \cdot u_*^2 + 0.023 \quad (18)$$

Sink of pollutants due to precipitation scavenging is represented by a linear process:

$$\frac{\partial C}{\partial t} = -\Lambda C \quad (19)$$

where the washout coefficient Λ depends on many parameters of both pollutants and precipitation. The models do not consider the complicated nature of the phenomena. The distribution of precipitations along the vertical is assumed to be uniform. The flux of wet deposition from the layer of h depth is equal to:

$$F = C\Lambda h \quad (20)$$

The same flux is represented as:

$$F = C_p I \quad (21)$$

where C_p is the concentration in precipitations and I is the precipitation intensity. Hence, it follows that:

$$\Lambda = \frac{C_p}{C} \frac{I}{h} = \frac{WI}{h} \quad (22)$$

where W is the scavenging ratio equal to that of concentration in precipitation to concentration in the air. Order of magnitude of W for heavy metal particles is 10^5 , which testifies to the effective scavenging. It is set equal to 500,000 for Pb and Cd. This value was also used in other long-range transport models for Europe (Alcamo et al., 1992; Bartnicki et al., 1993).

3 Examples of Deposition Monitoring Programs

3.1 EPA Deposition Monitoring Program

Sulphur and nitrogen oxides are emitted into the atmosphere primarily from burning fossil fuels. Sulfur and nitrogen oxides also have large natural sources. These emissions react in the atmosphere to form compounds that are transported long distances and are subsequently deposited in the form of pollutants such as particulate matter (sulphates and nitrates), SO₂, NO₂, and nitric acid. When it is reacted with volatile organic compounds (VOCs), it results in formation of ozone. The effects of atmospheric deposition include acidification of lakes and streams, nutrient enrichment of coastal waters and large river basins, soil nutrient depletion and decline of sensitive forests, agricultural crop damage, and impacts on ecosystem biodiversity. Toxic pollutants and metals can also be transported and deposited through atmospheric processes. Both local and long-range emission sources contribute to atmospheric deposition. Total atmospheric deposition is determined using both wet and dry deposition measurements. Wet deposition is the portion dissolved in cloud droplets and is deposited during rain or other forms of precipitation. Dry deposition is the part deposited on dry surfaces during periods of no precipitation as particles or in gaseous form. Although the term "acid rain" is widely recognized, the dry deposition portion ranges from 20 to 60 percent of total deposition.

The United States Environmental Protection Agency (EPA) is required by several Congressional and other mandates to assess the effectiveness of air pollution control efforts. These mandates include Title IX of the Clean Air Act Amendments (CAAA), the National Acid Precipitation Assessment Program (NAPAP), the Government Performance and Results Act, and the U.S. Canada Air Quality Agreement. One way to measure the effectiveness of these efforts is by determining whether sustained reductions in the amount of atmospheric deposition over broad geographic regions are occurring. However, changes in the atmosphere happen very slowly and trends are often obscured by the wide variability and climate. Numerous years of continuous and consistent data are required to overcome this variability, making long-term monitoring networks especially critical for characterizing deposition levels and identifying relationships among emissions, atmospheric loadings, and effects on human health and the environment. For wet and dry deposition, these studies typically include measuring concentration levels of key chemical components as well as precipitation amounts. For dry deposition, analyses must also include meteorological measurements that are used to estimate rate of the actual deposition, or “flux”. Data representing total deposition loadings (e.g., total sulphate or nitrate) are what many environmental scientists use for integrated ecological assessments.

The National Atmospheric Deposition Program (NADP) and the Clean Air Status and Trends Network (CASTNET), described in detail below, were developed to monitor wet and dry acid deposition, respectively. Monitoring site locations are predominantly rural by design to assess the relationship between regional pollution and changes in regional patterns in deposition. CASTNET also includes measurements of rural ozone and the chemical constituents of PM_{2.5}. Rural monitoring sites of NADP and CASTNET provide data where sensitive ecosystems are located and provide insight into natural background levels of pollutants where urban influences are minimal. The data provide needed information to scientists and policy analysts to study and evaluate numerous environmental effects, particularly those caused by regional sources of emissions for which long range transport plays an important role. Measurements from these networks are also important for understanding non-ecological impacts of air pollution such as visibility impairment and damage to materials, mainly those of cultural and historical importance.

National Atmospheric Deposition Network. The NADP was initiated in the late 1970s as a cooperative program between federal and state agencies, universities, electric utilities, and other industries to determine geographical patterns and trends in precipitation chemistry in the United States. Collection of weekly wet deposition samples began in 1978. The size of the NADP Network grew rapidly in the early 1980s when the major research effort by the NAPAP called for characterization of acid deposition levels. At that time, the network was known

as the NADP/NTN (National Trends Network). By the mid-1980s, the NADP had grown to nearly 200 sites where it stands today as the longest running national deposition monitoring network. The NADP analyzes the constituents important in precipitation chemistry, including those affecting rainfall acidity and those that may have ecological effects. The Network measures sulphate, nitrate, hydrogen ion (measure of acidity), ammonia, chloride, and base cations (calcium, magnesium, potassium). To ensure comparability of results, laboratory analyses for all samples are conducted by the NADP's Central Analytical Lab at the Illinois State Water Survey. A new sub-network of the NADP, the Mercury Deposition Network (MDN) measures mercury in precipitation.

Clean Air Status and Trends Network. The CASTNET provides atmospheric data on the dry deposition component of total acid deposition, ground-level ozone and other forms of atmospheric pollution. CASTNET is considered the nation's primary source for atmospheric data to estimate dry acidic deposition and to provide data on rural ozone levels. Used in conjunction with other national monitoring networks, CASTNET is used to determine the effectiveness of national emission control programs. Established in 1987, CASTNET now comprises over 70 monitoring stations across the United States. The longest data records are primarily at eastern sites. The majority of the monitoring stations are operated by EPA's Office of Air and Radiation; however, approximately 20 stations are operated by the National Park Service in cooperation with EPA. Each CASTNET dry deposition station measures: weekly average atmospheric concentrations of sulphate, nitrate, ammonium, sulphur dioxide and nitric acid, and hourly concentrations of ambient ozone levels. Meteorological conditions are required to calculate dry deposition rates. Dry deposition rates are calculated using atmospheric concentrations, meteorological data, and information on land use, vegetation, and surface conditions. CASTNET complements the database compiled by NADP. Because of the interdependence of wet and dry deposition, NADP's wet deposition data are collected at all CASTNET sites. Together, these two long-term databases provide the necessary data to estimate trends and spatial patterns in total atmospheric deposition.

National Oceanic and Atmospheric Administration. The NOAA also operates a smaller dry deposition network called Atmospheric Integrated Assessment Monitoring Network (AIRMoN) focused on addressing research issues specifically related to dry deposition measurement.

Rural Ozone. Ozone data collected by CASTNET are complementary to the larger ozone data sets gathered by the State and Local Air Monitoring Stations (SLAMS) and National Air Monitoring Stations (NAMS) networks. Most air quality samples at SLAMS/NAMS sites are located in urban areas, while CASTNET sites are in rural locations. Hourly ozone measurements are taken at each of the 50 sites operated by EPA. Data from these sites provide information to help characterize ozone transport issues and ozone exposure levels. The SLAMS can be visited at <http://www.epa.gov> and some examples are given below.

4 Examples of Air Quality Models

Models are tools that allow us to learn, and manage systems and processes. Both water and air models can contribute to our knowledge of the atmospheric deposition impacts on the Gulf of Mexico hypoxic zone. Models currently being used to investigate this issue include SPARROW, RADM and Extended RADM, Models-3/CMAQ, and REMSAD (Table 2).

Table 2. Models for Determining Atmospheric Deposition.

Model	Features	Limitations
SPARROW	<ul style="list-style-type: none"> • Statistical watershed model predictions based on actual stream measurements and source • Inputs: spatial scale—Chesapeake Bay 30 m² nation 1 km² • Explanatory factors include: <ul style="list-style-type: none"> ▪ Sources—fertilizer use, livestock wastes, non-agriculture non-point runoff, point sources, atmosphere deposition (wet nitrate plus additional wet and dry forms) • NOTE: Atmospheric inputs to the model are wet nitrate deposition, but there is strong evidence based on the land-to-water estimates of atmospheric delivery to streams that additional inputs from wet deposition of ammonium, organic nitrogen and dry deposition of inorganic nitrogen are also included in the SPARROW estimates. • Land to water delivery—soil permeability, stream density, temperature, and in-stream loss—water 	<ul style="list-style-type: none"> • Substantial stream monitoring data requirements • Difficult to describe detailed processes • The model is based on mean conditions and does not operate dynamically • Predictions at smaller scales are estimated with higher uncertainty

Model	Features	Limitations
	<p>velocity, stream channel size empirical estimates of rates of land to water delivery and in-stream loss of nutrients predictions accompanied by formal error bands</p>	
RADM	<ul style="list-style-type: none"> • Process air quality model • Full oxidant chemistry/cloud processes • Aqueous chemistry/dry deposition/particulate • Post-processing to define NO₃- oxidized N deposition (wet and dry deposition) • Eastern U.S./terrestrial area (watersheds) and coastal estuaries—80km grid resolution in eastern U.S. and 20 km grid resolution in mid- • Atlantic U.S. annual averages/warm season; cold season (climatological through aggregation method) • Used to define oxidized-N airsheds for coastal estuaries 	<ul style="list-style-type: none"> • Large grid size (urban influence not picked up in 80 km.) • No true ammonia cycling • Does not treat sea salt • No wet deposition over coastal ocean beyond 100 km • Older parameterizations of dry deposition • Bias in handling winter precipitation
Extended RADM	<ul style="list-style-type: none"> • Process air quality model • Full oxidant chemistry/cloud • Processes aqueous chemistry/dry deposition/fully integrated inorganic particle physics (NH_x cycling) • Oxidized and reduced N deposition (wet and dry deposition) • Eastern U.S./terrestrial area (watersheds) and coastal estuaries—80km grid resolution in eastern 	<ul style="list-style-type: none"> • Large grid size (urban influence not picked up in 80 km) • Does not treat sea salt • No wet deposition over coastal ocean beyond 100km • Older parameterizations of dry deposition • High resolution meteorology is interpolated • Bias in how handles

Model	Features	Limitations
	<p>U.S. and 20km grid resolution in mid-Atlantic U.S.</p> <ul style="list-style-type: none"> • Annual averages/warm season; cold-season (climatological) through computer-simulated aggregation method 	<p>winter precipitation</p>
Models-3/CMAQ	<ul style="list-style-type: none"> • Process air quality model • Full oxidant chemistry/cloud processes • Aqueous chemistry/updated dry deposition • Surface exchange/fully integrated particle physics (NO₃- and NH_x cycling; aerosol organics; sea salt influence) • Add mercury in a couple of years • Iron parameterized—based on global average • Oxidized and reduced N deposition (wet and dry deposition) • Continental U.S./Terrestrial area (watersheds) and coastal estuaries and coastal ocean waters—36km grid resolution for continental U.S. and 12km grid resolution for mid-Atlantic U.S., Gulf Coast U.S. and western U.S. • Annual averages/four-season averages (climatological)—deal with seasonality through aggregation method 	<ul style="list-style-type: none"> • Bi-directionality of ammonia deposition not yet accounted for (not sure how critical, but want to know about it) • Best estimates of deposition over ocean will come from 1-3 month study periods • Complex terrain effects will still be hard to simulate • Ability to model meteorology at 4km • Sufficient, spatially dense data to evaluate CMAQ
REMSAD	<ul style="list-style-type: none"> • System of models—consists of meteorological data preprocessor, the core Aerosol and Toxic 	<ul style="list-style-type: none"> • Uncertainties larger for shorter averaging time periods • Dependent on

Model	Features	Limitations
	Deposition Model, and post-processing programs <ul style="list-style-type: none"> • Designed to be a fast screening tool for control strategies for particulate matter (PM) • A continental-scale tool for PM and toxic deposition (regional-scale) • Grid model applicable over regional scales • Micro-mechanism chemistry including isoprene tracks PM and selected toxic species • Detailed representation of spatial and temporal distributions of PM concentrations and toxic deposition • Detailed deposition algorithm built into model • Treats meteorological influences on transport and removal directly • Responds to inventory-level control measures 	accuracy of emission inventories <ul style="list-style-type: none"> • Dependent on reliability of meteorological inputs • Coarse resolution in most situations

The SPARROW (SPATIally Referenced Regression On Watershed Attributes) watershed model divides a watershed using river reaches and it models mean annual total nitrogen yield by looking at upstream sources and computing the mass-balance between sites. SPARROW predictions of total nitrogen flux for the Mississippi Basin were based on the calibrations of the model to a national set of 374 stations, including 123 watersheds with monitoring locations. The model was used to look at the contributions of different sources to the Gulf of Mexico. The percent contribution of different sources in the Mississippi basin showed that approximately 60% of the nitrogen delivered to the Gulf originates from agricultural sources (fertilizer and livestock wastes) and approximately 18% from atmospheric deposition (the large error bars on the estimate yield a range of 6-28% for atmospheric deposition). The model was also used to look at origin of atmospheric contribution. Nearly 50%, of the atmospheric nitrogen was emanating from Ohio and upper Tennessee River basins. Agricultural sources seem to be the dominant feature in most of the Mississippi basin watersheds except in the western reach of the basin. Atmospheric input makes its largest contribution in the eastern portion of the basin. SPARROW predictions of in-

stream loss and nitrogen loads reflect long-term mean conditions. SPARROW is not a dynamic model; it addresses the issue of retention by assuming a steady-state and looking at the concentrations over a long time period. SPARROW can make seasonal predictions and for many management decisions, mean seasonal and annual estimates are satisfactory. Refinements will be required to make the model dynamic and these are planned for the future. Also, SPARROW currently has no way of handling sources of nitrogen stored in the system. Enhancements to the model were made to refine the in-stream delivery term to give a better estimate of in-stream loss in large rivers.

The next generation of SPARROW will expand on finer spatial resolution and land to water delivery. The developers are also adding output from the topographic models to get more information on subsurface flow. Future improvements to SPARROW will include explicit quantification of atmospheric inputs from dry deposition, descriptions of the types and locations of watershed sinks (e.g., ground water storage, subsurface transport), and it will account for temporal variability in flow, source inputs, and nitrogen transport within watersheds. The Regional Acid Deposition Model (RADM) and Extended RADM models process air quality models. These models can be used to look at a source region and see where atmospheric deposition of nitrogen, both oxidized and reduced, is falling. In the model, NH_3 travels about 2/3 as far as NO_3 but still farther than it was considered by conventional wisdom. The model can also estimate the percent-oxidized nitrogen deposition to a watershed explained by local airshed NO_x emissions vs. that from long-range transport. RADM has been operational since 1990. It models oxidized nitrogen deposition (wet and dry) in the eastern U.S. for terrestrial areas (watersheds) and coastal estuaries. It has been used by the Chesapeake Bay Program to help address atmospheric issues and used to define oxidized-nitrogen airsheds for coastal estuaries. The Extended RADM became operational in 1999. It models oxidized and reduced nitrogen deposition (wet and dry) in the eastern U.S./terrestrial area (watersheds) and coastal estuaries. The Extended RADM has been used to define oxidized nitrogen airsheds and now will be used to define reduced nitrogen airsheds for selected estuaries and in the Chesapeake Bay and North Carolina programs.

The Models-3/CMAQ is EPA's latest 1-atmosphere process model. It became available for testing in 1999 and will be operational in 2001. CMAQ will model oxidized and reduced nitrogen deposition (wet and dry), and will include sea salt influence, updated dry deposition information, and in a few years, mercury deposition. EPA is in the process of undergoing model evaluation on CMAQ and expects to apply it to Gulf Coast studies for year 2000 measurement campaigns in Tampa Bay (nitrogen deposition and ozone) and Houston (ozone and particle formation). To improve these and other models, more extensive characterization of the bias in NADP ammonia estimates and in weekly data (e.g., CASTNet) are needed. Other data issues include a lack of ammonia data (air concentration and deposition) resulting in inability to check models on NH_3/NH_4 split; a lack of data over water, particularly the Gulf of Mexico; and the need for good sea surface temperature data over the Gulf.

Models help characterize the problem—how much (help interpolate data or fill in for data gaps), from where (determine airsheds), from whom (which sector of nitrogen oxide emissions and which sector of NH₃ emissions), and what to expect of management options. However, there are some things that air quality models cannot tell us, or cannot tell us yet. It is difficult to get the deposition details (i.e., the actual deposition to a specific location or to a small watershed). The organic fraction of nitrogen atmospheric deposition is still beyond us by several years. Other challenges for future modeling efforts are modeling individual, multiple years of simulated nitrogen deposition and modeling the actual indirect nitrogen load attributable to the atmosphere. The biggest challenge is that we can't measure everything yet. The REgulatory Modelling System for Aerosols and Deposition (REMSAD) models atmospheric transport and deposition of nitrogen and mercury. The REMSAD platform is based on the UAM-V regional air quality model, which was extended to treat nitrogen transport, several toxics (mercury, dioxin, atrazine, and cadmium) and particulate matter. The model was extended vertically to the tropopause to look at longer-range transport. The model inputs include emissions, meteorological data, land uses, photolysis rates, and hydroxyl radical concentrations (for parameterized chemistry).

REMSAD can be used to assess the magnitude and patterns of total nitrogen deposition. Then the resulting data can be fed into watershed models to derive the nitrogen loadings into water bodies. The toxic deposition module within REMSAD simulates the atmospheric chemical and physical processes leading to mercury deposition and includes in-cloud transformation of mercury. REMSAD is being used in current EPA projects to model atmospheric deposition of nitrogen and mercury in the US, atmospheric concentrations of particulate matter, and deposition of pollutants including total oxidized nitrogen (NO_x), reduced nitrogen (NH₃), and acid species. It is also being used in an evaluation of nitrogen deposition comparing annual and monthly depositions with observations from the NADP.

The Total Maximum Daily Load (TMDL) evaluation in Wisconsin is using REMSAD for a management application. It will assess the effect of changes in the mercury emission levels on its deposition in the Great Lakes area. The model inputs will include meteorological input produced from the RUC model output from NOAA, the MM5 model, and the latest emission inventory from EPA that includes recent estimates of heavy duty diesel NO_x, air conditioning NO_x from light duty vehicles, and toxic emissions estimates. The assessment will aid EPA in determining the need to promulgate more stringent mobile source emission standards and evaluating the environmental consequences of alternative control strategies to reduce mercury deposition to designated areas. It will also look at the contribution to watersheds of mobile and other sources of nitrogen deposited on the Mississippi river basin and estuaries along the coasts.

5 Sensitivity Analysis by Using the OPANA Model

The air quality models can be used as tools to simulate the atmospheric behavior and reaction of the atmosphere system to different deposition parameterizations. Different atmospheric simulations and the sensitivity analysis of the atmosphere system to the different parameterizations will be presented by using the OPANA model.

OPANA, which stands for Operational ANA, is a model composed by 1) a non-hydrostatic mesoscale meteorological module REMEST - based on MEMO, Flassak and Moussiopoulos (1987), and MM5 (Grell et al., 1994); and 2) a chemical module CHEMA - based on the SMVGEAR (Jacobson and Turco, 1994) numerical solver, with the CBM-IV chemical mechanism (Gery et al., 1989).

In addition, an emission model EMIMA accounts for the anthropogenic and biogenic emissions in the model domain; biogenic emissions are based on the landuse classification from LANDSAT-5 satellite data for isoprene, monoterpene and natural NO_x emissions. A deposition module DEPO is based on the resistance approach (Wesely, 1989) and the experience of our group of deposition flux field experiments funded by DGXII (European Commission) (1993-1998).

OPANA model was properly applied into the EMMA project (DGXIII – EC, 1996-1998) and it is operating at the Madrid Community Environmental Office. OPANA model has also been applied at the following EU Projects: DECAIR (Development of an earth observation data converter with application to air quality forecast), CEO (Centre for Earth Observation, DGXII, 1999 - 2002), EQUAL (Electronic Services for a better Quality of Life, DGXIII; EU Commission, 1998-2001), and APNEE (Air Pollution Network for early warning and on-line information exchange in Europe Information Society Technology Programme, EU Commission, 2000-2001). OPANA is based on the Navier-Stokes equation system for the atmospheric flow and as a consequence it requires a 3D grid domain approach. The numerical accuracy of such type of model is quite high; however, the results are limited by the grid cell sizes since the meteorological and air concentrations are given as averages over the grid cell. Grid cell size is limited by the computer power since the Courant law limits the time step for the meteorological section of the air quality model OPANA. A sophisticated graphical user interface was developed in Tcl/Tk 8.0, which makes use of the VIS5D tool that was developed at the University of Wisconsin-Madison, Space Science and Engineering Center (SSEC) and also supported by NASA and EPA. VIS5D on-line with the OPANA-VIS package is capable of visualizing the 3D field for all meteorological variables and air concentrations and fluxes. Figure 3 shows a scheme of the OPANA model.

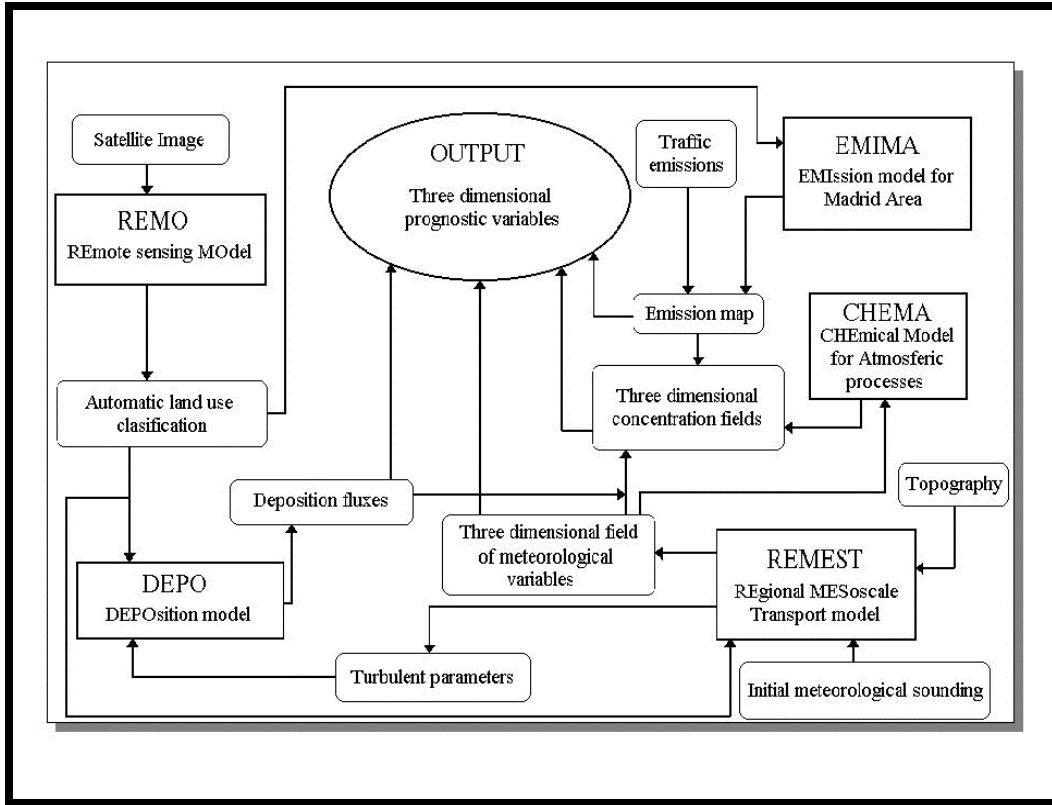


Figure 3. Schema of OPANA model.

Different deposition approaches were tested by using the OPANA air quality modeling system such as Wesely (1989) and Erisman et al. (1994). Primary ideas for these parameterizations are found in Baldocchi et al (1987) and Hicks et al. (1987). In Hicks et al. (1982) we found the preliminary ideas and concepts related to the resistance approach in deposition modeling. Wesely's (1989) contribution constitutes the reference for all air pollution modeling work for the 90's decade. The Erisman et al. (1994) contribution focuses on some specific aspects on the parameterization such as in-canopy resistance and relative humidity. On relation to in-canopy resistance as part of the total canopy resistance, Erisman et al. (1994) proposed a parameterization related to the Leaf Area Index (LAI) as follows:

$$R_{inc} = \frac{bLAIh}{u_*} \quad (23)$$

where LAI is the one-sided leaf area index, h the vegetation height - which we took as $10 z_0$, where z_0 is the roughness length, and b is an empirical constant taken as 14 m^{-1} . In winter when deciduous trees are leafless, all is set to one. This way, the exchange caused by penetration of gusts is accounted for in a straightforward way. For low vegetation, R_{inc} is assumed to be negligible. Results obtained by this equation are in reasonable agreement with those estimated by Wesely (1989). The resistance to uptake at the soil under the canopy

R_{soil} is modeled similarly to the soil resistance to bare solid. On the other hand, Nemani and Running (1989a) found a correlation between the NOAA AVHRR normalized differential vegetation index, $(\text{NIR} - \text{Red}) / (\text{NIR} + \text{Red})$, and estimated LAI of 53 coniferous forests in Montana (USA) as follows:

$$\begin{aligned} NDVI &= \text{Ln}(LAI / 1.625) * 0.34; \\ R^2 &= 0.88 \end{aligned} \quad (24)$$

From Nemani and Running (1989b) it is possible to hypothesize that by investigating the scategramm of NDVI and surface temperature T_s from the NOAA/AVHRR for a 20-25 km study area of conifer forest in Montana on July 14, after 5 weeks without rain (external leaf uptake resistance in Erisman et al. (1994), parameterization is taken as an exponential function with constants depending on the relative humidity), and August 6, after 3.2 cm of rain (in this case $R_{\text{ext}} = 1 \text{ sm}^{-1}$), the correlation between surface temperature and NDVI is found as follows:

$$\begin{array}{ll} \text{July, 14} & \text{August, 6} \\ T = -44NDVI + 55 & T_s = -28NDVI + 42 \\ R^2 = 0.91 & R^2 = 0.88 \end{array} \quad (25)$$

The regression relationship between the slope of $T_s/NDVI$ and surface resistance simulated and FOREST-BGC (the ecosystem simulation model from Running et al. (1989)) for 8 days during the summer of 1985 is:

$$\begin{aligned} R_c &= \text{Ln}(\sigma / 48 + 1) * (-10) \\ R^2 &= 0.92 \\ \sigma &= T_s / NDVI \end{aligned} \quad (26)$$

With these data sets, we can hypothesize that the higher surface temperature on July 14 results from higher Bowen ratio and that the slope of the $T_s/NDVI$ relationship can be used as a satellite derived estimate of surface energy partitioning.

By using these concepts and ideas, we planned a sensitivity experiment by using the OPANA air quality modeling system to see the reliability of using satellite information to generalize the deposition parameterization models since the parameterizations focused very much on local aspects and the application to mesoscale air quality modeling seemed to be questionable.

On Figure 4 and 5 we show an illustration of 5 km and 1 km spatial resolution Madrid OPANA model domain (with 80 x 100 km and located at 400000, 4431000 UTM for the south-west corner of the model domain). We have used data from U.S. Geological Survey's (USGS) Earth Resources Observation

System (EROS) Data Center, the University of Nebraska-Lincoln (UNL) and the Joint Research Centre of the European Commission. These Institutions generated a 1-km resolution global land cover characteristics database for use in a wide range of environmental research and modeling applications. The land cover characterization effort is part of the National Aeronautics and Space Administration (NASA) Earth Observing System Pathfinder Program and the International Geosphere-Biosphere Programme-Data and Information System's focused activity. Funding for the project is provided by the USGS, NASA, U.S. Environmental Protection Agency, National Oceanic and Atmospheric Administration, U.S. Forest Service, and the United Nations Environment Programme.

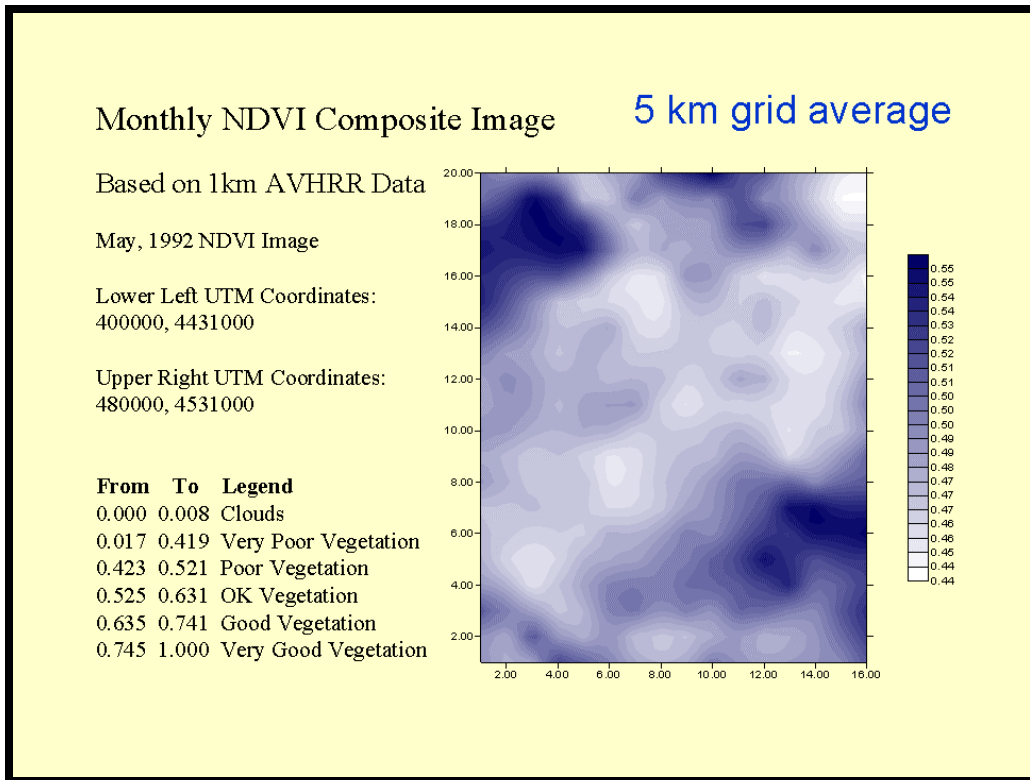


Figure 4. 5 km spatial resolution of Madrid OPANA model domain by using NDVI data from USGS.

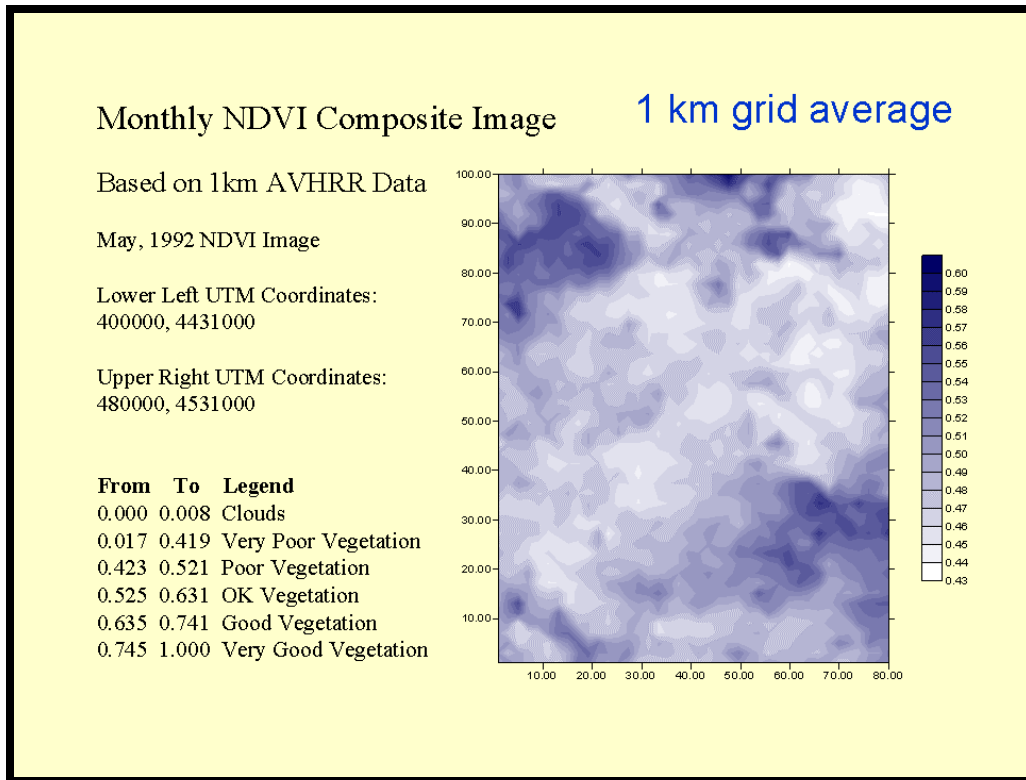


Figure 5. 1 km spatial resolution of Madrid OPANA model domain by using NDVI data from USGS.

The data set is derived from 1-km Advanced Very High Resolution Radiometer (AVHRR) data over a span of 12-month period (April 1992-March 1993). It is based on a flexible database structure and seasonal land cover regions concept. Seasonal land cover regions provide a framework for presenting the temporal and spatial patterns of vegetation in the database. The regions are composed of relatively homogeneous land cover associations (i.e., similar floristic and physiognomic characteristics), which exhibit distinctive phenology (that is, onset, peak and seasonal duration of greenness), and have common levels of primary production. One-kilometer AVHRR NDVI composites are the core data set used in land cover characterization. In addition, other key geographic data include digital elevation data, ecoregions interpretations, and country or regional-level vegetation and land cover maps. See Brown et al. (1993) for a detailed discussion of the role of ancillary data for land cover characterization. The base data used are the International Geosphere Biosphere Programme (IGBP) 1-km AVHRR 10-day composites from April 1992 through March 1993 (Eidenshink and Faundeen, 1994). Multitemporal AVHRR NDVI data are used to divide the landscape into land cover regions based on season. While the primary AVHRR data used in the classification is NDVI, the individual channel data sets are used for post-classification characterization of certain landscape properties. A data quality evaluation was conducted and is reported by Zhu and Yang (1996).

From Figures 4 and 5 we observe the importance of averaging the input data for air quality models (OPANA). In Figure 6 we observe a comparison between ozone surface concentrations when running OPANA model for May 1999 with different canopy parameterizations such as aerodynamic resistance (no canopy resistance), Erisman (1994) parameterization, and Nemani and Running (1989b) parameterization. The ozone concentrations obtained when using NOAA/AVHRR NDVI data and canopy resistance parameterization are expressed in 6.4 equation. Figure 7 also shows ozone surface concentrations but under stable conditions where the differences are higher than unstable conditions (Figure 6).

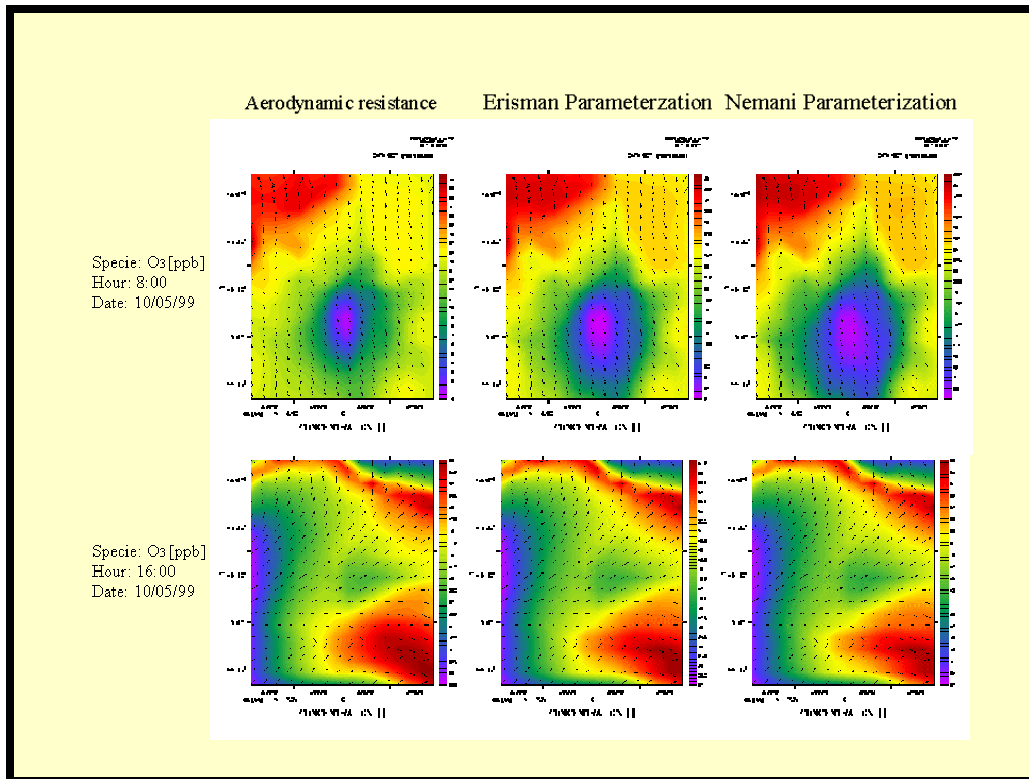


Figure 6. Ozone surface concentrations simulated by OPANA by using different deposition resistance approaches. Note that scales are different but colors are automatically scaled.

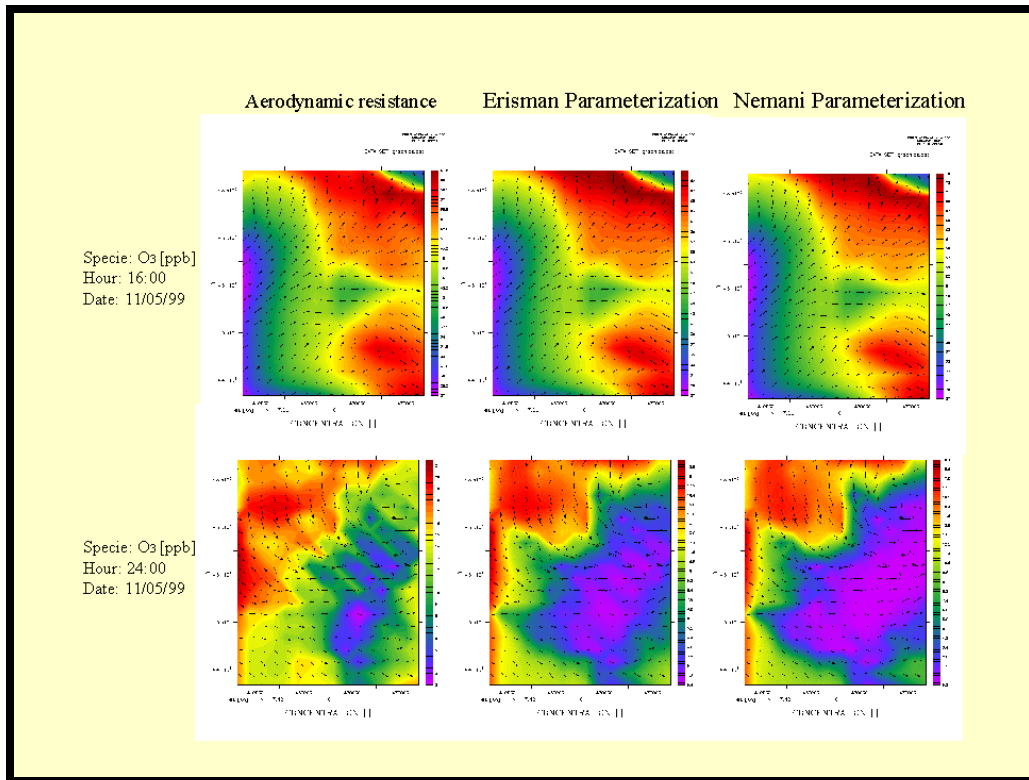


Figure 7. Ozone surface concentrations simulated by OPANA by using different deposition resistance approaches. Note that scales are different but colors are automatically scaled.

The results of this exercise show that a "global" canopy resistance approaches for deposition modeling based on data from NOAA/AVHRR or future microwave satellite series can be valid for mesoscale and continental air pollution simulation exercises since the differences between detailed parameterization approaches and satellite approaches are found to be minor.

References

- Alcamo J., Bartnicki J., Olendrzynski K. and Pacyna J. (1992) Results from a Climatological Model of Heavy Metal in Europe's Atmosphere. Proc. 19th Technical Meeting of NATO-CCMS on Air Pollution and Its Applications, September 29-October 4, Crete, Greece.
- Alexander, R.B., P.S. Murdoch, and R.A. Smith (1996). Streamflow-induced variations in nitrate flux in tributaries to the Atlantic coastal zone. *Biogeochem*, 33:149-177.
- Baldocchi D.D., Hicks B.B. and Camara P. (1987). A canopy stomatal resistance model for gaseous deposition to vegetated surfaces. *Atmospheric Environment*, 21, No. 1. Pergamon Journals Ltd., pp. 91-101.
- Bartnicki J., Modzelewski H., Szewczuk-Bartnicka H., Saltbones J., Berge E. and Bott A. (1993) An Eulerian model for atmospheric transport of heavy metals over Europe: model development and testing. DNMI. Tech.report N117. Norwegian Meteorological Institute, Oslo, Norway.

Brown, J.F., Loveland, T.R., Merchant, J.W., Reed, B.C., and Ohlen, D.O., (1993), Using multisource data in global land cover characterization: concepts, requirements and methods: Photogrammetric Engineering and Remote Sensing, v. 59, pp. 977-987.

Eidenshink, J.C. and Faundeen, J.L., (1994), The 1 km AVHRR global land data set-first stages in implementation: International Journal of Remote Sensing, v. 15, no. 17, pp. 3,443-3,462.

EPA <http://www.epa.gov/> .

Erismann, J.W., van Pul A. and Wyers P. (1994) Parameterization of surface resistance for the quantification of atmospheric deposition of acidifying pollutants and ozone. *Atmospheric Environment*, 28, 16. Elsevier Science Ltd., pp. 2595-2607.

Galloway, J.N., 1990. The intercontinental transport of sulfur and nitrogen. A.H. Knap (ed.), The Long-Range Atmospheric Transport of Natural and Contaminant Substances. Kluwer Academic Publishers, Netherlands.

Gery, M.W., Whitten G.Z., Killus J.P. and Dodge M.C (1989), A photochemical kinetics mechanism for urban and regional scale computer modelling, *Journal of Geophysical Research*, 94, D10, pp. 12925-12956.

Grell, G.A., Dudhia J. and Stauffer D.R. (1994) A description of the Fifth-Generation Penn State/NCAR Mesoscale Model (MM5). NCAR/TN-398+STR. NCAR Technical Note.

Hicks, B.B., Baldocchi D.D., Meyers T.P., Hosker Jr. R.P. and Matt D.R. (1987) A preliminary multiple resistance routine for deriving dry deposition velocities from measured quantities. In *Water, Air, and Soil Pollution*, 36, Ed. Reidel Publishing Company, pp. 311-330.

Hicks, B. B., Wesely, M.L., Coulter, R.L., Hart, R.L., Durham, J.L., Speer, R.E. and Stedman, D.H. (1982) An experimental study of sulphur deposition to grassland. In *Precipitation: Scavenging, dry deposition and Resuspension, Vol. 2*, (edited by Pruppacher, H.R., Semonin, R.G. and Slinn, W. G.N.) Elsevier, New York, pp. 933-942.

Hinrichsen, D., 1986. Multiple pollutants and forest decline. *Ambio*, 15:258-265.

Horstmann, M. and M.S. McLachlan (1998) Atmospheric deposition of semivolatile organic compounds to two forest canopies. *Atmospheric Environment*, v. 32, No 10, pp. 1799-1809.

Jacobs, C.M.J. and W.A.J. van Pul (1996) Long-range atmospheric transport of persistent organic pollutants, I: Description of surface - atmosphere exchange modules and Implementation in EUROS. National institute of public health and the environment, Bilthoven, the Netherlands. Report No 722401013.

Jacobson, M.Z. and Turco R.P. (1994) SMVGEAR: A sparse-matrix, vectorized gear code for atmospheric models, *Atmospheric Environment*, 28, 2, pp.273-284.

Lindfors, V., Joffre, S.M. and Damski, J. (1991) Determination of the wet and dry deposition of sulphur and nitrogen compounds over the Baltic sea using actual meteorological data. Finnish Meteorological Institute Contributions N 4, Helsinki.

Lippman, M., (1989). Health benefits of air pollution control: a discussion. Congressional Research Service (CRS) Report for Congress. The Library of Congress, Washington D.C.

Milford, J.B. and Davidson, C.I. (1985). The sizes of particulate trace elements in the atmosphere - a review. *Journal of the Air Pollution Control Association*, v. 35, No 12, pp. 1249-1260.

NADP <http://nadp.sws.uiuc.edu/>.

Oke, T.R. (1978). *Boundary Layer Climates*. Methuena Co. Ltd., London.

Paerl, H.W. (1993). Emerging role of atmospheric deposition in coastal eutrophication: biogeochemical and trophic perspectives. *Can. J. Fish. Aquat. Sci.*, 50:2254-2269.

Paerl, H.W., J. Rudek, and M.A. Mallin (1990). Stimulation of phytoplankton production in coastal waters by natural rainfall inputs: nutritional and trophic implications. *Marine Biol.*, 107:247-254.

Pekar, M. (1996) Regional models LPMOD and ASIMD. Algorithms, parametrization and results of application to Pb and Cd in Europe scale for 1990 MSC-E Report 9/96, September.

Puckett, L.J. (1994). Nonpoint and point sources of nitrogen in major watersheds of the United States. U.S.G.S. Water Investigations Report 94-4001. U.S. Geological Survey, Reston, Virginia.

Ruijgrok, W., Tieben, H., Eisinga, P. (1997) The dry deposition of particles to a forest canopy: a comparison of model and experimental results. *Atmospheric Environment* v. 31, No 3, pp. 399-415.

Salomons, W. and U. Forstner (1984). *Metals in the Hydrocycle*. Springer-Verlag, Heidelberg, Germany.

Schlesinger, W.H. (1991). *Biogeochemistry: An Analysis of Global Change*. Academic Press, Inc., San Diego, CA.

Sehmel, G. (1980) Particles and gas deposition: a review. *Atmos. Environ.*, v. 14, pp. 983-1011.

Sergeev, Yu.N. (Ed.), Kolodochka A.A., Krummel Hk.D., Kulesh V.P. and O.P. Savchuk (1979) Modelling of substance transport and transformation processes in the sea; Modelling of substance transport and transformation processes in the sea. L., published by Leningrad State University, p. 291.

Smith, R.L. (1990). *Ecology and Field Biology*. Harper Collins Publishers, NY.

Smith, R.A, G.E. Schwarz, and R.B. Alexander (1997). Regional interpretation of water-quality monitoring data. *Water Resources Research* 33(12): 2781-2798.

Thomas, G., Smith, K.E.C., Sweetman, A.J. and K.C. Jones (1998) Further studies on air-pasture transfer of polychlorinated biphenyls. *Environmental Pollution*, v.102, pp.119-128.

Tsyro, S. and L.Erdman (2000) Parameterization of aerosol deposition processes in EMEP MSC-E and MSC-W transport models. EMEP/MSW Technical Note, in preparation.

Vandenberg, J. (1994). *Air Quality Management Class Notes*. Duke University School of the Environment. Fall 1994.

Wesely M.K. (1989) Parameterization of surface resistances to gaseous dry deposition in regional-scale numerical models. In *Atmospheric Environment*, 23(6). Pergamon Press Ltd., pp. 1293-1304.

Williams, R.M. (1982) A model for the dry deposition of particles to natural water surfaces. *Atm. Env.*, 16, pp.1933-1938.

Zhu, Z., and Yang, L., (1996), Characteristics of the 1-km AVHRR data set for North America: International Journal of Remote Sensing, v. 17, pp. 1,915-1,924.

Pepper, D.W. and D.B. Carrington 2005. *Indoor Air Pollution Modeling*. Chapter 14 of *AIR QUALITY MODELING - Theories, Methodologies, Computational Techniques, and Available Databases and Software. Vol. II – Advanced Topics* (P. Zannetti, Editor). Published by The EnviroComp Institute (<http://www.envirocomp.org/>) and the Air & Waste Management Association (<http://www.awma.org/>).

Chapter 14

Indoor Air Pollution Modeling

Darrell W. Pepper ⁽¹⁾ and David B. Carrington ⁽²⁾

⁽¹⁾ Nevada Center for Advanced Computational Methods, University of Nevada Las Vegas, Las Vegas, Nevada (USA)

darrell.pepper@nscee.edu

⁽²⁾ Computer and Computational Sciences Division, Los Alamos National Laboratory, Los Alamos, New Mexico (USA)

dcarring@lanl.gov

Abstract: Indoor Air Pollution is a major concern to today's engineers, architects, and building occupants. More recent, stringent fire and smoke control ordinances, and concern for building occupants' health, have generated the need to understand the sources of indoor air pollution and predict indoor transport. Heating, ventilation, and air conditioning systems which try to maximize energy efficiency and maintain occupants' comfort and well-being, extensive use of man-made building materials, safety, health and recently encountered security risks have brought the idea of modeling indoor air pollution into the mainstay of building design and operation. Theories of air pollution modeling are presented below. Applicable source terms for indoor air pollution, from the simpler to the complex modeling techniques, are discussed here.

Key Words: indoor air quality, air-conditioning, second-hand smoke, ventilation, building contamination, building safety, numerical modeling, fluid dynamics, turbulence modeling, particulate transport, and resuspension.

Nomenclature

c_p	Specific heat at constant pressure
C_j	Concentration of the j^{th} species
$D_j; D_{jj}$	Fickian diffusivity of the j^{th} species
D	Deterministic forcing function

f_i	Body force in the i^{th} direction
g	Gravitational acceleration
g_{x_i}	Gravitational acceleration in the i^{th} coordinate direction
k	Thermal conductivity
κ	Von Karman constant of proportionality
$K_1 K_2 K_3$	Diagonal components of dispersion tensor in direction of principal axes
K_m	Turbulent exchange coefficient for momentum
L	Reference length
P	Pressure
Pr	Prandtl number
Q	Volumetric source term
q	Heat flux per unit area
$Q_{c,j}$	Concentration source for the j^{th} species
Q_s	Volumetric species source term
\dot{S}	Derivative of species or mass with respect to time
Sc	Schmidt number
T_{hot}	Reference temperature (hot or cold as indicated)
u_i	Velocity in i^{th} direction or i^{th} component
u'	Instantaneous value of fluctuation component of velocity in the x direction
u_*	Friction velocity
u_n	Initial guess or current time velocity
u^{n+1}	Velocity at next time step
u^n	Current or initial velocity
U_i	Velocity vector having components u, v, w
\hat{U}_i	Advection velocity
U_{f_i}	Diffusion velocity
v^*	Predicted velocity
v_{s_j}	Species settling velocity
x_i	i^{th} coordinate direction
$\overline{w'u'}$	Component of turbulent stress tensor

Greek Letter Symbols for Variables and Constants

κ	wave number
μ	Dynamic viscosity
ρ	Density
ρ_{fluid}	Fluid density

σ_{ij}	Stress tensor
ν	Kinematic viscosity
τ	Turbulent flux

Other Mathematical Notation

C^T	Vector transpose of gradient operators
K_{ij}	Dispersion tensor
$L()$	Linear operator L
\mathbf{n}	Vector normal to boundary surface
n_r	Normally distributed random number
Ω	Domain omega
$P_{x_i}(x_i, t)$	Probability distribution function for a three-dimensional space
σ	Standard deviation of a probability distribution
$\sigma(x(t))$	Standard deviation of a probability distribution
σ^2	Covariance of a probability distribution
Γ	Boundary of considered domain
W_i	Polynomial weighting function
$dW(t)$	Wiener process
$\{ \}$	Column vector
$[]$	Row vector or matrix
$\left\{ \begin{matrix} \bullet \\ \mathbf{v} \end{matrix} \right\}$	Time dependent vector of velocity variable
$[\mathbf{A}(\mathbf{u})]$	Advection Matrix
$[\mathbf{K}_v]$	Stiffness Matrix for velocity
$[\mathbf{K}_T]$	Stiffness Matrix for temperature
$[\mathbf{K}_C]$	Stiffness Matrix for concentration
$\{\mathbf{F}_v\}$	Load vector for velocity
$\{\mathbf{F}_T\}$	Load vector for temperature
$\{\mathbf{F}_C\}$	Load vector for concentration
$[\mathbf{M}]$	Mass matrix
N_k	Shape function

Mathematical Operators

$\bar{\mathbf{u}} \bullet \mathbf{n}$	Vector normal dot product
δ_{ij}	Kroneker delta
∇_x	Curl

$\nabla \bullet \vec{u}$	Vector dot product
Δ	First difference
$\frac{D}{Dt}$	Material derivative
$\frac{\partial}{\partial t}$	Time derivative
∇	Gradient operator

1 Introduction

Emission of pollutants and their accumulation due to poor ventilation and air exchange are serious problems that are currently under investigation by many researchers. Of particular concern are issues involving air quality within buildings. Toxic fumes and airborne diseases are known to produce undesirable odors, eye and nose irritations, sickness, and occasionally death. Other products such as tobacco smoke and carbon monoxide can also have serious health effects on people exposed to a poorly ventilated environment; studies indicate that indirect or passive smoking can also lead to lung cancer. Recommendations on outdoor airflow rates to dilute indoor polluted air vary considerably. Due to the demand for large air flow requirements, air quality is usually estimated during the design stage of a ventilation system.

1.1 General Ventilation Systems

Ventilation systems are designed to either prevent contaminants from entering a room or remove contaminants from interior sources within the room. Since ventilation systems are integral to the study of indoor air pollution, it is prudent to at least identify them. A ventilation system consists of several key components:

- (1) the contaminant source
- (2) an exhaust hood
- (3) an air mover
- (4) ducts and fittings
- (5) makeup air
- (6) exhaust air
- (7) a pollutant removal device
- (8) a discharge stack
- (9) air recirculation

Variations of these components are typically found in most ventilation systems designed to deal with indoor air quality and pollutant removal. Figure 1 shows a schematic of a general ventilation system.

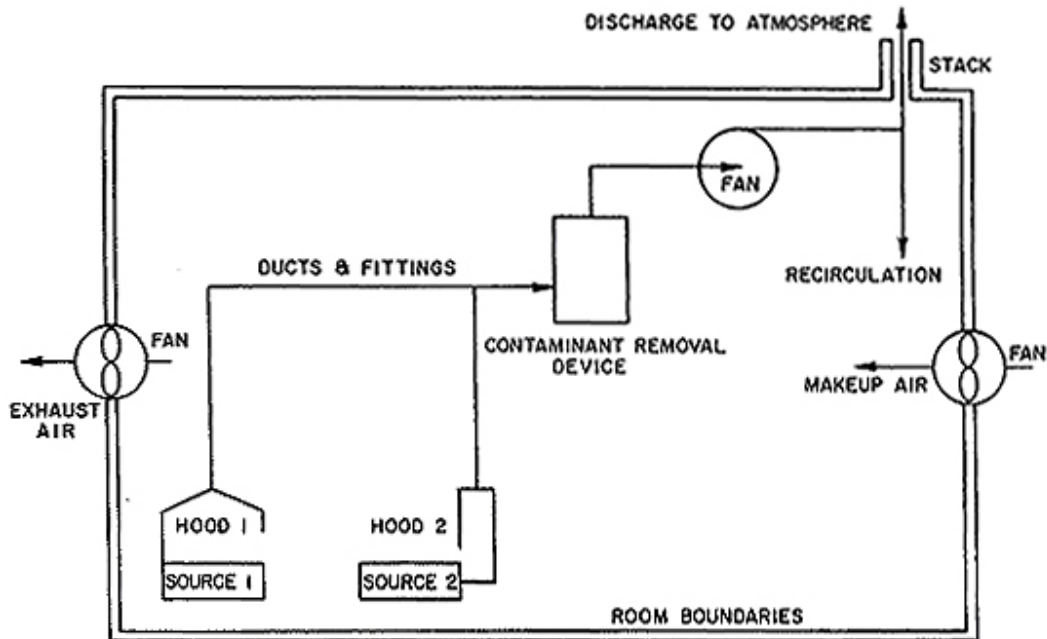


Figure 1. Schematic of a typical ventilation system (from *Industrial Ventilation*, R. J. Heinsohn, J. Wiley & Sons, New York, 1991, pg. 24).

- (1) the contaminant source typically consists of particulates, gases, and vapors generated by various activities
- (2) an exhaust hood is used to contain contaminants emitted from a source (e.g., hoods are used to cover grills in kitchens)
- (3) an air mover, or fan, is used to draw air into a hood
- (4) ducts and fittings make up the piping network connecting the hood to the fan
- (5) makeup air is air that is brought into the room from the outside – this air is usually temperature and humidity controlled
- (6) exhaust air is the air discharged from the room
- (7) a pollutant removal device is a specific piece of equipment used to remove excess contaminant from the room when environmental standards are exceeded
- (8) a discharge stack is a stack that exhausts air into the atmosphere
- (9) air recirculation is air that is returned into the room (clean air)

These components are fairly common in rooms containing ventilation systems, especially industrial settings that deal with dirty environments. More detail describing these components and their proper selection can be found in the ASHRAE Handbook (1981).

1.2 Exposure Risks

The assessment of risk, attributed to exposure to hazardous materials, is a formal field of study. A great deal of effort was spent in developing risk limits during the

early years of the nuclear industry (i.e., in the design and operation of nuclear reactors). A significant amount of mathematical development and theory exists on the subject (Brain and Beck, 1985).

Assessing risk requires information dealing with the types and amounts of material being used and the percent discharged to the environment. Before an accurate risk assessment can be made, it is essential that one have a good grasp of the materials and processes being undertaken. For example, there are over 56,000 manufactured or imported substances used in industrial operations (defined by the EPA in response to the Toxic Substances Control Act). The National Institute for Occupational Safety and Health (NIOSH) also lists a registry of toxic effects of chemical substances (RTECS). Likewise, the Occupational Safety and Health Administration (OSHA) maintains a list of toxic and hazardous materials. These registries are updated every few years and can be obtained from respective agency web sites.

Risk is generally depicted in terms of events per year (usually a small number) and uncertainty (%). Exposure limits are usually depicted in parts per million or billion (denoted as ppm or ppb, or mg/m^3). For example, the risk of getting cancer due to smoking cigarettes (1 pack/day) is 3.6×10^{-3} (annual risk) or a factor of 3 (order of magnitude) in percentage. The permissible exposure limit for acetone, for example, is 750 ppm; respirable dust from marble is $5 \text{ mg}/\text{m}^3$. Table 1 shows a list of some common materials and their permissible exposure limits.

Table 1. Permissible Exposure Limits of Several Materials and Activities.

<i>Material or Activity</i>	<i>Annual Event</i>	<i>%</i>	<i>ppm</i>	<i>mg/m³</i>
Smoking	3.6×10^{-3}	10^{-3}		
chloroform in drinking water	6×10^{-7}	10^{-7}		
Acetone			750	
Chlorine			0.5	
Fluorine			0.1	
Ozone			0.1	
mercury vapor				0.05
marble dust (respirable)				5
grain dust (oat, wheat, barley)				10
wood dust				5

While one can envision various techniques to establish risk, there is a simple technique to obtain a human exposure dose (Ames et al., 1987). This Human Exposure Dose index is related to the Rodent Potency Dose, or HERP, and relates the carcinogenicity of certain chemical agents to animal cancer tests. While one cannot use animal cancer tests to exactly predict human risk, the index does provide a good guide for establishing priorities and potential carcinogenic hazards. The HERP is defined as

$$\text{HERP} = \text{daily lifetime human dose (mg / kg)} \times \text{rodent TD}_{50} \text{ (mg / kg)}$$

where TD_{50} are values taken from a database for 975 chemicals (Ames et al., 1987). Table 2 lists several HERP values.

Table 2. Risk Based on HERP Index (from Ames et al., 1987).

<i>Daily Human Exposure</i>	<i>Dose ($\mu\text{g}/70\text{-kg person}$)</i>	<i>HERP (%)</i>
Chlorinated tap water	Chloroform	0.001
Swimming pool	Chloroform	0.008
Conventional home	Formaldehyde	0.6
Mobile home air	Formaldehyde	2.1
Beer (12 oz)	Ethyl alcohol	2.8
High exposure farm worker	Ethylene dibromide	140.0

1.3 Indoor Air Flow Modeling

In recent years there has been extensive activity in the development and use of Computational Fluid Dynamics (CFD) software and special programs for room air movement and contaminant transport applications. These investigations range from the prediction of air jet diffusion, air velocity and temperature distribution in rooms, spread of contamination in enclosures, to fire and smoke spread inside buildings. In most cases, the predicted results have been promising when compared to available experimental data. However, numerical modeling of ventilation problems is still at an early stage of development. A considerable amount of research and development work is still needed, particularly in the areas of computational schemes, irregular grids, turbulence modeling and wall functions, before CFD can replace physical modeling as a design tool.

One of the earliest attempts to numerically simulate airflow in rooms was conducted by Nielsen (1974) using the stream function-vorticity approach for the dependent variables, along with a two-equation ($k-\epsilon$) model for turbulence based on the numerical procedure developed by Gosman et al. (1969). The computations produced realistic room flows, but was limited to 2-D. Numerous papers have appeared over the years utilizing the stream function-vorticity approach for simulating 2-D flows within enclosures; however, the approach is *practically* limited to 2-D flows, and does not permit one to easily incorporate turbulence and 3-D effects inherent in actual ventilated enclosures. Efforts were later undertaken by Hjertager and Magnussen (1977), using the finite volume approach and the SIMPLE algorithm developed by Patankar and Spalding (1972), to solve the 3-D primitive equations of motion with the $k-\epsilon$ two-equation model for turbulence. They modeled the flow from an air jet exhausting into a rectangular room with two ceiling exits. While the point of jet separation from the ceiling was well predicted, the predicted velocity of the jet near the lower region of the room was higher than the measured value.

Gosman et al. (1980) extended their two-dimensional finite volume model to solve isothermal flows within 3-D enclosures with small ventilation openings.

They achieved good correlations of velocity profiles and jet velocity decay with measurements. Sakamoto and Matsuo (1980) similarly predicted 3-D isothermal flow in a room using the marker and cell (MAC) technique (Harlow and Welch, 1965) and two turbulence models: the k- ϵ approach and the large-eddy simulation (LES) technique (Deardorff, 1970). Results compared favorably with measured velocity profiles; they recommended that the k- ϵ approach for turbulence be used for room flow predictions over the LES model because it is simpler to use and requires less computing time for comparable accuracy. A computer program called CAFE, developed by Moulton and Dean (1980), was used to solve the 3-D velocity components, temperature, concentration, and k- ϵ turbulence parameters for flow in industrial enclosures and clean rooms. Results were in good agreement with measurements in regions where velocities were large.

Murakami et al. (1987) investigated the three-dimensional airflow and contamination dispersion in six (rectangular) types of ceiling supply clean rooms both numerically and experimentally for isothermal flow. They used the MAC method coupled with a central difference approach for the velocity components, and a second-order upwind scheme for k, ϵ , and concentration, to solve the transient transport equations. Results showed good agreement between prediction and measurement, as well as some interesting flow phenomena regarding the spread of a jet exhaust as it reached the floor. Awbi (1989) numerically solved 2-D air flow and temperature distributions within rooms with diffusers and various vent locations in an effort to simulate 3-D effects; the 2-D non-isothermal predictions compared well to the measured vertical velocity and temperature profiles in the room. A comprehensive historical discussion and descriptions of numerical methods for solving 2-D and 3-D ventilation and contaminant transport are given by Awbi (1991).

2 Fluid Flow Fundamentals

2.1 Governing Equations

The partial differential equations that describe the flow of fluid, heat, and concentration are all based on the conservation of mass, momentum, thermal energy, and species concentration. The dependent variables are the velocity components, temperature, concentration, and some turbulence variables to account for turbulent flow. These governing equations can be written as

Conservation of Mass

$$\frac{\partial \rho}{\partial t} + \frac{\partial \rho u}{\partial x} + \frac{\partial \rho v}{\partial y} + \frac{\partial \rho w}{\partial z} = 0 \quad (1)$$

Conservation of Momentum: x-direction

$$\rho\left(\frac{\partial u}{\partial t} + u\frac{\partial u}{\partial x} + v\frac{\partial u}{\partial y} + w\frac{\partial u}{\partial z}\right) = -\frac{\partial p}{\partial x} + \frac{\partial \sigma_{xx}}{\partial x} + \frac{\partial \sigma_{xy}}{\partial y} + \frac{\partial \sigma_{xz}}{\partial z} + f_x \quad (2)$$

Conservation of Momentum: y-direction

$$\rho\left(\frac{\partial v}{\partial t} + u\frac{\partial v}{\partial x} + v\frac{\partial v}{\partial y} + w\frac{\partial v}{\partial z}\right) = -\frac{\partial p}{\partial y} + \frac{\partial \sigma_{yx}}{\partial x} + \frac{\partial \sigma_{yy}}{\partial y} + \frac{\partial \sigma_{yz}}{\partial z} + f_y \quad (3)$$

Conservation of Momentum: z-direction

$$\rho\left(\frac{\partial w}{\partial t} + u\frac{\partial w}{\partial x} + v\frac{\partial w}{\partial y} + w\frac{\partial w}{\partial z}\right) = -\frac{\partial p}{\partial z} + \frac{\partial \sigma_{zx}}{\partial x} + \frac{\partial \sigma_{zy}}{\partial y} + \frac{\partial \sigma_{zz}}{\partial z} + f_z \quad (4)$$

Conservation of Energy

$$\rho c_p \left(\frac{\partial T}{\partial t} + u\frac{\partial T}{\partial x} + v\frac{\partial T}{\partial y} + w\frac{\partial T}{\partial z}\right) = \frac{\partial q_x}{\partial x} + \frac{\partial q_y}{\partial y} + \frac{\partial q_z}{\partial z} + Q \quad (5)$$

Species Concentration

$$\frac{\partial C}{\partial t} + u\frac{\partial C}{\partial x} + v\frac{\partial C}{\partial y} + w\frac{\partial C}{\partial z} = \frac{\partial}{\partial x}(D_{xx}\frac{\partial C}{\partial x}) + \frac{\partial}{\partial y}(D_{yy}\frac{\partial C}{\partial y}) + \frac{\partial}{\partial z}(D_{zz}\frac{\partial C}{\partial z}) + S \quad (6)$$

where ρ is density, u , v , and w are horizontal, lateral and vertical velocities, respectively, p is pressure, T is temperature, $f_{x,y,z}$ are velocity body force terms, Q and S are source/sink terms, and D_{xx} , D_{yy} , and D_{zz} are the species concentration diffusion coefficients. The normal and tangential viscous stress terms are defined as:

$$\begin{aligned} \sigma_{xx} &= \frac{2\mu}{3}\left(2\frac{\partial u}{\partial x} + \frac{\partial v}{\partial y} + \frac{\partial w}{\partial z}\right) & \sigma_{yy} &= \frac{2\mu}{3}\left(2\frac{\partial v}{\partial y} + \frac{\partial u}{\partial x} + \frac{\partial w}{\partial z}\right) \\ \sigma_{zz} &= \frac{2\mu}{3}\left(2\frac{\partial w}{\partial z} + \frac{\partial u}{\partial x} + \frac{\partial v}{\partial y}\right) & \sigma_{xy} = \sigma_{yx} &= \mu\left(\frac{\partial u}{\partial y} + \frac{\partial v}{\partial x}\right) \\ \sigma_{xz} = \sigma_{zx} &= \mu\left(\frac{\partial u}{\partial z} + \frac{\partial w}{\partial x}\right) & \sigma_{yz} = \sigma_{zy} &= \mu\left(\frac{\partial v}{\partial z} + \frac{\partial w}{\partial y}\right) \end{aligned} \quad (7)$$

with

$$q_x = \kappa\left(\frac{\partial T}{\partial x}\right) \quad q_y = \kappa\left(\frac{\partial T}{\partial y}\right) \quad q_z = \kappa\left(\frac{\partial T}{\partial z}\right) \quad (8)$$

where μ is dynamic viscosity and κ is thermal conductivity.

2.2 Ideal Fluids

As one can readily see from the complexity of the PDEs described in Equations (1)-(8) for general viscous fluid motion, obtaining solutions to these formidable equations are difficult, generally requiring a numerical approach (CFD). There are instances when one can make simple assumptions regarding overall fluid motion, and the solutions are fairly accurate. These assumptions are based on the premise of the flow being *ideal*, or that the flow is (1) incompressible, (2) inviscid, and (3) irrotational. If the flow under question can be considered ideal, analytical solutions may be used to obtain values for the components of flow, pressure, temperature, and even concentrations.

If the flow is incompressible, the density is constant. This helps in eliminating the effects of compressibility and density variation. An inviscid flow is one in which the viscosity is zero – hence there is no effects attributed to molecular or turbulent diffusion, i.e., no mixing. If these two criteria are valid, then the governing equations reduce to simpler, steady state conditions as shown below:

Conservation of Mass

$$\frac{\partial u}{\partial x} + \frac{\partial v}{\partial y} + \frac{\partial w}{\partial z} = 0 \quad (9)$$

Conservation of Momentum

x-direction

$$u \frac{\partial u}{\partial x} + v \frac{\partial u}{\partial y} + w \frac{\partial u}{\partial z} = -\frac{1}{\rho} \frac{\partial p}{\partial x} \quad (10)$$

y-direction

$$u \frac{\partial v}{\partial x} + v \frac{\partial v}{\partial y} + w \frac{\partial v}{\partial z} = -\frac{1}{\rho} \frac{\partial p}{\partial y} \quad (11)$$

z-direction

$$u \frac{\partial w}{\partial x} + v \frac{\partial w}{\partial y} + w \frac{\partial w}{\partial z} = -\frac{1}{\rho} \frac{\partial p}{\partial z} + g \quad (12)$$

Conservation of Energy

$$\rho c_p \left(u \frac{\partial T}{\partial x} + v \frac{\partial T}{\partial y} + w \frac{\partial T}{\partial z} \right) = \frac{\partial q_x}{\partial x} + \frac{\partial q_y}{\partial y} + \frac{\partial q_z}{\partial z} + Q \quad (13)$$

Species Concentration

$$u \frac{\partial C}{\partial x} + v \frac{\partial C}{\partial y} + w \frac{\partial C}{\partial z} = \frac{\partial}{\partial x} \left(D_{xx} \frac{\partial C}{\partial x} \right) + \frac{\partial}{\partial y} \left(D_{yy} \frac{\partial C}{\partial y} \right) + \frac{\partial}{\partial z} \left(D_{zz} \frac{\partial C}{\partial z} \right) + S \quad (14)$$

A further simplification can be made if the flow is irrotational. Irrotational flow is one in which there is no recirculation or rotation (i.e., the absence of vorticity). This implies a predominance of flow direction with no lateral components. Hence, the velocity components can be grouped into a single value, U , and the momentum equations reduce to Bernoulli's equation

$$\nabla \left(\frac{p}{\rho} + \frac{U^2}{2} + gz \right) = 0 \quad (15)$$

where ∇ is the gradient operator. The quantity $(p/\rho + U^2/2 + gz)$ is constant everywhere, and the flow is irrotational, steady, incompressible, and frictionless (i.e., the flow is *ideal*).

There are numerous solutions to cases involving ideal flow. By introducing the scalar potential functions,

$$u = -\frac{\partial \phi}{\partial x}; \quad v = -\frac{\partial \phi}{\partial y}; \quad w = -\frac{\partial \phi}{\partial z} \quad (16)$$

where ϕ is the scalar potential function. Substituting these expressions into the continuity equation, one obtains the Laplacian:

$$\frac{\partial^2 \phi}{\partial x^2} + \frac{\partial^2 \phi}{\partial y^2} + \frac{\partial^2 \phi}{\partial z^2} = 0 \quad (17)$$

Similarly, a scalar value for the stream function can be introduced for two dimensional flow where

$$u = -\frac{\partial \psi}{\partial y}; \quad v = \frac{\partial \psi}{\partial x} \quad (18)$$

and a Laplacian equation written as

$$\frac{\partial^2 \psi}{\partial x^2} + \frac{\partial^2 \psi}{\partial y^2} = 0 \tag{19}$$

Table 3 lists velocities and derivatives of the potential functions for two-dimensional planar and axisymmetric cylindrical and spherical coordinates.

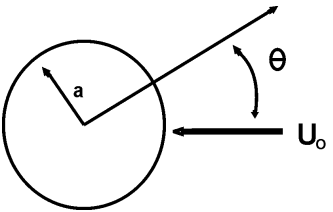
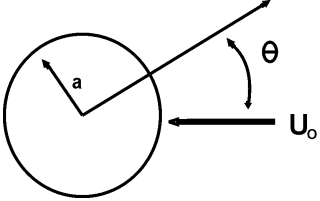
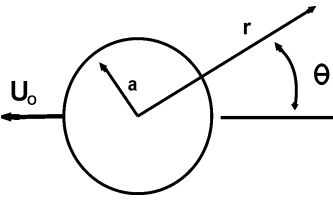
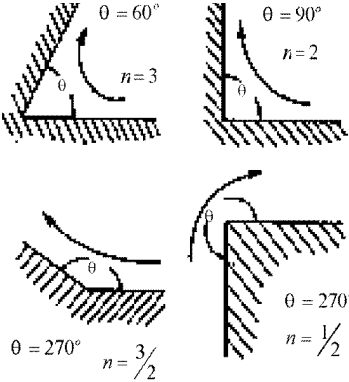
Table 3. Velocities as a Function of ϕ or ψ .

<i>Coordinate System</i>	<i>Velocities - ϕ</i>	<i>Velocities - ψ</i>
2-D Planar	$u = -\frac{\partial \phi}{\partial x}; \quad v = \frac{\partial \phi}{\partial y}$	$u = -\frac{\partial \psi}{\partial y}; \quad v = \frac{\partial \psi}{\partial x}$
2-D Axisymmetric	$u = -\frac{\partial \phi}{\partial r}; \quad v = -\frac{1}{r} \frac{\partial \phi}{\partial \theta}$	$u = -\frac{1}{r} \frac{\partial \psi}{\partial \theta}; \quad v = \frac{\partial \psi}{\partial r}$
3-D Spherical	$u = -\frac{\partial \phi}{\partial r}; \quad v = -\frac{1}{r} \frac{\partial \phi}{\partial \theta}$	$u = -\frac{1}{r^2 \sin \theta} \frac{\partial \psi}{\partial \theta};$ $v = \frac{1}{r \sin \theta} \frac{\partial \psi}{\partial r}$

Utilizing these two variables, potential flow solutions can be obtained for inlets and flanges.

Table 4. Potential Functions for Various Geometries (from *Industrial Ventilation*, R. J. Heinsohn, J. Wiley & Sons, New York, 1991, pg. 374).

Flow	Geometry	Potential relation
Flanged rectangular inlet		$\frac{x}{w} = \cosh\left(\frac{\phi}{k}\right) \cos\left(\frac{\psi}{k}\right)$ $\frac{y}{w} = \sinh\left(\frac{\phi}{k}\right) \sin\left(\frac{\psi}{k}\right); \quad k = q / L\pi$
Unflanged rectangular inlet		$\frac{x}{w} = \frac{1}{\pi} \left[\frac{2\phi}{k} + \exp\left(\frac{2\phi}{k}\right) \cos\left(\frac{2\psi}{k}\right) \right]$ $\frac{y}{w} = \frac{1}{\pi} \left[\frac{2\psi}{k} + \exp\left(\frac{2\phi}{k}\right) \sin\left(\frac{2\psi}{k}\right) \right]$ $k = Q / \pi$
Flanged circular inlet		$\phi = \frac{Q}{2\pi w} \sin^{-1} \left[\frac{2w}{a_1 + a_2} \right]$ $\psi = \frac{Q}{4\pi w} \left[4w^2 - (a_1 - a_2)^2 \right]^{1/2}$ $a_1 = \left[z^2 + (w + r)^2 \right]^{1/2};$ $a_2 = \left[z^2 + (w - r)^2 \right]^{1/2}$

Flow	Geometry	Potential relation
Flow around a stationary cylinder		$\phi = U_0 \cos \theta \left[r + \frac{a^2}{r} \right]$ $\psi = U_0 \sin \theta \left[r - \frac{a^2}{r} \right]$
Flow around a stationary sphere		$\phi = \frac{U_0 \cos \theta}{r^2} \left[r^3 + \frac{a^3}{2} \right]$ $\psi = \frac{U_0 \sin^2 \theta}{2r} \left[r^3 - a^3 \right]$
Flow around a sphere moving in a stationary fluid		$\phi = -\frac{U_0 a^3 \cos \theta}{2r^2}$ $\psi = \frac{U_0 a^3 \sin^2 \theta}{2r}$
Flow in corners		$\phi = -\left(\frac{a}{n}\right) U_w \left(\frac{r}{a}\right)^n \cos(n\theta);$ $U(a, 0) = U(a, \beta) = U_w$ $\psi = -\left(\frac{a}{n}\right) U_w \left(\frac{r}{a}\right)^n \sin(n\theta);$ $n = \pi / \theta$

Analytical solutions to Laplace's equation are harmonic functions (i.e., since the equation is linear and homogeneous, the combination of several solutions to subsets of the problem is also the solution to the overall problem). Hence, a flow field produced by two independent flow fields, each of which can be treated as ideal, can be combined (*superposition principle*) to yield the overall solution. For

example, if ϕ_1 and ϕ_2 are two independent solutions, then the horizontal velocity, u , can be obtained for the entire problem using the relation

$$u = -\frac{\partial\phi}{\partial x} = -\frac{\partial(\phi_1 + \phi_2)}{\partial x} = -\frac{\partial\phi_1}{\partial x} - \frac{\partial\phi_2}{\partial x} = u_1 + u_2 \quad (20)$$

Table 4 lists several potential functions and general cases of flow geometries where analytical solutions can be used to obtain overall values for ϕ and ψ . Several excellent texts that describe the use of potential functions for more complicated flow regimes include Pozrikidis (1999), Woo and Hwang (2000), and the ageless classic by Carslaw and Jaeger (1947).

2.3 Turbulence

A CFD code must be capable of modeling both laminar and turbulent fluid motion. Current approaches to modeling turbulence are based on either "first" or "second-order" closure models in which the governing equations are closed by equations for various turbulence correlation terms (kinetic energy, shear stress, etc.). Examples of such closure schemes are discussed in detail by Jones and Launder (1972). Results show that advanced turbulence closure schemes, incorporating more physics and less empiricism, provide the generality for modeling wider classes of problems and more accurately account for the irregular nature of turbulent flow.

An effective viscosity is usually employed to simplify the solution of the turbulent equations. This concept allows the turbulent stress terms to be conveniently combined with the molecular viscosity (laminar flow) into an overall viscosity term for numerical solution. The two most frequently used approaches to model the effective viscosity (and effective diffusion coefficients) are the Prandtl mixing length model and the k - ϵ two-equation model.

Although the mixing length hypothesis has been successfully applied to solving numerous turbulent flow problems, it has little application in complex flows due to the difficulty in specifying an appropriate length. The method is essentially unsuitable for situations in which recirculation occurs.

In an attempt to more accurately model turbulence within complex regions, especially when recirculation is present, a two-equation turbulence model was first proposed by Jones and Launder (1972). The most common two-equation model is one based on solution of the turbulent kinetic energy, k , and its dissipation rate, ϵ . This model is known as the k - ϵ scheme, and it is popular because of its applicability to a wide range of flow problems (as well as low computational demand over more complex models). The k - ϵ model has been applied to numerous flow problems with good predictive accuracy; also, it is the preferred choice for simulating flows where there is the potential for recirculation and/or swirl.

In the k- ε model, the equation for k (which is derived from the general Navier-Stokes equations) is written as:

$$\begin{aligned} \frac{\partial \rho k}{\partial t} + \frac{\partial \rho u k}{\partial x} + \frac{\partial \rho v k}{\partial y} + \frac{\partial \rho w k}{\partial z} = \\ \frac{\partial}{\partial x} \left(\Gamma_k \frac{\partial k}{\partial x} \right) + \frac{\partial}{\partial y} \left(\Gamma_k \frac{\partial k}{\partial y} \right) + \frac{\partial}{\partial z} \left(\Gamma_k \frac{\partial k}{\partial z} \right) + \mu_\tau \left(2 \left[\left(\frac{\partial u}{\partial x} \right)^2 + \left(\frac{\partial v}{\partial y} \right)^2 + \left(\frac{\partial w}{\partial z} \right)^2 \right] \right. \\ \left. + \left(\frac{\partial u}{\partial y} + \frac{\partial v}{\partial x} \right)^2 + \left(\frac{\partial u}{\partial z} + \frac{\partial w}{\partial x} \right)^2 + \left(\frac{\partial w}{\partial y} + \frac{\partial v}{\partial z} \right)^2 \right) - C_\mu \rho \frac{k^{1.5}}{L} + \beta g \frac{\mu_\tau \partial T}{\sigma_t \partial y} \end{aligned} \quad (21)$$

where $\mu_k = \mu_e / \mu_k$ with $\mu_k \sim 1$, μ_t is the turbulent Prandtl number (0.5 to 0.9) and C_μ is a constant ~ 0.09 . The last term represents the effect of buoyancy.

The transport equation for ε is as follows:

$$\begin{aligned} \frac{\partial \rho \varepsilon}{\partial t} + \frac{\partial \rho u \varepsilon}{\partial x} + \frac{\partial \rho v \varepsilon}{\partial y} + \frac{\partial \rho w \varepsilon}{\partial z} = \\ \frac{\partial}{\partial x} \left(\Gamma_\varepsilon \frac{\partial \varepsilon}{\partial x} \right) + \frac{\partial}{\partial y} \left(\Gamma_\varepsilon \frac{\partial \varepsilon}{\partial y} \right) + \frac{\partial}{\partial z} \left(\Gamma_\varepsilon \frac{\partial \varepsilon}{\partial z} \right) + C_1 \frac{\varepsilon}{k} \mu_\tau \left(2 \left[\left(\frac{\partial u}{\partial x} \right)^2 + \left(\frac{\partial v}{\partial y} \right)^2 \right. \right. \\ \left. \left. + \left(\frac{\partial w}{\partial z} \right)^2 \right] + \left(\frac{\partial u}{\partial y} + \frac{\partial v}{\partial x} \right)^2 + \left(\frac{\partial u}{\partial z} + \frac{\partial w}{\partial x} \right)^2 + \left(\frac{\partial w}{\partial y} + \frac{\partial v}{\partial z} \right)^2 \right) - C_2 \rho \frac{\varepsilon^2}{k} + C_3 \beta g \frac{\varepsilon}{k} \Gamma_t \frac{\partial T}{\partial z} \end{aligned} \quad (22)$$

Here, $\Gamma_t = \mu_e / \mu_\tau$ where μ_τ is a constant equal to 1.22, $C_1 = 1.44$, and $C_2 = 1.92$.

Likewise, the equation for concentration species can be written in similar fashion, i.e.,

$$\begin{aligned} \frac{\partial \rho C}{\partial t} + \frac{\partial \rho u C}{\partial x} + \frac{\partial \rho v C}{\partial y} + \frac{\partial \rho w C}{\partial z} = \frac{\partial}{\partial x} \left(D_{xx} \frac{\partial C}{\partial x} \right) + \frac{\partial}{\partial y} \left(D_{yy} \frac{\partial C}{\partial y} \right) + \frac{\partial}{\partial z} \left(D_{zz} \frac{\partial C}{\partial z} \right) \\ + \frac{\partial}{\partial x} (-\rho u'c') + \frac{\partial}{\partial y} (-\rho v'c') + \frac{\partial}{\partial z} (-\rho w'c') + S \end{aligned} \quad (23)$$

where c' is the deviation from the mean. The terms $-\rho u'c'$, $-\rho v'c'$, and $-\rho w'c'$ are the turbulent diffusion fluxes.

Attempts to simplify the Reynolds stress transport equations are usually made by approximating the advection and diffusion terms into algebraic expressions; such models are referred to as algebraic stress models (ASM). This technique reduces the computational time required to obtain a solution of the transport equations. However, these models have not found wide-scale application in fluid flow problems due to their complexity, and the fact that they still require a large

amount of computing time and do not always produce better predictions than the k - ϵ model.

In large eddy simulation (LES) models, large-scale turbulence fluctuations are solved directly by appropriate transport equations and only the small-scale fluctuations contribute to ϵ . The nonlinear interaction between large-scale and small-scale turbulence motion is approximated through a subgrid-scale turbulent viscosity model. Success of this type of turbulence modeling lies with the computational grid being fine enough to lie within the inertial subrange (Kolmogorov scale) where energy cascade takes place and the dissipation rate, ϵ , has a constant value. The LES method has the ability to freeze the flow at any moment in time; if mean flow quantities are required, the calculations must be conducted over a very long time scale. The application of LES has been relatively limited to isothermal flows in channels and over a cube. However, considerably more work is needed before the method can be applied to a wider range of flow problems.

The accuracy of the solution of the discretized turbulence equations depends on the accuracy of specifying the physical quantities at the boundaries of the flow domain, and on the methods of linking these relations to the bulk flow. Close to a solid boundary, the local Reynolds number is extremely small and turbulent fluctuations are damped out by the proximity of the surface - laminar shear becomes a locally dominant force as a result of the steep velocity gradient. Because of the damping effect of the wall, the transport equations for the turbulence quantities do not apply close to the wall. One way of dealing with this problem is to add extra source terms to the transport equations for k and ϵ , and use an extremely fine grid close to the surface so that the first few points are within the laminar sublayer. This technique is effective, but it requires a vast number of grid points (especially in three-dimensions).

An alternative, and more popular, approach is to use Couette flow analysis and apply algebraic relations (logarithmic laws or wall functions) close to the surface. This approach does not require an ultra-fine grid near the surface. At a point close to the wall, the momentum equation is reduced to a one-dimensional form with gradients in the direction normal to the surface.

Boundary conditions at vent inlets are usually set to fully developed profiles, unless specified directly by the user from experimental data. Likewise, at exits, the transverse velocity components are normally set to zero and the longitudinal exit velocity calculated from mass balance. Exit values for k and ϵ are usually not required because the Reynolds number at the exit is typically large; likewise, the gradients normal to the flow direction of the dependent variables may also be set to zero at the exit plane. A particularly nice feature when using finite element methods is the ability to set the traction terms (i.e., the RHS of the governing equations) equal to zero at the exit. This is the true mathematical formulation for proper specification of the outflow boundary conditions, and does not require a

priori judgment by the user (Gresho et al., 1984) when using finite volume or finite difference schemes.

2.4 Species Transport

It is well known that contamination produced in a ventilated room can quickly spread over the whole zone, especially in a mixing ventilation system with a large rate of entrainment and a circulatory motion created by jets. Normally, the transport equation for concentration is solved either in time-average form or time-dependent form after a converged solution has been achieved for the other transport equations (velocity, temperature, and k - ϵ turbulence parameters). When low concentration levels exist in a room environment (~ 100 ppm), the difference in density between the contaminant and air is usually ignored. This practice is fairly common in both research and industrial applications with regards to either gas or small particulate transport. Nielsen (1981) used this approach to model 2-D concentration distributions within enclosures to investigate the importance of room aspect ratios on concentration distribution; a decrease in height of the room air supply slot produced a decrease in concentration in the enclosure. *Higher room concentrations were found to exist when the contamination source was placed in a relatively stagnant region in the room.* Murakami et al. (1983) obtained similar conclusions from their three-dimensional simulations, and were later confirmed by Davidson (1989) using a 3-D, k - ϵ turbulence model.

The spread of smoke within an L-shaped (rectangular) shopping mall was investigated by Markatos and Cox (1986) using the PHOENICS finite volume code. Both steady-state and transient spread of smoke from a fire was modeled, and results compared with experimental measurements. Agreement between measurement and prediction was generally satisfactory with small differences in the velocity profiles near the top of the doorway openings and in the temperature profiles at the center of the doorways (where cold air entering from the lower region meets the hot smoke leaving the upper region).

Several commercially available CFD codes are being used for simulating room ventilation and contaminant dispersion. The code CFX, developed by AERE Harwell, is a variant of the SIMPLE technique (Patankar, 1980), and resembles the PHOENICS code. This code incorporates finite volumes and unstructured meshes to account for irregular surfaces, and was used to simulate the fire that occurred in Kings Cross Station in London several years ago. Likewise, the FLOVENT code, which is similar to the PHOENICS and CFX, allows one to perform 2-D and small-scale 3-D problems on high performance PCs. Unfortunately, the code does not allow one to handle irregular geometries - curved surfaces must be approximated by orthogonal grids (this effect leads to the stair-step appearance for irregular boundaries and can degrade the ability of a code to accurately resolve boundary layer effects and turbulence near surfaces).

3 Contaminant Sources

Contaminants in buildings generally consist of either particles or gases. Particles can either be in the form of solids or liquids. Gases are generally gaseous or exist as a vapor, both of which obey the perfect gas law. The Glossary of Fundamentals of Industrial Hygiene (1993) gives the following definitions for specific airborne contaminants:

Dusts: Solid particles typically created from crushing, handling, detonation, and impact of organic or inorganic materials; particles do not diffuse in air but settle under the influence of gravity.

Gas: Material state of matter with very low density and viscosity that responds to changes in temperature and pressure; gas diffuses and uniformly distributes itself throughout any enclosure.

Vapors: Gaseous form of substances normally in solid or liquid state at room temperature and pressure; vapors diffuse and mix with the environment – evaporation is the changing of a liquid into a vapor state.

Aerosols: Liquid droplets or solid particles that are dispersed in air with diameters generally in the range of 0.01 - 100 μm ; aerosols generally remain suspended in air for some time.

Fume: Particulate created from the evaporation of solid materials and dispersed into the air; fumes are usually less than 1 μm in diameter.

Mists: Suspended liquid droplets generated from condensation as a gas transforms to a liquid state or by a liquid dispersing into the air due to foaming, splashing, or atomizing; mist forms when a finely divided liquid becomes suspended in air.

Smoke: Particles (suspension of aerosols in air) created from combustion or sublimation, and consists of droplets as well as dry particles, (e.g., tobacco produces a wet smoke composed of tarry droplets); carbon or soot particles are generally less than 0.1 μ in size and result from incomplete combustion of carbon-based materials.

The mass of particles per unit volume of gas is known as the mass concentration (C), often referred to simply as concentration. A variety of units are used for concentration, but the most common is mg/m^3 .

The sources of building contamination and the multitude of contaminants are numerous. Many of the indoor pollution problems stem from construction activities of operations within a facility. Such contaminants include volatile organic compounds (VOCs), pesticides, biological contaminants promoted by moisture, asbestos, radon, lead, and PCBs.

3.1 Building Materials

A major portion of indoor air contaminants come from building materials and equipment. VOCs resulting from the manufacturing and installation processes typically migrate into the air. The majority of VOCs can be classified into the following categories (Hays et al., 1995).

Adhesives, sealants, and architectural coatings: these types of coatings are installed wet and dry or cure on the premises; the solvents used in the formulation of these materials directly relate to the VOCs emitted. The resins used in the base of adhesives are either natural or synthetic, and range from low to high emission rates; sealants consist of putties, caulking compounds, rubber, acrylic latexes, and silicones while architectural coatings include paints, stains, sealers, and varnishes.

Particleboard and plywood: particleboard is a composite produce made from wood chips or residues that are bonded together with adhesives and typically come from milling or woodworking waste. Plywood consists of several thin layers or plies of wood that are bonded by adhesive and are generally classified as either softwood or hardwood; the indoor air quality (IAQ) effects of softwood and hardwood vary with the adhesive (phenol-formaldehyde, PF, and urea-formaldehyde, UF, resins).

Carpet, resilient flooring, and wall covering: these types of materials bring VOC-emitting composition into the building interior along with the use of adhesives to attach the material to various surfaces. Carpets typically consist of fibers of either wool or synthetics. Resilient flooring is generally either tile or sheet (vinyl or rubber). Wall coverings are made from paper, fabric, and vinyl.

Table 5. Partial List of Building Materials and their Emissions (from Hays et al., 1995).

Material	Chemical emitted	Emission rate
Adhesives	Alcohols	
	Amines	
	Benzene	
	Toluene	
Sealants	Alcohols	
	Amines	
	Benzene	
	Xylenes	
Architectural coatings	paints – C4-benzene	
	paints - Toluene	
	stains/varnishes – Amines	
	stains/varnishes - Benzene	
Particleboard	Amines	
	Formaldehyde	0.2-2 mg/m ³ /h
	n-Hexane	15-26 µg/m ³ /h
Carpeting	4-Phenylcyclohexene	0.1 mg/m ³ /h(latex backed)
	Styrene	
Resilient Flooring	Amines	

	Alkanes	
	Linoleum - Trichloroethylene	3.6 $\mu\text{g}/\text{m}^2/\text{h}$
Wall Coverings	Amines	
	Xylenes	
Insulation	foam - Acetone	ND-0.02 $\text{mg}/\text{m}^2/\text{h}$
	Chloroform	ND-0.002 $\text{mg}/\text{m}^2/\text{h}$
Furnishings	Upholstery – Formaldehyde	

Insulation, acoustical ceiling tile, and furnishings: these types of materials include a variety of paints, adhesives, backing, fabrics, and fibrous materials all of which combine to contribute to VOCs. Insulation is commonly thermal oriented, but acoustical and fireproofing also are used; these usually exist in the form of batt and rigid foam consisting of fiberglass or mineral wool. Furnishings include such items as prefabricated movable partitions, workstations, desks, chairs, couches, photocopiers, computers, etc.

Table 5 is a partial list of materials and some of the chemicals emitted from their surfaces, along with emission rates when known. When building materials have a high-surface-area-to-room-volume ratio, it is important to quantify the emissions and their rates to avoid harmful effects to occupants.

3.2 Typical Operations

The most common carriers of pollutants are ventilation systems and the human body (general work activity and socialization). The ventilation system serves as an ideal transport mechanism for dispersing particulates and gaseous compounds throughout a building. Similarly, the human body acts as a repository from transporting all forms of pollutants within a room as well as to other humans.

Operations commonly found in many industrial and office environments include processes such as maintenance and housekeeping, which permit dust or particulate buildup that leads to indoor air contamination. Likewise, office equipment, including such devices as wet and dry copying machines, computers, laser printers, and color inkjet printers emit VOCs during operation. Pest control, construction activities in occupied buildings, moisture leaks, and many industrial activities including chemical spills, grinding, pouring, and sprays lead to indoor contamination. Operations involving food preparation and consumption are particularly sensitive to emissions and unsanitary conditions that lead to indoor air quality problems. Even the natural process of evaporation and diffusion of volatile liquids stored in rooms are common contributors to overall air quality.

3.3 Diffusion in Air

Contamination enters the air by either puff or continuous source emission. A puff is an instantaneous release, or burst, of material of short duration. A continuous emission occurs when a source of pollutant is emitted over a long time, leading to a discernable plume emanating from the source location. The transport physics

attributed to both occurrences obey the conservation of mass, as previously described by Equation (23). Much has been written on the atmospheric dispersion of puffs and plumes of contaminants (Pasquill and Smith, 1985), especially if one can reduce the PDE form of Equation (23) to a more manageable form that can be solved analytically. These analytical solutions are based on the use of Gaussian assumptions (i.e., statistical representations of the probability of concentration being found at specific locations). However, use of such reduced equation sets requires information from the user that may be unknown. This is discussed in more detail in the chapter on Gaussian and analytical solutions. For convenience, we restate the relations here:

Puff:

$$C(x, y, z) = \left(\frac{Q}{(2\pi)^{3/2} \sigma_x(t) \sigma_y(t) \sigma_z(t)} \right) \exp - \left[\frac{(x - Ut)^2}{2\sigma_x^2} + \frac{y^2}{2\sigma_y^2} + \frac{z^2}{2\sigma_z^2} \right] \quad (24)$$

Plume:

$$C(x, y, z) = \left(\frac{Q}{2\pi\sigma_y\sigma_z U} \right) \exp \left(\frac{-y^2}{2\sigma_y^2} \right) \left[\exp \left(\frac{-(z-H)^2}{2\sigma_z^2} \right) + \exp \left(\frac{-(z+H)^2}{2\sigma_z^2} \right) \right] \quad (25)$$

where Q is the source term, U is the principal velocity (or speed) of the air, x, y, z are spatial distances (from either the puff center or the plume source), H is the height of the release, and σ_x , σ_y , and σ_z are the standard deviations, or diffusion coefficients (which are found using empirical relations developed by Pasquill and Gifford – the Pasquill-Gifford curves - see Pasquill and Smith, 1985). Solutions for C from Equations (24)-(25) produce Gaussian probability values which yield circular distributions that can be plotted for specific deviations from the center of the puff or plume – these are usually calculated out to $\pm 3\sigma$ standard deviations.

The diffusion coefficient of particles of diameter D_p can be estimated from the relation (Fuchs, 1964)

$$D = \frac{\kappa TC}{3\pi\mu D_p} \quad (26)$$

$$\sigma = \sqrt{2Dt}$$

where κ is the Boltzmann constant, μ is the molecular viscosity of the carrier gas, C is a constant, D_p is the droplet diameter, t is time, and σ is the standard deviation, or diffusion coefficient. Table 6 shows particle size versus diffusion coefficient in air at STP.

Table 6. Particle Diffusion Coefficients in Air (STP) (from *Industrial Ventilation*, R. J. Heinsohn, J. Wiley & Sons, New York, 1991, pg. 180).

D_p (μm)	D (cm^2/s)
0.01	1.35×10^{-4}
0.05	6.82×10^{-6}
0.10	2.21×10^{-6}
0.50	2.74×10^{-7}
1.00	1.27×10^{-7}
5.00	2.38×10^{-8}
10.00	1.38×10^{-8}

There are numerous book sources that give the molecular diffusion coefficients for a variety of gases. One of the most commonly used source is the CRC Handbook of Physics and Chemistry, which can be found in nearly every library. An equation developed by Chen and Othmer (Vargaftik, 1975) can also be used to obtain the binary gas diffusion coefficient (D_{12} in cm^2/s)

$$D_{12} = \left(\frac{0.43}{K} \right) \left(\frac{T}{100} \right)^{1.81} \sqrt{ \left(\frac{1}{M_1} \right) + \left(\frac{1}{M_2} \right) } \quad (27)$$

$$K = EP \left(\frac{T_{c1} T_{c2}}{10000} \right)^{0.1405}, \quad E = \left[\left(\frac{v_{c1}}{100} \right)^{0.4} + \left(\frac{v_{c2}}{100} \right)^{0.4} \right]^2$$

where v_c and T are the critical volume ($\text{cm}^3/\text{g-mol}$) and temperature ($^{\circ}\text{K}$), M_1 and M_2 are the molecular weights, and pressure P is in atmospheres. To obtain the diffusion coefficient at temperatures and pressures other than STP,

$$D(P, T) = D(\text{STP}) \left(\frac{1}{P} \right) \left(\frac{T}{298} \right)^{1.81} \quad (28)$$

Table 7 lists some common diffusion coefficients in air for several chemical compounds.

Table 7. Diffusion Coefficients for Several Contaminants in Air (from *Industrial Ventilation*, R. J. Heinsohn, J. Wiley & Sons, New York, 1991, pg. 658).

Substance	M	D ($10^{-5} \text{ m}^2/\text{s}$)
Acetone	56	0.83
Ammonia	17	2.2
Benzene	78	0.77
Chloroform	119	0.87
Hexane	86	0.8
Methane	16	2.2
Sulfur dioxide	64	1.3
Toluene	92	0.71

3.4 Evaporation of Droplets

Drops of liquids are formed from a myriad of industrial and everyday operations. Droplets are basically formed as a result of spraying, aerating, or atomizing. In addition, gas rising through a liquid may ultimately collapse at the liquid's surface and produce liquid droplets. Every drop has a liquid-air interface; it is this interface through which the liquid of the drop, or the liquid contaminant within the drop, evaporates. The physics associated with droplet formation and evaporation are well known, and can be found in detail in various textbooks dealing with cloud physics – a well known reference is the work by Pruppacher and Klett (1978).

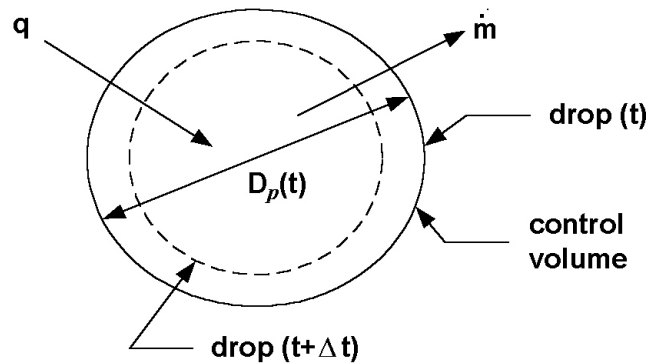


Figure 2. Schematic of an evaporating drop.

The physical processes associated with droplet evaporation can best be illustrated using Figure 2. Vapor escapes from the surface of the drop due to the vapor pressure of the saturated liquid being greater than the partial pressure of the vapor in the far field. The drop diameter, D_p , decreases as the liquid evaporates which in turn affects the rate of evaporation. The evaporating liquid removes energy from the drop and lowers the drop temperature below the ambient air temperature; this process lowers the drop pressure at the drop-air interface. Since evaporation lowers the drop temperature below the air temperature, energy is transferred to the drop by convection from the surrounding air. The mass and heat transfer are strongly coupled and thus control the rate of drop evaporation.

The set of differential equations that describe the evaporation rate, temperature, and diameter of a drop are fairly well established. These three simultaneous differential equations are typically written in the form

$$\begin{aligned} \dot{m} &= C_1 \pi M D_p \left(\frac{D_{ac}}{R_u} \right) Sc^{b_1} Re^{a_1} \left[\left(\frac{P_{r,i}}{T_p} \right) - \left(\frac{P_{v,o}}{T_o} \right) \right] \\ \dot{m} &= - \frac{\rho \pi D^2}{2} \frac{dD_p}{dt} \\ \frac{d(T_o - T_p)}{dt} &= - \left(\frac{6h_L}{\rho D_p c_v} \right) (T_o - T_p) + \frac{6mh_{fg}}{\rho \pi D_p^3 c_v} \end{aligned} \quad (29)$$

where Sc is the Schmidt number, Re is the Reynolds number, R_u is the universal gas constant, h_L is the average heat transfer coefficient, c_v is the specific heat at constant volume, and h_{fg} is the enthalpy of vaporization. The equation set in Equation (29) is best solved numerically. If the drop temperature at the liquid-air interface is known, the diameter of the drop can be calculated as a function of time by equating the first two relations. To compute the drop temperature, a simple energy balance as shown in Figure 2 gives the expression for q ,

$$q = \frac{mc_v dT_p}{dt} + u_f \frac{dm}{dt} + \dot{m} h_g(T) \quad \text{where} \quad m = \frac{\rho \pi D_p^3}{6} \quad (30)$$

where u_f is the internal energy of the saturated liquid and h_g is the enthalpy of the saturated vapor. For droplets with diameters less than 100 μm , the heat transfer within the drop is so rapid that the temperature within the drop can be considered to be uniform. For drops larger than 100 μm , the equation set (29) must be solved. The evaporation rate can be calculated from the first relation in Equation (29). Table 8 lists several drop sizes, mass, the mass flow rate (or evaporation rate), and temperature difference between ambient and drop temperatures.

Table 8. Particle diameter, mass, m, and temperature difference (from *Industrial Ventilation*, R. J. Heinsohn, J. Wiley & Sons, New York, 1991, pg. 216).

D_p (μm)	m (kg)	m (kg/s)	$T_o - T_p$ ($^{\circ}\text{C}$)
5	6.54×10^{-14}	1.08×10^{-10}	0.45
10	5.23×10^{-13}	2.16×10^{-10}	0.63
50	6.54×10^{-11}	1.18×10^{-9}	6.58
100	5.23×10^{-10}	2.74×10^{-9}	14.48

For particle sizes less than 10 μm , the particle temperature is essentially the same as the ambient temperature.

3.5 Resuspension of Particulate

Resuspension refers to the entrainment of a particulate into the air stream. The amount that is entrained into the air stream can be estimated using resuspension factors, resuspension rates, and fractional releases. Fractional releases provide an initial amount of contaminant injected into the fluid media.

Resuspension factors are defined as

$$\chi = \frac{C(\text{m}^3)}{C(\text{m}^2)} \quad (31)$$

where the quotient χ is airborne concentration per cubic meter of air divided by the surface concentration per square meter. Resuspension factors are not very useful for estimating quantities of particulate being entrained over time (changing or depleting surface concentration). However, they supply an effective method to evaluate the amount injected into the airflow by an activity at any one time, provided the surface concentration is known. Resuspension rates or mass fractions rates are defined as the fraction of contaminant released over time.

For low flow rates, resuspension coefficients must be specified. Approximations of resuspension rates or factors (mass flux into the domain) are based on the activity occurring and are listed below in this section. For disturbances from turbulent mixing, analytical calculation as developed by Martin et al. (1983) may be sufficient. An injection rate based on empirical evidence is desired.

Particulate entrainment is accomplished when attached particles move. A stream velocity large enough to accomplish this is defined as the threshold speed or threshold friction velocity $u_{*threshold}$. Once particles move, the adhesive forces are much weaker, and the particles are available for entrainment. The forces responsible for breaking the attachment are a function of shear stresses acting on the particle, particulate impingement from already suspended material, and adhesive forces between the surface and the particulate. Martin et al. (1983)

determined resuspension analytically, giving the resuspension rate as a function of friction velocity,

$$u_* = \sqrt{\frac{\tau_{wall}}{\rho_{fluid}}} \quad (32)$$

where τ_{wall} is the shear stress at the wall.

Threshold friction speed is determined from a semi-empirical relation as

$$A = (0.108 + 0.0323/B - 0.00173/B^2)(1 + 0.055/\rho_{fluid} g d_{part}^2)^{1/2} \quad (33)$$

where $A = u_{*threshold} / [(\rho_{part} - \rho_{fluid}) g d_p / \rho_{part}]^{1/2}$ and $B = u_{*threshold} d_{part} \rho_{fluid} / \mu_{fluid}$.

The equation is used for the range $0.22 \leq B \leq 10$.

For $B \leq 0.22$:

$$A = 0.266(1 + 0.055/\rho_{fluid} g d_{part}^2)^{1/2} (1 + 2.123/B)^{-1/2} \quad (34)$$

is used. Since $u_{*threshold}$ appears in both terms of the equality, iteration is required to obtain a solution.

Suspension occurs for particles having physical diameters smaller than $52 \mu\text{m}$ when the threshold velocity is reached. Particle suspension is assumed to occur when the terminal settling velocity, v_s , is equal to the friction velocity and the friction velocity is greater than the threshold velocity.

The amount of material suspended is given by

$$q_s = q_{horizontal} (c_{vert} / u_*^3 c_{hort}) \left[\left(\frac{u_*}{u_{*threshold}} \right)^{\text{Mass\%Suspended}/3} - 1 \right] \quad (35)$$

where: $q_{horizontal} = 2.61 \frac{\rho_{fluid}}{g} (u_* + u_{*threshold})^2 (u_* - u_{*threshold})$

and $c_{vert} = 2 \times 10^{-10}$ and $c_{hort} = 1 \times 10^{-6}$.

There are limitations on the use of this equation since the empirical constants were found by using light soil particles lying on flat thick beds without obstructions to disturb air flow. However, the equation form is proper, only needing experimental results for determining constants.

Threshold velocities for dense substances such as lead are calculated by Martin et al. (1983) to have a minimum value at about 0.3 m/sec for a 49 μm diameter particle. Smaller particles have much greater threshold friction velocities. Determination of the friction velocities on the walls in the laminar sublayer will allow for the incorporation of this resuspension equation provided the species is lying on a thick bed. Application of the above equation to other circumstances will require empirical data.

3.6 Coagulation of Particulate

Another source (and sink for particles) is by coagulation of smaller particles into larger particles as they collide. The time rate of change of concentration from agglomeration for particles with different sizes is given by (Reist, 1993)

$$\frac{dC}{dt} = \frac{-K_o}{2} C^2 \quad (36)$$

where $K_o = K_{12} = 2\pi (d_{part_1} + d_{part_2})(D_1 + D_2)$.

Over a relative short period of time, small particles will coagulate by diffusion into larger particles. For a monodispersed particulate ($D_1 = D_2$) of initial concentration of 1000 / cm^3 , the time for half the particles to coagulate is 55 hours. The time for the particle size to double for this case is 16 days. For an initial concentration of 100,000 / cm^3 , the coagulation half-life is 33 minutes and the size doubling time is 4 hours (Hinds, 1982). The time dependent relationship does not include source and sink terms that would also be affecting equations of concentration.

A deposition velocity by diffusion for particles with a micron aerodynamic diameter is insufficient to remove many of the small particles. However, time for coagulation is of the order of the air exchange rate. Therefore, any small particles would have a propensity to agglomerate to a size large enough for settling velocities to possibly be an effective scavenger. Typically, there will be some concentration of particles in the ambient air referred to as Total Suspended Particulate or TSP.

4 Design Criteria

Design for prevention or remediation of indoor air pollution requires expertise in optimizing geometrical configurations, knowledge of HVAC systems, perceived or expected contaminants and source locations, and economics. Much of the design concept involves ways in which to optimize benefits or balance the advantages and disadvantages of various configurations and equipment. The fact that a room or building will conceivably become contaminated is generally an

accepted fact – to what extent indoor air pollution will become critical is not really known until it happens. Most companies have a somewhat formal design process when developing preliminary designs and concepts – much of this relies on company administrative policies and the experience of the designer. In addition, consultants with specific areas of expertise can play a major role in orchestrating the overall design and configuration of equipment, materials, and potential exposures. In general, the designer must take into account the activities and processes being undertaken in the room or building, the movement of people, and the anticipated costs associated with using the best versus barely acceptable.

4.1 Exposure Levels

There are numerous agencies and organizations that have attempted to establish exposure limits to various chemicals and materials. These standards are typically referred to as threshold limit values (TLV), permissible exposure limits (PEL), and maximum acceptable concentrations (MAC). The American Conference of Governmental and Industrial Hygienists use TLV; the Occupational Safety and Health Administration (OSHA) publishes PEL values; the American National Standards Institute use MAC. While all three are generally compatible, PEL values are backed by law – it is usually prudent for the engineer or scientist to always check with OSHA for the PEL values. Table 9 shows a partial list of substances and the OSHA established PEL.

Table 9. Partial List of OSHA Permissible Exposure Limits.

Substance	PEL* (ppm)
Acetic acid	10
Benzene	10
Chloroform	2
Formaldehyde	3
Ozone	0.1
Turpentine	100

*TWA values

There are several limits that are commonly used in evaluating exposure. The first of these is the time-weighted average of concentration. This is the amount of concentration that workers are exposed to during a normal, 8-hr day, 5 days per week without causing adverse effects.

$$\begin{aligned} \text{TWA}(8\text{ - hr}) &= \left(\frac{1}{8}\right) \int_0^8 c(t) dt \\ \text{TWA}(40\text{ - hr}) &= \left(\frac{1}{40}\right) \int_0^{40} c(t) dt \end{aligned} \quad (37)$$

Short-term exposure limit is the maximum concentration to which workers can be exposed continuously up to 15 minutes without suffering from side effects.

$$\text{STEL} = \left(\frac{1}{15} \right) \int_0^{15} c(t) dt \quad (38)$$

Exposure hazards for a mixture of gaseous contaminants are defined by OSHA using an exposure parameter

$$\text{En} = \sum_i \left(\frac{c}{L} \right)_i \quad (39)$$

where c_i is the measured concentration and L_i is the PEL in comparable units of concentration. If $\text{En} > 1$, exposure is considered to be beyond acceptable limits.

An interesting contaminant that gets greatly overlooked is noise. Longitudinal pressure waves ranging from 20 – 20,000 Hz are known as sound waves. Hearing can be impaired when individuals are exposed to sound or noise above certain amplitudes and lengths of time. Sound power (W) is related to sound intensity by the relation

$$W = (4\pi r^2) \left(\frac{P^2}{\rho a} \right) \quad (40)$$

where a is the speed of sound, ρ is density, r is distance from the source, and P is pressure. Sound intensity (I) is usually used for the expression ($P^2/\rho a$). A sound-intensity level (L_I) can be defined as

$$L_I = 10 \log_{10} \left(\frac{I}{I_o} \right) \quad (41)$$

where $I_o = 10^{-12} \text{ W/m}^2$ and corresponds to the intensity at reference pressure ($P_o = 2 \times 10^{-5} \text{ N/m}^2$). Sound pressure (L_p) can be calculated at locations from a piece of equipment or process generating noise using the simple formula

$$L_p = L_w - 20 \log_{10} r(m) + 10 \log_{10} Q - 11 \quad (42)$$

where L_w is the sound power and Q is the directivity factor defined as the ratio of the sound power of a small omnidirectional hypothetical source to the sound power of an actual source at the same sound pressure level. The decibel (dB) is the unit used to express sound pressure level, sound intensity level, and sound power.

4.2 Economics

Economics is certainly a factor that must be considered when dealing with issues involving design and remediation of indoor air pollution. The two major costs are Total Capital Cost (TCC) and Total Revenue Requirements (TRR). TCC is essentially the initial costs consisting of money spent to design, build, and install various systems and equipment. TRR are monies spent that must be factored in to the TCC and the revenue needed to provide annual operating costs. Total Indirect Costs (TIC) are monies needed to pay for overhead, i.e., construction expenses, contractors fees, loan interest, building rental, etc. Total Direct Costs (TDC) consists of TCC plus TIC. The TIC is usually a fraction of the TDC. The equation is simply

$$TCC = TDC + TIC = TDC(1 + ICF) \quad (43)$$

where ICF is the Indirect Cost Factor. The TRR is composed of total variable costs (TVC) plus total fixed costs (TFC), or

$$TRR = TVC + TFC \quad (44)$$

Capital recovery cost (CRC) and the fixed cost factor (FCF) are calculated as follows:

$$CRC = TCC \times FCF$$

$$FCF = \frac{[i(1+i)^t]}{[(1+i)^t - 1]} \quad (45)$$

where i is the annual interest rate and t is the capital recovery period (years). Table 10 outlines the various costs and economic factors that should be considered.

Table 10. Cost factors for designing and building ventilation systems (from *Industrial Ventilation*, R. J. Heinsohn, J. Wiley & Sons, New York, 1991, pg. 154).

TCC	
TDC	TIC in % of TDC
Equipment	Construction expense (10-15%)
Labor	Contingencies (5-30%)
Materials	Contractors fees (4-6%)
Structures	Engineering (4-6%)
Consulting fees	Interest during construction (10-25%)
	Start-up costs (10-15%)
	Working capital (2-4%)
	Total ICF (45-100%)
TRR	
TVC	TFC in % of TCC
Administration	Capital recovery cost (11-23%)
Electric, gas, water	Taxes (3-7%)
Maintenance labor	Insurance (1-3%)
Maintenance material	Interim replacement (1-7%)
Operating labor	Tax credits (0-5%)
Supervision	
Raw materials	Total FCF (16-40%)

5 Simple Modeling Techniques

There are generally two concepts used when developing simple models for indoor air quality calculations: (1) well-mixed and (2) partially-mixed ventilation models. In a well-mixed model, the concentration is spatially uniform within the enclosure; in a partially-mixed model, the concentration is nonuniform generally due to poor mixing. In some situations, it is convenient and relatively safe to assume well-mixed conditions – this type of assumption leads to the use of simple analytical models. Unfortunately, most real world situations involve dealing with partially-mixed hypothesis. Analytical procedures are available for these situations as well, but they are somewhat limited; a mixing factor (m) is generally employed to modify the equations for a well-mixed model to account for the nonuniform distribution of concentration. It is usually preferable for these types of problems to employ CFD techniques and numerical models for dispersive transport.

5.1 Analytical Tools

Assume an enclosed space exists in which the concentration is considered to be spatially uniform. The mass concentration at $t = 0$ is c_0 . A source begins to generate contaminants at a constant rate (S). Outside air with contaminant c_a is

added to the enclosure at a constant volumetric flow rate Q – contaminated air is removed from the space at the same rate. Applying the equation for conservation of mass, the governing equations for the contaminant concentration entering and leaving the enclosure can be written as

$$V \frac{dc}{dt} = Qc_a - Qc + S \quad (46)$$

where V is the volume of the enclosure. Since the flow of air into and out of the enclosure is balanced, one only needs the expression for c . Integrating over time,

$$\int_{c_0}^{c(t)} \frac{dc}{[(Qc_a + S) - Qc]} = \frac{1}{V} \int_0^t dt \quad (47)$$

Solution of Equation (46) is

$$\frac{(c_{ss} - c(t))}{(c_{ss} - c_0)} = \exp\left(-\frac{Qt}{V}\right) \quad (48)$$

where c_{ss} is the steady state concentration (where $c_{ss} = c_a + S/Q$) obtained by setting the LHS of Equation (46) equal to zero. Assuming both initial and ambient concentrations are zero, one obtains the reduced form of Equation (48)

$$\frac{c(t)}{c_{ss}} = 1 - \exp(-Nt) \quad (49)$$

where $N = Q/V$ and is known as the number of room air changes per minute. To illustrate, if the ventilation rate is 10 room changes per hour, Equation (49) predicts that the concentration will be 64% of its steady state value in 6 minutes.

For a time-varying source or ventilation flow rate, Equation (46) can be rewritten as

$$\frac{dc}{dt} = -\frac{Qc}{V} + \frac{(S + Qc_a)}{V} \quad (50)$$

Equation (50) must be solved iteratively. Using a simple Runge-Kutta method, Equation (50) can be solved using the expression

$$c^{n+1} = \frac{\left(1 + \frac{A\Delta t}{2}\right)c^n + B\Delta t}{1 - \frac{A\Delta t}{2}} \quad (51)$$

where i is the iteration, $A = -Q/V$, $B = (S + Qc_a)/V$, and Δt is the time step. The solution begins with $t = 0$ and $i = 0$ where c_o is the initial concentration.

To account for wall losses (i.e., removal of contaminant by solid surfaces), Equation (46) can be modified to include the adsorption rate (k_{ad}) of contaminant on walls

$$V \frac{dc}{dt} = Qc_a + S - c(Q + A_s k_{ad}) \quad (52)$$

Equation (52) can be integrated to give

$$\frac{(c_{ss} - c(t))}{(c_{ss} - c_o)} = \exp\left(-\frac{(Q + A_s k_{ad})t}{V}\right) \quad (53)$$

assuming constant values for Q , S , and k_{ad} . For the case when $Q = S = 0$ (starting with a room contaminated), Equation (53) can be modified to

$$\frac{c(t)}{c_{max}} = \exp\left(-\frac{A t k_{ad}}{V}\right) \quad (54)$$

where c_{max} represents the maximum concentration at the beginning of the integration. Figure 3 shows the importance of adsorption of tobacco smoke (see Repace and Lowery, 1980; Heinsohn, 1991) and the effects of mixing in a room. In this instance, a single cigarette was burned and then extinguished in a 22 m³ room and the total mass of suspended particle matter measured during the entire period. Well-mixed conditions were produced by fans; the natural mixing occurred as a result of natural air currents. Notice that the concentration in the well-mixed experiment fell rapidly, as expected. The slope of the curve allows one to estimate the removal of contaminants by adsorption on solid surfaces. The rate of adsorption was found to be equivalent to an exhaust ventilation rate of 1.4 m³/min (50 CFM). It should also be pointed out that contaminants can also *desorb* from surfaces. In this case, desorption acts as a source term in Equation (48).

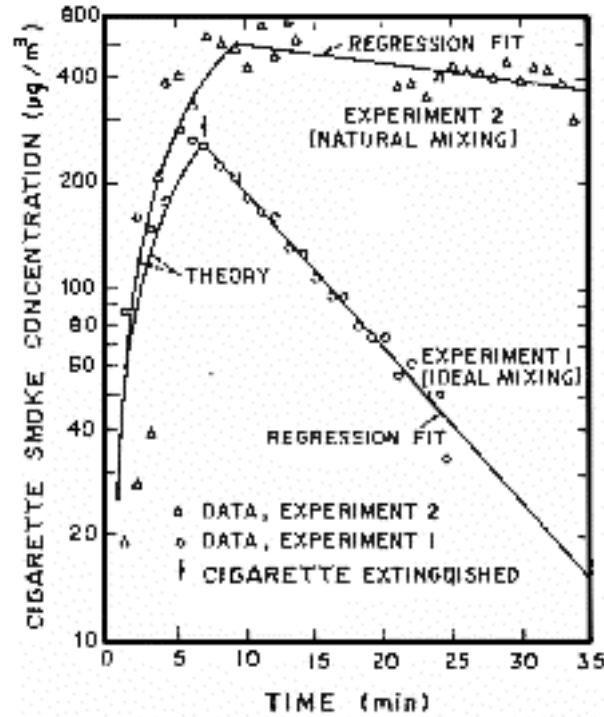


Figure 3. Smoke concentration within a room with and without internal mixing (from *Industrial Ventilation*, R. J. Heinsohn, J. Wiley & Sons, New York, 1991, pg. 245).

If only a fraction (f) of the return flow into an enclosed space is fresh air, Equation (46) can be modified to the following form

$$V \frac{dc}{dt} = -cQ[1 - (1-f)(1-\eta)] + S + Qfc_a(1-\eta) \quad (55)$$

where f is the makeup air fraction (makeup of fresh air/input air) and η is the efficiency of the air cleaning device. Integrating Equation (55),

$$\frac{(c_{ss} - c(t))}{(c_{ss} - c_o)} = \exp \left[- \left(\frac{Qt}{V} \right) \{1 - (1-\eta)(1-f)\} \right] \quad (56)$$

For variable source or volumetric flow rates, Equation (55) must be solved numerically.

For partially mixed conditions, the concentration varies both spatially and temporally. This condition is normally found in most industrial applications. The technique employed here is to introduce a mixing factor (m) to account for the spatial variations in concentration. Equation (46) now becomes

$$V \frac{dc}{dt} = S + (mQc_a) - (mQc) - (mc\eta Q_r) \quad (57)$$

where Q_r is the volumetric flow rate of recirculated air. Integration of Equation (57) gives

$$\frac{(c_{ss} - c(t))}{(c_{ss} - c_o)} = \exp\left[-\frac{mt(Q + Q_r\eta)}{V}\right] \quad (58)$$

For this particular type of situation, setting $m = 1$ indicates a well-mixed model while $m < 1$ implies nonuniform mixing and spatial variations in concentration (i.e., $m = 0.5$ is used for a perforated ceiling, $m = 0.166$ is for natural draft and ceiling exhaust fans, $m = 0.10$ is used for infiltration and natural drafts).

The source emission rate, or source strength (S), is usually not known and must be determined from experiment. A source can be released in a clean room and measurements made of the rise in concentration. The governing equation is

$$V \frac{dc}{dt} = S - c(Q_s + A_s k_{ad}) \quad (59)$$

where Q_s represents the volumetric flow rate through the sampling device. Immediately after the source is activated and while the concentration is small, Equation (59) reduces to the simple form

$$V \frac{dc}{dt} = S \quad (60)$$

and the source strength can be found from the slope of concentration versus time. A more accurate means of determining S is to measure two concentrations, c_1 and c_2 at two times t_1 and t_2 , and obtain S from the integration of Equation (59), i.e.,

$$S = -(A_s k_{ad} + Q_s) \left[c_1 \exp\left(\frac{-(A_s k_{ad} + Q_s)(t_2 - t_1)}{V}\right) - c_2 \right] / G \quad (61)$$

$$G = 1 - \exp\left[\frac{-(A_s k_{ad} + Q_s)(t_2 - t_1)}{V}\right]$$

Example:

An exhaust hood is installed within a few feet of a makeup air inlet in a room. Ethyl alcohol is evaporated in the hood. What is the steady state concentration of ethyl alcohol in the room and the amount of time before one begins to smell alcohol? Assume the threshold odor limit for ethyl alcohol is 40 mg/m^3 and the following criteria apply:

- V = volume of operating room (50 m^3)
 A_s = total area of adsorbing surfaces in operating room (85 m^2)
 k_{ad} = adsorption rate constant (0.001 m/s)
 S = rate at which ethyl alcohol is vaporized inside operating room
 (1 g/min)
 c_o = initial alcohol concentration inside operating room (10 mg/m^3)
 c_a = concentration of ethyl alcohol entering the makeup air duct
 (100 mg/m^3)
 Q_e, Q_r, Q_a, Q_s = volumetric flow rate of exhausted air, recirculated air,
 makeup air, and supply air ($Q_s = 20 \text{ m}^3/\text{min}$)
 $f = Q_a/Q_s$ = make up air fraction (0.9)
 η_1, η_2 = efficiencies of activated charcoal filter (0.5)

The governing equation to be solved is of the form

$$V \frac{dc}{dt} = S + Q_s c_s - c Q_e - c A_s k_{ad} \quad (62)$$

A mass balance for the air results in the expression

$$\begin{aligned} Q_s &= Q_a + Q_r \\ Q_e &= Q_s \end{aligned} \quad (63)$$

At the fan inlet, the mass balance for alcohol is

$$c_a Q_a (1 - \eta_2) + c Q_r (1 - \eta_1) = c_s Q_s \quad (64)$$

Using the definition of f ,

$$c_s = c_a f (1 - \eta_2) + c_r (1 - \eta_1) (1 - f) \quad (65)$$

The differential equation to be solved is of the form

$$\frac{dc}{dt} = Ac + B \quad (66)$$

where A and B are evaluated as

$$\begin{aligned} A &= \frac{\{-Q_s - A_s k_{ad} + Q_s (1 - f) (1 - \eta_1)\}}{V} = -\frac{25 \text{ m}^3 / \text{min}}{50 \text{ m}^3} = -0.5 \text{ min}^{-1} \\ B &= \frac{[S + f Q_s c_a (1 - \eta_2)]}{V} = 0.0218 \text{ g} / \text{m}^3 \text{ min} \end{aligned} \quad (67)$$

Setting $dc/dt = 0$ gives the steady state concentration,

$$c_{ss} = -\frac{B}{A} = 45.6 \text{ mg/m}^3 \quad (68)$$

Since A and B are known constants, the time can be calculated from the integral expression

$$\int_{10}^{40} \frac{dc}{[Ac + B]} = \int_0^t dt \quad (69)$$

$$t = 4.47 \text{ min}$$

5.2 Advection Model

Often, a source exists that is moving within a confined space. Examples of such situations are automobiles that are traveling through tunnels or a smoker walking from one room to another. In this instance, a simple control volume approach can be used to establish the governing equation for concentration. In many instances, make-up air consisting of fresh air is used to provide local ventilation, e.g., for tunnels less than 600 m in length.

A schematic of air and contaminant transport within a tunnel is shown in Figure 4. An elemental volume denoted by $A dx$ exists within a tunnel with uniform make-up air and exhausts. The conservation of mass for air within the volume gives the following expression

$$\frac{dU}{dx} = q_m - q_e \quad (70)$$

where $q_m = Q_m/LA$ and $q_e = Q_e/LA$. If q_m and q_e are constant, the air velocity in the tunnel at any location x is

$$\frac{U(x)}{U_o} = 1 + \frac{x(q_m - q_e)}{U_o} \quad (71)$$

where U_o denotes air entering the tunnel. If $q_m > q_e$, then $U(x)$ increases linearly with x ; if $q_e > q_m$, $U(x)$ decreases. The conservation of mass for contaminants can be written as

$$c \frac{dU}{dx} + U \frac{dc}{dx} = s + q_m c_m - c q_e - kc \quad (72)$$

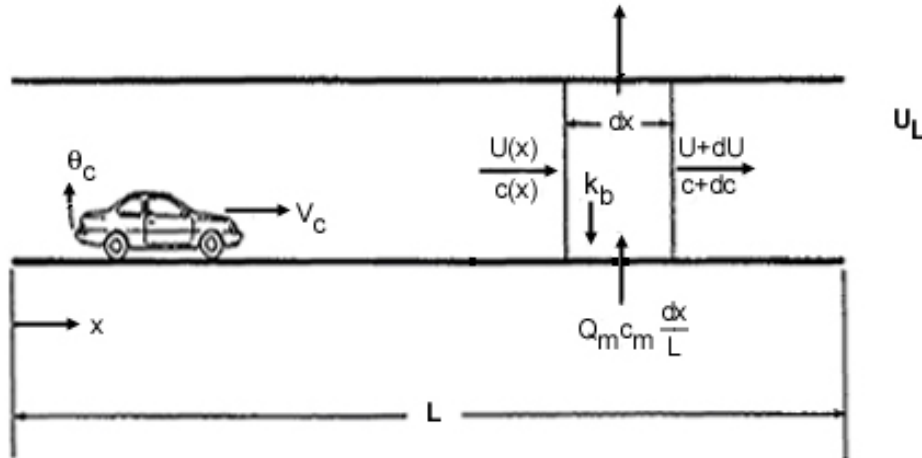


Figure 4. Air and concentration within a tunnel (from *Industrial Ventilation*, R. J. Heinsohn, J. Wiley & Sons, New York, 1991, pg. 567).

where $s = S/LA$ ($\mu\text{g}/\text{m}^3\text{-min}$) and $k = 4k_d/D$ (min^{-1}). D is the tunnel diameter, c_m is the contaminant, S is the source (mg/hr), and k_d (m/s) is the rate at which contaminant is deposited on the tunnel walls. Combining Equations (71)-(72), the equation for contaminant within the tunnel is

$$U \frac{dc}{dx} = s + q_m c_m - c(k + q_m) \quad (73)$$

which can be rewritten using Equation (71) as

$$\frac{dc}{(q_m c_m + s) - (k + q_m)c} = \frac{dx}{U_o + (q_m - q_e)x} \quad (74)$$

If q_m and q_e are constant (unequal and nonzero), Equation (74) can be integrated to

$$c(x) = \frac{s + q_m c_m}{k + q_m} + \left[c_o - \left(\frac{s + q_m c_m}{k + q_m} \right) \right] \left[\frac{U(x)}{U_o} \right]^{-b} \quad (75)$$

where $b = (k + q_m)/(q_m - q_e)$ and $U(x)/U_o$ can be replaced using Equation (71). If q_e and q_m vary with x , Equation (74) must be solved using a numerical approach, e.g., Runge-Kutta. If q_e and q_m are zero, Equation (74) cannot be used and Equation (73) must be integrated directly. When q_e and q_m are equal, the system is balanced. The usual case is for $q_m > q_e$.

5.3 Box Model

When the concentration within an enclosure is nonuniformly distributed, it is inaccurate to assume the enclosure can be treated as a well-mixed region. Although one could utilize partially mixed conditions and use mixing factors, the uncertainty in selecting values for m and the tendency of the partially mixed model to still predict spatially uniform concentrations would likely result in large inaccuracies. An alternative approach to the analytical tools utilized in the previous section is the *box model*, also sometimes referred to as the multi-cell well-mixed model (Heinsohn, 1991). Figure 5 shows a schematic of a partially mixed enclosure with two sources, two makeup air vents and two exhaust vents.

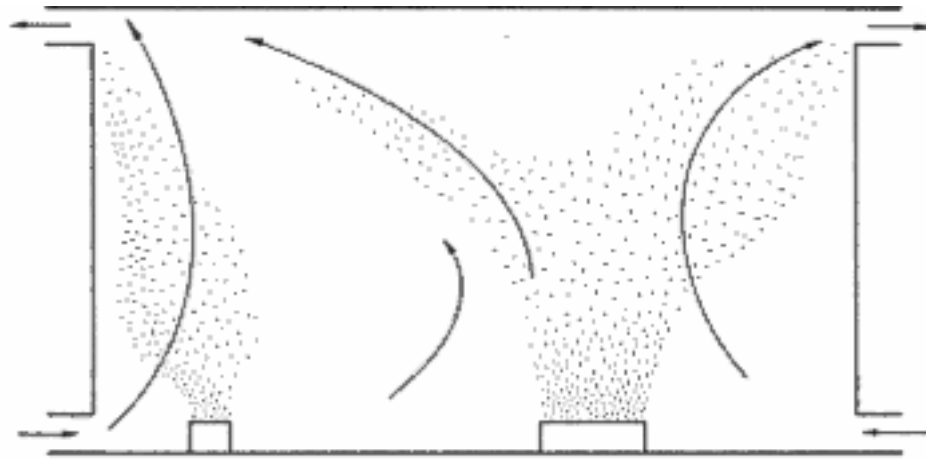


Figure 5. Partially mixed enclosure with two sources, two makeup air vents, and two exhaust vents (from *Industrial Ventilation*, R. J. Heinsohn, J. Wiley & Sons, New York, 1991, pg. 265).

Utilizing a box model approach, the domain is divided into two cells with contaminant that transfers between each cell. This is shown in Figure 6 for the two-cell model; the user can implement as many cells as desired – in this case, the problem domain is ideal for establishing a two-cell approach.

We begin by introducing the volumetric flow rates (Q) and fractions of those rates entering (x) and leaving (y) the cell boundaries.

Entering the enclosure:

$$\begin{aligned}
 Q_{1,i} &= x_1 Q \\
 Q_{2,i} &= x_2 Q \\
 Q &= Q_{1,i} + Q_{2,i} = Q(x_1 + x_2) \\
 x_1 + x_2 &= 1
 \end{aligned}
 \tag{76}$$

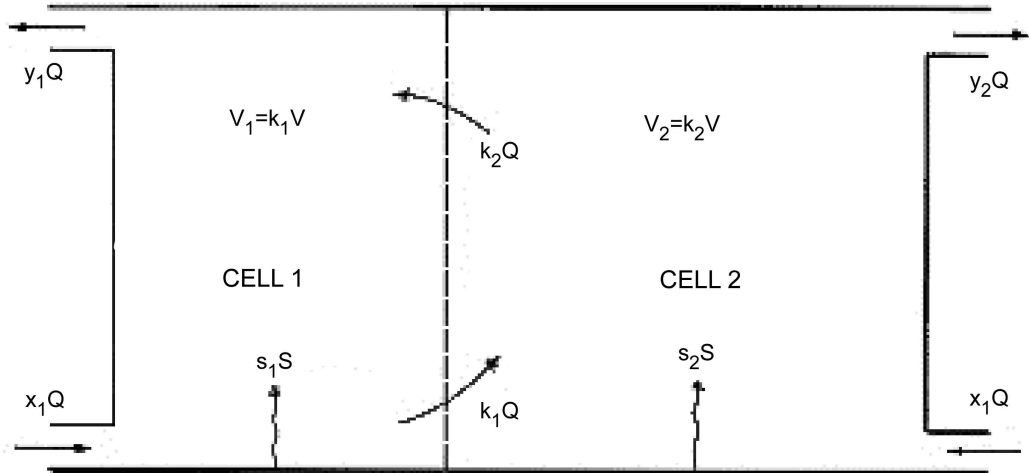


Figure 6. Two-cell box model (adapted from *Industrial Ventilation*, R. J. Heinsohn, J. Wiley & Sons, New York, 1991, pg. 266).

Leaving the enclosure:

$$\begin{aligned} Q_{1,o} &= y_1 Q \\ Q_{2,o} &= y_2 Q \\ y_1 + y_2 &= 1 \end{aligned} \quad (77)$$

The fractions are obtained from knowing the amounts of make-up air, recirculation, exhaust, and infiltration. The fraction of contaminant in each cell is designated as s_1 and s_2 , i.e.,

$$\begin{aligned} S &= S(s_1 + s_2) \\ s_1 + s_2 &= 1 \end{aligned} \quad (78)$$

and the volume of cells 1 and 2 expressed as fractions, v_1 and v_2 , of the total volume, V , as

$$\begin{aligned} V &= V(v_1 + v_2) \\ v_1 + v_2 &= 1 \end{aligned} \quad (79)$$

Fractional values for x , y , s , and v are input by the user.

The amount of volumetric flow rate transferred across the internal boundary between cells 1 and 2 is denoted through the use of exchange coefficients, k_1 and k_2 , which can vary from less than to greater than 1. Performing a conservation of mass balance yields the following expressions for cell 1 and 2,

$$\begin{aligned}
\text{Cell 1: } x_1Q + k_2Q - y_1Q - k_1Q &= 0 \\
x_1 - y_1 + k_2 - k_1 &= 0 \\
\text{Cell 2: } x_2Q + k_1Q - y_2Q - k_2Q &= 0 \\
x_2 - y_2 + k_1 - k_2 &= 0
\end{aligned} \tag{80}$$

The governing equations for the conservation of mass become

$$\begin{aligned}
v_1V \frac{dc_1}{dt} &= s_1S + x_1Qc_a + k_2Qc_2 - k_1Qc_1 - y_1Qc_1 \\
v_2V \frac{dc_2}{dt} &= s_2S + x_2Qc_a + k_1Qc_1 - k_2Qc_2 - y_2Qc_2
\end{aligned} \tag{81}$$

where c_a is the concentration in the air entering cells 1 and 2. The two sets of relations described by Equation (81) can be rewritten to the simpler pair of simultaneous, first-order differential equations by assuming $v = v_l$, $s = s_l$, and $k = k_l$ (and thus $k_2 = k + y - x$)

$$\begin{aligned}
\frac{dc_1}{dt} &= A + Bc_1 + Dc_2 \\
\frac{dc_2}{dt} &= E + Fc_2 + Gc_1
\end{aligned} \tag{82}$$

where the coefficients are defined as

$$\begin{aligned}
A &= \left(\frac{N}{v}\right) \left[x_1c_a + \left(\frac{sS}{Q}\right) \right]; \quad B = -\left(\frac{N}{v}\right) [k + y_1] \\
D &= \left(\frac{N}{v}\right) [x_2 - y_2 + k]; \quad E = \left(\frac{N}{(1-v)}\right) \left[x_2c_a + \left\{ (1-s) \frac{S}{Q} \right\} \right] \\
F &= -\left(\frac{N}{(1-v)}\right) [x_2 + k]; \quad G = \frac{Nk}{(1-v)}; \quad N = \frac{Q}{V}
\end{aligned} \tag{83}$$

The general solution to the pair of relations defined by Equations (82)-(83) is

$$\begin{aligned}
c_1(t) &= K_1 \exp(Ntw_1) + K_2 \exp(NTw_2) + c_{1,ss} \\
c_2(t) &= MK_1 \exp(Ntw_1) + LK_2 \exp(NTw_2) + c_{2,ss}
\end{aligned} \tag{84}$$

where $c_{1,ss}$ and $c_{2,ss}$ are the final (steady state) cell concentrations given as

$$c_{1,ss} = \frac{AF - ED}{DG - BF}; \quad c_{2,ss} = \frac{EB - AG}{DG - BF} \tag{85}$$

where

$$\begin{aligned}
 w_1 &= \left(\frac{1}{2N} \right) \left[(B+F) + \sqrt{(B-F)^2 + 4DG} \right] \\
 w_2 &= \left(\frac{1}{2N} \right) \left[(B+F) - \sqrt{(B-F)^2 + 4DG} \right] \\
 M &= \frac{Nw_1 - B}{D}; \quad L = \frac{Nw_2 - B}{D} \\
 I_1 &= c_1(0) - c_{1,ss}; \quad I_2 = c_2(0) - c_{2,ss} \\
 K_1 &= \left[L - \left(\frac{I_2}{I_1} \right) \right] \left[\frac{I_1}{(L-M)} \right]; \quad K_2 = \left[\left(\frac{I_2}{I_1} \right) - M \right] \left[\frac{I_1}{(L-M)} \right]
 \end{aligned} \tag{86}$$

where $c_1(0)$ and $c_2(0)$ are the initial cell concentrations. It is a simple matter to solve for the equation pair established by Equation (82). The only difficulty is in selecting an appropriate value for the exchange coefficient, k , which is difficult to establish. The best way is to use trial and error or some empirical judgment to determine a range of values for k . Note that as the value of k increases, the exchange between cells increases. When k reaches a value of around 15, the concentration in both cells approaches the equivalent of a single well-mixed cell, i.e., well-mixed conditions can be assumed throughout the entire enclosure. Although using two cells is crude, it is much better than assuming well-mixed conditions for the problem domain. Of course, one can always add more cells in an effort to refine the problem details and obtain a more accurate solution; however, the complexity of analyzing multiple cells increases proportionally to the square of the number of cells. If one winds up using many cells, it may be best to ultimately go to the use of numerical methods, i.e., CFD. The accuracy of the box model is limited by the inability to establish enough detail to describe the exchange of air among cells, especially if transient solutions are sought.

Box Model Example

Objects are to be cleaned in HCl solutions in one room before final assembly in an adjacent room. The liquid surface area is 75 ft² and HCl vapor is emitted at a rate of 0.02 gm/s-m². The room with HCl is 30 ft x 30 ft x 15 ft and has a doorway 10 ft x 15 ft into the adjacent room that is 50 ft x 30 ft x 15 ft. No HCl is generated in the adjacent room. The plant manager has reservations that placing an air curtain in the doorway will prevent HCl vapor from entering the adjacent room. Each room has its own HVAC system. Each room is well mixed and infiltration and exfiltration are equal to one change per hour. The ventilation system delivers 600 CFD of outside air to the adjacent room and 600 CFD of contaminated air is removed from the room containing HCl. What are the steady state concentrations in each room, how fast do the concentrations increase in time, and is the PEL (5 ppm ~ 7 mg/m³) exceeded in each room? Assume that no adsorption occurs and that HCl is initially zero.

Utilizing Equations (81)-(86), the following values for the various constants, assuming a two cell model, are calculated as shown in Table 11.

Table 11. Values for various parameters used in box model example.

Parameter	Value
x_1	0.1875
x_2	0.8125
y_1	0.6875
y_2	0.3125
S	1.0
V	0.375
Q	72,000 CFM
S	502 gm/hr
N	2 hr^{-1}
A	0.0372 gm/hr-m^3
B	$-5.33 (k+0.6875) \text{ hr}^{-1}$
D	$5.33 (k+0.5) \text{ hr}^{-1}$
E	0
F	$-3.2 (k+0.8125) \text{ hr}^{-1}$
G	$3.2 (k) \text{ hr}^{-1}$

Using Equation (71), a steady state concentration value of 175 ppm is obtained with a time constant of 0.5 hr, using a value of $k = 15$ (which is very conservative but allows one to place an upper bound on the exchange). Using this upper limit, the PEL would be exceeded during the working day. Figure 7 shows concentration values versus time within the two cells using $k = 0.2$ and $k = 1.8$. If $k = 0$, cell 1 is well mixed and cell 2 receives no HCl; as k increases, mixing increases. Steady state concentrations in both rooms approach values that would be predicted assuming well-mixed conditions throughout the rooms.

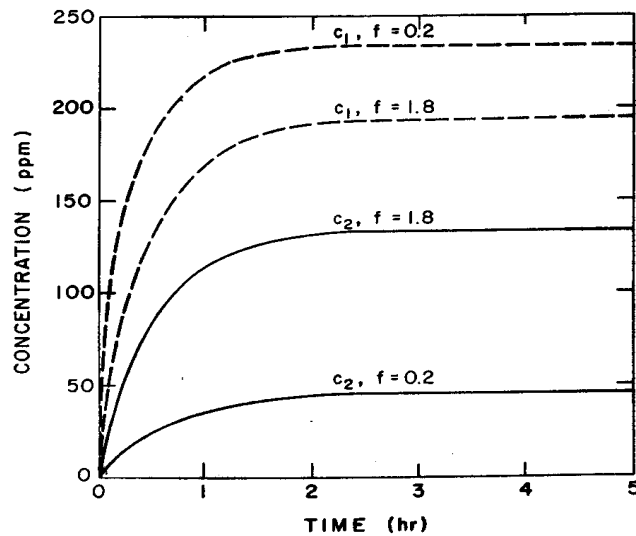


Figure 7. Box model example for mixing of HCL between two rooms (from *Industrial Ventilation*, R. J. Heinsohn, J. Wiley & Sons, New York, 1991, pg. 270).

6 Dynamics of Particles and Gases/Vapors

6.1 Drag, Shape, and Size of Particles

Analyzing the force on a particle in a flow field reveals the fluid to be exerting a force proportional to the particle's projected area, the square of the relative velocity of the particle to the fluid. This proportionality is known as Newton's resistance equation. In general form, Newton's resistance equation is

$$F_d = C_d \frac{\pi}{8} \rho_f d_p V^2 \quad (87)$$

where V is the relative velocity of the particle with diameter d_p having a drag coefficient C_d in a fluid with density ρ_f . This equation is valid for particle motion at subsonic speeds. Particles having Reynolds number (Re) less than one, $Re = d_p V \rho_f / \mu \ll 1$, the Stokes regime, the drag force is

$$F_d = 3\pi\mu d_p V \quad (88)$$

When substituted into Equation (87), the coefficient of drag is $C_d = 24 / Re$.

If particle size is of the order of the molecular mean free path, the particle no longer experiences the fluid as a continuum, but as individual molecules. Particles of this size invalidate the assumption of a no-slip boundary condition for the fluid on the particle's surface used in the Stokes flow analysis. The particle is able to slip through the fluid, reducing the drag experienced by the particle as predicted from a continuum analysis in Stokes' flow regimes. A slip factor (Cunningham slip correction factor) for particle drag factor corrects the Stokes drag coefficient

$$C_c = 1 + (2\lambda / d_p)(A_1 + A_2 e^{-A_3 d_p / \lambda}) \quad (89)$$

The variable λ is the molecular mean free path and is given by (Cooper and Alley, 1994)

$$\lambda = \frac{\mu}{0.499P \sqrt{8MW_f / \pi R T}} \quad (90)$$

where μ is the absolute viscosity of the fluid, MW_f is the molecular weight of the fluid, R is the universal gas constant, P is the pressure, and T is the absolute temperature. Any consistent set units will provide the length of the mean free path. The factors A_1, A_2, A_3 are dimensionless empirical constants for small particle drag (Martin et al., 1983).

The slip factor is used to augment the coefficient of drag in the force equation. The force of drag becomes

$$F_d = \frac{3\pi\mu V d_p}{C_c} \quad (91)$$

Particles of various shape and size are found in the indoor environment. Depending the molecular structure of the mineral or molecules forming the particle, it is possible to predetermine the shapes expected from some compounds (e.g., salt has a cubical shape and fibers are cylindrical in shape).

The Newton's resistance equation and Stokes flow analysis can be adjusted to account for non-spherical particles. By using an equivalent volume for the particle, that is, creating a sphere of equivalent volume that an irregular shaped particle would have if it were spherical, Stokes law becomes

$$F_d = 3\pi\mu V d_{pe} \quad (92)$$

where d_{pe} is the equivalent diameter of the particle.

An aerodynamic diameter is an equivalent diameter that is defined as the diameter of a spherical water droplet (a spherical particle with unit density) which has the same settling velocity v_s as the particle. The mathematical relation for aerodynamic diameter is

$$d_a = \sqrt{\frac{18\mu v_s}{C_c \rho_{\text{water}} g}} \quad (93)$$

Any equivalent set of units can be used to determine the aerodynamic diameter. The settling velocity, a terminal velocity of a particle in calm air, is determined by solving a particle's steady state rectilinear motion in a gravitational field, that is, by solving

$$F_g - F_d = m_p \frac{dv_p}{dt} \quad (94)$$

where F_g is the gravitational force exerted on the particle having mass m_p . Then solving this differential equation for the particles velocity, v_p , at steady state yields a terminal settling velocity

$$v_s = \frac{\rho_p d_p^2 C_c}{18\mu} g \quad (95)$$

6.2 Particle Motion

When the number of particles in the air is low, it is fair to assume that the particles do not influence the velocity field of the air. In other words, the average distance between any two particles is at least 10X the particle diameter. For water droplets, this would correspond to less than 4.2 kg/m³ in air. Table 12 shows upper limits for particle concentration influence on the flow field based on particle diameter and number density.

Table 12. Particle diameter versus density for influencing flow field.

Diameter (μm)	particles/m ³
1.0	8 x 10 ¹⁵
10.0	8 x 10 ¹²
100.0	8 x 10 ⁹

If knowledge of the velocity field of the air (or carrier gas) is known, then particle trajectories can be calculated. For situations when the density of a particle is 1000X greater than the density of air, buoyancy on a particle can be neglected. The motion of a single spherical particle can be expressed using the relation

$$\left(\frac{\pi D_p^3}{6}\right)\rho_p \frac{d\mathbf{v}}{dt} = -\left(\frac{C_D \rho}{2C}\right)\left(\frac{\pi D_p^2}{4}\right)(\mathbf{v} - \mathbf{U})|\mathbf{v} - \mathbf{U}| - \left(\frac{\pi D_p^3}{6}\right)\rho_p \mathbf{g} \quad (96)$$

where \mathbf{v} is the velocity of the particle, \mathbf{U} is the air velocity, C is a slip factor (~ 1 for $D_p \geq 10\mu\text{m}$), and \mathbf{g} is acceleration of gravity. Equation (96) is useful when calculating freely falling particles due to gravimetric settling, horizontal motion in quiescent air, and particles traveling through a moving stream.

For a particle settling in quiescent air ($\mathbf{U} = 0$) due to gravitation, motion is only downward. Hence, the vector velocity becomes $\mathbf{v} \equiv -v$ (where v denotes vertical motion). Likewise, the drag coefficient becomes $C_D = 24\mu/\rho D_p v$. Equation (96) can be simplified to the following form,

$$\frac{dv}{dt} = g - \frac{v}{\tau C} \quad (97)$$

where $\tau = \rho_p D_p^2 / 18\mu$, which is known as the relaxation time. If the particle starts from rest, the downward velocity is

$$v(t) = Cg\tau \left[1 - \exp\left(-\frac{t}{\tau C}\right) \right] \quad (98)$$

If $t \gg \tau$, then the settling, or terminal velocity (v_t), of the particle can be calculated using the simple relation

$$v_t = \tau g C \quad (99)$$

assuming that the Reynolds number ($Re = \rho U D_p / \mu$) is low. Figure 8 shows particle diameter versus settling velocity for three specific gravities (SG). Note that the settling velocity varies as the square of the particle diameter when $Re \leq 1$.

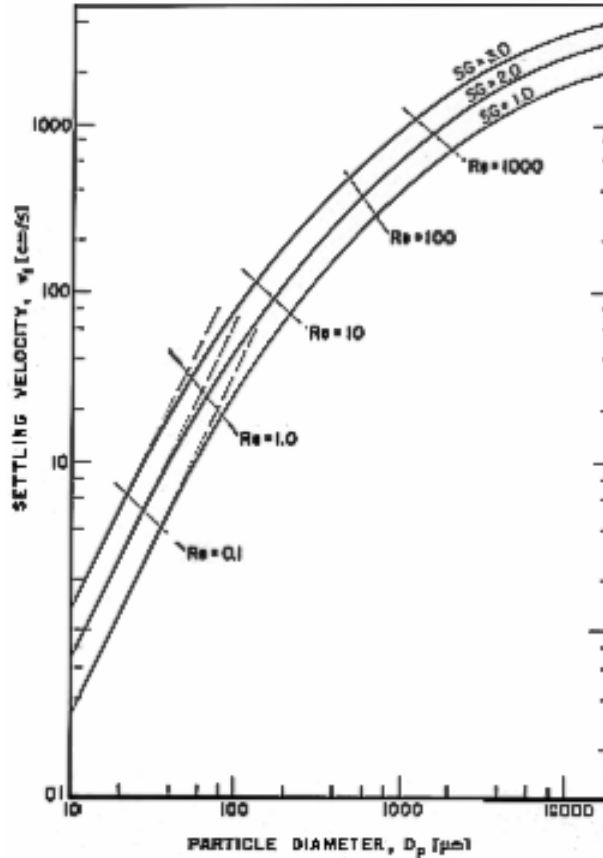


Figure 8. Settling velocity of spherical particles for three specific gravities (from *Industrial Ventilation*, R. J. Heinsohn, J. Wiley & Sons, New York, 1991, pg. 450).

When the particle is very large and $Re > 1000$, $C_D \sim 0.4$ and the settling velocity can be found from the relation

$$v_t = \sqrt{\left(\frac{4}{3}\right) \left(\frac{\rho_p D_p g}{0.4 \rho}\right)} \quad (100)$$

For a particle moving horizontally in quiescent air, we will assume that the horizontal velocity (u) of a sphere occurs when $Re \leq 1.0$. The differential equation for the horizontal motion is

$$\frac{du}{dt} = -\frac{u}{\tau C} \quad (101)$$

which can be integrated to yield

$$u(t) = u(0) \exp\left[-\frac{t}{\tau C}\right] \quad (102)$$

and the horizontal displacement (also known as stopping or penetration distance) calculated as

$$\int_0^{x(t)} dx = \int_0^t u dt = \tau C u(0) \left[1 - \exp\left(-\frac{t}{\tau C}\right)\right] \quad (103)$$

The maximum stopping distance is easily found by allowing $\tau \gg t$.

For particles traveling in a 2-D moving air stream, Equation (96) must be modified to the form

$$\frac{d\mathbf{v}}{dt} = -\left(\frac{3C_D}{4C}\right) \left(\frac{\rho}{\rho_p D_p}\right) (\mathbf{v} - \mathbf{U}) |\mathbf{v} - \mathbf{U}| - \mathbf{g} \quad (104)$$

which can be reduced to the following pair of coupled differential equations,

$$\begin{aligned} \frac{du}{dt} &= -\left(\frac{3C_D}{4C}\right) \left(\frac{\rho}{\rho_p D_p}\right) u_r (u_r^2 + v_r^2)^{1/2} \\ \frac{dv}{dt} &= -\left(\frac{3C_D}{4C}\right) \left(\frac{\rho}{\rho_p D_p}\right) v_r (u_r^2 + v_r^2)^{1/2} - g \end{aligned} \quad (105)$$

where u_r and v_r are relative velocities ($u-U$; $v-U$) and

$$C_D = 0.4 + \frac{24}{Re} + \frac{6}{(1 + Re^{1/2})}$$

$$Re = \rho D_p \frac{[u_r^2 + v_r^2]^{1/2}}{\mu}$$
(106)

For the case when the particle's motion is in a flow regime where $Re \leq 1.0$, the pair of equations reduce to the much simpler form

$$\frac{du}{dt} = -\left(\frac{u - U_x}{\tau C}\right)$$

$$\frac{dv}{dt} = -\left(\frac{v - U_y}{\tau C}\right) - g$$
(107)

which can be integrated, assuming $u(0) = v(0) = 0$, to

$$u(t) = u(0) \exp\left[-\frac{t}{\tau C}\right] + U_x(0) \left[1 - \exp\left(-\frac{t}{\tau C}\right)\right]$$

$$v(t) = v(0) \exp\left[-\frac{t}{\tau C}\right] - (g\tau C) \left[1 - \exp\left(-\frac{t}{\tau C}\right)\right]$$
(108)

where U_x and U_y denote components of the air velocity in the horizontal and vertical directions, respectively. If Re values are unknown and the flow regime is well beyond low flow levels, numerical methods (CFD) are required to compute the particle velocities and trajectories.

Particle motion is described by the time dependent convection-diffusion equation. For inviscid analysis or in laminar flow the transport equation can be easily adjusted to account for settling by incorporating a settling velocity into the advection-diffusion equation.

6.2.1 Deposition of Particulate with Aerodynamic Diameters $> 1\mu$ by Settling

The deposition of large particles by diffusion is extremely small as is evident by examining the equation for the velocity of deposition through a boundary layer of thickness δ_{part} , from diffusion alone. In the absence of thermophoretic velocities and turbulent dispersion, deposition velocity is a function of gravitational settling. The equation for species transport with settling becomes

$$\frac{\partial C_j}{\partial t} + u \frac{\partial C_j}{\partial x} + (v - v_{s_j}) \frac{\partial C_j}{\partial y} + w \frac{\partial C_j}{\partial z} = \frac{D_j}{\rho} \left[\frac{\partial^2 C_j}{\partial x^2} + \frac{\partial^2 C_j}{\partial y^2} + \frac{\partial^2 C_j}{\partial z^2} \right] + Q_c \quad (109)$$

This equation has a different advective velocity term in the y coordinate or direction of gravitational influence from Equation 1. The advective term $v - v_s$ in Equation (109) represents some relaxation of the particulate velocity versus the free stream velocity.

The deposition rate is given by

$$J = v_s \rho_p \quad (110)$$

For particles larger than $10 \mu\text{m}$ and Reynolds number between 2 and 500, the settling velocity is defined as (Cooper and Alley, 1994)

$$v_s = \frac{0.153 d_p^{1.14} \rho_p^{0.71} g^{0.71}}{\mu \rho^{0.29}} \quad (111)$$

Inertial deposition from laminar flow occurs for larger particles, which may be carried from the streamline flow onto an obstruction. The distance the particle would be carried from the streamline is dependent on the particle's momentum and size. The trajectory of the particle is initially a function of the fluid's trajectory.

Consider a distance a particle will travel from its inertia. Let that distance be just to a surface, a stopping distance of d_s . The velocity v_s of the particle normal to the surface multiplied by the time t , the relaxation time, is the stopping distance $d_s = v_s t$.

The rate of deposition from this stopping distance is determined by the concentration of particles with this relaxation time. As the particle size decreases, the distance traveled from inertia decreases, that is, the relaxation time is decreased. Relaxation time is defined as

$$t = \frac{C_c \rho_p d_p^2}{18\mu} \quad (112)$$

The particulate flux from the stopping distance d_s is

$$J_s = v_s C_j |_{d_s} \quad (113)$$

The value of C_j , is the value of the concentration at the stopping distance for that particular particulate density and size.

Inertial forces on large particles in turbulent flow are important mechanisms for deposition by impingement. Larger particles are carried into the boundary layer by inertia. The distance particles are carried into the transitional and laminar sublayers depends on the stopping distance which is dependent on the following factors: 1) particle size, 2) particle mass, and 3) degree of turbulence or energy of the flow.

If molecular diffusion is neglected, the velocity of deposition for particles is given by

$$V_{d+} = \frac{\mu_{\text{turb}}}{v_{\text{fluid}}} \frac{dc_+}{dy_+} = \frac{V_d}{u_*} \quad (114)$$

This equation is true for one-dimensional flow towards a flat plate. This equation provides a good approximation to flow within a cylinder where the radius of a surface is large compared to the scale of the turbulent boundary layer (Davies, 1966).

Consider, a particle travel distance just to a surface as the stopping distance of d_{s+} with a turbulent velocity v_{s+} normal to the surface, then

$$d_{s+} = v_{s+} t_+ \quad (115)$$

where $t_+ = t u_*^2 / \nu$ is the nondimensional relaxation time. The rate of deposition from this distance is determined by the concentration of particles with this relaxation time. As the particle size decreases, the distance traveled from inertial forces decreases, that is, the relaxation time is decreased. Relaxation time is defined as

$$t = \frac{C_c \rho_p d_p^2}{18\mu} \quad (116)$$

The non-dimensional particulate flux from the stopping distance d_{s+} is $J_{s+} = v_{s+} c_+|_{d_{s+}}$. The value of c_+ is the value of the concentration at the stopping distance for that particular particulate density and size.

6.2.2 Particle Motion in Electrostatic Field

Electrostatic forces can have very significant influence on the motion of aerosols. Most airborne particles are electrically charged, and when in the presence of electric potential, the resulting forces on the particles cause significant motion. So much so that this force is utilized by electrostatic precipitators for air cleaning and by aerosol measurement instruments.

Coulomb's law describes the electrostatic force as

$$F_e = \frac{1}{4\pi\epsilon_0} \frac{q_1 q_2}{r_{12}^2} \quad (117)$$

where q_1 is the particle's charge, q_2 is the surface's charge (or other point source), ϵ_0 is the permeability of a vacuum, and r_{12} is the distance between the charges.

A field strength E is the electrostatic force produced per unit charge of the particle. This field is then

$$E = \frac{F_e}{q_p} \quad (118)$$

where $q_p = ne$, n being the number or units of electron charge, e is 1.6×10^{-19} Coulombs.

The work required to move a particle distance 'x' in an electric field per unit charge is

$$W_p = \frac{F_e \Delta x}{q_p} \quad (119)$$

This work is the potential difference in the electric field and is measured in volts, e.g., the voltage between parallel plates in an electrostatic precipitator.

The difference between the drag force and the electrostatic force determines particle acceleration in an electric field

$$F_e - F_d = m_p \frac{dv_p}{dt} \quad (120)$$

6.2.3 Particle Motion Induced by Temperature Gradients

A temperature gradient will result in particles moving from the warmer region to the cooler region or surface. This phenomenon is the result of thermophoretic forces on the particles.

6.2.3.1 Thermophoretic Motion for Gases and Particles with Diameter Less Than the Molecular Mean Free Path

When the Knudsen number, $Kn = \lambda/d_p$, is greater than 1.0, the thermophoretic velocity is given by

$$V_{\text{Thermo}} = -0.55 \frac{\mu}{\rho T} \nabla T \quad (121)$$

where $\nabla T = \frac{T_{\text{hot}} - T_{\text{cold}}}{ds}$ and T is the ambient or bulk temperature of the fluid (Hinds, 1982).

6.2.3.2 Thermophoretic Transport for Particles with Diameter Greater Than the Molecular Mean Free Path

When $Kn < 1.0$, the particle is influencing inertial and thermodynamic states of nearby gas molecules. The thermophoretic velocity is found by equating resistive forces to the thermal force (Hinds, 1982) and is given by

$$V_{\text{Thermo}} = -\frac{3}{2} H \frac{\mu}{\rho T} \nabla T C_c \quad (122)$$

where T is the ambient or bulk temperature of the fluid, C_c is the Cunningham slip correction factor, and

$$H = \left[\frac{1}{1 + 6\lambda/d_p} \right] \left[\frac{\frac{k_f}{k_p} + 4.4\lambda/d_p}{1 + 2\frac{k_f}{k_p} + 8.8\lambda/d_p} \right] \quad (123)$$

where k_f and k_p are the thermal conduction of the fluid and particle, respectively.

Thermophoretic forces have an insignificant influence on the rate of deposition for particles of one micron physical diameter or larger. For very small particles, this velocity would add as a vector function to the settling velocity and the velocity of the air stream.

6.3 Particle Flow in Inlets and Flanges

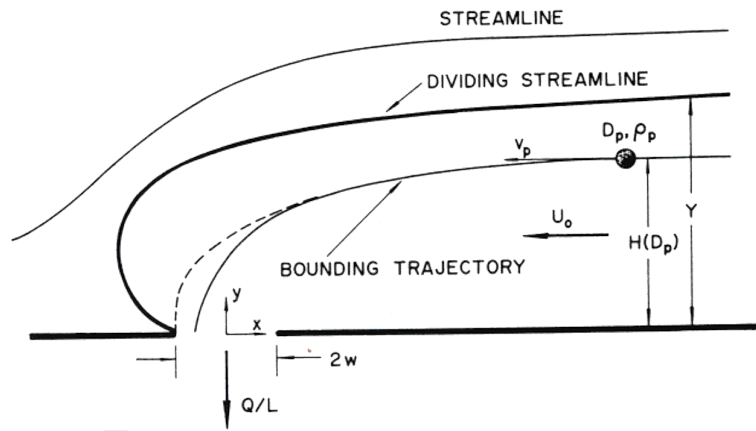
Contaminants and air are withdrawn by inlets of various shapes and sizes. The effectiveness of an inlet is basically how well it serves to capture contaminants. The locations of dividing streamlines and bounding trajectories of particles can be determined as a first guess using much of the analytical tools previously discussed. The quantitative measure of inlet effectiveness is generally referred to as *reach*. The reach defines the boundaries of the region from which the inlet reaches out and captures contaminants. In more definable terms, the reach can be defined as the ratio of the cross-sectional area of the stream tube of contaminants entering the inlet to the cross-sectional area of the stream tube of air entering the

inlet. The reach for particles is not always equal to one since some of the particles may not enter the inlet, even though all the air is pulled into the inlet. This is due to particle inertia and deflection. For gases and vapors, the reach is unity. Figure 9 (a-d) shows a set of dividing streamlines and bounding trajectories for several flanged inlet configurations.

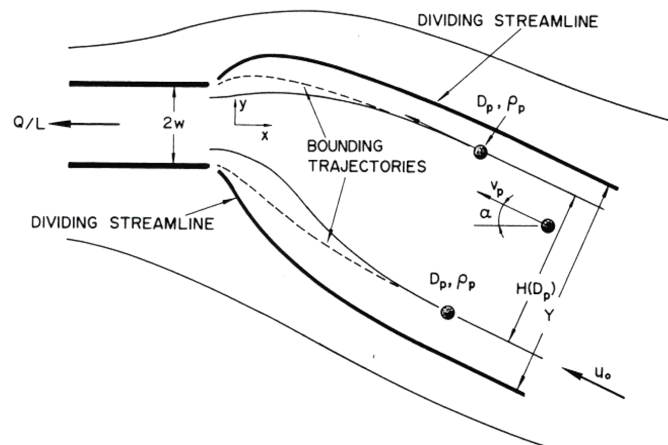
To find particle velocity, displacement, and its new location (x, y) , Equation (108) must first be solved. Once the velocities are determined, the location of the particle at the end of an interval of time can be found using the simple relations

$$\begin{aligned} x_j &= x_i + \Delta t u(x_i, y_i) \\ y_j &= y_i + \Delta t v(x_i, y_i) \end{aligned} \quad (124)$$

where i denotes initial (previous) position and j is the new position. Repeating solution of this pair of equations produces a table of x and y values that can be used to create a trajectory for the particle position. More details on this simple technique are given later in the section on Lagrangian Particle Transport.



(a)



(b)

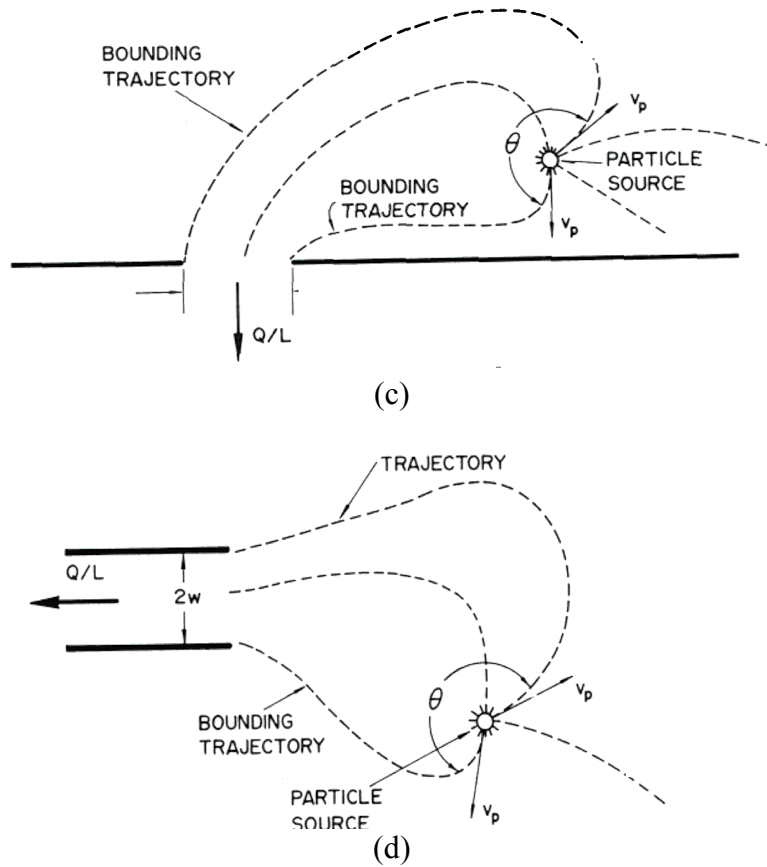


Figure 9. Dividing streamline and bounding trajectory for flanged inlets (from *Industrial Ventilation*, R. J. Heinsohn, J. Wiley & Sons, New York, 1991, pg. 518).

Figure 10 shows the dividing streamlines and bounding trajectories for particles of varying sizes entering an unflanged inlet.

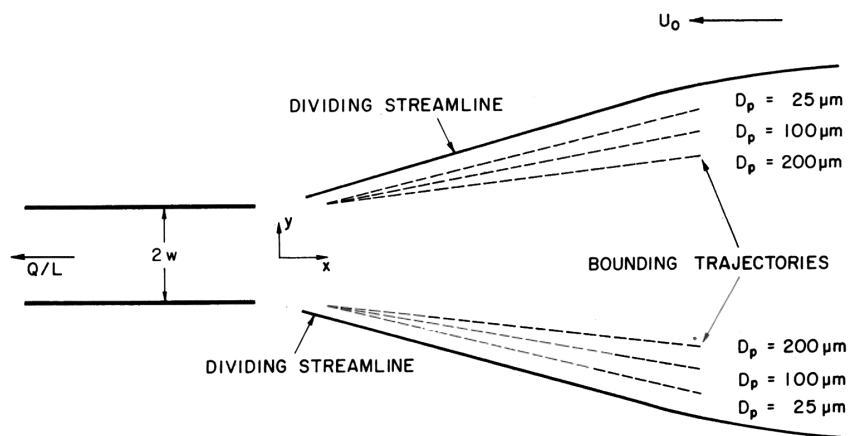


Figure 10. Reach of an unflanged inlet for several particle sizes (from *Industrial Ventilation*, R. J. Heinsohn, J. Wiley & Sons, New York, 1991, pg. 537).

7 Numerical Modeling - CFD

Indoor air quality can have a larger effect on human health than outdoor air quality. The common practice of relating measurements of outdoor pollutants to human exposure can be fundamentally wrong, especially with regards to hazardous material. Direct measurements of indoor air quality are the best way to evaluate the existence and the gravity of contaminants. In some instances, statistical data can be used to estimate flow rates. While such analyses lead to order of magnitude projections, they do not provide sufficient data for ventilation feedback and remediation. In order to obtain accurate assessments and forecasts of the effects on ventilation/air quality, modeling based on solution of the nonlinear equations of fluid motion (CFD) must be undertaken.

There are four fundamental numerical methods that are currently being used to model flow and species transport within enclosures. The two most popular and most prevalent methods are numerical models that utilize finite difference and finite volume techniques.

7.1 Finite Difference Method

Representing a derivative using a Taylor series and truncating higher order terms creates an approximation to that derivative. In this manner, when discrete distances and increments of time are employed in the Taylor series expansion, a finite difference approximation is made of the original differential equation. For example, looking at the 1-D equation for time dependent isotropic advection-diffusion,

$$\frac{d\phi}{dt} + u \frac{\partial\phi}{\partial x} = k \frac{\partial^2\phi}{\partial x^2} \quad (125)$$

we seek the derivatives of each term, found by Taylor series expansion.

Representing the derivative of f with respect to x we have

$$\phi_{x+1} = \phi_x + \frac{\partial\phi}{\partial x} \Delta x + \frac{1}{2!} \frac{\partial^2\phi}{\partial x^2} \Delta x^2 + \dots \quad (126)$$

Rearranging and dropping higher order terms, the first order derivative is represented in a discrete sense as

$$\frac{\partial\phi}{\partial x} = \frac{\phi_x - \phi_{x-1}}{\Delta x} \quad (127)$$

where a backward difference method is used.

Adding both the forward and backward Taylor series, the second order discrete derivative is

$$\frac{\partial^2 \phi}{\partial x^2} = \frac{\phi_{x+1} - 2\phi_x - \phi_{x-1}}{\Delta x^2} \quad (128)$$

Substituting these and the discrete time advancement

$$\frac{\partial \phi}{\partial t} = \frac{\phi_x^{t+1} - \phi_x^t}{\Delta t} \quad (129)$$

into the advection-diffusion equation results in the discrete representation of the governing equation

$$\frac{\phi_x^{t+1} - \phi_x^t}{\Delta t} + u \frac{\phi_x - \phi_{x-1}}{\Delta x} = k \frac{\phi_{x+1} - 2\phi_x - \phi_{x-1}}{\Delta x^2} \quad (130)$$

This equation is first order, accurate in time and space, although the diffusion term is second order accurate. Higher order discretization can be achieved with the use of various components of the Taylor series expansions. Also, notice this equation was developed based on an equal spacing of the discretization and could be modified for non-uniform grid spacing.

If this equation had been in 2-D, it would be apparent that the discretization had an orthogonality, the x and y discretization were perpendicular. This decomposition of the domain into grid points that can be connected by lines orthogonal is referred to as a structured grid. For complex domains the representation may suffer if there are curved surfaces or sides oblique to the discretization. Transformations can be constructed for complex domains that fit the complex boundaries and coordinates to an orthogonal discretization. This Boundary Fitted Coordinate (BFC) transformation can be complex but allows for the use of both FDM and structured FVM to solve problems on complex domains (Fletcher, 1991).

Upwinding of the advective term, i.e., a backward differencing, is employed since it is a stable discretization even for explicit time stepping. The stability constraint is the Courant-Friedrichs-Lewy (CFL) condition

$$C = u \frac{\Delta t}{\Delta x} \leq 1 \quad (131)$$

The condition states that a fluid molecule can travel no more than a spatial distance Δx in time Δt . It is interesting to write the upwinded term with a

numerical diffusion, thus indicating a damping of the 2nd order central difference scheme.

$$\frac{u}{\Delta x}(\phi_x - \phi_{x-1}) = \frac{u}{2\Delta x}(\phi_{x+1} - \phi_{x-1}) - \frac{u}{2\Delta x}(\phi_{x+1} - 2\phi_x + \phi_{x-1}) \quad (132)$$

This dampening is advantageous in capturing step gradients common to the advective term, the wave equation portion of the advection-diffusion model, as is indicated by its more stable nature (Fletcher, 1994).

Time advancement is accomplished either by implicit, semi-implicit or explicit formulation of the equation. When all the nodal values in each equation are being solved at the next time step, it is an implicit formulation. This formulation has no limiting value for the time increment (i.e., it is unconditionally stable).

Placing only the node being evaluated for time advancement in each equation on the left hand side (LHS) produces an explicit formulation. An explicit formulation's time increment is constrained by the CFL condition and also by diffusion, by the Fourier number

$$k \frac{\Delta t}{\Delta x^2} \leq \frac{1}{2} \quad (133)$$

Using a scheme, which averages in space the current and future time step is known as a semi-implicit scheme, the Crank-Nicholson averaging process, and is conditionally stable. Numerous other time marching schemes have been devised. An alternating direction implicit (ADI) scheme is particularly useful in separating multi-dimensional systems into time advancement for each dimension and is conditionally stable for this equation set.

7.2 Finite Volume Method

The majority of fluid flow simulations have been conducted using the finite volume approach (Patankar, 1980; Anderson et al., 1984), principally because of its ease of use and simplicity in establishing meshes for orthogonal regions (i.e., rectangles). Introduction of the Boundary Fitted Coordinates (BFC) technique to model irregular geometries helped in overcoming this handicap (Thompson et al., 1985). However, the computational accuracy of these simple difference schemes is limited to first order (spatially); in addition, such methods require extensive meshing effort and massive numbers of nodes (especially in three dimensions), and can become quite formidable for non-orthogonal problem domains. Modeling 3-D problems using finite volume (or finite difference) methods may typically require over 10^6 nodes, overwhelming the resources of the largest supercomputers.

Finite volume method (FVM) is a subset of the Method of Weighted Residuals (MWR) and in this sense is a cousin to the finite element method (FEM). It is an inner product projecting the residual to zero. Since the problem domain is a discrete system, the method seeks to minimize the error or residual, R , over the domain. Let the residual equation or relationship be determined by

$$R(L(\hat{u})) \quad (134)$$

where $L(\hat{u})$ is the approximation to any or some differential equation $L(u)$. The approximation of the function \hat{u} is given by

$$\hat{u}(x_i) = \sum_{i=1}^n u_i N_i \quad (135)$$

which is a polynomial expansion. The term N_i is the weight and \hat{u}_i is the trial value. For the FVM, this weight is just one or zero depending on if the elemental domain is being evaluated or not, and n is equal to 1.

The method seeks to minimize this residual over a domain. Requiring the residual to be zero on average is accomplished by multiplying the residual equation by the appropriate weighting function, w , and integrating over the entire domain

$$\int_{\Omega} w R(L(\hat{u})) d\Omega = 0 \quad (136)$$

When applied over a domain, which is discretized into finite volumes, the resulting set of algebraic equations can be solved for the unknowns, that is, the values of \hat{u} ,

$$\int_{\Omega} (R, w) d\Omega = 0 \quad (137)$$

where the residual R is the approximate solution and w is some appropriate weight or approximation. The residual is by definition approximate since only an approximation of the solution on the domain is possible with any discrete representation. It is possible however, to have an exact solution at the nodal points, known as superconvergence.

The difference between FEM and FVM is in the order of the interpolation polynomial where FEM has at least first order weighting functions and the variables are also represented as functions of higher order polynomials. The finite volume method uses zero order polynomials as both test and weight functions. The finite volume method is referred to as a subdomain method. To see how this works, we look at the equation for conservation of mass in integral form

$$L(u) = \nabla \cdot \rho \hat{v} = 0 \quad (138)$$

then

$$\int_{\Omega} L(u) \, d\Omega = \int_{\Omega} \nabla \cdot \rho \hat{v} \, d\Omega \quad (139)$$

Applying Green's Theorem, we have

$$\int_{\Omega} \nabla \cdot \rho \hat{v} \, d\Omega = \oint_{\Gamma} (\hat{n} \cdot \rho \hat{v}) \, d\Gamma \quad (140)$$

This integral equation evaluated over the domain Ω (shown in Figure 11) produces an expression for the conservation of mass given by

$$\rho_r u_r A_r - \rho_l u_l A_l + \rho_t u_t A_t - \rho_b u_b A_b = 0 \quad (141)$$

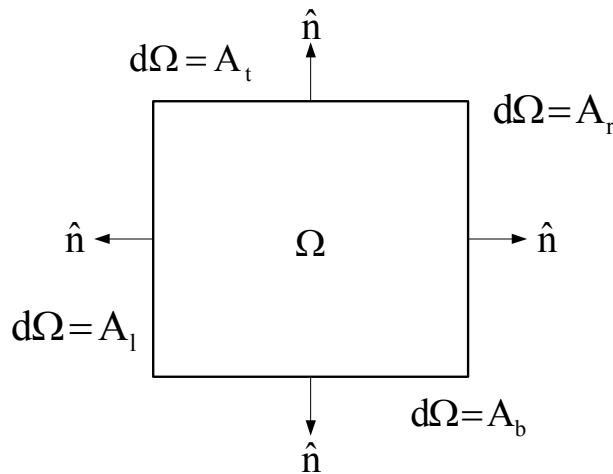


Figure 11. A finite volume.

If we assign and assume the values of ρ at the center of the cells, the values of velocity at the faces of each cell, an offset grid is created which avoids the difficulties associated with $2\Delta x$ instabilities (Hansen, 1996). This discretization is shown in Figure 12.

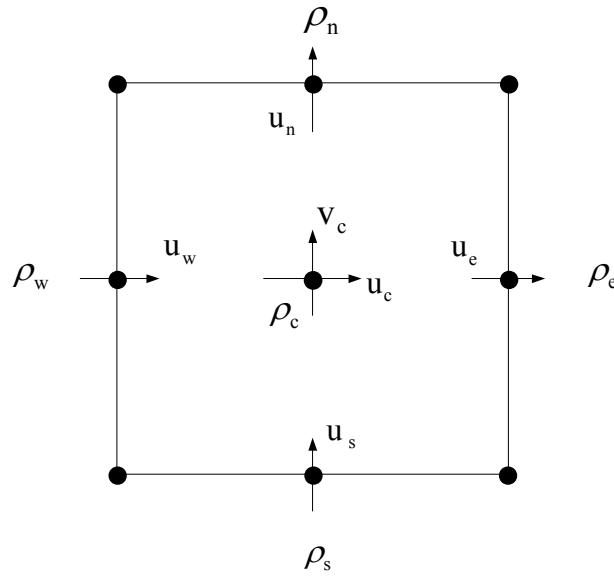


Figure 12. Discretization of a finite volume.

To avoid discretizations that might not have any physical meaning, an upwinding scheme is used. Only the center density belongs to the cell and is considered constant throughout the cell. Therefore ρ_w, ρ_e, ρ_s and ρ_n belong to the adjacent cells and are evaluated at the center of those cells. However, the velocities do belong to the points depicted on the faces of the cell. Upwinding is accomplished as follows

$$(\rho u)_e = \rho_c \text{Max}(u_c, 0) - \rho_e \text{Max}(-u_e, 0) \quad (142)$$

Noticing from Figure 12 that

$$\begin{aligned} A_t &= A_b = \Delta y \\ A_e &= A_w = \Delta x \end{aligned} \quad (143)$$

the discretized equation for mass conservation becomes

$$\int_{\Omega} \nabla \cdot \rho \hat{v} \, d\Omega \equiv \oint_{\Gamma} (\hat{n} \cdot \rho \hat{v}) \, d\Gamma \cong [(\rho u)_e - (\rho u)_w] \Delta y + [(\rho u)_n - (\rho u)_s] \Delta x \quad (144)$$

The momentum equations are developed similarly. If the elements are trapezoidal (2-D) or hexahedral (3-D), the surface areas and normal dot products must be calculated in order to evaluate the correct flux, thereby rendering this system capable of handling a non-orthogonal grid discretization.

7.3 The Finite Element Method

A numerical method that is capable of handling the wide variety of complex problems inherent in today's technology is the finite element method (Zienkiewicz, 1977). The reasons for its popularity include the ability to handle inhomogeneous or variable properties, irregular boundaries, and use of general-purpose algorithms that give high order accuracy. However, traditional finite element methods are not without their faults. The computational effort and storage requirements associated with traditional finite element methods rapidly become excessive when solving fluid flow problems. The bandwidth generated from the computational mesh and assembly procedure is critical when globally formulating the coefficient matrices. Problems involving a large number of nodes become difficult to solve on even the largest and fastest computers. Pepper (1987) and Pepper and Singer (1990) discuss accurate finite element algorithms that are computationally efficient, and are particularly advantageous in modeling large problems on small computers.

Bilinear isoperimetric quadrilateral elements are used to discretize 2-D problem domains; trilinear hexahedral elements are used for 3-D domains. The standard weak formulation of the Galerkin weighted residual technique is employed to cast Equations (1)-(6) into their integral form.

Conservation of Mass

$$\int_{\Omega} \left(\frac{\partial u}{\partial x} + \frac{\partial v}{\partial y} + \frac{\partial w}{\partial z} \right) W_i \, d\Omega = 0 \quad (145)$$

Conservation of Momentum

x-direction

$$\int_{\Omega} \left[\rho \left(\frac{\partial u}{\partial t} + u \frac{\partial u}{\partial x} + v \frac{\partial u}{\partial y} + w \frac{\partial u}{\partial z} \right) + \frac{\partial p}{\partial x} - \frac{\partial \sigma_{xx}}{\partial x} - \frac{\partial \sigma_{xy}}{\partial y} - \frac{\partial \sigma_{xz}}{\partial z} - f_x \right] W_i \, d\Omega = 0 \quad (146)$$

y-direction

$$\int_{\Omega} \left[\rho \left(\frac{\partial v}{\partial t} + u \frac{\partial v}{\partial x} + v \frac{\partial v}{\partial y} + w \frac{\partial v}{\partial z} \right) + \frac{\partial p}{\partial y} - \frac{\partial \sigma_{yx}}{\partial x} - \frac{\partial \sigma_{yy}}{\partial y} - \frac{\partial \sigma_{yz}}{\partial z} - f_y \right] W_i \, d\Omega = 0 \quad (147)$$

z-direction

$$\int_{\Omega} \left[\rho \left(\frac{\partial w}{\partial t} + u \frac{\partial w}{\partial x} + v \frac{\partial w}{\partial y} + w \frac{\partial w}{\partial z} \right) + \frac{\partial p}{\partial z} - \frac{\partial \sigma_{zx}}{\partial x} - \frac{\partial \sigma_{zy}}{\partial y} - \frac{\partial \sigma_{zz}}{\partial z} - f_z \right] W_i \, d\Omega = 0 \quad (148)$$

Conservation of Energy

$$\int_{\Omega} [\rho c_p \left(\frac{\partial T}{\partial t} + u \frac{\partial T}{\partial x} + v \frac{\partial T}{\partial y} + w \frac{\partial T}{\partial z} \right) - \frac{\partial q_x}{\partial x} - \frac{\partial q_y}{\partial y} - \frac{\partial q_z}{\partial z} - Q] W_i d\Omega = 0 \quad (149)$$

Species Concentration

$$\begin{aligned} & \int_{\Omega} \left[\frac{\partial C}{\partial t} + u \frac{\partial C}{\partial x} + v \frac{\partial C}{\partial y} + w \frac{\partial C}{\partial z} \right] W_i d\Omega + \\ & \int_{\Omega} \left[-\frac{\partial}{\partial x} \left(D_{xx} \frac{\partial C}{\partial x} \right) - \frac{\partial}{\partial y} \left(D_{yy} \frac{\partial C}{\partial y} \right) - \frac{\partial}{\partial z} \left(D_{zz} \frac{\partial C}{\partial z} \right) - S \right] W_i d\Omega = 0 \end{aligned} \quad (150)$$

where Ω denotes the computational domain and W_i is the weighting function. The u , v , w , p , T , and C variables are represented by the trial approximations

$$\begin{aligned} u(x, y, z, t) &= \sum N_i(x, y, z) \hat{u}(t) \\ v(x, y, z, t) &= \sum N_i(x, y, z) \hat{v}(t) \\ &\text{etc.} \end{aligned} \quad (151)$$

where N_i is the basis function; in this instance, $W_i = N_i$. The matrix equivalent formulations of Equation (152) are written as

$$\begin{aligned} C^T \vec{V} &= 0 \\ M \dot{\hat{u}} + [K + A(\vec{V})] \hat{u} + C^x p &= F_u \\ M \dot{\hat{v}} + [K + A(\vec{V})] \hat{v} + C^y p &= F_v \\ M \dot{\hat{w}} + [K + A(\vec{V})] \hat{w} + C^z p &= F_w \\ M \dot{\hat{T}} + [K + A(\vec{V})] \hat{T} &= F_T \\ M \dot{\hat{C}} + [K + A(\vec{V})] \hat{C} &= F_C \end{aligned} \quad (152)$$

where the $\dot{\cdot}$ refers to time differentiation, \wedge denotes trial function, and V is the velocity vector. The matrix coefficients are traditionally defined (using the Green-Gauss theorem)

$$\begin{aligned}
\mathbf{K} &= \int_{\Omega} \left(\frac{\partial N_i}{\partial x} \frac{\partial N_j}{\partial x} + \frac{\partial N_i}{\partial y} \frac{\partial N_j}{\partial y} + \frac{\partial N_i}{\partial z} \frac{\partial N_j}{\partial z} \right) d\Omega \\
\mathbf{A}(\vec{V}) &= \int_{\Omega} \left(u_k N_k N_i \frac{\partial N_j}{\partial x} + v_k N_k N_i \frac{\partial N_j}{\partial y} + w_k N_k N_i \frac{\partial N_j}{\partial z} \right) d\Omega \\
\mathbf{C}^x &= \int_{\Omega} N_i \frac{\partial N_j}{\partial x} d\Omega, \quad \mathbf{C}^y = \int_{\Omega} N_i \frac{\partial N_j}{\partial y} d\Omega, \quad \mathbf{C}^z = \int_{\Omega} N_i \frac{\partial N_j}{\partial z} d\Omega \quad (153) \\
\mathbf{C}^T &= \begin{Bmatrix} \mathbf{C}^x \\ \mathbf{C}^y \\ \mathbf{C}^z \end{Bmatrix}
\end{aligned}$$

$$\begin{aligned}
\mathbf{F}_u &= \int_{\Gamma_u} N_i \left(\frac{\partial u}{\partial x} \hat{n}_x + \frac{\partial u}{\partial y} \hat{n}_y + \frac{\partial u}{\partial z} \hat{n}_z \right) d\Gamma_u \\
\mathbf{F}_v &= \int_{\Gamma_v} N_i \left(\frac{\partial v}{\partial x} \hat{n}_x + \frac{\partial v}{\partial y} \hat{n}_y + \frac{\partial v}{\partial z} \hat{n}_z \right) d\Gamma_v \\
\mathbf{F}_w &= \int_{\Gamma_w} N_i \left(\frac{\partial w}{\partial x} \hat{n}_x + \frac{\partial w}{\partial y} \hat{n}_y + \frac{\partial w}{\partial z} \hat{n}_z \right) d\Gamma_w \quad (154) \\
\mathbf{F}_T &= \int_{\Gamma_T} \kappa N_i \left(\frac{\partial T}{\partial x} \hat{n}_x + \frac{\partial T}{\partial y} \hat{n}_y + \frac{\partial T}{\partial z} \hat{n}_z \right) d\Gamma_T \\
\mathbf{F}_C &= \int_{\Gamma_C} N_i \left(K_{xx} \frac{\partial C}{\partial x} \hat{n}_x + K_{yy} \frac{\partial C}{\partial y} \hat{n}_y + K_{zz} \frac{\partial C}{\partial z} \hat{n}_z \right) d\Gamma_C
\end{aligned}$$

where the i , j , and k subscripts denote summation over the local nodes within an element and $d\Gamma_u$, $d\Gamma_v$, $d\Gamma_w$, $d\Gamma_T$, and $d\Gamma_C$ represent boundary segments over which gradients of u , v , w , T , and C are specified.

The use of classical finite element methods to solve fluid flow problems generally requires large amounts of computational storage. The bandwidth generated as a result of the computational mesh and assembly procedures in formulating the coefficient matrices are critical. In addition, classical finite element methods tend to be slower in execution (but not necessarily in convergence to steady state) than finite difference methods as a result of repeated matrix multiplications and global assembly. Equations (153)-(154) are evaluated using Gaussian quadrature with 2 x 2 (2-D quadrilateral) or 2 x 2 x 2 (3-D hexahedral) Gauss points, and the overall global matrix solved via some form of Gaussian elimination. Figure 13 shows the 2-D (four node) and the 3-D (eight node) generic elements.

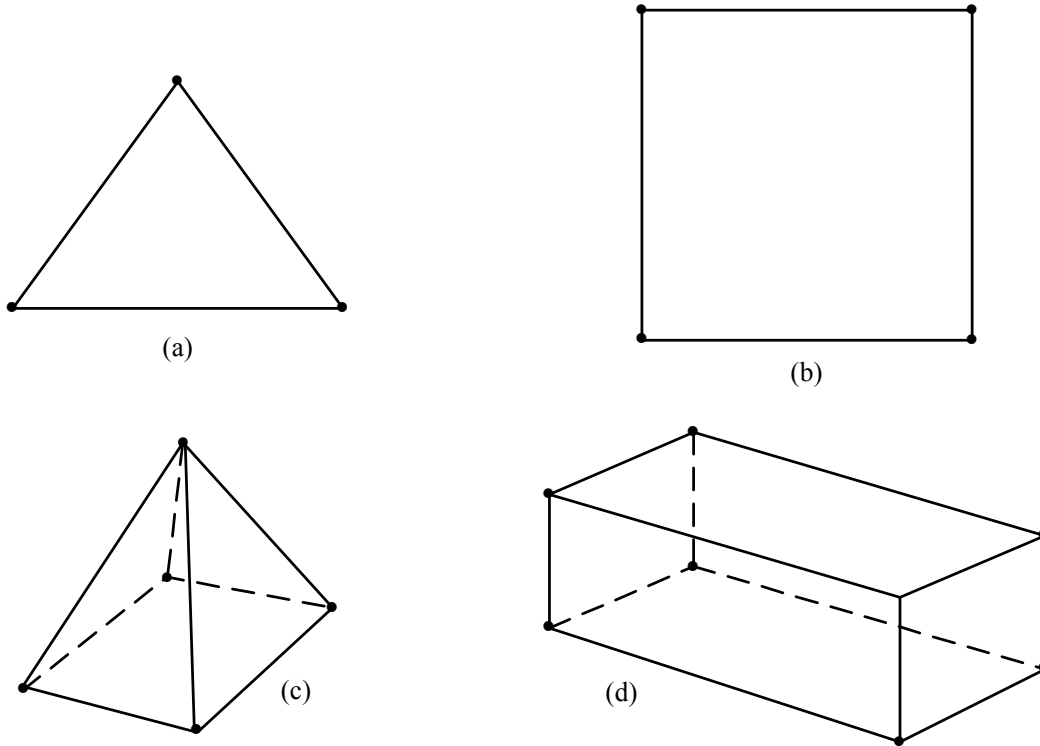


Figure 13. Generic finite elements: (a) 3 node triangle, (b) 4 node bilinear, (c) 5 node tetrahedral, (d) 8 node hexahedral.

7.3.1 Petrov-Galerkin

The Petrov-Galerkin formulation is obtained by perturbing the weighting for the advection term (only) such that

$$W_i = N_i + \frac{\alpha h_e}{2V} \left(u \frac{\partial N_i}{\partial x} + v \frac{\partial N_i}{\partial y} + w \frac{\partial N_i}{\partial z} \right) \quad (155)$$

where h_e is the element size, and α is defined as (Yu and Heinrich, 1986)

$$\alpha = \coth \frac{\beta}{2} - \frac{2}{\beta} \quad (156)$$

with $\beta = |V|h_e R_e / 2$, which is the cell Reynolds number. The use of this weighting function is particularly attractive when coupled with adaptive meshing.

The pressure is obtained from the "discrete" momentum equations and a time-difference version of the continuity equation. An explicit forward-in-time Euler scheme is used to advance the discretized equations in time.

7.4 Mesh Adaptation

Adaptive gridding methods concentrate computational cells in regions where the solution is rapidly changing and leave the grid coarse in regions where the solution is smooth. Because of the tremendous potential adaptive gridding has for reducing computational costs while maintaining the same level of accuracy, it is a forefront area in computational physics. Adaptation can occur within any element shape, i.e., triangles or quadrilaterals, tetrahedrals or hexahedrals (Pelletier and Ilinca, 1994; Pepper and Emery, 1994).

It is often necessary to resolve discontinuities or localized steep gradients in the computational domain; however, the cost of using enough closely spaced zones to resolve those regions as they move throughout the entire computational domain is high. Furthermore, such fine resolution is of no benefit in most of the domain. In these cases, adaptive gridding algorithms are used in which small computational cells are placed only in those regions with large gradients.

Refined localized gridding techniques for boundary layers in steady state calculations have been used for years. For many transient fluid problems with a fixed but complicated boundary geometry, adaptive gridding is used to obtain accurate answers with a modest number of grid points. These problems arise, for example, within interior flows and in external aerodynamics.

In the simplest application of adaptive gridding, equally spaced elements are established initially at the beginning of the calculation (see Figure 14, a-c). They are then adapted in time to the domain boundaries and to average properties of the flow. As the regions in the flow requiring the most accuracy become localized, the elements move relative to the localization, i.e., the gridding algorithm changes the mesh in the course of the calculation to keep the resolution localized where it is needed.

The criterion for clustering closely spaced elements is related to a local variable, such as velocity, temperature, or species concentration. The change in the variables, their derivatives, and their curvatures may be estimated to determine whether more or less resolution is needed, and the cell spacing can be adjusted (or divided as in Figure 14) to minimize the overall error.

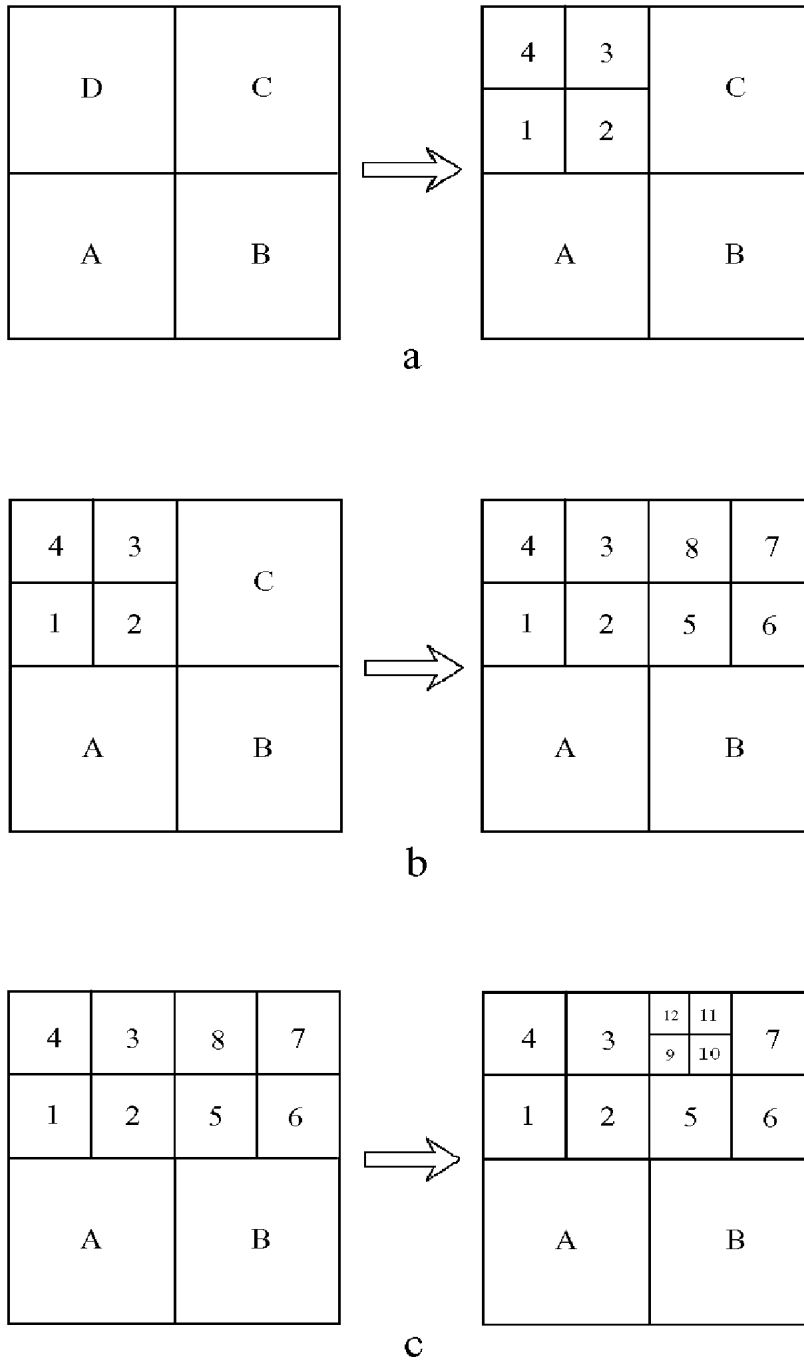


Figure 14. 2-D adaptive sequence.

7.5 Boundary Conditions for Mass Transport Analysis

Gas and particulate flux boundary conditions are of the form

$$q_{p_j} = h_{p_j} (C_{j \text{ at boundary}} - C_{\text{bluk}_j}) \quad (157)$$

where q_{p_j} is the flux rate of the j^{th} particle or substance, C_{bulk_j} is a bulk concentration in the fluid stream, and a boundary concentration $C_{j \text{ at boundary}}$ is just at the boundary.

Such an equation is basic; it is Newton's law of cooling applied to mass. The statement is general and is true for any substance. It is merely stating that the rate of transfer per unit area is the difference in concentration between one place and another multiplied by some constant. Only the convective coefficient h_{p_j} needs determining.

The convective coefficient h_{p_j} in the boundary condition above is determined by geometry, electrostatic forces, gravity, other forces affecting particulate inertia, diffusivities, partial pressures of vapors, chemical bonding, etc.

Another way of formulating the flux term for a strictly diffusion related flux is

$$J_j = D_j \nabla C_j \quad (158)$$

This is Fick's first law of diffusion (Reist, 1993) where J_i is mass flux and in one dimension.

Both forms of boundary conditions have units of mass per unit time per unit area. Different formulations are required as the significance of the forces acting on the mass changes and the type of mass in consideration. For an evaporating liquid, the first form is typically employed. For particulate depositing to a surface, or gases migrating without phase change at the boundary, the second form is more appropriate as it directly incorporates the diffusion coefficient. Particles with one-micron aerodynamic diameter or less do not experience gravitational settling or significant relaxation times. Therefore, a division at one-micron makes a natural delineation between the behavior of larger and smaller particles.

Diffusion, thermophoretic forces, and particle agglomeration (with associated increase in settling velocity) are responsible for deposition. For small particles, a settling velocity is essentially nonexistent. In the absence of inertial, thermophoretic forces and other forces, molecular diffusion through a boundary layer is responsible for most deposition of particles smaller than one micron.

If an analytic boundary layer solution were to be obtained, a deposition velocity could be calculated. The deposition velocity is given by the following diffusion velocity

$$V_d = \frac{\text{Rate of Deposition}}{C_{bulk} - C_{wall+}} \quad (159)$$

and for a concentration at the boundary or wall which is not affecting the rate of deposition (Davies, 1966)

$$V_d = \frac{J_j}{C_{\text{bulk}_j}} \quad (160)$$

For purely diffusive deposition, substituting for $\frac{dC_j}{dx} = \frac{C_{\text{boundary}} - C_{\text{bulk}_j}}{\delta_{p_j}}$, where dx is a boundary thickness over which there is a change in concentration, then

$$V_d = \frac{D_j}{\delta_{p_j}} \quad (161)$$

where V_d is deposition velocity and δ_{p_j} is a boundary layer thickness for the j^{th} particulate. This equation is for the case of sedimentation where the surface concentration is unimportant to the flow (Davies, 1966).

Rate of deposition is not affected by the flow. The difficulty with this equation is the determination of the boundary layer thickness, δ_{p_j} . It is essentially defined as the distance at which the gradient of concentration is zero. The bulk concentration is a function of distance changing in time as material is deposited from the flow.

Deposition of particulate in the numerical model is treated as a flux boundary. The mass flux to the wall has a value of the deposition equal to the deposition velocity. The mechanism for deposition is Fickian diffusion in the absence of other influencing forces. Deposition of inert gases onto a surface is zero. Other gases deposit via some reaction mechanisms for which rates must be specified. For deposition other than by diffusion, rates are generally determined experimentally.

Turbulence provides good mixing; therefore, if a homogenous concentration everywhere beyond the diffusive boundary layer is assumed, the deposition velocity becomes

$$V_d = \frac{\text{Rate of Deposition}}{C_\infty - C_0} = \frac{D_j}{\delta_{p_j}} \quad (162)$$

The difficulty again lies with the determination of δ_{p_j} .

The rate of transport in turbulent flow of a substance towards a surface in nondimensional form is (Davies, 1966)

$$\frac{R}{u_* c_o} = \left(\frac{D_j + \mu_{\text{turb}}}{v_{\text{fluid}}} \right) \frac{dc_+}{dy_+} \quad (163)$$

where:

$c_+ = c / c_o$ is nondimensional concentration at any given time

$y_+ = y u_* / v_{\text{fluid}}$ is nondimensional distance normal to a surface

$V_d = R / c_o$ is the deposition velocity

$u_* = \sqrt{\frac{\tau_w}{\rho_f}}$ is the friction velocity

By substituting these terms, an expression for the nondimensional V_+ is found as

$$\frac{V_+}{u_*} = \left(\frac{D_j + \mu_{\text{turb}}}{v_f} \right) \frac{dc_+}{dy_+} \quad (164)$$

The diffusive term is a linear combination of the turbulent eddy diffusivity μ_{turb} , and Fickian diffusivity, D_j . The deposition velocity is derived from the nondimensional deposition velocity by $V_+ = V_d / u_*$, where u_* is the friction velocity.

As previously mentioned, a numerical model for deposition of particulate is essentially treated as a flux boundary. The mechanism for deposition is Fickian diffusion only through the laminar sublayer. The mechanism for distribution into the turbulent sublayers is by turbulent diffusion. Unless a concentration is specified on the surface, the law of the wall is not necessary for calculation of the mass gradient.

7.6 Boundary Element Method

The boundary element method is a unique numerical scheme, which permits rapid and accurate solution of a specific class of equations (Brebbia and Dominguez, 1989). Employing Green's identity, the boundary element method (BEM) requires only the discretization of the boundary domain - no internal mesh is required as in the finite element method. The BEM reduces the dimensionality of a problem by one (i.e., a two-dimensional problem reduces to a line integral); a three-dimensional problem reduces to a two-dimensional surface formulation. Hence, input data processing consists only of the boundary geometry and boundary condition problem. The governing equation for advection-diffusion utilizing a scalar potential, ϕ , can be written as

$$L[\phi] \equiv \frac{\partial \phi}{\partial t} + \nabla \cdot (-k \nabla \phi) + (V \cdot \nabla) \phi - S \quad (165)$$

where V is the velocity vector, k is the dispersivity tensor, t is time, and S denotes the source density. Assuming steady-state, the governing operator $L[\phi]$ and its adjoint operator $L^*[\psi]$, in which ψ is the adjoint potential associated with ϕ to Green's second identity, can be written as

$$\int_{\Omega} (L[\phi]\psi - L^*[\psi]\phi) d\Omega = \int_{\Gamma} k \left(\phi \frac{\partial \psi}{\partial n} - \frac{\partial \phi}{\partial n} \psi \right) d\Gamma + \int_{\Gamma} V_n \phi \psi d\Gamma \quad (166)$$

where n is the outward normal to ϕ , and V_n is the normal component of V to Γ . If one introduces the fundamental solution ψ^* of $L^*[\psi] = 0$ instead of ϕ , Equation (166) can be rewritten as

$$c_i \phi(r_i) - \int_{\Gamma} q_n^* \phi d\Gamma = - \int_{\Gamma} \psi^* q_n d\Gamma + \int_{\Omega} S \psi^* \quad (167)$$

where c_i denotes a coefficient that depends on the position vector r_i , $q_n^* = n(-k \nabla \psi^* - V \psi^*)$, $q_n = n(-k \nabla \phi)$ and ψ^* is

$$\psi^*(r; r_i) = \exp\{-(V \cdot r' + |V| |r'|)/(2K)\} / (4\pi K |r'|) \quad (168)$$

in which $r' = r - r_i$, where r is the observation point, and $K_0[J]$ is the modified Bessel function of the second kind of order zero. The matrix equivalent form of Equation (167) is

$$[H]\{\Phi\} = [G]\{q\} + \{B\} \quad (169)$$

where $[H]$ and $[G]$ are banded sparse matrices, Φ , q , and B are vectors composed of nodal potentials ϕ , centroidal q_n and discretized domain integrals, respectively.

7.7 Lagrangian Particle Technique

Particle positions are calculated to simulate mass transport from both advection and diffusion. The transport equation can be written in the form

$$\frac{\partial C}{\partial t} + \frac{\partial U_i C}{\partial x_i} = 0 \quad (170)$$

where the velocity vector U_i is expressed in terms of advection and "flux" diffusion (Runchal, 1980)

$$U_i = \hat{U}_i + U_{f_i} \quad (171)$$

with U_i being the true advection velocity vector and the "flux" velocity defined as

$$U_{f_i} = -\sum_j \frac{K_{ij}}{C} \frac{\partial C}{\partial x_j} \quad (172)$$

By combining the advection and diffusion terms together, a total equivalent transport velocity can be obtained. The form of the transport equation becomes identical to the equation of continuity for a general compressible fluid. The original problem of turbulent diffusion is transformed into one describing the advective changes of fluid density in a compressible fluid moving in a velocity field of total equivalent transport velocities. Mass particles are synonymous with density and follow the fluid motion in the velocity field, i.e., they are Lagrangian particles in a non-solenoidal field of total equivalent transport velocity. Their number in any location (volume) determines the concentration of pollutant for the original diffusion problem.

The probability distribution function for a three-dimensional space is (Runchal, 1980)

$$P_{x_i}(x_i, t) = \frac{1}{(4\pi t)^{\frac{3}{4}} (K_1 K_2 K_3)^{\frac{1}{2}}} \exp\left\{-\sum_{i=1}^3 \frac{(x_i - U_i t)^2}{4K_{it}}\right\} \quad (173)$$

where x_i are the position vectors in the direction of the principal axes and $K_1 K_2 K_3$ are the diagonal components of the second-order dispersion tensor in the direction of the principal axes.

The transport equation for this distribution can be written as $P=P(x_i, t)$

$$\frac{\partial P}{\partial t} + \frac{\partial}{\partial x_i} (U_i P) = \frac{\partial}{\partial x_i} (K_{ij} \frac{\partial P}{\partial x_j}) \quad (174)$$

where the tensor summation convention has been employed and K_{ij} is a second-order dispersion tensor. The inclusion of particle decay, settling, and more complex dispersion processes involving specified turbulence correlations, and can be included in Equation (174).

The problem of transport of particles by advection and dispersion commonly represented by a deterministic transport equation such as Equation (174) can also be represented simply as a series of random walks. Each of these random walks is composed of a deterministic advection component and a random component.

For example, the increment in the position vector of a particle at any time t can be written as

$$x_t - x_o = \int_{t_o}^t U(x_{t'}, t') d't + \int_{t_o}^t D(x_{t'}, t') dw_{t'} \quad (175)$$

where D is a deterministic forcing function for the random component of motion. Equation (175) can be expressed simply as

$$\delta x(w, t) = \delta x_U + \delta x_D \quad (176)$$

with

$$\delta x_D(w, t) = \int_{t_o}^t n_r \sqrt{2K} d't \quad (177)$$

where D is assumed equivalent to K and n_r is a normally distributed random number with a mean value of zero, and a standard deviation of unity. The integral Equation (174) can be further simplified to

$$\begin{aligned} \delta x_D &= n_r \sigma \\ \sigma^2 &= \int_{t_o}^t 2K d't \end{aligned} \quad (178)$$

The variance obtained from Equation (175) is the same as that from Equation (174). Thus, Equation (172) can be written as

$$x_t - x_o = \int_{t_o}^t U(x_{t'}, t') d't + n_r \left\{ \int_{t_o}^t (2K(x_{t'}, t') d't) \right\}^{1/2} \quad (179)$$

For a rigorous application of the random walk method, the net particle displacement must be calculated by integration of Equation (179). However, with U and K as arbitrary functions of space and time, it is not always possible to obtain a closed form solution. It is generally sufficient to assume that the mean velocity and random components can be separately calculated and linearly superimposed.

For steady or quasi-steady flows, the time scale of particle motion is much smaller than the characteristic time scale of change in the mean velocity and the dispersion fields. In such a case, it is often more convenient to express U and K as functions of the position vector x_i , rather than as Lagrangian functions of time.

In the application of the random walk model, the particle displacement in each of the coordinate directions is independently calculated from the displacement algorithm, Equation (179). Before this is performed, however, the mean velocity, U , and the dispersion due to turbulence or other stochastic mechanisms must be specified. The velocity of any particle is obtained from the application of the BEM, which can be used to obtain velocity components anywhere within the problem domain without the need for a nodal mesh or interpolation. A general

probability distribution or correlation function for the random component of motion due to dispersion is utilized to account for the dispersivity tensor, K .

The calculation to advance the particle configuration in time proceeds in steps, or cycles, each of which calculates the desired quantities for time $t + \Delta t$ in terms of those at time t . Hence,

$$x_i(t + \Delta t) = x_i(t) + U_i \Delta t \quad (180)$$

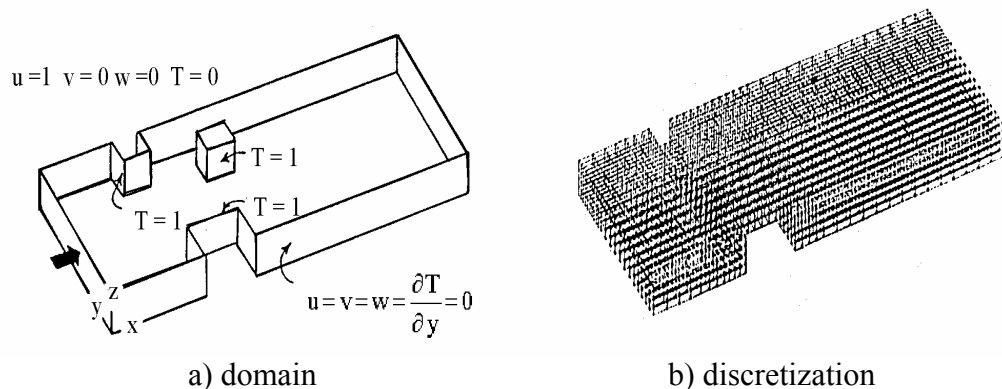
The velocity components are the fictitious total velocities determined for the beginning of the time interval and initial particle positions. Every particle is advanced in each cycle to a new position using Equation (180). Thus, the particle traces out in time a trajectory for the pollutant mass. Boundary conditions are introduced by modifications of the fictitious total velocities. Solid boundaries are simulated by not allowing particles to be transported across the boundaries. In each cycle, the fictitious total velocity for each cell is calculated as the sum of the advection velocity and the random turbulent flux velocity. The particle positions are updated using an interpolated total velocity. The concentration per unit volume is calculated from the particle masses.

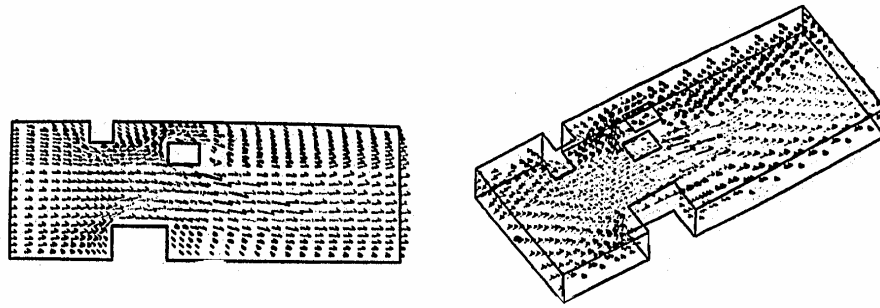
7.8 CFD Examples

Example 1: 3-D Airflow Around Heated Obstacles

For this problem, 3-D airflow is calculated around a set of heated obstacles. The physical domain and mesh are shown in Fig. 15 (a,b). The mesh consists of 2868 hexahedral elements; the Reynolds number is $Re = 10^3$ and $Pr = 1.0$. This type of problem commonly occurs in HVAC where obstructions are encountered within the flow domain.

Figure 15 (c,d) gives normal and perspective views of the 3-D velocity vectors within the channel. Recirculation of the flow occurs behind the blocks and small secondary cells develop in the corners. Thermal plumes emanate from the heated blocks; plume impingement from the left forward block occurs on the small mid-stream block. It is well known that when flow separates at the corners of blocks, horseshoe-like vortices are generated (Hunt et al., 1978).



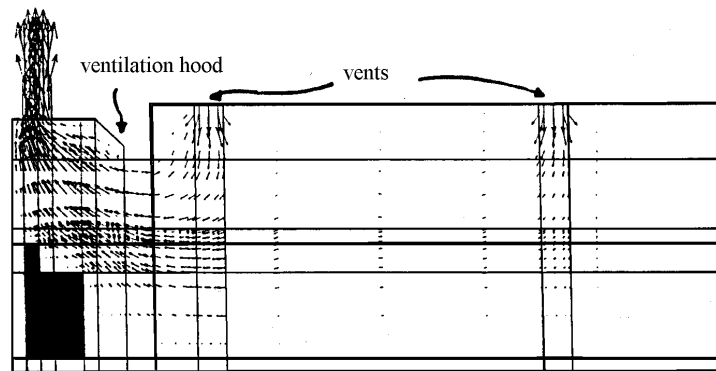


c) plane view of velocity vectors d) 3-D view of velocity vectors

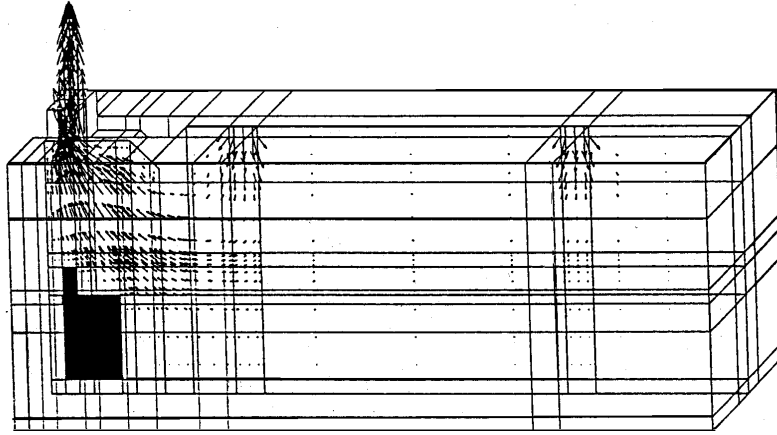
Figure 15. Airflow around heated obstacles.

Example 2: Air Flow over a Heated Oven within a Commercial Kitchen

In this simulation, air enters the kitchen from two ceiling vents (and entrainment from the right open boundary), passes over the heated surface of the oven, and exits through the upper left corner of the exhaust hood as shown in Figure 16 (a-c). The heated surface acts to enhance the air motion, eventually accelerating the room air out the domain, and illustrates the ability of the spectral-element method to accommodate mixed convection problems (where the flow transitions from motion due strictly to natural convection to strongly forced convection).



a) velocity vectors in side view of kitchen



b) velocity vectors in 3-D view of kitchen

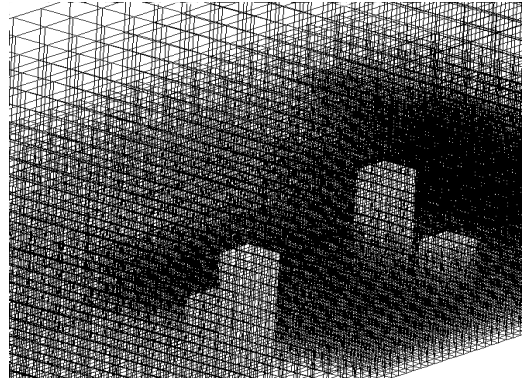


c) isotherms

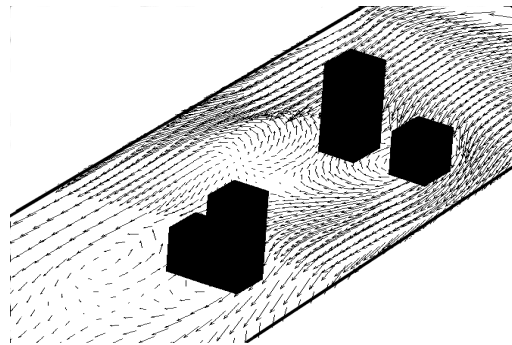
Figure 16. Flow over a heated oven in a commercial kitchen.

Example 3: 3-D Particulate Transport over Barriers

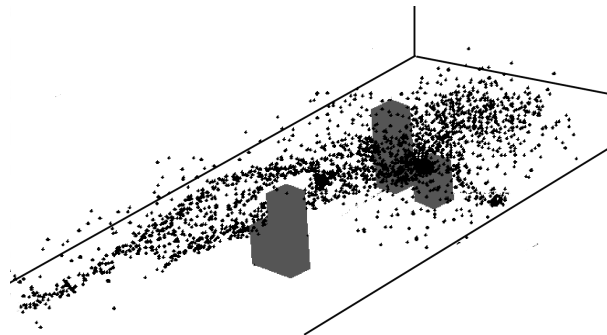
This example problem is modeled as a three-dimensional isothermal flow with a contaminant source located in front of the barriers. In this problem, the physical domain contains different size barriers. Three-dimensional hexahedrals are used to model the domain as shown in Figure 17 (a-c). The Petrov-Galerkin technique is used to eliminate numerical oscillations since there is a strong advection component to the problem. In this instance, the finite element method is used to establish the problem domain.



a) h-adapted finite element mesh



b) velocity vectors in horizontal plane



c) Lagrangian particles released into flow

Figure 17. 3-D particulate flow over a set of barriers.

A three-dimensional simulation of the airflow within the room is first calculated; mid-level velocity streak lines are shown in Figure 17 (b). A continuous source is released and the trajectory of the plume is illustrated using Lagrangian particles. In this simulation, two different particle sizes (light and heavy) are used, and the particles are advected and diffused in 3-D (Figure 17 c). Notice the plume of the light particles as they begin to disperse over the lower of the two barriers. The heavy particles eventually settle to the floor behind the first barriers. The simulations replicate the dispersion, and clearly show the spread of contaminant (e.g., smoke, based on particulate size).

Example 4: BEM-LPT model of particle dispersion

Figure 18 (a-c) shows the flow of air and particulate paths within a vented room. An [animation](#) is provided in the CD-ROM version of the book. Particles are released from a source located on the floor of the room. When the door on the right side of the room is opened, the plume bends towards the door, and begins to flow towards the lower pressure. The dispersion pattern of the particulates is more widely spread when the door is open – this is due primarily to the size of the opening.

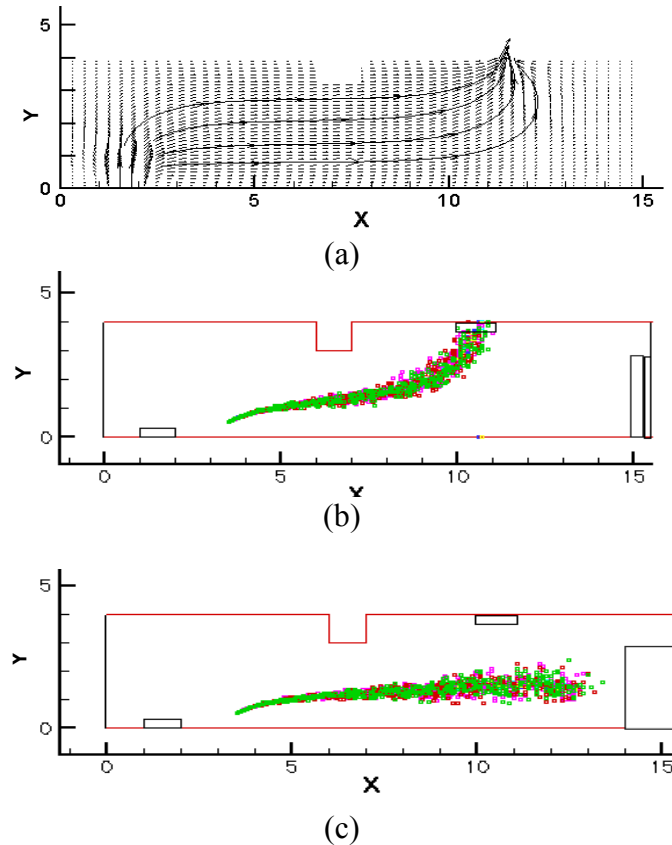


Figure 18. Indoor flow and particulate dispersion (a) velocities and streamlines, (b) door closed, and (c) door opened. An [animation](#) is provided in the CD-ROM version of the book.

7.9 Model Verification and Validation

A great deal of work has been done on verifying and validating results obtained with numerical models. Such efforts include comparing results between numerical and analytical models, sensitivity analyses, and seeing how well the numerical model predicts actual results obtained from experimental data. This latter comparison can be fairly tricky if some of the parameters, e.g., exchange coefficients, are not known in the actual experiment. A detailed discussion on model verification and validation can be found in the text by Roache (1998).

Efforts involved in validating and verifying numerical results with experimental data are not trivial - evaluations and comparisons must be carefully considered. These techniques include measures of difference, Pearson, Spearman, and Kendall correlations, skewness and kurtosis, tests for normality, and scatter diagrams (Pepper, 1981). These analyses help to provide insight into the physics of indoor air quality, and enable relations to be constructed to more reliably predict exposures.

References

- Anderson, D.A, Tannehill, J.C, and Pletcher, R.H., *Computational Fluid Mechanics and Heat Transfer*, Hemisphere, Wash., DC, 1984.
- American Society of Heating, Refrigerating and Air-Conditioning Engineers, *ASHRAE Handbook 1981 Fundamentals Volume*, Chpt. 22, Atlanta, GA, 1981, pp. 22.1-22.20
- Ames, B. N., Magaw, R., and Gold, L. S., "Ranking Possible Carcinogenic Hazards," *Science*, 236, 17 April 1987, pp. 271-280.
- Awbi, H. B., "Application of Computational Fluid Dynamics in Room Ventilation," *Build. Environ.*, 24, 1989, pp. 73-84.
- Awbi, H. B., *Ventilation of Buildings*, Chapman and Hall, London, 1991.
- Brain, J. D. and Beck, B. D., "Bioassays for Mineral Dusts and Other Particulates, *In Vitro Effects of Mineral Dusts*, E. B. Beck and J. Bignon (Eds.), NATO ASI Series Vol. G3, Springer Verlag, Berlin, 1985, pp. 323-335.
- Brebbia, C. A. and Dominguez, J., *Boundary Elements, An Introductory Course*, Comp. Mech. Pub., Southampton, U.K., 1989.
- Carrington, D. B., "Finite Elements with h-adaptation for Momentum, Heat, and Mass Transport with Application to Environmental Flow," Ph.D. Dissertation, University of Nevada - Las Vegas, Department of Mechanical Engineering, Las Vegas, NV, 2000.
- Carslaw, H. S. and Jaeger, J. C., *Conduction of Heat in Solids*, Oxford University Press, London, UK, 1947.
- Cooper, D. C., Alley, F. C., *Air Pollution Control A Design Approach*, 2nd edition, Prospect Heights, Illinois, Waveland Press, Inc., 1994.
- Davidson, L., "Numerical Simulation of Turbulent Flow in Ventilated Rooms," PhD. Thesis, Chalmers Univ. of Tech., Gotenborg, 1989.
- Davies, C. N., *Chapter XII Deposition from Moving Aerosols*, C. N. Davies (Ed.), *Aerosol Science*, NY, NY, Academic Press, 1966, pp. 409-428.
- Deardorff, J. W., "A Numerical Study of Three-Dimensional Channel Flow at Large Reynolds Numbers," *J. Fluid Mech.*, 41, 1970, pp. 453-480.
- Eguchi, Y., Yagawa, G., and Fuchs, L., "A Conjugate-Residual-FEM for Incompressible Viscous Flow Analysis," *Comp. Mech.*, Vol. 3, No. 1, 1988, pp. 59-72.

Fletcher, C.A.J., "Computational Techniques for Fluid Dynamics - Volume II," 2nd ed., Springer-Verlag, NY, 1991, pp. 47-78.

Fuchs, N. A., *The Mechanics of Aerosols*, Pergamon Press, NY, 1964.

Gosman, A. D., Pun, W. M., Runchal, A. K., Spalding, D. B., and Wolfshtein, M., *Heat and Mass Transfer in Recirculating Flows*, Academic Press, London, 1969.

Gosman, A. D., Nielsen, P. V., Restivo, A., and Whitelaw, J. H., "The Flow Properties of Rooms with Small Ventilation Openings," *Trans. ASME, J. Fluid Engr.*, 102, 1980, pp. 316-323.

Gresho, P. M., Chan, S. T., Lee, R. L., and Upson, C. D., "Modified Finite Element Method for Solving the Time-Dependent Incompressible Navier-Stokes Equations, Part 1, Theory," *Int. J. Num. Meth. Fluids*, 4, 1984, pp. 557-598.

Hansen, G. A., "Scalability of Preconditioners as a Strategy for Parallel Computation of Compressible Fluid Flow," Ph.D. Dissertation, University of Idaho, Department of Computer Science, Idaho Falls, ID, 1996.

Harlow, F. H. and Welch, J. E., "Numerical Calculation of Time-Dependent Viscous Incompressible Flow of Fluid with Free Surfaces," *Phys. Fluids*, 8, 1965, pp. 2182-2189.

Hayes, S. M., Gobbell, R. V., and Ganick, N. R., *Indoor Air Quality: Solutions and Strategies*, McGraw-Hill, Inc., NY, 1995.

Heinsohn, R. J., *Industrial Ventilation: Engineering Principles*, J. Wiley & Sons, NY, 1991.

Hjertager, B. H. and Magnussen, B. F., "Numerical Prediction of Three-Dimensional Turbulent Buoyant Flow in a Ventilated Room," *Heat Transfer and Turbulent Buoyant Convection*, D. B. Spalding and N. Afgan (Eds.), Vol. II, Hemisphere, Washington, DC, 1977, pp. 429-441.

Hunt, J.C., Abell, C.J., Peterka, J.A., and Woo, H., "Kinematical Studies of the Flows around Free or Surface Mounted Obstacles; Applying Topology to Flow Visualization," *J. Fluid Mech.*, 86, 1, 1978, pp.179-200.

Hinds, W.C., *Aerosol Technology – Properties, Behavior, and Measurement of Airborne Particles*, J. Wiley & Sons, NY, Inc., 1982, pp. 155-156.

Jones, W. P. and Launder, B. E., "The Prediction of Laminarization with a Two-Equation Model of Turbulence," *Int. J. Heat Mass Transfer*, 15, 1972, pp. 301-314.

Markatos, M. C. and Cox, G., "Hydrodynamics and Heat Transfer in Enclosures Containing a Fire Source," *Phys. Chem. Hydrodyn.*, 5, 1984, pp. 53-66.

Martin, R.A., Tang, P.K., Harper, A.P., Novat, J.D., and Gregory, W.S., *Material Transport Analysis for Accident-Induced Flow in Nuclear Facilities*, NUREG/CR-3527, Los Alamos, NM, Los Alamos National Laboratory, 1983.

Moult, A. and Dean, R. B., "CAFE-A Computer Program to Calculate the Flow Environment," CAD 80, *4th Int. Conf. on Computers in Design Engineering*, Brighton, UK, 1980.

Murakami, S., Tanaka, T., and Kato, S., "Numerical Simulation of Air Flow and Gas Diffusion in Room Model - Correspondence between Numerical Simulation and Model Experiment," *Proc. 4th CIB Int. Symp. on the Use of Computers for Environmental Engineering Related to Buildings*, Tokyo, 1983, pp. 90-95.

Murakami, S., Kato, S., and Suyama, Y., "Three-Dimensional Numerical Simulation of Turbulent Airflow in a Ventilated Room by Means of a Two-Equation Model," *ASHRAE Trans.*, 93(2), 1987, pp. 621-642.

Nielsen, P. V., "Flow in Air Conditioned Rooms," PhD Thesis, Tech. Univ. of Denmark, 1974.

Nielsen, P. V., "Contamination Distribution in Industrial Areas with Forced Ventilation and Two Dimensional Flow," *Int. Inst. of Refrigeration, Joint Meeting E1*, Essen, W. Germany, 1981, pp. 223-230.

Pasquill, F. and Smith, F. B., *Atmospheric Diffusion*, 3rd Ed., Ellis Horwood Ltd., Chichester, UK, 1985.

Patankar, S. V. and Spalding, D. B., "A Calculation Procedure for Heat, Mass, and Momentum Transfer in Three-Dimensional Parabolic Flows," *Int. J. Heat Mass Transfer*, 15, 1972, pp. 147-163.

Patankar, S. V., *Numerical Heat Transfer and Fluid Flow*, Hemisphere, NY, 1980.

Pelletier, D. and Ilinca, F., "An Adaptive Finite Element Method for Mixed Convection Heat Transfer," presented at the 32nd AIAA Aerospace Sci. Meeting, Jan. 10-13, 1994, Reno, NV, paper AIAA-94-0347

Pepper, D. W., "Modeling of Three-Dimensional Natural Convection with a Time-Split Finite Element Technique," *Num. Heat Transfer*, Vol. 11, 1987, pp. 31-55.

Pepper, D. W. and Singer, A. P., "A Modified Finite Element Method for the Personal Computer," *Num. Heat Transfer*, Vol. 11, 1990, pp. 31-55.

Pepper, D. W. and Emery, A. F., "Atmospheric Transport Prediction using an Adaptive Finite Element Method," *Proc. 5th Int. High Level Rad. Waste Manag. Conf.*, 1994, pp. 1946-1952.

Pepper, D. W., "Results from the Savannah River Laboratory Model Validation Workshop, Nov. 19-21, 1980," *Proceedings of the 5th Symp. on Turbulence, Diffusion, and Air Pollution*, March 9-13, 1981, Atlanta, GA.

Pozrikidis, C. (1999), *Little Book of Streamlines*, Academic Press, San Diego, CA.

Pruppacher, H. R. and Klett, J. D., *Microphysics of Clouds and Precipitation*, D. Reidel Pub. Co., Dordrecht, Holland, 1978.

Reist, P.C., *Aerosol Science and Technology*, 2nd Ed., McGraw-Hill, Inc., NY, 1993.

Repace, J. L. and Lowery, A. H., "Indoor Air Pollution, Tobacco Smoke, and Public Health," *Science*, 208, May 1980, pp. 464-472.

Roache, P. J., *Verification and Validation in Computational Science and Engineering*, Hermosa Pub., Albuquerque, NM, 1998.

Runchal, A. K., "A Random Walk Atmospheric Dispersion Model for Complex Terrain and Meteorological Conditions," *2nd AMS Joint Conf. on Appl. of Air Pollution Meteor.*, March 24-27, 1980, New Orleans, LA.

Sakamoto, Y. and Matsuo, Y., "Numerical Predictions of Three-Dimensional Flow in a Ventilated Room using Turbulence Models," *Appl. Math. Modelling*, Vol. 4, 1980, pp. 67-71.

Thompson, J. F., Warsi, Z. U. A., and Martin, C. W., *Numerical Grid Generation*, North-Holland, NY, 1985.

Vargaftik, N. B., *Tables on the Thermophysical Properties of Liquids and Gases*, 2nd Ed., Hemisphere Pub. Corp., Washington, DC, 1975.

Woo, T-C. and Hwang, C. C., *Classic Analytical Problems in Mechanical Engineering*, R. T. Edwards, Inc., Flouertown, PA, 2000..

Yu, C.C. and Heinrich, J.C., "Petrov-Galerkin Methods for the Time-Dependent Convective Transport Equation," *Int. J. Num. Methods in Engr.*, Vol. 23, 1986, p. 883-890.

Zienkiewicz, O.C., *The Finite Element Method*, McGraw Hill, London, 1977.

Chapter 15

Modeling of Adverse Effects

A brief introduction to the topic “Modeling of Adverse Effects” was presented in Volume I of this book series. A Chapter on this topic (15A – Modeling of Health Risks Associated with Combustion Facility Emissions) is included in the following pages. Other chapters are expected to be published in Volume III as follows:

15A - Modeling of Health Risks Associated with Combustion Facility Emissions

15B - Odor Modeling

15C - Visibility Modeling

15D - Ecological Adverse Effects

15E - Global Issues

For additional information, the reader can visit:

- <http://www.epa.gov/ebtpages/airairpollutioneffects.html>
The US EPA site on air pollution effects
- <http://www.cdc.gov/nceh/airpollution/>
The site of the Air Pollution and Respiratory Health Program of the National Center for Environmental Health, Centers for Disease Control and Prevention (CDC)
- <http://www.nywea.org/clearwaters/302140.html>
Models and methods for odor dispersion

- <http://www.epa.gov/oar/visibility/>
The US EPA site on visibility impairment due to air pollution
- http://www.hc-sc.gc.ca/hecs-sesc/air_quality/faq.htm
Frequently asked questions pertaining to the health effects of air pollution
- <http://www.arb.ca.gov/research/apr/past/health.htm>
Air Pollution Research Reports/Studies - Health Effects of Air Pollution
- <http://enhs.umn.edu/5103/vehicular/adverse.html>
Vehicular Exhaust and Air Pollution – Adverse Effects
- <http://www.ipcc.ch/index.htm>
Site of the Intergovernmental Panel on Climate Change (IPCC) assessment of climate change. Recognizing the problem of potential global climate change, the World Meteorological Organization (WMO) and the United Nations Environment Programme (UNEP) established the Intergovernmental Panel on Climate Change (IPCC) in 1988. It is open to all members of the UN and WMO. The role of the IPCC is to assess on a comprehensive, objective, open and transparent basis the scientific, technical and socio-economic information relevant to understanding the scientific basis of risk of human-induced climate change, its potential impacts and options for adaptation and mitigation
- <http://yosemite.epa.gov/oar/globalwarming.nsf/content/index.html>
The US EPA site on global warming
- http://www.ghcc.msfc.nasa.gov/MSU/hl_temp_ud.html
A discussion of the earth temperature variation and trends
- http://www.ssmi.com/msu/msu_data_description.html
Satellite measurements of the earth's temperature
- <http://www.giss.nasa.gov/data/update/gistemp/2004/>
Global Temperature Trends: 2004 Summation
- <http://www.aip.org/history/climate/index.html>
Discussion on global warming
- <http://www.envirocomp.org/html/publish/GlobalWarming/GWreport-text.pdf>
Debate issues on global climate change

Richter, R.O. and P.J. Sheehan 2005. *Modeling of Health Risks Associated with Combustion Facility Emissions*. Chapter 15A of *AIR QUALITY MODELING - Theories, Methodologies, Computational Techniques, and Available Databases and Software. Vol. II – Advanced Topics* (P. Zannetti, Editor). Published by The EnviroComp Institute (<http://www.envirocomp.org/>) and the Air & Waste Management Association (<http://www.awma.org/>).

Chapter 15A

Modeling of Health Risks Associated with Combustion Facility Emissions

Richard O. Richter ⁽¹⁾ and Patrick J. Sheehan ⁽²⁾

⁽¹⁾ *Exponent, Irvine, CA (USA)*

rrichter@exponent.com

⁽²⁾ *Exponent, Oakland, CA (USA)*

psheehan@exponent.com

Abstract: As part of the Resource Conservation and Recovery Act (RCRA) permitting process, the U.S. EPA regulates emissions from hazardous waste combustion facilities on a site-specific basis. The agency requires that human health and ecological risk assessment be conducted in order to evaluate the impacts of the chemicals emitted. To achieve consistency, the EPA has developed a protocol for estimating both human and ecological risks. In this chapter, the protocol developed by the EPA for human health risk assessment is described and the results of a case study, based on this protocol, are presented. Special attention is given to the uncertainties in risk estimates associated with the methods and default parameter values in the protocol.

Key Words: human health, risk assessment, combustion facilities, hazardous waste incinerators, fate and transport modeling, direct and indirect chemical exposures.

1 Introduction

Characterizing health risks associated with potential chemical exposures from combustion facility emissions is a complex process that generally involves modeling the emissions of hundreds of chemicals from multiple sources, modeling the airborne dispersion of the emitted chemicals, and modeling direct and indirect exposures for individuals at specific locations surrounding a facility. This chapter describes the process and methods that are used to estimate health

risks posed by emissions from combustion facilities. It also provides a risk assessment case study of a combustion facility.

Since 1990, the United States Environmental Protection Agency (EPA) has generated a series of documents to use in estimating carcinogenic risks and noncarcinogenic hazards, which are associated with both direct and indirect exposures to chemicals emitted from combustion facilities. This effort culminated in 1998 with EPA's publication of the Human Health Risk Assessment Protocol for Hazardous Waste Combustion Facilities (HHRAP) (U.S. EPA, 1998a). The three volumes with 2,000 pages of documents provide the approach, equations, and parameters necessary to calculate the concentrations of emitted chemicals in various environmental media, and to estimate the human health risks and hazards associated with their uptake by humans. The EPA uses the results of these risk assessments in permitting hazardous waste combustors and boiler/industrial furnaces that are regulated under the Resource Conservation and Recovery Act (RCRA). In addition, it is quite likely that this protocol will see greater use in permitting and evaluating of other emission sources, not just those permitted under the RCRA.

The HHRAP provides the framework and methods for evaluating risks, but application of the guidance requires collection and input of substantial site, land use, and chemical-specific information. This paper presents a case study describing the application of the HHRAP to a hazardous waste combustion facility and discusses some of the issues associated with its application.

1.1 Conceptual Site Model

The conceptual site model (Figure 1) graphically describes the pathways through which emitted chemicals enter various media by which humans can be exposed. Air dispersion modeling is used to model the transport of particles and vapors emitted from the combustion units and their associated equipment. Chemicals of potential concern (COPC) are partitioned between the particle and vapor phases as functions of their vapor pressures. At specific receptor locations around the facility, there are five modeled values for each chemical and source—vapor and particle concentrations, wet vapor deposition rates, and dry and wet particle deposition rates.

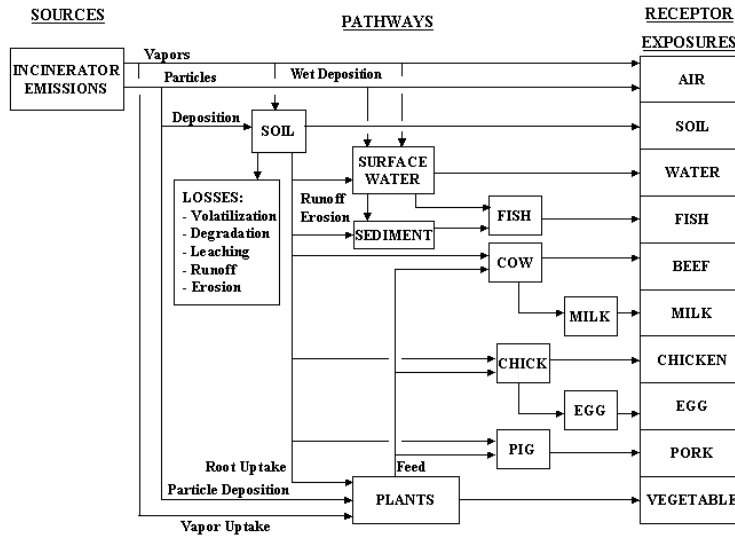


Figure 1. Conceptual site model.

The COPC enter soils, plants, and water bodies, where they accumulate over time. Farm animals bioaccumulate the chemicals from ingestion of affected soil and plants. Thus, chemical concentrations are calculated for beef, milk, pork, chicken, and eggs. Similarly, fish bioaccumulate the chemicals from the water and sediments, so chemical concentrations in edible fish tissues are estimated. Exposures are then calculated for adult and child residents, subsistence farmers, and subsistence fishers. The residential exposure pathways include direct inhalation of particles and vapors, incidental ingestion of affected soil, and consumption of homegrown vegetables and drinking water. The subsistence fisher exposure pathways are assumed to be the same as those for the resident, plus ingestion of fish. The subsistence farmer is assumed to be exposed via the same pathways as the resident, plus ingestion of homegrown beef, pork, milk, chicken, and eggs. In addition, the uptake rates of carcinogenic dioxins/furans via ingestion of mother's breast milk are evaluated for the infants of the resident, farmer, and fisher.

1.2 HHRAP Process

The HHRAP process requires numerous steps to estimate risks and hazards. They can be broken down into the following tasks:

1. Facility Characterization, in which the facility is evaluated to determine the sources, COPC emitted and emission rates.
2. Air Dispersion Modeling to determine the airborne concentrations and deposition rates at the media and receptor locations surrounding the facility.
3. Exposure Scenario Identification, which selects the locations and types of receptors to be evaluated.

4. Estimation of Media Concentrations, in which the concentrations of the various COPC are estimated in the air, water, soil, sediments, and biota.
5. Exposure Quantification, in which the intake rates of the affected media are used to estimate the doses of chemicals received by the receptors.
6. Toxicity Assessment, in which the quantitative relationship between dose and effect is determined for each chemical, and the toxicity criteria for COPC are determined.
7. Risk and Hazard Characterization, in which the estimated risks and hazards are estimated based on the average daily doses and the toxicity criteria for all of the chemicals.
8. Uncertainty Interpretation, wherein the uncertainties and limitations associated with the risk assessment process are discussed.

2 Case Study

The case study is based on a risk assessment for a chemical plant with a hazardous waste combustion unit facility in the southeastern United States that was evaluated in accordance with EPA's HHRAP.

2.1 Facility Characterization

The goal of the facility characterization is to identify and quantify the emissions released from the sources at the site. The characterization includes identification of sources, identification of COPC, and estimation of emission rates in grams per second (g/s).

2.2 Source Identification

The first step in characterizing the facility is identifying all potential emission sources related to the burning of hazardous wastes. Stack emissions are point sources that release chemicals under normal operating and control conditions of the combustion units. Fugitive emissions are those from other regulated sources associated with the combustion process. Generally area sources, fugitive emissions sources, include tanks, piping, and material-handling equipment used with the combustion units. Fugitive emissions are also considered from sources associated with the post-process treatment and handling of residues from the combustion process.

For this case study, two point sources and two area sources were identified. The point sources, S-1 and S-2, are two 30-meter stacks associated with combustors that recover energy from liquid organic wastes to heat boilers. The two area sources, A-1 and A-2, are the piping and tanks associated with the incineration units.

2.3 COPC Identification

COPC are selected based on knowledge of the wastes fed to the incinerator, the products of incomplete combustion, and the air pollution control system being used. For existing or similar facilities, COPC can be identified from the results of stack testing conducted during risk assessments or trial burns. The EPA HHRAP requires that COPC be identified “based on their potential to pose an increased risk or hazard via one or more direct or indirect exposure pathways”.

The following steps describe the COPC selection process:

1. Prepare a list that includes all of the analytes from the stack tests and any fugitive emissions.
2. Evaluate the list against the waste-feed streams and potential fugitive emissions to determine whether any non-detects should be deleted.
3. Delete compounds that are non-detect, not in the waste-feed stream, and do not have toxicological data.
4. Delete compounds that are non-detect, not in the waste-feed stream, and/or are not likely to be products of incomplete combustion (PIC).
5. Evaluate the 30 tentatively identified compounds with the greatest emissions to determine whether they should be evaluated qualitatively.
6. Keep any non-detect compounds that could possibly be emitted based on site-specific conditions.

For this site, 192 possible COPC were identified. Using the above procedures, 60 non-detects were eliminated. Thus, the final list included 132 COPC: the 17 congeners of polychlorinated dibenzo-*p*-dioxins (PCDD) and polychlorinated dibenzofurans (PCDF) for which toxicity data exist, 2 polycyclic aromatic hydrocarbons (PAH), 64 halogenated organic compounds, 36 other organic compounds, 10 metals, chlorine, hydrogen chloride, and carbon disulfide.

2.4 Emission Rates

For the two point sources, S-1 and S-2, the emission rates under normal operating conditions were derived based on an evaluation of the data from stack tests. For the area sources, A-1 and A-2, their total emission rates were estimated based on measurements of fugitive volatile organic compounds (VOC) emitted from pumps, valves, flanges, and release valves. All of the emission rates were calculated in terms of g/s.

2.5 Air Dispersion Modeling

The goal of the air dispersion modeling is to estimate the average concentrations and deposition rates at the specific locations of the media and receptors surrounding the facility. Typically, the Industrial Source Complex Short-Term (ISCST) Model is used to model each source. The model requires site-specific information about the sources, surrounding terrain and land uses, receptors, and meteorologic conditions. The HHRAP requires a rectangular receptor grid out to 50 km in each direction from the center of the sources. The spacing between nodes is 100 m from the source out to 3 km, 500 m from 3 to 10 km, and 1,000 m from 10 to 50 km. Typically, 15 model runs may be required for each source—five 1-year runs each for vapor phase, particle phase, and particle-bound emissions. The modeling runs are all based on a unit emission rate of 1 g/s for each source.

For this case study, the runs for the stacks included vapor, particle phase (mass-weighted), and particle-bound (area-weighted) modeling, while the runs for the area sources included only vapor modeling. From the output, the following 5-year average unit concentrations and deposition rates were calculated from each source for each receptor location.

- Vapor-phase concentrations ($\mu\text{g}/\text{m}^3$ per g/s) and wet vapor deposition rates ($\text{g}/\text{m}^2\text{-yr}$ per g/s)
- Particle-phase concentrations ($\mu\text{g}/\text{m}^3$ per g/s) and dry and wet deposition rates ($\text{g}/\text{m}^2\text{-yr}$ per g/s)
- Particle-bound concentrations ($\mu\text{g}/\text{m}^3$ per g/s) and dry and wet deposition rates ($\text{g}/\text{m}^2\text{-yr}$ per g/s)

As shown in Figures 2a through 2t, the contours for the 5-year average values form two distinct patterns. The contours were hourglass-shaped with maximums north and south of the facility for the concentrations and dry deposition rates related to the stacks. The contours were centered about the site for the concentrations related to the area sources and for the wet deposition rates for all the sources. The former patterns are due to the fact that the prevailing winds are from the north and south, and that maximums for a stack are at a distance from the source, while the latter patterns are caused by rain washing out both particles and vapors before they can travel far from the source.

2.6 Exposure Scenario Identification

Exposure scenarios are based on characterizing the surrounding area, evaluating recommended exposure scenarios, and establishing the locations of the receptors. Each exposure scenario consists of a receptor and various pathways by which the receptor can be exposed to chemicals emitted from the facility. The exposure pathways can be either direct or indirect. In this case, the only major direct pathway of potential consequence is the inhalation of COPC in the vapor and particulate phases. Indirect pathways include ingestion of affected media,

including: soil, homegrown produce, drinking water, beef, milk, chicken, eggs, pork, and fish. For infants, the uptake of dioxins and furans is via ingestion of breast milk.

In accordance with the HHRAP, nine human exposure scenarios were evaluated:

- Resident: adult, child, and breast-fed infant
- Subsistence fisher: adult, child, and breast-fed infant
- Subsistence farmer: adult, child, and breast-fed infant

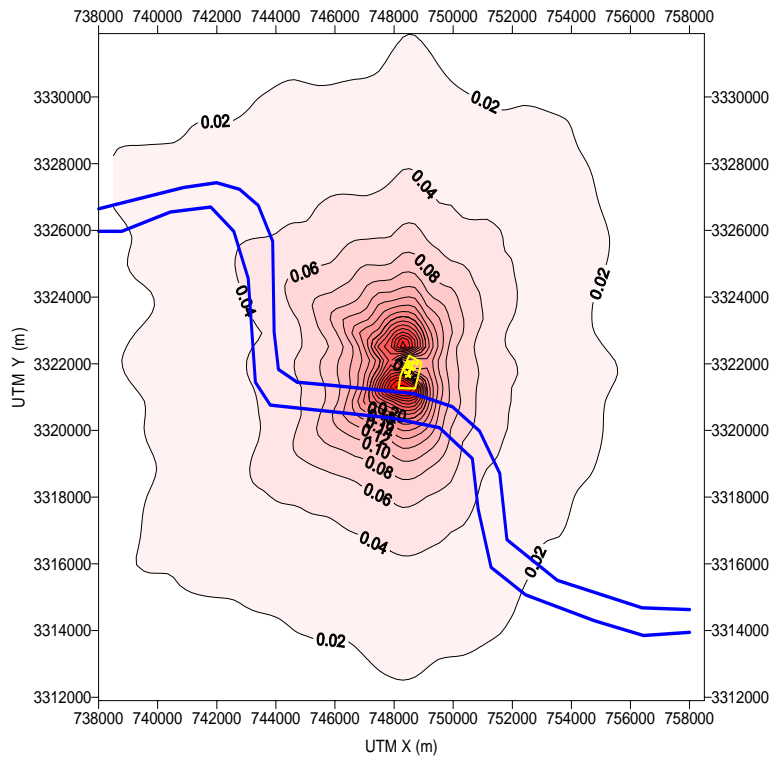


Figure 2a. Predicted normalized 5-year average concentration for vapor phase for incinerator stack S-1.

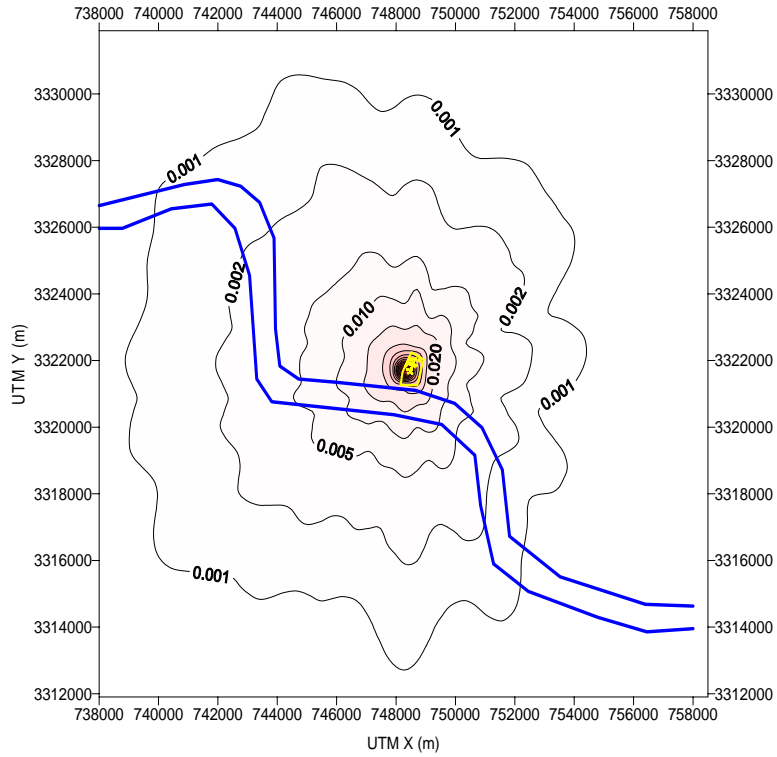


Figure 2b. Predicted normalized 5-year wet deposition for vapor phase for incinerator stack S-1.

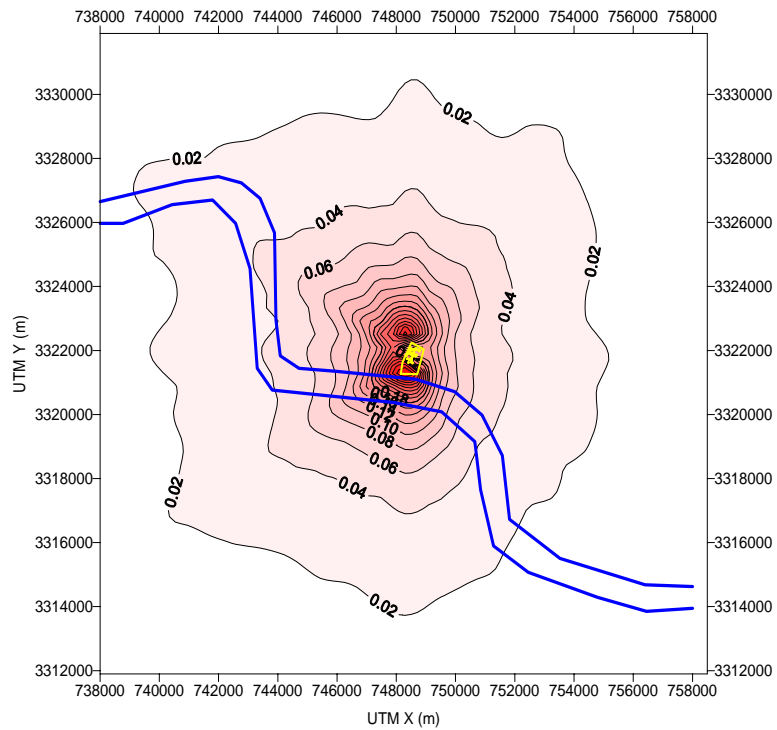


Figure 2c. Predicted normalized 5-year average concentration for particulate phase for incinerator stack S-1.

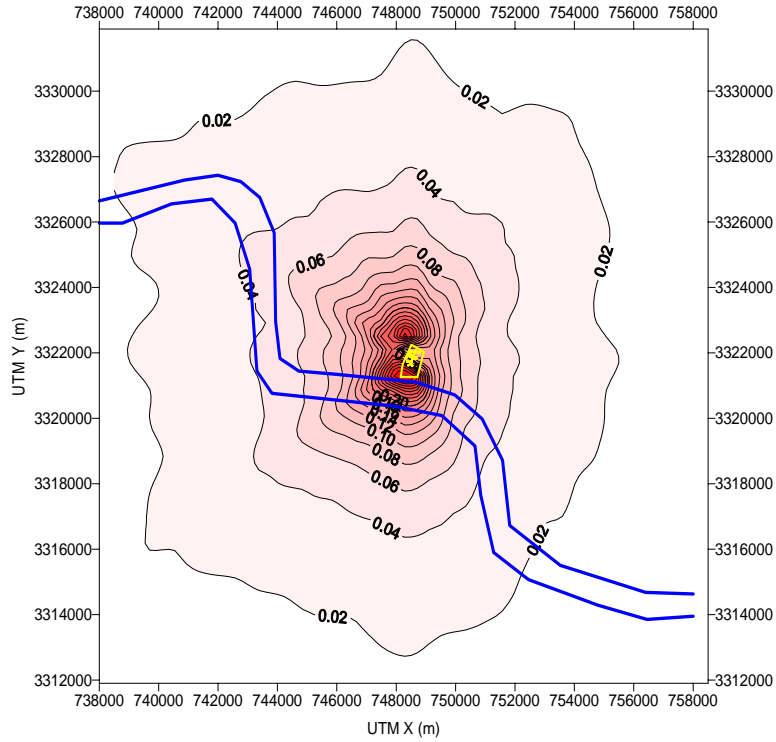


Figure 2f. Predicted normalized 5-year average concentration for particle-bound phase for incinerator stack S-1.

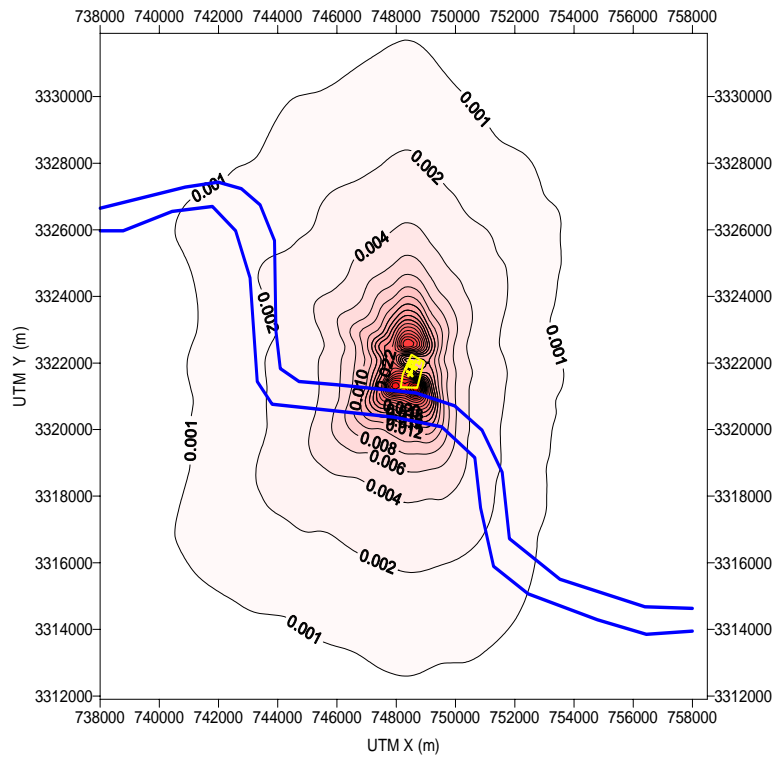


Figure 2g. Predicted normalized 5-year dry deposition for particle-bound phase for incinerator stack S-1.

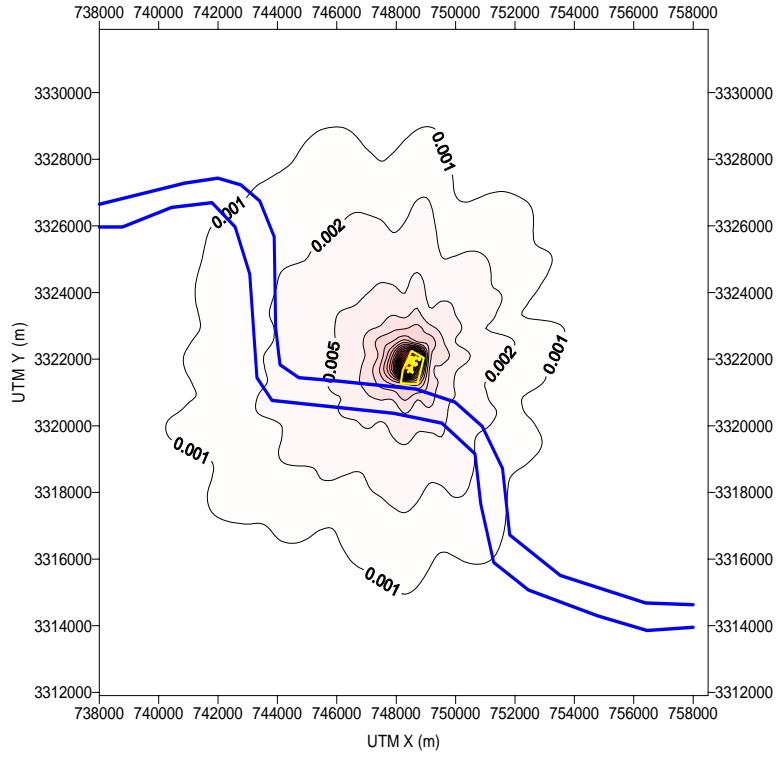


Figure 2h. Predicted normalized 5-year wet deposition for particle-bound phase for incinerator stack S-1.

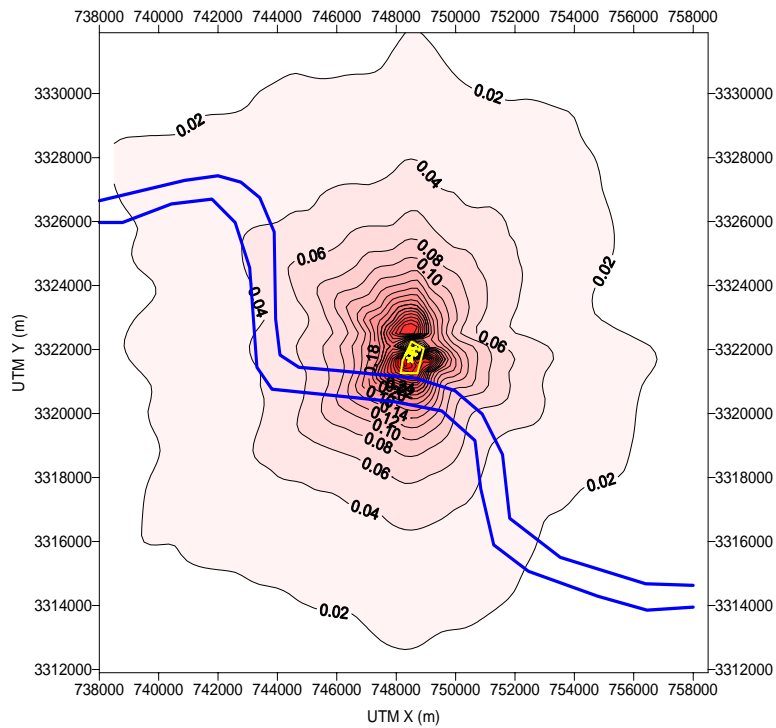


Figure 2i. Predicted normalized 5-year average concentration for vapor phase for incinerator stack S-2.

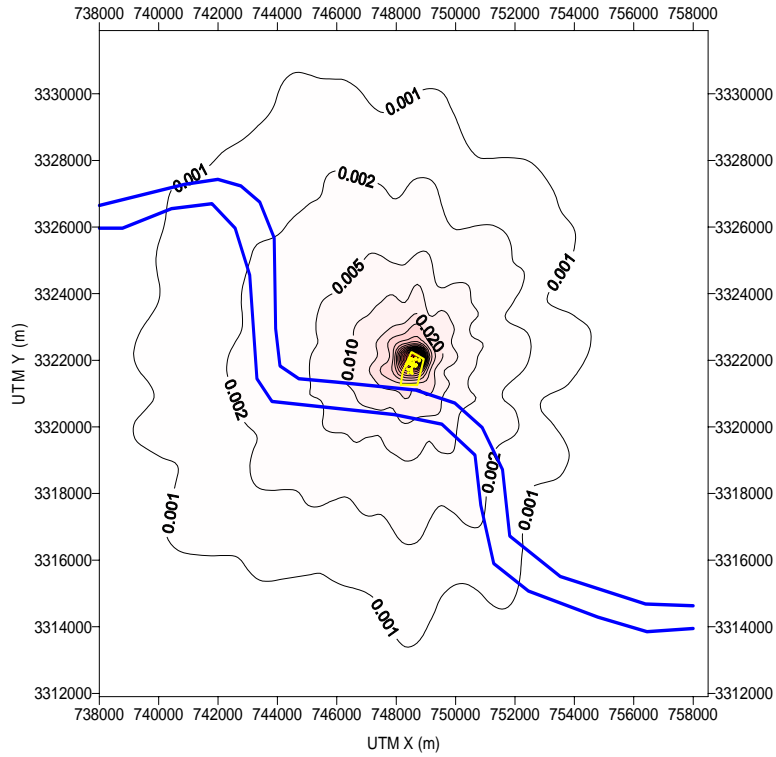


Figure 2j. Predicted normalized 5-year wet deposition for vapor phase for incinerator stack S-2.

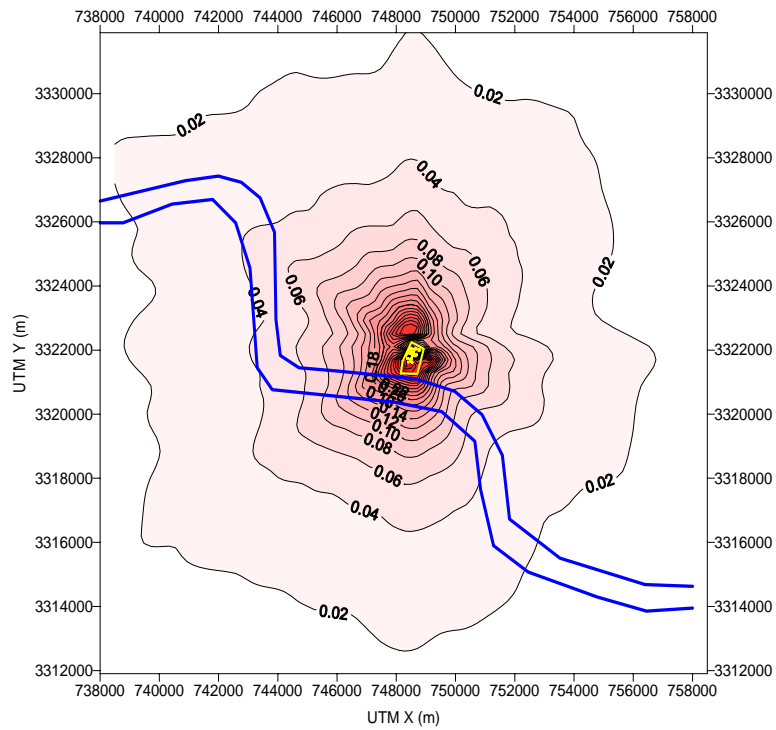


Figure 2k. Predicted normalized 5-year average concentration for particulate phase for incinerator stack S-2.

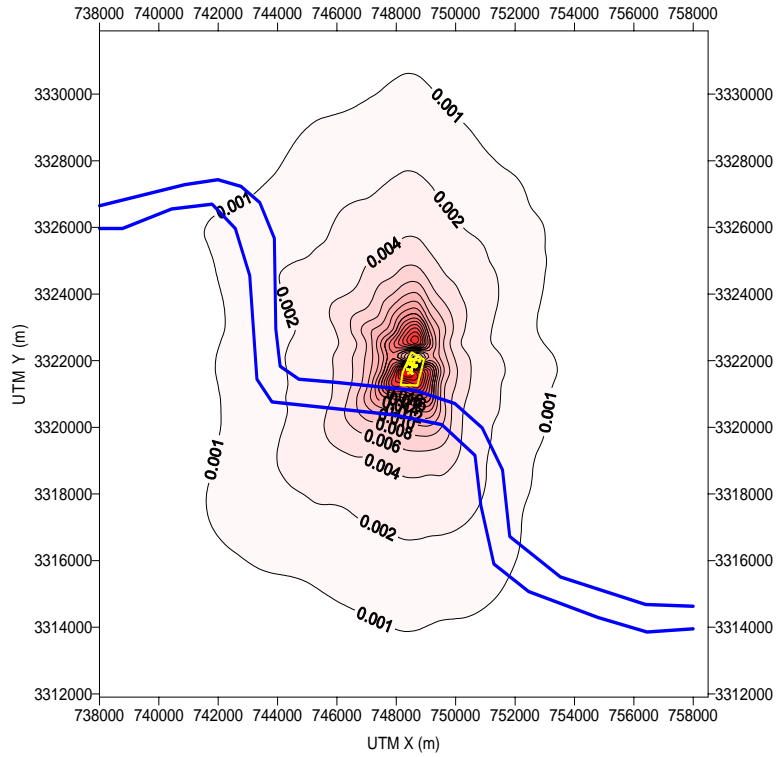


Figure 2l. Predicted normalized 5-year dry deposition for particulate phase for incinerator stack S-2.

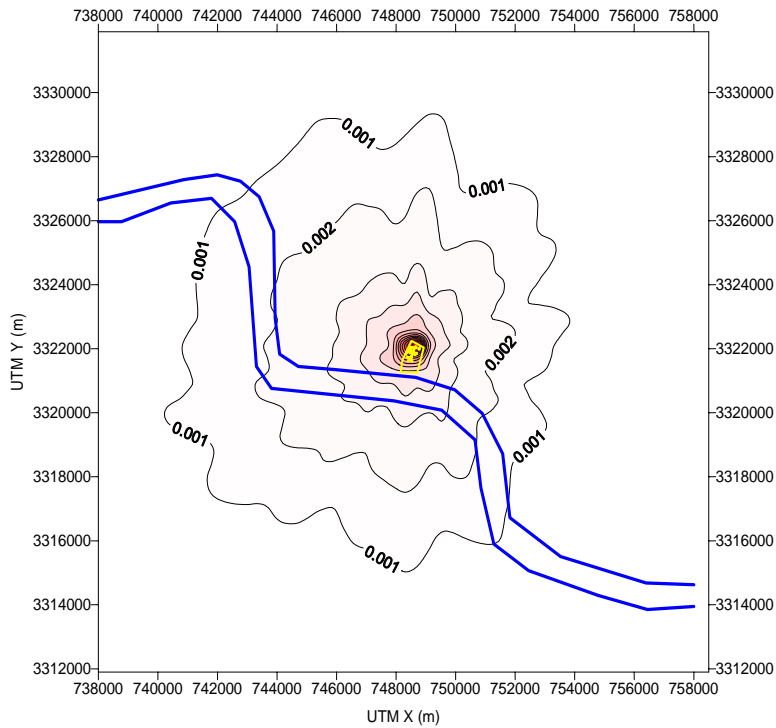


Figure 2m. Predicted normalized 5-year wet deposition for particulate phase for incinerator stack S-2.

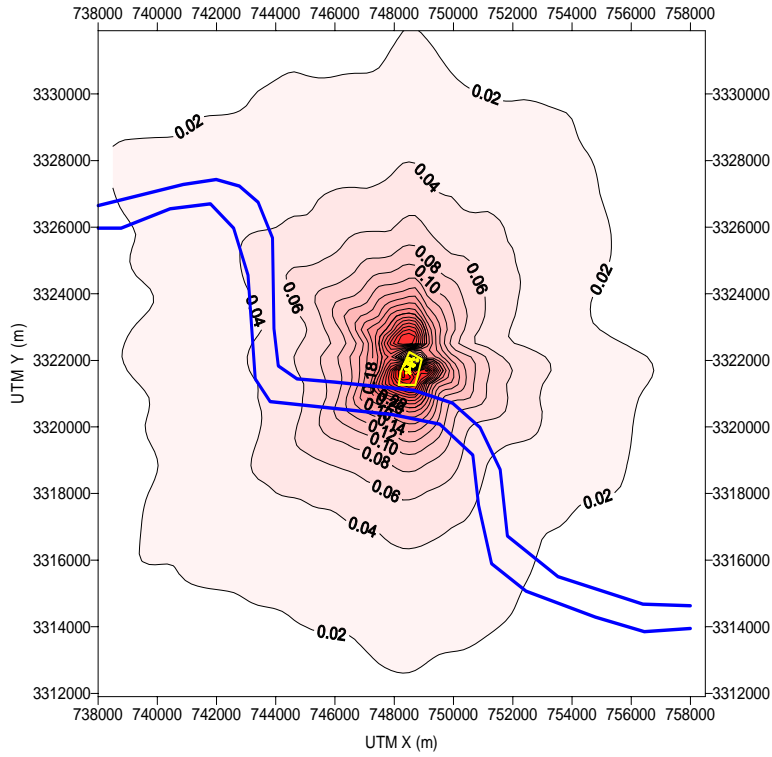


Figure 2n. Predicted normalized 5-year average concentration for particle-bound phase for incinerator stack S-2.

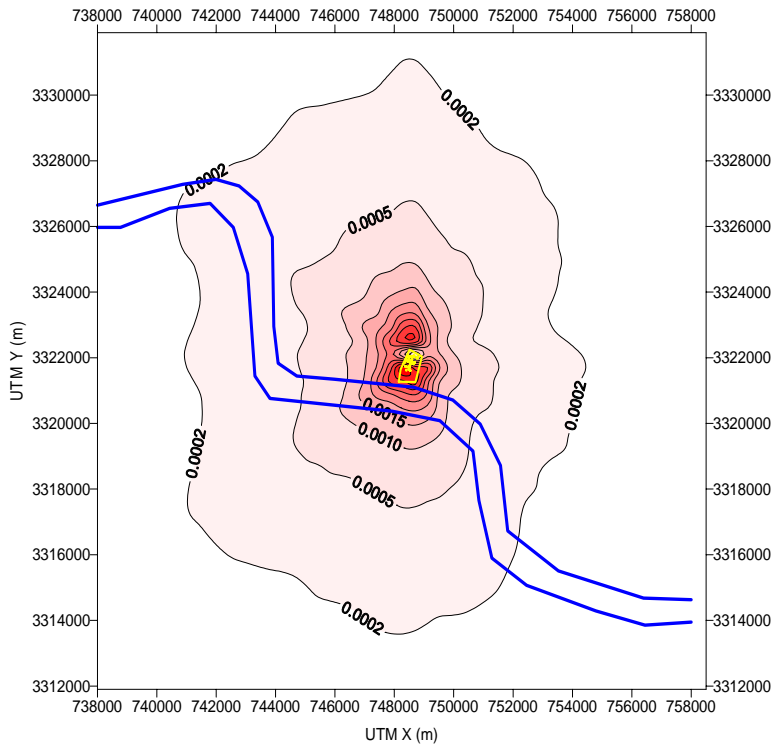


Figure 2o. Predicted normalized 5-year dry deposition for particle-bound phase for incinerator stack S-2.

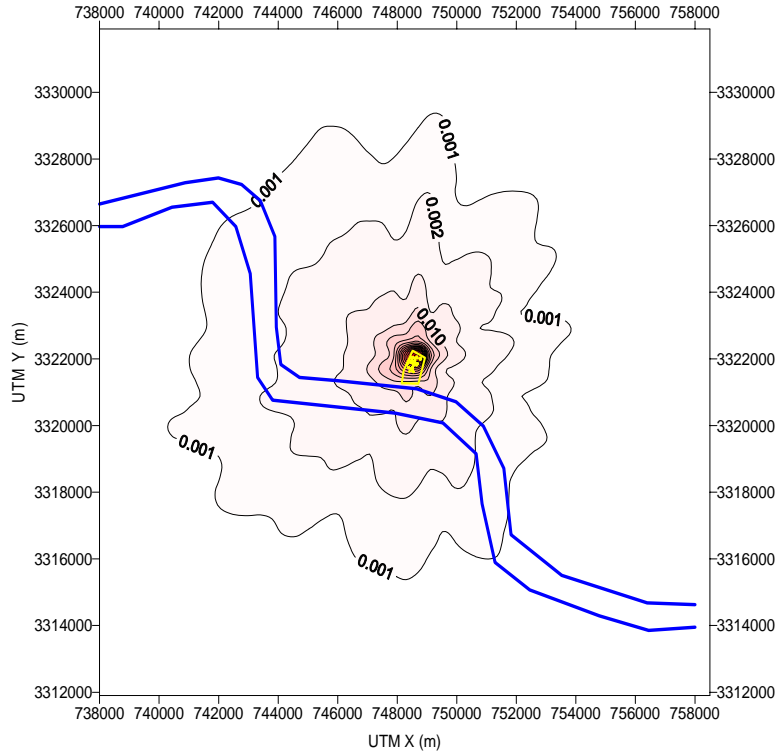


Figure 2p. Predicted normalized 5-year wet deposition for particle-bound phase for incinerator stack S-2.

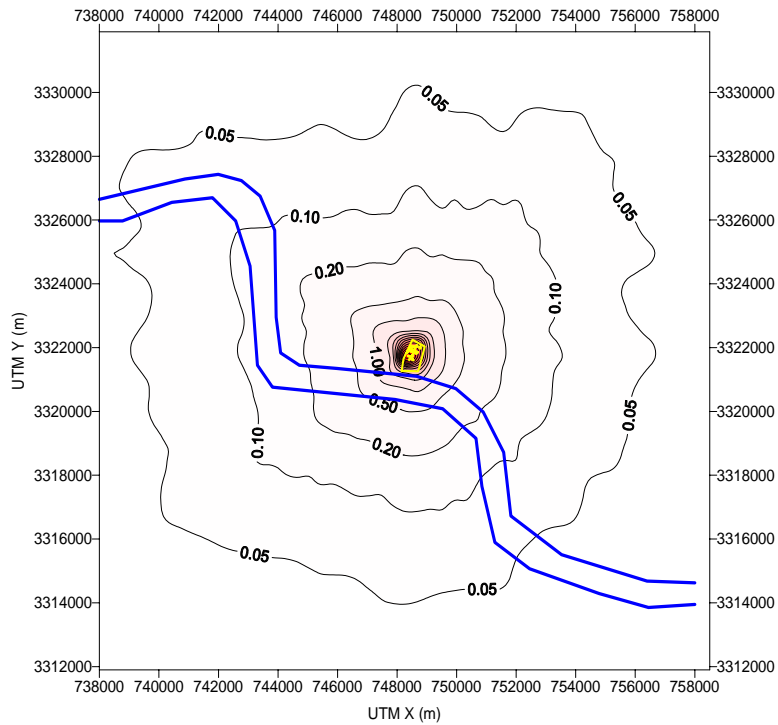


Figure 2q. Predicted normalized 5-year average concentration for vapor phase for fugitive source A-1.

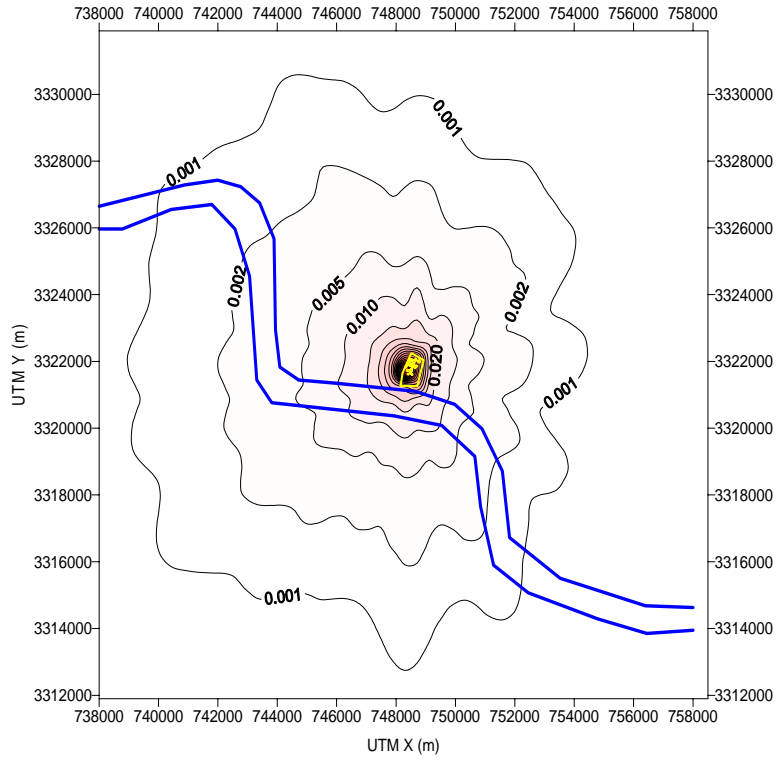


Figure 2r. Predicted normalized 5-year wet deposition for vapor phase for fugitive source A-1.

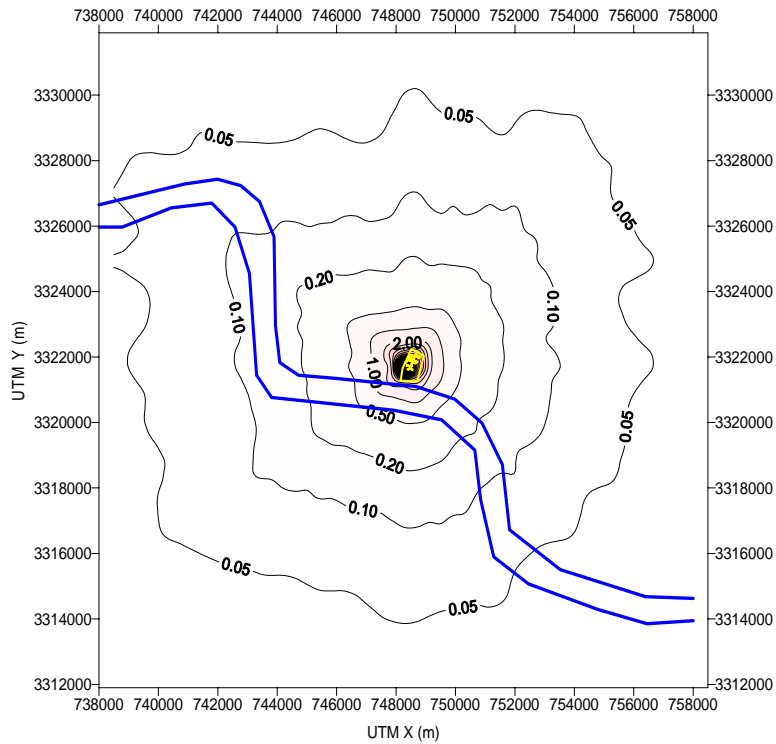


Figure 2s. Predicted normalized 5-year average concentration for vapor phase for fugitive source A-2.

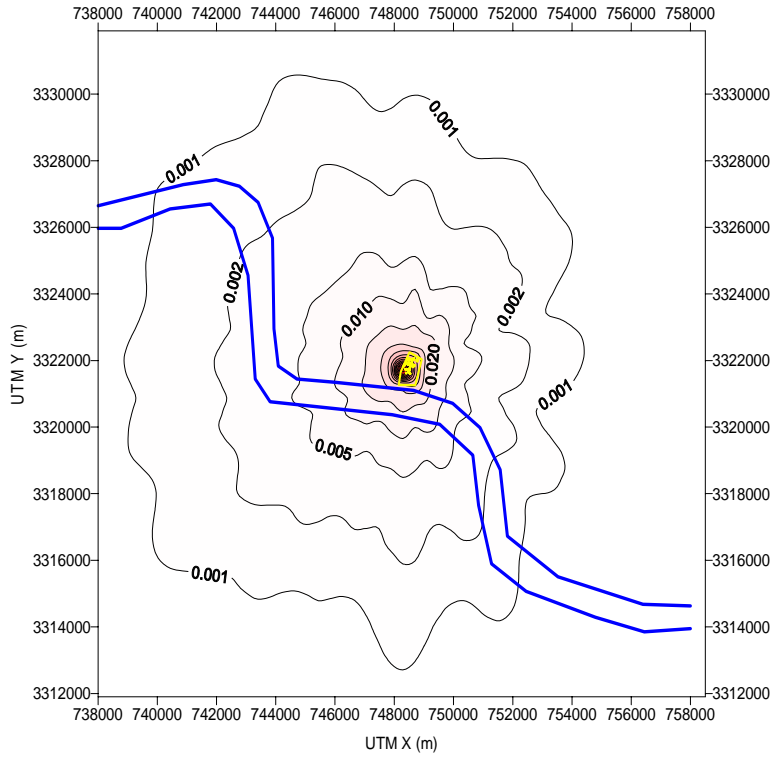


Figure 2t. Predicted normalized 5-year wet deposition for vapor phase for fugitive source A-2.

Table 1 lists the exposure pathways for each of the nine scenarios.

Table 1. Exposure scenarios for evaluation.

Exposure Pathways	Receptors ^a						
	Adult Farmer	Child Farmer	Adult Fisher	Child Fisher	Adult Resident	Child Resident	Breast-Fed Infants ^b
Inhalation of vapors and particulates	•	•	•	•	•	•	
Incidental ingestion of soil	•	•	•	•	•	•	
Ingestion of drinking water from surface-water sources	•	•	•	•	•	•	
Ingestion of breast milk							•
Ingestion of homegrown produce	•	•	•	•	•	•	
Ingestion of homegrown beef	•	•					
Ingestion of milk from homegrown cows	•	•					
Ingestion of homegrown chickens	•	•					
Ingestion of eggs from homegrown chickens	•	•					
Ingestion of homegrown pork	•	•					
Ingestion of fish			•	•			

Source: U.S. EPA (1998a)

^a Exposure scenarios as the combinations of exposure pathways evaluated for a particular receptor.

^b Infant exposure to polychlorinated dibenzo-*p*-dioxins and polychlorinated dibenzofurans via the ingestion of their mother’s breast milk is evaluated as separate exposure pathway.

Based on land-use patterns, concentrations, and deposition rates, the maximum likely human receptors were determined to exist at one of three general locations, as shown on Figure 3. Theoretical receptors were placed at 100-m intervals in each area. Residential locations A-1 through A-12, which are the closest possible residences west of the site, are approximately 3 km away from the facility. Residential locations E-13 through E-34, the closest possible residences south of the site, are approximately 1.5 km away, across a river. Residential locations F-35 through F-54, the closest possible residences to the eastern border of the facility, are directly adjacent to the facility.

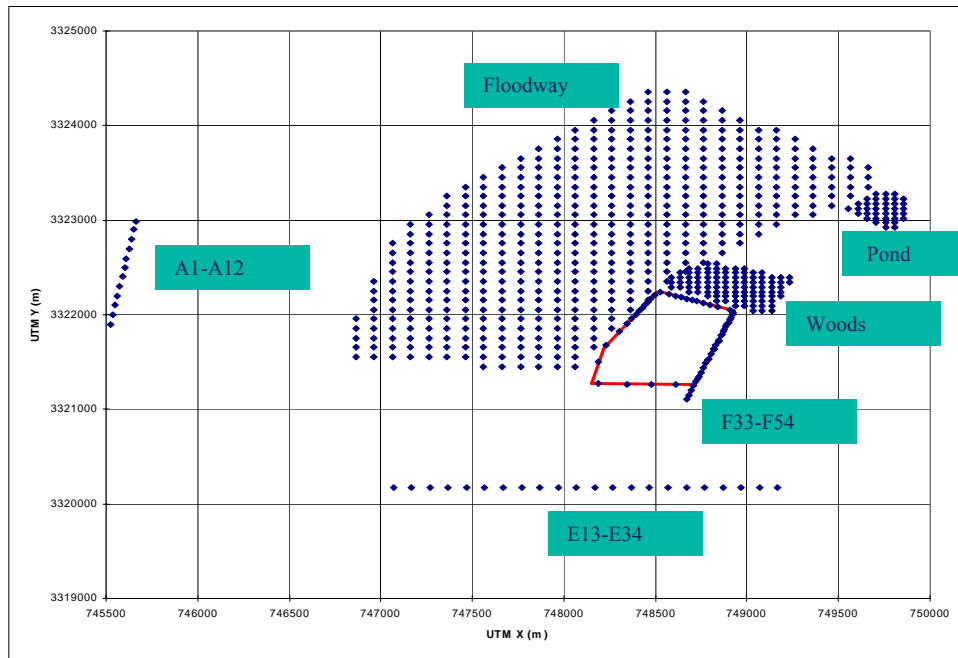


Figure 3. Receptor locations.

In order to estimate chemical concentrations in drinking water and fish, the two watersheds nearest the site were modeled—the river as a drinking-water source and a small stream north of the site as a source of fish. The river and stream were modeled as plug flow reactors using their average flow rates and dimensions. The average concentrations and deposition rates were used as input for determining the loading from runoff and direct deposition.

For the purpose of this risk assessment, subsistence farmers were assumed to live in the residences described above (A-1 through F-54). Because the residential properties west of the site (A-1 to A-12) and south of the river (E-13 to E-34) are sufficiently large to raise cattle, these locations were assumed to be the grazing areas for their beef and dairy cattle. The properties east of the facility are not large enough to support grazing; therefore, it was assumed that their beef and milk came from a commercial grazing area located several miles southwest of the site.

2.7 Estimation of Media Concentrations of COPC

The next step in the risk assessment process is calculating the concentrations of COPC in the media based on combustor emissions. Figure 1, the conceptual site model, shows the pathways by which the compounds emitted from the combustion facility enter various media that are potentially consumed by the receptors. The following describes the equations and parameters from the HHRAP guidance that are required to calculate the media concentrations.

2.7.1 Calculation of COPC Concentrations in Air and Deposition Rates

Because the air dispersion modeling assumes a unit emission rate of 1.0 g/s for all chemicals, the results are unitized and must be converted to chemical-specific concentrations and deposition rates based on the actual emission rates from each source. For multiple sources, the COPC concentrations and deposition rates for each source are added to get the total concentrations and deposition rates for each chemical.

The guidance assumes that the COPC partition between the vapor phase and either the particle-bound phase or the particle phase. All metals except mercury are assumed to be completely incorporated into the particle phase. For most organic compounds, it is assumed that the partitioning is between the vapor phase and the surface of the particles (i.e., particle bound). However, for the few organic compounds with low vapor pressures, ($< 1 \text{ E-9 mmHg}$), it is assumed that the partitioning is between the vapor phase and the internal particle matrix. For organic compounds, the fraction of the COPC concentration that is in the vapor phase, F_v , is calculated per Junge (1977):

$$F_v = \frac{c \times S_T}{p_L \times (c \times S_T)} \quad (1)$$

where:

- F_v = fraction of COPC in vapor phase
- c = Junge constant (1.74 E-4 atm-cm)
- S_T = Whitby's average surface area of particulates
($= 3.3 \text{ E-6 cm}^2/\text{cm}^3$)
- p_L = liquid phase vapor pressure (atm)

Similarly, the fraction associated with the particle is simply:

$$F_p = (1 - F_v) \quad (2)$$

where F_p is the fraction of COPC on or in particle.

The chemicals are assumed to be divided between the vapor and particle phases, so the vapor concentration, C_v , of a given chemical at a specific location due to a specific source is calculated as follows:

$$C_v = Q \times F_v \times C_{yv} \quad (3)$$

where:

- C_v = vapor-phase concentration of COPC at location X,Y from a given source ($\mu\text{g}/\text{m}^3$)
- Q = COPC source emission rate (g/s)
- F_v = fraction of COPC emitted in vapor phase from source (unitless)
- C_{yv} = unitized 5-year average vapor-phase air concentration at location X,Y from the source ($\mu\text{g}\cdot\text{sec}/\text{g}\cdot\text{m}^3$)

Similarly, the particulate concentration, C_p , is calculated as follows:

$$C_p = Q \times (1 - F_v) \times C_{yp} \quad (4)$$

where C_p is the particle-phase concentration of COPC at location X,Y from a given source ($\mu\text{g}/\text{m}^3$) and C_{yp} is the unitized 5-year average particle-phase air concentration at location X,Y from the source ($\mu\text{g}\cdot\text{sec}/\text{g}\cdot\text{m}^3$).

For wet vapors, the location- and chemical-specific deposition rate is calculated as follows:

$$D_{wv} = Q \times F_v \times D_{ywv} \quad (5)$$

where D_{wv} is the wet vapor deposition rate of COPC at location X,Y from a given source ($\text{g}/\text{m}^2\cdot\text{year}$), and D_{ywv} is the unitized 5-year average wet vapor deposition rate at location X,Y from the source ($\text{g}\cdot\text{s}/\text{g}\cdot\text{m}^2\cdot\text{year}$).

For wet particle deposition, the location- and chemical-specific deposition rate is calculated as follows:

$$D_{wp} = Q \times (1 - F_v) \times D_{ywp} \quad (6)$$

where D_{wp} is the wet particle deposition rate of COPC at location X,Y from a given source ($\text{g}/\text{m}^2\cdot\text{year}$), and D_{ywp} is the unitized 5-year average wet particle deposition rate at location X,Y from the source ($\text{g}\cdot\text{s}/\text{g}\cdot\text{m}^2\cdot\text{year}$).

For dry particle deposition, the location- and chemical-specific deposition rate is calculated as follows:

$$Ddp = Q \times (1 - Fv) \times Dydp \quad (7)$$

where Ddp is the dry particle deposition rate of COPC at location X,Y from a given source ($\text{g}/\text{m}^2\text{-year}$), and Dwp is the unitized 5-year average dry particle deposition rate at location X,Y from the source ($\text{g-s}/\text{g-m}^2\text{-year}$).

The COPC concentrations and deposition rates from each source are added to get the total values for each chemical at each X,Y location. The values used throughout the rest of this risk assessment are the totals for each receptor location from all four sources at the site.

2.7.2 Calculation of COPC Concentrations in Soil

EPA guidance uses two different approaches to determine concentrations of COPC in soils—one for carcinogens and one for noncarcinogens. It should be noted that these concentrations in soil must be calculated for each residence (which is where soil is ingested, produce is grown, and pigs and chickens are raised), for the drinking water and fishing watersheds, and for the grazing areas for cattle.

For carcinogens, the COPC concentration in soil (C_{soil}) is the average value during the exposure duration:

for $Td \geq T2$:

$$C_s = \frac{D_s}{k_s \times (T_d - T_1)} \times \left[\left[T_d + \frac{\exp(-k_s \times T_d)}{k_s} \right] - \left[T_1 + \frac{\exp(-k_s \times T_1)}{k_s} \right] \right] \quad (8)$$

for $T_1 < T_d < T_2$:

$$C_s = \frac{\left(\frac{(D_s \times T_d) - C_{sT_d}}{k_s} \right) + \left[\frac{C_{sT_d}}{k_s} \times (1 - \exp[-k_s \times (T_2 - T_d)]) \right]}{(T_2 - T_1)} \quad (9)$$

For noncarcinogens, the concentration is taken as the maximum value, which occurs at the end of the combustion period:

$$C_s = \frac{D_s \times [1 - \exp(-k_s \times T_d)]}{k_s} \quad (10)$$

where:

C_s = average concentration in soil over exposure duration (mg/kg)

C_{STd}	=	soil concentration at time Td (mg/kg)
D_s	=	deposition term (mg/kg-year)
k_s	=	soil loss coefficient (1/year)
T_d	=	period over which deposition (combustion) occurs (year)
T_1	=	beginning of combustion period (year)
T_2	=	length of exposure duration (year)

The deposition term, D_s , is determined from the particle and vapor deposition rates as follows:

$$D_s = \frac{100}{Z \times BD} \times [0.31536 \times V_{dv} \times C_v + D_{wv} + D_{wp} + D_{dp}] \quad (11)$$

where:

Z	=	soil mixing-zone depth (cm)
BD	=	soil dry bulk density (g/cm^3)
V_{dv}	=	dry deposition velocity (cm/s)
0.31536	=	unit conversion factor (m-g-s/cm- μ g-year)

The soil loss constant, k_s , is COPC- and site-specific. It is the sum of losses from five sources—leachate, erosion, runoff, degradation, and volatilization:

$$k_s = k_{sl} + k_{se} + k_{sr} + k_{sg} + k_{sv} \quad (12)$$

where:

k_s	=	COPC-specific soil loss constant from all processes (1/year)
k_{sl}	=	COPC-specific soil loss constant from leaching (1/year)
k_{se}	=	COPC-specific soil loss constant from erosion (1/year)
k_{sr}	=	COPC-specific soil loss constant from surface runoff (1/year)
k_{sg}	=	COPC-specific soil loss constant from degradation (1/year)
k_{sv}	=	COPC-specific soil loss constant from volatilization (1/year)

The derivation of these constants is described in detail in the HHRAP.

2.7.3 Calculation of COPC Concentrations in Above-Ground Produce

The same equations are used to calculate the chemical concentrations in plants for assessing human ingestion of homegrown produce and in the plants eaten by grazing livestock. The total COPC concentrations in the plant tissue of above-ground produce, P_t , are assumed to be due to three mechanisms—deposition of particles on plant surfaces, vapor transfer through the leaves, and root uptake:

$$P_t = P_d + P_v + P_r \quad (13)$$

where:

- P_t = total COPC concentration in plant (mg/kg)
 P_d = COPC concentration in plant due to direct deposition (mg/kg)
 P_v = COPC concentration in plant due to air-to-plant transfer (mg/kg)
 P_r = COPC concentration in plant due to root uptake from soil (mg/kg)

The COPC concentration in plants due to direct deposition is determined as follows:

$$P_d = \frac{1,000 \times [D_{dp} + (F_w \times D_{wp})] \times R_p \times [(1 - \exp(-k_p \times T_p))]}{Y_p \times k_p} \quad (14)$$

where:

- F_w = fraction of wet deposition that adheres to plant (unitless)
 R_p = interception fraction of edible portion of plant (unitless)
 k_p = plant surface loss coefficient (1/year)
 T_p = time plant is exposed before harvest (year)
 Y_p = yield for the edible portion of the plant (kg dw/m²)

The COPC concentration in plants, for both produce and forage, due to air-to-plant transfer is determined as follows:

$$P_v = \frac{C_v \times B_v \times V_G}{\rho_a} \quad (15)$$

where:

- B_v = air-to-plant biotransfer factor for above-ground produce and forage ([mg COPC/kg plant dw] per [mg COPC/kg air])
 V_G = empirical correction factor for above-ground produce and forage (unitless)
 ρ_a = density of air (g/m³)

The COPC concentration in above-ground plants, for both produce and forage, due to root uptake from soils is determined as follows:

$$P_r = C_s \times B_r \quad (16)$$

where B_r is the plant-soil bioconcentration factor (BCF) for above-ground produce (unitless).

For below-ground produce, the COPC concentration is:

$$Pr = Cs \times Brrootveg \times VGrootveg \quad (17)$$

where $Brrootveg$ is the plant-soil BCF for below-ground produce (unitless) and $VGrootveg$ is the empirical correction factor for below-ground produce (unitless).

It should be noted that most of the partitioning factors used for organic chemicals are based on correlations of uptake to the octanol-water partitioning coefficients for just a few organic compounds.

2.8 Calculation of COPC Concentrations in Animal Products

The COPC concentrations in beef, milk, pork, chicken, and eggs are estimated from the modeled levels in the soil and plant material that is ingested and bioconcentrated by the farm animals.

For beef, the COPC tissue concentration is:

$$A_{beef} = B_{beef} \times MF \times \left[\left(\sum_i^n (F_i \times Q_{p_i} \times P_i) \right) + (Q_s \times C_s \times B_s) \right] \quad (18)$$

where:

- A_{beef} = COPC concentration in beef tissue (mg/kg fresh weight [FW])
- B_{beef} = COPC biotransfer factor for beef (day/kg FW)
- F_i = fraction of plant “i” eaten by animal that contains COPC (unitless)
- Q_{p_i} = quantity of plant “i” eaten by animal each day (kg dw/day)
- P_i = total concentration of COPC in each plant “i” eaten by the animal (mg/kg dw)
- Q_s = quantity of soil eaten by animal each day (kg/day)
- B_s = soil bioavailability (unitless)
- MF = metabolism factor (unitless); this value is 1.0 for all of the chemicals evaluated

The COPC concentration in milk is calculated in a similar manner:

$$A_{milk} = B_{milk} \times MF \times \left[\left(\sum_i^n (F_i \times Q_{p_i} \times P_i) \right) + (Q_s \times C_s \times B_s) \right] \quad (19)$$

where A_{milk} is the COPC concentration in milk (mg/kg) and B_{milk} is the biotransfer factor for milk (day/kg net weight animal tissue).

The COPC concentration in pork is calculated as follows:

$$A_{\text{pork}} = B_{\text{pork}} \times MF \times \left[\left(\sum_i^n (F_i \times Q_{p_i} \times P_i) \right) + (Q_s \times C_s \times B_s) \right] \quad (20)$$

where A_{pork} is the COPC concentration in pork tissue (mg/kg FW) and B_{pork} is the biotransfer factor for pork (day/kg FW).

The COPC concentration in poultry meat is calculated as follows:

$$A_{\text{chick}} = B_{\text{chick}} \times \left[\left(\sum_i^n (F_i \times Q_{p_i} \times P_i) \right) + (Q_s \times C_s \times B_s) \right] \quad (21)$$

where A_{chick} is the COPC concentration in poultry (mg/kg FW) and B_{chick} is the biotransfer factor for poultry (unitless).

The COPC concentration in eggs is calculated as follows:

$$A_{\text{egg}} = B_{\text{egg}} \times \left[\left(\sum_i^n (F_i \times Q_{p_i} \times P_i) \right) + (Q_s \times C_s \times B_s) \right] \quad (22)$$

where A_{egg} is the COPC concentration in eggs (mg/kg FW) and B_{egg} is the biotransfer factor for eggs (unitless).

Similar to the plant partitioning coefficients, most of the biotransfer factors for the organic compounds are based on correlations with octanol-water partitioning coefficients for a small group of chemicals.

2.8.1 Calculation of COPC Concentrations in Drinking Water and Fish

Surface-water COPC concentrations were calculated for the water bodies based on their physical and chemical characteristics and the mass loadings of COPC. These values were then used to determine the COPC concentrations in drinking water and fish as appropriate.

The total COPC mass loading to a water body is the sum of five pathways:

$$L_t = L_{\text{dep}} + L_{\text{dif}} + L_{\text{ri}} + L_{\text{r}} + L_{\text{e}} + L_{\text{i}} \quad (23)$$

where:

L_t = total COPC mass loading to the water body (g/year)

Ldep =	total wet particle phase, dry particle phase, and wet vapor deposition directly to the water body (g/year)
Ldif =	vapor-phase diffusion load to water body (g/year)
Lri =	runoff load from impervious surfaces (g/year)
Lr =	runoff load from pervious surfaces (g/year)
Le =	soil erosion load (g/year)
Li =	internal transfer (g/year)

The equations used to calculate the above mass loading rates are in Appendix B of the HHRAP.

From the total mass loading, the total water-body concentration, which includes both the water column and the bed sediment, is calculated as follows:

$$C_{wtot} = \frac{L_t}{V_{fx} \times f_{wc} + k_{wt} \times A_w \times (d_{wc} + d_{bs})} \quad (24)$$

where:

Cwtot =	total COPC concentration in water body (g/m ³ = mg/L)
Vfx =	average volumetric flow rate through water body (m ³ /year)
fwc =	fraction of total water-body COPC concentration that occurs in the water column (unitless)
kwt =	overall total water-body dissipation rate constant (1/year)
Aw =	surface area of water body (m ²)
dwc =	depth of water column (m)
dbs =	depth of upper benthic sediment layer (m)

The equations and parameters used to determine the above values are contained in Appendix B of the HHRAP.

From the concentration in the water body, the total concentration in the water column is calculated as follows:

$$C_{wctot} = f_{wc} \times C_{wtot} \times \frac{d_{wc} + d_{bs}}{d_{wc}} \quad (25)$$

where Cwt is the total COPC concentration in water column (mg/L).

The dissolved water-column concentration is then calculated as follows:

$$C_{dw} = \frac{C_{wctot}}{1 + (K_{dsw} \times TSS \times 10^{-6})} \quad (26)$$

where:

- C_{dw} = dissolved-phase water concentration (mg/L)
 K_{dsw} = suspended sediments/surface-water partition coefficient (L/kg)
 TSS = total suspended solids in water column (mg/L)
 10^{-6} = conversion factor for mg to kg

The COPC dissolved-phase water concentrations are the values used to assess exposure associated with the ingestion of drinking water, because it is assumed that surface water would be treated to remove suspended solids prior to its distribution to consumers.

The COPC concentrations in the bed sediments of the water bodies are used to estimate fish uptake of chemicals that readily bioaccumulate and for use in the ecological risk assessment. The bed-sediment concentration is calculated as follows:

$$C_{sb} = f_{bs} \times C_{wtot} \times \frac{K_{dbs}}{\theta_{bs} + (K_{dbs} \times C_{bs})} \times \frac{d_{wc} + d_{bs}}{d_{bs}} \quad (27)$$

where:

- C_{sb} = COPC concentration in bed sediments (mg/kg)
 f_{bs} = fraction of total water-body COPC concentration in bed sediments (unitless)
 K_{dbs} = bed-sediment and pore-water partition coefficient (L/kg)
 θ_{bs} = bed-sediment porosity (L water/L sediment)
 C_{bs} = bed-sediment concentration (kg/L)

The COPC concentrations in fish are calculated based on concentrations in either the dissolved water or the bed sediments. The source for a specific COPC is based on the availability of a specific accumulation factor for water or sediment.

For dissolved water-to-fish transfer based on a BCF, the following equation is used:

$$C_{fish} = C_{dw} \times BCF_{fish} \quad (28)$$

where C_{fish} is the COPC concentration in fish (mg/kg FW) and BCF_{fish} is the BCF for COPC in fish (L/kg).

For dissolved water-to-fish transfer based on a BAF, the COPC concentration in fish is calculated as follows:

$$C_{fish} = C_{dw} \times BAF_{fish} \quad (29)$$

where BAF is the bioaccumulation factor (L/kg).

For dioxins, furans, and polychlorinated biphenyls (PCB), the COPC concentration in fish is assumed to be a function of the COPC concentration in sediments and is calculated as follows:

$$C_{\text{fish}} = \frac{C_{\text{sb}} \times \text{flipid} \times \text{BSAF}}{\text{OC}_{\text{sed}}} \quad (30)$$

where:

- flipid = fish lipid constant (unitless)
- BSAF = biota-sediment accumulation factor (unitless)
- OC_{sed} = fraction of organic carbon in bottom sediment (unitless)

Like the bioaccumulation factors for farm animals, most of the values for fish are based on correlations with octanol-water partitioning coefficients for a relatively few organic chemicals.

2.9 Exposure Quantification

The goal of this section is to quantify the potential receptor exposures to the COPC (in mg/kg-day) by the various pathways. The exposures are calculated as average daily doses (ADD) for noncarcinogens and as lifetime average daily doses (LADD) for carcinogens.

The two major routes of exposure are inhalation of particles and vapors, and ingestion of affected media. The daily doses are a function of the estimated media concentrations, intake rates of the various media, and receptor exposure parameters that define the frequency and duration of expected exposures.

2.9.1 Calculation of Intake Rates

The intake rate, IR, of a COPC in food, water, or soil is a function of the rate of consumption of the medium per unit body weight, fraction of the medium that contains the COPC, and the COPC concentration in the medium:

$$\text{IR} = \text{CR} \times f \times C \quad (31)$$

where:

- IR = intake rate of COPC in food, water, or soil (mg/kg-day)
- f = fraction of medium that contains the COPC
- C = chemical concentration in environmental food or soil (mg/kg) or water (mg/L)
- CR = consumption rate of medium (kg/kg-day)

It should be noted that the EPA uses several different definitions for the consumption rates. For produce, beef, milk, chicken, eggs, and fish, the consumption rates are given in kg/kg-day. For soil and water, the consumption rates are in kg/day and L/day, respectively. Therefore, these latter consumption rates must be divided by the body weight of the receptor to properly calculate the intake rates

$$CR = \frac{CR}{BW} \quad (32)$$

where BW is the body weight of receptor (kg).

Table 2 presents the media consumption rates used in the HHRAP guidance.

Table 2. Intake rates and fractions of contaminated media used in exposure scenarios.

Contaminated Food or Media	Exposure Scenario											
	Adult Farmer		Child Farmer		Adult Fisher		Child Fisher		Adult Resident		Child Resident	
	Rate	Fraction	Rate	Fraction	Rate	Fraction	Rate	Fraction	Rate	Fraction	Rate	Fraction
Beef (kg FW/kg-day)	0.00114	1	0.00051	1	NA	NA	NA	NA	NA	NA	NA	NA
Milk (kg FW/kg-day)	0.00842	1	0.01857	1	NA	NA	NA	NA	NA	NA	NA	NA
Chicken (kg FW/kg-day)	0.00061	1	0.000425	1	NA	NA	NA	NA	NA	NA	NA	NA
Eggs (kg FW/kg-day)	0.00062	1	0.000438	1	NA	NA	NA	NA	NA	NA	NA	NA
Pork (kg FW/kg-day)	0.00053	1	0.000398	1	NA	NA	NA	NA	NA	NA	NA	NA
Fish (kg FW/kg-day)	NA	NA	NA	NA	0.00117	1	0.000759	1	NA	NA	NA	NA
Above-ground produce (kg DW/kg-day)	0.0003	1	0.00042	1	0.0003	0.25	0.00042	0.25	0.0003	0.25	0.00042	0.25
Protected above-ground produce (kg DW/kg-day)	0.00057	1	0.00077	1	0.00057	0.25	0.00077	0.25	0.00057	0.25	0.00077	0.25
Below-ground Produce (kg DW/kg-day)	0.00014	1	0.00022	1	0.00014	0.25	0.00022	0.25	0.00014	0.25	0.00022	0.25
Soil (kg/day)	100	1	200	1	100	1	200	1	100	1	200	1
Drinking water (L/day)	1.4	1	0.67	1	1.4	1	0.67	1	1.4	1	0.67	1
Air (m3/hour)	0.63	1	0.3	1	0.63	1	0.3	1	0.63	1	0.3	1

Source: U.S. EPA (1998a) DW-dry weight FW-fresh weight NA-not applicable

2.9.2 Calculation of Doses

Consistent with the current EPA risk assessment guidance, variations of the following general equation were used to assess the ADD for each combination of chemical “i” and indirect exposure pathway “j” to be considered in the human health assessment:

$$\text{ADD}_{ij} \text{ or } \text{LADD}_{ij} = \frac{\text{IR}_{ij} \times \text{EF} \times \text{ED} \times \text{BMF}_i}{365 \times \text{AT}} \quad (33)$$

where:

- ADD = average daily dose (mg/kg-day) for noncarcinogenic chemicals
- LADD = lifetime average daily dose (mg/kg-day) for carcinogenic chemicals
- IR = intake rate of medium of concern (mg/kg-day)
- EF = exposure frequency (days/year)
- ED = exposure duration (years)
- BMF = biometabolism factor
- 365 = conversion factor for years to days
- AT = averaging time (years) (for noncarcinogenic effects, AT = exposure duration; for carcinogenic effects, AT = 70 years)

For exposure via inhalation, the following general dose equation was used to assess uptake for each chemical “i” to be considered in the human health assessment:

$$\text{ADI}_i \text{ or } \text{LADI}_i = \frac{\text{Ca}_i \times \text{IR}_i \times \text{ET} \times \text{EF} \times \text{ED} \times \text{BMF}_i \times 0.001}{365 \times \text{BW} \times \text{AT}} \quad (34)$$

where:

- ADI = average daily inhalation dose (mg/kg-day) for noncarcinogenic chemicals
- LADI = lifetime average daily inhalation dose (mg/kg-day) for carcinogenic chemicals
- Ca = COPC concentration in air ($\mu\text{g}/\text{m}^3$)
- IR = inhalation intake rate (m^3/hour)
- ET = exposure time (hours/day)
- EF = exposure frequency (days/year)
- ED = exposure duration (years)
- BMF = biometabolism factor (unitless)
- 365 = conversion factor for years to days
- AT = averaging time (years) (for noncarcinogenic effects, AT = exposure duration; for carcinogenic effects, AT = 70 years)

The exposure parameters are presented in Table 3.

Table 3. Exposure parameters.

Variable Description	Adult Farmer	Child Farmer	Adult Fisher	Child Fisher	Adult Resident	Child Resident
Exposure duration (year)	40	6	30	6	30	6
Exposure frequency (days/year)	350	350	350	350	350	350
Body weight (kg)	70	15	70	15	70	15
Averaging time (year) carcinogens	70	70	70	70	70	70
Averaging time (year) noncarcinogens	40	6	30	6	30	6

Source: U.S. EPA (1998a)

2.10 Toxicity Assessment

The purpose of the toxicity assessment is to determine the quantitative relationship between the dose of a chemical and the incidence of the adverse effect associated with exposure to that chemical. The toxicity assessment, sometimes referred to as the Dose-Response Assessment, is the process of characterizing the quantitative relationship between the dose of an agent and the probability of adverse health effects occurring in exposed populations (NRC/NAS, 1983). The dose-response relationship is evaluated separately for non-carcinogenic and carcinogenic effects.

For most chemicals, the Dose-Response Assessment has already been completed, and quantitative toxicological criteria are available from EPA and other health agency sources. The selected criteria, cancer slope factors (CSF) for carcinogens, and reference doses (RfD) for noncarcinogens, for both oral and inhalation exposures, should reflect the appropriate routes of exposure for the chemicals of concern at the site (U.S. EPA, 1989). The hierarchy of sources for identifying toxicological criteria is:

1. Draft guidance from EPA on hazardous waste incinerators (U.S. EPA, 1998a and 1999a)
2. Integrated Risk Information System (IRIS) (U.S. EPA, 1999b)
3. Health Effects Assessment Summary Tables (HEAST) (U.S. EPA, 1995)
4. EPA criteria documents
5. Agency for Toxic Substances and Disease Registry Toxicological Profiles (ATSDR, 1999)
6. Environmental Criteria and Assessment Office
7. Other sources

It should be noted that the 1998 incinerator guidance, in order to provide toxicity criteria in cases where specific studies were unavailable, uses numerous route-to-route extrapolations when there is no RfD or CSF for one route of exposure, but

there is an RfD or CSF for the other route. This approach appears contrary to EPA's own policy, which requires a detailed evaluation of the literature to determine whether such a route extrapolation is appropriate for the chemical. Because most of the toxicity criteria selected for this evaluation are from the EPA's 1998 guidance, this route extrapolation can introduce uncertainty into the risk assessment results by predicting risks for a given chemical and intake route when there are no studies to support the toxicity via that exposure route.

2.11 Risk Characterization

The final step in the risk assessment is to quantify the effects of potential exposure to COPC emitted from the combustion facility. In this risk characterization step, three different effects are evaluated. For carcinogens, the estimated upper-bound excess lifetime cancer risk is estimated. For noncarcinogens, the hazard index is estimated. For breast-fed infants, exposure to dioxins and furans from facility emissions is compared to exposures from background levels.

2.11.1 Calculation of Potential Carcinogenic Risk

For carcinogens, potential risk is estimated as the statistical upper bound of the incremental probability of an individual developing cancer over a lifetime as a result of exposure to the carcinogen. The lower bound of this incremental probability is zero; therefore, cancer risks range from the lower bound of zero to the upper-bound risks reported in this assessment.

Lifetime incremental cancer risks associated with the LADD are calculated as the product of the LADD and the cancer potency for each chemical "i" and exposure pathway "j," as shown below:

$$\text{RISK}_{ij} = \text{CSFo}_i \times \text{LADD}_{ij} \quad (35)$$

where:

$$\begin{aligned} \text{RISK}_{ij} &= \text{lifetime incremental cancer risk due to chemical "i" and exposure pathway "j"} \\ \text{CSFo}_{ij} &= \text{oral cancer slope factor for chemical "i" (mg/kg-day)}^{-1} \\ \text{LADD}_{ij} &= \text{lifetime average daily dose for chemical "i" and exposure pathway "j" (mg/kg-day)} \end{aligned}$$

For ingestion pathways, the risk for each pathway and chemical is found by substituting into the above equation for the LADD:

$$\text{RISK}_{ij} = \frac{I_{ij} \times \text{EF} \times \text{ED} \times \text{BMF}_i \times \text{CSFo}_i}{365 \times \text{AT}} \quad (36)$$

For inhalation, the risk for each chemical is:

$$\text{RISK}_i = \frac{\text{Ca}_i \times \text{IR} \times \text{ET} \times \text{EF} \times \text{ED} \times \text{BMF}_i \times 0.001 \times \text{CSF}_i}{365 \times \text{BW} \times \text{AT}} \quad (37)$$

The results of quantitative risk estimates for carcinogens and suspected carcinogens are expressed as the incremental risk, over the course of a 70-year lifetime, of contracting cancer above the background rate of approximately 3 in 10 (3×10^{-1}). The total upper-bound cancer risk is calculated by combining risks across exposure pathways and chemicals as follows:

$$\text{RISK}_{\text{TOT}} = \sum_{i=1}^m \sum_{j=1}^n \text{RISK}_{ij} \quad (36)$$

where:

RISK_{TOT}	=	total risk of all chemicals and pathways
m	=	number of chemicals
n	=	number of pathways

In the Superfund program, EPA established an acceptable excess lifetime cancer risk range from one in ten thousand to one in one million. This range may be expressed as 1×10^{-4} to 1×10^{-6} . For example, a risk of 1×10^{-6} means that one person in one million could develop cancer as a result of a lifetime exposure to emissions from a facility studied in an assessment. In supplemental guidance to the HHRAP, the EPA has recommended that risks from a single facility should not exceed 1×10^{-5} (U.S. EPA, 1998b).

2.11.2 Calculation of Hazard Quotients and Indices

Noncarcinogenic effects for each exposure route and chemical are evaluated by comparing an average dose over a specified time period with an RfD derived for a similar time period. This ratio of exposure to toxicity is called a hazard quotient (U.S. EPA, 1989):

$$\text{HQ}_{ij} = \frac{\text{ADD}_{ij}}{\text{RfD}_{ij}} \quad (39)$$

where:

- $ADD_{i,j}$ = average daily dose (mg/kg-day) by chemical and exposure pathway
 $RfD_{i,j}$ = reference dose (mg/kg-day) by chemical and exposure pathway
 (RfDo for oral exposures and RfDi for inhalation exposures)
 i = chemical
 j = exposure pathway

The hazard quotient assumes that there is a dose (i.e., the RfD) below which adverse health effects are unlikely (U.S. EPA, 1989). If the exposure levels are below the threshold (ratio <1), it is unlikely that noncarcinogenic effects would occur (U.S. EPA, 1989). To assess the overall potential for noncarcinogenic effects, hazard quotients for the individual exposure pathways (e.g., dermal contact, ingestion, and inhalation) and chemicals are summed for specific individuals to obtain the hazard index:

$$HI = \sum_{i=1}^m \sum_{j=1}^n HQ_{ij} \quad (40)$$

where:

- HI = hazard index for all chemicals and pathways
 m = number of chemicals
 n = number of pathways

To account for background contributions, the EPA has recommended that the hazard index from a single facility should not exceed 0.25 (U.S. EPA, 1998b).

2.11.3 Evaluating Breast-Fed Infant Exposure to Dioxins and Furans

Potential risk to breast-fed infants due to the intake of dioxins and furans is evaluated by a comparison to background exposures. The HHRAP guidance lists procedures and equations to estimate 1) the concentration of dioxin-like contaminants in the mother's milk, and 2) the average daily dose for a breast-fed infant, calculated on the basis of an averaging time of one year. The estimated ADD of 2,3,7,8-TCDD Toxicity Equivalent (TEQ) due to the combustion facility is then compared to that of a dose of 60 pg/kg-day due to background levels.

The concentration in mother's breast milk is calculated as follows:

$$C_{milkfat} = \frac{m \times 1E9 \times h \times f1}{0.693 \times f2} \quad (41)$$

where:

$C_{milkfat}$	=	TCDD TEQ concentration in milk fat of mother's breast milk (pg/kg)
m	=	maternal intake rate of TEQs for dioxins and furans (mg/kg-day)
$1E9$	=	conversion factor for mg to pg = 10^9
h	=	half-life of dioxins and furans in adults
$f1$	=	fraction of dioxins and furans stored in fat (0.9)
$f2$	=	fraction of mother's weight that is fat (0.3)

The infant's average daily dose is then:

$$ADD_{inf} = \frac{C_{milkfat} \times f3 \times f4 \times IR_{milk} \times EDI}{BW_{inf} \times AT} \quad (42)$$

where:

ADD_{inf}	=	infant's average daily dose from breast milk (pg TEQ/kg-day)
$f3$	=	fraction of breast milk that is fat (0.04)
$f4$	=	fraction of TEQ absorbed by infant (0.9)
IR_{milk}	=	daily intake rate of breast milk (0.8 kg/day)
EDI	=	exposure duration for infant (1 year)
BW_{inf}	=	body weight of infant (10 kg)
AT	=	averaging time (1 year)

2.12 Results of the HHRA

The results of the HHRA are presented below.

2.12.1 Identification of Maximum Exposure Locations

Rather than discuss the risks in detail for each of the 54 theoretical residences, it was decided to focus the discussion on the maximum receptor locations in the three groups (A, E, and F). First, all 54 scenarios were run to identify the maximum receptor locations for total risks, hazards, and dioxin/furan uptakes by infants for each of the three receptor groups.

A total of six maximum receptor locations were identified—one in group A, two in group E, and three in group F. Based on the modeling results, the maximum receptors in each group were identified as:

- Group A: A-10 had the maximum cancer risks for all six exposure scenarios. A-11 had the maximum hazard indices, along with the maximum dioxin/furan intake rates for the

resident and fisher infant scenarios. A-1 had the maximum dioxin/furan intake rate for the farmer infant exposure scenario.

- Group E: E-28 had the maximum cancer risks for all six scenarios. E-27 had the maximum hazard indices for all six scenarios, as well as the maximum dioxin/furan intake rates for the three infant scenarios.
- Group F: F-48 had the maximum cancer risks for all six scenarios. F-38 had the maximum hazard indices for all six scenarios. F-40 had the maximum dioxin/furan intake rates for the three infant scenarios.

The total theoretical cancer risks and hazard indices for these scenarios are presented in Table 4.

Table 4. Summary of human health risks and hazard indices.

Maximum Receptor	UTM X (m)	UTM Y (m)	Adult Resident		Child Resident		Adult Farmer		Child Farmer	
			Risk	HI	Risk	HI	Risk	HI	Risk	HI
A-10	745638	3322796	5.E-07	5.E-02	2.E-07	1.E-01	2.E-06	5.E-02	6.E-07	1.E-01
A-11	745651	3322899	5.E-07	5.E-02	2.E-07	1.E-01	2.E-06	5.E-02	6.E-07	1.E-01
E-27	748468	3320176	1.E-06	1.E-01	4.E-07	3.E-01	5.E-06	1.E-01	1.E-06	3.E-01
E-28	748568	3320176	1.E-06	1.E-01	5.E-07	3.E-01	5.E-06	1.E-01	1.E-06	3.E-01
F-38	748709	3321248	5.E-06	2.E-01	2.E-06	5.E-01	8.E-06	2.E-01	2.E-06	5.E-01
F-48	748844	3321729	8.E-06	2.E-01	4.E-06	4.E-01	1.E-05	2.E-01	4.E-06	4.E-01

Maximum Receptor	UTM X (m)	UTM Y (m)	Adult Fisher		Child Fisher	
			Risk	HI	Risk	HI
A-10	745638	3322796	1.E-06	6.E-02	3.E-07	1.E-01
A-11	745651	3322899	1.E-06	6.E-02	3.E-07	1.E-01
E-27	748468	3320176	2.E-06	1.E-01	5.E-07	3.E-01
E-28	748568	3320176	2.E-06	1.E-01	5.E-07	3.E-01
F-38	748709	3321248	5.E-06	2.E-01	2.E-06	5.E-01
F-48	748844	3321729	9.E-06	2.E-01	4.E-06	4.E-01

2.12.2 Risk Drivers

The risk drivers are the pathways and chemicals that are the main contributors to estimated risks. A review of all 54 exposure scenarios indicates that the drivers are consistent. For the adult and child residents, the major risks are associated with direct inhalation of chlorinated VOC, arsenic, and hexavalent chromium (Cr[VI]). For the adult and child farmers, the major risks are associated with direct inhalation of the same chemicals, plus indirect exposures associated with

PCDD/F in beef, milk, chicken, and eggs. For the adult and child fishers, major risks are again associated with direct inhalation of the same chemicals, followed by minor amounts of arsenic and PCDD/F due to ingestion of fish.

The major sources of the chlorinated VOC are the fugitive emissions from the two area sources (fugitive emissions from valves, flanges, pumps, and relief valves). The sources for the metals (arsenic and Cr[VI]) and the PCDD/F are the emissions from the two stacks.

2.12.3 Hazard Drivers

The hazard drivers are the pathways and chemicals that are the major contributors to the hazard indices. A review of all 54 exposure scenarios indicates that the drivers are consistent. Direct inhalation of chlorine is the hazard driver for all of the receptors, with metals in fish causing slight increases in the hazard indices for the adult and child fishers. In the errata to the HHRAP (U.S. EPA, 1999a), the provisional reference concentration for chlorine has decreased by a factor of 1,750. Thus, using the earlier reference concentration from the 1998 guidance would result in 80-90% reduction in the hazard indices.

The major sources of the chlorine and metals are the emissions from the stacks for S-1 and S-2.

2.12.4 Dioxin Exposure in Infants

Table 5 contains the estimated intakes of 2,3,7,8-TCDD TEQs for infants via ingestion of breast milk. The maximum doses are 0.04 pg/kg-day for the resident infant at F-40, 2.0 pg/kg-day for the farmer infant at E-27, and 0.07 pg/kg-day for the fisher infant at F-40. These doses are all much less than the dose of 60 pg/kg-day due to background levels.

Table 5. Summary of dioxin intake by infants.

Maximum Receptors	UTM X (m)	UTM Y (m)	Infant TCDD TEQs (pg/kg)		
			Resident	Farmer	Fisher
A-1	745524	3321898	7.E-03	6.E-01	4.E-02
A-11	745651	3322899	7.E-03	6.E-01	4.E-02
E-27	748468	3320176	2.E-02	2.E+00	5.E-02
F-40	748736	3321344	4.E-02	7.E-01	7.E-02

2.13 Uncertainty Characterization

Risk assessment inherently attempts to err on the side of safety, public health, and protection of the environment. Therefore, risk assessment methodology, particularly for screening-level assessments, generally is based on the application of conservative parameters and assumptions in all phases. Because direct

measurements are not available for many of the parameters upon which the risk estimates depend (e.g., accumulation factors, media concentrations, human exposure parameters, and toxicity criteria), conservative assumptions and default values must be employed to essentially eliminate the possibility of underestimating risk. This practice, although commonly used in the risk assessment process, necessarily introduces a significant level of conservatism in the risk estimate by relying on upper-bound values rather than statistically based or best-estimate values. It is quite common to find that risks calculated using conservative upper-bound parameters are more than 10- to 100-fold greater than those calculated using best-estimate parameter values.

The following sections provide brief discussions of the more important uncertainties associated with this risk assessment.

2.13.1 COPC Selection

The selection of COPC to be evaluated in this risk assessment was based on knowledge of the chemicals in the waste feed and compounds that are or could be formed in the combustion process. Their selection is based on our ability to detect, identify, and quantify them using standard analytical methods. The sampling and analytical methods used are by nature designed to identify and quantify compounds that are thought to be hazardous. There may be other compounds in the emissions that are also hazardous, but have not yet been identified as such, or for which there are no approved sampling and analysis methods. Except for chemicals mandated for inclusion, if a chemical was never detected either in the waste feed or in any of the stack samples, it was eliminated from the COPC list. Thus, the risk assessment may not include compounds that are present but have unknown toxicological effects. The contribution of such chemicals to risk is unknown, but they are probably low because the hundreds of chemicals evaluated as COPC are relatively toxic compounds known to contribute substantially to human health and ecological risks.

2.13.2 Estimated Emission Rates

The emission rates used in this risk assessment are based on knowledge of the combustion process and limited sampling, and analysis of the incinerator stack emissions and fugitive emissions from related equipment. Several factors affect our ability to quantify long-term emission rates.

The sampling and analysis of stack and fugitive emissions are point-in-time estimates. The results are then used to estimate the long-term average emission rates. In the present case, the company sampled the stack gases under the most severe operating conditions (and so, presumably, maximum pollutant emission rate conditions). Thus, for those pollutants where the emission-rate data were used directly, the contribution to incremental risk from the pollutants would tend to be higher than long-term average risks. For those pollutants where a long-term

average emission rates were estimated, the contribution to the average long-term risk could be higher or lower, depending on the validity of the model used to adjust the test emission rates to long-term average emission rates.

Many of the chemicals analyzed were reported as being below their detection limits in one or more samples. Thus, it was necessary to assume that these chemicals could be present and to develop a protocol for converting the non-detects to estimated values, which were used to estimate emission rates. For detected compounds, either their maximums or 95% upper confidence limits (UCL) of the mean of the detected values were used. It is noted that the population of data available for determining the 95% UCL was small (typically ranging from 3 to 12 data points). Normally, a population of at least 20–30 points is necessary to derive valid statistics. Therefore, uncertainty is introduced.

For non-detect compounds that were retained as COPC, emissions were estimated using laboratory method detection limits (MDL) that were then multiplied by a factor of 2.63. Because the MDL are typically greater than the estimated detection limit for a specific analysis, and because of the factor of 2.63, the emission rates are exaggerated upper-bound estimates, which contribute to higher estimates of risk.

Even though field measurements indicated that there were no detectable emissions from process equipment, EPA default “no-leak” values were used to estimate fugitive emissions. These values, while small, are not “zero.” Thus, predicted risks for offsite receptors from VOC inhalation are probably overestimated.

2.13.3 Air Dispersion Modeling

Several air modeling factors contribute to uncertainty in this risk assessment. Specifically, there are uncertainties with regard to selected model parameters and the level of conservatism incorporated into the dispersion modeling.

The modeling of three emission phases (i.e., particle, particle-bound, and vapor) is required. Model studies are needed to confirm that mass is being conserved and not created by applying this approach. The ISCST3 plume depletion algorithm was limited to one field test. The representativeness of meteorologic conditions and site characteristics needs to be established. Incorporating dry gas deposition in the ISCST3 model is questionable because there is limited information on dry gas deposition velocities.

The ISCST3/PCRAMMET models compute deposition velocities for terms that cannot be directly computed in applied studies (i.e., Bowen ratios, minimum Monin-Obukhov scaling length, net radiation, and albedo). The present subjective nature of inputting such values and using broadly defined surface characteristics (not site specific) creates a need to justify the use of specific

parameters. A more objective way of computing the Monin-Obukhov scaling has been successful using surface roughness and atmospheric stability class, and similar procedures could be implemented easily.

The ISCST3 wet deposition algorithm is based on measured rainfall amount, not rainfall intensity. The EPA assumes that the wet deposition rate is linear with the precipitation rate. Model tests show that the ISCST3 wet deposition amounts vary by at least a factor of 2 from other model algorithms. Scavenging coefficients used by ISCST3 for wet deposition are based on a field study that evaluated particle scavenging during convective storms. The applicability of these coefficients for long-term wet deposition estimates has not been demonstrated.

The ISCST3 model dry and wet deposition algorithms need to be tested rigorously against experimental data. The resuspension algorithm within ISCST3 also needs to be tested. Not considering resuspension of deposited material at deposition “hot spots” would likely result in overestimating exposure.

The ISCST3/BPIP building wake algorithms do not address open or rounded structures well. Open pipeline support structures and storage tanks do not have the same building wake characteristics as solid block structures. The use of block-like structures and lack of accounting for smoother aerodynamic structures such as rounded and spherical storage tanks would likely result in higher predicted ground-level concentrations.

It should be made clear that the use of alternative methods to more accurately represent site-specific conditions should not also have to be proven more conservative than the default guideline methods. Such conservatism is counterproductive to accurately estimating the downwind concentrations and deposition rates in the modeling/exposure assessment. The result of using default conditions rather than site-specific conditions is an overstatement of ground-level concentrations near the sources.

2.13.4 Receptors

The receptor locations used in this risk assessment were selected to provide an upper bound to the risk estimates. There was no attempt to evaluate the average risk to people living in the area.

Residents were assumed to live in areas with the highest offsite COPC concentrations and deposition rates. Subsistence fishers were assumed to live in these same residences and to get all of their fish from the most highly affected water body in the area. Subsistence farmers were assumed to live in these same residences, and to raise all of their own produce, pork, chicken, and eggs at home, and to get their beef and dairy products from cattle raised either at home or at the

nearest affected grazing area. These highly artificial receptor “models” tend to overestimate risk.

2.13.5 Exposure Scenarios and Pathways

Exposure scenarios and pathways used in this assessment are generally quite conservative, and are typical for a screening-level assessment. Parameters for chemical intake rates and the frequency and duration of exposure are very conservative, as recommended by the EPA. For example, this assessment assumes that the adult resident and fisher reside in the same location (i.e., the maximum residential exposure location, 24 hours/day, 350 days/year) for 30 years, and the adult farmer for 40 years. These values are for individuals in the upper bounds of exposure frequency and duration. Bioavailability (amount of the chemical absorbed into the body following inhalation or ingestion) is assumed to be 100% for all chemicals except phthalates, again a highly conservative assumption for many of the COPC included in the risk assessment.

2.13.6 Estimation of Media Concentrations

The environmental fate and transport modeling used in this risk assessment is a conservative screening-level methodology, consistent with the draft guidance. Unit emission rates were determined for vapors and particulates, considering both wet and dry deposition and the adherence of chemicals to emitted particulates. The parameters selected for modeling the transport of these emissions are specified in the guidance, and are consistent with standard modeling procedures for risk assessment.

Several parameters or calculation procedures used in the risk assessment are based on the assumption of long-term, “steady-state” conditions. Steady-state conditions represent the approximate highest sustained concentration in a particular medium (e.g., in plants, sediments, fish tissues, beef, milk) that occur because of the balance between long-term accumulation and loss processes that affect that particular medium. Steady-state conditions are generally important only for more persistent organic chemicals (e.g., dioxin-like compounds) and metals (e.g., mercury) that may tend to accumulate in environmental media (e.g., bioconcentrate or bioaccumulate). In this risk assessment, most of the indirect risks attributable to the site are related to persistent chemicals for which exposures and risks are controlled by the assumption of steady-state conditions. The critical parameters include: 1) the air-to-plant transfer factor (or B_v), which affects chemical concentrations in plants fed to cattle and the above-ground produce consumed by each resident; 2) the BAF for calculating chemical concentrations in livestock (e.g., in the meat and milk of locally raised cattle); 3) the bioconcentration terms for determining sediment and fish concentrations of persistent chemicals; and 4) the biotransfer factor for calculating chemical concentrations in human breast milk and infant exposures and risks.

Almost all BAF are based on the octanol-water partitioning (K_{ow}) values of the chemicals. The assumption is that there is a direct correlation between the BAF and the affinity of a chemical for octanol. Typically, researchers have measured chemical uptake into several plants or animals, and then correlated the uptake to the K_{ow} values. This correlation is then used to predict the bioaccumulation of other chemicals by the same plants and animals. The higher the K_{ow} of a chemical, the higher its BAF. Even greater uncertainty is associated with BAF for some pathways that are based solely on the ratios of the fat contents between two animal products, without regard to morphological or physiological differences between species. For example, the BAF for pork are obtained by multiplying the BAF for beef by the ratio of fat in pork to fat in beef.

Although the assumption of steady-state conditions is an important and useful concept, in certain instances it can create problems that considerably overstate the reasonably expected exposures and health risks due to facility emissions. This is because an exponential term is used in the calculation procedures for steady-state parameters, and simplified forms of these calculations will dramatically overstate the annual average dose and cumulative risks. For most of the media, it may take years or decades of consistent exposure to achieve a steady-state condition. Steady state is rarely achieved in certain media. For example, chemical concentrations in pasture grasses can be dramatically limited by seasonal growth and consumption patterns that determine whether steady state is ever achieved in a particular location. Similarly, chemical concentrations in sediments and fish can be strongly influenced by fish mobility and seasonal or incidental changes in sediment deposition and loss. In these cases, the assumption of steady-state concentrations in environmental media or the food chain result in considerable overstatement of the chemical concentrations, exposures, and risks.

2.13.7 Intakes and Doses

The estimates of media intakes and doses for both humans and the animals that they consume affect the estimated risks. While there is a high degree of variability in the intake rates, this risk assessment assumes that all consumption rates are constant across a given population. The result would be to overestimate risks for those who have lower intakes and to underestimate the risks for those with higher intake rates.

2.13.8 Toxicity Criteria

The risk assessment included conservative EPA toxicity criteria for each of the chemicals that had available CSF and/or noncancer RfD. These toxicity criteria are generally based on animal or human data that provide a dose-response interpretation that tends to overstate the actual or likely risks.

If a given chemical did not have a published EPA CSF or RfD in the IRIS (U.S. EPA, 1999b) or the most current HEAST (U.S. EPA, 1995), the 1998 EPA

guidance (U.S. EPA, 1998a) used route-to-route extrapolations, disregarding its own procedures. The effect is to increase the risk estimates and hazard indices by assuming that chemicals are equally toxic regardless of exposure route.

In addition, the errata to the 1998 guidance (U.S. EPA, 1999a) contained numerous provisional toxicity values from the EPA's National Center for Exposure Assessment (NCEA). These values have not undergone the same level of scientific review as those contained in IRIS. The results in this risk assessment were strongly influenced by the use of NCEA's provisional reference concentration for chlorine. IRIS has only an oral RfD of 0.1 mg/kg-day. Using route-to-route extrapolation, the 1998 guidance has an inhalation reference concentration of 0.35 mg/m³. NCEA's provisional reference concentration is 0.0002 mg/m³. The use of NCEA's value increased the hazard index for chlorine by a factor of 1,750 over using the value in the 1998 guidance. Without the use of the NCEA value for chlorine, the total hazard indices would decrease from 60% to 95%.

The noncancer hazards from chemical exposures in the risk assessment (except lead) were evaluated using the hazard index approach, wherein the estimated dose is divided by an established EPA safe dose, an oral RfD, or an inhalation reference concentration. The RfD and reference concentrations are typically 100 to 10,000 times less than the highest no-observed-adverse-effects levels (NOAEL) observed in the most sensitive animal species. This approach is likely to overstate the potential for noncancer hazards in humans.

2.13.9 Risk Characterization

Because the risk characterization relies on all of the previous factors, it will have an even higher degree of uncertainty. Also, most of the input is based on conservative assumptions, so the resulting risks and hazards will tend to be even more conservative. This is the purpose of a screening-level risk assessment—to produce upper-bound estimates of risks, not to characterize risks that are most likely for individuals or the population at large.

2.14 Summary and Conclusions

RCRA regulations require that potential risks be evaluated when permitting facilities that produce emissions from the burning of hazardous wastes. Thus, the development of the HHRAP guidance has been driven by the permitting needs of the regulatory community, especially the EPA. While there are a large number of uncertainties associated with the risk assessment process, it is obvious that the risk estimates are likely to be conservative and err on the side of safety and protection of human health.

References

- ATSDR. 1999. ATSDR's toxicological profiles on CD-ROM. CRCnetBASE 1999. U.S. Department of Health and Human Services, Agency for Toxic Substances and Disease Registry, Public Health Service, Atlanta, GA.
- Junge, C.E. 1977. Fate of pollutants in the air and water environments, Part I. Suffet, I.H. (Ed.). John Wiley & Sons, New York, pp. 7–26.
- NRC/NAS. 1983. Risk assessment in the federal government: Managing the process. National Research Council and the National Academy of Science, Washington, DC.
- U.S. EPA. 1989. Risk assessment guidance for Superfund: Volume I – Human health evaluation manual. Interim Final. EPA/540/1-89/002. U.S. Environmental Protection Agency, Office of Solid Waste, Office of Emergency and Remedial Response, Washington, DC.
- U.S. EPA. 1995. Health effects assessment summary tables. EPA/540/R-95/036. U.S. Environmental Protection Agency, Office of Emergency and Remedial Response, Washington, DC.
- U.S. EPA. 1998a. Human health risk assessment protocol for hazardous waste combustion facilities. Peer Review Draft. Volumes 1, 2, and 3. EPA-530-D-98/001A, B, and C. U.S. Environmental Protection Agency Region 6, Center for Combustion Science and Engineering, Multimedia Planning and Permitting Division, and Office of Solid Waste and Emergency Response, Washington, DC. www.epa.gov/epaoswer/hazwaste/combust/risk.htm.
- U.S. EPA. 1998b. Region 6 risk management addendum – Draft human health risk assessment protocol for hazardous waste combustion facilities. EPA-R6-98-002. U.S. Environmental Protection Agency, Region 6, Multimedia Planning and Permitting Division, and Office of Solid Waste and Emergency Response, Dallas, TX. www.epa.gov/epaoswer/hazwaste/combust/risk.htm.
- U.S. EPA. 1999a. Errata to human health risk assessment protocol for hazardous waste combustion facilities. Peer Review Draft. U.S. Environmental Protection Agency, Region 6, Center for Combustion Science, and Engineering and Office of Solid Waste and Emergency Response, Washington, DC. www.epa.gov/epaoswer/hazwaste/combust/risk.htm.
- U.S. EPA. 1999b. Integrated risk information system (IRIS). U.S. Environmental Protection Agency, Cincinnati, OH. <http://www.epa.gov/iris/index.html>.

Chapter 16

Statistical Modeling

A brief introduction to the topic “Statistical Modeling” was presented in Volume I of this book series. Two chapters on this topic:

16A – Air Quality Forecast and Alarm Systems

16B – Receptor Models

are included in the following pages.

BRANK P 2000

Finzi, G. and G. Nunnari 2005. *Air Quality Forecast and Alarm Systems*. Chapter 16A of *AIR QUALITY MODELING - Theories, Methodologies, Computational Techniques, and Available Databases and Software. Vol. II – Advanced Topics* (P. Zannetti, Editor). Published by The EnviroComp Institute (<http://www.envirocomp.org/>) and the Air & Waste Management Association (<http://www.awma.org/>).

Chapter 16A

Air Quality Forecast and Alarm Systems

Giovanna Finzi ⁽¹⁾ and Giuseppe Nunnari ⁽²⁾

⁽¹⁾ *Dipartimento di Elettronica per l'Automazione, Università di Brescia, Brescia (Italy)*

finzi@ing.unibs.it

⁽²⁾ *Dipartimento di Ingegneria Elettrica Elettronica e dei Sistemi, Università di Catania, Catania (Italy)*

gunnari@dees.unict.it

Abstract: The following chapter reports a review of different stochastic and statistical modelling approaches, and the results obtained by their application to actual case studies both in urban and in industrial areas. The assessment of the results, in terms of daily and hourly forecast performance indexes and statistical indicators, is presented, compared and discussed. The structure of the chapter is the following. After a preliminary section summarizing the most significant stochastic and statistical modelling techniques (Section 1), some literature results are reported in Section 2. A more detailed mathematical description of the main techniques considered for air quality modelling is given in Section 3. Section 4 gives guidelines on how to build a model for air quality forecast and evaluate its performances. Some case studies concerning the modelling of tropospheric ozone concentrations, both in urban and industrial areas, are given in Section 5. In Section 6 the application of the selected techniques to the implementation of an operational decision support system (DSS) is described. Also, the performance of the system for two different metropolitan areas in the Northern part of Italy (namely Brescia and Milan) is evaluated. Finally, a short survey of the available software packages to implement the modelling techniques described is given in Appendix.

Key Words: stochastic models, air quality forecast, tropospheric ozone, decision support system.

1 Introduction

Stochastic and statistical models are based on semi-empirical relationships between available data and measurements. The distinction between stochastic and statistical models is not always clear in literature since these models share several common features. Usually models are referred to as stochastic when the time variability is taken into account explicitly, and they are referred to as statistical if based on the use of some stationary statistical approaches (such as the clustering techniques or the Bayesian inference mechanism).

Models taking uncertainty into account, instead of deterministic ones, do not aim to describe the level of pollution as a phenomenology-driven, cause-effect problem; instead, their identification is based on the direct use of air quality measurements. In particular, statistical models are generally useful when the information available from measured concentration trends is more relevant than the one obtained from the deterministic analyses. The use of statistical models may also be encouraged by the presence of a significant amount of data, recorded by several monitoring networks, in the territory of interest.

Some general information about basic statistical and stochastic models for air pollution data is given in Gilbert (1987) and Zannetti (1990). More recent techniques are described by Finzi et al. (2001) and Jorquera et al. (2004).

In the development of such models, measurements of pollutants and related meteorological variables have been considered as time series and analysed by means of a wide variety of methods, including:

- spectral analysis
- component approach (trend + seasonal + residuals)
- regression analysis
- trend analysis
- clustering analysis
- principal component analysis
- hybrid models
- *black-box* ARIMA models
- *grey-box* (non linear and non stationary) models
- Bayesian models

More recently other statistical approaches have been published generically referenced as AI (*Artificial Intelligence*) or *Soft-computing* techniques, including:

- *neural models*
- *fuzzy models*
- *neuro-fuzzy models*

Statistical modelling approaches can be used in a *black box* mode (i.e., pollutant concentration time series analysed without any phenomenological information),

to evaluate their intrinsic statistical variations without attempting any physical explanation. Otherwise, they can be used in a *grey box* mode, in which other information (such as meteorological or emission variables, seasonal cycles) may be taken into account explicitly or implicitly, although always in an uncertain environment.

In the following each model class will be shortly referenced, pointing out its main features with respect to a possible use as air pollutant concentrations predictor.

- **Spectral analysis** (Jenkins and Watts, 1968) allows the identification of cycles in meteorological and air quality time series measurements. Early applications of spectral analysis of SO₂ concentration were carried out by Tilley and McBean (1973) and Trivikrama et al. (1976). They showed the existence of semi-diurnal, diurnal and three-and-half-day period oscillations in SO₂ and wind time series recorded in the study area (Northern USA). Semidiurnal cycles were interpreted in terms of local phenomena, such as sea breezes. Longer periods seem to be induced by synoptic weather variations. More recently, spectral analysis has been applied by Schlink et al. (1997) for analysing SO₂ data recorded at Leipzig in the years 1980-1993.
- **Component models** are based on a spectral decomposition of time series into a trend component, a periodic component, and a residual component. Each component shows a peculiar behaviour; in particular, trend one is very smooth and slowly varying with fixed periods for the cyclic components. Each component is predicted on the basis of its features and the final forecast is a combination of all of them (Schlink et al., 1997). In spectral decomposition, low-pass and band-pass filters are used to quantify the components. Young et al. (1991) gave very convenient and flexible filtering algorithms based on the Kalman filter.
- **Regression analysis** is a particular type of stationary multiple input time-series analysis, in which meteorological measurements are statistically related to air quality concentrations by means of a linear model.
- **Trend analysis** allows evidencing and eliminating any *a priori* significant trend or seasonal variation in time series (see contribution by Buishand et al., 1988).
- **Clustering analysis** allows finding a set of *a priori* unknown data categories (or clusters), based on available set elements and observations. Formally, a clustering process orders observations in clusters (i.e., subsets with high degree of association among members of the same group and low among members of different groups). Clustering analysis for modelling pollution data has been considered for instance by Sanchez et al. (1990) and Huang (1992).

- **Principal component analysis** allows reduction of multivariate data through transformation of the original variables into a new set of uncorrelated ones, progressively accounting for decreasing proportions of explained variance in the data. Aim of this methodology is to reduce the dimensionality of the model. The new variables (principal components), are defined as linear functions of the original ones. If a limited number of components account for a large percentage of explained variance in the observations, they can be used to simplify the subsequent analysis. Principal components have been used by many authors (e.g., Lins, 1987).
- **Hybrid models**, mainly the ones based on Kalman filters, have been frequently used for updating the forecast capabilities of a deterministic predictor based on the availability of real-time measurement of pollutants. For instance, the application proposed by Melli et al. (1981) suggested this approach for real-time control of SO₂ emissions in the industrial area of Porto Marghera, which is located in the Venetian lagoon region (Italy).
- **Black-box ARIMA and ARMAX models** (Box and Jenkins, 1970, 1976; Box et al., 1994) have been considered as one of the most cost-effective approaches for time series analysis. Many authors have been inspired to apply this technique in developing pollutant forecast models for SO₂ time series as well as for other pollutants such as ozone, NO_x, etc. (see Finzi et al., 1983).
- **Grey-box models** are extended ARMAX (Auto Regressive Moving Average with eXogenous inputs) models, which allow the user to take into account the non-stationarity of the process through parameters depending on time-varying classes in order to treat the complexity of air pollution dynamics (a first example of application to SO₂ urban pollution forecast is illustrated in Finzi and Tebaldi, 1982).
- The **neural approach** consists of using artificial neural networks (ANN) to identify air quality prediction models. Neural networks are virtually parallel computational architecture based on the emulation of the human brain. Applications of similar computational architectures to the prediction of SO₂ concentration have been described by Boznar et al. (1993), Arena et al. (1996), Finzi et al. (1998), and Nunnari et al. (2001).
- The **fuzzy approach** aims to describe the behaviour of dynamic systems by using linguistic representation (i.e., the system model is represented by a set of rules, the rule base, in the “if...then” form). A similar methodology has been proposed to implement NARX (Non-linear Auto Regressive with eXogenous inputs) models of pollutant time series (e.g., Nunnari et al., 1998; Nunnari, 2000), allowing an easily understandable way to model complex air quality phenomena.

- In **neuro-fuzzy** systems, neural networks are used to tune the *membership functions* of the fuzzy system and to automatically extract *fuzzy rules* from numerical data (see Finzi and Volta, 2000).
- **Bayesian models** are recent techniques applied to forecast critical pollution episodes. Some contributions referring to this topic are reported by Maffei (1999), Cossentino et al. (2003), and Nunnari and Cannavò (2004). The peculiarity of this approach is that the prediction problem is formalised in terms of a Bayesian Network (BN). Deep *a priori* knowledge about the model structure is not required to build a BN; instead, heuristic knowledge that is usually available can easily be taken into account. Bayesian models can work even in the presence of partially missing input information. When some input values are missing, they can simply be neglected or replaced by surrogates such as the corresponding probability distributions. Finally, BNs can operate in the so-called *diagnostic mode* in order to infer the causes of poor air quality.

2 Some Literature Results

Some of the most significant results, which appeared in the literature referred above, are shortly reported in the following: they mainly concern the application of statistical and stochastic models to predict critical pollutant concentrations both in industrial and urban areas.

Regression analysis was employed by Bringfelt (1971) to assess significant variables driving SO₂ concentrations in Central Stockholm. One of the aims of the study was to set up a warning system for SO₂ episodes based on the forecast of atmospheric mixing layer height and wind speed. SO₂ mean daily concentrations, averaged over four monitoring sites in Central Stockholm, were compared with temperature, wind speed and mixing height by means of a multiple regression analyses for the winter periods of 1967-1969. Different methods to extract the best meteorological predictors from routine weather data were compared. As temperature predictor, the difference of mean daily temperature monitored at the local airport was used when below a threshold of 25°C. The mixing height was estimated on the basis of night and day radio sounding measures (01 and 13 hours) and the minimum temperature in the city. The multiple correlation coefficient came out quite high (0.84). The daily SO₂ levels were predicted with a standard error of about 25%.

A **Kalman filtering** approach was proposed by Melli et al. (1981) for modelling SO₂ emissions in the Venetian Lagoon industrial area (Northern Italy) with the aim of implementing a real time system for emission control; the authors considered real-time emission control as an air quality strategy alternative to permanent emission reduction. They proposed an emission control scheme characterised by the following steps:

- Collect current concentration and meteorological measurements from monitoring networks.
- Forecast future values of relevant local meteorological variables, by means of simple stochastic mathematical predictors.
- Predict future concentrations on the basis of information from current concentration values, forecast meteorology and scheduled emissions. The predictor model is based on a complex forecast algorithm (Kalman predictor) derived from the “stochastic version” of the numerical solution of the advection-diffusion partial differential equation.
- If future concentrations exceed some reference level, the scheduled emissions are reduced. The assumed control policy consists of mixing fuel with a cleaner one, under the constraint of maintaining the production scheduled by each polluting plant.

The results of the case study are supplied as cost-effectiveness curves (cost versus effectiveness of the control action). The authors showed that real-time emission control was economically cheaper and technically possible.

Finzi and Tebaldi (1982) applied a non-stationary and non-linear **grey-box** autoregressive model with exogenous inputs to predict daily SO₂ average concentration in Milan urban area (Northern Italy). This city is now using mostly methane or low sulphur fuels for domestic heating, but at the time when the study was performed (late 1970s), there were serious problems with SO₂ pollution due to low quality fuels widely used for domestic heating. Data analysis carried out on historical time series allowed the authors to evidence that the urban pollution level was particularly high during cold season with anti-cyclonic synoptic conditions, low ambient temperature, and low wind. So they implemented a forecast model for daily SO₂ DAP (Dosage Area Product) computed over Milan urban area. In particular, two different meteorological categories were defined respectively, corresponding to cyclonic and anti-cyclonic synoptic regimes over Northern Italy; the local wind velocity and temperature were considered as non-linear exogenous inputs. The model was validated comparing predicted and measured data during the winter season of 1975-1976, with fairly good agreement mainly during severe critical episodes.

A more complex *grey-box* model was further applied in a study concerning SO₂ air pollution forecast in Madrid metropolitan area (Hernandez et al., 1983; Finzi et al., 1983). In this study the role of meteorological variables in statistical pollution forecasting models was highlighted. A comparison was also performed between *black-box* and *grey-box* models, showing how the use of basic physical knowledge of the phenomenology allows a higher cleverness in episodes prediction.

Another statistical model to forecast SO₂ concentrations in the surroundings of a thermal power plant was studied by Brusasca and Finzi (1986) with the purpose of emission real-time control. The plant taken as a case study, with a nominal

power of 1365 MW, is located at Turbigo (in the Po Valley near the Alps Mountains, the Ticino River Natural Park, and not far from the city of Milan) and managed by ENEL (the Italian National Electricity Board). The authors implemented a **Cyclostationary** Auto Regressive model (referred also as ARCX in the following Sections) to forecast half-hourly and daily mean concentrations of SO₂ at some hours in advance during the day. Thanks to a recursive computation scheme, the prediction of half-hourly average concentrations was performed and updated starting from the morning data considered for the study. They recorded at 5 stations around the plant (in the range of 5 Km) during the cold seasons of 1982/83, 1983/84 and 1984/85. The real-time daily SO₂ forecast model was compared with a more trivial one, the so-called persistent model; the results evidenced that the stochastic predictor performed much better in terms of a statistical analysis of the forecast errors, and allowed the power plant managers to prevent critical episodes and meet law standards.

Boznar et al. (1993) carried out one of the first studies that appeared in the literature concerning a comparison between a deterministic and a **neural network** based approach. They modelled SO₂ concentrations due to Slovenian thermal power plant emissions and pointed out the difficulties in using deterministic models when the terrain is not flat. Moreover, they stressed the fact that also the simplest stationary Gaussian model needs several input parameters to work properly. Since it is often difficult to get inputs and a reliable parameterisation in real time, deterministic models may give unrealistic estimates, mostly based on the assumption of a stationary emission and meteorological scenario. Alternatively, they proposed a **neural network** based approach for short-term prediction.

Artificial neural networks have also been taken into consideration by Arena et al. (1996) to set up a model of SO₂ time series monitored in an industrial area very close to Siracusa (Sicily). In particular, a short-term prediction (six hours ahead) of the SO₂ pollutant mean value has been performed. A neural architecture was implemented, based essentially on a *Multilayer Perceptron* devoted to predict alarming situations and to estimate the mean pollutant value. The results showed that **neural network** based strategies for short-term prediction of SO₂ levels are promising.

Statistical methods have also been developed by Schlink et al. (1997) to set up an advanced smog warning system in central Leipzig (Germany) by modelling winter time SO₂ concentrations recorded during 1980-1993. The authors essentially use a **recursive Kalman algorithm**, based on a preliminary spectral analysis of the SO₂ concentration time series; the smog episodes with low frequencies and time-dependent power spectra were well represented by the trend component alone. This component was therefore investigated in the phase space, where it exhibited a typical trajectory feature. One data subset was used to identify the model parameters and another was left for validation; the results were still not satisfactory. So a modified method was proposed to extrapolate the time-

dependent spectrum of the trend component, namely a local harmonic approximation. This method was tested and compared with simple linear extrapolation. It provided a generalization, producing closer correspondence between predicted and observed concentration values.

Another study concerning **neural network** models, applied to SO₂ pollution, has been reported by Reich et al. (1999). They address the problem of the apportionment of a small number of SO₂ sources from a data set of ambient concentrations. A three layer feed-forward artificial **neural network** trained with a back-propagation algorithm was employed. A subset of hourly meteorological conditions and measured concentrations constituted the input patterns to the network, which was mainly designed to identify relevant emission parameters of unknown sources as outputs. The remaining model data were degraded by adding noise to some meteorological parameters and the effectiveness of the method was tested. The model was applied to a realistic case where 24 h SO₂ concentrations were previously measured. Some of the limitations of the artificial **neural network** approach and its capabilities are discussed in this paper.

The role of statistical and stochastic modelling techniques as a practical tool for air quality prediction and forecasting has been recognized by the European Union in the framework of the Fifth Framework Program funded projects devoted to develop and test a variety of advanced statistically based modelling techniques. Among these, it is worth to mention the APPETISE project (*Air pollution episodes: modelling tools for improved smog management*, <http://www.uea.ac.uk/env/appetise/>). This work has been carried out over a period of two years (Greig et al, 2000) by a consortium of 9 institutions from 5 different European Countries. The project has focused essentially on four key pollutants: nitrogen oxides, particulates, ground level ozone and sulphur dioxide.

A significant number of statistical modelling techniques were applied to model pollutant time series of a rich database representing different meteorological and emission conditions throughout Europe. The performances of the considered techniques were inter-compared rigorously. The variety of inter-compared techniques together with the different locations of the area considered, and different kind of sites (i.e., urban, suburban, rural, industrial) and targets make the results of this inter-comparison exercise more general and interesting. The main results of the project have been published by Schlink et al. (2003) for ground level O₃, by Kukkonen et al. (2003) for NO₂ and PM₁₀, and by Nunnari et al. (2004) for SO₂.

In Section 5, *grey-box* models, *neural*, *fuzzy* and *neuro-fuzzy* networks will be taken into consideration and applied to other recent real case studies, and their performance will be compared as real time predictors for atmospheric urban pollutant concentrations. As introduced above, all the approaches are based on the analysis of time series of pollutant concentration measures recorded by air quality control networks. The first methodology requires a minimum physical

understanding of the phenomenon in order to drive the model to the description of the non-linearity and non-stationarity of the process by means of a limited number of parameters, while the other ones can be applied by a non-expert user by means of largely automatic procedures (*black-box* approach).

3 Time Series Modelling

Techniques for modelling time series can be roughly classified as linear and non-linear.

3.1 Linear Techniques

Linear techniques represent the simplest way to model statistical time series. Despite the fact that the largest part of natural phenomena are non-linear (e.g., Kantz and Schreiber, 1997), several ideas can be generalised from the theory of linear modelling techniques.

Until recently, linear multi-variate methods have been considered to be one of the most cost-effective approaches for time series analysis. Many authors have been inspired to apply these techniques, after some appropriate modifications, in developing pollutant forecasting models. These techniques have been applied to modelling SO₂ time series as well as other pollutants such as O₃, NO_x etc. The original Box-Jenkins approach (Box and Jenkins, 1976; Box et al., 1994) has been adapted by some authors in order to treat the complexity of air pollution data such as non-stationarity (e.g., Finzi et al., 1998).

The basic structure of linear techniques is outlined as follows. Let us denote a discrete time random process by $\{y(t)\}$ and a discrete purely random process with zero mean and variance σ^2 by $\{e(t)\}$. A process $\{y(t)\}$ is said to be a moving average process of order q , and indicated as MA(q) if

$$y(t) = e(t) + \gamma_1 e(t-1) + \dots + \gamma_q e(t-q) = (1 + \gamma_1 B + \dots + \gamma_q B^q) e(t) \quad (1)$$

where γ_i are constants and B is the backward shift operator. Similarly a process is said to be an autoregressive process of order p , and indicated as AR(p) if

$$y(t) = \alpha_1 y(t-1) + \dots + \alpha_p y(t-p) + e(t) \quad (2)$$

where α_i are constants and $|\alpha_i| < 1$.

A very simple AR model is the so-called persistent model (i.e., $y(t) = y(t-1)$, tomorrow equals today) that is often considered as a reference model during inter-comparison exercises.

By combining the AR and the MA structures, it is possible to obtain an ARMA process of order (p,q) as follows:

$$y(t) = \alpha_1 y(t-1) + \dots + \alpha_p y(t-p) + e(t) + \gamma_1 e(t-1) + \dots + \gamma_q e(t-q) \quad (3)$$

Such structure is sometimes useful to model linear stationary univariate time series. To handle linear non-stationary time series, the ARMA model can be appropriately extended in order to obtain the ARIMA model (Box and Jenkins, 1970). An ARIMA(p, d, q) model is a particular ARMA model where the original time series $\{y(t)\}$ is substituted by the d-times differenced series $\{B^d y(t)\}$.

Multivariate time series (i.e., time series in which one variable is related to others), referred to as exogenous variables (or inputs), can be modelled by using the ARMAX models. As an example, if we want to model the ozone time series recorded at a given point, we can try to use as exogenous variables (the solar radiation and the concentration of Nitrogen Dioxide, NO₂) since it is known that these variables play a role in the ozone cycle. The structure of the ARMAX process is the following:

$$y(t) = \alpha_1 y(t-1) + \dots + \alpha_p y(t-p) + \beta_1 u(t-1) + \dots + \beta_r u(t-r) + e(t) + \gamma_1 e(t-1) + \dots + \gamma_q e(t-q) \quad (4)$$

Equation (4) has been considered in the presence of an individual exogenous variable $u(t)$, also referred to as the input variable, but the generalization to the case of a generic number of exogenous variables is trivial. Furthermore, the above-mentioned structure can be generalised to the case when the stochastic variables $y(t)$ and $u(t)$ are vectors. ARMAX models lead to a simpler but quite useful representation. The ARX model is given by:

$$y(t) = \alpha_1 y(t-1) + \dots + \alpha_p y(t-p) + \beta_1 u(t-1) + \dots + \beta_r u(t-r) + e(t) \quad (5)$$

Identification of parameters of ARX models (i.e., the determination of constants α_i and β_i from experimental data), can be obtained by the standard Least Square (LS) method. Identification of ARMAX models can be performed instead using the Generalized Least Square (GLS) approach (e.g., Soderstrom and Stoica, 1989).

Finzi et al. (1982) proposed a particular kind of ARMAX models referred to as *cyclo-stationary* or *grey-box* ARMAX model that are able to deal with particular (cyclic) non-stationary phenomena that often affect pollution time series. The structure of a *cyclo-stationary* ARMAX model is as follows:

$$y(t) = \sum_{i=1}^p \alpha_i [s(t)] \cdot y(t-i) + \sum_{j=1}^r \beta_j [s(t)] \cdot u_j(t-k_j) + \sum_{h=1}^q \gamma_h [s(t)] \cdot e(t-h) + e(t) \quad (6)$$

where $s(t)$ is a properly defined category at time t and k_j is the lag time. These kinds of models can be useful when the process to be modelled is affected by some underlying periodic (daily, weekly, seasonal or yearly) components.

3.2 Non-Linear Techniques

Linear methods allow interpreting all the regular structure in a data set such as dominant frequencies. However, the linear paradigm, which can be roughly stated as “small causes lead to small effects”, is not always true for natural phenomena. This can be explained by bearing in mind that linear differential equations can only lead to exponentially growing or periodically oscillating solutions. This means that all irregular behaviours of a given system must be attributed to some random external input. However, it is known from the *System Theory* that random inputs are not the only ones responsible for irregular behaviours of the system output; nonlinearities or chaos can produce very irregular data even with purely deterministic equation. So, it is better to try to explain irregularities in a given time series with both the presence of random inputs and nonlinearities (Kantz and Schreiber, 1997). The literature about non-linear modelling techniques is very rich and we will deal with the most widely considered ones here.

3.2.1 NARX Models

A general way to represent nonlinear systems is the NARX (Non-linear Auto Regressive with eXogenous inputs) representation, which can be considered as a generalization of the ARX model:

$$y(t) = f(y(t-1), \dots, y(t-p), u_1(t-1), \dots, u_1(t-r_1), u_2(t-1), \dots, u_2(t-r_2), \dots, u_n(t-1), \dots, u_n(t-r_n)) + e(t) = f(X) + e(t) \quad (7)$$

Here f is an unknown non-linear function, $y(t)$ is the system output, u_1, u_2, \dots, u_n are related input variables (e.g., meteorological and/or emission variables), and $e(t)$ is a random term. In expression (7) the variable X is expressed as:

$$X^T(t) = [y(t), y(t-1), \dots, y(t-n_y+1), u_1(t), \dots, u_1(t-n_1+1), \dots, u_q(t), \dots, u_q(t-n_1+1)] \in R^d \quad (8)$$

in order to indicate the data vector, also referred to as the model input pattern.

Several of the most powerful time series modern techniques - such as the Multi-layer Perceptron (MLP) artificial **neural networks**, the *Fuzzy* and *Neuro-Fuzzy*

techniques - can be considered for approximating the unknown function f , given an appropriate set of measured data, as explained below.

3.2.1.1 The MLP Modelling Technique

Multi-layer Perceptron (MLP) Neural Networks are parallel computational architectures where their structure is based on the emulation of the human brain. If suitably “trained” using a set of examples, they can “learn”; that is, they can extract the link between the input data and the corresponding output data (Lippmann, 1987). MLPs can thus be used to solve a number of problems of classification, and more generally, *black-box* identification, in which *a priori* knowledge of the model is not needed (Chen and Billings, 1992). Moreover, operations are relatively simple and can be performed quite systematically; the learning phase is entrusted to special optimisation algorithms such as the *back-propagation* algorithm (Rumelhart et al., 1986). Properties of MLPs in non-linear system identification are described in Sioberg et al. (1994). From the mathematical point of view, MLPs perform automatic search of models in the class of NARX structure. It has to be stressed that such a modelling approach can be equally applicable for both scalar and vector sequences. The use of this non-linear auto-regression can be justified as follows. For a wide class of deterministic systems, it can be assumed a *diffeomorphism* (i.e., a one-to-one differential mapping) between a finite window of the time series [$y(t-1)$, ... $y(t-p)$, $u(t-1)$, ... $u(t-n)$] and the underlying state of the dynamic system which gives rise to the time series. This implies the existence of the non-linear auto-regression of the form (7). The MLP neural network thus forms an approximation of the ideal function $f(\cdot)$. Furthermore, it has been shown (Cybenko, 1989) that a feed-forward **neural network**, with an arbitrary number of neurons in the hidden layer, can approximate any uniformly continuous function with an arbitrary degree of accuracy.

The internal model representation by using a *Multi-layer Perceptron* structure is based on the expression:

$$N_i(U) = \Gamma(W_i \cdot U + B_i) \quad (9)$$

which is used in a recursive frame. The meaning of the symbols is as follows:

- U = output of the (i-1)th layer
- W_i = weight matrix associated to the ith layer
- B_i = bias vector corresponding to the ith layer
- Γ = an appropriate activation function

Formally, the output of the **neural network** can be expressed as follows:

$$Y = F(U) = \Gamma(W_n (\Gamma(W_{n-1} (\dots \Gamma(W_1 \cdot U)))) \quad (10)$$

In the expression above, the biases have not been reported for sake of simplicity. Since a MLP with one hidden layer can solve the same class of problems that can be solved by using MLP with more than one hidden layer, below we will refer to MLP with one hidden layer only. Under this hypothesis, expression (10) assumes the following simpler form:

$$Y = F(U) = \Gamma(W_2 (\Gamma(W_1 \cdot U + B_1) + B_2)) \quad (11)$$

MLPs have been considered in the literature for air pollution time series modelling by several authors such as Boznar et al. (1993), Arena et al. (1996), Nunnari et al. (1998), Gardner and Dorling (1998, 1999), Schlink et al. (2003), Kukkonen et al. (2003), and Nunnari et al. (2004).

A problem with using MLP trained by the traditional back-propagation algorithm is, apart from the often excessively low speed of convergence (e.g., Sarkar, 1995), the possibility of obtaining configurations of the weights corresponding to a local minimum. The literature reports numerous variations of this algorithm aimed at improving the performance (see Gori and Tesi, 1992). Another problem using MLP is the choice of the most appropriate number of neuron in the hidden layers. A small number of hidden neurons yields low accuracy models; on the other hand, a large number produces the problem of over fitting, which means poor generalization capabilities of the model. Since there are no *a priori* formulas to compute the best number of hidden neurons (Barron, 1993), this is usually done by a trial and error approach by searching for a trade-off between accuracy and generalization capabilities of new input data. In order to correctly evaluate the generalisation capabilities of MLP trained by using the traditional back-propagation (BP) algorithm, the so-called *Early Stopping* approach (Sjoberg and Ljung, 1995) can be considered.

Despite the fact that BP algorithm is the most widely considered **neural networks** for training MLP, others algorithms are available such as the conjugate gradient optimisation approach. Moreover, the traditional Sum of Squares Error (SSE) that is the standard cost function minimised by the BP algorithm is sometimes replaced by other kinds of cost function. As an example, Dorling et al. (2003) proposed to use the *maximum likelihood* cost functions to model air quality data.

3.2.1.2 The Fuzzy Modelling Technique

The fuzzy set theory represents a different approach to dealing with uncertainty than the traditional probabilistic and statistical methods. The essential feature of the fuzzy logic is the concept of membership function, which ranges between 0 and 1 and represents the degree of membership of an individual element to a given set, referred to as a fuzzy set. From the seminal paper by Zadeh (1965), a lot of work has been carried out in the field of fuzzy logic, and it is beyond the purpose of this chapter to deal with the huge amount of theoretical and practical aspects of this theory. Here, we only deal with the problem of approximating a NARX model of the form (7) by using a fuzzy rule base of the form:

$$\begin{aligned}
 R_i : \text{if } y(t) \text{ is } A_{i,1} \text{ and } y(t-1) \text{ is } A_{i,2} \text{ and, } \dots, y(t-n_y+1) \text{ is } A_{i,n_y} \text{ and} \\
 u_1(t) \text{ is } A_{i,n_y+1} \text{ and } u_1(t) \text{ is } A_{i,n_y+2} \text{ and, } \dots, u_1(t) \text{ is } A_{i,n_y+n_1} \text{ and} \\
 \dots \\
 u_q(t) \text{ is } A_{i,n_y+n_1+\dots} \text{ and } u_q(t) \text{ is } A_{i,n_y+2} \text{ and, } \dots, u_q(t) \text{ is } A_{i,p} \\
 y(t+1) \text{ is } B_i \quad (i=1, \dots, k)
 \end{aligned} \tag{12}$$

where $A_{i,j}$ ($j=1, \dots, p$) and B_i ($i=1, \dots, K$) are fuzzy sets. Particularly in the case considered below, the consequent fuzzy sets B_i are assumed to be *singletons* (i.e., real numbers).

The fuzzy modelling approach consists of the following steps:

1. Positioning of the membership functions $A_{i,j}$ in their respective universe of discourse. This step is based on the determination of the matrix centres of the input data clusters by using one of the clustering algorithms described in the subsequent Section 3.2.6, or it can be simply performed on a trial and error basis. The shape of the membership function must also be selected among a large variety (e.g., trapezoidal, Gaussian, etc.)
2. Generation of all possible rules according with the input patterns available
3. Pruning of the unnecessary rules; this step is based on approximating the input patterns with the closest cluster centre
4. Determination of the consequent part of each rule; this is done by using an appropriate optimisation approach. It can be demonstrated that for rules of the form (12), the consequent part of each rule can be also obtained by using the least square algorithm (e.g., Nunnari, 2000)
5. Further pruning phase (last step is optional) according to a statistical criterion which takes into account the number of activation of each rule

More details about this algorithm for modelling air pollution time series can be found in (Nunnari, 2000). A quite similar approach, based on the use of the *Fuzzy C-means* clustering algorithm, is described in Section 3.2.6.

3.2.1.3 The *Neuro-Fuzzy* Technique

In *neuro-fuzzy* systems, **neural networks** are used to tune the *membership functions* of the fuzzy system and to automatically extract *fuzzy rules* from numerical data (Shing and Jang, 1993). The internal structure of a *neuro-fuzzy* network is illustrated in Figure 1. The nodes of the first layer represent the *crisp* inputs. The activation functions of the second layer nodes are Gaussian and act as membership functions. Each neuron of the third layer acts as a *rule node* so that this layer provides the fuzzy rule base. The output of this layer determines the activation level at the output memberships. As ordinary neural nets, the *neuro-fuzzy* one learns on a training data set, tuning membership functions and rules by means of a *back-propagation* algorithm.

When x_i is the i^{th} node in layer A , O_j^L is the j^{th} output of generic layer L , and W_{ij}^L is the weight of the link between j^{th} neuron at layer $L+1$ and i^{th} neuron at layer L , each layer output can be described as follows:

$$\text{Layer B: } O_j^B = \left(1 + \exp\left(-\frac{x_i - w_{ij}^{Ap}}{W_{ij}^{Al}}\right) \right)^{-1}$$

$$\text{Layer C: } O_j^C = \min_i (w_{ij}^B \cdot O_j^B)$$

$$\text{Layer D: } O_j^D = \frac{\sum_i w_{ij}^C \cdot O_i^C}{\sum_i O_i^C}$$

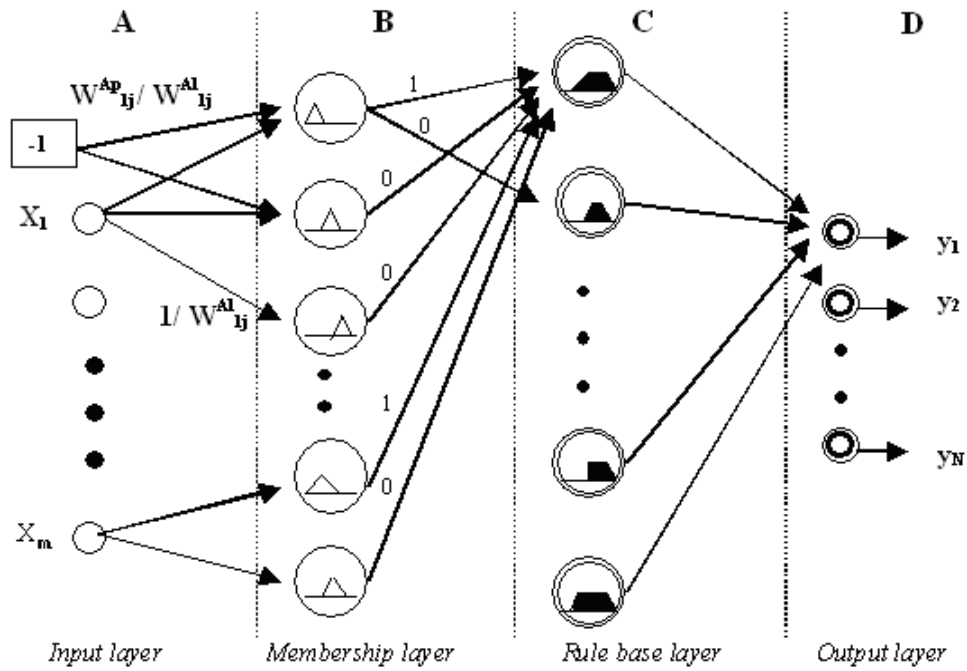


Figure 1. Neuro-fuzzy network architecture.

3.2.1.4 The Wavelet based Modelling Technique

Wavelet functions have been reported in the literature due to their capability of modelling transient phenomena occurring in particular geophysical time series (e.g., earthquakes). Some insights on the use of wavelets for system identification improvements can be found in Zhang (1997). A strategy, based on wavelets for modelling air pollution data, was proposed by Nunnari (2003). The mentioned approach can be summarised as follows. Let $\psi(t)$ be a basic wavelet function and let s ($s \neq 0$) and u be real numbers; the family of wavelets corresponding to $\psi(t)$ is

$$\Psi_{s,u}(t) = \frac{1}{\sqrt{s}} \Psi\left(\frac{t-u}{s}\right) \quad (13)$$

Here s represents the dilatation and u gives the translation. With reference to expressions (7) and (8), let us introduce the scalar quantities t_j ($j=1, \dots, M$) as a map between the vectorial argument of expression (7) and the scalar argument t of the generic j -th wavelet function (13):

$$t_j = \frac{[A_j \otimes (X(t) - U_j)] \cdot [A_j \otimes (X(t) - U_j)]^T}{s_j} \quad (14)$$

where A_j and U_j are appropriate vectors of unknown parameters. The WAG approach consists of approximating $y(t+1)$ in expression (7) as:

$$y(t+1) = \sum_{j=1}^M w_j \cdot \Psi_j(t_j) \quad (15)$$

In the WAG approach, the number of approximating wavelet functions M is obtained by a *trial and error* iterative procedure, a trade-off between accuracy and generalisation capabilities, while the remaining model parameters, namely A_j , U_j , s_j , and w_j ($j=1, M$) are searched by using a genetic algorithm (GA) optimisation approach (Holland, 1975). The reason for using GAs is that they are capable of finding the global minimum of a function with many variables, overcoming the limitation of typical gradient-based optimisation techniques (Goldberg, 1989). Even though by using a search algorithm, such as GAs, the modeller can define very complicated cost functions, good results can still be obtained by the traditional minimisation of the sum of error squares.

3.2.2 The Generalized Additive Modelling Technique

The Generalised Additive Model (GAM) uses smoothing techniques, such as locally weighted regression, to identify and represent possible non-linear relationships between the output and the model inputs (i.e., the explanatory variables).

This approach represents an alternative to considering polynomial terms or searching for the appropriate transformations of both output and input variables. By using these models, the link function of the expected output value variable is modelled as a sum of a number of smooth functions of the explanatory variables as expressed by (16) rather than in terms of explanatory variables themselves:

$$y(t+1) = f_1(u_1(t)) + f_2(u_2(t)) + \dots + f_k(u_k(t)) + e(t) \quad (16)$$

GAM is discussed in Breiman and Friedman (1985), Cleveland (1979), Davis et al. (1998), Davis and Speckman (1999), Hastie and Tibshirani (1986, 1987), and Wood (2000). Applying the GAM technique, the non-linear functions f_i in equation (16) are specified in a nonparametric fashion by means of scatterplot smoothers (i.e., weighted average of neighbouring observations). Cubic or fourth order splines functions were applied for instance by Schlink et al. (2003) to model tropospheric ozone and SO₂ time series (Nunnari et al., 2004)

3.2.3 Local Prediction in Phase Space

Local Prediction in Phase Space is a method for non-linear time series analysis, which is based on the paradigm of deterministic chaos (Kaplan and Glass, 1995;

Abarbanel, 1996; Kantz and Schreiber, 1997). The chaos theory offers completely new concepts and algorithms to model irregular behaviour and anomalies in systems, which do not seem to be inherently stochastic. An original reference on phase space embedding is Takens (1981).

The first step of the Local Prediction in Phase Space (LPH) technique is phase space embedding of the observed pollution data $y(t)$. This is done by forming delay vectors

$$\bar{y}(t) = (y(t - (m - 1)d), \dots, y(t - d), y(t))^T \quad (17)$$

with m representing the embedding dimension and d representing the delay time. Methods for estimating the optimal embedding parameters are discussed by Grassberger and Procaccia (1983), Kennel et al. (1992), and Sugihara and May (1990).

The second step is the local non-parametric extrapolation in the phase space, beginning at a starting point $\bar{y}(t)$. In a neighbourhood $U_\varepsilon(\bar{y}(t))$ of this point, all points and their tracks are considered. According to Equation (18), the forecast is calculated as the average of these tracks

$$y(t + 1) = \frac{1}{|U_\varepsilon(\bar{y}(t))|} \sum_{\bar{y}(s) \in U_\varepsilon(\bar{y}(t))} y(s + 1), \quad \text{with } s < t \quad (18)$$

A peculiarity of the LPH technique is that it requires time series without missing values. Application of this technique for modelling O_3 and SO_2 time series were considered by Schlink et al. (2003).

3.2.4 The Kalman Filtering Approach

The Kalman filtering approach is based on the assumption that the linearization and discretization - of the differential equation that describes the concentration of a given pollutant - are described by a system of equations of the form (19):

$$\begin{aligned} X(t + 1) &= A \cdot X(t) + B \cdot U(t) + C \cdot V(t) \\ Y(t) &= D \cdot X(t) + E \cdot Z(t) \end{aligned} \quad (19)$$

where A , B , C , D and E are matrices of parameters of appropriate dimensions, $X(t)$ and $U(t)$ are the state and input vectors respectively, and $V(t)$ and $Z(t)$ are purely random signals with zero mean and known covariance. The first part of Equation (19) is referred to as the state equation since it allows computation of the system state at time $t+1$ on the basis of information available up to time t . The second equation is referred to as the output (or the observation equation), and reflects the

fact that the state of the system is considered as an internal variable (i.e., it may not be directly observed, but it can be computed based on an appropriate measurement process) involving the variables $Y(t)$ and $U(t)$. The presence of the random variables, $V(t)$ and $Z(t)$, is the way to represent the incomplete knowledge of the process. Interested readers can find details about methods available to estimate the unknown parameters of the model (19) in several books, including Brown and Hwang (1996). A comprehensive framework for analysing time series of environmental data, based on the use of recursive Kalman filters, was proposed by Young et al. (1991) and further improved by Young et al. (1997) and Young (1998). Application of such a methodology has been proposed by Schlink et al. (1997) and Ng and Yan (1998).

3.2.5 Clustering Approaches

A statistical model to predict episodes of poor air quality can be formalized as a classification problem. To understand this, it is necessary to bear in mind that often we are not interested to know the *exact* value that will assume the concentration of a given pollutant, but rather if the value will belong to a certain class. For instance, we might classify air quality in classes such as (excellent, good, acceptable, worse, or bad) and we may be interested to forecast the class of air quality for tomorrow. Or we might classify the concentration of a given pollutant in classes according to threshold levels suggested by actual legislation (e.g., the attention level of the alarm level) and we want to know if the concentration of a given pollutant will exceed the attention level tomorrow. Classification models can be obtained using a large variety of approaches. For instance, a traditional MLP **neural network** can be *trained* as a classifier to forecast if the concentration of a given pollutant will exceed the attention level or not, rather than try to predict the *exact* value. In this case, it would be possible to use well-known algorithms such as the back-propagation to find the model parameters. However, more appropriately, the classification can be achieved by using one of the numerous algorithms proposed in literature, such as the K-means developed by MacQueen in 1967 and the Hard C-Means. For a description of these algorithms, see Anderberg (1973) and Hartigan (1975), respectively, or the good synthesis made by Jorquera et al. (2004). A K-means clustering approach was considered by Sanchez et al. (1990), who presented results of a synoptic meteorological classification oriented at forecasting particulate matter in the city of Valladolid (Spain). Clustering was also used by Huang (1992) to predict air quality in the city of Xiamen (China).

The advent of Fuzzy Logic has stimulated the development of other clustering algorithms such as the Fuzzy C-Means developed by Dunn (1973), further improved by Bezdek (1981). This method is based on minimizing the following objective function:

$$J_m = \sum_{i=1}^N \sum_{j=1}^C u_{ij}^m \|x_i - c_j\|^2, \quad 1 \leq m < \infty \quad (20)$$

where m is any real number greater than 1, u_{ij} is the degree of membership of x_i in the cluster j , x_i is the i^{th} of d -dimensional measured data, c_j is the d -dimension centre of the cluster, and $\|*\|$ is any norm expressing the similarity between any measured data and the centre. The real number m is referred to as the fuzzyfication parameter. If m is zero, the clusters are conventional. However, the larger the parameter value, the fuzzier the cluster will be. The recommended value for m is 2, which also assures convergence of the algorithm.

Fuzzy partitioning is carried out through an iterative optimisation of the objective function shown above, with the update of membership u_{ij} :

$$u_{ij} = \frac{1}{\sum_{k=1}^C \left(\frac{\|x_i - c_j\|^2}{\|x_i - c_k\|^2} \right)^{\frac{2}{m-1}}} \quad (21)$$

and the cluster centres c_j .

$$c_j = \frac{\sum_{i=1}^N u_{ij}^m \cdot x_i}{\sum_{i=1}^N u_{ij}^m} \quad (22)$$

This iteration will stop when:

$$\max_{ij} \{ |u_{ij}^{k+1} - u_{ij}^k| \} < \varepsilon \quad (23)$$

where ε is a termination criterion (between 0 and 1) and k is the iteration steps. This procedure converges to a local minimum or a saddle point of J_m .

3.2.6 Identification of Air Quality Models by Using Fuzzy C-Means

The Fuzzy C-means algorithm can be used to identify non-linear air quality models using the approach proposed by Sugeno and Yasukawa (1993). This approach allows minimization of the number of rules in the fuzzy rule base thus avoiding the drawback of traditional fuzzy model identification, where the number of fuzzy rules increases exponentially with the number of inputs. This is obtained by partitioning the input universe of discourse based on the Fuzzy C-means.

The method can be stated as follows. Let B represent a fuzzy cluster defined in the output variable universe and A the projection of B in the input space. The projection of A in the axes of the input variables x_j , ($i = 1, \dots, p$) yields the fuzzy sets A_j . The projection must satisfy the following relation:

$$A_1(x_{1k}) = A_2(x_{2k}) = \dots = A_p(x_{pk}) = B_i(y_{1k}) \quad (24)$$

where $A_j(x_{jk})$ is the degree of membership of the k^{th} sample of the input variable x_j to the fuzzy set and A_j and $B_i(y_k)$ are the degree of membership of the k^{th} sample to the cluster B_i . Expression (24) gives the following fuzzy rule:

$$\text{if } x_1 \text{ is } A_1 \text{ and } x_2 \text{ is } A_2 \text{ and } \dots \text{ and } x_p \text{ is } A_p \text{ then } y \text{ is } B_1 \quad (25)$$

Note that in order to avoid generating two or more fuzzy rule for each input variable, it is necessary to assume that the fuzzy clusters cannot be convex. After generating the fuzzy set A , the fuzzy sets A_j are approximated by trapezoidal-type set. Hence, the consequent part of the rule generated from equation (24) is changed by consequents in the typical Takagi-Sugeno form:

$$y^i = c_0^i + \sum_{j=1}^p c_j^i \cdot x_j \quad (26)$$

The unknown parameters c_j^i are identified by using the traditional least square approach.

The original Takagi-Sugeno approach has a number of drawbacks. It performs the clustering process using only the information from the output space, thus ignoring the input space. Furthermore, non-convex clusters in the input space must be split into two or more sets. Some of these limitations were overcome by other authors such as Briseño and Cipriano (1996).

3.2.7 Bayesian Air Quality Models

Bayesian models, also known as Directed Acyclic Graphs (DAGs), are of increasing interest to the scientific community since they provide a natural tool for dealing with uncertainty and complexity (Jordan, 1999). They are essentially graphical models obtained as a combination of graph theory and probability theory. Bayesian models have been considered, in particular, in the machine learning and statistics communities. More recently, they have been applied to modelling dynamic systems because they can encode the time variable (Dynamic Bayesian Networks, DBNs). A very simple DAG is represented in Figure 2. It consists of two nodes labelled as X and Y respectively, which represent two

random variables. The arrows from X to Y can be informally interpreted as indicating that X causes Y . This model can be represented as:

$$P(X, Y) = P(X) \cdot P(Y | X) = P(Y) \cdot P(X | Y) \quad (27)$$

where $P(X, Y)$ represents the joint probability, $P(X)$ and $P(Y)$ are *a priori* probabilities, and $P(Y|X)$, $P(X|Y)$ are conditional probabilities. If we consider Y as the observed variable and X as the hidden variable, one goal of the model could be to infer X given Y (i.e., to invert the causal arrow).

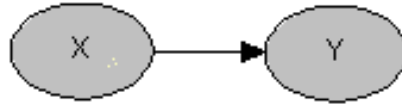


Figure 2. A very simple DAG.

This ability is referred to as inference. In order to make inferences, it is necessary to estimate the model parameters (learning) that can be represented as a conditional probability table (CPT). There are two main kinds of inference: exact and approximate. Exact inference, in the sense of having a closed form solution, is only possible in a very limited set of cases, most notably when all hidden nodes are discrete or when all nodes (hidden and observed) have linear Gaussian distributions. One of the most relevant exact inference algorithms for DAG models is the “chain-rule” decomposition that is illustrated by the following expression:

$$\begin{aligned} p(X) &= p(X_1, X_2, \dots, X_n) = p(X_1) \cdot \prod_{i=2}^n p(X_i | X_1, \dots, X_{i-1}) = \\ &= p(X_1) \cdot p(X_2 | X_1) \cdot \dots \cdot p(X_n | X_1, \dots, X_{n-1}) \end{aligned} \quad (28)$$

This algorithm essentially pushes sums inside products to marginalize the irrelevant hidden nodes efficiently; this is the so-called variable elimination algorithm (Pearl, 2000). The result of the computation is a single marginal $P(X_i | X_j)$. However, even in cases where exact inference is possible, it might not be computationally feasible; the cost of inference depends on the width of the inference tree. In this case, or when a closed form does not exist for the inference, one can use approximate inference. Several algorithms for approximate inference have been proposed, including the Expectation Maximization (EM) algorithm. The reader is referred to the recent book by Neapolitan (2004) for deeper insight into learning Bayesian Networks.

An example of Dynamic Bayesian Network is shown in Figure 3. This network was considered by Nunnari and Cannavò (2004) to model SO_2 daily mean time series at Melilli (Siracusa, Italy).

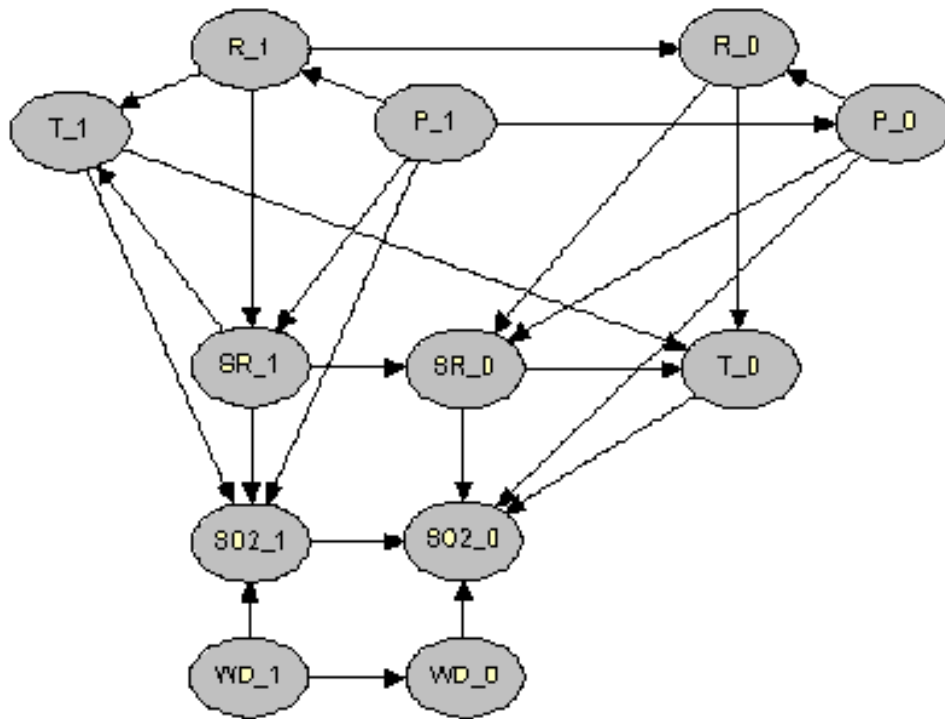


Figure 3. Example of Dynamic Bayesian Network. The meaning of the variables at the nodes is as follows: (T) air temperature, (P) atmospheric pressure, (SR) Solar Radiation, (WD) wind direction, (R) level of rain, (SO_2) sulphur dioxide. The symbol $_0$ or $_1$ close to the variable indicates that it is evaluated at time t (the day of prediction) or at time $t-1$ (the day before).

In this figure, the output node is $SO_2(t)$ (represented as $SO2_0$ in Figure 3), which allows us to compute the probability that the output belongs to one of the four classes defined for this variable. Hence, the model output is represented by the most probable class. Software packages such as Matlab® or Netica® can be used to learn the CPT for each node in the DAG.

4 Building a Model for Air Quality Forecast

Since statistical models for air quality forecast are based on extracting semi-empirical relationships from pollution time series, they are strictly dependent on the point where information is recorded. Furthermore, they depend on several factors such as the type of pollutant (e.g., primary or secondary pollutant), the type of target (e.g., prediction of the daily mean values, daily maximum value, or hourly mean values), the horizon of the forecast (e.g., 1 day, 12 hours, etc.), the type of area (e.g., urban, suburban, rural, industrial) and so on. We assume that the designer has already chosen these elements and is aware about the current normative about the limit values for the considered pollutant. An example of

normative is the EC–Council directive 1999/30/EC of 22 April 1999 that provides the limit values for sulphur dioxide, nitrogen dioxide, oxide of nitrogen, particulate matter, and lead in ambient air.

Furthermore, we assume that an adequate set of data is available in order to build and test the model under development. It is not easy to give rules for judging if a given available data set is adequate or not, since this depends on numerous factors enumerated above. Roughly speaking, we assume that a data set spanning over at least two years is available. The data set should concern both pollution and meteorological data. Emission data are in general unavailable, but in some cases one can try to use information related with emissions. As an example, in an urban area one can assume, as a surrogate of emissions data, the information from traffic flow data (if available).

4.1 Structure of Prediction Models

When building a short-term air quality forecast model, a crucial step is finding the most appropriate set of arguments of the unknown function in expression (7). In other terms, we have to establish the exogenous inputs (sometimes referred to as the “explanatory variables”) and the number of regressions for each considered variable. It is necessary to stress here that the solution of this problem is perhaps one of the major problems for the modelers. First, all the candidate variables are often numerous and not necessarily known *a priori*. Moreover, the link between the pollutant concentration and the exogenous inputs is nonlinear and depends on the investigated geographical area. In addition, the selected variables depend on the particular target (daily maximum, daily mean, hourly mean, etc.). Finally, we must stress that the observed data are affected by various kinds of noises. Although several authors have addressed the problem of input variable selection, it is still resolved in an unsatisfactory way. This problem has been studied by Zickus et al. (2001) who evaluated which of 20 input variables are relevant for predicting exceedances of the European PM₁₀ daily average limit value in the Helsinki Metropolitan Area. These authors showed good agreement with some selected predictors, but also variability among different methods. Aware of the high level of complexity in the variable selection problem, the designer can try to have some rough indication about candidate exogenous variables by using correlation analysis and calculation of typical days. Correlation and typical days can be computed as explained below.

4.1.1 Correlation Analysis

The internal correlation $\rho(\tau)$ of the observation in a time series $y(t)$ is expressed as a function of the time lag τ between observations and is defined mathematically as:

$$\rho_y(\tau) = \frac{E(y_t - \mu_y)(y_{t+\tau} - \mu_y)}{E(y_t - \mu_y)^2} \quad (29)$$

where y_t , $t = 0, \pm 1, \pm 2, \dots$ represent the values of the series $y(t)$ and μ_y is the mean of the series. The symbol E denotes the expected value. Expression (29) can be calculated as:

$$\rho_{yc}(\tau) = \frac{\sum_{i=1}^{n-\tau} (y_i - \mu_{yc})(y_{i+\tau} - \mu_{yc})}{\sum_{i=1}^n (y_i - \mu_{yc})^2} \quad (30)$$

where μ_{yc} is the mean of the observed values y_1, y_2, \dots, y_n . A plot of the values of the autocorrelation against the lag is known as the autocorrelation function. Similarly, the correlation between two time series $y(t)$ and $u(t)$ is defined as:

$$\rho_{yu}(\tau) = \frac{E(y_t - \mu_y)(u_{t+\tau} - \mu_u)}{E(y_t - \mu_y)(u_t - \mu_u)} \quad (31)$$

and can be computed as:

$$\rho_{yc}(\tau) = \frac{\sum_{i=1}^{n-\tau} (y_i - \mu_{yc})(u_{i+\tau} - \mu_{uc})}{\sum_{i=1}^n (y_i - \mu_{yc})(u_i - \mu_{uc})} \quad (32)$$

A serious limitation using correlation analysis is that with this technique, it is possible to identify only linear associations between the considered pollutant and other explanatory variables (e.g., meteorological variables) when we expect that the associations are non-linear.

4.1.2 Typical Day Analysis

A typical day is calculated using series of average hourly values as follows: 24 averages are calculated, one for each hour of the day being considered, for each day of the year. Each average is therefore calculated on 365 values (366 in a leap year) recorded at the same time of the day; this is expressed in a formula as:

$$\bar{y}(k) = \frac{1}{364} \sum_{h=0}^{364} y(k + h \cdot 24), \quad k = 1, \dots, 24 \quad (33)$$

As an example of a typical day, SO_2 concentrations recorded at the station referred to as Melilli in the industrial area of Siracusa (Italy) from 1995 to 1999, are shown in Figure 4a. Typical days of SO_2 plotted with typical days of wind direction (WD) are shown in Figure 4b.

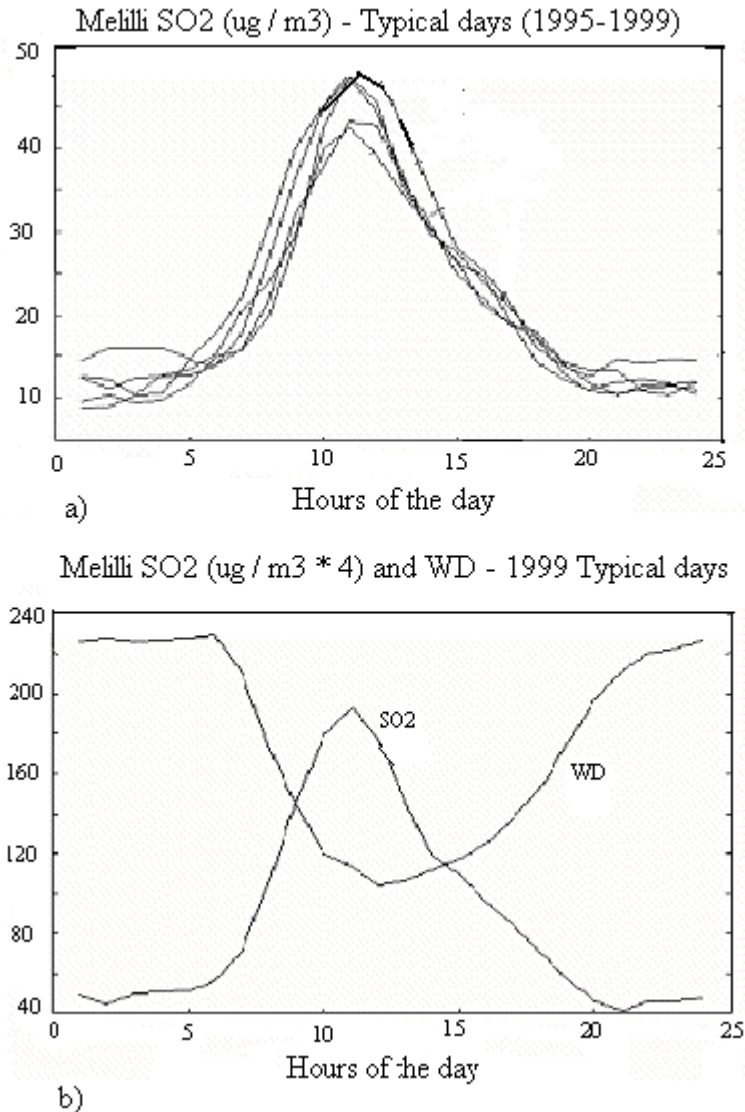


Figure 4. Example of typical day a) SO_2 b) SO_2 and wind direction.

The typical day SO_2 concentration at Melilli (Figure 4a) shows peaks between 10 a.m. and 12 p.m. local time that are somewhat surprising. In fact, pollution in this area is mainly due to oil refinery industries that are characterized by almost constant emission rates during 24 h. Hence, it seems reasonable to attribute the peaks to local atmospheric condition and, in particular, to the wind regime as suggested by Figure 4b. From Figure 4b, one can easily conclude that wind direction could be a candidate to explain the behaviour of SO_2 in this area. A

possible explanation of what has been observed was studied by Nunnari et al. (2004).

4.2 An Iterative Procedure for Building Models

Let us assume that, depending on the considered pollutant and target, a set of candidate explaining variables has been obtained by using correlation analysis and/or day type analysis, or any other *a priori* knowledge. Furthermore, let us suppose that a representative data set is available.

Independently of the modelling technique considered, the identification of a model for short term forecast of air quality involves an iterative process consisting of the following steps:

1. Divide the data set into (at least) two subsets: 1) a calibration data set which will be used to identify the model parameters; and 2) a testing data set that will be used to test the model performance (i.e., test its generalization capabilities). If possible, depending on the extension of the data set available, it is more suitable dividing that data set into three subsets. The first will be referred to as the calibration (or the learning) data set, the second as the validation set and the third as the test set that will be used to finally evaluate the model performance. The presence of the third data set is justified by the fact that in an iterative process, the second data set (i.e., the test) is in some sense still used to find an optimal set of model parameters, as it will be clear after reading the following steps.
2. Identify the model parameters by using one of the available methods (e.g., those enumerated in Section 3).
3. Validate the model against the validation data set.
4. Modify the model structure when it does not perform satisfactorily. In this case, go back to step 2 and repeat the whole process.

4.3 Evaluating the Model Performances

From the procedure outlined in the previous section, it is evident that the problem of evaluating the model performance plays a crucial role in the success of the model. It is important to consider indices that are able to evaluate performances in an objective manner. Indices usually considered for evaluating statistical air quality models can be grouped into two separate sets: 1) global fit indices, for example, those indices that give measures of the fit of the overall time series (i.e., RMSE error); and 2) those that give a measure of the capability of a given model to predict critical episodes, referred to as exceedance indices. A list of the considered performance indices is reported below. Interested readers can find detailed information about performance indices in Willmott (1982) and Willmott et al. (1985). Further insights can be found in Van Aalst and De Leeuw (1997).

4.3.1 Global Fit Indices

Let us indicate μ_o and μ_p as the mean of the observed time series (O) and predicted time series (P), and σ_o and σ_p as the corresponding standard deviations. The most widely considered global fit indices are the following:

Bias

$$\frac{1}{N} \sum_{i=1}^N (P_i - O_i) \quad (34)$$

The mean bias error is the degree of correspondence between the mean forecast and the mean observation. Lower numbers are best. Values < 0 indicate under-forecasting.

MAE

$$\frac{1}{N} \sum_{i=1}^N |P_i - O_i| \quad (35)$$

The Mean Absolute Error is the mean of the absolute value of the residuals from a fitted statistical model. Lower numbers are best.

RMSE (the Root Mean Square Error)

$$\sqrt{\frac{1}{N} \sum_{i=1}^N (P_i - O_i)^2} \quad (36)$$

σ_e^2 (the variance of the error)

$$\sigma_e^2 = \frac{1}{N} \sum_{i=1}^N (P_i - O_i)^2 \quad (37)$$

σ_{un}^2 (the unexplained variance in percent)

$$\sigma_{un}^2 = \frac{\sigma_e^2}{\sigma_O^2} \cdot 100 \quad (38)$$

where σ_O^2 represents the variance of the observed time series.

d (the index of agreement)

$$d = 1 - \frac{\sum_{i=1}^N (P_i - O_i)^2}{\sum_{i=1}^N (|P_i - \mu_O| + |O_i - \mu_O|)^2} \quad (39)$$

It gives the measure of the degree of which predictions are error-free. With respect to a good model, the index of agreement should approach one.

ρ (the correlation coefficient observed-predicted)

$$\rho = \frac{\sum_{i=1}^N (O_i - \mu_O)(P_i - \mu_P)}{\sigma_O \sigma_P} \quad (40)$$

4.3.2 Exceedance Indices

This kind of performance indices were adopted by the European Environment Agency (Van Aalst and de Leeuw, 1997) to test the capabilities of a short term forecast model to predict exceedances of photochemical smog episodes, with particular attention to tropospheric ozone concentrations. These indices are defined according to the following standard *contingency table* (Table 1):

Table 1. The EEA contingency table.

Alarms	Observed		Total
	Yes	No	
Forecasted			
Yes	A	$f-a$	f
No	$m-a$	$N+a-m-f$	$N-f$
Total	M	$N-m$	N

where:

- N = total number of data points
- f = total number of forecast exceedances
- m = total number of observed exceedances
- a = number of correctly forecast exceedances

Using these definitions, the following indices can be defined:

SP (the probability of detection)

$$SP = \frac{a}{m}100 \quad (41)$$

SP is the *fraction of correct forecast* of critical events. Its values range from 0 to 100 (100 being the best value).

SR (the percentage of predicted exceedances actually occurred)

$$SR = \frac{a}{f}100 \quad (42)$$

SR is the *fraction of realised forecast* critical events (range from 0 to 100 with a best value of 100).

FA (the false alarm rate)

$$FA = (100 - SR) \quad (43)$$

FA is the percentage of instances when predicted exceedances do not occur. With respect to a good model, FA should approach zero.

SI (the success index)

$$SI = \left(\frac{a}{m} + \frac{N + a - m - f}{(N - m)} - 1 \right) \cdot 100 \quad (44)$$

SI indicates how well the exceedances were predicted. N is the total samples in the time series. Since SI is not affected by a large number of correctly forecasted non-exceedances, it is useful for evaluating rare events. SI ranges from -100 to 100 (100 being the best value).

5 Identification of Statistical Air Quality Models

In this Section we report some case studies concerning the application of statistical modelling techniques to different areas. Results refer to different time-horizon (from hours to 1 day), targets (e.g., 1 hour average, 1 day average, 1 day maximum, etc.), and modelling techniques.

5.1 Ozone *Grey-Box* and MLP at Brescia and Catania (Italy)

The application of *grey-box* and *artificial neural networks* models has been performed in two Italian urban areas: 1) Brescia in the Northern part of Italy and 2) Catania in the Southern part (Finzi et al., 1998). See Figure 5.



Figure 5. Location of Brescia and Catania.

For each city, the examined data records consist of 1 h average O_3 , CO, NO and NO_2 concentrations measured by the urban air quality monitoring network. In particular, tropospheric *ozone* is a photochemical oxidant that may cause serious health problems to people and damage to materials and crops. The European Community directive 92/72/EEC, following the WHO guidelines, prescribes air quality standards for ozone in terms of threshold values for health protection, population information and warning (Sluyter and Van Zantvoort, 1996). The critical anthropogenic emissions (mainly traffic and combustion processes), the frequent stagnating meteorological conditions and the high solar radiation in Mediterranean regions cause ozone peaks, especially during the summer months. In order to take short-term abatement actions to prevent critical episodes, a proper real time concentration exceedances alarm system was set up for population information and warning; different forecast modelling methodologies have been used and compared.

Due to the particular relevance of photochemical pollution during summer season, two time series of hourly data measured during June-August 1996 and 1997 respectively have been taken into account for both cities. The first one has been used as the training set in identifying the model stage, while the validation of the predictors has been performed on the second one.

A pre-processing phase was required to remove the patterns containing incomplete data due to non-working or re-calibration of the measuring instruments.

5.1.1 Grey-Box Model Identification

Different classes of *grey-box* models have been considered and identified for O₃ concentration among stationary and cyclo-stationary autoregressive models having as inputs other chemical compounds taking part in the photochemical reactions. The most significant phenomenon in explaining O₃ dynamics is the 24 h period of solar radiation, which is directly connected to the photochemical atmosphere reactivity and indirectly to the regular variation of vehicular urban traffic emissions throughout the day.

The particular *grey box* model examined is cyclo-stationary with period of 24 h and assigned ranges of internal stationarity of the parameters during sub-periods of the day (night, sunrise, morning, afternoon, sunset). Model performances were evaluated in terms of Bias, σ_e , σ_{un}^2 , and ρ . The results obtained are reported in Table 2 and 3 for Brescia and Catania respectively.

Table 2. Performance indexes for *grey-box* predictors at Brescia.

Performance Indexes	Identification (1996)	Test (1997)		
		1 hour	3 hours	6 hours
<i>Bias</i>	0	0.32	0.79	1.68
σ_e	7.25	8.78	11.53	12.56
σ_{un}^2	0.13	0.32	0.54	0.63
ρ	0.93	0.83	0.69	0.62

Table 3. Performance indexes for *grey-box* predictors at Catania.

Performance Indexes	Identification (1996)	Test (1997)		
		1 hour	3 hours	6 hours
<i>Bias</i>	0	0.65	0.25	3.61
σ_e	4.57	5.64	9.73	11.31
σ_{un}^2	0.06	0.08	0.23	0.31
ρ	0.97	0.96	0.86	0.83

5.1.2 MLP Neural Network Model Identification

It is well known that there are no practical criteria for the definition of the topology of the MLP solving a given problem. Hence, the best network topology has been searched by a trial and error procedure. As a first attempt, the input pattern has been defined as:

$$y(t), y(t-1), \dots, u_1(t), u_1(t-1), \dots, u_1(t-n_1), \dots, u_p(t), u_p(t-1), \dots, u_p(t-n_p)$$

where $y(t)$ is the ozone concentration recorded at time t and $u_1(t), \dots, u_p(t)$ are exogenous inputs representing other pollutants of the nitrogen cycle recorded with the ozone (e.g., NO, NO₂, NMHC). The structure of the output pattern has been defined as $[y(t+k_a)]$, k_a being the number of steps ahead of the prediction model. Several attempts have been performed varying the parameters p , n_1, \dots, n_p , and the number of units in the hidden layer n_h . The parameter k_a has been set to 1, 3 and 6. For each attempt, the back-propagation algorithm has been used to train the network. At the end of the trial-and-error procedure, the network topology has been obtained as the one giving the best set of performance indexes. In this application, Auto Regressive non-linear models have been investigated. The best network topology for the considered problem was a MLP of the type 3-12-1 (i.e., 3 neurons in the input layer, 12 neurons in the hidden layer and 1 neuron in the output layer). This result is reliable, independently from the value of k_a . In Table 4 and 5, the performance indexes are reported.

Table 4. MLP neural network predictors at Brescia.

Performance Indexes	Learn (1996)	Test (1997)		
		1 hour	3 hours	6 hours
<i>Bias</i>	-0.49	-0.53	-0.18	2.86
σ_e	4.84	5.92	6.71	8.50
σ_{un}^2		0.15	0.06	0.30
ρ		0.92	0.97	0.90

Table 5. MLP neural network predictors at Catania.

Performance Indexes	Learn (1996)	Test (1997)		
		1 hour	3 hours	6 hours
<i>Bias</i>	0.01	-0.45	-1.19	-3.68
σ_e	4.68	5.55	9.06	11.73
σ_{un}^2	0.07	0.08	0.21	0.34
ρ	0.97	0.96	0.89	0.86

5.1.3 Discussion of Results

The performance indexes reported in Tables 2 to 5 show that the mean square error, the ratio of the unexplained variance and the correlation coefficient in the considered case are generally more satisfying for the neural model. This is evident from the validation concerning the Brescia data set. In particular, the last index reveals a greater efficiency of neural models to *capture* the deterministic and persistent part of the historical time series.

In order to test the capabilities of the predictors to predict episodes of poor air quality threshold, the SP and FA indices were computed for different time horizon and thresholds. The results are shown in Table 6 and 7 for Brescia and Catania respectively.

Table 6. Performance indexes corresponding to different O₃ concentration threshold value at Brescia.

Forecast Step	Threshold value	Outl. N.	Grey box		Neural network	
			SP	FA	SP	FA
3 hours	50 ppb	443	77.9	27.2	74.7	12.7
6 hours			75.4	30.4	81.0	34.1
3 hours	70 ppb	34	55.9	7.0	52.9	2.3
6 hours			64.7	9.0	38.2	1.8

Table 7. Performance indexes corresponding to different O₃ concentration threshold value at Catania.

Forecast Step	Threshold value	Outl. N.	Grey box		Neural network	
			SP	FA	SP	FA
3 hours	50 ppb	240	88.7	12.9	88.7	11.1
6 hours			86.2	13.2	80.4	9.1
3 hours	70 ppb	30	23.3	1.6	6.7	0.0
6 hours			0.0	0.0	0.0	0.0

For the cleverness of the two classes of models in foreseeing the O₃ peaks correctly, the results show that the *grey-box* models tend to have a higher performance in forecasting critical episodes, although they give a larger number of false alarms. This fact can be related to the different features of the two model classes; in particular, the considered *grey-box* models are time-variant while the identified neural models have a stationary structure. So it seems that neural models give more *conservative* predictions than *grey-box* models. The comparison between temporal O₃ patterns (measured and forecast values), reported in Figures 6 and 7 for Brescia and Catania respectively, looks quite

satisfying. The two periods (10-15 August 1997 for Brescia and 3-7 July for Catania) have been chosen as significant both for their criticality with respect to ozone pollution over Europe and for their typical photochemical feature.

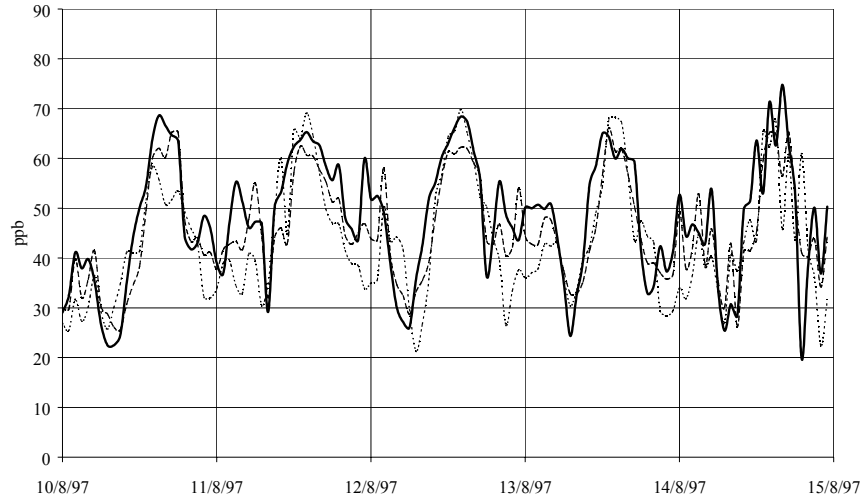


Figure 6. Brescia O₃ patterns: measured concentrations (—), 3 hours ahead forecast by means of *grey-box* model (· ·) and neural network (- -).

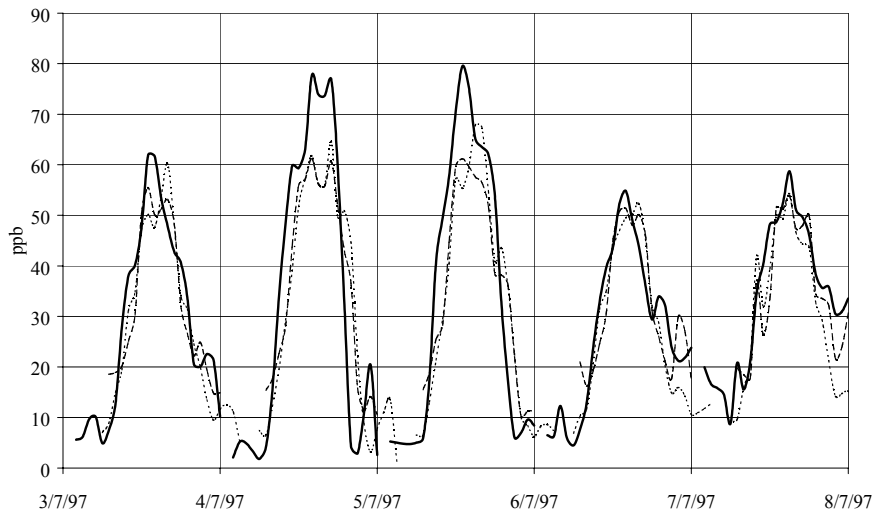


Figure 7. Catania O₃ patterns: measured concentrations (—), 3 hours ahead forecast by means of *grey-box* model (· ·) and neural network (- -).

5.2 Ozone Fuzzy and Neuro-Fuzzy Model at Brescia and Siracusa (Italy)

In this Section, *fuzzy* and *neuro-fuzzy* models for ozone at Brescia and Siracusa (industrial area) are considered. The industrial area of Siracusa is located in the eastern coast of Sicily, about 50 Km south of Catania (Figure 5). In the post-WWII

period, one of the largest concentrations of petrochemical industries in Europe developed here and it is considered to be an area of high environmental risk.

5.2.1 Brescia Metropolitan Area

The examined data records consist of O₃, CO, NO and NO₂ hourly concentrations measured by the urban air quality monitoring station in the city of Brescia. Local temperature monitored and forecast data were available from the meteorological office. The models were identified on 1994-1998 and validated on 1999 summer season data (May to September).

The *neuro-fuzzy* network forecast is performed on the maximum expected hourly concentration value during the afternoon. The model has been identified assuming triangular membership functions and *sum-prod* inference mechanism. The *crisp* model inputs are O₃ concentrations and the most relevant meteorological parameter (temperature) taking part in the photochemical reactions during the day (Finzi and Volta, 2000).

Table 8 shows the inputs and their respective fuzzy set number for the best model as a trade-off between a satisfying forecast performance and a possible operational implementation.

Table 8. The *neuro-fuzzy* model inputs.

Inputs	Value	Fuzzy sets
O ₃ conc.	10 a.m.-12a.m. average	3
O ₃ gradient	12 a.m.-6 a.m. difference	4
Temperature	10 a.m.-12a.m. average	3
Temperature	12am- 6a.m. difference	2

The rule base came out to be a set of 30 rules. The *persistent model* skill parameters have been also computed as lower bound performance indexes. The forecast evaluation has been related to an O₃ threshold value of 140 µg/m³. Figure 8 compares the European skill parameters computed for the persistent and the *neuro-fuzzy* predictor. The *neuro-fuzzy* model seems worthy to be used mainly for its cleverness in avoiding false alarms, while the *SP* index claims for a forecast improvement in enhancing some episodes.

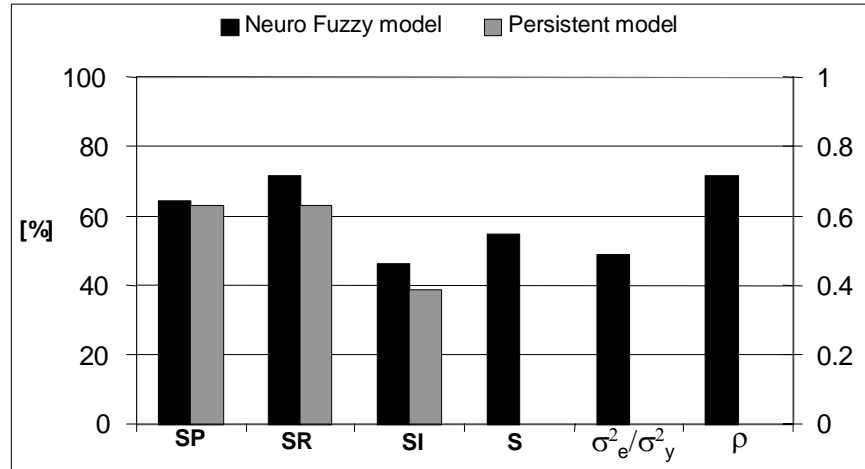


Figure 8. Performance indexes referred to the persistent model.

5.2.2 Siracusa Industrial Area

Fuzzy models have been obtained by using the approach described in Section 3.2.1.2. Data for model identification were recorded during 1995-1998, while the test was done using data recorded in 1999. The *fuzzy* model forecasts are performed at 8 p.m., giving the maximum expected hourly concentration value during the day after. The inputs of the *fuzzy* prediction model studied for the Siracusa industrial area are shown in Table 9.

Table 9. The *fuzzy* model inputs.

Inputs	Value	Fuzzy sets
O ₃ conc.	1 a.m. – 8 p.m. average	3
NO ₂	1 a.m. – 8 p.m. average	3
NO _x	1 a.m. – 8 p.m. average	3
Temperature	10 a.m. – 6 p.m. average	3
Solar Radiation	10 a.m. – 6 p.m. average	3
Pressure	10 a.m. – 6 p.m. average	3
Wind Direction	10 a.m. – 6 p.m. average	3

The proposed model was compared with a persistent model. The *fuzzy* model identified consist of 42 rules (3 fuzzy sets of trapezoidal type for each considered). The results of the comparison carried out with the persistent model for a threshold of 140 $\mu\text{g}/\text{m}^3$ are reported in Figure 9.

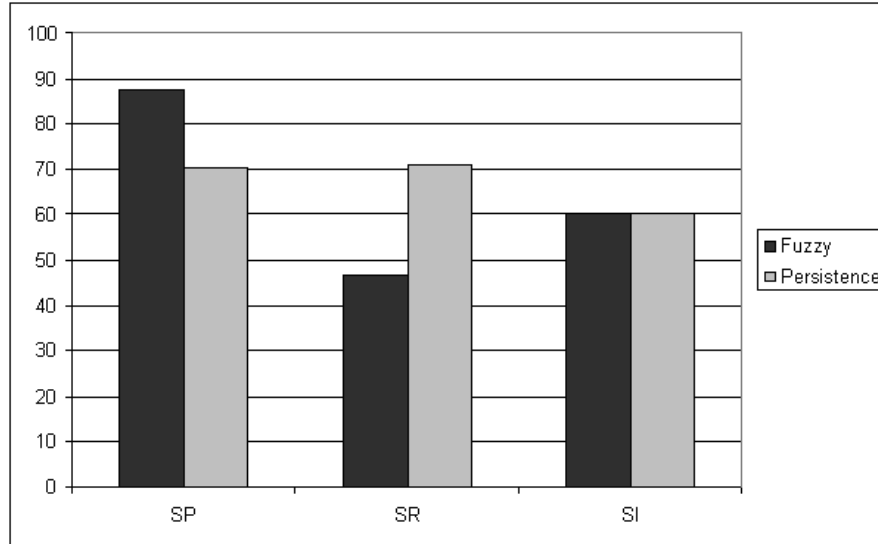


Figure 9. Performance indices for the Fuzzy model compared with the persistent model for the Siracusa industrial area.

5.2.3 Comments on Results

The *neuro-fuzzy* model identified for the Brescia metropolitan area, which was designed specifically to predict critical episodes, shows a satisfying performance both in forecasting exceedances of the threshold level and in avoiding *false alarms*.

The *SP* index obtained for the *fuzzy* model identified for the Siracusa industrial area is considerably better than the one exhibited by the persistent model. On the contrary, the *fuzzy* model shows worse performances in terms of *SR*, which results in a larger number of false alarms. This is due to the fact that the performances of the *fuzzy* model have been optimised with respect to the *SP* parameters.

Finally, it must be observed that:

- *fuzzy* and *neuro-fuzzy* predictors perform better than persistent model (i.e. linear ones)
- *fuzzy* and *neuro-fuzzy* model complexity and flexibility allow the optimization of model performances, stressing the capability to forecast exceeding values or avoiding *false alarms*
- *neuro-fuzzy* models, although they are non-linear, are more *readable* (due to the typical “if ... then” form) than the MLP neural network models, and can suggest physical explanation of pollutant processes.

5.3 Inter-Comparison Among ARCX, MLP, NFU and FU Forecast Models

In the preceding Section 5.2 *grey-box* and **neural networks** predictors were compared to each other, while in Section 4.2 the pair of *neuro-fuzzy* and *fuzzy*

models were considered. In this Section, a wider inter-comparison exercise involving *grey-box* (ARCX), **neural networks** (NN), *neuro-fuzzy* (NFU) and *fuzzy* (FU) models will be reported. The selected areas are still Brescia and Siracusa, and the target is the forecast of ozone daily maximum concentration. For all the considered models, exogenous inputs were:

- the average ozone concentration computed between 4 p.m. and 8 p.m. of the day before
- the maximum temperature between 1 a.m. and 8 p.m.
- the NO₂ average concentration between 4 p.m. and 8 p.m. of the day before

The data set for both areas was represented by meteo-chemical measures recorded in the years 1995 to 2001. Instead of splitting the data into two different sets (the so called *learning* set and *validation* set), as it is usual among the neural network practitioners, in order to take the generalisation capabilities of the prediction models into account, the data set was divided into three subsets: the *learning* set, the *validation* set and the *testing* set. It has been pointed out indeed (e.g., Sjoberg and Ljung, 1995) that the validation error rate, periodically computed during the *learning* phase, is not a good estimate of the *generalisation* error. One way to evaluate an unbiased estimate of this last error is to run the prediction model on a third set of data, the *test* set, not used at all before for the training process. In the inter-comparison exercise, the *learning* set, the *validation* set and the *testing* set were composed respectively by data recorded in 1995 to 1998, 1999, 2000 and 2001. The results, referring to a threshold of 140 µg/m³ in terms of forecasting performances, are shown in Figures 10 and 11 for Brescia and Siracusa respectively.

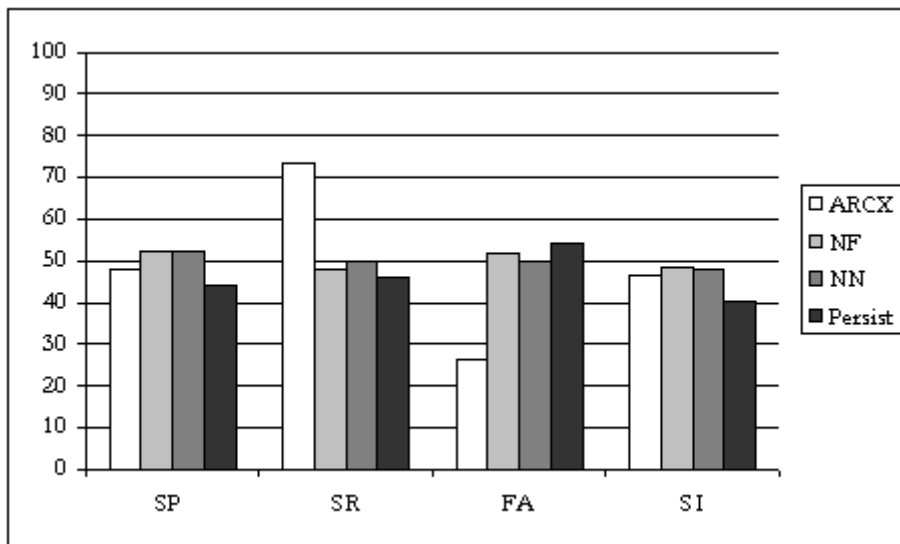


Figure 10. Performance indices for Brescia.

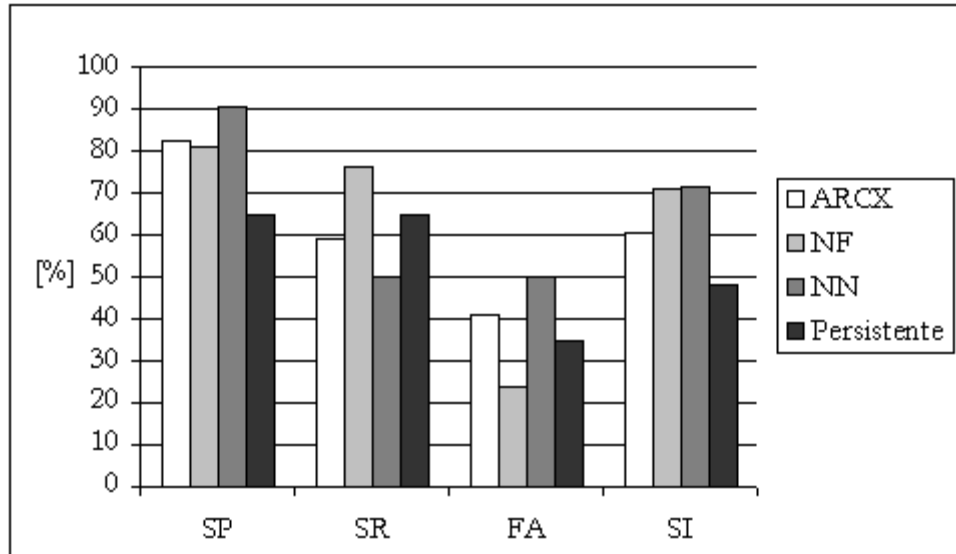


Figure 11. Performance indices for Siracusa.

Based on the reported results, the following considerations can be made:

- The forecasting performances are generally better for Siracusa than for Brescia. This means that the performance levels are point dependent no matter what modelling technique is considered. This fact can be easily explained by taking the different geographic meteo-climatic conditions of the two areas into account. Probably there were ozone accumulations in Siracusa that depend on a quite regular sea breeze regime. The concentration daily peaks can be predicted more easily with respect to Brescia.
- ARCX, NF and NN predictors work better than the persistent model in terms of SP and SI indices.
- While NN and NF usually perform slightly better than ARCX in terms of SP and SI, ARCX performs better in terms of FA in some cases.

5.4 Conclusive Remarks

At the end of this Section some further remarks are made referring to the results reported in the preceding Sections 5.1 to 5.3. The first consideration is that there is no single modelling approach exhibiting all the performance indices at the best level. The structure of a model, as well as its performance, is strictly dependent on the particular monitoring site. The forecast performance is usually higher if reliable meteorological information is provided as inputs. This means that, when information about pollutant emissions is not available, meteorological conditions play a key role in improving the reliability of predictions. The results reported show that not all observed critical episodes can be explained on the basis of historical concentration time series and meteo-climatic data measured at ground level. Neural based approaches, even the *neuro-fuzzy* version, seem more promising (though moderately) to critical events forecast.

6 An Operational Decision Support System

As example of possible operational use of forecast models, a prototype of Decision Support System (DSS) for short-term emission reduction measures, is described in Figure 12 (Finzi, 2001). It implements two feedback loops, which may be based on different methodologies taken into consideration. Air quality status forecast, given by the daily model, is supplied to the Control Authority in order to support the decisions relevant to the emission abatement strategies (vehicle traffic reduction or restriction in different metropolitan areas, temporary adoption of closer industrial emission limits, health prevention policies, etc.). These measures can prevent smog episodes if they are planned ahead of time. It is also possible to inform the population by means of media, in order to limit the unhealthy exposures; in this way, the feedback can prevent and reduce both pollution and sanitary risks.

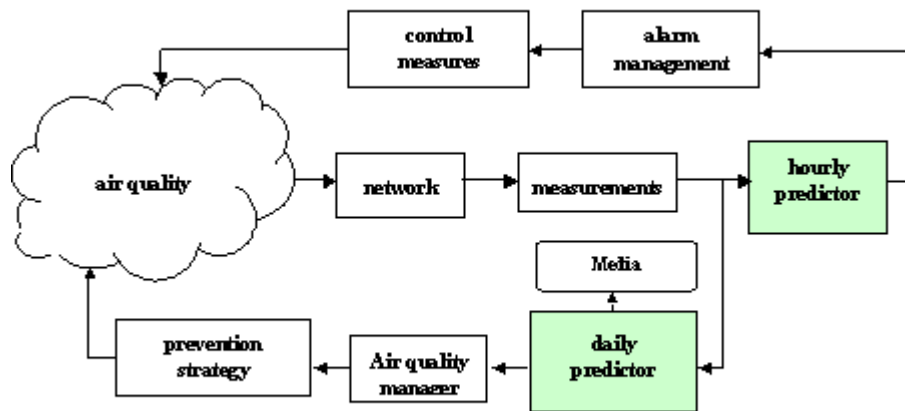


Figure 12. A Decision Support System for Air Quality Alert.

The designed system has a second internal feedback improving operational effectiveness in the short term (hours). The information, provided both by the hourly predictor model and the on-line meteo-chemical networks, allows the air quality managers to monitor the current pollutant evolution with a high confidence.

Moreover, any exceedance of the threshold, if not correctly forecast a day in advance, can be quickly recognised in the morning by the alarm system in order to apply short-term pollution control measures (traffic information through road panels, mobilisation of the metropolitan police, traffic control by means of a computerised system of traffic lights, etc.).

The metropolitan areas of Brescia and Milan have been considered as case studies and the performance of the designed DSS in both cities is examined in the following paragraphs.

6.1 Brescia Metropolitan Area Case Study

The examined data records consist of O₃, CO, NO and NO₂ hourly concentrations measured by the urban air quality monitoring station in the centre of Brescia (see Figure 13). The city is located in the Po Valley in Northern Italy and is characterised by high industrial, urban, and traffic emissions, and continental climate.

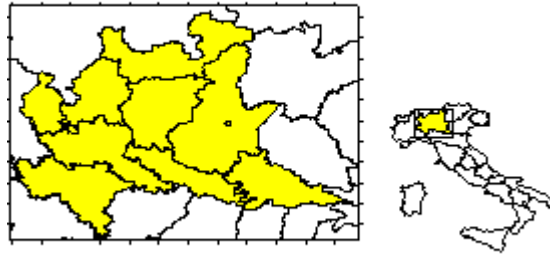


Figure 13. The Brescia area (in yellow).

Local temperature monitored and forecast data are available from the meteorological office. Both classes of models were identified on the period 1994-1998, and validated on 1999 summer season data (May to September). A pre-processing phase was required to remove the patterns containing incomplete data due to non-working or re-calibration of the measurement instruments.

Two alternative alarm DSS (see Figure 12) were set up:

- a) *neuro-fuzzy* network forecasts were performed on the maximum expected hourly concentration value one day in advance, while *grey-box* predictors provided 4 hour ahead forecast of O₃ concentrations from sunrise to noon during the same day
- b) *grey-box* forecast was performed on the maximum expected hourly concentration value one day in advance, while *neuro-fuzzy* network predictor provided the maximum expected hourly concentration value at noon for the afternoon during the same day.

Case a)

The *neuro-fuzzy* model has been identified for O₃ maximum daily concentration, assuming Gaussian membership functions and max-min inference mechanism. The *crisp* model inputs were the chemical compounds (O₃ and NO₂ concentrations) and the most relevant meteorological parameter (temperature) taking part in the photochemical reactions during the day. Table 10 shows the inputs and their respective fuzzy set number for the best model as a trade-off between a satisfying forecast performance and a possible operational implementation. The rule base came out to be composed by 135 rules.

Table 10. The neuro-fuzzy model inputs.

Inputs	Value	Fuzzy sets
O ₃ conc.	Max concentration	6
O ₃ conc.	4p.m. - 8p.m. average	4
NO ₂ conc.	4p.m. - 8p.m. average	4
Temperature	Max forecast for the following day	3
Temperature	Max	5

Different *grey-box* models have been considered and identified for O₃ hourly concentration in the classes of stationary and cyclo-stationary autoregressive models (Finzi and Volta, 2000).

The most significant phenomenon in explaining O₃ hourly value dynamics appears to be the 24 h period of solar radiation, which is directly connected to the photochemical atmosphere reactivity and indirectly to the regular variation of vehicular urban traffic emissions throughout the day. So, the particular *grey-box* model considered is a *cyclo-stationary* one of 24 h period, with assigned sub-period internal stationarity ranges for the parameters (night, sunrise, morning, afternoon, and sunset).

The *persistent model* (tomorrow equals today) skill parameters have also been computed as lower bound performance indices. The indices, related to an O₃ threshold value of 140 µg/m³, have been estimated for both daily *neuro-fuzzy* and hourly *grey-box* models. On the basis of the skill parameters computed for the persistent, the *neuro-fuzzy* and *grey-box* predictor, the second model seems worthy to be used mainly for its cleverness in avoiding false alarms, while *SP* index claims for a forecast improvement in enhancing some episodes. The hourly *grey-box* model provides a second internal system feedback, improving operational effectiveness in the short term (hours). The results (Figure 14)

underline the improvement mainly in forecasting ozone threshold exceedances (*SP*) and in performing *success index* (*SI*).

The comparison among temporal O₃ patterns (measured and forecast values), reported in Figure 15, points out the improvement provided in detecting alarms by the hourly model during a particular critical episode between 28 June and 7 July 1999.

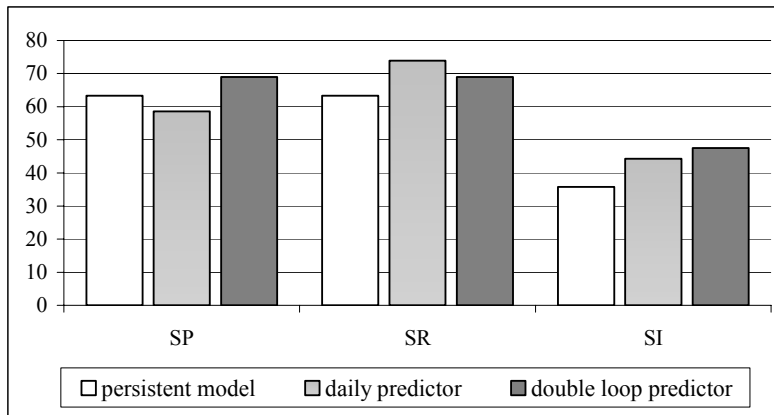


Figure 14. The estimated forecast skill parameters.

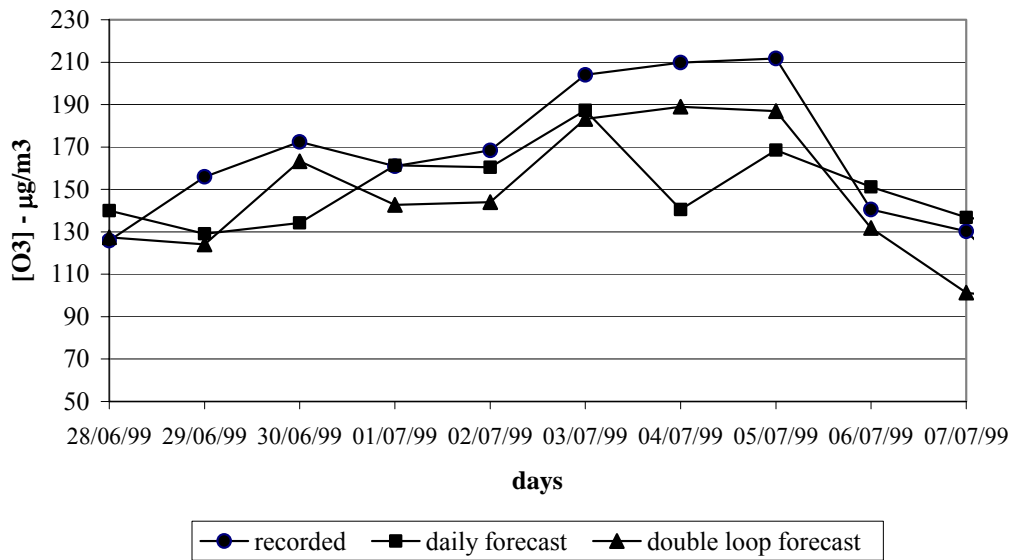


Figure 15. Ozone patterns: measured concentrations, daily forecast by means of single loop *neuro-fuzzy* model and double loop 4 hour ahead *grey-box* predictor.

Case b)

Different *grey box* models have been considered and identified for O₃ maximum daily concentration forecast. The most significant phenomena in explaining O₃ maximum value dynamics appear to be the solar radiation and temperature, directly connected to the photochemical atmosphere reactivity, and the regular variation of vehicular urban traffic emissions during the day. So, the particular *grey box* model considered is a *non-linear* ARX(1), with assigned temperature categories (Table 11).

Table 11. The *grey-box* model inputs.

Inputs	Value
O ₃ concentration	4 p.m. to 8 p.m. average
NO ₂ concentration	4 p.m. to 8 p.m. average
Temperature	Daily maximum value squared

The *neuro-fuzzy* approach has been used to forecast the maximum expected hourly concentration value during the afternoon. The model has been identified assuming *triangular* membership functions and *sum-prod* inference mechanism. The *crisp* model inputs were O₃ concentrations and the most relevant meteorological parameter (temperature) taking part in the photochemical reactions during the day.

Table 12 shows the inputs and their respective fuzzy set number for the best model as a trade-off between a satisfying forecast performance and a possible operational implementation. In this case, the rule base came out to be composed by 30 rules.

Table 12. The *neuro-fuzzy* model inputs.

Inputs	Value	Fuzzy sets
O ₃ conc.	10 a.m. to noon average	3
O ₃ conc.	8 a.m. to noon gradient	4
Temperature	10 a.m. to noon average	3
Temperature	6 a.m. to noon gradient	2

The performance indices, related to the O₃ threshold value of 140 µg/m³, have been estimated for both *neuro-fuzzy* and *grey-box* models. The *persistent model* (tomorrow equals today) skill parameters have also been computed as lower bound performance indices.

Figure 16 compares the skill parameters computed for the four models: the daily (*grey-box*) and hourly (*neuro-fuzzy*) predictors, their combination in the air quality system and the persistent model. The first two predictors have good performance in avoiding false alarms, while the *SP* index for daily model provides a forecast improvement in enhancing some episodes. The *neuro-fuzzy* predictor matches the persistent model in correctly forecasting smog events.

The air quality system of Figure 12, implementing the second internal feedback, improves operational effectiveness in the short term (hours), taking into account all recent available meteo-chemical measurements. The results underline the system synergy, mainly in forecasting ozone threshold exceedances (*SP*) and in global performance (*SI*).

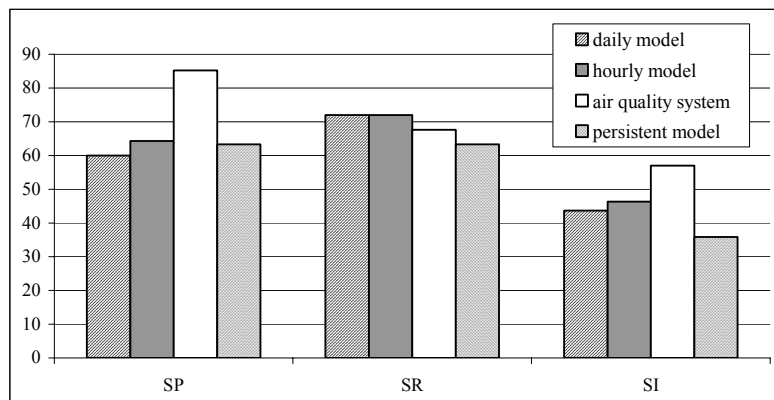


Figure 16. The estimated forecast skill parameters.

6.2 Milan Metropolitan Area Case Study

The examined data records consist of photochemical pollutants hourly concentrations measured by the urban air quality monitoring network in Milan during 1994-1999. Local and synoptic meteorological data are also available from the meteorological office. The assessment of the results, in terms of forecast performance indices and statistical indicators, according to European Environment Agency guidelines, is presented in the following.

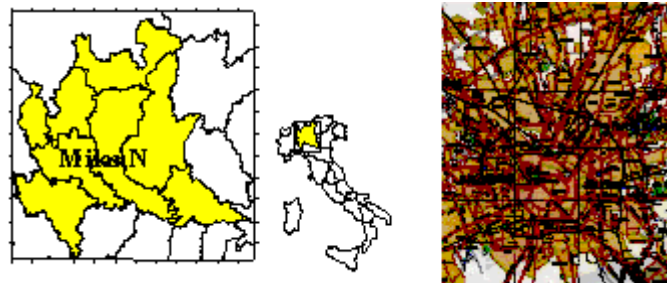


Figure 17. The Milan metropolitan area (in yellow).

The Milan metropolitan area, the city and its suburbs (see Figure 17), is a very industrialised and populated region in the Po Valley. The data records examined in this study consist of O₃, CO, NO and NO₂ hourly concentrations measured by three urban and suburban air quality monitoring stations (Parco Lambro, Via Juvara, Piazza Zavattari). Local temperature monitored and forecast data are available from the meteorological office. The models have been identified during the period 1994-1998 and validated during 1998-1999. A pre-processing phase was required to remove the patterns containing incomplete data due to non-working or re-calibration of the measuring instruments.

Different predictors have been considered and identified for O₃ and NO₂ maximum daily concentrations in the classes of stationary and cyclo-stationary auto-regressive models (Finzi, 2001).

The most significant phenomenon in explaining O₃ hourly value dynamics appears to be the 24 h period of solar radiation, which is directly connected to the photochemical atmosphere reactivity and indirectly connected to the regular variation of vehicular urban traffic emissions along the day. So, the particular *grey box* model considered is an auto-regressive model with exogenous inputs and categories. The inputs are O₃ average concentrations measured from 4 p.m. to 8 p.m. and the maximum temperature recorded during the day. The categories are defined for the future trend of the maximum temperature. The model has been identified for use in the summer seasons.

The model, referring to the maximum NO₂, is similar to the preceding one. The particular *grey box* model considered is an auto-regressive model with exogenous inputs and categories; the inputs are NO₂ average concentrations measured mostly in the morning (from 7 a.m. to 2 p.m.) and the maximum temperature recorded during the day. The categories are built for the future trend of the maximum temperature. The model has been identified for use in the winter seasons.

The *persistent model* (tomorrow equals today) skill parameters have been also computed as lower bound performance indices. The assessment of the results is presented in the following Figures 18 (*a, b, c, d*), both in terms of statistical indicators and real-forecast series comparison examples. All the indices have been computed with reference to a O₃ threshold value of 150 µg/m³ and to a NO₂ threshold value of 135 µg/m³. As it can be seen, *grey-box* models, although structurally simple, give more reliable alarm forecasts with respect to persistent models for all the examined pollutant measurement locations.

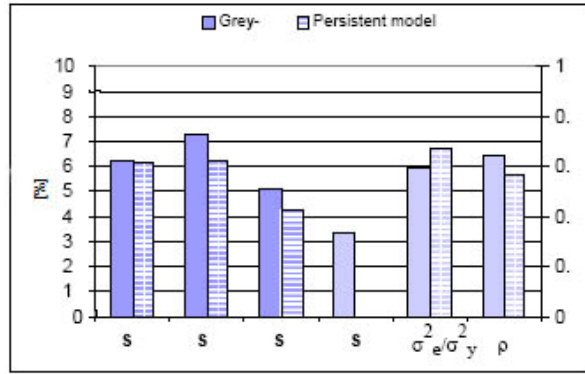


Figure 18a. Forecast System Validation Juvara station. NO₂ skill parameters (winter 1998).

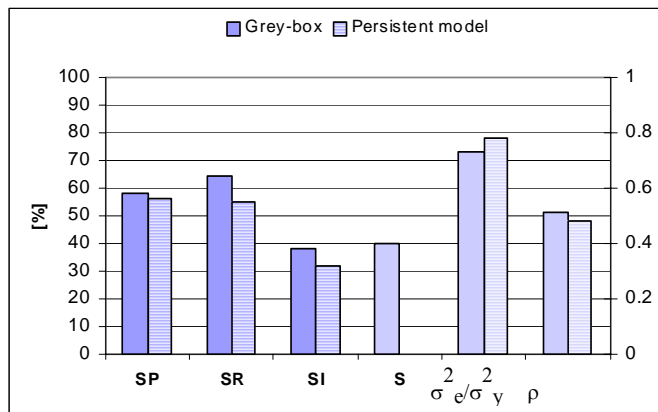


Figure 18b. Zavattari station. NO₂ skill parameters (winter 1998).

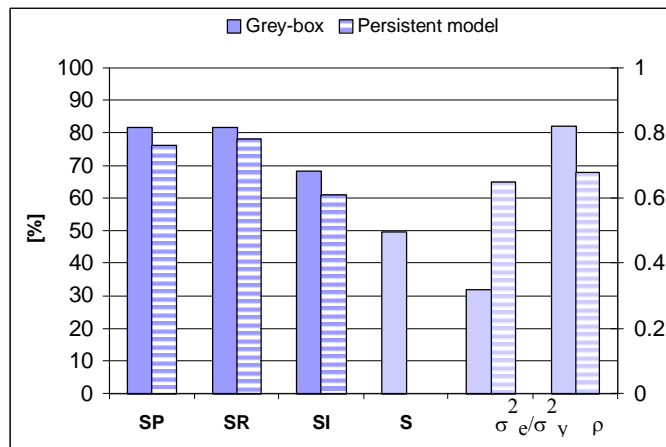


Figure 18c. P. Lambro station. O₃ skill parameters (summer 1999).

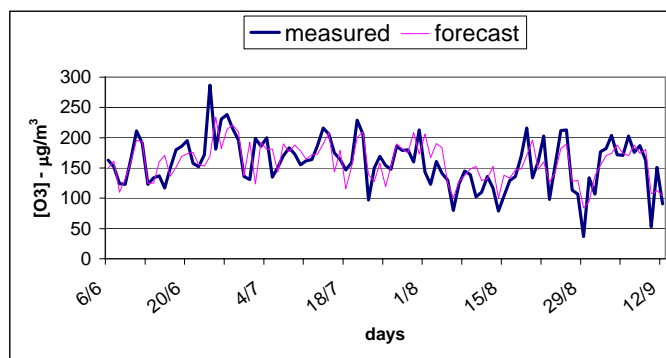


Figure 18d. P. Lambro station. O₃ real and forecast. Time series along the validation season (summer 1999).

7 Conclusions

Statistical modelling approaches have been the object of a growing interest among researchers involved in air quality modelling. This is proved by the large amount of studies published in literature, partially outlined in the first part of this chapter. This is also a consequence of the gradually increasing number of pollution data available from the monitoring networks. In addition, unlike deterministic models requiring a lot of input information (in most cases not available from monitoring networks in real time), statistical approaches represent a straightforward way to fit available pollution and meteorological time series.

As shown in the preceding paragraphs, the statistical models' performance in real cases is strictly point dependent and may require some time and trials to be properly tuned. However, a statistical approach provides an excellent and easy way to capture the global dynamics involved with the complex phenomena of air pollution, overcoming the drawbacks of using deterministic models when predictors have to work in real time (hours, few days).

Also, statistical models are good ways to approach the problem of pollution peaks prediction. The results show that the number of critical episodes correctly forecast ranges from 60% to 90%, depending on the particular target, area and statistical modelling technique considered, while the rate of false alarms ranges from 30% to 50%. This apparently large number of false alarms can be ascribed to the lack of emission data in real time and correctly reflect the fact that not all critical episodes can be interpreted using the ground-recorded meteo-chemical information. However, a false alarm rate around 40% appears to be acceptable if the total number of critical episodes along the year is limited. Moreover, there is a reasonable evidence that these results can be further improved taking into account, when available, vertical profiles of significant meteorological variables (e.g., wind, temperature, etc.). The analysis carried out also highlights the role of meteorological forecasts as inputs to reliable predictors of pollutant critical episodes.

In the last section, the implementation of statistical models in decision support systems (DSS) is suggested as one of the actual possible use in real time. The two case studies reported show how the contribution of peculiar statistical approaches may be integrated in a feedback loop system, increasing the operational effectiveness of the DSS as a whole.

Finally, it must be observed that all the examined models perform better globally than the persistent model, as indicated by the skill score indices computed as lower bound performance thresholds.

Acknowledgements

This research has been partially supported by Italian MURST and Provincia di Brescia, in the frame of EUROTRAC-2/SATURN European scientific project.

The Siracusa industrial area case study has been carried out in the framework of the European Union Project APPETISE (Contract N. IST-99-11764).

References

- Abarbanel, H.D.I., *Analysis of observed chaotic data*, Springer, New York, 1996.
- Anderberg, M.R., *Cluster Analysis for Applications*, Academic Press, New York, 1973.
- Arena, P., Baglio, S., Castorina, C., Fortuna, L., Nunnari, G., A Neural Architecture to Predict Pollution in Industrial Areas, *Proc. of the International Conference on Neural Network - ICNN*, Vol. 4, pp. 2107-2112, 1996, Washington, USA.
- Barron, A.R., Universal Approximation Bounds for Superposition of a Sigmoidal Function, *IEEE Trans. on Information Theory*, vol. 39, pp. 930-945, 1993.
- Bezdek, J.C., *Pattern Recognition with Fuzzy Objective Function Algorithms*, Plenum Press, New York, 1981.
- Box, G.E.P., Jenkins, G.M., *Time Series Analysis, Forecasting and Control*, Holden Day Inc., S. Francisco, 1970, new edition 1976.
- Box, G.E.P., Jenkins, G.M., Reinsel, G.C., *Time Series Analysis, Forecasting and Control*, Prentice Hall, 1994.
- Boznar, M., Lesjak, and P. Mlakar, A Neural Network-Based Method for Short-Term Predictions of Ambient SO₂ Concentrations in Highly Polluted Industrial Areas of Complex Terrain, *Atmospheric Environment*, Vol. 27B, No. 2, pp. 221-230, 1993.
- Breiman, L. and Friedman, J.H., Estimating Optimal Transformations for Multiple Regression and Correlation, *American Statistical Association*, Vol. 80, No. 391, pp. 580-598, 1985.
- Bringfelt, B., Important Factors for the Sulphur Dioxide Concentration in Central Stockholm, *Atmospheric Environment*, Vol. 5, pp. 949-972, 1971.

Briseño, H., Cipriano, A., Clustering methods applied to fuzzy model identification, *Proc. of the 7th Latin American Congress of Automatic Control*, September 9-13, Buenos Aires, pp. 760-765, 1996.

Brown, R.G., Hwang, P.Y.C., Introduction to Random Signals and Applied Kalman Filtering with Matlab exercises and solutions, Wiley, 3rd Edition, 1996.

Brusasca, G., Finzi, G., Stochastic Models for Real-Time Sulphur Dioxide Pollution Forecast around Thermal Power Plants, in *Proc. of ENVIROSOFT86. Comp Mech. Publications*, pp. 177-191, 1986.

Buishand, T.A., Kempen, G.T., Frantzen, A.J., Reijnders, H.F. and Van den Eshof, A.J. Trend and Seasonal variation of precipitation chemistry data in the Netherlands, *Atmospheric Environment*, Vol. 22(2), pp. 339-348, 1988.

Chen, S., Billings, S.A. "Neural networks for nonlinear dynamic system modelling and identification", *Int. Journal Control*, **56**, No. 2, pp. 319-346, 1992.

Cleveland, W. S., Robust Locally Weighted Regression and Smoothing Scatterplots, *Journal of the American Statistical Association*, **74**, No. 368, pp. 829-836, 1979.

Comrie, A.C. Comparing Neural Networks and Regression Models for Ozone Forecasting, *Air & Waste Management Association*, Vol. **47**, pp. 653-663, 1997.

Cossentino, M., Damiani, A., Gaglio, S., Raimondi, F.M., Vitale, M.C., Exploring the use of Soft-computing and artificial intelligence techniques in atmospheric pollution modelling, *Air Pollution XI*, WIT press (Brescia, C.A. and Patania, F., Editors), 2003.

Cybenko, G. Approximation by superpositions of a sigmoidal function, *Mathematics of Control, Signals and Systems*, Vol. 2, pp. 303-314, 1989.

Dorling, S.R., Foxall, R.J., Mandic, P.D., Cawley, G.C. Maximum likelihood cost functions for neural networks models of air quality data, *Atmospheric Environment*, Vol. 37, pp. 3435-3443, 2003.

Davis, J.M., Eder, B.K., Nychka, D. and Yang, Q., Modelling the effects of meteorology on ozone in Houston using cluster analysis and generalised models, *Atmospheric Environment*, 32(14/15), pp. 2505-2520, 1998.

Davis, J.M. and Speckman, P., A model for predicting maximum and 8 h average ozone in Houston, *Atmospheric Environment*, 33, pp. 2487-2500, 1999.

Dunn, J.C., A Fuzzy Relative of the ISODATA Process and Its Use in Detecting Compact Well-Separated Clusters, *Journal of Cybernetics*, 3, pp. 32-57, 1973.

Finzi G., Tebaldi G., A mathematical model for air pollution forecast and alarm in an urban area", *Atmospheric Environment*, Vol.16, 2055- 2059, 1982.

Finzi, G., Hernandez, E., Garcia, R., "The SO₂ pollution in Madrid. Part II: A comparison between two stochastic models for real-time forecast purposes", *Il Nuovo Cimento*, Vol. 6C, No.6, pp. 605-617, 1983.

Finzi, G., Bonelli, P., Bacci, G., "A stochastic model of surface wind speed for air quality control purposes", *Journal of Climate and Applied Meteorology*, Vol. 23, pp. 1354-1361, 1984.

Finzi, G., Volta, M., Nucifora, A., Nunnari, G., Real-Time Ozone Episode Forecast: a Comparison between Neural Network and Grey-Box Models, *Proc. International ICSC/IFAC Symposium on Neural Computation - NC'98*, Vienna, 1998.

Finzi, G., Volta, M., Real time urban ozone alarm system including neuro-fuzzy networks and grey box models, *Proc. Second International ICSC/IFAC Symposium on NEURAL COMPUTATION-NC2000*, ICSC Academic Press, pp. 659-663, 2000.

Finzi, G., An air quality alarm system for Milan Metropolitan Area, *proc. EUROTRAC Symposium 2000*, P.M. Midgley, M. Reuther, M. Williams (Eds.), Springer Verlag Berlin, Heidelberg, 2000.

Finzi, G., Pirovano, G., Volta, M., Gestione della Qualità dell'Aria - Modelli di Simulazione e Previsione, McGraw-Hill Libri Italia Srl, Milano, (in Italian), 2001.

Gardner, M.W., S.R. Dorling, Artificial neural networks (the multilayer perceptron), A review of applications in the atmospheric sciences, *Atmospheric Environment*, Vol. 32, No. 14, pp. 2627-2636, 1998.

Gardner, M.W., S.R. Dorling, Neural network modelling and prediction of hourly NO_x and NO₂ concentration in urban air in London, *Atmospheric Environment*, Vol. 33, pp. 709-719, 1999.

Gilbert, R.O., Statistical Methods for Environmental Pollution Monitoring, Van Nostrand Reinhold, New York, 1987.

Gori, M., Tesi, A. On the problem of local minima in backpropagation, *IEEE trans. Patt. Anal. Machine Intell.* Vol. PAMI-14, No. 1, pp 76-86, 1992.

Grassberger, P. and Procaccia, I., *Characterisation of strange attractors*, Physical Review Letters, Vol. 50, pp. 346, 1983.

Greig, A.J., Cawley, Dorling S., Eben, K., Fiala, A. J., Karppinen, A., Keder, J., Kolehmainen, M., Kukkonen, J., Bertuccio, L., Macoun, J., Niranjani, M., Nucifora, A., Nunnari, G., Palus, M., Pelikan, E., Ruuskanen, J., Schlink, U., Air pollution episodes: modelling tools for improved smog management (APPETISE), *Proc. of the Eighth International Conference AIR POLLUTION 2000*, New Hall, Cambridge University, UK, 24 – 26, pp. 89-98, 2000.

Hartigan, J., *Clustering Algorithms*, John Wiley & Sons, New York, 1975.

Hastie, T.J. and Tibshirani, R.J., *Generalized Additive Models*, Chapman & Hall, London, 1986.

Hastie, T.J. and Tibshirani, R.J., *Generalized Additive Models: Some Applications*, *Journal of the American Statistical Association*, Vol. 82, No. 398, pp. 371-386, 1987.

Hernandez, E., Garcia, R., Finzi, G., The Sulphur Dioxide Pollution in Madrid. Part 1: A Study of the Meteorological and Statistical Aspects, *Il Nuovo Cimento*, 6C(6), pp. 595-604, 1983.

Holland, J.H. *Adaptation in Natural and Artificial System*, University of Michigan Press, 1975.

Huang, G., A stepwise cluster analysis method for predicting air quality in a urban environment, *Atmospheric Environment*, Vol. 26B, pp. 349-357.

Jenkins, G.M, Watts, D.G., *Spectral Analysis and Its Applications*, Holden-Day, San Francisco, 1968.

Jordan, M.I., Editor, *Learning in graphical Models*, Mit Press, 1999.

Jorquera, H., Perez-Correa, R., Cipriano, A., Acuna, G., Short Term Forecasting of Air Pollution Episodes, Chapter 3 of Environmental Sciences and Environmental Computing, Vol. II (P. Zannetti, Editor), The EnviroComp Institute, 2004.

Kantz, H., Schreiber, T., Nonlinear Time Series Analysis, Cambridge Nonlinear Science Series 7, Cambridge University Press, 1997 (reprinted 2000, 2002).

Kaplan, D. and Glass, L., Understanding Nonlinear Dynamics, New York: Springer, 1995.

Kennel, M.B., Brown, R. and Abarbanel, H.D.I., Determining embedding dimension for phase space reconstruction using a geometrical construction, *Phys. Rev.*, Vol. A 45, pp. 3403, 1992.

Kukkonen, J., Partanen, L., Karppinen, A., Ruuskanen, J., Junninen, H., Kolehmainen, M., Niska, H., Dorling, S., Chatterton, T., Foxall, R., Cawley, G., Extensive evaluation of neural network models for the prediction of NO₂ and PM₁₀ concentration, compared with deterministic modelling system and measurements in central Helsinki, *Atmospheric Environments*, Vol. 37, pp. 4539-4550, 2003.

Lins, H.F., Trend analysis of monthly sulfur dioxide emissions in the conterminous United States, *Atmospheric Environment*, 21, 11, pp. 2297-2309, 1987.

Lippmann, R.P., An introduction to computing with neural nets, *IEEE ASSP Magazine*, Vol. 4, No. 2, pp. 4-22, 1987.

Ljung L., System Identification Toolbox for use with MATLAB, The Math Work Inc., Natick, Massachusetts, 1991.

Maffei, G., Prediction of carbon monoxide acute air pollution episodes. Model formulation and first application in Lombardy, *Atmospheric Environment*, Vol. 33, pp. 3859-3872, 1999.

Melli, P., Bolzern, P., Fronza, G., Spirito, A., Real-Time Control of Sulphur Dioxide Emissions from an Industrial Area, *Atmospheric Environment*, 15, 5, pp. 653-666, 1981.

Ng, C.N. and Yan, T.L., Recursive modelling and adaptive forecasting of air quality data in C.A. Brebbia, C.F., Ratto, and H. Power (Eds.), *Air Pollution VI*, Boston, Computational Mechanics Publications, pp 869-877, 1998.

Neapolitan, R.E., Learning Bayesian Networks, Prentice Hall series in artificial intelligence, 2004.

Nunnari, G., Nucifora, A., Randieri, C., The application of neural techniques to the modelling of time-series of atmospheric pollution data", *Ecological Modelling*, Vol. 111, pp. 187-205, 1998.

Nunnari G., (2000) Fuzzy models of pollutant time-series with reduced number of rules, *Neural Network World*, No. 6, pp. 983-1000.

Nunnari, G., Bertucco, L, Milio, D., Predicting Daily Average SO₂ Concentrations in the Industrial Area of Syracuse (Italy), *Proceedings of ICANNGA 2001*, 5th International Conference on Artificial Neural Networks and Genetic Algorithm, Prague, Czech Republic, April 22-25, 2001.

Nunnari, G., Modelling air pollution time-series by using wavelet functions and genetic algorithms, *Soft Computing*, Springer Verlag, Vol. 8, No. 3, pp. 173-178, 2004.

Nunnari, G., Dorling, S., Schlink, U., Cawley, G., Foxall, R., Chatterton, T., Modelling SO₂ Concentration at a Point with Statistical Approaches, *Environmental Modelling and Software*, Vol. **19/10**, pp. 887-905, 2004.

Nunnari, G., Cannavò, F., A Bayesian approach to model pollution time series, Proc. of the ANDIS 2004 International Symposium (CR-ROM), Taormina (Italy), June 2004, pp. 1-6, 2004.

Pearl, J., (2000), *Causality: Models, Reasoning and Inference*, Cambridge Univ. Press.

Reich, S.L., Gomez, D.R. and Dawidowski, L.E., Artificial neural network for the identification of unknown air pollution sources, *Atmospheric Environment*. Vol. 33, pp. 3045-3052, 1999.

Rumelhart, D.E., Hinton, G.E., McLelland, L., Parallel Distributed Processing Exploration in the Microstructure of Cognition. MIT Press, Cambridge, Mass. Vol. 1, pp. 45-76, 1986.

Sanchez, M.L., Pasqual, D., Ramos, C., Perez, I., Forecasting particulate pollutant concentrations in a city from meteorological variables and regional weather patterns, *Atmospheric Environment*, Vol. 24A, pp. 1509-1519, 1990.

Sarkar, D., Methods to speed-up error backpropagation learning algorithm, *ACM Computing Surveys*, Vol. 27, No. 4, pp. 520-542, 1995.

Schlink, U., Herbarth, O. and Tetzlaff, G., A component time-series model for SO₂ data: forecasting, interpretation and modification, *Atmospheric Environment*, Vol. 31, No. 9, pp. 1285-1295, 1997.

Schlink, U., Dorling, S., Pelikan, E., Nunnari, G., Cawley, G., Junninen, H., Greig, A., Foxall, R., Eben, K., Chatterton, T., Vondráček, J., Richter, M., Dostal, M., Bertuccio, L., Kolehmainen, M. and Doyle, M., A rigorous inter-comparison of ground-level ozone predictions, *Atmospheric Environment*, Vol. **37**, pp. 3237-3253, 2003

Shing, J., R. Jang, "ANFIS: Adaptive-Network-based Fuzzy Inference System", *IEEE trans. on System, Man and Cybernetics*, Vol. 23, pp. 665-683, 1993.

Sjoberg J., Hjalmarsson H., Ljung L., Neural Networks in System Identification, *Proceedings of the Sysid '94*, Copenhagen, Denmark, 1994.

Sjoberg, J., Liung, L., Overtraining, regularisation and searching for a minimum, with application to neural networks, *International Journal of Control*, 62(6), pp. 1391-1407, 1995.

Sluyter, R., E. van Zantvoort, Information Document concerning Air Pollution by Ozone. Overview of the situation in the European Union during the 1997 summer season, Report to the commission by European Environment Agency, European Topic Centre on Air Quality, 1997.

Sugihara, G. and May, R., Nonlinear forecasting as a way of distinguishing chaos from measurement error in time series, *Nature*, Vol. 344, pp. 734, 1990.

Sugeno, M. and Yasukawa, T., A fuzzy-logic based approach to qualitative modeling, *IEEE Transactions on Fuzzy Systems*, **1**, pp. 7-31.

Takens, F., Detecting strange attractors in turbulence. Lecture notes in Math. Springer, New York, Vol. 898, 1981.

Tilley, T., McBean, T.A., An application of spectrum analysis to synoptic-pollution data, *Atmos. Environment*, No. 7, pp. 793-801, 1973.

Trivikrama, S.R., Samson, P.I., Pedadda, A.R., Spectral analysis approach to the dynamics of air pollutants, *Atmos. Environment*, No. 10, pp. 375-379.

TRW, Inc. Air Quality Display Model, Prepared for NAPCA, PHS, U.S. DHEW, Washington DC, NTIS PB-189-194, 1976.

Van Aalst, R.M., F.A.A.M. de Leeuw (Eds.), National Ozone Forecasting System And International Data Exchange In Northwest Europe, *European Topic Centre on Air Quality*, 1997.

Volta, A., Nucifora, G., G. Nunnari. "Real time ozone episode forecast: a comparison between neural network and grey box models", *Proc. International ICSC/IFAC Symposium on NEURAL COMPUTATION-NC '98*, ICSC Academic Press, pp. 854-860, 1998.

Willmott, C.J., Some comments on the evaluation of model performance. *Bulletin American Meteorological Society*, 63 (11), pp. 1309-1313, 1982.

Willmott, C.J., et al., Statistics for the evaluation and comparison of models. *Journal of Geophysical Research*, 90 (C5), pp. 8995-9005, 1985.

Wood, S.N., Modelling and smoothing parameter estimation with multiple quadratic penalties, *J.R. Statistic. Soc. B*, Vol. 62, Part 2, pp. 413-428, 2000.

Young, P.C., Ng, C.N., Lane, K., Parker, D. Recursive forecasting, smoothing and seasonal adjustment of non-stationary environmental data, *Journal of Forecasting*, Vol. 10, pp. 57, 1991.

Young, P.C., Jakeman, A.J. and Post, D.A., Recent advances in data-based modelling and analysis of hydrological systems, *Water Science & Tech.* **36**, pp. 99-116, 1997.

Young, P.C., Data-based mechanistic modelling of environmental, ecological, economic and engineering systems, *Env. Modelling and Software*, **13**, pp. 105-122, 1998.

Van Aalst, R.M. and De Leeuw, F.A.A.M., National Ozone Forecasting System and International Data Exchange in Northwest Europe, *European Topic Centre on Air Quality*, 1997.

Zadeh, L.A. Fuzzy sets, *Information and Control*, **8**, pp. 338-353, 1965.

Zadeh, L.A. The concept of a linguistic variable and its application to approximate reasoning, Part I, *Inf. Sci.*, **8**, pp. 199-249, 1975.

Zadeh, L.A. The concept of a linguistic variable and its application to approximate reasoning, Part II, *Inf. Sci.*, **8**, pp. 301-357, 1975.

Zadeh, L.A. The concept of a linguistic variable and its application to approximate reasoning, Part III, *Inf. Sci.*, **9**, pp. 43-80, 1976.

Zannetti, P., Air Pollution Modeling, Theories, Computational Methods and Available Software, Van Nostrand Reinhold (Ed.), New York, 1990.

Zhang, Q., Using wavelet network in non parametric estimation, *IEEE trans on Neural Networks*, **8**, pp. 227-236, 1997.

Zickus, M., Greig, A.J. and M. Niranjana, Evaluating the Variable Selection and Prediction Performance of Several Machine Learning Algorithms Applied to a PM₁₀ Data Set, *Proceedings of 3rd International Conference on Urban Air Quality*, Loutraki, Greece, March 2001.

BRANKLEY
P. 200

Appendix

A Survey of Software Packages for Developing Forecast Models

In this appendix, we give some information concerning the software packages for building forecasting models by using the techniques described in Section 3.

ARX, ARIMA, and ARMAX models can be identified and simulated by using the Matlab® developed by Ljung (1991).

Cyclo-stationary or *grey-box* ARMAX models can easily be implemented by using the Matlab® programming features. However, a specific tool for *cyclo-stationary* models, referred to as Winast, was developed by the book of Finzi et al. (2001) and it is in the CD as part of the referenced book.

MLP **neural networks** devoted to implement NARX model for air quality forecast can be applied using the general purpose Matlab® Neural Network Toolbox, which gives the user the possibility of using the high level graphical and training features. However, a large number of other tools are available through the Internet such as JANN (a Java Artificial Neural Network) developed at the University of Catania in the framework of the APPETISE project (IST - 99-11746). This tool is available for interactive use at the following URL: <http://www.dees.unict.it/users/gnunnari/appetise/jann/index.html>.

Fuzzy and *Neuro-Fuzzy* models can be implemented by using the Matlab® *Fuzzy* Toolbox

Wavelet based models can be implemented by using the Matlab® Wavelet Toolbox. A specific tool has been coded as a Matlab script by G. Nunnari.

Generalised Additive Models (GAM) and Local Prediction in Phase Space (LPH) models can be implemented by using a tool called TISEAN, which is free and available at the following URL: www.mpiPKS-dresden.mpg.de/~tisean/TISEAN_2.1/index.html.

Such software tool allows the analysis of time series with methods based on the theory of nonlinear deterministic dynamical systems, or chaos theory. The software has grown, with contributions from various groups, during the last few years and was put into distributable form for <http://www.mpiPKS-dresden.mpg.de/~tisean98>, held in Dresden, 11-21 Feb 1998. Some of the routines built around the programs are given in the book by Kantz and Schreiber (1997).

Kalman Filtering models can be implemented by using Mathematica®: <http://www.wolfram.com/products/mathematica/index.html>.

Cluster analysis and modelling can be performed with routines available in the Matlab® Fuzzy tool box, or by using one of the available statistical software packages such as Mathematica® <http://www.wolfram.com/products/mathematica/index.html> or XLstat <http://www.xlstat.com/>.

Bayesian Modelling can be performed by using a number of software tools such as the Bayes Net toolbox for Matlab® developed by K. Murphy (see the following URL: <http://www.ai.mit.edu/~murphyk/Software/BNT/bnt.html> or Netica <http://www.norsys.com/>), which is one of the world's most widely used Bayesian network development software.

Watson, J.G. and J.C. Chow 2005. *Receptor Models*. Chapter 16B of *AIR QUALITY MODELING - Theories, Methodologies, Computational Techniques, and Available Databases and Software. Vol. II – Advanced Topics* (P. Zannetti, Editor). Published by The EnviroComp Institute (<http://www.envirocomp.org/>) and the Air & Waste Management Association (<http://www.awma.org/>).

Chapter 16B

Receptor Models

John G. Watson ⁽¹⁾ and Judith C. Chow ⁽¹⁾

⁽¹⁾ *Desert Research Institute, Reno, NV (USA)*

John.Watson@dri.edu

Judy.Chow@dri.edu

Abstract: Receptor models complement source models by independently identifying sources and quantifying their contributions using ambient measurements of different observables at different times and locations. Source apportionment is accomplished by solution of the mass balance equations that express concentrations of several measured pollutants as a linear sum of products of pollutant abundances in source emissions and source contributions. These equations can be solved by several methods, including maximum likelihood weighted least squares, singular value decomposition eigenvectors, and positive matrix factorization. A viable solution does not guarantee physical reality, so internal and external validation measures must be evaluated. Receptor models are best used in conjunction with source models to create a “weight of evidence” for justifying emission reduction measures on different source types.

Key Words: receptor model, source apportionment, chemical mass balance (CMB), ambient measurement, source profile, particulate matter (PM), volatile organic compound (VOC).

1 Introduction

1.1 Receptor Model Definition

Receptor models (Brook et al., 2003; Watson and Chow, 2002a; Watson et al., 2002a) include a wide range of multivariate analysis methods that use ambient air measurements to infer the source types, source locations, and source contributions that affect ambient pollutant concentrations. Receptor models contrast with the source models explained in other chapters. Source models begin with source emissions and calculate ambient concentrations using mathematical

representations of meteorological dispersion, chemical transformation, and deposition. Applying source and receptor models to the same situation reveals deficiencies in each that, when remedied, lead to a better assessment of pollution sources.

1.2 Use and Applicability

Receptor models have been used to quantify source contributions from direct emissions of suspended particulate matter (PM) (Chow and Watson, 2002a) and volatile organic compounds (VOC) (Watson et al., 2001a), evaluate the zone of influence of source emissions (Watson and Chow, 2001a), determine limiting precursors for ammonium nitrate (Blanchard et al., 2000), estimate contributions to secondary sulfate from nearby emitters (Watson et al., 2002b), evaluate the effects of sulfate reductions on ammonium nitrate levels (Ansari and Pandis, 1998), identify uninventoried sources (Henry et al., 1997), improve emission inventories (Mendoza-Dominguez and Russell, 2000), and track the long-term effectiveness of pollution control strategies (Malm et al., 2002).

In addition to outdoor air applications, receptor models have been used to evaluate personal and animal exposure (Godleski et al., 2000), estimate source contributions to urban and regional haze (Chow et al., 2002a; Pitchford et al., 1999; Watson, 2002a, b), identify causes of nuisance and acid deposition (Anttila et al., 1994; Motelay-Massei et al., 2003), apportion toxic materials in water to their emitters (Pena-Mendez et al., 2001; Stout et al., 2001), and identify pollution sources in hazardous soil remediation (Murphy, 2000; Sims and Sims, 1995).

Receptor models complement, rather than replace, source models by providing an independent method of assessing the influence of nearby and distant sources. Their results are part of the “weight of evidence” (U.S. EPA, 2001a) that needs to be assembled to define and justify cost-effective emission reduction strategies. All air quality models are imperfect representations of reality, and input data are seldom complete. Using several types of models helps to identify and quantify model inaccuracies and to focus further investigation on the areas of greatest uncertainty. Watson et al. (2002a) present a framework for using receptor and source models to solve air quality problems that consists of: 1) formulating a conceptual model; 2) identifying potential sources; 3) characterizing source emissions; 4) obtaining and analyzing ambient gas and particle samples for major components and source markers; 5) confirming source types with multivariate receptor models; 6) quantifying source contributions with chemical mass balance (CMB); 7) estimating source profile changes and the limiting precursor gases for secondary aerosols; and 8) reconciling receptor modeling results with source models, emission inventories, and receptor data analyses. These steps systematize the weight of evidence approach.

1.3 Previous Receptor Model Reviews

This chapter summarizes and updates results from, rather than replicates, previous reviews and specialty conference proceedings that present theory, application examples, and measurement requirements for receptor models (Brook et al. [2003], Chow [1985], Chow and Watson [2002a], Cooper and Watson [1980], Gordon [1980, 1988], Gordon et al. [1984], Henry et al. [1984], Henry [1997, 2002], Hopke [1985, 1991, 1999, 2003], Hopke and Dattner [1982], Javitz and Watson [1988], Javitz et al. [1988], Pace [1986], Watson [1979, 1984], Watson et al. [1981, 1989, 2001a, 2002a], and Watson and Chow [2002a]). Watson et al. (2002a) classified more than 500 citations of receptor modeling theory and applications, and this list is still incomplete. Chow and Watson (2002a) summarized the results of 22 PM_{2.5} and PM₁₀ (particles with aerodynamic diameters <2.5 μm and <10 μm, respectively) source apportionment studies conducted between 1990 and 1998. Watson et al. (2001a) presented a similar summary for VOC receptor models.

Early receptor model research was motivated by the need to develop emission reduction strategies for the attainment of the Total Suspended Particulate (TSP, mass of particles with aerodynamic diameters < ~ 40 μm) standards and PM₁₀ National Ambient Air Quality Standards (NAAQS) in many urban areas. Receptor modeling studies showed the importance of long-range sulfate transport (Lioy et al., 1982 and Mueller et al., 1983), fugitive dust (Gatz et al., 1981), vegetative burning (Watson, 1979), meat cooking (Rogge et al., 1996), and cold start/high emitting vehicles (Watson et al., 1998a) to ambient PM. These sources were previously omitted from local emission inventories, so no form of source-oriented modeling would estimate their contributions. When applied to VOCs (Fujita et al., 1992, 1994, 1995), receptor modeling resulted in major improvements to mobile source emission estimates (California Air Resources Board, 2000).

2 Receptor Model Types

Figure 1 categorizes receptor models based on their use of multivariate PM or VOC properties, measured at a receptor, and by their combination with source modeling concepts. Each receptor model type can be applied independently or in combination with other model types. Table 1 lists the types, strengths, and weaknesses of the different model types.

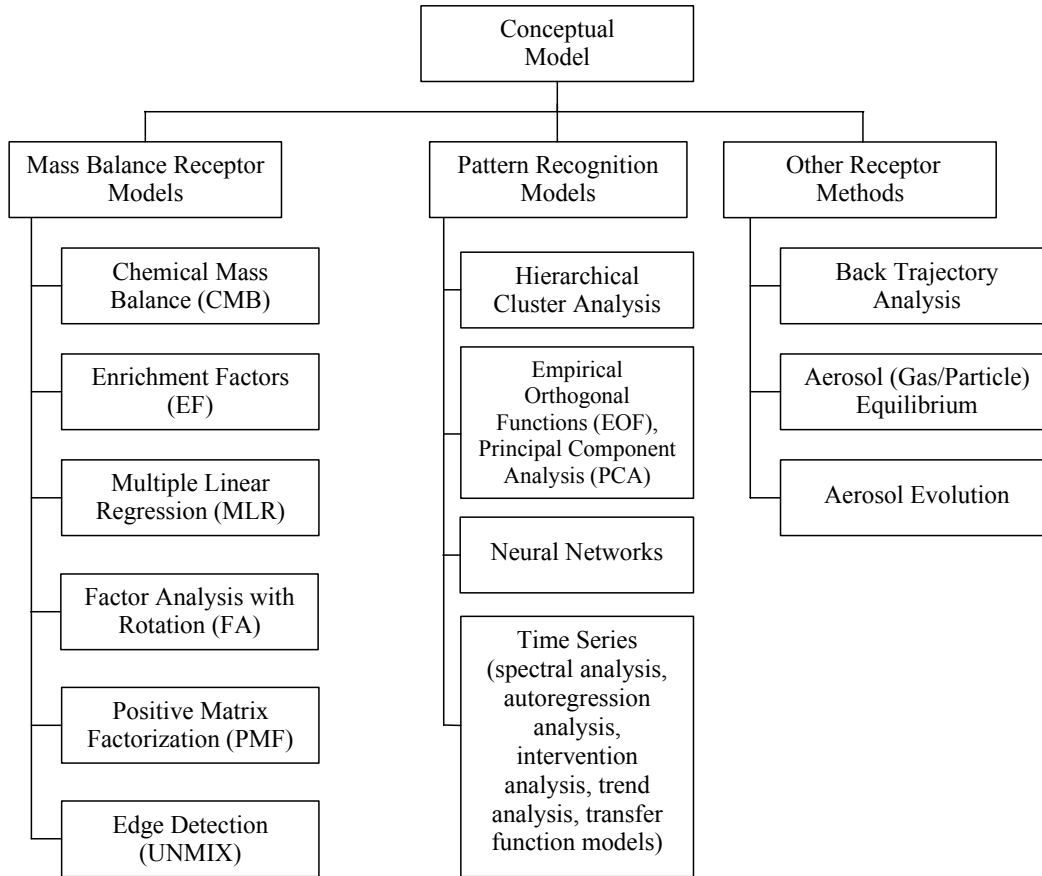


Figure 1. Summary of receptor models and source/receptor techniques.

Table 1. Strengths and weaknesses of different receptor model types (based on Brook et al., 2003 and Watson et al., 2002a). Citations given below are illustrative rather than comprehensive and are recommended for further details.

Receptor Model	Description	Strengths	Weaknesses
Chemical Mass Balance (CMB) (Hidy and Friedlander [1971], Watson [1979], and Watson et al. [1984, 1991])	Ambient chemical concentrations are expressed as the sum of products of species abundances and source contributions. These equations are solved for the source contribution estimates when ambient concentrations and source profiles are used as input. Several different solution methods have been applied, but the effective variance least squares estimation method is most commonly used because it incorporates precision estimates for both source and ambient input data into the solution and propagates these errors to the model outputs. The tracer solution is also commonly used, in which one chemical component is assumed to be unique and in a constant abundance in each source type.	<ul style="list-style-type: none"> • Simple to use, software available. • Quantifies major primary PM source contributions with element, ion, and carbon measurements, and VOC contributions with > 50 non-methane hydrocarbon measurements. • Quantifies contributions from source types with single particle and organic compound measurements. • Provides quantitative uncertainties on source contribution estimates based on input concentrations, measurement uncertainties, and collinearity of source profiles. • Has potential to quantify secondary sulfate contributions from single sources with gas and particle profiles when profiles can be “aged” by chemical transformation models. 	<ul style="list-style-type: none"> • Requires representative source profiles, and common source and receptor measurements of observables, that are not always available. • Assumes all observed mass is due to the sources selected in advance, which involves some subjectivity. • Does not directly identify the presence of new or unknown sources. • Chemically similar sources may result in collinearity without more specific chemical markers. • Typically does not apportion secondary particle constituents to sources. Must be combined with profile aging model to estimate secondary PM.
Enrichment Factor (EF) (Dams et al. [1971] and Reimann and de Caritat [2000])	The ratios of atmospheric concentrations of elements to a reference element are compared to the same ratios in geological material, marine	<ul style="list-style-type: none"> • Simple, no software needed. • Indicates presence or absence of emitters. • Inexpensive. • Provides evidence of secondary PM 	<ul style="list-style-type: none"> • Semi-quantitative method, often not source specific. • Requires source composition data. • More useful for source/process identification than for

Receptor Model	Description	Strengths	Weaknesses
	<p>aerosol, or vehicle exhaust. Higher ratios are attributed to anthropogenic sources or secondary aerosol. Local soil and road dust compositions often differ from global crystal compositions. Heavy metal enrichments are attributed to industrial emitters. Potassium enrichment is attributed to burning and cooking. Sulfur enrichment is attributed to secondary sulfate. OC enrichment is attributed to secondary organics.</p>	<p>formation and changes in source impacts by changes in ambient composition.</p>	<p>quantification.</p>
<p>Multiple Linear Regression (MLR) (Kleinman et al. [1980], Morandi et al. [1991], and Malm and Gebhart [1997])</p>	<p>Mass, chemistry, or light extinction is expressed as linear sums of regression coefficients times source marker concentrations measured at a receptor. The regression coefficients represent the inverse of the chemical abundance of the marker species in the source emissions. The product of the regression coefficient and the marker concentration for a specific sample is the tracer solution to the CMB equation that yields the source contribution.</p>	<ul style="list-style-type: none"> • Implemented by many statistical software packages. • Operates without source profiles. • Abundance of marker species in source is determined by inverse of regression coefficient. • Apportions secondary PM to primary emitters when primary markers are independent variables and secondary component (e.g., sulfate) is dependent variable. 	<ul style="list-style-type: none"> • Requires a large number of ambient measurements. • Marker species must be from only the sources or source types examined. • Limited to sources or source areas with markers. • Abundance of marker species in emissions is assumed constant with no variability.
<p>Hierarchical Cluster Analysis (Gether and Seip)</p>	<p>Multivariate statistical procedure to group data based</p>	<ul style="list-style-type: none"> • Simple, software available. • Detects natural 	<ul style="list-style-type: none"> • Semi-quantitative method. • Requires large data

Receptor Model	Description	Strengths	Weaknesses
[1979], Hopke et al. [1976], Saucy et al. [1987], and Wilkinson [1990])	on similarities between observables. Usually presented by a Euclidian distance between each pair of observables.	data groupings without prior knowledge of group characteristics. <ul style="list-style-type: none"> • Can be used for either spatial or temporal analysis. 	sets. <ul style="list-style-type: none"> • Requires prior knowledge of sources to select key species indicative of potential emission sources in the study area.
Eigenvectors (Principal Component Analysis [PCA], Factor Analysis [FA], Empirical Orthogonal Functions [EOF]) (Blifford and Meeker [1967], Henry and Hidy [1982], Henry [1987], Henry et al. [1991], Hopke [1988], Thurston and Spengler [1985], and White [1999])	Correlations or covariances are calculated from chemical measurements taken on simultaneous samples at a large number of locations. Eigenvectors of this correlation or covariance matrix represent a spatial distribution of source influence over the area, providing that the samplers have been located to represent the gradients in source contributions.	<ul style="list-style-type: none"> • Models such as PCA and FA identify major source types, and relate secondary components to source via correlations or covariances. • Sensitive to the influence of unknown and/or minor sources. • Influenced by extreme values. Can be used to identify data outliers. 	<ul style="list-style-type: none"> • Large data sets required. • Most models are based on statistical associations (e.g., common variations or associations among groups of variables) rather than a derivation from physical and chemical principles. • Vectors or components are usually related to broad source types as opposed to specific categories or sources. • Many subjective rather than objective decisions and interpretations of eigenvectors as sources. • Do not always produce unique, physically valid solutions.
Non-Negative Least Squares (Positive Matrix Factorization [PMF]) (Hopke et al. [2003], Kim and Hopke [2004], Kim et al. [2004], Paatero and Tapper [1994] and Poirot et al. 2002)	Mass balance equations are solved by least squares minimization for many samples, not just for a single one. This provides an overdetermined set of equations that allows source profile abundances, as well as source contribution estimates, to be calculated.	<ul style="list-style-type: none"> • Software available. • Requires uncertainty estimates of ambient measurements. Can handle missing or below-detection-limit data. • Weights species concentrations by their analytical precisions. • Constrained to non-negative species concentrations or source contributions. 	<ul style="list-style-type: none"> • Requires large ambient data sets. • Need to judge the number of retained sources. • Requires measured source profiles to assign categories to derived profiles. • Weights only by uncertainty of receptor measurements, not by uncertainties in source profiles. • Several adjustable parameters and initial

Receptor Model	Description	Strengths	Weaknesses
		<ul style="list-style-type: none"> • Provides solution evaluation tool (e.g., R^2, Chi-square). • Derives source profiles from ambient measurements as they would appear at the receptor. 	<p>conditions must be selected, often based on trial and error.</p>
Edge Detection (RMAPS, UNMIX) (Henry [1997], and Henry et al. [1999])	Edges are constant ratios among chemical components that are detected in multi-dimensional space. Some samples in the input data must have no contribution from the sources to define an edge. The edges detected by models such as UNMIX are extensions of self-modeling curve resolution to n dimensions sources.	<ul style="list-style-type: none"> • Software available. • Does not require assumptions about number or composition of sources. • Provides source contribution estimate to each sample. • Provides evaluation tool (e.g., R^2, S/N ratio). 	<ul style="list-style-type: none"> • Requires large ambient data sets. • Does not make explicit use of errors or uncertainties in ambient concentrations or source profiles. • Can produce an infinite number of solutions with the same root mean square error. • Need to assume or predetermine number of retained sources. • May result in no solution.
Time Series (e.g., spectral analysis, auto regression analysis, intervention analysis, trend analysis, transfer function models) (Perrier et al. [1995], Somerville and Evans [1995], Hies et al. [2000], Jorquera et al. [2000], and Watson and Chow [2001a])	Provides understanding of temporal variation of mass and chemical concentrations that coincide with meteorology and source information. Assists in formulating conceptual models and selecting sources for further modeling. Assumes that different source types or sub-types may have some periodicity to their emissions that allows separation of different source impacts.	<ul style="list-style-type: none"> • Can be used to determine statistical trends in data sequences. • Provides clues to influences from meteorology and sources. 	<ul style="list-style-type: none"> • Requires continuous measurements. • Semi-quantitative descriptive data analysis does not provide specific source impact information.
Neural Networks (Bishop [1995], Chelani et al.	Attempts to simulate pattern recognition processes of the	<ul style="list-style-type: none"> • Makes no prior assumptions about data distributions. 	<ul style="list-style-type: none"> • Semi-quantitative method. • Requires large

Receptor Model	Description	Strengths	Weaknesses
[2002], and Gao et al. [1994])	human brain by creating classification rules. Known inputs and outputs are presented to a neural network that simulates the human thought process. The network assigns weights to the inputs that reproduce the outputs. Once these patterns have been established for cases where outputs are known, weights can be applied to input data to estimate outputs.	<ul style="list-style-type: none"> • Deals with nonlinear relationships. • Neural networks can provide function relationships and represent a solution to the CMB equations. 	ambient data sets. <ul style="list-style-type: none"> • Requires training set containing known source/receptor relationships. • Subjective association of outputs with sources.
Backward Trajectory Analysis (Ashbaugh [1983], Draxler [1999], and Green and Gebhart [1997])	Estimates the path and location of the air reaching a receptor based on prior wind movements. The simplest form classifies pollutant concentrations or source contributions by surface wind direction in a pollution rose. More complex backward trajectories add hourly wind vectors generated by a meteorological model.	<ul style="list-style-type: none"> • Traces or projects the route of air mass transport over hundreds to thousands of kilometers, and on the order of several days. • Can generate multiple trajectories with different time intervals. • Can represent plume spread from vertical wind shear at different hours of day, and provide better understanding of day/night transition. 	<ul style="list-style-type: none"> • Relies on wind observations with limited temporal and spatial density. • Highly dependent on wind interpolation algorithm and start height/vertical dispersion parameters. • Accuracy and precision of the wind measurements dictate the model output. • Unable to resolve small-scale turbulence. • Provides history of air parcel travel path, but cannot tell how much pollution was picked up along the way or differentiate between pollutant contributions. • More useful in regional than in urban-scale applications.
Aerosol (Gas/Particle) Equilibrium (Ansari and Pandis [1998],	The portions of a semi-volatile species in the gas and particle phase are estimated based on receptor	<ul style="list-style-type: none"> • Estimates partitioning between gas and particle phases for ammonia, nitric acid, 	<ul style="list-style-type: none"> • Highly sensitive to temperature and relative humidity. Short duration samples are not

Receptor Model	Description	Strengths	Weaknesses
Blanchard and Hidy [2003], Blanchard et al. [2000], Stelson and Seinfeld [1982], and Watson et al. [1994a])	measurements to determine which precursor is in excess and which needs to be diminished in order to reduce concentrations in the particle phase. The theory is most highly developed for ammonium nitrate/ammonium sulfate and has been used to determine the extent to which ammonia or oxides of nitrogen/sulfur dioxide reductions are needed to reduce ambient ammonium nitrate levels.	ammonium nitrate, and aerosol water content. <ul style="list-style-type: none"> • Allows evaluation of effects of precursor gas reductions on ammonium nitrate levels. 	usually available. <ul style="list-style-type: none"> • Gas-phase equilibrium depends on particle size, which is not often known in great detail. • Sensitivity to aerosol mixing state, which is not completely understood or quantified.
Aerosol Evolution (Lewis and Stevens [1985], Stockwell et al. [2001], and Watson et al. [2002b])	Source profiles containing particle chemical components and gaseous precursors are mathematically “aged” using a chemical reaction scheme. Source profile evolution has been done using Lagrangian source models to simulate the conditions that a profile might encounter en route between source and receptor.	<ul style="list-style-type: none"> • Can be used parametrically to generate several profiles for typical transport and meteorological situations that can be used as input to mass balance equations. 	<ul style="list-style-type: none"> • Very data-intensive. Input measurements are often unavailable. • Derives relative, rather than absolute, concentrations. • Level of complexity may not adequately represent profile transformations.

Receptor as well as source models start with a conceptual model that proposes plausible theories about the causes of an elevated pollutant concentration or effect. The conceptual model is formed from previous experience (e.g., tests on similar sources, gas and particle transport and transformation under similar meteorological conditions), the nature of the problem (e.g., exceeding an air quality standard, consistently poor visibility over a local area or large region), and available measurements (e.g., ambient, source, and meteorological). A conceptual model (Pun and Seigneur [1999], Watson et al. [1998b], Watson and Chow [2002b]) provides reasonable, though not necessarily accurate, explanations of: 1) potential sources; 2) precursor gas and particle emission characteristics; 3) meteorological conditions that affect emissions, transport, and transformation; 4)

size, chemical, and temporal characteristics of precursor gas and particle emissions; and 5) frequency, magnitude, and composition of the PM or VOC levels. The conceptual model is used to design a measurement program that considers the location and number of monitoring sites, sampling frequencies and periods, sampling durations, properties that are quantified, samples that are selected for laboratory analysis, and the modeling and data analysis methods that will be applied.

Trajectory, aerosol evolution, and equilibrium models are described from a source-oriented point of view in other chapters and are not examined in detail here, except to note that they can also be used in a receptor-oriented mode, as cited in the references. An ammonium nitrate chemical equilibrium model, for example, can be used as a source model within the context of an air quality model. It can also be used as a receptor model to determine whether nitric acid (HNO_3) or ammonia (NH_3) limits ammonium nitrate formation when NH_3 , HNO_3 , hydrochloric acid (HCl), sulfur dioxide (SO_2), sulfuric acid (H_2SO_4), ammonium (NH_4^+), nitrate (NO_3^-), sulfate ($\text{SO}_4^{=}$), temperature, and relative humidity measurements are available at a receptor. Wind models have source-oriented forward trajectory modes and receptor-oriented backward trajectory modes.

Chemical and physical analysis methods are often termed receptor models, but they serve as inputs to models. Carbon 14 (^{14}C) single particle microscopic analysis, gas chromatograms, x-ray spectra, and many other analytical outputs are analogous to source profiles (mass fractions of emitted chemical components) in that they represent a pattern that might allow a source contribution to be identified and quantified. Without the receptor model mathematics and applications framework, however, these methods do not provide valid, quantifiable source apportionments.

3 Multivariate Receptor Model Mathematics

Receptor models are incorrectly referred to as “statistical” methods (e.g., Seinfeld and Pandis, 1998). This is inaccurate because the statistical distributions, often-missing data, and variable uncertainties of the input measurements do not conform to the rigorous assumptions required for statistical tests. Furthermore, statistical significance tests are rarely used, and are not useful, for source apportionment studies. This misconception partially arises because much of the receptor modeling mathematics is also used to determine and test statistical associations in other areas of science. There are also situations where the physical basis for the receptor model formulation has not yet been clearly understood or demonstrated.

The derivation presented below (Watson, 1984) shows the physical and mathematical relationships between emission models, source models, and receptor models and the simplifying assumptions that are made when these models are applied.

Summation indices (lower case) are defined as follows:

- i = Pollutant, representing any quantifiable property such as an element (e.g., aluminum, arsenic, selenium, etc.), water soluble ions (e.g. SO_4^- , NO_3^- , NH_4^+ , etc.), an operationally defined carbon fraction (organic carbon [OC], elemental carbon [EC]), a specific volatile or organic carbon compound (e.g., benzene, benzo(a)pyrene), an isotopic abundance (e.g., ^{14}C , lead 210 [^{210}Pb], sulfur 34 [^{34}S]), or particle property (e.g., vanadium- and nickel-rich particle, S-shaped spiny particle).
- j = Source type, a grouping of individual source emissions with similar compositions that differ from the compositions of other source types. Common source types include geological material, sea salt, vegetative burning, cooking, motor vehicle exhaust, evaporated gasoline, and architectural coatings.
- k = When the sample was taken (i.e., continuous hourly averages to days representing different seasons, days of the week, and times of day).
- l = Receptor location, often selected to be source dominated (e.g., near roadways or other emitters), exposure dominated (where people live, work, and play), transport dominated (between major source areas), and boundary dominated (to determine what is entering a monitoring domain). Source-dominated samples may be used to obtain source profiles.
- m = Source subtype, a specific source or groups of emitters within a source type that have similar source compositions or locations. Paved roads, unpaved roads, agricultural soil, and industrial dust are geological source subtypes. Diesel and gasoline engine exhaust are vehicle exhaust subtypes. Source subtypes may become source types with the measurement of additional chemical components or directional sampling that allow them to be distinguished by the receptor model.

Upper case indices designate the total number. Symbols used in the model equations and typical units are described as follows:

- A_{jkm} = Activity that causes emissions for source type j corresponding to time period k for subtype m (unit of activity/sec). Typical activities are vehicle miles traveled, amount of fuel consumed, or amount of product produced. Population densities are often used as surrogates for area source activities.
- C_{ikl} = Concentration of pollutant i for time period k at location l (unit of $\mu\text{g}/\text{m}^3$, ng/m^3 , ppm, or ppb). This is the receptor concentration.
- D_{klm} = Dispersion and mixing of emissions from source type between subtype m and receptor l corresponding to time period k (sec/m^3).
- F_{ij} = Fractional quantity of pollutant i in source type j (unitless). These are elements of the source profile for different source types. For PM measurements, profile abundances are usually normalized to mass emissions from a source in the desired size range. They may also be normalized to the weighted sum of the major species emitted or to an individual element that is present in all of the source types being modeled. Owing to the large number of species, total VOC is not usually available

for normalization. Options for VOC source normalization are discussed below.

- Q_{jkm} = Emission rate from subtype m of source type j corresponding to time period k ($\mu\text{g}/\text{sec}$).
- R_{jkm} = Rate of emissions (emission factor) per unit of activity for subtype m of source type j corresponding to time period k ($\mu\text{g}/\text{unit of activity}$).
- T_{ijklm} = Transformation of pollutant i between source subtype m of type j and receptor l corresponding to time period k (unitless).
- S_{jkl} = Contribution from source type j for time period k at receptor l ($\mu\text{g}/\text{m}^3$, ng/m^3 , ppm, or ppb).
- W_{ik} = Weighting of differences between measured and calculated concentrations for pollutant i on sample k .

3.1 Emission Model

Emission rates for a pollutant from a source are usually estimated in an inventory by:

$$Q_{jkm} = R_{jkm} A_{jkm} \quad (1)$$

The R_{jkm} emission factors are derived from a limited number of tests on representative emitters, and are applied over a wide range of emitters that may constitute M individual sources or J source types. An emission inventory may include a category of “electrical generation” that consists of emissions from diesel generators, coal-fired power stations, natural gas burners, and residual oil combustors. Each of these would be classified as a separate source type for receptor modeling. Diesel generators would be grouped with other diesel emissions from heavy-duty trucks, farm equipment, and construction equipment because their chemical source profiles would be similar. The activity level might be specific to location and time, but this is true only of specially constructed, gridded inventories. Most inventories for mobile and area sources are compiled as annual averages over countywide and statewide areas. Large point sources can usually be associated with a specific location.

Source models take the form of:

$$C_{ikl} = \sum_{j=1}^J \sum_{m=1}^M D_{klmn} T_{ijklm} F_{ij} Q_{jkm} \quad (2)$$

All of the values on the right side of Equation (2) are inputs that estimate the concentration of a specific pollutant i at a specific time k and location l . Other chapters in this book show that the linear form of this equation is a large, but necessary, simplification to show the relationship between the source and receptor models.

Receptor models used for source apportionment are based on the chemical mass balance equations:

$$C_{ikl} = \sum_{j=1}^J F_{ij} S_{jkl} \quad (3)$$

For this to be of use, species i must be such that $T_{ijlm} = 1$, meaning that there is little change in the F_{ij} between source and receptor, or that such changes can be adequately estimated with an aerosol evolution model and have been incorporated into the F_{ij} . A comparison of Equations (2) and (3) also implies that:

$$S_{jkl} = \sum_{m=1}^M D_{klm} Q_{jkm} \quad (4)$$

In contrast to the source model, the ambient concentrations (C_{ikl}) are known and the source contributions (S_{jkl}) are to be calculated. The mass balance equations (Equation 3) can be solved for single samples if the source profiles (F_{ij}) have been measured by minimizing the weighted sum of the squares of the differences between measured and calculated concentrations for individual samples:

$$\sum_{i=1}^I \left\{ \left(C_{ikl} - \sum_{j=1}^J F_{ij} S_{jkl} \right) / W_{ik} \right\}^2 = \text{Minimum} \quad (5)$$

The weights (W_{ik}) can be set to 1, but they are usually selected to represent uncertainties in the ambient measurements and variability of the source profile abundances (Watson et al., 1984). This minimization takes the same form as a multiple linear regression equation, but it is not used in the statistical sense that is usually associated with regression.

Positive matrix factorization (PMF) attempts to derive source profiles from the ambient data themselves. The PMF solution to the mass balance equations (Paatero and Tapper, 1994) minimizes the weighed sum of squares of the difference between measured and calculated concentrations over many samples:

$$\sum_{k=1}^K \sum_{i=1}^I \left\{ \left(C_{ikl} - \sum_{j=1}^J F_{ij} S_{jkl} \right) / W_{ik} \right\}^2 = \text{Minimum} \quad (6)$$

With multiple samples and with rigorous assumptions, there are sufficiently more equations than unknowns to estimate values of source profiles as well as source contributions. The derived profiles need to be associated with measured source compositions that can be determined only from source tests.

Watson (1984) showed how the eigenvector and multiple linear regression (MLR) models are derived from the mass balance equations and the simplifying assumptions that need to be made. When source profiles are not measured, unique solutions to Equation (6) do not exist, and subjective interpretation is needed to judge the validity of the derived source profiles.

4 Model Input Measurements

Receptor models require multivariate measurements that are specific to gaseous precursors, particle sizes, chemical/physical/optical characteristics, temporal variations, and source locations. Several sampling and analytical methods provide time-integrated samples of PM (ACGIH [2001], Baron and Willeke [2001], Chow [1995], Landsberger and Creatchman [1999]) and VOC (Zielinska and Fujita, 1994) that are collected in the field and analyzed in the laboratory. In-situ measurement systems (McMurry [2000], Middlebrook et al. [2003], Wang et al. [1999], Watson et al. [1998c], Yamamoto et al. [2002]) provide the opportunity to better associate ambient concentrations with specific wind directions and distances from the receptor. Source emissions need to be measured for the same pollutants with methods comparable to those used at receptors.

4.1 Source Profiles

Source profiles are intended to represent a category or type of source, rather than individual emitters. All receptor models require measured source profiles, even those that intend to derive these profiles from the ambient measurements. The derived profiles must always be compared and evaluated against measured profiles that represent a source type. The number and definition of these categories are limited by the degree of similarity between the profiles. Mathematically, this similarity is termed “collinearity” (Henry, 1992), which means that two or more of the CMB equations are redundant and the set of equations cannot be solved. Owing to measurement error, however, CMB equations are never completely collinear in a mathematical sense. When two or more source profiles are collinear, standard errors on source contributions are often very high. Some source contributions may be unrealistically high, while others may be negative. Determining the degree of collinearity is one of the main objectives of receptor model validation (Watson et al., 1998d).

4.1.1 Common Emission Sources

Emission inventories need to be examined before a receptor model is applied to determine which source profiles are needed, and which chemical components must be measured in local source emissions and ambient air. These inventories can be less quantitative than those needed for source modeling. Receptor models only need to identify potential emitters, not the individual emission rates. Source types that are often combined due to its similarity or collinearity for PM and VOCs are:

- Vegetative burning and cooking: Subtypes include fireplaces, wood stoves, prescribed burns, wildfires, char-broiling, and meat cooking. Some of these source subtypes may be separated when appropriate organic compounds are measured.
- Diesel exhaust: Subtypes include heavy- and light-duty cars and trucks, off-road equipment, stationary engines for pumps and generators, ship generators, and locomotives.
- Gasoline exhaust: Subtypes include heavy- and light-duty cars and trucks, and small engines. Emission inventories do not usually contain breakdowns by cold-starts and visible smoking vehicles, although these subtypes might be discriminated by certain organic compounds in a profile. Two-stroke engine profiles may differ from four-stroke engine profiles.
- Gasoline evaporative emissions: Subtypes include fueling stations and hot-soak vehicles.
- Fugitive dust: Subtypes include paved roads, unpaved roads, agricultural tilling, dairy/feedlot soil, construction, wind erosion, and industrial aggregate. These subtypes can sometimes be separated based on single particle profiles or the measurement of specific mineral composition (Ashbaugh et al. [2003], Chow et al. [2003]).
- Solvents and coatings: Subtypes include evaporation from paints, degreasers, and solvents. These subtypes can be separated when the specific solvent compounds are known.
- Metals: Subtypes include copper smelters, lead smelters, steel mills, and aluminum mills. These often have similar metal emissions but in different abundances depending on the process.
- Aggregate handling: Subtypes include cement, quarrying, and mining. Ores are often enriched in the materials being extracted, thereby allowing their separation. When low-level measurements of trace elements such as copper, zinc, and lead are made, metal processing operations that use these materials can be classified into separate source types.

Vehicle-related VOC emissions, including exhaust, evaporated fuel, and liquid fuel, are ubiquitous in all urban areas. Architectural (e.g., paints) and industrial solvents (e.g., cleaning and process solvents, as in printing) are also common, but highly variable, in most urban areas. Petrochemical production and oil refining are more specific to certain urban settings, such as the Texas coast, where these activities are numerous. Biogenic emissions are larger in the eastern U.S., where forests are lush, in contrast to the arid west. VOC emissions in inventories are often reported in equivalent units of methane or propane. Comparisons of relative source attributions to emission inventories require appropriate reconciliation between the inventory and source contribution units.

4.1.2 Source Profile Normalization Options

Both gaseous and particulate species can be included in a source profile. As noted in the definition of F_{ij} above, one of the difficulties in combining VOC and $PM_{2.5}$ in a source apportionment is that there are some particle sources (e.g., suspended dust) that have negligible VOC components and some VOC sources (e.g., solvents, evaporated gasoline, biogenics) that have negligible particle components. There are many sources, such as vehicle exhaust, cooking, and wood combustion, that have large VOC and PM components, and profiles that normalize both gas and particle components to $PM_{2.5}$ mass may increase the utility of the profiles for both VOC and PM source apportionment studies.

Individual profiles are formed from individual source samples, and the precisions of the numerator and denominator are propagated (Watson et al., 2001b) to obtain the individual profile uncertainties. These individual profiles are further combined to obtain the source profiles used as CMB model input or for comparison with those derived from ambient data. Chow et al. (2003) established a framework that uses statistical measures to composite similar profiles. The simplest composite consists of the averages and standard deviations of abundances for all individual profiles within a group. Outlier tests are applied to remove individual profiles that unduly bias the averages and standard deviations. There are always some outliers in any series of source tests owing to the difficulties in field sampling and emission variability. For this reason, it is important to obtain five or more samples that run the range of operating conditions and fuels for a given source type to obtain representative source profiles.

VOC abundances are defined by several different methods. Watson et al. (2001a) summarize VOC terms in common use that represent different fractions of atmospheric organic material. These include reactive organic gases (ROG), total organic gases, photochemical assessment monitoring station (PAMS) species, non-methane hydrocarbons (NMHC), heavy hydrocarbons (C_{10} - C_{20}), carbonyl compounds, non-methane organic compounds (NMOG), semi-volatile organic compounds (SVOC), and total VOC. Non-standard variable definitions and units are an impediment to VOC source apportionment. VOC concentrations are usually reported in ppbC or $\mu\text{g}/\text{m}^3$ at local temperature and pressure. Either unit is acceptable for receptor modeling, but the source profile ratios must be consistent with the ambient measurements. VOC fractional abundances have been normalized by: 1) NMHC, consisting of ROG and an unidentified fraction; 2) the sum of the quantified or most abundant measured compounds, which varies depending on the study; 3) the sum of all canister measurements, including non-reactive gases such as halocarbons; and 4) NMOG, the sum of all VOCs measured from all applied methods. These profile differences preclude the comparability and use of profiles from different studies. Watson et al. (2001a) advocate normalization to the sum of the 56 PAMS species in ppbC that are almost universally quantified in canister samples by the U.S. Environmental Protection

Agency (EPA) TO-14 method¹. Measurements from other canister analyses, Tenax and 2,4-dinitrophenylhydrazine (DNPH), can also be normalized to this sum. With this common convention, re-normalization to NMOG or other categories is straightforward.

4.1.3 Requirements for a Source Profile Library

The current SPECIATE database (U.S. EPA, 1999) includes 376 PM and 610 VOC source profiles, most of which are dated before 1989. These source profiles need to be updated with more contemporary data to enhance their usefulness for both source and receptor models. The objectives of compiling source profile libraries are to: 1) identify chemical and physical characteristics of primary PM and VOC emissions; 2) tabulate and document chemical abundances and variabilities from source tests; and 3) provide data interfaces to receptor models and speciated emission inventories. These databases can be used to: 1) create speciated emission inventories for regional haze, PM_{2.5}, and ozone modeling; 2) estimate hazardous and toxic air pollutant emissions from primary PM and VOC emissions; 3) provide input to mass balance receptor models; and 4) verify profiles derived from ambient measurements by the multivariate receptor models listed in Table 1.

The minimum source profile requirements to compile a library are:

- No hot stack samples or hot stack/impinger analyses should be included. Only dilution sampler results come close to representing ambient air concentrations. Method 201/202 certification results (U.S. EPA [1996, 1997]) for PM₁₀ do not represent actual, condensed, particle emissions (England et al., 2000).
- VOC profiles should include, at a minimum, the 56 PAMS species (U.S. EPA, 2001b), plus other available species (additional light hydrocarbons from canisters, heavy hydrocarbons from Tenax, and carbonyls from DNPH). PM profiles should include, at a minimum, major elements (at least those reported by the National Park Service [NPS], Interagency Monitoring of Protected Visual Environments [IMPROVE] [Malm et al., 2000], and EPA's PM_{2.5} Speciation Trends Network [STN]); major water-soluble ions (SO₄²⁻ and NO₃⁻ at a minimum—preferably NH₄⁺, water-soluble sodium, magnesium, potassium, calcium, chloride, fluoride, and phosphate); and carbon fractions (total carbon, OC, and EC, preferably with other fractions that are defined by the method such as the eight IMPROVE fractions [Chow et al., 1993, 2001, 2004a], and carbonate carbon [Chow and Watson, 2002b]). Organic functional groups, organic compounds, isotopic abundances, and single particle properties should be included where they are reported, well-defined, and can be normalized to PM mass or the sum of PAMS VOCs.
- Profiles must include their chemical abundances and variabilities (Chow et al. [2003, 2004b], Watson and Chow [2001b], Watson et al. [2001c]).

¹ <http://www.epa.gov/ttnamti1/files/ambient/airtox/to-14ar.pdf>

Preference should be given to profiles that represent an average and standard deviation of individual samples. Analytical uncertainties for individual source profiles should be identified as such; they are typically smaller than the variability among several samples taken at different times from the same emitter or from samples taken from different, but similar, emitters (Chow et al., 2003). The method for estimating variabilities should be documented. Some references report emission rates instead of emission profiles. Emission rates that are not normalized are not useful for receptor modeling.

Necessary profile documentation includes:

- The primary reference document for the profile. Secondary references should be supplied when original profiles have been modified (i.e., by aerosol aging, different sample compositing, etc.). Gray literature reports should be scanned and made available with the database. Copyrighted journal articles and book chapters can be obtained from libraries.
- The profile database should include (in the notes column or other fields) the specific size fraction, type of source sampling (e.g., hot stack [presumably excluded], dilution stack, diluted plume [e.g., airborne], source dominated, grab/resuspension), background corrections, chemical analysis methods, sample compositing criteria and methods, and number and types of profiles in a composite.

4.2 Ambient Measurements

Receptor observables are a subset of the source profile species and must include at least those species in the source profiles that allow sources to be separated by the receptor model.

4.2.1 Physical and Chemical Characteristics of Receptor Concentrations

Table 2 associates VOC, semi-volatile organic compounds (SVOC), and PM measurements with measurement methods. For gas- and particle-phase organics, a standard set of species is needed for all studies. Table 3 contains C₂ to C₁₂ VOCs that can be obtained by canister sampling, C₈ to C₂₀ VOCs by Tenax sampling, and SVOC and PM organic compounds by Teflon-coated glass-fiber filter and PUF/XAD-4/PUF solid adsorbent sampling. These compounds are determined by thermal desorption/cryogenic preconcentration, followed by gas chromatography (GC) separation and flame ionization or electron capture detection and/or combined GC/mass spectrometry/Fourier transform infrared detection. One of the difficulties with organic compound measurements is that different researchers measure different compounds by different methods, so that ambient and source concentrations are not always compatible. Seinfeld and Pandis (1998) and Watson et al. (2002a) discuss which species are useful for identifying different source types and provide more extensive references to applications and analytical techniques.

Table 2. Inorganic and organic species and measurement methods commonly used for receptor modeling.

Observables	Chemical Analysis Method
Particulate mass on filters	Gravimetry
Particulate elements (Na to U) on filters	X-ray fluorescence (XRF) Proton-induced x-ray emission (PIXE) Instrumental neutron activation analysis (INAA) Inductively coupled plasma / emission spectroscopy (ICP/ES) Inductively coupled plasma / mass spectrometry (ICP/MS)
Particulate water-soluble anions on filters (F^- , Br^- , Cl^- , NO_3^- , PO_4^{3-} , SO_4^{2-})	Ion chromatography (IC) Automated colorimetry (AC)
Particulate cations on filters (NH_4^+ , Na^+ , Mg^{++} , K^+ , Ca^{++})	Ion chromatography (IC) Atomic absorption spectrophotometry (AAS) (flame or graphite) Automated colorimetry (AC)
Particulate carbon (organic carbon [OC], elemental carbon [EC], carbonate, other fractions defined by thermal or optical properties)	Thermal/optical reflectance (TOR) Thermal/optical transmission (TOT) Thermal manganese oxidation (TMO)
Particulate single-particle morphology on filters	Computer-controlled scanning electron microscopy (CCSEM) Electron Microprobe Transmission Electron Microscopy
C_2 - C_{10} organics, volatile organic compounds (VOC)	Canister and gas chromatography measurement with various detectors
C_{11} - C_{20} organics, VOCs and semi-volatile organic compounds (SVOC)	Tenax cartridge with thermal desorption and gas chromatography with various detectors
SVOC (polycyclic aromatic hydrocarbons [PAH])	Filter/PUF/XAD/PUF with extraction in solvents of different polarities and gas chromatography with various detectors
Carbonyl VOCs	2, 4-dinitrophenylhydrazine (DNPH)-coated C_{18} cartridge and gas or liquid chromatography
Oxygenated VOCs (e.g., alcohol, ethers, esters)	Carbotrap canister, solvent extraction, derivitization, and gas chromatography with various detectors

Table 3. List of volatile organic compounds (VOCs), photochemical assessment monitoring station (PAMS) target compounds, semi-volatile organic compounds (SVOCs), and particulate organic compounds.

1. C₂ to C₁₂ VOC samples acquired by canister samplers using gas chromatography (GC) with mass spectrometry (MS) for analysis of 123 VOCs:

propene	4-methyl-1-pentene	1-methylcyclopentene	2,3-dimethylhexane	n-nonane	indene
propane	3-methyl-1-pentene	benzene	2-methylheptane	isopropylbenzene	1,3-diethylbenzene
isobutane	cyclopentane	3,3-dimethylpentane	4-methylheptane	isopropylcyclohexane	1,4-diethylbenzene
1,3-butadiene	2,3-dimethylbutane	cyclohexane	3-methylheptane	2,6-dimethyloctane	n-butylbenzene
n-butane	methyl-t-butylether	4-methylhexene	2,2,5-trimethylhexane	alpha-pinene	1,2-diethylbenzene
methanol	2-methylpentane	2-methylhexane	1-octene	3,6-dimethyloctane	1,3-dimethyl-4-ethylbenzene
t-2-butene	2,2-dimethylpentane	2,3-dimethylpentane	1,1-dimethylcyclohexane	n-propylbenzene	isopropyltoluene
1&2-butyne	3-methylpentane	cyclohexene	n-octane	m-ethyltoluene	nonanal
c-2-butene	2-methyl-1-pentene	3-methylhexane	2,3,5-trimethylhexane	p-ethyltoluene	1-undecene
3-methyl-1-butene	1-hexene	1,3-dimethylcyclopentane	2,4-dimethylheptane	1,3,5-trimethylbenzene	n-undecane
ethanol	n-hexane	3-ethylpentane	4,4-dimethylheptane	o-ethyltoluene	1,2,4,5-tetramethylbenzene
isopentane	t-3-hexene	1-heptene	2,6-dimethylheptane	octanal	1,2,3,5-tetramethylbenzene
1-pentene	t-2-hexene	2,2,4-trimethylpentane	2,5-dimethylheptane	beta-pinene	1,2,3,4-tetramethylbenzene
2-methyl-1-butene	2-methyl-2-pentene	t-3-heptene	3,3-dimethylheptane	1-decene	2-methylindan
n-pentane	cis-3-methyl-2-pentene	n-heptane	ethylbenzene	1,2,4-trimethylbenzene	1-methylindan
isoprene	c-3-hexene	2,4,4-trimethyl-1-pentene	m- & p-xylene	n-decane	1-dodecene
t-2-pentene	c-2-hexene	methylcyclohexane	2-methyloctane	isobutylbenzene	naphthalene
c-2-pentene	trans-3-methyl-2-pentene	2,5-dimethylhexane	3-methyloctane	sec-butylbenzene	n-dodecane
2-methyl-2-butene	methylcyclopentane	2,4-dimethylhexane	styrene	1,2,3-trimethylbenzene	
2,2-dimethylbutane	2,4-dimethylpentane	2,3,4-trimethylpentane	o-xylene	limonene	
cyclopentene	2,2,3-trimethylbutane	toluene	1-nonene	indan	

2. Photochemical Assessment Monitoring Stations (PAMS) monitor 56 target VOCs:

ethylene	1-pentene	n-hexane	2,3,4-trimethylpentane	n-propylbenzene
acetylene	n-pentane	methylcyclopentane	toluene	m-ethyltoluene
ethane	isoprene	2,4-dimethylpentane	2-methylheptane	p-ethyltoluene
propylene	t-2-pentene	benzene	3-methylheptane	1,3,5-trimethylbenzene
propane	c-2-pentene	cyclohexane	n-octane	o-ethyltoluene
isobutane	2,2,-dimethylbutane	2-methylhexane	ethylbenzene	1,2,4-trimethylbenzene
1-butene	cyclopentane	2,3-dimethylpentane	m&p-Xylenes	n-decane
n-butane	2,3-dimethylbutane	3-methylhexane	styrene	1,2,3-trimethylbenzene
t-2-butene	2-methylpentane	2,2,4-trimethylpentane	o-xylene	m-diethylbenzene
c-2-butene	3-methylpentane	n-heptane	n-nonane	p-diethylbenzene
isopentane	2-methyl-1-Pentene	methylcyclohexane	isopropylbenzene	n-undecane

3. C₈ to C₂₀ VOC samples acquired by glass cartridges filled with Tenax-TA (a polymer of 2,6-diphenyl-p-phenylene oxide) solid adsorbent. Samples were analyzed by the thermal desorption/cryogenic preconcentration method followed by high-resolution GC separation and flame ionization detection (FID) and/or combined MS/Fourier transform infrared (FTIR) detection for 63 VOCs:

1,2,4,5-tetramethylbenzene	1-methyl-3-ethylbenzene	1,3-di-n-propylbenzene	benzaldehyde
1(1,1-dimethylethyl)3-5-dimethylbenzene	1-methyl-4-ethylbenzene	2-methylnaphthalene	acetophenone
(1-methylethyl)benzene	4-methylindan	1-methylnaphthalene	2,5-dimethylbenzaldehyde
1-methyl-4-(1-methylethyl)benzene	2-methylindan	hexanal	ethanone-1(3-methoxyphenol)
1,4-diethylbenzene	5-methylindan	heptanal	t-2,4-decadienal
1,2-diethylbenzene	1,3-dimethyl-4-ethylbenzene	octanal	undecane
1,3-diethylbenzene	1,2-dimethyl-3-ethylbenzene	nonanal	dodecane
(1-methylpropyl)benzene	1,3-dimethyl-5-ethylbenzene	decanal	tridecane
1,2,3,4-tetramethylbenzene	1,2-dimethyl-4-ethylbenzene	undecanal	tetradecane
2,3-dihydroindene (indan)	1-methyl-2-n-propylbenzene	dodecanal	pentadecane
1,2,3,5-tetramethylbenzene	1-methyl-3-n-propylbenzene	tridecanal	hexadecane
1-methyl-2-(1-methylethyl)benzene	1-methyl-4-n-propylbenzene	tetradecanal	heptadecane
1-methyl-3-(1-methylethyl)benzene	1-methyl-2-n-butylbenzene	pentadecanal	octadecane
n-pentylbenzene	1,4-dimethyl-2-ethylbenzene	hexadecanal	nonadecane
(2-methylpropyl)benzene	1,3-dimethyl-2-ethylbenzene	octadecanal	eicosane
1-methyl-2-ethylbenzene	1-ethyl-2-n-propylbenzene	2-furaldehyde	

4. Carbonyl samples were acquired by carbonyl samplers containing dinitrophenylhydrazine (DNPH) cartridges, followed by high-performance liquid chromatography (HPLC) analysis of 14 carbonyls:

formaldehyde acetaldehyde acetone acrolein	propanal crotonal methyl ethyl ketone methacrolein	butanal pentanal glyoxal hexanal	benzaldehyde and m-tolualdehyde
---	---	---	------------------------------------

5. SVOCs and particulate organics acquired with a sampling train consisting of a Teflon-impregnated glass fiber filter backed up with a PUF/XAD-4/PUF sandwich solid adsorbent. Samples were analyzed by GC/MS for 151 SVOCs and particulate organic compounds:

<u>Naphthalene</u> 2-menaphthalene 1-menaphthalene 2,6+2,7-dimenaphthalene 1,7+1,3+1,6-dimenaphthalene 2,3+1,4+1,5-dimenaphthalene 1,2-dimenaphthalene 1,8-dimenaphthalene biphenyl 2-methylbiphenyl 3-methylbiphenyl 4-methylbiphenyl trimethylnaphthalene Isomers ethyl-Methylnaphthalenes acenaphthylene acenaphthene phenanthrene fluorene methylfluorenes Isomers 1-methylfluorene methylphenanthrenes Isomers 2-methylphenanthrene	4Hcyclopenta(def)phenanthren benzo(c)phenanthrene perylene quinoline dibenzo[a,e]pyrene dibenzo[a,h]pyrene dibenzo[a,i]pyrene dibenzo[a,l]pyrene dibenz[a,j]acridine dibenz[a,h]acridine 7H-dibenzo[c,g]carbazole 5-methylchrysene dibenz[a,h]anthracene 7,12-dimethylbenzanthracene 3-methylcholanthrene oxy-PAH 9-fluorenone xanthone acenaphthenequinone perinaphthenone Anthraquinone 9-anthraldehyde	<u>Hopanes&Steranes</u> 18(H)-22,29,30-trisnorneohopane 17(H)-22,29,30-trisnorhopane 17(H)-21(H)-29-norhopane 17(H)-21(H)-hopane 20R,5(H),14(H),17(H)-cholestane 20R,5(H),14(H),17(H)-cholestane 20R&S,5(H),14(H),17(H)- ergostane 20R&S,5(H),14(H),17(H)- sitostane <u>Carpanes</u> 8, 13-dimethyl-14-n- butylpodocarpane 8, 13 dimethyl-14-[3'-methylbutyl] podocarpane n-alkanoic Acids octanoic acid nonanoic acid decanoic acid undecanoic acid	<u>Alkanes</u> n-pentadecane n-hexadecane n-heptadecane n-octadecane n-nonadecane n-eicosane n-heneicosane n-docosane n-tricosane n-tetracosane n-pentacosane n-hexacosane n-heptacosane n-octacosane farnesane norpristane norfarnesane pristane phytane
---	--	--	--

1-methylphenanthrene 3,6-dimethylphenanthrene 1,7-dimethylphenanthrene anthracene 9-methylanthracene fluoranthene pyrene methylpyrene/fluoranthenes 4-methylpyrene retene benzonaphthothiophene benz(a)anthracene 7-methylbenz[a]anthracene chrysene/triphenylene benzo(b+j+k)FL BeP BaP 7-methylbenzo[a]pyrene indeno[123-cd]pyrene dibenz(ah+ac)anthracene benzo(b)chrysene benzo(ghi)perylene coronene	benzanthrone benz(a)anthracene-7,12-dione 1,4-chrysenequinone 9,10-dihydrobenzo(a)pyren-7(8H)-one nitro-PAH 1-nitronaphthalene 2-nitronaphthalene methylnitronaphthalenes 2-nitrobiphenyl 4-nitrobiphenyl 5-nitroacenaphthene 2-nitrofluorene 9-nitroanthracene 1-nitropyrene 4-nitropyrene 3-nitrofluoranthene 7-nitrobenz(a)anthracene 6-nitrochrysene 6-nitrobenzo(a)pyrene 1,8-dinitropyrene 1,6-dinitropyrene 1,3-dinitropyrene	dodecanoic acid tridecanoic acid tetradecanoic acid heptadecanoic acid octadecanoic acid nonadecanoic acid eicosanoic acid alkanedioic acids octadecanedioic acid nonadecanedioic acid <u>Aromatic acids</u> benzoic acid methylbenzoic acid	<u>Saturated</u> <u>Cycloalkanes</u> tridecylcyclohexane tetradecylcyclohexane pentadecylcyclohexane hexadecylcyclohexane heptadecylcyclohexane octadecylcyclohexane nonadecylcyclohexane <u>Lower priority</u> <u>cycloalkanes</u> heptylcyclohexane octylcyclohexane nonylcyclohexane decylcyclohexane undecylcyclohexane dodecylcyclohexane eicosylcyclohexane heneicosylcyclohexane
---	---	--	---

4.2.2 Receptor Measurement Databases

Air quality monitoring networks in the U.S. are not designed for the application of receptor or source models (Demerjian, 2000). The major emphasis of networks is on NAAQS compliance rather than on the broader range of purposes that might include air quality forecasting, episode alerts, health studies, atmospheric process studies, evaluating source zones of influence, evaluating long-term effectiveness of control strategies, and source apportionment modeling (Chow et al. [2002b], U.S. EPA [2002]).

At least three levels of monitoring are needed:

- **Level III:** Portable, inexpensive filter and continuous sampling at a large number of locations with a minimum investment in site infrastructure and maintenance (Baldauf et al., 2001, 2002). Some accuracy and precision are traded for greater spatial coverage. Temporary, dense networks of this type surrounding Level I and Level II sites would establish the zones of representation for the permanent monitors.
- **Level II:** Fixed sites with proven technology, similar to compliance sites, but with observables and locations intended to serve the multiple purposes described above. Resources directed at urban sites that are no longer needed for compliance could be used to establish background, boundary, and transport sites.
- **Level I:** Fixed sites with proven, novel technology, similar to those of the U.S. EPA's current supersites program. These would have instrumentation similar to that of Level II and Level III sites to determine comparability, as well as detailed size distributions, PM chemistry, and precursor gases.

Special studies have been conducted to obtain data at representative receptors during periods when PM and/or VOC concentrations have been found to be excessive. Chow and Watson (1989), Liou et al. (1980), and Watson and Chow (1992) summarize several chemically speciated data sets for suspended particles. The most complete chemical database to which receptor modeling can be applied is the IMPROVE network, which has acquired elemental, ionic, and carbon measurements at national parks and wilderness areas since 1987 (Eldred et al., 1989). The recently established STN may also be a source of data for receptor models in urban areas. The most comprehensive VOC data, derived from the PAMS, takes canister or continuous gas chromatographic measurements at urban and suburban sites during the summer.

4.2.3 Receptor Model Application Levels

There is no single sampling and analysis design that will permit successful receptor modeling in every urban area. Since measurements can be costly, it is useful to examine existing samples and data to assist in forming a conceptual model prior to designing a full-scale source apportionment study. Three sequential stages of complexity (U.S. EPA, 1984) can be applied, with each stage being progressively more costly, but providing more accurate and precise results than the previous stage.

Stage I uses existing data or data that can be readily obtained from analyses of existing samples (Gordon et al., 1984). Source profiles, related to local sources that were measured elsewhere, are also used. This effort confirms the selection of contributing sources from the preliminary analysis and eliminates minor contributors from further scrutiny. If the sources contributing to the high concentrations of PM or VOC are apparent and sufficiently certain, no further work will be needed. Alternatively, this step serves to reduce the areas to be studied in greater detail under an intermediate (Stage II) analysis.

Stage II involves additional chemical analyses on existing samples or the acquisition of additional samples from existing sampling sites. It is intended to fill the gaps in model input data that may have been discovered in Stage I, so as to reduce uncertainty in results of the Stage I source apportionment. This may require new source and ambient sampling activities. Local fugitive dust samples are acquired, resuspended, and analyzed, at a minimum. Ground-based vehicle exhaust and vegetative burning profiles may also be acquired. Industrial source profiles from other studies can often be adapted. C₂ to C₁₂ hydrocarbons are measured for VOC apportionment studies, while elements, ions, and carbon are quantified for PM studies. Where additional sampling is possible, monitoring locations and times are selected to bracket suspected contributors.

Stage III analysis is applied only in the most complex airsheds, where the costs of emission reduction are high and their effectiveness is uncertain. A Stage III study involves original source testing and measurements beyond the basic PM or VOC species. C₁₀ to C₂₀ hydrocarbons and PM organic species are measured at source and receptor.

Many of the receptor modeling techniques described in Table 1 are appropriate for all three stages of PM or VOC assessment. Precision and validity estimates define the measurement requirements for the next level of analysis. These estimates can also be used to determine whether the model results at a given stage of PM or VOC assessment adequately eliminate the need for more extensive assessment.

4.3 Meteorological Variables

Concurrent with air quality measurements, meteorological measurements at the same or nearby locations are needed to better characterize the meteorological regimes affecting the sampled area. Meteorological measurements (typically at 10 meters above ground level) such as wind speed, wind direction, temperature, relative humidity, dew point, atmospheric pressure, cloud cover, solar radiation, mixing height, and precipitation are commonly used in principle component analysis (PCA) and factor analysis (FA). Temperature has been shown to be related to the intensity of photochemical reactions (Wolff and Lioy, 1978). Absolute humidity is related to the partial pressure of water vapor and can be associated with smog precursors. Inverse relative humidity is theoretically related to aerosol water content and is related to aerosol hygroscopic growth factors. Poor atmospheric dispersion (horizontal and vertical) is indicated by low wind speeds/mixing height and poor ventilation during cold winter periods. These variables are often correlated with atmospheric constituents that can also be used in time series and other receptor analyses. Nearby rawinsonde or radar profiler upper-air meteorology data can be used for backward air mass trajectory analysis (Draxler and Hess, 1997). These trajectories indicate the regions over which an air mass traveled, during the previous 12 to 120 hours, before arriving at the receptors.

4.4 Chemical Transformation Parameters

Appropriate gas and particle processes (Lewis and Stevens [1985], Watson et al. [2002b]) can be used for atmospheric “aging” of source profiles. “Aging” is assumed to occur in a confined “box” or “puff” from source to receptor along a trajectory path. Temperature, relative humidity, precursor gas concentrations, and particle composition affect changes in chemical abundances for different aging times. Watson et al. (2002a) provide an example of how to simulate changes in source profiles from nearby coal-fired power stations and how to use these aged profiles in receptor model applications for data acquired from the Mt. Zirkel Wilderness Area in northwestern Colorado. Watson et al. (1994b) also provide an example of the aerosol equilibrium model and the non-linearity of inorganic aerosol. These chemical transformation/equilibrium models require concurrent air quality and meteorological measurements of PM and their precursor gases such as NH_3 , HNO_3 , SO_2 , HCl , VOC, temperature, and relative humidity. Shorter duration sampling of 1 to 6 hours is preferable to minimize the uncertainties of model simulation.

5 Receptor Model Assumptions, Performance Measures, and Validation Procedures

5.1 CMB Model Validation and Application Protocol

CMB software provides outputs and performance measures (Table 4) that can be adapted to other receptor models that follow the mass balance equations. The seven-step applications and validation protocol (Watson et al., 1998d) can also be applied to these receptor models (Watson, 2002c). The steps are: 1) determine the applicability of the receptor model; 2) format input files and perform initial model runs; 3) evaluate outputs and performance measures; 4) evaluate deviations from model assumptions; 5) modify model inputs to remediate problems; 6) evaluate the consistency and stability of the model results; and 7) corroborate receptor model results with other modeling and analyses. Elaborations are given below.

Table 4. Chemical mass balance (CMB) receptor model outputs and performance measures.

Output/Statistic/Code	Abbreviation	Description
Source Contribution Estimate	SCE	Contribution from the source type to the profile-normalizing component (usually PM mass or sum of PAMS VOCs).
Standard Error	STD ERR	The uncertainty of the source contribution estimate (SCE), expressed as one standard deviation of the most probable SCE. This is an indicator of the precision or certainty of each SCE. The STD ERR is estimated by propagating the precisions of the ambient measurements and source profiles through the effective variance least-squares calculations. Its magnitude is a function of the uncertainties in the input data and the amount of collinearity (i.e., degree of similarity) among source profiles. When the SCE is less than the STD ERR, the STD ERR is interpreted as an upper limit of the source contribution.
t-Statistic	TSTAT	Ratio of the SCE to its STD ERR. A high TSTAT suggests a non-zero SCE.
R-square	R-SQUARE	Variance in ambient species concentrations explained by the calculated species concentrations. A low R-SQUARE (<0.8) indicates that the selected source profiles have not accounted for the variance in the selected receptor concentrations. Ranges from 0 to 1.0.
Percent Mass Accounted For	PERCENT MASS (% MASS)	The sum of SCE divided by the PM mass or VOC concentration. A value approaching 100% is desired.

Output/Statistic/Code	Abbreviation	Description
Degrees of Freedom	DF	The number of species minus number of sources in fit. Solutions with larger degrees of freedom are typically more stable and robust than ones with small degrees of freedom.
Chi-square	CHI SQUARE	CHI SQUARE is the square root of the sum of the squares of the RATIO R/U that correspond to fitting species divided by the DF. Similar to R-SQUARE except that it also considers the uncertainties of the calculated species concentrations. A large CHI SQUARE (>4.0) means that one or more of the calculated species concentrations differ from the measured concentrations by several uncertainty intervals. The values for these statistics exceed their targets when: 1) contributing sources have been omitted from the calculation; 2) one or more source profiles have been selected which do not represent the contributing source types; 3) precisions of source profiles or ambient data are underestimated; and/or 4) source profiles or ambient data are inaccurate.
Ratio of Calculated to Measured Species	RATIO C/M	Ratio of calculated to measured concentrations and its uncertainty. Used to identify species that are over- or under-accounted for by the model. The ratios should be near 1.00 if the model has accurately explained the measured concentrations. Ratios that deviate from unity by more than two uncertainty intervals suggest that an incorrect set of profiles is being used to explain the measured concentrations.
Ratio of Residual to its Uncertainty	RATIO R/U	Ratio of the signed difference between the calculated and measured concentrations (i.e., the residual) divided by the uncertainty of that residual (i.e., square root of the sum of the squares of the uncertainty in the calculated and measured concentrations). Used to identify species that are over- or under-accounted for by the model. The RATIO R/U specifies the number of uncertainty intervals by which the calculated and measured concentrations differ. When the absolute value of the RATIO R/U exceeds two, the residual is significant. If it is positive, then one or more of the profiles is contributing too much to that species. If it is negative, then there is an insufficient contribution to that species and a source may be missing.

5.1.1 Determine the Receptor Model Applicability

The following conditions must be met for a receptor model to be applicable:

- A sufficient number of PM or VOC receptor samples have been taken with accepted sampling methods to fulfill study objectives. If objectives are to determine how to attain ambient air quality standards, samples should represent annual average and maximum concentrations for PM_{2.5} and PM₁₀, and correspond to maximum 8-hour average ozone concentrations for VOCs. At least one ambient sample is needed for a CMB run, with the other methods in Table 1 requiring at least 50 to 100 ambient samples that encompass the variability of source contributions.
- Samples are amenable to or have been analyzed for a variety of chemical species. As noted above, elements, ions, and carbon are the minimal measurements for PM apportionment while the PAMS species listed in Table 3 are the minimal requirements for VOC apportionment.
- Potential source contributors can be identified and grouped into source types of distinct chemical compositions with respect to the available receptor species.
- Source profiles are available from the study area or from similar sources that represent the source compositions as they would appear at the receptors. Changes in source composition between source and receptor must be accommodated in order for the model to be physically meaningful.

5.1.2 Format Input Files and Perform Initial Model Runs

Modern receptor modeling software (Henry [2000], Hopke et al. [1983], Paatero [1998, 2000], Watson et al. [1997]) allows input data files to be prepared in spreadsheet or word processor formats and, with contemporary computer memories, there is no practical limit to the number of source profiles, chemical species, or individual samples that can be included in a single file. It is convenient, however, to group input data by site or season when data sets are large.

The initial model runs should include sensitivity tests (Watson et al., 1994b). For the CMB, this involves evaluating the effects of different combinations of source profiles and fitting species. For eigenvector, edge detection, and PMF models, this involves different selections of chemical species and subsets of the ambient samples, different selections of the number of factors, different rotation methods, and different settings for selectable variables.

In selecting source profiles for inclusion in a CMB or for associating a derived factor with a source type, wind direction data can be reviewed to disregard downwind sources that have little opportunity to contribute detectable concentrations. Source types that are likely to be dormant, such as wood smoke

emissions during hot summer months, can also be eliminated, or they should be interpreted as wildfires or prescribed burning that might occur during that period.

Some sources have emissions that are chemically similar or consistent over time – that is, although the absolute magnitude of the emissions may vary, the abundances of the measured species may be stable. However, the chemistry of some species could be variable if an industrial source alternates its operating conditions, feedstock, or fuel. This variability must be reflected in the uncertainties that are assigned to each species abundance in the profile. These concerns about source profile variability are analogous to those faced by the dispersion modeler when estimating emission rates or dispersion parameters.

Because receptor models use the analytical results from all included species, mis-estimation of a single species, even so-called “tracer” species, may not appreciably affect the source contribution estimates. This is especially true if these species have been assigned and are inversely weighted by uncertainties, which reflect their variability in source emissions. When these uncertainties are adequately estimated, other less variable species abundances provide a larger influence on the source contribution estimates.

5.1.3 Evaluate Outputs and Performance Measures

Model outputs and performance measures are described in Table 4. These are examined for different combinations of profiles and species to determine the optimal fit to the data.

5.1.4 Evaluate Deviations from Model Assumptions

The performance measures and tests can often indicate when deviations from model assumptions may have occurred. These deviations do not necessarily invalidate the receptor model result, but they point out the potential for invalidity. This is why a separate step is necessary in the applications and validation protocol that evaluates the effects of these deviations from assumptions and determines whether these effects can be tolerated.

5.1.5 Modify Model Inputs to Remediate Problems

Receptor modeling results may be compromised by: 1) insufficient receptor measurements; 2) insufficient or non-representative source measurements; 3) incorrect profile combinations; and 4) source profile collinearity. Because of the complex interactions of all the data in a least squares estimate that occur in some CMB solutions (including the PMF solution), statistics or diagnostics may not always be adequate to conclusively isolate a problem with model input. Remedies for unacceptably high uncertainties due to collinearity include:

- Measure additional species that are abundant in one source, but not so abundant in other sources.

- Reduce the uncertainties in the source profiles of the collinear sources. This is applicable only if the uncertainties estimated for a composite profile are believed to be overestimated, owing to outliers in the compositing process.
- Combine the collinear source profiles into a single profile of a “composite source type” that chemically represents the source types identified by the estimable linear combinations of inestimable sources. For example, resuspended road dust and windblown soil dust are chemically similar, and some modelers include a single term to represent “crustal material” instead of the two individual source types. This aggregate source contribution estimate (SCE) might then be partitioned into its components by another method (e.g., source modeling, microscopy, or wind trajectory analysis).

5.1.6 Evaluate the Consistency and Stability of the Model Results

SCEs should not differ by more than two standard errors, with changes in input data (number of samples, number of species, and number of profiles). Portions of the input data may be perturbed randomly or systematically in proportion to their uncertainty. The sensitivity of SCEs to the species can be evaluated by eliminating and adding species to the calculation, and determining the change in source contributions.

5.1.7 Corroborate Receptor Model Results with Other Modeling and Analyses

The receptor analysis is considered valid if four criteria are met: 1) the receptor model is determined to be applicable; 2) the performance measures are generally within target ranges; 3) there are no significant deviations from model assumptions; and 4) the sensitivity tests reveal no unacceptable instabilities or inconsistencies. If uncertainties associated with source contributions are too high for decision-making purposes even after taking the steps recommended here, then the source compositions being used do not represent the sources in the airshed or they are too uncertain.

Source and receptor models may be used in a collaborative manner to perform an apportionment, provided that the source model is applicable and the receptor model is valid for the particular application. Spatial and time series distributions should be examined to determine that magnitudes of SCEs are consistent with the locations and timing expected from those sources.

5.2 Model Sensitivity Tests

An example of sensitivity testing for PM₁₀ source apportionment along the Baja California, California (CA) border (Chow and Watson, 1997) is given in Table 5. Initial tests with different combinations of source profiles were done to determine which profiles best explained the data at the Calexico, CA, site. Several test CMB runs were performed for 24-hour samples collected on 12/02/92 with PM₁₀ mass concentrations of $222.7 \pm 11.2 \mu\text{g}/\text{m}^3$. CMB performance measurements were examined to determine how well the ambient concentrations were explained by the SCEs. The results of these initial trials were used as guidance in CMB analysis of the entire sample set.

Based on the emission inventory and site survey, primary geological material, primary marine aerosol, salt flats or alkaline dust, primary vegetative burning, and primary motor vehicle sources were expected to be important contributors in the study area. Ambient measurements showed that high ambient concentrations of crustal species (e.g., aluminum, silicon, iron), marine and alkaline species (e.g., sodium, chloride), as well as OC, EC, and lead were observed. PM₁₀ OC concentrations were enriched relative to EC in many samples. To account for this “excess” OC, either an agricultural burning profile, a charbroil cooking emission profile, or a composite of the two was used. Secondary ammonium nitrate and ammonium sulfate profiles explained NO₃⁻, SO₄⁼, and NH₄⁺, which were unaccounted for by the primary emission profiles. Although soluble sodium was used in place of elemental sodium, magnesium was below the lower quantifiable limits (LQLs) in many of the source profiles. PM₁₀ SO₄⁼ was used in place of sulfur (S), and chloride (Cl⁻) was used in place of chlorine (Cl), because the soluble fractions of these species are more typical of secondary sulfate and marine aerosol, or playa salt sources, than the total elemental fractions.

The test results of the source apportionments at each site are presented by a series of trials representing different combinations of source profiles in Table 5. The “best fit” or “default fit” is presented first as a reference. The SCEs and CMB performance measurements are shown for each trial.

Table 5 indicates that primary geological material was the largest contributor, followed by primary motor vehicle exhaust and vegetative burning emissions. The “best fit” was obtained using the Imperial County, CA, composite road dust profile (ICRDC) and the asparagus burning profile (ICABC2). While the Imperial County composite motor vehicle profile (ICRSC) produced a “good fit,” the Mexicali, Mexico, motor vehicle profile (IMRSUC) gave better results because it accounted for more of the unusually high lead concentration ($0.127 \pm 0.0007 \mu\text{g}/\text{m}^3$) in this sample. Meteorological data on 12/02/92 suggests that this sample was indeed impacted by cross-border transport.

Table 5. Example of sensitivity tests in chemical mass balance (CMB) receptor modeling (sample from Calexico, CA, on 12/02/94).

PROFILE ^a	BEST FIT	TRIAL 1	TRIAL 2	TRIAL 3	TRIAL 4	TRIAL 5	TRIAL 6
ICRDC (Road Dust)	143.6 ± 11.1	138.1 ± 11.1				136.0 ± 11.2	136.3 ± 13.4
ICBDC (Bulk Soil)			149.7 ± 15.6				
ICBD27 (Salt Flats)				74.5 ± 6.3			
IMRDC2 (Road Dust)					140.8 ± 6.6		
IMRSUC (Vehicle Exhaust)	18.1 ± 8.1						
ICRSBC (Vehicle Exhaust)		23.8 ± 7.4	33.6 ± 8.3	25.9 ± 10.1	27.0 ± 7.4		
ICRSIC3 (Vehicle Exhaust)						36.6 ± 13.5	
ICRSIC2 (Vehicle Exhaust)							60.5 ± 12.0
MARIP (Marine Aerosol)	2.1 ± 1.3	2.2 ± 0.5	1.7 ± 2.5	-17.3 ± 3.0	2.0 ± 0.7	1.9 ± 0.6	1.4 ± 0.6
ICABC2 (Ag Burn)	30.2 ± 12.2	28.5 ± 11.6	17.7 ± 12.3	74.1 ± 20.4	24.0 ± 10.6	25.9 ± 12.2	14.4 ± 9.1
BAMAJC (Wood Stove)							
IMTSAC (Charbroiling)							
AB75TAL (Ag Burn/Cooking)							
ICPPMC (Power Station)							
IMGPEC (Glass Plant)							
AMSUL (Amm Sulfate)	4.2 ± 1.8	3.6 ± 1.6	2.0 ± 4.3	-15.9 ± 3.0	3.1 ± 1.1	2.6 ± 2.0	
AMNIT (Amm Nitrate)	17.6 ± 1.9	15.9 ± 2.1	14.9 ± 2.5	17.5 ± 2.4	15.7 ± 2.2	13.7 ± 5.0	1.2 ± 8.1
CHI SQUARE ^b	0.95	1.08	0.69	19.6	1.19	1.03	0.64
R SQUARE ^b	0.96	0.96	0.95	0.46	0.97	0.94	0.96
PERCENT MASS ^b	96.8	95.2	98.6	71.3	95.4	97.3	96.0
COLLINEARITY ^c			ICBDC	ICBD27			ICRDC
			ICABC2	MAR100			ICRSIC
			ICRSBC	AMSUL			ICABC2

<u>PROFILE^a</u>	<u>TRIAL 7</u>	<u>TRIAL 8</u>	<u>TRIAL 9</u>	<u>TRIAL 10</u>	<u>TRIAL 11</u>	<u>TRIAL 12</u>	<u>TRIAL 13</u>
ICRDC (Road Dust)	142.9 ± 12.1	142.0 ± 11.8	144.6 ± 11.3	147.2 ± 12.1	138.6 ± 11.2	137.7 ± 11.4	137.7 ± 11.2
ICBDC (Bulk Soil)							
ICBD27 (Salt Flats)							
IMRDC2 (Road Dust)							
IMRSUC (Vehicle Exhaust)							
ICRSBC (Vehicle Exhaust)			33.1 ± 11.5	44.4 ± 9.0	24.1 ± 7.6	23.9 ± 7.4	23.5 ± 7.4
ICRSC (Vehicle Exhaust)							
ICRSHC (Vehicle Exhaust)							
ICRSIC3 (Vehicle Exhaust)	32.5 ± 9.9						
ICRSIC2 (Vehicle Exhaust)		38.2 ± 19.1					
MARIP (Marine Aerosol)	2.4 ± 1.0	1.8 ± 0.8	3.3 ± 0.5	3.7 ± 0.6	2.2 ± 0.5	2.2 ± 0.5	2.1 ± 0.5
ICABC2 (Ag Burn)	20.6 ± 11.3	30.2 ± 14.4				28.2 ± 11.6	28.8 ± 11.7
BAMAJC (Wood Stove)			17.8 ± 12.0				
IMTSAC (Charbroiling)				-6.8 ± 14.9			
AB75TAL (Ag Burn/Cooking)					29.0 ± 12.4		
ICPPMC (Power Station)						0.26 ± 1.12	
IMGPEC (Glass Plant)							0.81 ± 0.62
AMSUL (Amm Sulfate)	3.0 ± 1.7	3.4 ± 1.9	3.3 ± 1.8	3.2 ± 1.8	3.6 ± 1.7	3.4 ± 1.8	3.2 ± 1.7
AMNIT (Amm Nitrate)	14.3 ± 3.1	16.8 ± 3.4	15.7 ± 2.5	15.1 ± 2.8	15.9 ± 2.1	15.9 ± 2.1	16.0 ± 2.1
CHI SQUARE ^b	ICRSIC3	ICRSIC2	ICRSBC	ICRSDC		AMSUL	AMSUL
R SQUARE ^b	ICABC2	ICABC2	BAMAJC	ICRSBC		AMNIT	AMNIT
PERCENT MASS ^b	AMSUL	ICRDC		IMTSAC		ICPPMC	IMAR100
COLLINEARITY ^c	AMNIT						IMGP15C

^a See Chow and Watson (1997) for source profile descriptions.

^b See Table 4 for details.

^c Similar profiles representing subtypes that need to be combined into a single source type. Determined by the method of Henry (1992).

PM₁₀ Na⁺ and Cl⁻ concentrations were both present in elevated concentrations (1.13 ± 0.07 and 6.5 ± 0.4 µg/m³, respectively). Because the Cl⁻/Na⁺ ratio is actually higher than ratios found in seawater, the “pure” unreacted marine profile (MARIP) was used to fit these species. The secondary ammonium nitrate profile (AMNIT) was the fourth largest component of PM₁₀, following the contributions from primary geological material (143.6 ± 11.1 µg/m³), primary agricultural burning (30.2 ± 12.2 µg/m³), and primary motor vehicle emissions (18.1 ± 8.1 µg/m³).

The asparagus burning profile (ICABC2) was needed to fit OC, which had a concentration in this sample 5.6 times greater than that of EC. In the “best fit” case, the performance measurements, shown in Table 5, are excellent with a “CHI SQUARE” of 0.95, an “R-SQUARE” of 0.96, and a “PERCENT MASS” of 97%.

The first trial results in Table 5 were similar to the “best fit” solution except that an Imperial Valley motor vehicle profile (ICRSBC) was used. The major difference was a poorer fit for lead. In Trial 2, the Imperial County bulk soil profile (ICBDC) was substituted for the Imperial County road dust profile (ICRDC). This solution shows a potential collinearity among bulk soil composite (ICBDC), asparagus burning (ICABC2), and motor vehicle exhaust (ICRSBC) profiles, but the source contribution estimates are similar to those of the best fit solution.

For Trial 3, the bulk salt flats profile (ICBD27) was used by itself to represent fugitive dust contributions. The “CHI SQUARE” was high (19.6) and the “PERCENT MASS” was low (71.3%) in this case. The substitution of the Mexicali composite road dust profile (IMRDC2) for the “best fit” Imperial County road dust profile (ICRDC) caused little variation in the source contributions (Trial 4). This was also the case for Trial 5, where the Imperial County composite motor vehicle profile (ICRSC) was used, although less of the lead was accounted for in this case.

Substitution of the Imperial County motor vehicle profile with profile “ICRSHC” in Trial 6 resulted in a potential collinearity among road dust (ICRDC), motor vehicle exhaust (ICRSHC), asparagus burning (ICABC2), and ammonium nitrate (AMNIT) profiles. Similar results and higher “CHI SQUAREs” (2.21 and 2.64, respectively) were obtained by substituting the motor vehicle profiles with the profiles “ICRSIC3” and “ICRSIC2” in Trials 7 and 8, respectively.

Trial 1 combination was modified in Trial 9 by substituting the Bakersfield residential wood combustion (i.e., fireplace) profile (BAMAJC) for the asparagus burning profile (ICABC2). The solution is degraded, with a higher “CHI SQUARE” (3.54), lower “R-SQUARE” (0.88), and a potential collinearity among motor vehicle exhaust (ICRSBC) and residential wood combustion (BAMAJC). Substituting the taco restaurant charbroil cooking profile (IMTSAC) for the asparagus burning profile (ICABC2) produced a similar result, with potential

collinearity among the road dust (ICRDC), motor vehicle exhaust (ICRSBS), and charbroil cooking (IMTSAC) profiles in Trial 10.

A composite profile (AB75TA25) constructed by combining 75% of asparagus burning (ICABC2) and 25% of charbroil cooking (IMTSCA) is tested in Trial 11. The results in this trial are similar to those obtained in Trial 1. The manure-fueled power plant profile (ICPPMC) was added to the Trial 1 combination in Trial 12. The SCEs from the manure-fueled power plant (ICPDMC) were not significant ($0.26 \pm 1.12 \mu\text{g}/\text{m}^3$) and a cluster was formed containing the ammonium sulfate (AMSUL), ammonium nitrate (AMNIT), and manure-fueled power plant (ICPPMC) profiles.

Finally, Trial 13 added the glass plant profile (IMGPEC) to the Trial 1 combination. Again, the SCEs from the glass plant (IMGPEC) were small ($0.81 \pm 0.62 \mu\text{g}/\text{m}^3$), and this profile was potentially collinear with the ammonium sulfate (AMSUL), ammonium nitrate (AMNIT), and marine (MARIP) profiles. The “best fit” source combination provided a robust source apportionment because similar solutions were obtained using different combinations of profiles. The results shown in Table 5 for Trials 1, 4, 5, and 11 indicate similarly high performance indices and potential profile collinearities.

Therefore, the “best fit” solution shown in Table 5 is realistic, but the ICABC2 profile must be interpreted as a broader “vegetative burning” source that includes several source-types (e.g., agricultural field burning, backyard and trash burning, residential wood combustion, and restaurant charbroiler) rather than the asparagus field burning from which it was derived. SCEs calculated from either the charbroil cooking or asparagus burning source profile may represent more than any single source.

6 Summary and Conclusions

Receptor models are complementary to source models in that they infer source contributions from ambient concentrations, whereas source models estimate them from emissions. Agreement between the two independent models provides a weight of evidence in favor of the validity of both models. Disagreement points to areas where further measurements or more representative modeling is needed.

All multivariate receptor models are based on and are solutions to the CMB equations, which express ambient concentrations as a linear sum of source contributions and chemical abundances in those contributions. When there are substantial differences in the chemical abundances in the emissions, source contributions can be distinguished from each other with appropriate mathematical deconvolutions and simplifying assumptions. A wide variety of chemical and physical properties can be measured at source and receptor to distinguish one

source type from another, but these measurements are not available from current compliance-oriented monitoring networks.

An application and validation protocol should be applied to all receptor model applications, including those that derive source profiles. This protocol includes performance measures and sensitivity tests that evaluate the extent to which simplifying assumptions are complied with, and how variability in the ambient and source measurements adds uncertainty to the source contribution estimates. Ultimately, the comparison between receptor and source models provides the most important estimate of the validity of both methods.

References

- ACGIH (2001). *Air Sampling Instruments for Evaluation of Atmospheric Contaminants*, 9th ed., B.S. Cohen and C.S.J. McCammon, Eds. American Conference of Governmental Industrial Hygienists, Cincinnati, OH.
- Ansari, A.S., and S.N. Pandis. 1998. Response of inorganic PM to precursor concentrations. *Environ. Sci. Technol.*, **32**(18):2706-2714.
- Anttila, P., P. Paatero, U. Tapper and O. Järvinen. 1994. Application of positive matrix factorization to source apportionment: Results of a study of bulk deposition chemistry in Finland. *Atmos. Environ.*, **29**:1705-1718.
- Ashbaugh, L.L. 1983. A statistical trajectory technique for determining air pollution source regions. *J. Air Pollution Control Assoc.*, **33**(11):1096-1098.
- Ashbaugh, L.L., O.F. Carvacho, M.S. Brown, J.C. Chow, J.G. Watson and K.L. Magliano. 2003. Soil sample collection and analysis for the Fugitive Dust Characterization Study. *Atmos. Environ.*, **37**(9-10):1163-1173. doi: 10.1016/S1352-2310(02)01022-1.
- Baldauf, R.W., D.D. Lane, G.A. Marotz and R.W. Wiener. 2001. Performance evaluation of the portable MiniVol particulate matter sampler. *Atmos. Environ.*, **35**:6087-6091.
- Baldauf, R.W., R.W. Wiener and D.K. Heist. 2002. Methodology for siting ambient air monitors at the neighborhood scale. *J. Air & Waste Manage. Assoc.*, **52**(12):1433-1442.
- Baron, P.A., and K. Willeke. 2001. *Aerosol Measurement: Principles, Techniques and Applications*, 2nd ed., P.A. Baron and K. Willeke, Eds. John Wiley & Sons, New York, NY.
- Bishop, C.M. 1995. *Neural Networks for Pattern Recognition*. Clarendon Press, Oxford, UK.
- Blanchard, C.L., P.M. Roth, S.J. Tanenbaum, S.D. Ziman and J.H. Seinfeld. 2000. The use of ambient measurements to identify which precursor species limit aerosol nitrate formation. *J. Air & Waste Manage. Assoc.*, **50**(12):2073-2084.
- Blanchard, C.L., and G.M. Hidy. 2003. Effects of changes in sulfate, ammonia, and nitric acid on particulate nitrate concentrations in the southeastern United States. *J. Air & Waste Manage. Assoc.*, **53**(3):283-290.
- Blifford, I.H., and G.O. Meeker. 1967. A factor analysis model of large scale pollution. *Atmos. Environ.*, **1**:147-157.

Brook, J.R., E. Vega and J.G. Watson. 2003. Chapter 7: Receptor methods. In *Particulate Matter Science for Policy Makers, A NARSTO Assessment, Part 2*. NARSTO, Pasco, WA, pp. 7-1-7-48.

California Air Resources Board. 2000. EMFAC2000 emission factor model, release 2.02. California Air Resources Board, Sacramento, CA. <http://www.arb.ca.gov/msei/msei.htm>.

Chelani, A.B., D.G. Gajghate and M.Z. Hasan. 2002. Prediction of ambient PM₁₀ and toxic metals using artificial neural networks. *J. Air & Waste Manage. Assoc.*, **52**(7):805-810.

Chow, J.C. (1985). *A composite modeling approach to assess air pollution source/receptor relationships*. Sc.D. Dissertation, Harvard University, Cambridge, MA.

Chow, J.C., and J.G. Watson. 1989. Summary of particulate data bases for receptor modeling in the United States. In *Transactions, Receptor Models in Air Resources Management*, J.G. Watson, Ed. Air & Waste Management Association, Pittsburgh, PA, pp. 108-133.

Chow, J.C., J.G. Watson, L.C. Pritchett, W.R. Pierson, C.A. Frazier and R.G. Purcell. 1993. The DRI Thermal/Optical Reflectance carbon analysis system: Description, evaluation and applications in U.S. air quality studies. *Atmos. Environ.*, **27A**(8):1185-1201.

Chow, J.C. (1995). Critical review "Measurement methods to determine compliance with ambient air quality standards for suspended particles". *J. Air & Waste Manage. Assoc.*, **45**(5):320-382.

Chow, J.C., and J.G. Watson. 1997. Imperial Valley/Mexicali Cross Border PM₁₀ Transport Study. Report No. 4692.1D1. Prepared for U.S. Environmental Protection Agency, Region IX, San Francisco, CA, by Desert Research Institute, Reno, NV.

Chow, J.C., J.G. Watson, D. Crow, D.H. Lowenthal and T. Merrifield. 2001. Comparison of IMPROVE and NIOSH carbon measurements. *Aerosol Sci. Technol.*, **34**(1):23-34.

Chow, J.C., and J.G. Watson. 2002a. Review of PM_{2.5} and PM₁₀ apportionment for fossil fuel combustion and other sources by the chemical mass balance receptor model. *Energy & Fuels*, **16**(2):222-260. doi: 10.1021/ef0101715.

Chow, J.C., and J.G. Watson. 2002b. PM_{2.5} carbonate concentrations at regionally representative Interagency Monitoring of Protected Visual Environment sites. *J. Geophys. Res.*, **107**(D21):ICC 6-1-ICC 6-9. doi: 10.1029/2001JD000574.

Chow, J.C., J.D. Bachmann, S.S.G. Wierman, C.V. Mathai, W.C. Malm, W.H. White, P.K. Mueller, N. Kumar and J.G. Watson. 2002a. 2002 Critical review discussion - Visibility: Science and regulation. *J. Air & Waste Manage. Assoc.*, **52**(9):973-999.

Chow, J.C., J.P. Engelbrecht, J.G. Watson, W.E. Wilson, N.H. Frank and T. Zhu. 2002b. Designing monitoring networks to represent outdoor human exposure. *Chemosphere*, **49**(9):961-978.

Chow, J.C., J.G. Watson, L.L. Ashbaugh and K.L. Magliano. 2003. Similarities and differences in PM₁₀ chemical source profiles for geological dust from the San Joaquin Valley, California. *Atmos. Environ.*, **37**(9-10):1317-1340. doi: 10.1016/S1352-2310(02)01021-X.

Chow, J.C., J.G. Watson, L.W. Chen, W.P. Arnott, H. Moosmüller and K.K. Fung, K.K., 2004a. Equivalence of elemental carbon by Thermal/Optical Reflectance and Transmittance with different temperature protocols. *Environ. Sci. Technol.*, **38**(16):4414-4422.

- Chow, J.C., J.G. Watson, H.D. Kuhns, V. Etyemezian, D.H. Lowenthal, D. Crow, S.D. Kohl, J.P. Engelbrecht and M.C. Green. 2004b. Source profiles for industrial, mobile, and area sources in the Big Bend Regional Aerosol Visibility and Observational (BRAVO) Study. *Chemosphere*, **54** (2): 185-208.
- Cooper, J.A., and J.G. Watson. 1980. Receptor oriented methods of air particulate source apportionment. *J. Air Pollution Control Assoc.*, **30**(10):1116-1125.
- Dams, R., J.A. Robbins, K.A. Rahn and J.W. Winchester. 1971. Quantitative relationships among trace elements over industrialized N.W. Indiana. In *Nuclear Techniques in Environmental Pollution*. International Atomic Energy Agency, Vienna, Austria, pp. 139-145.
- Demerjian, K.L. 2000. A review of national monitoring networks in North America. *Atmos. Environ.*, **34**(12-14):1861-1884.
- Draxler, R.R., and G.D. Hess. 1997. Description of the HYSPLIT_4 Modeling System. *Report No. NOAA Technical Memorandum ERL ARL-224*. National Oceanic and Atmospheric Administration, Air Resources Laboratory, Silver Spring, MD. <http://www.arl.noaa.gov/data/models/hysplit4/win95/arl-224.pdf>.
- Draxler, R.R. 1999. HYSPLIT User's Guide. *Report No. NOAA Technical Memorandum ERL ARL-230*. National Oceanic and Atmospheric Administration, Air Resources Laboratory, Silver Spring, MD. http://www.arl.noaa.gov/data/models/hysplit4/win95/user_man.pdf.
- Eldred, R.A., T.A. Cahill, L.K. Wilkinson, P.J. Feeney and W.C. Malm. 1989. Particulate characterization at remote sites across the U.S.: First year results of the NPS/IMPROVE Network. In 82nd Annual Meeting of the Air & Waste Management Association, Anaheim, CA.
- England, G.C., B. Zielinska, K. Loos, I. Crane and K. Ritter. 2000. Characterizing PM_{2.5} emission profiles for stationary sources: Comparison of traditional and dilution sampling techniques. *Fuel Processing Technology*, **65**:177-188.
- Fujita, E.M., B.E. Croes, C.L. Bennett, D.R. Lawson, F.W. Lurmann and H.H. Main. 1992. Comparison of emission inventory and ambient concentration ratios of CO, NMOG, and NO_x in California's South Coast Air Basin. *J. Air & Waste Manage. Assoc.*, **42**(3):264-276.
- Fujita, E.M., J.G. Watson, J.C. Chow and Z. Lu. 1994. Validation of the chemical mass balance receptor model applied to hydrocarbon source apportionment in the Southern California Air Quality Study. *Environ. Sci. Technol.*, **28**(9):1633-1649.
- Fujita, E.M., J.G. Watson, J.C. Chow and K.L. Magliano. 1995. Receptor model and emissions inventory source apportionments of nonmethane organic gases in California's San Joaquin Valley and San Francisco Bay Area. *Atmos. Environ.*, **29**(21):3019-3035.
- Gao, N., M.D. Cheng and P.K. Hopke. 1994. Receptor modeling of airborne ionic species collected in SCAQS, 1987. *Atmos. Environ.*, **28**(8):1447-1470.
- Gatz, D.F., G.J. Stensland, M.V. Miller and A.C.D. Leslie. 1981. Sources of airborne calcium in rural central Illinois. In *Atmospheric Aerosol: Source/Air Quality Relationships*, E.S. Macias and P.K. Hopke, Eds. American Chemical Society, Washington, DC, pp. 303-325.
- Gether, J., and H.M. Seip. 1979. Analysis of air pollution data by the combined use of interactive graphic presentation and a clustering technique. *Atmos. Environ.*, **13**:87-96.

Godleski, J.J., R.L. Verrier, P. Koutrakis and P. Catalano. 2000. Mechanisms of morbidity and mortality from exposure to ambient air particles. *Report No. 91*. Health Effects Institute (HEI), Cambridge, MA.

Gordon, G.E. 1980. Receptor models. *Environ. Sci. Technol.*, **14**:792-800.

Gordon, G.E., W.R. Pierson, J.M. Daisey, P.J. Liroy, J.A. Cooper, J.G. Watson and G.R. Cass. 1984. Considerations for design of source apportionment studies. *Atmos. Environ.*, **18**(8):1567-1582.

Gordon, G.E. 1988. Receptor models. *Environ. Sci. Technol.*, **22**(10):1132-1142.

Green, M.C., K.A. Gebhart. 1997. Clean air corridors: A geographic and meteorologic characterization. *J. Air & Waste Manage. Assoc.*, **47**(3):403-410.

Henry, R.C., and G.M.Hidy. 1982. Multivariate analysis of particulate sulfate and other air quality variables by principal components - Part II, Salt Lake City, Utah and St. Louis, Missouri. *Atmos. Environ.*, **16**:929-943.

Henry, R.C., C.W. Lewis, P.K. Hopke and B.J. Williamson. 1984. Review of receptor model fundamentals. *Atmos. Environ.*, **18**(8):1507-1515.

Henry, R.C. 1987. Current factor analysis receptor models are ill-posed. *Atmos. Environ.*, **21**(8):1815-1820.

Henry, R.C., Y.J. Wang and K.A. Gebhart. 1991. The relationship between empirical orthogonal functions and sources of air pollution. *Atmos. Environ.*, **25A**(2):503-509.

Henry, R.C. 1992. Dealing with near collinearity in chemical mass balance receptor models. *Atmos. Environ.*, **26A**(5):933-938.

Henry, R.C. 1997. History and fundamentals of multivariate air quality receptor models. *Chemom. Intell. Lab. Sys.*, **37**(1):37-42.

Henry, R.C., C.H. Spiegelman, J.F. Collins and E.S. Park. 1997. Reported emissions of organic gases are not consistent with observations. *Proc. Natl. Acad. Sci. USA*, **94**:6596-6599.

Henry, R.C., Y. Mi and W. Moran. 1999. Multivariate receptor modeling of SCAQS VOC and airborne particle composition data. Report No. ARB-R-99/683; ARB-A832-131. Prepared for California State Air Resources Board, Sacramento, CA, by University of Southern California, Los Angeles, CA.

Henry, R.C. 2000. *UNMIX Version 2 Manual*. Ronald C. Henry, Ph.D., West Hills, CA.

Henry, R.C. 2002. Multivariate receptor models - Current practice and future trends. *Chemom. Intell. Lab. Sys.*, **60**(1-2):43-48. doi:10.1016/S0169-7439(01)00184-8.

Hidy, G.M., and S.K. Friedlander. 1971. The nature of the Los Angeles aerosol. In *Proceedings of the Second International Clean Air Congress*, H.M. Englund and W.T. Beery, Eds. Academic Press, New York, pp. 391-404.

Hies, T., R. Treffeisen, L. Sebald and E. Reimer. 2000. Spectral analysis of air pollutants Part 1. Elemental carbon time series. *Atmos. Environ.*, **34**(21):3495-3502.

- Hopke, P.K., E.S. Gladney, G.E. Gordon, W.H. Zoller and A.G. Jones. 1976. The use of multivariate analysis to identify sources of selected elements in Boston urban aerosol. *Atmos. Environ.*, **10**:1015-1025.
- Hopke, P.K., and S.L. Dattner. 1982. *Receptor Models Applied to Contemporary Pollution Problems*. Air & Waste Management Association, Pittsburgh, PA.
- Hopke, P.K., D.J. Alpert and B.A. Roscoe. 1983. FANTASIA - A program for target transformation factor analysis to apportion sources in environmental samples. *Computers & Chem.*, **7**(3):149-155.
- Hopke, P.K. 1985. *Receptor Modeling in Environmental Chemistry*. John Wiley & Sons, Inc., New York.
- Hopke, P.K. 1988. Target transformation factor analysis as an aerosol mass apportionment method: A review and sensitivity study. *Atmos. Environ.*, **22**(9):1777-1792.
- Hopke, P.K. 1991. *Receptor Modeling for Air Quality Management*, P.K. Hopke, Ed. Elsevier Press, Amsterdam, The Netherlands.
- Hopke, P.K. 1999. An introduction to source receptor modeling. In *Elemental Analysis of Airborne Particles*, S. Landsberger and M. Creatchman, Eds. Gordon and Breach Science, Amsterdam, pp. 273-315.
- Hopke, P.K. 2003. Recent developments in receptor modeling. *J. Chemometrics*, **17**(5):255-265.
- Hopke, P.K., Z. Ramadan, P. Paatero, G.A. Norris, M.S. Landis, R.W. Williams and C.W. Lewis. 2003. Receptor modeling of ambient and personal exposure samples: 1998 Baltimore Particulate Matter Epidemiology-Exposure Study. *Atmos. Environ.*, **37**(23):3289-3302. doi: 10.1016/S1352-2310(03)00331-5.
- Javitz, H.S., and J.G. Watson. 1988. Feasibility study of receptor modeling for apportioning utility contributions to air constituents, deposition quality and light extinction. Prepared for Electric Power Research Institute, Palo Alto, CA, by SRI International, Menlo Park, CA.
- Javitz, H.S., J.G. Watson, J.P. Guertin and P.K. Mueller. 1988. Results of a receptor modeling feasibility study. *J. Air Pollution Control Assoc.*, **38**(5):661-667.
- Jorquera, H., W. Palma and J. Tapia. 2000. An intervention analysis of air quality data at Santiago, Chile. *Atmos. Environ.*, **34**(24):4073-4084.
- Kleinman, M.T., B.S. Pasternack, M. Eisenbud and T.J. Kneip. 1980. Identifying and estimating the relative importance of sources of airborne particulates. *Environ. Sci. Technol.*, **14**(1):62-65.
- Kim, E. and P.K. Hopke., 2004. Source apportionment of fine particles at Washington, DC, utilizing temperature-resolved carbon fractions. *J. Air & Waste Manage. Assoc.*, **54**(7):773-785.
- Kim, E., P.K. Hopke, and E.S. Edgerton. 2004. Improving source identification of Atlanta aerosol using temperature resolved carbon fractions in positive matrix factorization. *Atmos. Environ.*, **38**(20):3349-3362.
- Landsberger, S., and M. Creatchman. 1999. *Elemental Analysis of Airborne Particles*, S. Landsberger and M. Creatchman, Eds. Gordon and Breach, Newark, NJ.
- Lewis, C.W., and R.K. Stevens. 1985. Hybrid receptor model for secondary sulfate from an SO₂ point source. *Atmos. Environ.*, **19**(6):917-924.

Lioy, P.J., J.G. Watson and J.D. Spengler. 1980. APCA specialty conference workshop on baseline data for inhalable particulate matter. *J. Air Pollution Control Assoc.*, **30**(10):1126-1130.

Lioy, P.J., R.P. Mallon, M. Lippmann, T.J. Kneip and P.J. Samson. 1982. Factors affecting the variability of summertime sulfate in a rural area using principal component analysis. *J. Air Pollution Control Assoc.*, **32**(10):1043-1047.

Malm, W.C., and K.A. Gebhart. 1997. Source apportionment of sulfur and light extinction using receptor modeling techniques. *J. Air & Waste Manage. Assoc.*, **47**(3):250-268.

Malm, W.C., M.L. Pitchford, M. Scruggs, J.F. Sisler, R.G. Ames, S. Copeland, K.A. Gebhart and D.E. Day. 2000. Spatial and seasonal patterns and temporal variability of haze and its constituents in the United States: *Report III. Report No. ISSN: 0737-5352-47*. Cooperative Institute for Research in the Atmosphere, Colorado State University, Ft. Collins, CO. http://vista.cira.colostate.edu/IMPROVE/Publications/improve_reports.htm.

Malm, W.C., B.A. Schichtel, R.B. Ames and K.A. Gebhart. 2002. A ten-year spatial and temporal trend of sulfate across the United States. *J. Geophys. Res.*, **107**(D22):ACH 11-1-ACH 11-20. doi:10.1029/2002JD002107.

McMurry, P.H. 2000. A review of atmospheric aerosol measurements. *Atmos. Environ.* **34** (12-14):1959-1999.

Mendoza-Dominguez, A., and A.G. Russell. 2000. Iterative inverse modeling and direct sensitivity analysis of a photochemical air duality model. *Environ. Sci. Technol.*, **34**(23):4974-4981.

Middlebrook, A.M., D.M. Murphy, S.H. Lee, D.S. Thompson, K.A. Prather, R.J. Wenzel, D.Y. Liu, D.J. Phares, K.P. Rhoads, A.S. Wexler, M.V. Johnston, J.L. Jimenez, J.T. Jayne, D.R. Worsnop, I. Yourshaw, J.H. Seinfeld and R.C. Flagan, R.C. 2003. A comparison of particle mass spectrometers during the 1999 Atlanta Supersite Project. *J. Geophys. Res.*, **108**(D7):SOS 12-1-SOS 12-13.

Morandi, M.T., P.J. Lioy and J.M. Daisey. 1991. Comparison of two multivariate modeling approaches for the source apportionment of inhalable particulate matter in Newark, NJ. *Atmos. Environ.*, **25A**(5/6):927-937.

Motelay-Massei, A., D. Ollivon, B. Garban and M. Chevreuil. 2003. Polycyclic aromatic hydrocarbons in bulk deposition at a suburban site: assessment by principle component analysis of the influence of meteorological parameters. *Atmos. Environ.*, **37**(22):3135-3146.

Mueller, P.K., G.M. Hidy, R.L. Baskett, K.K. Fung, R.C. Henry, T.F. Lavery, N.J. Nordi, A.C. Lloyd, J.W. Thrasher, K.K. Warren and J.G. Watson. 1983. Sulfate Regional Experiment (SURE): Report of findings. *Report No. EA-1901*. Electric Power Research Institute, Palo Alto, CA.

Murphy, B.L. 2000. Allocation by contribution to cost and risk at superfund sites. *Environ. Forensics*, **1**(3):117-120.

Paatero, P., and U. Tapper. 1994. Positive matrix factorization: A non-negative factor model with optimal utilization of error estimates of data values. *Environmetrics*, **5**:111-126.

Paatero, P. 1998. User's guide for positive matrix factorization programs PMF2 and PMF3 *Part I: Tutorial*. University of Helsinki, Helsinki, Finland.

- Paatero, P. 2000. User's guide for positive matrix factorization programs PMF2 and PMF3 *Part 2: Reference*. University of Helsinki, Helsinki, Finland.
- Pace, T.G. 1986. *Transactions, Receptor Methods for Source Apportionment: Real World Issues and Applications*, T.G. Pace, Ed. Air Pollution Control Association, Pittsburgh, PA.
- Pena-Mendez, E.M., M.S. Astorga-Espana and F.J. Garca-Montelongo. 2001. Chemical fingerprinting applied to the evaluation of marine oil pollution in the coasts of Canary Islands (Spain). *Environ. Poll.*, **111**(2):177-187.
- Perrier, V., T. Philipovitch and C. Basdevant. 1995. Wavelet spectra compared to Fourier spectra. *J. Math. Phys.*, **36**(3):1506-1519.
- Pitchford, M.L., M.C. Green, H.D. Kuhns, I.H. Tombach, W.C. Malm, M. Scruggs, R.J. Farber, V.A. Mirabella, W.H. White, C. McDade, J.G. Watson, D. Koracin, T.E. Hoffer, D.H. Lowenthal, J.C. Vimont et al. 1999. Project MOHAVE, Final Report. U.S. Environmental Protection Agency, Region IX, San Francisco, CA. <http://www.epa.gov/region09/air/mohave/report.html>.
- Poirot, R.L., P.R. Wishinski, P.K. Hopke and A.V. Polissar. 2002. Errata: Comparative application of multiple receptor methods to identify aerosol sources in northern Vermont (vol. 35, pg 4622, 2001). *Environ. Sci. Technol.*, **36**(4):820.
- Pun, B.K., and C. Seigneur. 1999. Understanding particulate matter formation in the California San Joaquin Valley: Conceptual model and data needs. *Atmos. Environ.*, **33**(29):4865-4875.
- Reimann, C., and P. de Caritat. 2000. Intrinsic flaws of element enrichment factors (EFs) in environmental geochemistry. *Environ. Sci. Technol.*, **34**(24):5084-5091.
- Rogge, W.F., L.M. Hildemann, M.A. Mazurek, G.R. Cass and B.R.T. Simoneit. 1996. Mathematical modeling of atmospheric fine particle-associated primary organic compound concentrations. *J. Geophys. Res.*, **101**:19379-19394.
- Saucy, D.A., J.R. Anderson and P.R. Buseck. 1987. Cluster analysis applied to atmospheric aerosol samples from the Norwegian Arctic. *Atmos. Environ.*, **21**:1649-1657.
- Seinfeld, J.H., and S.N. Pandis. 1998. *Atmospheric Chemistry and Physics: From Air Pollution to Climate Change*. John Wiley & Sons, New York, NY.
- Sims, R.C., and J.L. Sims. 1995. Chemical mass-balance approach to field-evaluation of bioremediation. *Environ. Prog.*, **14**(1):F2-F3.
- Somerville, M.C., and E.G. Evans. 1995. Effect of sampling frequency on trend detection for atmospheric fine mass. *Atmos. Environ.*, **29**(18):2429-2438.
- Stelson, A.W., and J.H. Seinfeld. 1982. Relative humidity and temperature dependence of the ammonium nitrate dissociation constant. *Atmos. Environ.*, **16**(5):983-992.
- Stockwell, W.R., H. Geiger and K.H. Becker. 2001. Estimation of incremental reactivities for multiple day scenarios: An application to ethane and dimethoxymethane. *Atmos. Environ.*, **35**:929-939.
- Stout, S.A., A.D. Uhler and K.J. McCarthy. 2001. A strategy and methodology for defensibly correlating spilled oil to source candidates. *Environ. Forensics*, **2**(1):87-98.
- Thurston, G.D., and J.D. Spengler. 1985. A quantitative assessment of source contributions to inhalable particulate matter pollution in metropolitan Boston. *Atmos. Environ.*, **19**(1):9-25.

U.S. EPA. 1984. Receptor model technical series, vol. V: Source apportionment techniques and considerations in combining their use. *Report No. EPA-450/4-84-020*. U. S. Environmental Protection Agency, Research Triangle Park, NC.

U.S. EPA. 1996. *Method 202 - Determination of condensable particulate emissions from stationary sources*. U.S. Environmental Protection Agency, Office of Air Quality Planning and Standards, Technical Support Division, Research Triangle Park, NC. <http://www.epa.gov/ttn/emc/promgate/m-202.pdf>.

U.S. EPA. 1997. *Method 201A - Determination of PM_{10} emissions (constant sampling rate procedure)*. U.S. Environmental Protection Agency, Office of Air Quality Planning and Standards, Technical Support Division, Research Triangle Park, NC. <http://www.epa.gov/ttn/emc/promgate/m-201a.pdf>.

U.S. EPA. 1999. *SPECIATE: EPA's repository of total organic compound and particulate matter speciated profiles for a variety of sources for use in source apportionment studies*. U.S. Environmental Protection Agency, Office of Air Quality Planning and Standards, Research Triangle Park, NC. <http://www.epa.gov/ttn/chief/software/speciate/>.

U.S. EPA. 2001a. *Draft guidance for demonstrating attainment of air quality goals for $PM_{2.5}$ and regional haze*. U.S. Environmental Protection Agency, Research Triangle Park, NC. <http://vistas-sesarm.org/tech/draftpm.pdf>.

U.S. EPA. 2001b. *PAMS information*. U.S. Environmental Protection Agency, Research Triangle Park, NC. <http://www.epa.gov/ttn/amtic/pams.html>.

U.S. EPA. 2002. *National ambient air monitoring strategy (Second draft)*. U.S. Environmental Protection Agency, Research Triangle Park, NC. <http://www.epa.gov/ttn/amtic/files/ambient/monitorstrat/compms.pdf>.

Wang, J.L., C.J. Chang, W.D. Chang, C. Chew and S.W. Chen. 1999. Construction and evaluation of automated gas chromatography for the measurement of anthropogenic halocarbons in the atmosphere. *J. Chromatogr.*, **844**:259-269.

Watson, J.G. 1979. *Chemical element balance receptor model methodology for assessing the sources of fine and total suspended particulate matter in Portland, Oregon*. Ph.D. Dissertation, Oregon Graduate Center, Beaverton, OR.

Watson, J.G., R.C. Henry, J.A. Cooper and E.S. Macias. 1981. The state of the art of receptor models relating ambient suspended particulate matter to sources. In *Atmospheric Aerosol: Source/Air Quality Relationships*, E.S. Macias and P.K. Hopke, Eds. American Chemical Society, Washington, DC, pp. 89-106.

Watson, J.G. 1984. Overview of receptor model principles. *J. Air Pollution Control Assoc.*, **34**(6):619-623.

Watson, J.G., J.A. Cooper and J.J. Huntzicker. 1984. The effective variance weighting for least squares calculations applied to the mass balance receptor model. *Atmos. Environ.*, **18**(7):1347-1355.

Watson, J.G., J.C. Chow and C.V. Mathai. 1989. Receptor models in air resources management: A summary of the APCA International Specialty Conference. *J. Air Pollution Control Assoc.*, **39**(4):419-426.

Watson, J.G., J.C. Chow and T.G. Pace. 1991. Chemical mass balance. In *Receptor Modeling for Air Quality Management*, P.K. Hopke, Ed. Elsevier Press, New York, NY, pp. 83-116.

Watson, J.G., and J.C. Chow. 1992. Data bases for PM₁₀ and PM_{2.5} chemical compositions and source profiles. In *Transactions, PM₁₀ Standards and Nontraditional Particulate Source Controls*, J.C. Chow and D.M. Ono, Eds. Air & Waste Management Association, Pittsburgh, PA, pp. 61-91.

Watson, J.G., J.C. Chow, F.W. Lurmann and S. Musarra. 1994a. Ammonium nitrate, nitric acid, and ammonia equilibrium in wintertime Phoenix, Arizona. *J. Air & Waste Manage. Assoc.*, **44**(4):405-412.

Watson, J.G., J.C. Chow, Z. Lu, E.M. Fujita, D.H. Lowenthal and D.R. Lawson. 1994b. Chemical mass balance source apportionment of PM₁₀ during the Southern California Air Quality Study. *Aerosol Sci. Technol.*, **21**(1):1-36.

Watson, J.G., N.F. Robinson, C.W. Lewis, C.T. Coulter, J.C. Chow, E.M. Fujita, D.H. Lowenthal, T.L. Conner, R.C. Henry and R.D. Willis. 1997. *Chemical mass balance receptor model version 8 (CMB) user's manual*. Prepared for U.S. Environmental Protection Agency, Research Triangle Park, NC, by Desert Research Institute, Reno, NV. <ftp://eafs.sage.dri.edu/cmb80/model/>.

Watson, J.G., E.M. Fujita, J.C. Chow, B. Zielinska, L.W. Richards, W.D. Neff and D. Dietrich. 1998a. *Northern Front Range Air Quality Study. Final report*. Prepared for Colorado State University, Fort Collins, CO, by Desert Research Institute, Reno, NV. <http://charon.cira.colostate.edu/DRIFinal/ZipFiles/>.

Watson, J.G., D.W. DuBois, R. DeMandel, A.P. Kaduwela, K.L. Magliano, C. McDade, P.K. Mueller, A.J. Ranzieri, P.M. Roth and S. Tanrikulu. 1998b. *Field program plan for the California Regional PM_{2.5}/PM₁₀ Air Quality Study (CRPAQS)*. Prepared for California Air Resources Board, Sacramento, CA, by Desert Research Institute, Reno, NV. <http://sparc2.baaqmd.gov/centralca/publications.htm>.

Watson, J.G., J.C. Chow, H. Moosmüller, M.C. Green, N.H. Frank and M.L. Pitchford. 1998c. Guidance for using continuous monitors in PM_{2.5} monitoring networks. *Report No. EPA-454/R-98-012*. Prepared for U.S. Environmental Protection Agency, Research Triangle Park, NC, by Desert Research Institute, Reno, NV. <http://www.epa.gov/ttn/amtic/pmpolgud.html>.

Watson, J.G., N.F. Robinson, C.W. Lewis, C.T. Coulter, J.C. Chow, E.M. Fujita, T.L. Conner and T.G. Pace. 1998d. CMB8 applications and validation protocol for PM_{2.5} and VOCs. *Report No. 1808.2D1*. Prepared for U.S. Environmental Protection Agency, Research Triangle Park, NC, by Desert Research Institute, Reno, NV.

Watson, J.G., and J.C. Chow. 2001a. Estimating middle-, neighborhood-, and urban-scale contributions to elemental carbon in Mexico City with a rapid response aethalometer. *J. Air & Waste Manage. Assoc.*, **51**(11):1522-1528.

Watson, J.G., and J.C. Chow. 2001b. Source characterization of major emission sources in the Imperial and Mexicali valleys along the U.S./Mexico border. *Sci. Total Environ.*, **276**(1-3):33-47.

Watson, J.G., J.C. Chow and E.M. Fujita. 2001a. Review of volatile organic compound source apportionment by chemical mass balance. *Atmos. Environ.*, **35**(9):1567-1584. <ftp://ftp.cgenv.com/pub/downloads/Watson.pdf>.

Watson, J.G., B.J. Turpin and J.C. Chow. 2001b. The measurement process: Precision, accuracy, and validity. In *Air Sampling Instruments for Evaluation of Atmospheric Contaminants*, 9th ed., B.S. Cohen and C.S.J. McCammon, Eds. American Conference of Governmental Industrial Hygienists, Cincinnati, OH, pp. 201-216.

Watson, J.G., J.C. Chow and J.E. Houck. 2001c. PM_{2.5} chemical source profiles for vehicle exhaust, vegetative burning, geological material, and coal burning in northwestern Colorado during 1995. *Chemosphere*, **43**(8):1141-1151.

Watson, J.G. 2002a. Visibility: Science and regulation. *J. Air & Waste Manage. Assoc.*, **52**(6):628-713.

Watson, J.G. 2002b. Visibility: Science and regulation - A summary of the 2002 Critical Review. *EM*, (June):36-43.

Watson, J.G. 2002c. Appendix S: Independent Review. In *Source Apportionment Analysis of Air Quality Data: Phase 1 - Final Report*. Mid-Atlantic Regional Air Management Assoc., Baltimore, MD, pp. S1-S63.

Watson, J.G., and J.C. Chow. 2002a. Particulate pattern recognition. In *Introduction to Environmental Forensics*, B.L. Murphy and R. Morrison, Eds. Academic Press, New York, NY, pp. 429-460.

Watson, J.G., and J.C. Chow. 2002b. A wintertime PM_{2.5} episode at the Fresno, CA, supersite. *Atmos. Environ.*, **36**(3):465-475.

Watson, J.G., T. Zhu, J.C. Chow, J.P. Engelbrecht, E.M. Fujita and W.E. Wilson. (2002a). Receptor modeling application framework for particle source apportionment. *Chemosphere*, **49**(9):1093-1136.

Watson, J.G., J.C. Chow, D.H. Lowenthal, N.F. Robinson, C.F. Cahill and D.L. Blumenthal. 2002b. Simulating changes in source profiles from coal-fired power stations: Use in chemical mass balance of PM_{2.5} in the Mt. Zirkel Wilderness. *Energy & Fuels*, **16**(2):311-324.

White, W.H. 1999. Phantom spatial factors: An example. *J. Air & Waste Manage. Assoc.*, **49**(3):345-349.

Wilkinson, L. 1990. *SYSTAT: The System for Statistics*. SYSTAT Inc., Evanston, IL.

Wolff, G.T., and P.J. Liroy. 1978. An empirical model for forecasting maximum daily ozone levels in the northeastern U.S. *J. Air Pollution Control Assoc.*, **28**(10):1034-1038.

Yamamoto, N., M. Fujii, O. Endo, K. Kumagai and Y. Yanagisawa. 2002. Broad range observation of particle deposition on greased and non-greased impaction surfaces using a line-sensing optical microscope. *J. Aerosol Sci.*, **33**(12):1667-1679.

Zielinska, B., and E.M. Fujita. 1994. Organic gas sampling. In *Environmental Sampling for Trace Analysis*, B. Markert, Ed. VCH Publishers, New York, NY, pp. 163-184.

Blank Page

Canepa, E. and J. Irwin 2005. *Evaluation of Air Pollution Models*. Chapter 17 of AIR QUALITY MODELING - *Theories, Methodologies, Computational Techniques, and Available Databases and Software*. Vol. II – *Advanced Topics* (P. Zannetti, Editor). Published by The EnviroComp Institute (<http://www.envirocomp.org/>) and the Air & Waste Management Association (<http://www.awma.org/>).

Chapter 17

Evaluation of Air Pollution Models

Elisa Canepa ⁽¹⁾ and John S. Irwin ⁽²⁾

⁽¹⁾ *INFM (National Institute for the Physics of Matter), Department of Physics - University of Genova, Genova (Italy)*

elisa.canepa@fisica.unige.it

⁽²⁾ *John S. Irwin and Associates¹, Raleigh, NC (USA)*

jsirwinetal@nc.rr.com

Abstract: Information is given about model evaluation, the overall system of procedures designed to measure model performance, and in particular, the process of statistical performance evaluations. Statistical performance evaluation is an assessment of model performance based on the comparison of model outputs with experimental data. Some performance measures, consisting of statistical indices and graphical methodologies, currently used are described. Problems related to uncertainty analysis are highlighted.

Key Words: model quality assurance, model evaluation, statistical model evaluation, uncertainty analysis, statistical indices, performance measures.

1 Introduction

Model quality assurance is a collection of activities one should perform in order to promote the development and application of good air quality simulation models (discussed in more detail in Section 8 below). One of the elements of model quality assurance is model evaluation. Model evaluation² is a collection of activities one should perform in order to understand how a model behaves and how a model compares with observations (discussed in more detail in Section 6).

¹ From 1975 to 2004, John Irwin was a NOAA employee, on assignment to the U.S. Environmental Protection Agency, Research Triangle Park, NC 27711.

² Readers will see that we have avoided the use of the term “validation”. Fox (1981) and Olesen (1996) define “validation” as a conclusion resulting from detailed and copious evidence that leads to formal recognition, which might include several evaluations.

One of the elements of model evaluation is statistical model evaluation. Statistical model evaluation, also called “statistical performance evaluation”, is an assessment of model performance based on the comparison of model outputs with experimental data (discussed in more detail in Section 7).

It is our experience and conclusion from a comprehensive review of past model evaluation exercises that it is not profitable to provide a “cookbook” with series of steps that one must accomplish in order to adequately implement a statistical model evaluation. Models are used in a variety of ways, many of which were never anticipated when the model was first developed and made available. Models are often used in situations that, in principle, they are incapable of handling as they are lacking characterization of relevant physical processes. For example, although most operational air quality models provide estimates of ensemble average concentrations, they are typically used to estimate maximum (peak) concentration values (which are extreme values within an ensemble).

Instead of a series of steps, we provide a framework (Section 4) within which one can understand why modeling results and observations differ. We believe that by following the ideas expressed in this framework, one can develop a successful evaluation of any model regardless of whether it is being applied in a manner consistent with its designed physics and modeling assumptions. In Section 5, we summarize those performance measures that are in common usage, and then in Section 7, we discuss concepts that can be employed in developing a statistical model evaluation.

2 Terminology

A review of recent evaluation exercises reveals³ that various characteristics of atmospheric dispersion models have been tested, and often the methods have used application-specific schemes with various performance measures. In fact, in the literature it is possible to find widely diverse definitions concerning topics related to model evaluation. To avoid confusion and misunderstandings, we believe that it would be useful to achieve a harmonization about terminology and its use. The etymology of the terms we use is important for understanding by both scientists and decision-makers. Hence, we have tried not to depart too much from the etymological word meanings (Schlunzen, 1997).

³ Of the large available number, we list a few for example. **Methods/Review:** U.S. Environmental Protection Agency (1992), Hanna et al. (1993), Poli and Cirillo (1993), Ward (1994), Weil et al. (1997), **Long Range Transport:** Bellasio et al. (1998), Brandt et al. (1998), Carhart et al. (1989), Mosca et al. (1998); **Complex Terrain:** Cox et al. (1998), Desiato (1991), Gronskei et al. (1993), Luhar and Rao (1994), Ross and Fox (1991), Thuillier (1992); **Plume Dispersion:** Brusasca et al. (1989), Carruthers et al. (1999), Hanna and Paine (1989), Hanna and Chang (1993), Olesen (1995), **Regional Grid:** Davis et al. (2000), Dennis (1986), Hanna et al. (1996), Hass et al. (1997), Kumar et al. (1994), **Low Winds/Street Canyons:** Kumar Yadav and Sharan (1996), Lanzani and Tamponi (1995), Okamoto et al. (1999).

Atmospheric air quality model: an idealization of atmospheric physics to calculate the magnitude and location of pollutant concentrations. This may take the form of an equation, algorithm, or series of equations/algorithms used to calculate average or time-varying concentration. They may take the form of a deterministic model or a statistical model. The model may involve process descriptions and numerical methods for solution.

Calibration (or model calibration): a procedure used to make, at the model development stage, estimates of the parameters of model equations, which best fit the general model structure to a specific observed data set.

Data assimilation: a numerical technique, which makes it possible to combine model results and observations in one integrated system, with the purpose of minimizing the discrepancy between model predictions and observations.

Data quality assessment: the scientific and statistical evaluation of data to determine if data obtained from environmental data operations are of the right type, quality and quantity to support their intended use.

Data quality objective: a range of acceptability for data used in modeling analyses for a specific application.

Deterministic model: a model is deterministic when it is assumed that all possible behaviors are determined by the set of equations comprising the model. These models are based on fundamental mathematical descriptions of atmospheric processes, in which effects (i.e., air pollution) are generated by causes (i.e., emissions).

Diffusion, absolute: the characterization of the spreading of material released into the atmosphere based on a coordinate system fixed in space.

Diffusion, relative: the characterization of the spreading of material released into the atmosphere based on a coordinate system that is relative to some local position of the dispersing material (e.g., center of mass).

Dispersion: the combined effects of eddy diffusion and advection (transport).

Evaluation (or model evaluation): the overall system of procedures designed to measure the model performance.

Evaluation objective: a feature or characteristic which can be defined through an analysis of the observed concentration pattern (e.g., maximum centerline concentration or lateral extent of the average concentration pattern as a function of downwind distance) for which one desires to assess the skill of the models to reproduce.

Evaluation procedure: the analytical steps to be taken to compute the value of the evaluation objective from the observed and modeled patterns of concentration values.

Fate: the destiny of a chemical or biological pollutant after release into the atmosphere.

Model intercomparison: a process where several models, all presumably appropriate for some chosen situations (idealized or real), simultaneously have their performances assessed and compared.

Performance measures (or statistical comparison metrics): evaluation tools (quantitative and/or qualitative) like statistical indices and graphical methodologies, used to compare model outputs with observed values.

Process model: an idealization of atmospheric physics envisioned as being composed of a series of inter-related processes to calculate the magnitude and location of pollutant concentrations based on fate, transport, and diffusion in the atmosphere. These models most often are deterministic models, but in principle, could attempt to characterize the stochastic process effects.

Quality assurance: all those planned and systematic actions necessary to provide adequate confidence that a product or service will satisfy given requirements for quality.

Sensitivity analysis: a process for identifying the magnitude, direction, and form (e.g., linear or non-linear) of the effect of the variation of one or more model parameters or model inputs on the model result.

Statistical model: a model of a stochastic process that represents the dependence of successive or neighboring events in response to variation in an external influence on the process. These models are parsimonious using the fewest number of parameters capable of explaining quantitative variation in some observed data. They are based upon semi-empirical statistical relations among available data and measurements.

Statistical model evaluation: the analysis of model performance based on the comparison of model outputs with experimental data (evaluation objectives). Statistical model evaluations involve summarizing model performance in an overall sense (typically called performance evaluation), and testing the simulation of specific processes within a model (typically called diagnostic evaluations).

Stochastic process: a continuous causal process in time, space, or both, responding to variation in an external influence, and producing a varying series of measured states or events.

Uncertainty: a difference (or differences) between what is modeled and what is observed. It is a consequence of a lack of knowledge in model formulation, and errors (or omissions) in data and observations. In principle, uncertainty can be reduced with either improved theory or observations; however, it is generally accepted that there is a limit to how much of the natural variability can be explicitly simulated by models. The portion of natural variability that is beyond the reach of modeling is referred to as inherent variability⁴.

Uncertainty analysis: a process for estimating model uncertainty.

Variability: is what happens in the natural system; the observable variations.

Verification: is the checking of the computer code to ensure that it is a true representation of the conceptual model upon which it is based. This includes checking whether the mathematical equations involved have been solved correctly and comparing the numerical solutions with idealized cases for which an analytic solution exists.

3 Background

Air quality simulation models have been used for many decades to characterize the transport and diffusion of materials in the atmosphere (Pasquill, 1961; Randerson, 1984; Hanna et al., 1982). The wider use of atmospheric models in scientific studies for regulatory purposes and for describing air quality scenarios requires assessing the degree of reliability of model results. Generally, such an assessment is performed through the comparison of model outputs against field measurements. Tracer experiments are particularly helpful in evaluating the capability of these models to properly simulate transport and diffusion. Comparisons between model outputs and measurements are performed using both qualitative data analysis techniques and quantitative statistical methods.

Up until the early 1980s, comparing modeling results with observations was considered simple. The outputs of dispersion models were plotted against measurements (using traditional scatter plots of the values) and simple performance measures such as the correlation coefficient were computed (Clarke, 1964; Martin, 1971; Hanna, 1971). High correlation values were interpreted as an indication that the model was performing well; low correlation (a not uncommon case) was interpreted to mean that the model was performing poorly.

As air quality models came into more common use, concerns were raised that early statistical performance evaluation had been naive. Little consideration had been given to the consequences and sources of uncertainty and variability. As

⁴ What we are labelling “inherent variability” is what Fox (1984) and others discuss as “inherent uncertainty”, and what Hanna (1993) discuss as the “irreducible scatter caused by stochastic fluctuations”.

discussed in Sections 4 and 6, the sources of uncertainty can be envisioned as being composed of: model formulation uncertainty, representativeness uncertainty, measurement uncertainty, and inherent variability⁴.

- Model formulation uncertainty is composed of theory uncertainty (there may be more than one theory that adequately describes available data) and numerical uncertainty (conversion of mathematical algorithms to numerical code may involve approximations that could lead to spurious noise in the solutions if not well-treated);
- Representativeness uncertainty arises whenever there is a lack of agreement in the data used as model input or the data used for comparison with model output⁵ to satisfy the spatial and temporal assumptions of the model;
- Measurement uncertainty results from errors in measurements, which can affect model inputs⁶ and can affect observed concentrations used for comparison with model outputs;
- Inherent variability arises because models only characterize a portion of the naturally occurring variations.

In the early comparisons, measurement uncertainties were assumed to be small in comparison to the “real world fluctuations”, when in fact that was not always a safe assumption. More importantly, even hypothetically error-free measurements possess space and time limitations that prevent them from being good approximations of the time and space assumptions used in the construction of the model. For instance, the comparison of measurements taken at an isolated receptor with grid-averaged model outputs is inappropriate (Davis et al., 2000).

The early statistical performance evaluations failed to address the fact that models provide estimates of ensemble means, whereas the observations are individual realizations from imperfectly defined ensembles (Lamb from Longhetto, 1980; Venkatram, 1988). Furthermore, reliance on linear regressions and correlation coefficient can provide misleading results (Zannetti and Switzer, 1979). Lastly, models rely on emission and meteorological inputs whose uncertainties could justify disagreements between predictions and observations (Irwin et al., 1987).

In the early eighties, several attempts were made to develop standard methodologies for judging air quality model performance (Bornstein and Anderson, 1979; Venkatram, 1982 and 1983; Willmot, 1982). The American

⁵ Differences from not properly satisfying the model input assumptions are referred to by some as “data representativeness uncertainty”, and by other as “input uncertainty”; differences in properly satisfying the model output assumptions are most often referred to as “data representativeness uncertainties”.

⁶ Uncertainties in emission data may result from measurement or formulation uncertainties since a wrong methodology might have been used for emission estimation.

Meteorological Society sponsored two workshops in an attempt to provide specific guidelines on the use of statistical tools in air quality applications. A summary of their recommendations is provided in two papers by Fox (1981, 1984).

The most interesting comments and recommendations from the above workshops were:

- the concern about the absolute, rather than statistical nature of U.S. air quality standards
- the possibility of computing statistics between measured data values and model predicted values even when these values are not coupled in time and/or in space
- the identification of reducible errors and inherent variability
- the recommendations to decision-makers to educate themselves and accept the challenge of decision making with quantified uncertainty

Following these two workshops, a series of studies were undertaken to continue to investigate the problem of statistically evaluating the performance of air quality models. Interesting methods were proposed at the DOE Model Validation Workshop, October 23-26, 1984, Charleston, South Carolina, and by Alcamo and Bartnicki (1987) and Hanna (1989a). Major operational evaluations of air quality models were sponsored by EPRI (Reynolds et al., 1984; Ruff et al., 1984; Moore et al., 1985; Reynolds et al., 1985).

Further development of the evaluation methodologies proposed in the early eighties was needed, as it was found that the rote application of performance measures, such as those listed in Fox (1981), was incapable of discerning differences in model performance (Smith, 1984). Whereas if the evaluation results were sorted by stability and distance downwind, then differences in modeling skill could be discerned (Irwin and Smith, 1984). It was becoming increasingly evident that the models were characterizing only a small portion of the observed variations in the concentration values (Hanna, 1988). To better deduce the statistical significance of differences seen in model performance in the face of small sample sizes and unknown uncertainties, investigators began to explore the use of bootstrap techniques (Hanna, 1989). By the late 1980s, most of the model evaluations involved the use of bootstrap techniques in comparing the maximum values of modeled and observed cumulative frequency distributions of the concentration values (Cox and Tikvart, 1990).

Even though the procedures and measures are still evolving to describe performance of models that characterize atmospheric fate, transport and diffusion (Weil et al., 1992; Dekker et al., 1990; Cole and Wicks, 1995), there has been a general acceptance for a need to address the large uncertainties inherent in atmospheric processes. There has also been a consensus reached on the philosophical reasons that models of earth science processes can never be verified

(in the sense of claiming that a model is truly representative of natural processes). General empirical proposition about the natural world cannot be certain since there will always remain the prospect that future observations may call the theory in question (Oreskes et al., 1994). It is seen that numerical models of air pollution are a form of a highly complex scientific hypothesis concerning natural processes that can be confirmed through comparison with observations, but never verified.

4 Framework

To set the context for the following discussion (Irwin, 2000), it is important to realize that most of the model evaluation results currently available in the literature are for applied air quality models that use ensemble average characterizations of the transport and diffusion, the chemical transformations, and the physical removal processes. Thus, these applied air quality models only provide a description of the average fate of pollutants to be associated with each possible ensemble of conditions (or “regime”). Natural variability that is not characterized by the model can result in large deviations when comparing individual observations (which are individual realizations from an ensemble of realizations) with modeling results (which are characterizing the ensemble average result).

The differences seen in comparison between model predictions and observations of atmospheric air concentrations may largely reflect inherent variability. Likely, this component of variability is inherent in that it cannot be simulated explicitly by improving the physics of the air quality models. At best, air quality models provide an unbiased estimate of the average concentration expected over all realizations of an ensemble. An estimate of an ensemble can be developed from a set of experiments having fixed external conditions (Lumley and Panofsky, 1964). To accomplish this, the available concentration values are sorted into classes characterizing ensembles. For each of the ensembles thus formed, the difference between the ensemble average and any observed realization (experimental observation) is then ascribed to inherent variability where its variance, σ_n^2 , can be expressed as (Venkatram, 1988):

$$\sigma_n^2 = \overline{(C^o - \overline{C^o})^2} \quad (1)$$

where C^o is the observed concentration seen within a realization; the over-bars refer to an average over all available realizations within a given ensemble, so that $\overline{C^o}$ is the estimated ensemble average. In (1), the ensemble refers to the ideal infinite population of all possible realizations meeting the (fixed) characteristics of the chosen ensemble. In practice, we will only have a small sample from this ensemble. Measurement uncertainty in C^o in most tracer experiments is typically

a small fraction of the measurement threshold, and when this is true, its contribution to σ_n can usually be deemed negligible.

Defining the characteristics of the ensemble in (1) using the model's input values, α , one can view the observed concentrations as:

$$C^o = C^o(\alpha, \beta) = \overline{C^o}(\alpha) + c(\Delta c) + c(\alpha, \beta) \quad (2)$$

where β are the variables needed to describe the unresolved transport, fate and diffusion processes. The over-bar represents an average over all possible values of β for the specified set of model input parameters α ; $c(\Delta c)$ represents the effects of concentration representativeness and measurement uncertainty, and $c(\alpha, \beta)$ represents ignorance in β , unresolved deterministic processes and stochastic fluctuations (Hanna, 1988; Venkatram, 1988). Since $\overline{C^o}(\alpha)$ is an average over all β , it is only a function of α , and in this context, $\overline{C^o}(\alpha)$ represents the ensemble average that the model is ideally attempting to characterize.

The modeled concentrations, C^s , can be envisioned as:

$$C^s = C^s(\alpha) = \overline{C^o}(\alpha) + d(\Delta\alpha) + f(\alpha) \quad (3)$$

where $d(\Delta\alpha)$ represents the effects of uncertainty in specifying the model inputs and $f(\alpha)$ represents the effects of uncertainty in the model theory and numerical implementation.

The method we propose for performing an evaluation of modeling skill is separately averaging the observations and modeling results over a series of non-overlapping limited-ranges of α , which are called "regimes". Averaging the observations provides an empirical estimate of what most of the current models are attempting to simulate, $\overline{C^o}(\alpha)$. A comparison of the respective observed and modeled averages over a series of α -groups provides an empirical estimate of the combined deterministic error associated with input uncertainty and formulation errors.

Given this framework, designing a model evaluation can be envisioned as a two-step process. Step one, we analyze the observations to provide average patterns for comparison with modeled patterns. Step two, given the uncertainties in estimating the average patterns, we test to see whether differences seen in a comparison of performance of several models are statistically significant. In order to place confidence bounds on conclusions reached in step two, bootstrap resampling is recommended (see Section 5.4). Within the American Society for

Testing and Materials (ASTM), a standard guide⁷ has been developed that outlines this strategy for designing statistical evaluations of dispersion model performance (a statistical evaluation of performance).

This process is not without problems, as grouping data together for analysis requires large data sets of which there are few. Sorting the data into groups requires sufficient knowledge of the experimental conditions to determine how the data collected on different days or during different time periods should be grouped together. In reality, the external forcing conditions are imperfectly known, and hence the groups are imperfectly composed.

Another problem is that air quality models only explain a small portion of the observed variations, and there are large uncertainties involved in any air quality modeling assessment. Earlier in this chapter, we mentioned that there are essentially four sources of uncertainty: formulation uncertainty, representativeness uncertainty, measurement uncertainty, and inherent variability. We now take a moment to provide some perspective as to the size and nature of inherent variability and model input uncertainty.

From Equation (2), we see that natural variation that is not explained by the model is the term $c(\alpha, \beta)$, and we have referred to this as the inherent variability. It has been estimated that the portion of natural variability that is not accounted for by atmospheric transport and diffusion models is of order of the magnitude of the regime averages (Weil et al., 1992; Hanna, 1993). Thus, small sample sizes in the groups, which are used in the statistical evaluation to form pseudo-ensembles, could lead to large uncertainties in the estimates of the ensemble averages.

An illustration of unexplained concentration variability is presented in Figure 1. Project Prairie Grass (Barad, 1958; Haugen, 1959) is a classic tracer dispersion experiment where sulfur-dioxide (SO_2) was released from a small tube placed 46 cm above the ground. Seventy 20-minute releases were conducted during July and August 1956, in a wheat field near O'Neil, Nebraska. Sampling arcs were positioned on semicircles centered on the release, at downwind distances of 50, 100, 200, 400 and 800 m. The samplers were positioned 1.5 m above the ground, and provided 10-minute concentration values. For the purpose of illustrating concentration variability, two small ensembles of six experiments along the 400-m arc have been grouped together in Figure 1 using the inverse of Monin-Obukhov length, L , a stability parameter (as $1/L$ approaches zero, the surface layer of the atmosphere approaches neutral stability conditions). Concentration values from near-surface point sources are inversely proportional to the transport wind speed, U , and directly proportional to the emission rate, Q . To group the results of the six experiments together, the concentration values were normalized by multiplying the concentration values by U/Q , where U was defined as the

⁷ Standard Guide for the Statistical Evaluation of Atmospheric Dispersion Model Performance, D6589, Annual Book of Standards Volume 11.03, American Society for Testing and Materials, West Conshohocken, PA 19428 (<http://www.astm.org>).

value observed at 8 m above the ground. The solid line shown for each group is a Gaussian fit to the results for the six experiments in the group. The scatter of the normalized concentration values about this Gaussian fit can be statistically analyzed to provide an estimate of the concentration variability not characterized by the Gaussian fit. From this analysis and other tracer studies, the stochastic fluctuations (inherent variability) were investigated by analyzing the distribution of $C^o/\overline{C^o}$ for centerline concentration values. The distribution was found to be approximately lognormal, with a standard geometric deviation of order 1.5 to 2 (Irwin and Lee, 1997; Irwin, 1999). These results suggest that centerline concentration values from individual experiments may typically deviate from the ensemble average maximum by as much as a factor of two.

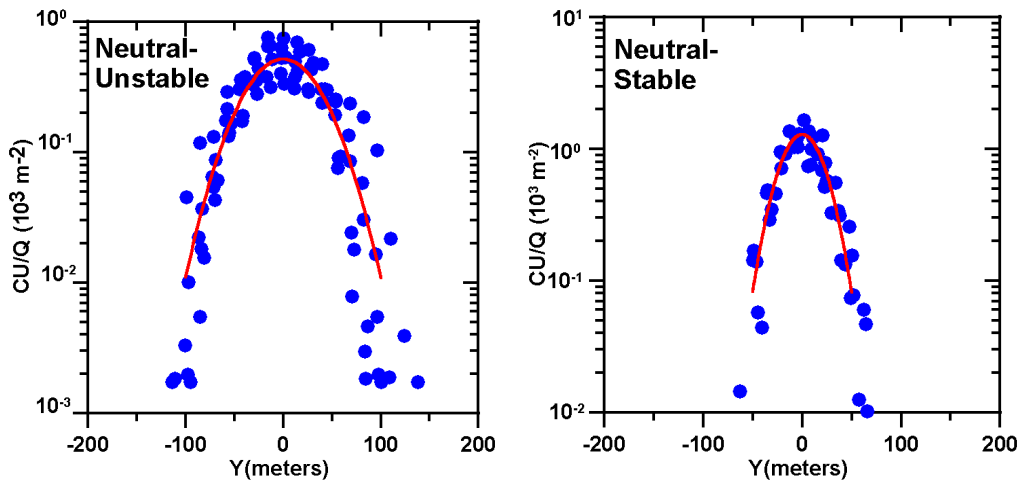


Figure 1. Near-neutral unstable (left) and near-neutral stable (right) normalized concentration values at the 400-meter arc. The neutral-unstable experiments are 6, 11, 34, 45, 48 and 57, with Monin-Obukhov lengths ranging from -263 m to -82 m. The neutral-stable experiments are 21, 22, 23, 24, 42, and 55, with Monin-Obukhov lengths ranging from 164 m to 359 m.

The use of wind tunnel measurements can be useful towards providing data for a model evaluation process (Schatzmann and Leitzl, 1999). The work of Stein and Wyngaard (2000) investigates the relationship between inherent variability in laboratory and atmospheric boundary layer flows. For a given averaging time, they show that the inherent variability in laboratory flows is smaller than in the atmospheric boundary layer flows under the same stability and statistical conditions.

Characterizing the model input is another source of uncertainty. The variance in modeled concentration values due to input uncertainty can be quite large. Using a Gaussian plume model, Irwin et al. (1987) investigated the uncertainty in estimating the hourly maximum concentration from elevated buoyant sources during unstable atmospheric conditions due to model input uncertainties. A numerical uncertainty analysis was performed using the Monte-Carlo technique to propagate the uncertainties associated with the model input. Uncertainties were

assumed to exist in four model input parameters: wind speed, standard deviation of lateral wind direction fluctuations, standard deviation of vertical wind direction fluctuations, and plume rise. It was concluded that the uncertainty in the maximum concentration estimates is approximately double the uncertainty assumed in the model input. For instance, if half of the input values are within 30% of their error-free values, then half of the estimated maximum concentration values will be within 60% of their error-free values. Using a photochemical grid model, Hanna et al. (1998) investigated the uncertainty in estimating domain-wide hourly maximum ozone concentration values near New York City for July 7-8, 1988. Fifty Monte-Carlo runs were made in which the emissions, chemical initial conditions, meteorological input and chemical reaction rates were varied within expected ranges of uncertainty. The amount of uncertainty varied, depending on the variable. Those variables with the least assumed uncertainty (most of the meteorological inputs) were assumed to be within 30% of their error-free values 95% of the time. Larger uncertainties were generally assumed for the emissions and reaction rates. They found that the domain-wide maximum hourly averaged ozone ranged from 176 to 331 ppb (almost a factor of two range). These two investigations reveal that the sensitivity to model input uncertainties is quite large, regardless of whether the model is a Gaussian plume model, a photochemical grid model, or whether the specie being modeled is inert or chemically reactive.

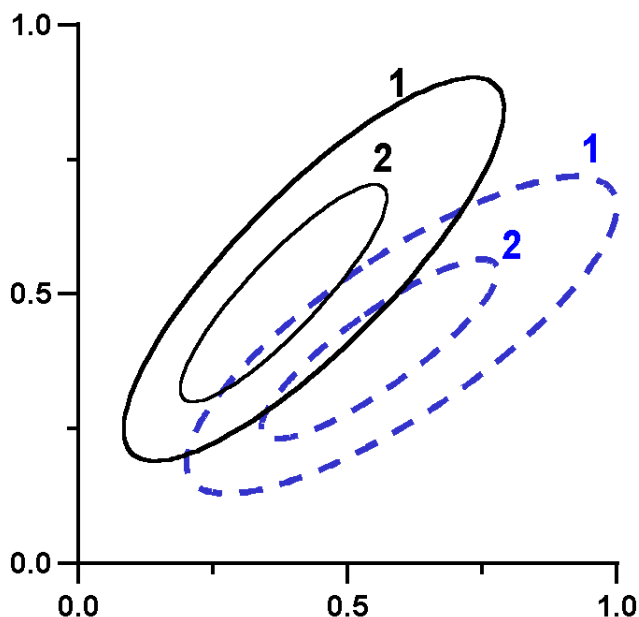


Figure 2. Illustration of displacement of observed (solid lines) and predicted (dashed lines) ground-level concentration patterns. Isopleths represent points with the same concentration. The point-by-point correlation is poor, but the patterns are clearly similar (adapted from Hanna, 1988 [Reprinted with permission from the Air Pollution Control Association]).

Irwin and Smith (1984) warned that the disagreement between the indicated wind direction and the actual direction of the path of a plume from an isolated point source is a major cause for disagreement between model predictions and observations. As a plume is transported downwind, it typically expands at an angle of approximately 10 degrees, and this angle is seldom larger than 20 degrees. With such narrow plumes, even a 2-degree error in estimating the plume transport direction can cause very large disagreement between modeled and observed surface concentration values. Weil et al. (1992) analyzed nine periods from the EPRI Kincaid experiments, where each period was about 4 hours long. They concluded that for short travel times (where the growth rate of the plume's width is nearly linear with travel time), the uncertainty in the plume transport direction is of the order of 1/4 of the plume's total width. Farther downwind, where the growth rate of the plume's width is less rapid, the uncertainty in the plume transport direction is larger than 1/4 of the plume's total width. Figure 2 illustrates that any point-to-point comparison of modeled and observed concentration values (e.g., correlation, bias, mean squared error) would suggest poor performance. It is clearly seen that the basic pattern is modeled well if the observed pattern is shifted over to better correspond with that modeled. In conclusion, the uncertainties of plume transport direction are substantial, and likely will preclude, especially for isolated source comparisons, a meaningful evaluation of modeled and observed concentration values paired in time and space.

This section presented a framework providing a means for understanding why modeled and observed values differ. The observations are envisioned as being composed of an ensemble mean about which there are deviations either resulting from representativeness and measurement uncertainty, or uncharacterized natural variability, $c(\alpha, \beta)$. Examples were provided that suggest that for maximum surface concentrations, uncharacterized variability, $c(\alpha, \beta)$, is on the order of the ensemble mean, (i.e., could easily account for factor of two deviations from the mean). The model values are envisioned as being composed of an ensemble mean about which there are deviations either resulting from input (representativeness and measurement) uncertainty, or model theory and numerical implementation errors. Examples were provided that suggest that the effects of input uncertainty can be amplified within the model (e.g., doubled), and can lead to variations on the order of a factor of two. As a pragmatic mean for assessing systematic errors in the model formulations, it was recommended that pseudo-ensembles be formed by grouping evaluation data into time periods where conditions can be assumed to be similar. Then it was recommended that comparisons be made of the group averages, because this insulates the comparisons from many of the sources of uncertainties. Other issues will be addressed, such as how to cope with uncertainties in the direction of transport, as discussed in Section 7. First, we will discuss in the next section the kinds of performance measures one might choose in developing an evaluation procedure.

5 Performance Measures

The preceding section described a philosophical framework for understanding why observations differ from model simulation results. This section provides definitions of the performance measures and methods often employed in current evaluations of air quality models. Proper model evaluation involves the application of both statistical indices and graphical methodologies. The list of possible performance measures is extensive (e.g., Fox, 1981), but it has been illustrated that a few well-chosen simple-to-understand performance measures can provide adequate characterization of a model's performance (e.g., Hanna, 1988). Therefore, the selection of performance measures to compare model outputs against observed values is a fundamental step. Statistical indices and graphical methodologies emphasize specific model characteristics (e.g., Canepa and Builtjes, 1999); therefore, outlining the characteristics of each performance measure is useful. The following discussion is not meant to be exhaustive. The key is not in how many performance measures are used, but is in the statistical design used when the performance measures are applied (e.g., Irwin and Smith, 1984).

For convenience, we discuss the comparison of the observed and modeled concentration values in the following discussion. In reality, model evaluation can involve comparisons of observed and modeled plume rise, building wake dimensions, etc. Any feature (evaluation objective) that can be deduced from an analysis of the concentration pattern and converted to a numeric value can be substituted for the word "concentrations" in the following discussion.

5.1 Basic Performance Measures

MEAN of both the observed and simulated concentrations is defined as:

$$MEAN_{observed} = \overline{C^o} = \sum_i \frac{C_i^o}{N} \quad MEAN_{simulated} = \overline{C^s} = \sum_i \frac{C_i^s}{N} \quad (4)$$

where N is the total number of the values being averaged, C_i^o (C_i^s) is the i^{th} observed (simulated) concentration value. A perfect model would give $MEAN_{observed} = MEAN_{simulated}$. Note, the values being averaged may be for the same time period (an average over a set of receptors), or the values being averaged may be at a fixed receptor location, either relative or absolute (an average over some time period).

SIGMA (standard deviation) of both the observed and simulated concentrations is defined as:

$$SIGMA_{observed} = \sigma^o = \sqrt{\frac{\sum_i (C_i^o - \bar{C}^o)^2}{N}} \quad (5)$$

$$SIGMA_{simulated} = \sigma^s = \sqrt{\frac{\sum_i (C_i^s - \bar{C}^s)^2}{N}} \quad (6)$$

a perfect model would give $SIGMA_{observed} = SIGMA_{simulated}$.

5.2 Description of Some Paired Performance Measures

Often the evaluation procedure involves a comparison that logically involves pairing of the observed and modeled values. This might be: the maximum concentration over a domain seen for an hour or a day, or the maximum concentration seen on receptor arcs centered on a tracer release location, etc.

It is not possible to assume that uncertainty in both the observations and the modeled values is small in comparison to the variations seen in their mean values (Irwin et al., 1987; Weil et al., 1992; Hanna, 1993; Hanna et al., 1998). Unless the uncertainties are small in comparison to the variations in their mean values, one cannot confidently make comparisons of raw observations with modeled values.

However, the paired comparison of group averages is meaningful, especially if the groups are well formulated and provide representative estimates of the ensemble average concentration for each group.

BIAS is defined as:

$$BIAS = \bar{C}^s - \bar{C}^o \quad (7)$$

A perfect model would give $BIAS = 0$. If $BIAS > 0$ (< 0), the model on average overestimates (underestimates) the observed concentrations. We have followed here and elsewhere the convention that a positive BIAS indicates a model over-prediction. This has been found to be better understood by decision-makers and users of model evaluation results (whereas, having to explain a negative BIAS as a model over-prediction was a constant problem). We mention this because one may find in some literature that the opposite convention is sometimes used.

FB (Fractional Bias) is defined as:

$$FB = \frac{\bar{C}^s - \bar{C}^o}{(\bar{C}^s + \bar{C}^o)/2} \quad (8)$$

FB ranges between -2 and $+2$. For a perfect model, $FB = 0$. If $FB > 0$ (< 0), the model on average overestimates (underestimates) the observed concentration values.

The **MEAN**, **BIAS** and **FB** only characterize the “on average” model behavior. One can directly judge the average model performance by looking at the $MEAN_{\text{observed}}$ and $MEAN_{\text{simulated}}$ values simultaneously. From the value of the **BIAS**, one has an idea of whether the model underestimates ($BIAS < 0$) or overestimates ($BIAS > 0$) the observed values. However, the **BIAS** value does not convey any sense of how large the average difference is relative to the average magnitude of the observed values. For example, if one is dealing with two data sets, characterized by $\overline{C_A^o} = 10$ and $\overline{C_B^o} = 100$ (in appropriate units), and using a model obtains $\overline{C_A^s} = 20$ and $\overline{C_B^s} = 110$, the **BIAS** value, in both cases, is 10. However, the “on average” behavior of the model is better in case B, because the percentage difference is less in case B. To address this issue, the **FB** can be helpful. The **FB** is the **BIAS** normalized by the average value of $\overline{C^o}$ and $\overline{C^s}$. As far as the previous example is concerned, $FB_A = 0.67$ and $FB_B = 0.095$. Thus, better model performance is evident in case B.

FS (Fractional Standard deviation) is defined as:

$$FS = \frac{\sigma^s - \sigma^o}{(\sigma^s + \sigma^o)/2} \quad (9)$$

FS ranges between -2 and $+2$. For a perfect model, $FS = 0$. If $FS > 0$ (< 0), the spreading of the simulated concentration values is larger (smaller) than the spreading of the observed concentration values.

The **SIGMA** and **FS** provide information about the spread (variance) in the modeled and observed concentration values. One can directly judge the model performance looking at the $SIGMA_{\text{observed}}$ and $SIGMA_{\text{simulated}}$ values simultaneously. The **FS** index is analogous to the **FB** index, except it is only related to the relative difference in the variances.

COR (linear **COR**relation coefficient) is defined as:

$$COR = \frac{\overline{(C^o - \overline{C^o})(C^s - \overline{C^s})}}{\sigma^o \sigma^s} \quad (10)$$

which ranges between -1 and $+1$ and a perfect model would give $COR = +1$.

COR provides information on the strength of the linear correlation between the modeled and the observed concentration values. For a value of + 1, the so-called “complete positive correlation”, there is correspondence between all pairs of modeled and observed concentration values (C_i^o, C_i^s). If the values were plotted against one another in a scatter diagram, all points would lay along a straight line with positive slope. The “complete negative correlation” corresponds to all the pairs on a straight line with negative slope, and $COR = -1$. A value of COR near zero indicates the absence of linear correlation between the variables. A model will have $COR = +1$ if $\overline{C_i^o - C^o} = \overline{C_i^s - C^s}$ for any (C_i^o, C_i^s). Because it is possible that $\overline{C^o} \neq \overline{C^s}$, the previous equality does not mean $C_i^o = C_i^s$ for any (C_i^o, C_i^s) as we should expect for a perfect model. Furthermore, it should also be pointed out that a high correlation coefficient does not necessarily indicate a direct dependence between the variables. Two variables may have no true relationship to one another, but may be correlated to a third variable (“spurious correlation”).

FA2 (fraction within a Factor of 2) is defined as:

$$\text{fraction of data with } 0.5 \leq \frac{C_i^s}{C_i^o} \leq 2 \quad (11)$$

A perfect model would give $FA2 = 1$.

NMSE (Normalized Mean Square Error) is defined⁸:

$$NMSE = \frac{\overline{(C^s - C^o)^2}}{\overline{C^s} \overline{C^o}} \text{ or, if for every } i, C_i^o \neq 0 \text{ then, } NMSE = \frac{\sum_i s_i^2 (1 - k_i)^2}{\sum_i s_i k_i} \quad (12)$$

where $k_i = C_i^s / C_i^o$ and $s_i = C_i^o / \overline{C^o}$; a perfect model would give $NMSE = 0$. The value of this index is always positive.

WNNR (Weighted Normalized mean square error of the Normalized Ratios) is defined as:

⁸ RMSE (Root Mean Square Error) is defined:

$RMSE = \sqrt{\overline{(C^s - C^o)^2}}$. A perfect model would give a $RMSE = 0$, and the value of this index is always positive. Note, preference is given to using the RMSE rather than the NMSE when there are large uncertainties in $\overline{C^o}$ (which typically occurs when the observed concentration values are close to the measurement threshold).

$$WNNR = \frac{\sum_i s_i^2 (1 - \hat{k}_i)^2}{\sum_i s_i \hat{k}_i} \quad (13)$$

where $\hat{k}_i = 1/k_i$ (if $k_i > 1$) and $\hat{k}_i = k_i$ (if $k_i \leq 1$). A perfect model would give $WNNR = 0$. The value of this index is always positive.

NNR (Normalized mean square error of the distribution of Normalized Ratios) is defined as:

$$NNR = \frac{\sum_i (1 - \hat{k}_i)^2}{\sum_i \hat{k}_i} \quad (14)$$

A perfect model would give $NNR = 0$. The value of this index is always positive.

The **FA2**, **NMSE**, **WNNR** and **NNR** indices give information about the ratios between simulated and measured concentrations. Only the FA2 and NNR indices, out of all indices considered, depend solely on the ratios between simulated and measured concentrations, and not on the data set itself, so they are the only indices strictly usable to compare simulations of different experiments. NMSE attributes more weight to model errors concerning the estimates of the highest measured concentrations in some cases, of the lowest ones in other cases; WNNR attributes more weight to model errors concerning the estimates of the highest measured concentrations; and NNR attributes the same weight to model errors independently of the position of the data within the concentration range (Poli and Cirillo, 1993; Canepa and Modesti, 1997).

SCATTER DIAGRAM, **FOEX**, and **FA α** again give information about the ratios between simulated and measured concentrations. SCATTER DIAGRAM is a graph where predicted values are plotted versus measured ones (see Figure 3). The $y = x$ line represents the perfect agreement between predictions and measured values. A value above (below) the $y = x$ line indicates a situation of over-prediction (under-prediction). FOEX is defined as

$$FOEX = \left[\frac{N_{(C_i^s > C_i^o)}}{N} - 0.5 \right] \cdot 100 \quad (15)$$

where $N_{(C_i^s > C_i^o)}$ is the number of over-predictions (i.e. the number of pairs

where $C_i^s > C_i^o$). It ranges between -50% and $+50\%$. If $FOEX = -50\%$, all the points are below the $y = x$ line and if $FOEX = +50\%$, all the points are above the $y = x$ line. The best value is 0% , which means that there are half under-predictions and half over-predictions. FOEX does not take into account the

magnitude of the over-predictions; it evaluates only the number of events of over-prediction. Representing the scatter diagram on logarithmic paper, the FA α band is the region between the two lines of equation $y - y_0 = (x - x_0) \pm \ln(\alpha)$, where x_0 and y_0 are the coordinates of the origin of the axes. If $\alpha = 2$, then FA $\alpha = \text{FA}2$ (see above).

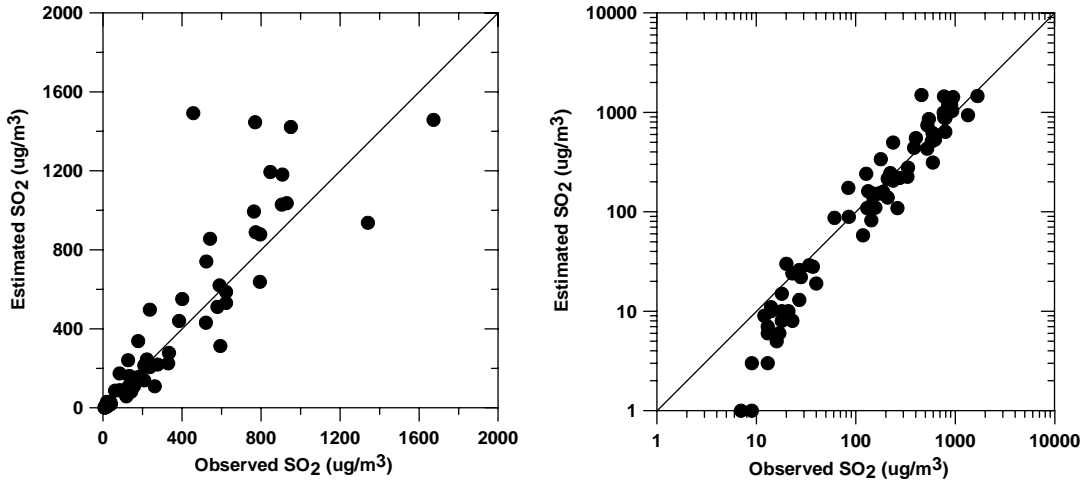


Figure 3. Example of SCATTER DIAGRAM: linear axes (left), log axes (right).

PERCENTILES and **BOX PLOT** give information about the cumulative probability. The n^{th} percentile of a distribution of values is defined as the cumulative probability in percent, that is, the value that bounds the $n\%$ of values below and the $(100 - n)\%$ above it. Looking at the box plot (see Figure 4), the general features of the distribution of the considered values can be distinguished.

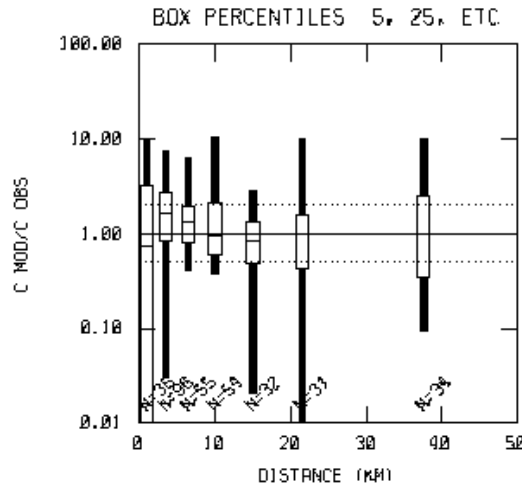


Figure 4. Example of C_i^s / C_i^o BOX PLOTS stratified with respect to the distance from the source.

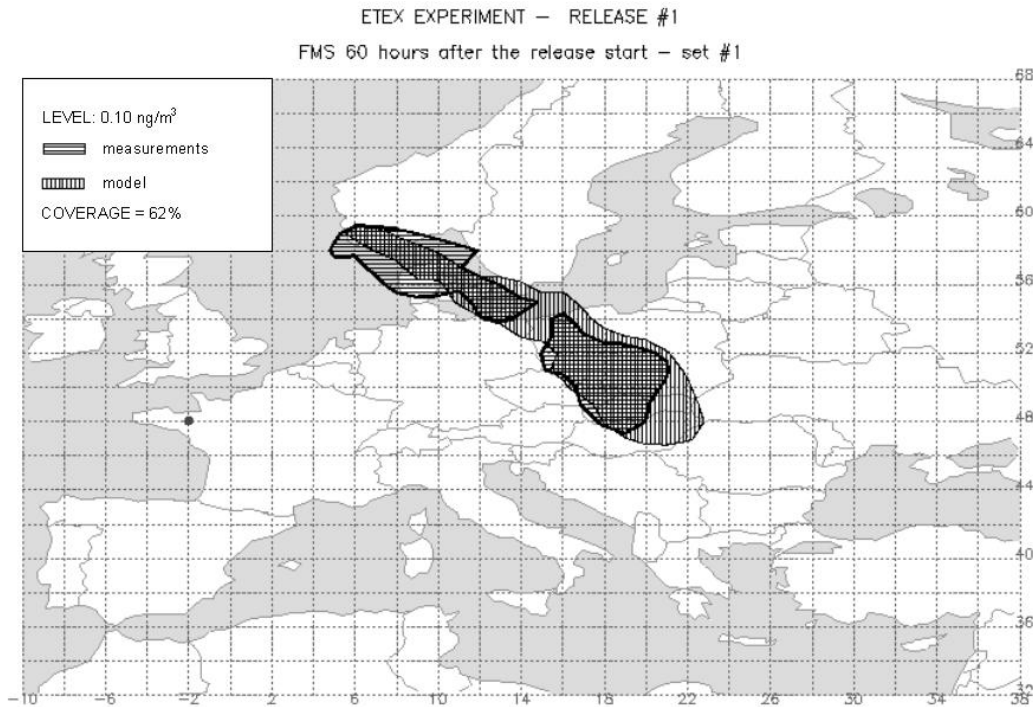


Figure 5. Example of FMS [from Graziani et al. (1998), courtesy of EI/JRC].

FMS (Figure of Merit in Space) gives information about the space analysis (see Figure 5), and is defined as

$$FMS = 100 \frac{A_1 \cap A_2}{A_1 \cup A_2} \quad (16)$$

FMS is calculated at a fixed time for a fixed concentration level (significant level). FMS is the percentage of overlap between the measured (A_1) and predicted (A_2) areas. A shift in space of the concentration patterns can reduce the FMS significantly (e.g., Figure 2).

FMT (Figure of Merit in Time) gives information about the time analysis, and is defined as

$$FMT_x = 100 \frac{\sum_j \min\{C_x^o(t_j), C_x^s(t_j)\}}{\sum_j \max\{C_x^o(t_j), C_x^s(t_j)\}} \quad (17)$$

FMT is calculated at a fixed location \bar{x} for a time series of data. FMT evaluates the overlap of the observed and predicted concentration patterns in time. A temporal shift of the time series can reduce the FMT significantly.

5.3 Description of Some Unpaired Performance Measures

An evaluation procedure often involves a comparison that logically involves unpairing of the observed and modeled values. An underlying assumption here is that we have two samples, presumably drawn from the same distribution. If the samples are representative and from the same distribution, then they should both have similar distributions. We have shown in Equations (2) and (3) that the observed and modeled concentration values have different sources of variance, and thus are not from the same distribution. However, if we have groups that are well-formulated and provide representative samples for a series of ensembles, then we can anticipate that the observed and modeled group averages are from the same underlying distribution, and hence have similar frequency distributions.

The **QUANTILE-QUANTILE PLOT** is constructed by plotting the ranked concentration values against one another (e.g., highest concentration observed versus the highest concentration modeled, etc.; see Figure 6). If the observed and modeled concentration frequency distributions are similar, then the plotted values will lie along the 1:1 line on the plot. By visual inspection, one can easily see if the respective distributions are similar, and whether the observed and modeled concentration maximum values are similar.

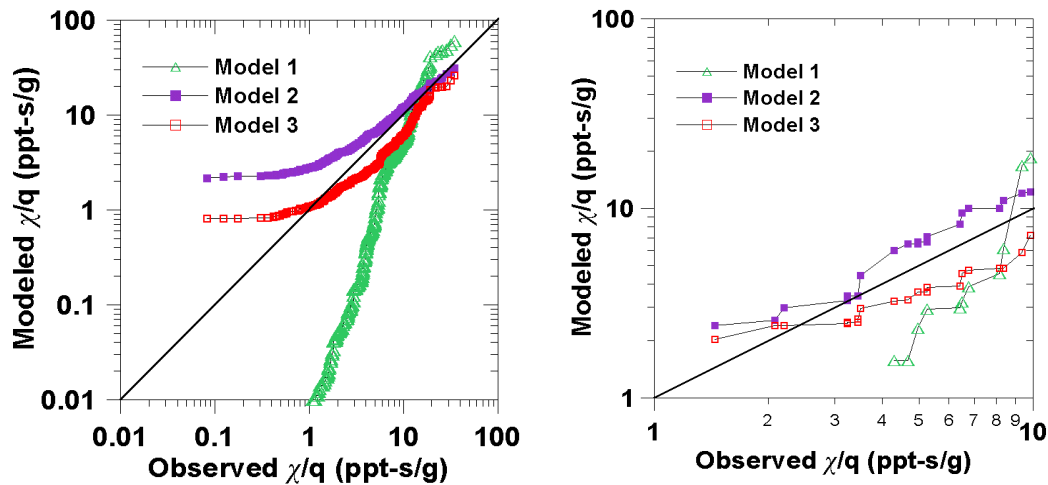


Figure 6. Example of QUANTILE-QUANTILE PLOTS comparing: on the left side, observed and modeled centerline concentration values (not recommended); on the right side, observed and modeled regime average centerline concentration values (as recommended by the ASTM guide cited in Section 4).

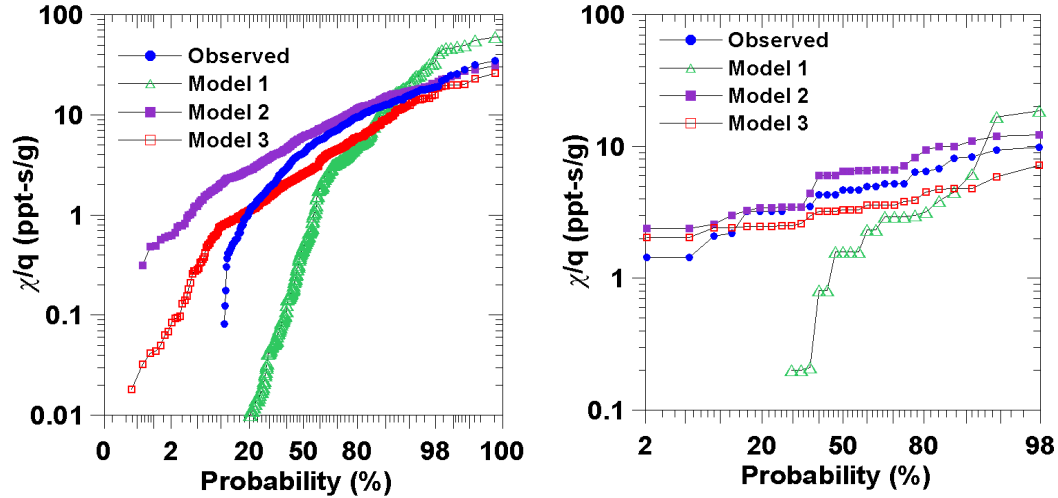


Figure 7. Example of CUMULATIVE FREQUENCY PLOTS comparing: on the left side, observed and modeled centerline concentration values (not recommended); on the right side, observed and modeled regime average centerline concentration values (as recommended by the ASTM D6589 cited in Section 4).

The CUMULATIVE FREQUENCY PLOT (Figure 7) is constructed by plotting the ranked concentration values (lowest to highest) against the plotting position frequency, f (typically in percent), where p is the rank (1 = lowest), N is the number of values and f is defined as (Larsen, 1969):

$$f = 100\% - 100\%(N - p + 0.6)/N \quad \text{for } p > N/2$$

$$f = 100\%(p - 0.4)/N \quad \text{for } p < N/2$$
(18)

As with the QUANTILE-QUANTILE PLOT, a visual inspection of the respective CUMULATIVE FREQUENCY DISTRIBUTION PLOTS (observed and modeled) is usually sufficient to suggest whether the two distributions are similar, and whether there is a bias in the model to over- or under-estimate the maximum concentration values observed.

The RHC (Robust Highest Concentration) index is often used where comparisons are being made of the maximum concentration values, and is envisioned as a more robust statistical test than direct comparison of maximum values. The RHC is based on an exponential fit to the highest $R - 1$ values of the cumulative frequency distribution, where R is typically set to 26 for frequency distributions involving a year's worth of values (averaging times of 24 hours or less) (Cox and Tikvart, 1990). The RHC is computed as:

$$RHC = C(R) + \Theta \cdot \ln\left(\frac{3R - 1}{2}\right)$$
(19)

where Θ is the average of the $R-1$ largest values minus $C(R)$, and $C(R)$ is the R^{th} largest value. The value of R may be set to a lower value when there are fewer values in the distribution to work with; the RHC of the observed and modeled cumulative frequency distributions are often compared using an FB index, see Cox and Tikvart (1990).

5.4 Bootstrap Resampling

The standard analytical formulas for confidence intervals on performance measures from statistics textbooks may be inappropriate (Fox, 1984) since air quality data and model performance measures are not necessarily normally-distributed nor can they always be transformed to a normal distribution. The bootstrap resampling procedure (Heidam, 1987; Hanna, 1989; Cox and Tikvart, 1990; Efron and Tibshirani, 1993) was suggested as an alternative method, since it did not depend on the form of the underlying distribution function.

Following the description provided by Efron and Tibshirani (1993), suppose one is analyzing a data set x_1, x_2, \dots, x_n , which for convenience is denoted by the vector $x = (x_1, x_2, \dots, x_n)$. A bootstrap sample, $x^* = (x_1^*, x_2^*, \dots, x_n^*)$, is obtained by randomly sampling n times with replacement from the original data points $x = (x_1, x_2, \dots, x_n)$. For instance, with $n = 7$ one might obtain $x^* = (x_5, x_7, x_5, x_4, x_7, x_3, x_1)$. From each bootstrap sample, one can compute some statistics s (median, average, RHC, etc.). By creating a number of bootstrap samples, m , one can compute the mean, \bar{s} , and standard deviation, σ_s , of the statistic of interest. For estimation of standard errors, m is typically on the order of 50 to 500.

Often, the bootstrap resampling procedure can be improved by blocking the data into two or more blocks or sets, with each block containing data having similar characteristics. This prevents the possibility of creating an unrealistic bootstrap sample where all the members are the same value (Hanna, 1989).

When performing model evaluations and model intercomparisons, for each hour there are not only the observed concentration values, but also the modeling results from all the models being tested. In such cases, the individual members, x_i , in the vector $x = (x_1, x_2, \dots, x_n)$ are vectors themselves, composed of the observed value and its associated modeling results (from all models, if there are more than one). Thus, the selection of the bootstrap sample x^* also includes each model's estimate for this case.

For example, suppose confidence limits are desired on the NMSE calculated from a set of n couples (C^s, C^o) , where C^s is the model simulation estimate and C^o is the corresponding observed value. In the bootstrap procedure, a new set of n couples (C^s, C^o) is randomly drawn from the original set. If a given (C^s, C^o) is

drawn, it is replaced before the next draw is made. Thus, it is possible (but not very probable) that all n “draws” consist of the same couple (C^s, C^o) . For each resample set of size n , the NMSE is calculated. If m resamples are drawn, the cumulative distribution function of the m values of NMSE will provide estimates of confidence limits on NMSE. For example, the 95% confidence interval on NMSE will range from 2.5% to 97.5% points on the NMSE distribution.

For assessing differences in model performance, one often wishes to test whether the differences seen in a performance measure computed between Model #1 and the observations (say, $NMSE_1$), is significantly different when compared to that computed for another model (say Model #2, $NMSE_2$) using the same observations. For testing whether the difference between performance measures is significant, the following procedure is recommended. Let each bootstrap sample be denoted x^{*b} , where “*” indicates this is a bootstrap sample and “ b ” indicates this is sample b of a series of bootstrap samples (where the total number of bootstrap samples is B). From each bootstrap sample, x^{*b} , one computes the respective values for $NMSE_1^b$ and $NMSE_2^b$. The difference $\Delta^{*b} = NMSE_1^{*b} - NMSE_2^{*b}$ can then be computed. Once all B samples have been processed, compute from the set of B values of $\Delta^* = (\Delta^{*1}, \Delta^{*2}, \dots, \Delta^{*B})$, the average and standard deviation, $\bar{\Delta}$ and σ_{Δ} . The null hypothesis is that $\bar{\Delta}$ is not equal to zero with a stated level of confidence, α , and the t -value for use in a Student’s t -test is:

$$t = \frac{\bar{\Delta}}{\sigma_{\Delta}} \quad (20)$$

For illustration purposes, assume the level of confidence is 90% ($\alpha = 0.1$). Then for large values of B , if the t -value from the above equation is larger than Student’s $t_{\alpha/2}$ equal to 1.645, it can be concluded with 90% confidence that $\bar{\Delta}$ is not equal to zero, and hence there is a significant difference in the NMSE values for the two models being tested.

6 Model Evaluation

Model evaluation is one of the elements of model quality assurance (see Section 8). Model evaluation is itself a system of procedures designed to measure performance (Model Evaluation Group, 1994a, 1994b; U.S. Environmental Protection Agency, 1997). Following Borrego et al. (2001b), model evaluation is composed of: model algorithm verification, sensitivity analysis, uncertainty analysis, statistical model evaluation, and model inter-comparison. Therefore, statistical model evaluation is one of the fundamental steps to achieve model evaluation.

- **Model algorithm verification** is the process of checking the computer code to ensure the code is a true representation of the conceptual model on which it is based. This includes: checking that the mathematical equations involved have been solved correctly, and comparing numerical solutions with idealized cases for which an analytic solution exists (“verification of numerical solutions”) to demonstrate that the two match over the particular range of conditions under consideration.
- **Sensitivity analysis** is a process of characterizing the response of a model to changes in input and parameter values. The purpose is to identify the magnitude, direction, and form (e.g., linear or non-linear) of the effect of such variations. Sensitivity tests can be performed with respect to: 1) uncertainty of physics/chemistry model parameters, and 2) uncertainty of emission and meteorological model input data. In either case, one can use two methods: a) systematically vary one or more of the model inputs to determine the effect on the modeling results (Hilst, 1970), or b) perform a Monte-Carlo study with random sampling (Irwin et al., 1987). In traditional sensitivity studies (item a), each input would be varied over a reasonable range likely to be encountered. These studies were routinely performed in the early years of air pollution modeling to develop a better understanding of the performance of plume dispersion models simulating the transport and diffusion of inert pollutants. Monte-Carlo studies (item b) are becoming more common, as they provide a sense of the overall response of the modeling system to known uncertainties throughout the system. They are especially useful for models simulating chemically reactive species where there are strong nonlinear couplings between the model input and the output (Hanna et al, 1998). Results from traditional sensitivity and Monte-Carlo studies provide useful guidance on which inputs should be most carefully prescribed because they account for the greatest sensitivity in the modeling output. Sensitivity analysis can also provide insight into how a model will behave when it is applied to conditions outside of the severely limited supply of available evaluation data.
- **Uncertainty analysis** (Section 4) is a process of estimating the model uncertainty. The total model uncertainty consists of three terms: 1) model formulation uncertainty in theoretical and numerical description of physics/chemistry parameters and processes (possibly systematic or random, assessable using traditional sensitivity or Monte-Carlo studies); 2) representativeness and measurement uncertainty in emission and meteorological model input data (both systematic and random, assessable using traditional sensitivity or Monte-Carlo studies); and 3) inherent variability associated with those physical processes which are not characterized within the model (both systematic and random, requires an extensive observational database and the estimation of ensemble averages). While the first and second contributions can in principle be reduced, it has

been recognized that inherent variability is not reducible, as it relates to the stochastic nature of the turbulent atmospheric motions (Fox, 1984).

- **Statistical model evaluation** (Section 7) is the comparison of model outputs with experimental data. It is also referred to as a statistical performance evaluation (ASTM D6589). It is preferred that the comparison data have not been used to develop the model.
- **Model intercomparison** is a process where several models, all presumably appropriate for some chosen situations (idealized or real), simultaneously have their performance assessed. This is a necessary step if one is to objectively select those models (from a list of possible candidate models), which perform best for some chosen situations. It is becoming increasingly more common for model intercomparisons to involve bootstrap resampling in order to arrive at an objective determination of whether differences seen in performance are statistically significant (see discussion in Section 5.4).

7 Statistical Model Evaluation

Statistical model evaluation is the analysis of model performance based on the statistical comparison of the model outputs with the experimental data (evaluation objectives). Although we can recommend specific steps one should accomplish, the details in how these steps are accomplished typically cannot be defined until:

1. the evaluation goal is defined,
2. the model is defined (or models if one is interested in performing model intercomparison), and
3. the databases are defined.

The sequence shown is a natural consequence that one cannot define which models to apply until the goal is defined. For instance, are we testing the performance of models to estimate the maximum concentrations near an industrial facility with one or several tall stacks next to buildings? Are we testing the performance of models to estimate the peak daily ozone concentration near a large city that is downwind of several even larger cities? The evaluation databases to be employed cannot be defined until one knows which model (or models) is selected and the task (objective) to be evaluated. Models require certain inputs, which may limit the usefulness of certain field data. Certain tasks require particular sampling plans (otherwise, one cannot evaluate the model's performance).

7.1 Before Evaluation

7.1.1 Defining the Evaluation Goal

To statistically assess model performance, one must define an overall evaluation goal or purpose. This will suggest features (evaluation objectives, see Section 7.2.1) within the observed and modeled concentration patterns to be compared (e.g., maximum surface concentrations, lateral extent of a dispersing plume). The selection and definition of evaluation objectives are typically tailored to the model's capabilities and intended uses. The very nature of the problem of characterizing air quality and the way models are applied make it impossible to define one single or absolute evaluation objective suitable for all purposes. The definition of evaluation objectives will be restricted by the limited range of conditions in the available comparison data. A procedure needs to be defined that allows definition of an evaluation objective from available observations of concentration values.

The evaluation goal can be process oriented (diagnostic); in this case one will have to make a selection of the model characteristics/modules to be validated. The evaluation goal may concern the overall model (integrated). It can be episodic or climatological depending on the time scale. The goal should be specific enough that it can be converted into one or more objective comparisons, which allows construction of null hypotheses that can be tested.

The evaluation goal may be to assess the performance of models to characterize what they were intended to characterize, namely ensemble estimates. Alternatively, the goal may be to assess the performance of models to characterize something different from their design capabilities, like maximum values as seen in the observations. There are consequences in choosing the latter, as good correspondence in this case may be indicative of a systematic flaw in a model, rather than a well-performing model. We recommend including, in all model evaluations, an assessment of how well models perform their designed capabilities.

When the intent is to select, among several models, a model able to perform as intended, the goal can be to determine which of several models has the lowest combination of bias and scatter, when modeling results are compared with observed values of the evaluation objectives. For this assessment, we recommend using the **NNR** or the **NMSE** (other performance measures may also provide useful insights). We first define the model having the lowest value for the **NNR** as the base-model. Then to assess the relative skill of the other models, the null hypotheses would be that the **NNR** values computed for the other models are significantly different when compared to that computed for the base-model (see Section 5.4).

7.1.2 Understanding Models to be Validated

Another part of statistical model evaluation is in having a fundamental understanding of what a model is capable of estimating (what physical processes are included or excluded from explicit treatment). All models are a compromise in what physical processes are chosen for explicit treatment. If the objective is to estimate the pattern of concentration values in the near vicinity of one (or several) source, then typically chemistry is of little importance. For such situations, the travel times from the sources to the receptor locations of interest are too short for chemistry formation and destruction to greatly affect the results. However, such situations demand that the air quality model properly treat near-field source emission effects such as: building wakes, initial characterization of source release conditions and size, rates of diffusion of pollutants released as they transport downwind, terrain and land use effects on plume transport, etc. If chemistry is to be explicitly treated, then initial source release effects are typically unimportant, as the pollutants are well-mixed over some volume of the atmosphere by the time the chemistry of interest has greatly affected the results. First attempts to treat both near-field dispersion effects and chemistry have been found to be inefficient and slow on today's computers that are available for routine use.

One might ask why more than one model is often involved in a statistical model evaluation exercise. There are several pragmatic reasons. Often, there is already an "accepted" model, and the purpose of statistical model evaluation is to prove whether a candidate model's performance is significantly better than the "accepted" model. Models differ in the characterized physical processes, the sophistication of input data required, and the numerical processor required. If several models can be shown to have statistically similar performance, then one might select from these a model for use that best meets available resources in input data, computer expertise, processing time, etc. Parsimony (economy or simplicity of assumptions) is a desired trait in modeling. As illustrated in Figure 8, as the model formulation increases in complexity (to explicitly treat more physical processes), we increase the number of input variables, which increases the likelihood of degrading the model's performance due to input data and model parameter uncertainty. Underlying the model formulation and input uncertainty, there is the inherent variability that the model does not characterize (represented as the line labeled "noise").

Alternatively, one might select from a group of models having similar performance, a model that is known to handle a specific process (deposition, sulfate chemistry, etc.). For testing certain specific processes, there may be very few databases suitable for use in an evaluation. This is not a desirable situation, but one often faces less evaluation data than is needed. Thus, part of model evaluation is an artful use of sparsely available field data. A corollary is to have a working knowledge of the field data that possibly could be used, and knowing the strengths and weaknesses of each field experiment's data.

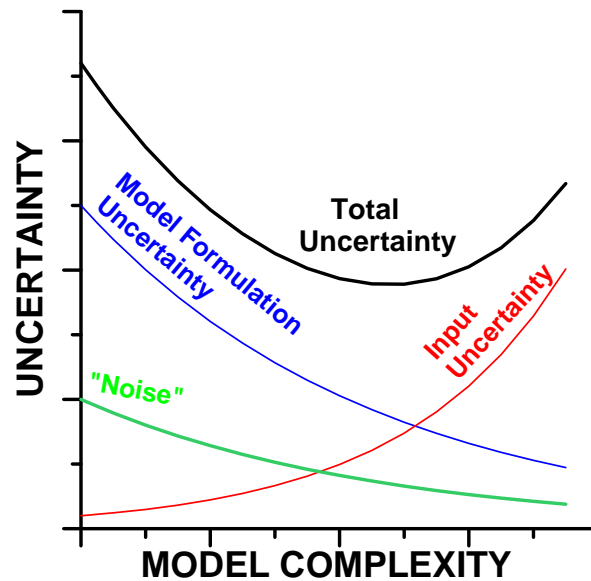


Figure 8. Illustration of relationship of model formulation uncertainty and input uncertainty, and the combined effect on total model uncertainty. [Adapted from Hanna (1989b). Reprinted with permission from the Butterworth-Heinemann Publishing Company].

7.1.3 Selecting Field Data for Use in the Model Evaluation

Model evaluation is mostly constrained by the amount and quality of available observational data for comparison with modeling results. The simulation models are capable of providing estimates of a larger set of conditions than for which there are observations. Furthermore, most models do not provide estimates of directly measurable quantities. For instance, even if a model provides an estimate of the concentration at a specific location, it is most likely an estimate of an ensemble average result which has an implied averaging time; for grid models, it represents an average over some volume of air (e.g., grid average). Hence, in establishing what abilities of the model are to be tested, one must first consider whether there are sufficient data available that can provide (either directly or through analysis) observations of what is being modeled.

Some fundamental understanding of the sampler limitations (operational range), background concentration values, and stochastic nature of the atmosphere is necessary for developing effective evaluation methodologies. All samplers have a detection threshold; below this threshold, observed values either are not provided, or are considered suspect. It is possible that there is a natural background of the tracer, which either has been subtracted from the observations, or needs to be considered in using the observations. Some samplers have a saturation point that limits the maximum value that can be observed. The user of concentration observations should address these limitations, as needed, in designing the evaluation procedures.

It is often worthwhile to perform a preliminary data set review in order to learn the “structure” of the data, and thereby identify appropriate strengths and limitations within a field experiment (U.S. Environmental Protection Agency QA/G-9, 1998). This review could include calculations of basic statistical quantities - number of observations and data capture, average, median (P50), range, standard deviation, coefficient of variation, P99, and P95 - and graphical representation of the data. The preliminary data set review should include considerations about quality of the data as well (for more details see Section 8.2).

We recommend viewing a model’s performance, in relative terms, in comparison to several available models over a variety of circumstances. As new field data becomes available, the selection of the best performing model may change, as the models may be validated for new conditions and in new circumstances. This argues for using a variety of field data sets to provide hope for developing robust conclusions as to which of several models can be currently deemed to perform best.

The following series of steps should be considered in choosing data sets for model evaluation studies:

- select field data sets appropriate for the applications for which the model is to be evaluated, taking the quality of the data into account
- note the model input values that require estimation for the selected data sets
- determine the required levels of temporal detail (e.g., minute-by-minute or hour-by-hour) and spatial detail (e.g., vertical or horizontal variation in the meteorological conditions) for the models to be evaluated, as well as the existence and variations of other sources of the same material within the modeling domain
- ensure that the samplers are sufficiently close to one another and in sufficient numbers for definition of the evaluation objectives
- find or collect appropriate data to estimate the model inputs and to compare with model outputs

7.2 Evaluation Strategy

7.2.1 Defining Evaluation Procedures

Performing a statistical model evaluation involves defining those evaluation objectives (features or characteristics) within the pattern of observed and modeled concentration values that are of interest to compare. As yet, no single feature or characteristic has been found, that can be defined within a concentration pattern, that can fully test a model’s performance. For instance, the maximum surface concentration may appear unbiased through a compensation of errors in estimating the lateral extent of the dispersing material and in estimating the vertical extent of the dispersing material. Considering that other biases may exist (e.g., in treatment of the chemical and removal processes during transport, in

estimating buoyant plume rise, in accounting for wind direction changes with height, in accounting for penetration of material into layers above the current mixing depth, and in systematic variation in all of these biases as a function of atmospheric stability), one can appreciate that there are many ways that a model can falsely give the appearance of good performance.

In principle, modeling diffusion involves characterizing the size and shape of the volume into which the material is dispersing as well as the distribution of the material within this volume. Volumes are three dimensional, so a model evaluation will be more complete if it tests the model's ability to characterize diffusion along more than one of these dimensions. In practice, there are more observations available on the downwind and crosswind concentration profiles of the dispersing material than are available on vertical concentration profiles of the dispersing material.

Developing evaluation objectives involves having a sense of what analytical procedures might be employed. This involves a combination of understanding the modeling assumptions, knowledge of possible comparison measures, and knowledge of the success of previous practices. For example, to assess the performance of the skill of a model to simulate the areal extent of a dispersing puff of tracer emissions from a comparison of isolated measurements with the estimated concentration pattern, Brost (1988) used evaluation objectives and procedures developed for measuring the skill of mesoscale meteorological models to forecast the areal extent of a tropical cyclone from a comparison of isolated pressure measurements to the estimated pressure pattern (Anthes, 1983). In particular, the surface area where concentrations were predicted to be above a certain threshold was compared to the surface area deduced from the available monitoring data. The lesson here is that evaluation objectives and procedures developed in other earth sciences can often be adapted for use in evaluating air dispersion models.

7.2.2 Developing Evaluation Procedures

Having selected evaluation objectives for comparison, the next step would be to define an evaluation procedure (or series of procedures), which defines how each evaluation objective will be derived from the available information. Development of statistical model evaluation procedures begins by providing technical definitions of the terminology used in the goal statement. In the following discussion, we use a plume dispersion model example, but, as discussed in Section 7.4, the thought process is also valid for grid models.

For instance, suppose that the evaluation goal is to test the ability of models to replicate the average centerline concentration as a function of transport downwind and as a function of atmospheric stability. The stated goal involves several items which require definition, namely: 1) what is an "average centerline

concentration”, 2) what is “transport downwind”, and 3) how will “stability” be defined?

What questions arise in defining the average centerline concentration? Given a sampling arc of concentration values, a decision is needed of whether the centerline concentration is the maximum value seen anywhere along the arc, or whether the centerline concentration is that seen near the center of mass of the observed lateral concentration distribution. If one chooses the latter concept, then a definition is needed of how “near” the center of mass one has to be, in order to be representative of a centerline concentration value. One might decide to select all values within a specific range (nearness to the center of mass). In such a case, either a definition or a procedure will be needed to define how this specific range will be determined. A decision will have to be made on the treatment of observed zero (and near measurement threshold) concentrations. Discarding such values is saying that low concentrations cannot occur near a plume’s center of mass, which is a dubious assumption. One might test to see if conclusions reached regarding “best performing model” are sensitive to the decision made on the treatment of near-zero concentrations.

What questions arise in defining “transport downwind”? During near-calm wind conditions when transport may have favored more than one direction over the sampling period, “downwind” is not well described by one direction. If plume models are being tested, one might exclude near-calm conditions since plume models are not meant to provide meaningful results during such conditions. If puff models or grid models are being tested, one might sort the near-calm cases into a special regime for analysis.

What questions arise in defining the “stability”? For surface releases, surface-layer Monin-Obukhov length, L , has been found to adequately define stability effects, whereas, for elevated releases, Z_i/L , where Z_i is the mixing depth, has been found to be a useful parameter for describing stability effects. Each model likely has its own meteorological processor. It is likely that different processors will have different values for L and Z_i for each of the evaluation cases. There is no one best way to deal with this problem. One solution might be sorting the data into regimes using each of the model’s input values, and seeing whether or not the previous conclusions as to the best performing model are affected.

What questions arise if one is grouping data together? If one is grouping data together for which the emission rates are different, one might choose to resolve this by normalizing the concentration values by dividing by the respective emission rates. Dividing by the emission rate requires either a constant emission rate over the entire release, or the downwind transport must be sufficiently obvious that one can compute an emission rate based on travel time that is appropriate for each downwind distance.

We discussed earlier the difficulty in properly characterizing the plume transport direction. A decision will have to be made as to how one will compare a feature

(or characteristic) in a concentration pattern, when uncertainties in transport direction are large. Will the observed and modeled patterns be shifted, and if so, in what manner?

Even defining the “observed” pattern is problematic, because one must decide where the “edge” of the pattern occurs. Will the reported concentration be used, even though it is near (or below) the measurement threshold? If one includes for analysis only concentration greater than zero, the testing may favor models that overestimate the extension in space and/or in time of the pollution episode. On the contrary, if the statistic includes all data (including zeros), the performance of a model, that in general underestimates the extension in space and/or in time of the pollution episode, is improved. Furthermore, one can imagine that adding a number of receptor points far from the area of interest of the pollutant, obviously measuring zero concentration, would artificially improve the performance of any model. An approach might consist of including all the points where either measured or simulated values give non-zero concentration. However, this criterion generates different ensembles of selected data that are dependent on each model’s results. To try to overcome the outlined difficulties, a filter like that used by Mosca et al. (1998) dealing with the ETEX (European Tracer EXperiment) can be applied. They selected pairs (C^o, C^s) showing a non-zero measured concentration that occur not earlier than two time intervals (6 h) before the model predicts the arrival of the cloud, and not later than two time intervals after the model predicts the departure of the cloud.

This discussion is not meant to be exhaustive, but to illustrate how the thought process might evolve. By defining terms, other questions arise and, when resolved, will eventually develop an analysis that will compute the evaluation objective from the available data. There likely is more than one answer to the questions that develop. This may cause different people to develop different objectives and procedures for the same goal. If the same set of models is chosen as the best performing, regardless of which path is chosen, one can likely be assured that the conclusions reached are robust.

7.3 Summarizing Evaluation Results

Summarizing model evaluation results usually involves both performance and diagnostic evaluations, and both are needed to establish credibility within the client and scientific community. Performance evaluations allow determination of relative model precision and accuracy in comparison with data and alternative modeling systems. Performance evaluations allow us to answer the question, how well does the model simulate the temporal and spatial patterns seen in the observations, and typically employ large spatial/temporal scale data sets (e.g., large field experiments, national data sets). A performance evaluation might involve a summary of one or more evaluation objectives over all conditions experienced within a particular field experiment. Performance evaluations can be done with or without stratification of the evaluation data into regimes; however,

we have recommended the use of modeled and observed regime averages, as this improves the likelihood of detecting bias in the models' ability to perform as intended. Diagnostic evaluations allow determination of the model precision and accuracy in simulating intermediate processes that affect the final results. Diagnostic evaluations allow us to answer the question, do we get the right answer for the right reason, and usually employ smaller spatial/temporal scale data sets (e.g., field studies). A diagnostic evaluation might involve comparison of observed and modeled values (evaluation objectives) as a function of one or more model input variables, with a focus on a particular process (e.g., plume rise, production of chemical species).

7.3.1 Detecting Trends in Modeling Bias

In this discussion, references to observed and modeled values refer to the observed and model evaluation objectives (e.g., regime averages). A plot of the observed and modeled values as a function of one of the model input parameters is a direct means for detecting model bias. Such comparisons have been recommended and employed in a variety of investigations (e.g., Fox 1981; Weil et al., 1992; and Hanna, 1993). In some cases, the comparison is the ratio formed by dividing the modeled value by the observed value, plotted as a function of one or more of the model input parameters. If the data have been stratified into regimes, one can also display the standard error estimates on the respective modeled and observed regime averages. If the respective averages are encompassed by the error bars (typically plus and minus two times the standard error estimates), one can assume that the differences are not significant (Irwin, 1998). As described by Hanna (1988), this is "seductive" inference. A more robust assessment of the significance of the differences would be to use the analysis discussed in Section 5.4.

7.3.2 Overall Summary of Performance

As an example of overall summary of performance, we will discuss a procedure constructed using the scheme introduced by Cox and Tikvart (1990) as a template. The design for statistically summarizing model performance over several regimes is envisioned as a five-step procedure.

1. Form a replicate sample using concurrent sampling of the observed and modeled values for each regime. Concurrent sampling associates results from all models with each observed value so that selection of an observed value automatically selects the corresponding estimates by all models.
2. Compute the average of observed and modeled values for each regime.
3. Compute the **NNR** using the computed regime averages, and store the value of the **NNR** computed for this pass of the bootstrap sampling.
4. Repeat steps 1 through 3 for all B bootstrap sampling passes.

5. Implement the procedure described in Section 5.4 to detect: a) which model has the lowest computed **NNR** value (call this the “base” model); b) which models have **NNR** values that are significantly different from the “base” model.

In the Cox and Tikvart (1990) analysis, the data were sorted into regimes (defined in terms of Pasquill stability category and low/high wind speed classes), and bootstrap resampling was used to develop standard error estimates on the comparisons. The performance measure was the **RHC** (computed from the raw observed cumulative frequency distribution), which is a comparison of the highest concentration values (maxima), which most models do not contain the physics to simulate. This procedure can be improved if the performance measure is the **NNR** computed from the modeled and observed regime averages of centerline concentration values.

The data demands are much greater for using regime averages than for using individual concentrations. Procedures that analyze groups (regimes) of data require intensive tracer field studies, with a dense receptor network, and many experiments. Whereas, Cox and Tikvart (1990) devised their analysis to make use of very sparse receptor networks having one or more years of sampling results. With dense receptor networks, attempts can be made to compare average modeled and “observed” centerline concentration values, but there are only a few of these experiments that have sufficient data to allow stratification of the data into regimes for analysis. With sparse receptor networks, there are more data for analysis, but there is insufficient information to define the observed maxima relative to the dispersing plume’s center of mass. Thus, there is uncertainty as to whether or not the observed maxima are representative of centerline concentration values. As discussed earlier, observed concentrations for inert gas can easily vary by a factor of two in magnitude about their respective ensemble averages. It is not obvious that the average of the N (say 25) observed maximum hourly concentration values (for a particular distance downwind and narrowly defined stability range) is the ensemble average centerline concentration the model is predicting. In fact, one might anticipate that the average of the N maximum concentration values is likely to be higher than the ensemble average of the centerline concentration. Following the testing procedure outlined by Cox and Tikvart (1990) may favor selection of poorly formed models that routinely underestimate the lateral diffusion (and thereby overestimate the plume centerline concentration). This in turn may bias the performance of such models in their ability to characterize concentration patterns for longer averaging times. We see evaluations, using field data from sparse networks, as a useful extension to further explore the performance of a well-formulated model for other environs and for use of the model for other purposes.

7.4 Evaluation of Eulerian Grid Models

For the most part, the preceding discussion and the examples provided were explicitly discussed from the viewpoint that the models being validated were for inert species (e.g., sulfur dioxide, primary emissions of particulate, carbon monoxide, etc.). In addition, the examples were discussed in terms of plume and puff modeling concepts. Evaluation of grid models is not governed by different principles. All of the philosophy and principles discussed in the previous sections apply equally to grid models.

The problems and uncertainties of characterizing the inert pollutant patterns and transport are just as severe for a grid model as for plume or puff models. In recent years, more attention has been given to assessing the performance of Eulerian grid models in characterizing concentrations of primary pollutants. Studies such as Kumar et al. (1994) suggest that large differences are seen when comparisons are made involving primary pollutants. Differences seen in comparisons involving primary pollutants are typically an order of magnitude larger than those seen for reactive (secondary formed) pollutants. The surface concentration values of primary pollutants are typically one of localized maxima or minima, surrounded by strong gradients. The observed pattern is one stochastic realization from some imperfectly defined ensemble. The simulation results are strongly dependent on proper characterization of the emissions, and on the sophistication brought to bear on the analysis and characterization of the time and space varying three-dimensional wind field. To further complicate the problem for grid models, the spatial and temporal characterization of the precursor emissions are highly uncertain (e.g., Hanna et al., 1998), as they are most often deduced from assumptions of land use, activity patterns, traffic flows, etc., rather than on direct measurements of emissions.

Unlike primary pollutants, the spatial pattern for surface concentration values of secondary pollutants (like ozone) is typically a broad flat maximum with weak spatial gradients. Localized areas with strong gradients in ozone concentration are found in the near vicinity of sources emitting large amounts of nitrogen oxides, which can locally deplete the ozone. Given a reasonably good precursor inventory, one would expect the ozone pattern to be well simulated. Sources with large emissions of nitrogen oxide should be easy to identify. As discussed in Hogrefe et al. (2001b), the production of ozone within and downwind of a large urban area correlates with the diurnal course of available sunlight and the precursor emissions are often correlated with the diurnal course of the surface temperatures, so the model estimates are forced somewhat to show good correlation in time.

Photochemical grid models should be validated using extensive and detailed field data (e.g., see Section 7.1.3) to determine if the models adequately represent the ozone processes. However, there are few (if any) field studies that have collected ozone data over an extensive length of time with a reasonably dense network of

receptors. Without such data, the formal statistical approaches where null hypotheses are constructed and tested are of little value.

Photochemical model intercomparison is of interest. In order to perform such intercomparisons, it is necessary to design the base runs for the various models so that they are as comparable as possible (i.e. using the same grid domain, the same emissions files, the same meteorological inputs, and the same initial and boundary conditions) while still preserving the advanced features available in the technical components of each of the models. In any case, if the database is not extensive and detailed, it is difficult to discern significant differences between models (e.g., Hanna et al., 1996).

It is also of interest to determine how well models simulate important variables, such as NO₂, VOC and other precursors, at the surface and aloft. Uncertainties involving the initial conditions and boundary conditions should be assessed, and it should be determined whether models perform better with initial and boundary conditions provided by larger scale models, or with values derived from intensive observations. It is of interest to know whether the models respond differently to changes in VOC and NO_x emissions, or whether the predictions are improved by using prognostic rather than diagnostic meteorological model input.

7.4.1 The “Threshold” Methods

Traditionally, Tesche et al. (1990) and the U.S. Environmental Protection Agency (1991) have recommended statistical analysis of the residuals to evaluate photochemical models. The final acceptance criteria are arbitrary, requiring the calculated model biases and variances to be within certain bounds or “thresholds”. For completeness, we shall review these methods in this section. However, as described by Arnold et al. (1998), recent analyses have shown that “acceptable” performance has been determined using these bias and threshold criteria in spite of the existence of fundamental errors in the model inputs of emissions and meteorology. Currently, an effort is underway to develop a new generation of model evaluation methods for assessing the performance of chemical grid models, and we have summarized some of the methods being examined in Section 7.4.2.

Hanna et al. (1996) photochemical model evaluation exercise was founded on two steps, suggested by Tesche et al. (1990) and U.S. Environmental Protection Agency (1991):

- the first step involved visual inspections of the various contour plots, vertical profiles, and time series, to look for obvious signs of correlation, trends, biases, and scatter
- the second step made use of the average normalized bias

$$\text{average normalized bias} = \overline{(C^s - C^o)} / C^o \quad (21)$$

and average normalized absolute bias

$$\text{average normalized absolute bias} = \overline{|C^s - C^o|} / C^o \quad (22)$$

It is worth noting that it is not possible to deal with zero observed concentrations using these indices. U.S. Environmental Protection Agency (1991) recommends the average normalized bias be less than about 10-15%, and the average normalized absolute bias be less than about 30-35%, for data sets in which the daily maximum ozone predictions and observations are paired in time and space.

Hanna et al. (1996) performed a statistical analysis concerning: 1) peak 1 h averaged ozone concentration for a given day anywhere in the domain; 2) 1 h averaged ozone concentrations larger than 60 ppb at all monitors and hours (i.e. paired in space and time).

Following U.S. Environmental Protection Agency (1991), U.S. Environmental Protection Agency (1996) presents a compilation of a series of photochemical model simulations and evaluation exercises conducted within the United States. These evaluations focused on the models' ability to predict the domain-wide peak ozone concentration, and the concentrations at all locations with observed ozone concentrations above 60 ppb. The performance measures used are:

- the normalized accuracy of domain-wide maximum 1-hour concentration unpaired in space and time

$$A_u = 100 \left(\frac{C^s \text{ domain-wide peak} - C^o \text{ domain-wide peak}}{C^o \text{ domain-wide peak}} \right) \quad (23)$$

- mean normalized bias of all simulated and observed concentration pairs with $C_i^o > 60$ ppb

$$NBIAS_{60} = \frac{100}{N} \sum_{i=1}^N \frac{(C_i^s - C_i^o)}{C_i^o} \quad (24)$$

where N includes all the simulated and observed concentration pairs with $C_i^o > 60$ ppb

- mean normalized error of all simulated and observed concentration pairs with $C_i^o > 60$ ppb

$$NERROR_{60} = \frac{100}{N} \sum_{i=1}^N \frac{|C_i^s - C_i^o|}{C_i^o} \quad (25)$$

Again following U.S. Environmental Protection Agency (1991), Lurmann and Kumar (1997) and SAIC (1997) presented an evaluation of the ability of the UAM-V model (Morris et al., 1993) to estimate 1-hour and 8-hour average ozone concentrations, respectively.

7.4.2 Advanced Methodologies

Data representativeness problem

Davis et al. (2000) deal with the problem of the data representativeness using spatial statistical techniques to compare observed ozone fields with the surface level ozone forecast fields from grid models. The 8-hour average daily observed ozone at the monitoring sites was interpolated to the model grid cells using a spatial statistical method, and then differences between the model output fields and the spatially interpolated observed fields were compared.

Scale analysis methodologies

Hogrefe et al. (2001a, 2001b) and Biswas et al. (2001) suggest that there are several shortcomings in using traditional performance measures, such as: if data assimilation is applied, the required statistical independence of the observed and simulated data sets is violated; traditional statistics provide little insight into the physical behavior of the model (i.e. they do not give any insight into the model's ability to reproduce the spatial and temporal correlation structures embedded in the observations on various scales). Therefore, to analyze meteorological input parameters, ozone predictions, predictions of ozone precursors, and predictions of ozone-precursors relationship, they introduced additional model evaluation methods based on the concept of scale analysis. To this end, a spectral decomposition technique is applied. It then becomes evident that model performance is time-scale specific and, therefore, the outcome of model evaluation on different time scales can be tied to the model formulation of the relevant processes on these time scales.

Time series of ozone observations contain fluctuations occurring on many different time scales (e.g., Vukovich, 1997; Sebald et al., 2000). Since ozone observations are taken at discrete intervals, the highest and lowest frequencies that can be estimated for any particular time series are determined by the sampling interval and the length of data record, respectively. The choice of the different frequency bands used by Hogrefe et al. (2001a, 2001b) and Biswas et al. (2001) was performed both on the recorded power spectrum and on *a priori* knowledge about different physical processes of interest to the simulation of air quality. They choose: the intra-day (ID) range (periods less than 12 hours), the diurnal (DU) range (periods of 24 hours), the synoptic (SY) range (periods of 2-21 days), and long-term baseline (BL) fluctuations (containing periods greater than 21 days).

The intra-day fluctuations are determined by the effects of turbulent horizontal and vertical mixing, and ozone response to fast-changing emissions patterns during traffic rush hours. Diurnal fluctuations are associated with the diurnal variation of the solar flux, and the resulting differences between the daytime photochemical production and the nighttime removal of ozone as well as the diurnal cycle of boundary layer evolution and decay. The variations of ozone on the synoptic scale are caused by changing meteorological conditions such as the presence of a nearly stagnant high pressure system or the passage of frontal systems. Fluctuations in baseline are caused by seasonal variations of the solar flux, changing large-scale flow patterns, and change in vegetation coverage and biogenic emissions.

Hogrefe et al. (2001a, 2001b) and Biswas et al. (2001) used the Kolmogorov-Zurbenko (KZ) filter (Zurbenko, 1986) because of its powerful separation characteristics, simplicity, and ability to handle missing data. This technique is described in more detail in Eskridge et al. (1997), Rao et al. (1997) and Hogrefe et al. (2000). In the following, we give only an outline.

The temporal components mentioned previously are estimated as follows:

$$ID(t) = \ln[O_3(t)] - KZ_{3,3} \{ \ln[O_3(t)] \} \quad (26)$$

$$DU(t) = KZ_{3,3} \{ \ln[O_3(t)] \} - KZ_{13,5} \{ \ln[O_3(t)] \} \quad (27)$$

$$SY(t) = KZ_{13,5} \{ \ln[O_3(t)] \} - KZ_{103,5} \{ \ln[O_3(t)] \} \quad (28)$$

$$BL(t) = KZ_{103,5} \{ \ln[O_3(t)] \} \quad (29)$$

where $KZ_{m,k}$ is the KZ filter with a window size of m hours and k iterations. Thus, by adding all components as defined in Equations (26), (27), (28), and (29), the ozone process is represented as

$$\ln[O_3(t)] = ID(t) + DU(t) + SY(t) + BL(t) \quad (30)$$

where the intra-day, diurnal and synoptic components are zero-mean processes. The actual ozone concentration in the ppb scale can be obtained as

$$O_3(t) \approx e^{ID(t)} \times e^{DU(t)} \times e^{SY(t)} \times e^{BL(t)} \quad (31)$$

As far as the model's ability to simulate ozone fields is concerned, Hogrefe et al. (2001b) first compared the relative importance of the individual components to the overall ozone process for both observations and model predictions. For this purpose, the variance of each component is computed and compared to the overall variance for both observations and model predictions. Then, to compare the

absolute amount of energy on different time scales between observation and model predictions, Hogrefe et al. (2001b) listed the ratios of the variances of the modeled to the observed time series for different time scales. They concluded that the models characterize best those variations having time scales longer than several days. They suggested that to increase confidence in the regulatory modeling process, the modeling period should be several synoptic cycles in duration rather than the 2-3 days of a single ozone pollution episode.

Process oriented methodologies

As we have already said, the evaluation goal may concern the overall model (integrated), or can be process oriented (diagnostic). In this case, one will have to make a selection of the model characteristics/modules to be validated. Several authors (e.g., Hass et al., 1997; Dennis et al., 1999; Tonnesen and Dennis, 2000a and 2000b; Luecken et al., 1999) have been asking that model evaluation of complex grid models be process oriented. In other words, they want to know if the model is describing how things happen correctly without too much emphasis on whether the magnitude of the changes predicted are correct. Therefore, they do not believe that a photochemical model has been fully evaluated if comparisons are only observed versus predicted ozone. They are worried that a model can give the correct result for the wrong reason. So, they want the evaluation to “look inside” the model, and to analyze modules to see if the model has modeled the right causes for the effects seen.

7.4.3 Final Remarks

It is concluded that validating the performance of Eulerian grid models is not philosophically different than validating the performance of plume or puff models. The pattern for inert species is just as difficult to characterize for any of the various model types. To validate performance for characterizing the inert species pattern, the same thought process would be followed, regardless of the model being validated. For reactive species, the pattern appears to have fewer anomalies, but characterization of the chemistry, initial and boundary conditions, and characterization of the precursor emission rates are very uncertain. The logistics of running several Eulerian grid models for the same field studies are found to have their own sets of problems and constraints. Furthermore, field studies of reactive species rarely provide a time series long enough for developing confidence bounds to formally test whether differences seen in comparing different models is significant.

8 Model Quality Assurance

Confidence in using air quality models in scientific studies, as well as in operational decision-making applications is founded on a program of quality assurance. The definition of quality assurance can be inferred from different sources. From ISO 14000 (International Standards on Environmental

Management), the definition of quality assurance is all those planned and systematic actions necessary to provide adequate confidence that a product or service will satisfy given requirements for quality. From U.S. Environmental Protection Agency QA/G-5 (1998) and EUROTRAC (<http://www.gsf.de/eurotrac/organisation/g-qa-qc.htm>), quality assurance is defined as an integrated system of management activities involving planning, implementation, assessment, reporting, and quality improvement to ensure that a process, item or service is of the type and quality needed and expected by the user.

8.1 Overview of Model Quality Assurance

Model quality assurance can be envisioned as documentation of the following items (e.g., Borrego and Tchepel, 1998; Borrego et al., 2001b): definition of purpose and scope of the modeling, model description, database description, selection of performance measures, model evaluation, scientific peer review, and user oriented assessment. Therefore, model evaluation (see Section 6), which in turn includes statistical model evaluation (see Section 7), is a basic component of model quality assurance.

- **Definition of purpose and scope of the modeling.**
 - Identification of the type of model under evaluation: long range transport models, photochemical models at continental scale, photochemical models at urban scale (without obstacles), street canyon models (urban scale with obstacles), stack models, concentration fluctuation models, dense gas models, indoor pollution, and other models⁹.
 - Identification of the purpose of the modeling: air quality assessment (determine impact on human health, ecosystems), regulatory purpose (e.g., calculation of a minimum stack height for new installation), policy support (e.g., scenario studies on effect of emission abatement measures), emergency planning (estimation of hazardous gas concentration), public information (e.g., online information on the possible occurrence of smog episodes), and scientific research (better understanding of physical/chemical processes involving air pollution).
- **Model description.** Availability of extended description of the model is important for quality assurance procedures. The model description should include a detailed description of the physics and chemistry contained in the model. The description should include a summary of the model characteristics (e.g., model approximations, time and space resolution, modeling scale). Furthermore, it should contain details of the model such as: model name, version number, date of first release, area of application,

⁹ For example, mesoscale flow models (that are the necessary support for dispersion in complex terrain), chemical modules, chemical heterogeneous reactions, cloud formation models, models for aerosol transformation and growth, model for turbulence, etc. Some of these models are for the purposes mentioned, others are only used to understand physical phenomena and eventually are inserted as sub-models in some of the mentioned models.

originating organization, source of model (from the originators, through third parties, or in particular whether it is an improved version of an earlier model), model type, hardware requirements, software requirements, and references.

- **Database description.** Database description first identifies the data used to construct the model parameters at the development stage. Then it identifies the data used during the process of both “model algorithm verification” and “model evaluation”. It contains details as data ownership/accessibility and origin of the data (from analytic results, simulated by higher-order models, laboratory experiments, field experiments, incident reports). Database selection includes consideration of factors such as: data quality assurance, completeness, appropriateness, model features/parameters covered, data uncertainties (which concern both data used as model inputs, e.g., emission and meteorological data, and data used to make a comparison against model outputs, e.g., pollutant concentrations), and data representativeness.
- **Selection of performance measures.** This would include selection of evaluation tools (quantitative or/and qualitative) as statistical indices and graphical methodologies to compare model outputs with observed values. Performance measures reflect the ability of a model to simulate real world phenomena; it helps in understanding a model’s limitations and provides support for model inter-comparisons.
- **Model evaluation.** Model evaluation is the overall system of procedures designed to measure the model performance, and includes: model algorithm verification, sensitivity analysis, uncertainty analysis, statistical model evaluation, and model inter-comparisons (see Section 6).
- **Scientific peer review.** Scientific peer review includes: an assessment of the appropriateness of the scientific content; the limits of applicability of the model; limitations and advantages of the model; and possible improvements. A further objective of a scientific peer review is to guarantee that all steps of model evaluation were implemented in agreement with a model’s requirements. For example, good models will likely exhibit poor correlation with observations if applied in a manner inconsistent with their physics assumptions. For instance, the modeled concentration values from a mesoscale photochemical model will compare poorly with observations from an urban station directly affected by traffic emissions. Scientific peer review may involve expert external analysis.
- **User oriented assessment.** User oriented assessment provides information on: availability of the model, associated documentation, installation procedures, user interface, ease of use, guidance in selecting model options and input data, limitations on the applicability of the model, explanations concerning the output, clarity of warnings and error messages, computational costs, and possible improvements.

8.2 Related Topics

The following items describe some topics related to model quality assurance.

- **Quality assurance of emission inventories.** Harmonization of the methodology for the compilation of emission inventories is needed. Furthermore, an effort should be focused on developing objective estimates of the uncertainties in emission inventories.
- **Data quality assessment and data quality objectives.** Data quality assessment (DQA) is the scientific and statistical evaluation of data to determine if the data obtained from environmental data operations are of the right type, quality and quantity to support their intended use (U.S. Environmental Protection Agency QA/G-9, 1998). A data quality objective (DQO) is a range of acceptability of measured data for a specific application. The definition of DQO depends on the project scientific objectives and on intended use of the data. Different monitoring programs have distinct DQOs. To estimate the quality of measurements, the data quality indicators (DQI) are used. DQI are (Borrego et al., 2001a): bias (systematic error); precision (random error); accuracy (combination of systematic and random errors); and completeness (percent of valid measurements). The uncertainties of measurements have to be reported and considered in data application.
- **Model calibration.** Model calibration is a procedure used to make, at the model development stage, estimates of parameters within the model equations, which best fit the general model structure to a specific observed data set. Note that successful model calibration only indicates that the structure of the model includes the important variables that influence behavior (or correlated well with variables that influence behavior) under the conditions prevailing for the calibration data set. Model calibration does not ensure that the model will predict well under conditions that are quite different than were used in the calibration. For this reason, as new data become available, models almost invariably need additional calibration. When updating calibrated values within a model, one should consider previously used data, as well as the newly acquired data. Finally, use of any model beyond its proven range of application will involve expert judgment, knowledge of the physical processes being modeled, and an awareness of the sensitivity of the model's output to changes in input.
- **Data assimilation.** Data assimilation is a numerical technique, which makes it possible to combine model results and observations in one integrated system. Observations are input to the numerical system, which consists of the model combined with the data assimilation technique. To several parameters (either internal model parameters or input data), noise factors are added. The system will attempt to minimize the discrepancy between calculated concentrations and observations. An essential consideration in this process is

to balance the “accepted range of disparity” (noise factors) with the data representativeness of the observations in time and space.

9 Guidelines for Model Evaluation: Towards Harmonization in Model Evaluation Methodology

Although presently the evaluation methodology is generally left to the user to define, it is important to realize that efforts are underway to standardize evaluation methodologies. This would allow comparison of model evaluation results performed by different users. It would also provide a standard manner for gaining acceptance of models for various operational uses. As experience increases, it is hoped that consensus will be reached in certain evaluation goals, evaluation objectives and associated evaluation methodologies, and data sets to be employed. The ultimate goal will be to define a standard evaluation methodology for each evaluation goal.

9.1 The USA Effort

Within the United States, the emphasis has been on the development, evaluation and application of air quality simulation models that allow development of air quality management plans to achieve defined national air quality goals. These plans involve development of emission control strategies sometimes for individual sources (“primary” impacts associated with pollutants emitted directly into the atmosphere) and sometimes for classes of sources (“secondary” impacts associated with pollutants formed during transport). Part of the decision on which model to select is dictated by ensuring that the appropriate physical processes are addressed by the model. However, another part of the decision in model selection is the recognition that every model is a compromise in that not all processes are included or else the computational demands would become excessive. Hence, model selection often involves expert judgment based on actual experience in the use and application of the various models available.

The American Society for Testing and Materials (ASTM) has published a “Standard guide for statistical evaluation of atmospheric dispersion models” (ASTM D6589). This guide provides a general philosophy that can be used to design statistical model evaluation procedures, either for the comparison of modeled concentrations with observations, or to assess one model’s performance relative to other candidate models.

Founded in 1995, NARSTO¹⁰ (<http://www.cgenv.com/Narsto/>) is a public/private partnership, whose membership spans the government, utilities, industry, and academy throughout Mexico, the United States, and Canada. Its primary mission is to coordinate and enhance policy-relevant scientific research, and assess

¹⁰ Formerly an acronym for “North American Research Strategy for Tropospheric Ozone”.

tropospheric pollution behavior; its activities provide input for science-based decision-making and determination of workable, efficient, and effective strategies for local and regional air-pollution management. NARSTO has an ongoing activity to evaluate regional air-pollution models by comparing output from multiple models as well as by testing against data obtained from NARSTO field intensives.

9.2 The European Effort

During the last few years in Europe, many insights have been given about the need to improve model evaluation quality. Excellent examples are the ETEX campaigns on the real-time assessment of the long-range atmospheric dispersion of harmful releases (Mosca et al., 1998, <http://rem.jrc.cec.eu.int/etex/>) and the RTMOD exercises (Bellasio et al., 1998, <http://rtmod.jrc.it/rtmod/>). The need to understand the differences between operational uses of air quality models and the desire to reduce the disparity between different models when applied to the same problem was highlighted in recent International Conferences. These conferences (there have been seven so far) were organized with the aim of “Harmonization within Atmospheric Dispersion Modeling for Regulatory Purposes” (<http://www.harmono.org/>), and attracted an increasingly large scientific participation (Olesen, 1996, 2001). A central activity of the "Harmonization" initiative is the distribution of a Model Validation Kit¹¹. The Model Validation Kit is a collection of three experimental data sets accompanied by software for model evaluation. It is a practical tool meant to serve as a common frame of reference for modelers. The experience gained from these conferences together with that in the field of long-range dispersion for accidental releases points in the direction of inter-comparing mesoscale flow models. This is the content of MESOCOM (<http://java.ei.jrc.it/Projects/MESOCOM>), which is currently ongoing. The EUROTRAC-2 subprojects GLOREAM¹² and SATURN (<http://aix.meng.auth.gr/saturn/>) are aimed at the formulation of suitable evaluation methodologies for regional and urban scale air pollution models, respectively. The German organization BWPLUS (<http://bwplus.fzk.de/>) is presently promoting an inter-comparison of methods for the prediction of the air pollutant concentrations in a specific street canyon using usually available input data.

Furthermore, it is useful to recall the Data Sets for Atmospheric Modeling (DAM) initiative of the JRC (<http://java.ei.jrc.it/Projects/DAM>). DAM's objective is to facilitate the accessibility of datasets, presently available to the Scientific Community for atmospheric model evaluation, to any model developer or user that intends to validate his/her modeling tool. DAM is intended as an interface between modelers and the information available through existing web sites or other contact points.

¹¹ http://www.dmu.dk/atmosphericenvironment/Harmoni/M_V_KIT.htm.

¹² <http://www.dmu.dk/AtmosphericEnvironment/gloream/>.

Acknowledgements

Prof. Carlos Borrego, Prof. Peter Builtjes, Dr. Ana Cristina Carvalho, Dr. Jerry Davis, Dr. Giovanni Graziani, Mr. Ariel Stein, Dr. Oxana Tchepel, Dr. Steve Warner, and WIT press (Southampton) are gratefully acknowledged. Dr. Canepa's contribution to this work was supported by the MURST COFIN 99 project ACME CUE, and the INFM PA project GEPAGG01. The information in this document has been funded in part by the United States Environment Protection Agency under an Interagency Agreement (139-384-83) to the National Oceanic and Atmospheric Administration. It has been subjected to Agency review for approval for publication. Mention of trade names or commercial products does not constitute endorsement or recommendation for use.

References

- Alcamo, J., and J. Bartnicki (1987): A framework for error analysis of a long-range transport model with emphasis on parameter uncertainty. *Atmos. Environ.*, **21**(10): 2121-2131.
- Anthes, R.A. (1983): Review - regional models of the atmosphere in middle latitudes. *Monthly Weather Review*, **111**: 1306-1335.
- Arnold, J.R., Dennis, R.L., and Tonnesen, G.S., (1998): Advanced techniques for evaluating Eulerian air quality models: background and methodology. Proceeding of the 10th Joint Conference on the Application of Air Pollution Meteorology with the A&WMA, Phoenix, AZ., pp. 1-5.
- Barad, M.L., Editor (1958): Project Prairie Grass, A Field Program in Diffusion. Geophysical Research Paper, No. 59, Vol I and II, Report AFCRC-TR-58-235, Air Force Cambridge Research Center, 439 pp.
- Bellasio, R., R. Bianconi, G. Graziani, and S. Mosca (1998): RTMOD: An Internet based system to analyze the predictions of long-range atmospheric dispersion models. *Computer Geosciences* **25**: 819-833.
- Biswas, J., S.T. Rao, P. Kasibhatla, W. Hao, G. Sistla, R. Mathur, and J. McHenry (2001): Evaluating the performance of regional-scale photochemical modeling systems: part III – precursor predictions and ozone-precursor relationship. *Atmos. Environ.*, **35**: 6129-6149.
- Bornstein, R.D., and S.F. Anderson (1979): A survey of statistical techniques used in validation studies of air pollution prediction models. Technical Report No. 23, Stanford University, Stanford, California.
- Borrego, C., and O. Tchepel (1998): Quality assurance/quality control in SATURN: a first approach. Hamburg Workshop, August 1998.
- Borrego, C., N. Barros and O. Tchepel (2001a): Data Quality Assessment: Lisbon experimental field campaign LisbEx 96. Transport and Chemical Transformation in the Troposphere. Proceedings from the EUROTRAC-2 Symposium 2000, 27-31 March 2000, Garmisch-Partenkirchen, Germany. P.M. Midgley, M. Reuther, M. Williams (Eds.). Springer-Verlag Berlin, Heidelberg, Germany, on CD-ROM.
- Borrego, C., O. Tchepel and A.C. Carvalho (2001b): Model Quality Assurance. Transport and Chemical Transformation in the Troposphere. Proceedings from the EUROTRAC-2 Symposium 2000, 27-31 March 2000, Garmisch-Partenkirchen, Germany. P.M. Midgley, M. Reuther, M. Williams (Eds.). Springer-Verlag Berlin, Heidelberg, Germany, pp. 21-26.

- Brandt, J., A. Bastrup-Birk, J.H. Christensen, T. Mikkelsen, S. Thykier-Nielsen, and Z. Zlatev (1998): Testing the importance of accurate meteorological input fields and parameterizations in atmospheric transport modeling using DREAM – validation against ETEX-1. *Atmos. Environ.*, **32**(24): 4167-4186.
- Brost, R.A., P.L. Haagensohn, and Y.H. Kuo (1988): The effect of diffusion on tracer puffs simulated by a regional scale Eulerian model. *Journal of Geophysical Research*, **93**(D3): 2389-2404.
- Brusasca, G., G. Tinarelli, and D. Anfossi (1989): Comparison between the results of a Monte Carlo atmospheric diffusion model and tracer experiments. *Atmos. Environ.*, **23**(6): 1263-1280.
- Canepa, E., and F. Modesti (1997): Considerations about statistical indices used in the evaluation of air quality models. Air Pollution 97, 16-18 September 1997, Bologna, Italy, *Air Pollution V*, pp. 607-616, H. Power, T. Tirabassi and C.A. Brebbia editors, Computational Mechanics Publications, Southampton, UK.
- Canepa, E., and P.J.H. Bultjes (1999): Methodology of model testing and application to dispersion simulation above complex terrain, *Conference Proceedings on CD-ROM, 6th International Conference on Harmonization within Atmospheric Dispersion Modeling for Regulatory Purposes*, 11-14 October 1999, INSA de Rouen, France. [to be published in *Int. J. Environ. Pollut.*]
- Carhart, R.A., A.J. Policastro, M. Wastag, and L. Coke (1989): Evaluation of eight short-term long-range transport models using field data. *Atmos. Environ.*, **23**(1): 85-105.
- Carruthers, D.J., A.M. Mckeown, D.J. Hall, and S. Porter (1999): Validation of ADMS against wind tunnel data of dispersion from chemical warehouse fires. *Atmos. Environ.*, **33**: 1937-1953.
- Clarke, J.F. (1964): A Simple Diffusion Model for Calculating Point Concentrations from Multiple Sources. *Journal of the Air Pollution Control Association*, **14**(9): 347-352.
- Cole, S.T., and P.J. Wicks, Editors (1995): Model Evaluation Group: Report of the Second Open Meeting. EUR 15990 EN, European Commission, Directorate-General XII, Environmental Research Programme, L-2920 Luxembourg, 77 pp.
- Cox, W.M., and J.A. Tikvart (1990): A statistical procedure for determining the best performing air quality simulation model. *Atmos. Environ.*, **24A**(9):2387-2395.
- Cox, R.M., J. Sontowski, R.N. Fry Jr., C.M. Dougherty, and T.J. Smith (1998): Wind and diffusion modeling for complex terrain. *J. Appl. Meteor.*, **37**: 996-1009.
- Davis, J.M., D. Nychka and B. Bailey (2000): A comparison of regional oxidant model (ROM) output with observed ozone data. *Atmos. Environ.*, **34**: 2413-2423.
- Dekker, C.M., A. Groenendijk, C.J. Sliggers, and G.K. Verboom (1990): Quality Criteria for Models to Calculate Air Pollution. Lucht (Air) 90, Ministry of Housing, Physical Planning and Environment, Postbus 450, 2260 MB Leidschendam, The Netherlands, 52 pp.
- Dennis R.L. (1986): Issue, design and interpretation of performance evaluations: ensuring the emperor has clothes. *Air Pollution Modeling and Its Application V*, edited by DeWispelaere V.C., Schiermeier F.A. and Gillani N.V., pp. 411-424, Plenum Press, New York.
- Dennis, R.L., Arnold, J.R., Tonnesen, G.S., Y. Li (1999): A new response surface approach for interpreting Eulerian air quality model sensitivities. *Computer Physics Communications*, **117**: 99-112.

Desiato, F. (1991): A dispersion model evaluation study for real-time application in complex terrain. *J. Appl. Meteor.*, **30**: 1207-1219.

Efron, B., and R.J. Tibshirani (1993): *An Introduction to the Bootstrap*. Monographs on Statistics and Applied Probability 57, Chapman & Hall, New York, 1993, 436 pp.

Eskridge, R.E., J.Y. Ku, S.T. Rao, P.S. Porter, and I.G. Zurbenko (1997): Separating different scales of motion in time series of meteorological variables. *Bull. Amer. Meteor. Soc.*, **78**: 1473-1483.

Fox, D.G. (1981): Judging air quality model performance: a summary of the AMS workshop on dispersion model performance. *Bull. Amer. Meteor. Soc.*, **62**: 599-609.

Fox, D.G. (1984): Uncertainty in air quality modeling. *Bull. Amer. Meteor. Soc.*, **65**(1): 27-36.

Graziani G., W. Klung and S. Mosca (1998): Real-time long-range dispersion model evaluation of ETEX first release, EUR 17754 EN, ISBN 92-828-3657-6.

Gronski, K.E., S.E. Walker, and F. Gram (1993): Evaluation of a model for hourly spatial concentration distributions. *Atmos. Environ.*, **27B**(1):105-120.

Hanna, S.R. (1971): A simple method of calculating dispersion from urban area sources. *Journal of the Air Pollution Control Association*, **21**(22): 774-777.

Hanna, S.R. (1988): Air quality model evaluation and uncertainty. *Journal of the Air Pollution Control Association*, **38**: 406-412.

Hanna, S.R. (1989a): Confidence limits for air quality model evaluation as estimated by bootstrap and jackknife resampling methods. *Atmos. Environ.*, **23**(6): 1385-1398.

Hanna, S.R. (1989b): Plume dispersion and concentration fluctuations in the atmosphere. P.N. Cheremisinoff (Editor). *Encyclopedia of Environmental Control Technology, Volume 2, Air Pollution Control*. Gulf Publishing Company, Houston, TX, pp. 547-582.

Hanna, S.R. (1993): Uncertainties in air quality model predictions. *Boundary-Layer Met.* **62**: 3-20.

Hanna, S.R., and R.J. Paine (1989): Hybrid Plume Dispersion Model (HPDM) development and evaluation. *J. Appl. Meteor.*, **28**: 206-224.

Hanna, S.R., and J.C. Chang (1993): Hybrid plume dispersion model (HPDM) improvements and testing at three field sites. *Atmos. Environ.*, **27A**(9): 1491-1508.

Hanna, S.R., G.A. Briggs, and R.P. Hosker (1982): *Handbook on Atmospheric Diffusion*. DOE/TIC-11223 (NTIS Document DE82002045), National Technical Information Service, U.S. Department of Commerce, Springfield, VA, 102 pp.

Hanna, S.R., J.C. Chang, and D.G. Strimaitis (1993): Hazardous gas model evaluation with field observation. *Atmos. Environ.*, **27A**(15): 2265-2285.

Hanna, S.R., G.E. Moore, and M.E. Fernau (1996): Evaluation of photochemical grid models (UAM-IV, UAM-V, and the ROM/UAM-IV couple) using data from the Lake Michigan Ozone Study (LMOS). *Atmos. Environ.*, **30**(19): 3265-3279.

Hanna, S.R., J.C. Chang, and M.E. Fernau (1998): Monte Carlo Estimates of Uncertainties in Predictions by a Photochemical Grid Model (UAM-IV) Due to Uncertainties in Input Variables. *Atmos. Environ.*, **32**: 3617-3628.

Hass, H., P.J.H. Builtjes, D. Simpson, and R. Stern. (1997): Comparison of model results obtained with several European regional air quality models. *Atmos. Environ.*, **31**(19): 3259-3279.

Haugen, D.A. Editor (1959): Project Prairie Grass, A Field Program in Diffusion. Geophysical Research Paper, No. 59, Vol III, Report AFCRC-TR-58-235, Air Force Cambridge Research Center, 673 pp.

Heidam, N.Z. (1987): Bootstrap estimates of factor model variability. *Atmos. Environ.*, **21**(5): 1203-1217.

Hilst, G.R. (1970): Sensitivities of Air Quality Prediction to Input Errors and Uncertainties. Proceedings of Symposium on Multiple-Source Urban Diffusion Models, Air Pollution Control Office Publication No. AP-86, U.S. Environmental Protection Agency, Research Triangle Park, NC, Chap. 8, 41 pp.

Hogrefe, C., S.T. Rao, I.G. Zurbenko, and P.S. Porter (2000): Interpreting the information in ozone observation and model predictions relevant to regulatory policies in the Eastern United States. *Bull. Amer. Meteor. Soc.*, **81**: 2083-2106.

Hogrefe, C., S.T. Rao, P. Kasibhatla, G. Kallos, G.J. Tremback, W. Hao, D. Olerud, A. Xiu, J. McHenry, and K. Alapaty (2001a): Evaluating the performance of regional-scale photochemical modeling systems: part I – meteorological predictions. *Atmos. Environ.*, **35**: 4159-4174.

Hogrefe, C., S.T. Rao, P. Kasibhatla, W. Hao, G. Sistla, R. Mathur, and J. McHenry (2001b): Evaluating the performance of regional-scale photochemical modeling systems: part II – ozone predictions. *Atmos. Environ.*, **35**: 4175-4188.

Irwin, J.S., (1998): "Statistical evaluation of atmospheric dispersion models," 5-th International Conference on Harmonization with Atmospheric Dispersion Modeling for Regulatory Purposes, May 18-21, 1998, Rhodes, Greece (Preprints pp. 46-53, to be published in International Journal of Environment and Pollution), 8 pp.

Irwin, J.S. (1999): Effects of concentration fluctuations on statistical evaluation of centerline concentration estimates by atmospheric dispersion models, *Conference Proceedings on CD-ROM*, 6th International Conference on Harmonization within Atmospheric Dispersion Modeling for Regulatory Purposes, 11-14 October 1999, INSA de Rouen, France. [to be published in *Int. J. Environ. Pollut.*]

Irwin, J.S. (2000): Modeling Air Quality Pollutant Impacts. Air Quality Management In Urban Areas In the Light Of EU Legislation, November 6-7, Krakow, Poland. (EURASAP Newsletter, Number 40, pages 2-28, ISSN-1026-2172, available at <http://www.meteo.bg/EURASAP/Newsletter.html>).

Irwin, J.S. and M.E. Smith (1984): Potentially Useful Additions to the Rural Model Performance Evaluation, Bulletin American Meteorological Society, Vol 65, pp. 559-568.

Irwin, J.S., and R.F. Lee (1997): Comparative evaluation of two air quality models: within-regime evaluation statistic. *Int. J. Environ. Pollut.*, **8**(3-6): 346-355.

Irwin, J.S., S.T. Rao, W.B. Peterson, and D.B. Turner (1987): Relating error bounds for maximum concentration estimates to diffusion meteorology uncertainty. *Atmos. Environ.*, **21**(9): 1927-1937.

Kumar, N., A.G. Russel, T.W. Tesche, and D.E. McNally (1994): Evaluation of CALGRID using two different ozone episodes and comparison to UAM results. *Atmos. Environ.*, **28**(17): 2823-2845.

Kumar Yadav, A., and M. Sharan (1996): Statistical evaluation of sigma schemes for estimating dispersion in low wind conditions. *Atmos. Environ.*, **30**(14): 2595-2606.

Lanzani, G., and M. Tamponi (1995): A microscale Lagrangian particle model for the dispersion of primary pollutants in a street canyon: sensitivity analysis and first validation trials. *Atmos. Environ.*, **29**(23): 3465-3475.

Larsen, R.I. (1969): A new mathematical model of air pollution concentration averaging time and frequency. *Journal of the Air Pollution Control Association*, **19**: 24-30.

Longhetto, A., Editor (1980): *Atmospheric Planetary Boundary Layer Physics*. Elsevier, New York.

Luecken, D.J, Tonnesen, G.S., and Sickles, J.E., II (199): Differences in NO_x speciation predicted by three photochemical mechanisms. *Atmos. Environ.*, (33): 1073-1084.

Luhar, A.K., and K.S. Rao (1994): Lagrangian stochastic dispersion model simulations of tracer data in nocturnal flows over complex terrain. *Atmos. Environ.*, **28**(21): 3417-3431.

Lumley, J.L., and H.A. Panofsky (1964): *The structure of atmospheric turbulence*. Wiley Interscience, New York, 239 pp.

Lurmann, F.W., and N. Kumar (1997): Evaluation of the UAM-V model performance in OTAG simulations phase I: summary of performance against surface observations. Final Report STI-996120-1605-FR, Sonoma Technology, Inc., Santa Rosa, CA. Prepared for: Science Applications International Corporation, McClean, VA.

Martin, D.O. (1971): An Urban Diffusion Model for Estimating Long Term Average Values of Air Quality. *Journal of the Air Pollution Control Association*, **21**(1): 16-19.

Model Evaluation Group (1994a): Guidelines for model developers. Can be requested from Dr. S. Cole, DG XII/D1, Rue de la Loi 200, B-1049 Belgium. Fax +32 2 296 3024.

Model Evaluation Group (1994b): Model Evaluation Protocol. Can be requested from Dr. S. Cole, DG XII/D1, Rue de la Loi 200, B-1049 Belgium. Fax +32 2 296 3024.

Moore, G.E., M.K. Liu, and R.J. Londergan (1985): Diagnostic validation of Gaussian and first-order closure plume models at a moderately complex terrain site. Systems Applications, Inc., Final Report EA-3760, San Rafael, California.

Morris, R.E., M. Yocke and T.C. Myers (1993): Application of the nested grid urban airshed model to the Lake Michigan region. Presented at AW&MA International Conference and Course, Tropospheric Ozone: Nonattainment and Design Value Issues, 27-30 October, Boston, Massachusetts. (UAM-V is available at: <http://uamv.saintl.com/>).

Mosca, S., G. Graziani, W. Klug, R. Bellasio, and R. Bianconi (1998): A statistical methodology for the evaluation of long-range dispersion models: an application to the ETEX exercise. *Atmos. Environ.*, **32**(24): 4307-4324.

Okamoto, S., H. Ohnishi, T. Yamada, T. Mikami, S. Momose, H. Shinji, and T. Itohiya (1999): A model for simulating atmospheric dispersion in a low-wind condition. *Conference Proceedings on CD-ROM*, 6th International Conference on Harmonization within Atmospheric Dispersion

Modeling for Regulatory Purposes, 11-14 October 1999, INSA de Rouen, France. [to be published in *Int. J. Environ. Pollut.*]

Olesen, H.R., (1995): The model validation exercise at Mol: overview of results. Workshop on Operational Short-range Atmospheric Dispersion Models for Environmental Impact Assessment in Europe, Mol, November 1994, published in: *Int. J. Environ. Pollut.*, **5**(4-6): 761-784.

Olesen, H.R. (1996): Toward the establishment of a common framework for model evaluation. In: Air Pollution Modeling and Its Application XI, pp. 519-528. Edited by S-E. Gryning and F. Schiermeier, Plenum Press, New York.

Olesen, H.R. (2001): Ten years of harmonization: past, present, and future. Presentation at the 7th International conference on Harmonisation within Atmospheric Dispersion Modelling for Regulatory Purposes, May, 2001, Belgirate, Italy. 10 pp.
(<http://www.dmu.dk/atmosphericenvironment/harmoni.htm>)

Oreskes, N., K. Shrader-Frechette and K. Belitz (1994): Verification, validation, and confirmation of numerical models in the earth sciences. *Science*, **263**: 641-646.

Pasquill, F. (1961): The estimation of the dispersion of windborne material. *Meteorological Magazine*, **90**: 33-49.

Poli, A.A., and M.C. Cirillo (1993): On the use of the normalized mean square error in evaluating dispersion model performance. *Atmos. Environ.*, **15**: 2427-2434.

Randerson, D., Editor (1984): Atmospheric Science and Power Production. DOE/TIC-27601 (NTIS Document DE84005177). National Technical Information Service, U.S. Department of Commerce, Springfield, VA, 850 pp.

Rao, S.T., I.J. Zurbenko, R. Neagu, P.S. Porter, J.Y. Ku, and R.F. Henry (1997): Space and time scales in ambient ozone data. *Bull. Amer. Meteor. Soc.*, **78**: 2153-2166.

Reynolds, S.D., C. Seigneur, T.E. Stoeckenius, G.E. Moore, R.G. Johnson, and R.J. Londergan (1984): Operational validation of Gaussian plume models at a plain site. System Applications, Inc., Final Report EA-3076, San Rafael, California.

Reynolds, S.D., T.C. Myers, J.E. Langstaff, M.K. Liu, G.E. Moore, and R.E. Morris (1985): Operational validation of Gaussian and first-order closure plume models at a moderately complex terrain site. System Application, Inc., Final Report EA-3759, San Rafael, California.

Ross, D.G., and D.G. Fox (1991): Evaluation of an air pollution analysis system for complex terrain. *J. Appl. Meteor.*, **30**(7): 909-923.

Ruff, R.E., K.C. Nitz, F.L. Ludwig, C.M. Bhumralkar, J.D. Shannon, C.M. Sheih, I.Y. Lee, R. Kumar, and D.J. McNaughton (1984): Regional air quality model assessment and evaluation. SRI International Final Report EA-3671, Menlo Park, California.

SAIC (1997): Summary of the UAM-V model performance in OTAG simulations phase II: 8-hour performance statistics. Science Applications International Corporation, Final Report, Raleigh, North Carolina.

Schatzmann, M., and B. Leitl (1999): Quality assurance of urban dispersion models. *Conference Proceedings on CD-ROM*, 6th International Conference on Harmonization within Atmospheric Dispersion Modeling for Regulatory Purposes, 11-14 October 1999, INSA de Rouen, France (to be published in *Int. J. Environ. Pollut.*).

Schlunzen, K.H. (1997): On the validation of high-resolution atmospheric mesoscale models. *J. Wind Eng. Ind. Aerod.*, **67&68**: 479-492.

Sebald, L., R. Treffeisen, E. Reimer, and T. Hies (2000): Spectral analysis of air pollutants. Part 2: ozone time series. *Atmos. Environ.*, **34**: 3503-3509.

Smith, M.E. (1984): Review of the attributes and performance of 10 rural diffusion models. *Bull. Amer. Meteor. Soc.*, **65**: 554-558.

Stein, A.F., and J.C. Wyngaard (2000): Fluid modeling and the evaluation of inherent uncertainty. GMU Transport and Dispersion Modeling Workshop, 11-12 July 2000, George Mason University, Fairfax, Virginia.

Stein, A.F., and J.C. Wyngaard (2001): Fluid modeling and the evaluation of inherent uncertainty. *Journal of Applied Meteorology*. Vol. 40(10): 1769-1774.

Tonnesen, G.S., and R.L. Dennis (2000a): Analysis of radical propagation efficiency to assess ozone sensitivity to hydrocarbons and NO_x 1. local indicators of instantaneous odd oxygen production sensitivity. *J. of Geophys. Res.*, **105**, D7: 9213-9225.

Tonnesen, G.S., and R.L. Dennis (2000b): Analysis of radical propagation efficiency to assess ozone sensitivity to hydrocarbons and NO_x 2. long-lived species as indicators of ozone concentration sensitivity. *J. of Geophys. Res.*, **105**, D7: 9227-9241.

Tesche, T.W., P. Georgopoulos, J.H. Seinfeld, F. Lurmann, and P.M. Roth (1990): Improvements in procedures for evaluating photochemical models. Report A832-103, California Air Resources Board, Sacramento, California.

Thuillier, R.H. (1992): Evaluation of a puff dispersion model in complex terrain. *J. Air Waste & Manage. Assoc.*, **42**: 290-297.

U.S. Environmental Protection Agency (1991): Guideline for regulatory applications of the Urban Airshed Model. EPA-450/4-91-013, U.S. Environmental Protection Agency, Research Triangle Park, NC 27711.

U.S. Environmental Protection Agency (1992): Protocol for Determining the Best Performing Model, EPA-454/R-92-025, Office of Quality Planning and Standards

U.S. Environmental Protection Agency (1996) Compilation of Photochemical Models' Performance Statistic for 11/94 Ozone SIP Applications. EPA-454/R-96-004. U.S. Environmental Protection Agency, Office of Air Quality Planning and Standards, Research Triangle Park, NC 27711, 156 pp.

U.S. Environmental Protection Agency (1997): Evaluation of Modeling Tools for Assessing Land Use Policies and Strategies. EPA 420/R-97-007. U.S. Environmental Protection Agency, Ann Arbor, MI, 60 pp. (available at http://www.epa.gov/orcdizux/transp/publicat/pub_sust.htm).

U.S. Environmental Protection Agency QA/G-5 (1998): Guidance for Quality Assurance Project Plans. http://www.epa.gov/quality/qa_docs.html.

U.S. Environmental Protection Agency QA/G-9 (1998): Guidance for the Data Quality Assessment: Practical Methods for Data Analysis. http://www.epa.gov/quality/qa_docs.html.

Venkatram, A. (1982): A framework for evaluating air quality models. *Boundary-Layer Meteor.*, **24**: 371-385.

Venkatram, A. (1983): Uncertainty in predictions from air quality models. *Boundary-Layer Meteor.*, **27**: 185-196.

Venkatram, A. (1988): Inherent uncertainty in air quality modeling. *Atmos. Environ.*, **22**(6): 1221-1227.

Vukovich, F.M. (1997): Time scales of surface ozone variations in the regional, non-urban environment. *Atmos. Environ.*, **31**: 1513-1530.

Ward, A.C. (1994): A simple procedure for ranking the performance of several air-quality models across a number of different sites. *Atmos. Environ.*, **28**(18): 2909-2915.

Weil, J.C., R.I. Sykes, and A. Venkatram (1992): Evaluating air-quality models: review and outlook. *J. Appl. Meteor.*, **31**: 1121-1145.

Weil, J.C., L.A. Corio, and R.P. Brower (1997): A PDF dispersion model for buoyant plumes in the convective boundary layer. *J. Appl. Meteor.*, **36**: 982-1003.

Willmot, C.J. (1982): Some comments on the evaluation of model performance. *Bull. Amer. Meteor. Soc.*, **63**: 1309-1313.

Zannetti, P., and P. Switzer (1979): Some problems of validation and testing of numerical air pollution models. Proceedings, Fourth Amer. Meteor. Soc. Symp. on Turbulence, Diffusion, and Air Pollution, January, Reno, Nevada, pp. 405-410.

Zurbenko, I.G. (1986): *The spectral analysis of time series*. North Holland.

Irwin, J. 2005. *A Historical Look at the Development of Regulatory Air Quality Models for the United States Environmental Protection Agency*. Chapter 18 of *AIR QUALITY MODELING - Theories, Methodologies, Computational Techniques, and Available Databases and Software*. Vol. II – *Advanced Topics* (P. Zannetti, Editor). Published by The EnviroComp Institute (<http://www.envirocomp.org/>) and the Air & Waste Management Association (<http://www.awma.org/>).

Chapter 18

A Historical Look at the Development of Regulatory Air Quality Models for the United States Environmental Protection Agency

John S. Irwin

John S. Irwin and Associates¹, Raleigh, NC (USA)

jsirwinetal@nc.rr.com

Abstract: Information about the development and use of regulatory air quality models, with an emphasis on those whose development was sponsored or promoted by the United States Environmental Protection Agency (EPA), is provided. A broad definition of regulatory is used here to include not only modeling used for setting specific emission limits, but also modeling used in developing EPA's agenda. The review outlines the major events in U.S. air quality legislation, noting the resulting influence on air quality model development. This partial review is meant to augment critical science reviews available elsewhere.

Key Words: air quality, Clean Air Act and its Amendments, model development.

1 Introduction

What caused the development of mathematical simulation models that describe the transport and fate of pollutants as they move through the atmosphere? Was this simply a consequence of intellectual curiosity? Was there a military need for characterization of poison gas dispersion, smoke obscuration effectiveness, or

¹ From 1975 to 2004, John Irwin was a NOAA employee, on assignment to the U.S. Environmental Protection Agency, Research Triangle Park, NC 27711.

radioactive fallout? Were such models spawned as a result of a fear of nuclear power generation facilities? Was it recognized as fundamental to developing objective strategies for the mitigation of hazards to human health from industrial emissions? If the answers to these questions were known, it would likely be attributable to all of the above concerns and to many not listed. Certainly the Atomic Energy Act in 1954 (which ultimately founded the Nuclear Regulatory Agency) and Public Law 159 in 1955 (which ultimately founded the Environmental Protection Agency) were instrumental in stimulating research activities. As fundamental as the causes for development, it is also important to recognize as with the development of all science understanding, many individuals contributed with partial solutions, which have been cobbled together to form what are called air quality simulation models. Even today, air quality models characterize the outward observable effects more so than the fundamental manner in which the processes happen. Thus, most of today's air quality models are rightfully characterized as first-order characterizations of the mean effects of transport, dispersion and fate. Even the emission characterizations are model estimates that are in many instances first-order approximations.

The current air quality model is really a system of models or sub-models. Each of the sub-models performs a function when needed. For buoyant emissions, the plume rise model attempts to estimate how high the mass of emissions will rise before stabilizing at some distance above the ground. A meteorological model (which in itself is a collection of models) characterizes the mean and turbulent properties of the atmosphere. A dispersion model estimates how the cloud of emissions expands as it moves downwind. A chemistry model simulates chemical transformations. There can be a wet deposition model to estimate the removal of mass by rainfall, and a dry deposition model to estimate the removal of mass to the ground and vegetation. As described by Peters et al. (1995), there is a jargon developing that is used to describe the level of sophistication in a modeling system. The first-generation models have first-order chemistry (with only a few primary reactions simulated). The transport and dispersion are founded on steady-state approximations in time and space. The second-generation models typically add removal processes, increase the level of sophistication in the parameterizations and chemistry simulations, and allow transport and dispersion to vary as a function of time and space. The third-generation models have yet to be realized, and currently are called the next-generation models. They will consist of select processes coupled together so that interactions and feedbacks can be investigated (e.g., aerosol formation attenuation of incoming radiation, which could alter aerosol formation rates).

There have been a number of reviews on the subject of the history of the development of air quality models. The five volumes edited by Stern (1976, 1977) cover the development of almost all of the aspects associated with air quality management, of which modeling is but a part. DeMarrais (1974), Turner (1979), and Randerson (1984) summarized the early years with emphasis on the characterization of the transport and fate of inert pollutants. Seinfeld (1988)

reviewed the early years in photochemical modeling. The transition from thinking that photochemical problems could be resolved with local-scale models to requiring regional-scale models can be seen in the reviews by Eliassen (1980), Fisher (1983), Eliassen et al. (1982), Peters et al. (1995), and Russell and Dennis (2000). The recent review by Seigneur et al. (1999) provides a review of particulate matter models.

There are several reviews that focus particularly on the Environmental Protection Agency (EPA), its history and the development of its programs. Jasanoff (1990) reviews several science policy disputes that involved EPA regulatory decisions, and the redress of increased use of science peer reviews and Science Advisory Boards. U.S. Environmental Protection Agency (1996) provides a summary of the first 25 years of EPA, its people and the legislative events of note. National Research Council (1991a) provides an excellent overview of EPA's attempts to devise legislative tools and modeling tools to assess ozone impacts. National Research Council (1991b) provides a review of how EPA envisioned an increased emphasis on reducing human health risks through exposure and how risk assessment would require revision of the modeling systems to address several new issues (e.g., the difference between ambient concentration values versus human exposures, the variability of human susceptibility to health risks, the increased uncertainties associated with such modeling systems). National Research Council (1994) provides a review of EPA's problems to successfully respond to legislative requirements to formally identify and then institute programs to reduce ambient concentrations of hazardous air pollutants.

The purpose of this discussion is to review the development of regulatory air quality models within the United States as viewed from the EPA perspective. EPA uses results from air quality modeling to define emission limits for new sources and for existing sources that are considering upgrades or changes to their process that would change their emissions. EPA also uses results from air quality modeling to investigate the consequences of alternative national pollution control strategies. In the discussion that follows, we use a broad definition of the term regulatory modeling to include both of these purposes. This review is intended to complement the cited critical science reviews. Since the inception of the EPA in 1970, the atmospheric scientists who provided EPA meteorological and air quality modeling support were with the Air Resources Laboratory (ARL) of the National Oceanic and Atmospheric Administration (NOAA)². This resulted from a tradition within

² The Weather Bureaus Special Projects Research Field Office had three Field Research Divisions in 1948 to provide support to the emerging atomic energy program. Two of these Divisions served as a source of meteorological information and expertise for nuclear research facilities located near Oak Ridge, TN and Idaho Falls, ID. The Washington D.C. Division provided meteorological expertise regarding nuclear tests conducted around the world. In 1955, a division was established in Cincinnati, OH to provide meteorological consultation to the Public Health Service (PHS). In 1957, a Division was established in Las Vegas, NV to provide weather support for nuclear testing. In 1965, President Johnson consolidated two long-standing Department of Commerce agencies into the Environmental Sciences Services Administration (ESSA), the Coast and Geodetic Survey (established by President Jefferson in 1807) and the Weather Bureau (established by Congress in

the U.S. Weather Bureau to provide direct support to all Federal agencies needing meteorological information, which was passed on to the NOAA when it was formed. Most of the ARL scientists initially assigned to the EPA were former Weather Bureau scientists who had participated in many of the early investigations to construct operational transport and dispersion models. Therefore, it is easier to discuss the early years of air quality modeling if we start some years before the EPA was formally established.

Describing historical development poses a dilemma. For discussion purposes, it is easier if we focus on one topic; however, it creates a false sense of order, which is more related to the wisdom of hindsight. In reality, since everything is happening at once, it is difficult to determine the significance of individual developments when viewed in context. At various points, we will attempt to make some of the connections, but most of this work is left for the reader to assimilate. Section 2 of this discussion will focus on the legislative events that influenced and simulated the development of air quality models. Section 3 reviews the development of the early plume models for non-reactive pollutants, their evolution and specialization for characterizing dispersion from large individual industrial sources, and the current trend towards puff models. Section 4 summarizes the development of long-term air quality models that provide estimates of seasonal and annual average concentration for an urban area for non-reactive³ pollutants. In the early to mid-1970s, these long-term models proved the feasibility of designing emission control strategies for entire cities for non-reactive pollutants, and thus offered a basis for considering development of air quality regulations. During the late 1990s as computers became more powerful, the use of long-term approximate solutions and long-term models seems to have declined. Section 5 reviews the development of tropospheric chemistry models, which were first designed solely for estimating ozone impact for cities. As experience and understanding were gained, it became clear that all secondary pollutants (e.g., ozone, sulfate, nitrates, etc.) involved regional-scale formation and transport. Section 6 attempts to summarize the issues (some resolved, many still pending) that are influencing current model development.

1891). In 1970, President Nixon combined ESSA with seven other earth science programs to establish the NOAA. By then, the ARL had five Divisions: Idaho Falls, Las Vegas, Oak Ridge, Washington D.C., and Research Triangle Park. The Cincinnati Office was moved to Research Triangle Park, NC in 1969 specifically to provide support to the EPA.

³ In truth, all emissions undergo chemical transformations. The emphasis here is on those emitted directly into the atmosphere that undergo slow chemical transformations (if any).

2 Legislative History of Air Pollution Modeling

There are more than a dozen major statutes or laws that form the legal basis for the Environmental Protection Agency (EPA)⁴ programs. There is a natural cause and effect linkage between legislation and air pollution model development, and we focus here on those that seem to directly affect air pollution model development. Air pollution models are used primarily for planning, as opposed to reacting to some emergency or accident. Albeit in an idealized sense, air pollution models provide a cost effective means for investigating the current and future possible conditions given certain assumptions. Given the expense of industry (and ultimately to the industry's customers) to install and maintain emission control equipment and procedures, air pollution models have been developed with new capacities as new requirements are either proposed for legislation or promulgated by legislation.

The Atomic Energy Act of 1954 required the Atomic Energy Commission (AEC), whose programs are now administered by the Nuclear Regulatory Commission (NRC) and the Department of Energy (DOE), to make a detailed environmental assessment before a nuclear construction permit and final operation license were issued. This was the first federal requirement for a systematic assessment of environmental impact that resulted in the routine use of mathematical simulation models for the characterization of the transport and fate of materials through the atmosphere.

Public Law 159, dated July 14, 1955, gave the Surgeon General of the Public Health Service (PHS), under the supervision of the Secretary of Health, Education, and Welfare (HEW), the responsibility of mitigating air pollution. Through an interagency agreement between the PHS and the National Weather Bureau, three meteorologists (Jack Lovett, Francis Pooler and Raymond Wanta) were assigned to support the PHS Air Pollution Engineering Center at the Taft Sanitary Engineering Center in Cincinnati, Ohio. Over the years, the Weather Bureau division in Cincinnati increased in number to 26 by 1967.

In 1963 the Clean Air Act (CAA) was passed. This act gave limited enforcement authority to the federal government, increased the availability of research and development money, and called for the development of air quality criteria (for when air is deemed adverse to public health or welfare).

The 1965 Amendments to the Clean Air Act provided federal authority to control emissions from new automobiles. The Air Quality Act of 1967 emphasized state control of air pollution problems and called for an expanded federal program. Friedlander and Seinfeld (1969) mentioned that the United States was being divided into about 100 air quality control regions. A major emphasis was to be

⁴ (<http://www.epa.gov/epahome/laws.htm>) provides a list of these laws and links to the text of these laws and regulations.

placed on diffusion modeling in the delineation of the regions. Still there were no National Ambient Air Quality Standards (NAAQS)⁵. With no NAAQS and no time frames defined for attaining air quality standards, there was no national consistency in the approaches being considered.

In 1970, under Reorganization Plan Number 3⁶, President Richard Nixon formed the U.S. Environmental Protection Agency using parts of HEW, the Department of Interior, U.S. Department of Agriculture, and the AEC. The Weather Bureau having earlier evolved into the Environmental Science Services Administration (ESSA) became the National Oceanic Atmospheric Administration (NOAA) under Reorganization Plan Number 4⁷. On December 31, 1970, the Clean Air Act was again amended. The amendments of 1970 revolutionized federal policies by establishing philosophies that dominate the EPA today; air quality was identified as a major public health problem, quantitative air quality management (e.g., modeling) was introduced, and the partnership between the federal and state agencies was clarified. The states were required to develop State Implementation Plans (SIP) to demonstrate, using air quality modeling, how they intended to attain and maintain the specified NAAQS within a specified time frame. NAAQS were instituted for six pollutants: carbon monoxide, total suspended particulates, sulfur dioxide, oxidants (revised to photochemical ozone and non-methane hydrocarbons in 1977), nitrogen dioxide and lead. Process-based models for ozone were yet to be developed, so an empirical method called Appendix J was used to estimate the percentage reduction (rollback) needed in total and non-methane hydrocarbon emissions to reduce maximum afternoon ozone concentration values. Congress set 1975 as the deadline for attaining these NAAQS. Section 112 of the 1970 Clean Air Act required EPA to set emission standards for hazardous air pollutants so as to protect public health with an ample margin of safety. As will be seen in the following discussion, EPA found control of ozone an elusive problem, and by 1984, EPA had listed only eight pollutants as hazardous⁸.

By 1977, 2 years after the 1975 deadline specified in 1970, many areas were still in violation of the ozone NAAQS. The Clean Air Act Amendments of 1977 set a new compliance date of 1982 for attainment of the ozone and carbon monoxide

⁵ National primary ambient standards are set to protect the public health and secondary standards are set to protect the public welfare. Each standard specifies an averaging time, frequency of occurrence and concentration value (e.g., a 1-hour concentration average not to be exceeded more than once per year). EPA is required by the 1970 Clean Air Act to review the primary and secondary standards at least once every five years to determine whether revisions to the standards are necessary to continue protecting public health and the environment. For more information, see <http://www.epa.gov/ttn/oarpg/naaqsfinaaq.html>.

⁶ See <http://www.epa.gov/history/publications/origins6.htm>.

⁷ See <http://www.history.noaa.gov/eo11564.html> and <http://www.history.noaa.gov/index.html>.

⁸ The chemicals listed as hazardous air pollutants under the National Standards for Hazardous Air Pollutants (NESHAP), with month/year of public notice in parenthesis, were: asbestos (3/71), beryllium (3/71), mercury (3/71), vinyl chloride (12/75), benzene (6/77), radionuclides (12/79), inorganic arsenic (6/80), and coke-oven emissions (9/84).

NAAQS, and areas that demonstrated they could not meet the 1982 deadline were given extensions until 1987. The Clean Air Act Amendments of 1977 established the formal regulatory use of air quality dispersion models. These amendments established the concept of Prevention of Significant Deterioration (PSD) to be applied before construction of all new or modified major emitting facilities. Projected emissions from these facilities were to be modeled to determine if these sources (in combination with existing sources) would cause unacceptable ambient sulfur dioxide and particulate concentration values. Since PSD review is conducted before construction, the focus is on air quality modeling. Recognizing the burden placed on models by these legislative amendments, EPA was required to hold national modeling conferences at 3-year intervals to review modeling practices. EPA was further instructed to describe with reasonable particularity the modeling procedures and requirements. This led to the development of modeling guidance that described which air quality simulation model to use, how the meteorological conditions were to be processed for analysis, and the manner in which the modeling assessment was to be conducted.

Evidence was mounting by 1977 that ozone formation for the Eastern United States had a significant regional component that was beyond the reach of the Clean Air Act and its Amendments. Concerns were also being raised that regional transport might also be responsible for the observed elevated levels of sulfate. In 1980, President Carter signed the Acid Precipitation Act of 1980 (Public Law 96-294). The Acid Precipitation Act gave the government 10 years to perform a comprehensive assessment of the fate of sulfate. To address this requirement, the National Acid Precipitation Assessment Program (NAPAP) was established⁹. Looking back, 1980 can be viewed as a turning point for the EPA. From this point and on, the emphasis was to be on regional model development and evaluation issues.

By 1983, EPA had listed only six air pollutants as hazardous under the National Standards for Hazardous Air Pollutants (NESHAP), which was evidence of the difficulty of defining and implementing risk-based emission standards. In response to a directive from the Congress, the Food and Drug Administration (FDA), contracted with the National Academy of Sciences to examine whether alterations in institutional arrangements or procedures, particularly the organizational separation of risk assessment from regulatory decision-making and the use of uniform guidelines for inferring risk from available scientific information, could improve federal risk assessment activities. The Committee on the Institutional Means for Assessment of Risks to Public Health was formed in the National Research Council's Commission on Life Sciences in October 1981 and completed its work in January 1983 (National Research Council, 1983). As a general conclusion, the Committee believed that the basic problem in risk assessment was the sparseness and uncertainty of the scientific knowledge of the health hazards addressed, and this problem was seen as having no ready solution. These National

⁹ See <http://www.oar.noaa.gov/organization/napap.html>.

Research Council recommendations planted the seed within the EPA culture to conduct risk assessments that include a formal uncertainty assessment on the methods and conclusions reached. A key goal of these risk assessments would be to maintain a clear separation between science and policy, and in which transparency (all assumptions explicitly stated) was a stated goal.

By 1990, 3 years after the extended deadline of 1987, more than 133 million Americans were living in the 96 areas that were not in attainment of the ozone NAAQS defined in 1977. The 1990 Clean Air Act Amendments (CAAA) required redefinition of ozone non-attainment into five classifications: extreme, severe, serious, moderate, or marginal. The classification and jurisdictional boundaries of the non-attainment areas required extensive analyses of monitoring and modeling results. Section 182 of the amendments stipulates for areas designated serious (16 in number), severe (8), or extreme (1), that within 4 years after the date of the enactment of the CAAA of 1990, the State shall submit a revision to the applicable implementation plan that includes "...a demonstration that the plan, as revised, will provide for attainment of the ozone national ambient air quality standard by the applicable date. This attainment demonstration must be based on photochemical grid modeling or any other analytical method determined by the Administrator ... to be at least as effective". Section 184 of the 1990 CAAA established an interstate ozone transport region extending from Washington D.C. metropolitan area to Maine. The amendments also provided for creation of interstate transport commissions, to in effect, serve the role as broker between the several States included within an interstate ozone transport region, who were ultimately responsible for compliance with the provisions of the Clean Air Act and its Amendments.

In 1990, Congress revised the 1970 CAA procedures to be used to reduce health impacts from hazardous pollutants, by rewriting Section 112 in Title III of the 1990 Clean Air Act Amendments, and prescribing a two-stage program. Congress defined 189 compounds and compound classes as hazardous (subject to possible additions and deletions). In the first-stage of pollutant reduction, EPA was required to define technology standards and maximum available control technology (MACT) on sources of those chemicals. Section 112(f) defined the second-stage of the program, which required EPA to assess the residual risks associated with any emissions remaining, following installation of the MACT on the affected sources. A second-stage of controls is triggered only if EPA determines that an ample margin of safety has not been obtained by the technology-based emission reductions.

Title IV of the 1990 CAAA was the first national effort to use market-based incentives to achieve environmental goals, rather than the command-and-control approach employed to this point. To reduce the adverse effects of acid deposition, reductions in annual emissions of its precursors, and sulfur dioxide and oxides of nitrogen from combustion of fossil fuels, a program of alternative control measures was initiated that included technology adaptation (e.g., scrubbers and

higher-efficiency boilers), created a fuel switching, and emission allowance trading and banking system. With the use of market-based incentives to reduce adverse effects of acid deposition, the pressure to complete an operational acid deposition model was reduced, and the direction in model development turned away from sulfate acid deposition to developing characterizations of fine particles of all origins.

The Clean Air Act Amendments of 1990 defined new procedures for attaining pollution reductions for sulfur dioxide and toxics, which avoided direct use of modeling, and this had an impact on the development of air quality modeling. As will be discussed later, support for local-scale model development gradually diminished as more attention was given to development of large-scale grid models that could treat the chemistry of several pollutants simultaneously. The 1990 amendments required EPA to determine if local-scale plume models were systematically underestimating the impact of fugitive emissions (from roadways and dredging operations) associated with large surface coal mines. This provided a basis for minor improvements to be made in algorithms used in local-scale modeling for dry deposition. The regulatory importance of modeling was expanded from demonstrating compliance, as expressed in the amendments of 1977 and assessment of ozone abatement strategies, to being needed for assessment of the annual atmospheric deposition of toxic substances (sources and relative contributions) to the "Great Waters" (Great Lakes, Chesapeake Bay, Lake Champlain, coastal waters).

During the decade following the enactment of the CAAA of 1990, EPA completed reviews of the ozone and particulate NAAQS. In March of 1993, notice was given with a final decision not to revise the existing primary and secondary ozone NAAQS (58 FR 13008). Both were of the form of a 1-hour average not to be exceeded more than once per year, based on an analysis of 3 years of data. In July 1997, EPA made known its intention to revise the primary and secondary ozone NAAQS (Federal Register Vol. 62 No. 138) to the form of a 3-year average of the fourth highest maximum daily 8-hour average. In July 1997, EPA made known its intention to revise the primary and secondary particulate matter NAAQS. Lawsuits filed questioning whether the EPA had been given too much authority by the 1970 CAA were set aside by a Supreme Court Decision in February 2001¹⁰. The primary PM_{2.5}¹¹ particulate matter NAAQS was to have the form of a 3-year average of the 98th percentile of 24-hour PM_{2.5} concentration values. The primary PM₁₀¹⁰ particulate matter NAAQS was to have the form of a 3-year average of the 99th percentile of 24-hour PM₁₀ concentration values. The secondary particulate matter NAAQS were revised to be identical to the proposed primary standards. Of interest to air quality modeling was that these proposed revisions to the ozone and particulate matter NAAQS continued the need for multi-year modeling

¹⁰ See <http://www.epa.gov/airlinks/airlinks4.html> and <http://www.epa.gov/ttn/oarpg/naaqsfm/>.

¹¹ PM_{2.5} refers to particulate matter with a diameter of 2.5 microns or less, and PM₁₀ refers to particulate matter with a diameter of 10 microns or less.

assessments of the upper percentile values of the respective concentration distributions.

In summary, the legislation that has most stimulated the regulatory use of air quality modeling are: 1) Atomic Energy Act of 1954, as it established the requirement for Weather Bureau Field Offices to provide technical services in environmental impact assessment which ultimately established the linkage between NOAA and EPA; Public Law 159 in 1955, as it created the Public Health Service that ultimately became the Environmental Protection Agency; 2) the Clean Air Act Amendments of 1970 and 1977, which relied on air quality modeling as a means for demonstrating compliance for the development of State Implementation Plans and for permits required by the New Source Review program; and finally, 3) the Clean Air Act Amendments of 1990, which formalized the requirement to use tropospheric chemistry air quality models for demonstrating a plan for attainment of the ozone NAAQS.

3 Air Quality Models for Individual Industrial Facilities

The PSD/NSR defined in the CAA amendments of 1977 established a need for air quality models that could be applied for major emitting facilities (to be constructed or to be modified) in order to determine if these sources (in combination with existing sources) would cause unacceptable ambient sulfur dioxide and particulate concentration values. As discussed initially in this section, the early models for sulfur dioxide and particulate emissions evolved from models constructed earlier for assessment of gas warfare and dispersion of nuclear fallout from atomic explosions. Based on predicted impacts from these dispersion models, the amounts of emissions allowed from each stack were estimated, such that the ambient air quality standards defined in the PSD/NSR program were attained. Before the PSD/NSR program, whether an area was in attainment was defined through air quality monitors. The PSD/NSR program allowed attainment to be defined through air quality modeling. In this section, we provide a brief review of the dispersion models used prior to 1977, and then follow the evolution of these models. It is sometimes distracting to follow a time sequence, and in these places we summarize the time sequence of the development of some major sub-model used in point source dispersion modeling.

In the early 1950s, there was great interest in nuclear fallout. Hyde (1952) used a trajectory analysis to show that radioactive debris from bomb tests in Nevada in October and November were detected in rainfall in France in November and December of 1951. List (1954) provided a detailed trajectory analysis for eight bomb tests conducted in the spring of 1952, including a discussion of fallout from three of the tests, with daily maps showing isolines of activity and areas of precipitation for several days following each of the tests. In discussing the possible relationships between detonations of atomic bombs and weather, Machta and Harris (1955) concluded that it was unlikely that such explosions affected the

weather. Both Bob List and Lester Machta were meteorologists assigned to the Washington D.C. Weather Bureau Field Division.

In 1955, the first addition of *Meteorology and Atomic Energy* (U.S. Weather Bureau, 1955) was published. The editor of this work was Harry Wexler who was then the Chief of the Scientific Services Division in the Weather Bureau. Personnel from the Scientific Services Division assisted in the collection and preparation of this report, many of which became commonplace names within air pollution research (e.g., F. A. Gifford Jr., B. List¹², L. Machta⁶, D. Pack, F. Pooler). Written for the characterization of the transport and dispersion of nuclear radiation, this was the first compendium dealing with all the facets of air pollution meteorology. It included information on sources, development of dispersion patterns, methods and nomograms for computing downwind concentrations, meteorological instruments and their proper use and climatological data pertinent to air pollution meteorology.

At this point in time, the practical method for characterizing dispersion from a point source followed the ideas of Sutton (1947)¹³. During the summer of 1956, an experimental program to study micrometeorology and dispersion from near-surface releases was conducted near the town of O'Neil in north central Nebraska. This comprehensive turbulence and diffusion program of 70 tracer experiments was given the name Project Prairie Grass, and was instrumental in providing a basis for the development of practical methods for the characterization of atmospheric dispersion. One of the first papers to discuss these data was by Cramer (1957), in which a Gaussian plume model was described that related the horizontal and vertical dispersion to the observed standard deviations of lateral and elevation angles of the wind fluctuations. Barad and Haugen (1959) used the Project Prairie Grass results to specifically investigate the veracity of Sutton's model for plume dispersion. Not long thereafter, Pasquill (1961) offered a pragmatic technique to estimate Gaussian plume vertical and lateral dispersion that could be implemented with easily acquired meteorological observations, namely: insolation and wind speed. By 1958, F. Pasquill was corresponding with F.A. Gifford (who was then with the Oak Ridge Field Research Division), and R. McCormick and D.B. Turner (who were then with the Cincinnati Field Research Division) prior to 1961. So, Gifford (1961) offered a conversion of Pasquill's angular spread values to standard deviations of plume spread, and Turner (1961) offered a conversion of Pasquill's

¹² In 1949, Bob List edited sixth edition of the Smithsonian Meteorological Tables, which is now in its fifth reprint (List, 1971), a fundamental meteorological handbook. Lester Machta was hired at the inception of the Weather Bureau Field Offices in 1948, and was Director of the NOAA Air Resources Laboratories from 1968 to 1991, renamed in 1982 to NOAA Air Resources Laboratory.

¹³ "... The incidence of gas warfare in 1916 gave an impetus to the investigation of atmospheric diffusion, which ultimately led to the formation of a special meteorological research team at the Chemical Defense Experimental Station, Porton, Wiltshire. The present paper is an integrated account of certain mathematical investigations carried out by the writer between 1932 and 1938. Some parts of this work were published in 1932 and 1934, but hitherto no connected account has existed outside of official reports."

stability classification criteria that employed hourly airport observations. These extensions to Pasquill's scheme simplified its use, and made it practical for it to be converted to a numerical algorithm.

Development of an air quality simulation model for use in air quality planning, involved the combination of two important concepts besides the characterization of plume dispersion. Industrial stacks emit heated gases that tend to rise, which requires a plume rise model. Elevated temperature inversions were known to contribute to the buildup of smoke and air pollution (smog) (Schrenk et al., 1949; Wilkins, 1953; Lucas, 1958), which requires a mixing height model. Characterizing the emission and dispersion of pollutants in an entire city involves treating hundreds of individual stack emissions in conjunction with low-level diffuse emissions. An early proof of concept was Turner's (1964) simulation of sulfur dioxide emissions for Nashville, TN, which illustrated that it was feasible to combine the concepts of Pasquill plume dispersion with the Holland (1953) plume rise and mixing heights using Holzworth's (1964) concepts, into a practical air quality simulation model. These results were based on a one-year study of Nashville, TN, where data from a network of 32 sampling stations were used. Results showed that the 24-hour sulfur dioxide concentrations and the aerial extent of the pollution impacts from multiple sources could be analyzed using a source inventory coupled with a numerical dispersion model. Turner (1967) explained the details of this type of model in a handbook with example problems and solutions for teaching the concepts.

The development of mixing height models is hampered by the fact that the depth through which emissions are mixed is an asymptotic result, that is best observed by analysis of vertical profiles of inert tracers released specifically for the purpose. Holzworth (1964) published a climatology of urban morning and afternoon mixing depths for the contiguous United States¹⁴. This report popularized the idea of using easy to determine mixing depths in air pollution evaluations. This report also illustrated the usefulness of numerical methods for the processing of large quantities of data for the practical evaluation of air pollution problems. Mixing depth data is rarely a primary focus of field studies; and thus, there are few quality data sets for use. Since Holzworth's investigations, EPA has not invested resources toward developing improved mixing height algorithms for use in its air quality models, but has chosen to select algorithms developed by others. As discussed in a recent review, Seibert et al. (2000), all available methods have strengths and weaknesses.

The early plume rise formulas were based on an integral model, in which the differential equations governing the total fluxes of mass, momentum and energy

¹⁴ The morning urban mixing depth was determined as the intersection of a morning urban minimum potential temperature (the observed minimum temperature plus 5° C) with the morning potential temperature profile (defined from a morning upper-air observation). The afternoon maximum mixing depth was determined as the intersection of the afternoon maximum potential temperature with the morning potential temperature profile.

through a plume cross section are closed using an entrainment assumption. Typically, the entrainment assumption¹⁵ specifies that the average rate at which outside air enters the plume surface is proportional to the characteristic vertical velocity of the plume at any given height, and assumes that dilution by atmospheric turbulence is negligible in comparison to other factors (Taylor, 1945). Holland (1953), in describing the micrometeorology associated with the Oak Ridge, TN area, provided a plume rise formula that became known as the Holland formula. Scorer (1959) presented formulas for computing plume rise, claiming the existing formulas were too complicated for practical use. Then Briggs (1965), using dimensional arguments introduced a new plume rise for buoyant plumes. Nonhebel (1965) reviewed many plume rise formulae and noted the confusion. By 1969, there were 30 plume rise models to choose from, so the critical review by Briggs (1969), which offered a simplified alternative, was well received. G.A. Briggs extended his works over the time period from 1969 to 1975, which by then had become the primary plume rise model of choice (Briggs, 1975). As discussed by Weil (1988) and Netterville (1990), the plume rise model of Briggs was chosen to embody the primary physical processes of buoyant plume rise, when the ambient turbulence is small, and thus the dilution of the buoyant plume is dominated by its own motion, which is an apt characterization of plume rise in thermally neutral and stable atmospheric conditions. There are other conditions when these assumptions prove to be inadequate; namely, the penetration of buoyant fluid into an elevated inversion (where the thickness and strength of the elevated inversion complicates the characterization of the plume rise), and buoyant rise in a strongly convective boundary layer (where the strength of the convective eddies can exceed the buoyancy forces within the plume). To date, the models used routinely in air pollution assessments have continued to employ Briggs' plume rise model, and to treat the effects of penetration and rise in a convective boundary layer as special cases. This is in contrast to adopting plume rise models with a broader range of applicability. In part, this relates to the fact that, regardless of the plume rise model employed, the estimated rise characterizes the ensemble average plume rise, and there is little skill perceived (more variance explained) through the use of the more comprehensive plume rise models.

Soon after the move of the Cincinnati office to Research Triangle Park, NC in 1969, W. Snyder joined the NOAA staff on assignment to support the EPA. W. Snyder was a specialist in the operation and use of wind tunnels. Since there was no wind tunnel when he first arrived, his early years were devoted to constructing a wind tunnel, and establishing criteria for its use in simulating atmospheric turbulence and dispersion. Snyder (1972) laid the groundwork by defining the similarity criteria for modeling atmospheric flows in air and water using wind tunnels and water towing tanks.

¹⁵ A reasonable assumption, since the focus was on characterizing the rise of a heated plume resulting from an atomic bomb blast.

One of the first questions posed to the EPA Wind Tunnel and Fluid Modeling Facility was whether flow around scale models of buildings could be used to investigate the potential for stack gas emissions to be captured in the lee wake of the buildings. Using results from wind tunnel simulations, Snyder and Lawson (1976) showed that for stacks close to buildings, designing a stack to be 2.5 times the building height was adequate for a building whose width perpendicular to the wind direction was twice its heights, but defined stack heights greater than needed for tall thin buildings. These investigations were extended by Huber and Snyder (1976) towards development of algorithms that could be incorporated into plume dispersion models to simulate the enhanced dispersion of plumes caught in building wakes.

By the early 1970s, D.B. Turner had a collection of numerical algorithms that were written in FORTRAN, and provided a means for simulating plume dispersion. Using an existing nationwide computer network, UNAMAP (User's Network for Applied Modeling of Air Pollution) came into being in 1972 (Turner et al., 1989), and consisted of six air quality simulation models. The computer network was only available to a limited few who had access, so it was decided to distribute the models as FORTRAN code on a magnetic tape, with the National Technical Information Service (NTIS) as the provider of the tape to the public. In 1989, the EPA Office of Air Quality Planning and Standards took over the responsibility of distributing the models to the user community using a dial-up Bulletin Board Service, which evolved to what is called today the Support Center for Regulatory Air Models (<http://www.epa.gov/scram001/>).

By 1977, the primary features of the models being used for characterizing dispersion from isolated point sources was: the vertical and lateral dispersion were characterized using the Pasquill-Gifford dispersion curves of 1961 for rural environs, the six¹⁶ stability categories ranging from very unstable (A) to very stable (F) were characterized using D.B. Turner's 1961 criteria, the plume rise was characterized using the Briggs 1975 modeling equations, and the mixing height was characterized using the Holzworth 1964 model. For urban environs, the stability categories at night are forced to neutral (D). The model for modeling individual point sources was CRSTER (U.S. Environmental Protection Agency, 1977)¹⁷. A Gaussian plume for multiple sources, called RAM, was released in 1978 (Turner and Novak, 1978; U.S. Environmental Protection Agency, 1978a)¹⁸.

¹⁶ Pasquill (1961) had seven stability categories, and had envisioned the neutral category as being composed of two cases, adiabatic for when the surface is actively heated (daytime) and subadiabatic for when the surface is not heated (overcast and nighttime). EPA chose to use the subadiabatic category and its dispersion characterization for all neutral cases. This may explain, in part, a tendency for the resulting models to underestimate surface concentrations from tall stacks during daytime neutral conditions.

¹⁷ EPA desired to quickly develop the FORTRAN code for modeling a single point source, and it became known as the crash (CRS) program for its tight time deadlines. When the scope was expanded to include terrain interactions, the model name was coined, CRSTER.

¹⁸ Named after Robert A. McCormick who was the Director of the NOAA Meteorological Sciences

RAM was one of the first operational models used by the EPA to employ the St. Louis dispersion curves (McElroy and Pooler, 1968)¹⁹ for characterizing urban dispersion effects. Using EPA wind tunnel research results for modeling building wake effects, CRSTER was adapted to become the first version of the Industrial Source Complex (ISC) model (U.S. Environmental Protection Agency, 1979).

Responding to the Clean Air Act Amendments of 1977, the *Guideline on Air Quality Models* (U.S. Environmental Protection Agency, 1978b) was published, which was to be used by EPA, States, and industry to prepare and review PSD air quality modeling assessments and State implementation plans. The Guideline of 1978 was intended to ensure consistent air quality analyses for modeling activities.

This Guideline was developed and published for the specific purpose of complying with the 1977 Clean Air Act amendments that required EPA to prescribe with "reasonable particularity" the modeling procedures to be used in PSD assessments.

The Guideline of 1978, in order to be reasonably prescriptive, had identified for each perceived situation, the model that would be recommended for regulatory assessments. With updates to the Guideline new situations were added. Example situations included: relatively flat terrain with rural or urban conditions, complex terrain with rural or urban conditions, long range transport, dispersion in the vicinity of the shoreline or ocean. The Guideline further stipulated the procedures an applicant would have to follow in order to employ an alternative model to that which was specified for use in the Guideline. Basically, the model had to be demonstrated to perform as well or better than the model prescribed in the Guideline for the particular situation. This proved to be an almost insurmountable requirement, except in a few circumstances where the applicant had sufficient resources and perseverance.

Around this time, EPA was sued by private industry for requiring the use of the Pasquill stability, a dispersion curves for the characterization of dispersion from isolated industrial sources having tall stacks. From 1976 through 1980, this lawsuit made its way through the court proceedings. The court ruled in favor of the EPA's position (FR, 1980). This ruling did not review the technical decision to use the Pasquill-Gifford dispersion curves for elevated releases (and in particular the dispersion curve associated with very unstable conditions, stability category A). What the courts did in coming to this decision was scrutinize EPA's decision making process to insure that EPA's decisions had not been arbitrary or capricious. The courts upheld EPA's decision making process.

The publication of the Guideline in 1978 had several consequences. It recommended specific models for use in complying with the modeling required by the EPA for the Prevention of Significant Deterioration (PSD) and New Source Review (NSR) programs. It defined the EPA Regional Offices as having the final

Modeling Division when it was established in Research Triangle Park, NC in 1970.

¹⁹ A reanalysis by G.A. Briggs of the St. Louis dispersion curves resulted in the Briggs urban curves, which were used in subsequent releases of EPA's dispersion models (Gifford, 1976).

authority for interacting with the public, and reviewing and accepting PSD/NSR modeling results. It defined the process by which new models would be considered, and process by which the Guideline would be periodically updated. Through the years, the system defined in the 1978 Guideline for managing the PSD/NSR modeling requirements has proven itself to be highly effective and workable, both for regulators and those regulated²⁰. There were two negative consequences resulting from the 1978 Guideline. First, the procedures for using alternative models required one to determine that the alternative model being proposed would perform better than that recommended in the Guideline. In his critical review of dispersion modeling, Turner (1979) noted that there were no recognized model performance standards (metersticks)²¹. With no accepted measure for defining a difference in performance, arguing the case for use of an alternative model was difficult. Secondly, in order to introduce a new model or replace an existing Guideline model, EPA had to follow the administrative requirements for publication of a proposed revision, a public review and comment time period, and then publication of the final revisions to the Guideline. This imposes an inertia in the revision of the modeling guidance that is at least 18 months or more in length. Even though results from research studies during the period from 1975 to 1995 proved to be one of the more exciting, providing many improved methods for the characterization point source dispersion, the structure and form of the models used for regulatory assessments remained largely unchanged.

Section 123 of the CAA Amendments of 1977 states that construction of tall stacks for the principal purpose of reducing pollutant impacts at the surface was not acceptable. It was considered good-engineering practice (GEP) to build stacks to avoid being captured within the wake effects of nearby buildings and obstacles (terrain effects). Guidance was published by the EPA on how to use a wind tunnel to determine the stack height needed to avoid building effects (Lawson and Snyder, 1983) and terrain effects (U.S. Environmental Protection Agency, 1985a) that enhance dispersion (result in concentration maxima that are 40% higher than would otherwise occur if the building or terrain were not affecting the flow).

²⁰ Since its inception, J.A. Tikvart of the US EPA has provided oversight and management of all activities associated with the drafting, updating and implementation of the Guideline. He foresaw that the purpose of the Guideline would be realized by the people who implemented the guidance. Through his efforts, various programs and activities were established, as the EPA Model Clearinghouse to resolve problematic technical questions, and annual workshops were held to ensure communication between the EPA Regional modeling contacts.

²¹ J.A. Tikvart of the US EPA and L. Niemeyer of the ASMD established a Cooperative Agreement with the American Meteorological Society in 1979 to provide expertise and assistance in evaluating technical aspects of air quality models that may be used for applications as required by the Clean Air Act Amendments of 1977. The AMS Steering Committee for the EPA Cooperative Agreement fostered improved model evaluation metersticks through workshops and reviews (Randerson, 1979; Fox, 1981; Fox, 1984; Smith, 1984; Irwin and Smith, 1984). This committee also attempted to foster development of improved methods for characterizing transport and diffusion, which culminated in the formation of the AMS EPA Regulatory Model Improvement Committee (AERMIC), which developed AERMOD (Weil, 1992).

Another area where the EPA Wind Tunnel and Fluid Modeling Facility had a major impact was in developing a pragmatic method for characterizing the flow and dispersion around an isolated hill. Through a combination of wind tunnel and fluid towing tank experiments, Hunt and Snyder (1980) developed the dividing streamline concept, which suggests that unless the flow has sufficient energy, it will flow around an obstacle rather than flow directly over the obstacle. Full-scale tracer field studies confirmed these findings at Cinder Cone Butte, ID in 1980; Hogback Ridge, NM in 1982, and the Tracy Power Plant, NV in 1984 (Snyder et al., 1985). From these results, the EPA complex terrain dispersion model, CTDM/PLUS, was developed (Perry, 1992a, b).

During the period from 1975 to 1990, a new understanding was reached concerning dispersion within the convective boundary layer (CBL). The convective tank experiments by Willis and Deardorff (1976, 1978, 1981) revealed that the surface releases tended to slide along the surface until captured within a convective updraft. A surface release thus captured would appear to have an accelerated vertical dispersion in comparison to its lateral dispersion, as suggested by the Pasquill stability category A curve for vertical dispersion during very unstable conditions. An elevated release tended to slowly descend towards the surface, being caught within the general downdraft area surrounding the isolated convective updrafts. This view argued for a more complex dispersion model than was possible by the simple Gaussian plume model. These fluid modeling results were confirmed by the Convective Diffusion Observed by Remote Sensors (CONDORS) field experiments conducted at the NOAA facilities in Boulder, CO during August and September 1983 (Eberhard et al., 1988; Briggs, 1989, 1993a, b). Operational plume dispersion models were developed to address this new understanding of convective dispersion by the Maryland Power Plant Research Program (Weil and Brower, 1984; Weil and Corio, 1988); the EPA (Turner et al., 1986; Gryning et al., 1987), and EPRI (Hanna and Paine, 1989; Hanna and Chang, 1991). The most recent proposals have been ADMS (Carruthers et al., 1994, Bennet and Hunter, 1997, Owen et al., 2000) and AERMOD (Weil, 1992; Perry et al., 1994; Lee et al., 1996).

EPA has always had models to propose for use for short-range dispersion, but there has been a continuing need for models that could handle the more complex effects associated with dispersion involving transport beyond the near-field, say 15 to 20 km. Starting in 1975, EPA has supported the development of a series of models starting with MESOPUFF (Benkley and Bass, 1979), which was extended by the North Dakota State Department of Health to become MSPUFF (Schock and Weber, 1984). Petersen (1982) provided a model for handling an instantaneous release as a puff, which he then extended to handle a time-varying emission rate (possibly moving source, like a ship in a harbor) by a multi-source Gaussian puff model called INPUFF (Petersen and Lavdas, 1986). EPA supported the development of a multi-layer model, MESOPUFF II (Scire et al., 1984), that could better address wind shear effects on dispersion (variation of wind direction with height). MESOPUFF II was revised to become CALPUFF (Scire et al., 2000a, 2000b),

which has since received further development support (e.g., State of Victoria, Australia funded development of Graphical User Interfaces; U.S. National Forest Service inclusions of algorithms for treatment of forest fires; EPA funded aqueous phase chemistry and near-field dispersion enhancements; Aluminum Industry funded inclusion of buoyant line source algorithms; California energy commission funded inclusion of convective dispersion algorithms). Puff models can directly address the inhomogeneity in the meteorological conditions, which is impossible to address in the context of a steady-state plume dispersion model. Developing the terrain induced flows, storing the time-varying three-dimensional meteorological fields, and tracking possibly tens of thousand puffs have restricted puff models to large mainframe computers until recent times.

In 1999, EPA proposed that the ISC plume dispersion model be replaced with the second-generation plume dispersion model, AERMOD. It was also proposed that the Gaussian puff model, CALPUFF, be accepted for all refined modeling involving transport with distances greater than 50 km, and on a case-by-case basis for any situation involving complex winds (e.g., calms and stagnation, narrow valley channeling, dispersion near shorelines of large lakes and oceans). Application of either of these models anticipates a more sophisticated user than that envisioned in the development of the ISC modeling systems. As experience is gained in the use of the CALPUFF modeling system, it is anticipated that the realism provided by treating the time-variations of the three-dimensional wind and turbulence fields along with transformation and deposition will become highly desired, such that plume models may fall into disuse. For this to occur, various enhancements will be necessary in order to allow ready application of this modeling system to the variety of situations now handled by plume dispersion models.

There are several scientists whose names are distinguished in the development and use of models for simulating the impacts of individual industrial facilities in regulatory assessments. F. Pasquill and F.A. Gifford offered a pragmatic update of O.G. Sutton's model for characterizing the vertical and lateral extent of stack emissions as they disperse downwind. Through the publication of a practical handbook (a conversion of the subjective criteria for defining Pasquill's stability categories into objective criteria capable of being implemented in computer software, and establishment of a system for distribution of the numerical dispersion models), D.B. Turner popularized the use and application of Gaussian plume models in regulatory assessments. G.A. Briggs offered a pragmatic description of buoyant plume rise that could be easily used with limited definition of the meteorological conditions. W. Snyder's wind tunnel studies provided a basis for developing models of how the swirl of eddies around buildings and hills affect the plume rise and the dispersion of buoyant stack emissions. The efforts of these scientists formed the basis and use of industrial source dispersion models in regulatory assessments, not only within the United States, but also in other countries.

4 The Development of Urban-Scale Long-Term Air Quality Models

The Clean Air Act is a federal law covering the entire country, with the states doing much of the work. Under this law, EPA sets limits on how much of a pollutant can be in the air anywhere in the United States. This ensures that all Americans have the same basic health and environmental protections. The law allows individual states to have stronger pollution controls; but, states are not allowed to have weaker pollution controls than those set for the whole country. The law recognizes that it makes sense for states to take the lead in carrying out the Clean Air Act, because pollution control problems often require special understanding of local industries, geography, housing patterns, etc. States have to develop state implementation plans (SIP) that explain how each state will ensure that the limits set by the EPA will be reached or maintained. These plans invariably involved the use of air quality models to relate the control of emissions with estimated air quality impacts.

In the early years of air dispersion modeling (say, prior to 1968), most calculations were completed with paper, pencil and hand calculators. Early computers were limited in their memory capabilities. This spawned the development of a particular type of dispersion model, which employed a statistical summary of meteorological conditions, which then required a special algorithm for characterizing the resulting dispersion. These models came to be known as long-term models, as they were designed to provide annual or seasonal-average concentration values. These models have historical importance as they provided the early demonstrations of how air pollution dispersion models could be used to design emission control programs. They came into being around 1965 and survived for about 30 years, until computer memory and speed made them unnecessary.

Early examples of this type of model were described by Meade and Pasquill (1958) and Lucas (1958). The idea was relatively simple, but most of the algorithms for characterizing the basic processes (e.g., buoyant plume rise, plume dispersion, depletion, etc.) were simplistic (first-generation) with little experimental verification. Basically, a computation was made for each expected wind speed and stability condition, whose probability of occurrence was computed for wind sectors surrounding the source (varying from 12 to 16 wind sectors). The average concentration was computed by summing for each wind sector, the computed concentration at each downwind distance, multiplied by the frequency of occurrence of each wind speed and stability combination. Over the next 20 years, a series of climatological or long-term models were developed and tested that were based on this algorithm.

Pooler (1961) used the long-term algorithm, and was one of the first investigators to employ numerical methods for automating the computations (IBM 650 computer) to provide estimates of monthly average concentration values for

comparison with observations of sulphur dioxide (SO₂) collected daily from November 1958 through March 1959 at 123 sampling sites in Nashville, TN. We have to temper Pooler's evaluation results, as regressions were performed with the observed concentration values to provide best estimates of the variation of the monthly emission rates from the known sources. That said, the model overestimated²² the observed values by a factor of 1.37 with 110 of the 122 values within a factor of two of the observed values, with 74 of the 122 values within 30%.

Gifford and Hanna (1970) offered an alternative to employing Gaussian plume modeling for simulating pollutant impacts from area source emissions. They demonstrated, through comparisons with other algorithms, that one can rely on compensation from adjacent area sources such that the lateral dispersion can be neglected. This was called the narrow-plume hypothesis by Calder (1969, 1977), and relies on the area source emissions to be something like a checker-board, with similar emissions in adjacent grid squares. Gifford and Hanna (1973) extended their discussion and demonstrated that annual or seasonal average concentrations might be approximated for an entire urban area using a simple relationship of $C = kQ/U$, where C is the average concentration (grams per cubic meter), k is the proportionality constant, Q is the average emission rate of the pollutant (grams per second per square meter, estimated as the total emissions for the city divided by the area of the city, which in their studies was typically of order 7 to 18 km in radius), and U is the annual or seasonal average wind speed (meters per second). The proportionality constant was determined to be mostly a function of stability (day versus night, etc.), and to a lesser extent city size (increasing as city size increased).

For the purposes of estimating an annual average concentration, it was found that k should be specified based on whether the emissions being characterized are elevated or near-surface, and for near-surface emissions, whether the receptors are very near or somewhat away. For near-surface releases, k is equal to 600 for receptors located very near the emissions (like roadway emissions of carbon monoxide), and k is equal to 250 for receptors located away from the emissions. For elevated releases, k is equal to 30 (Gifford and Hanna, 1973; Hanna et al., 1982).

Martin (1971) continued the development of the model used by Pooler with a comparison of results computed (IBM 1130) for a winter season of the average sulfur dioxide concentration values for comparisons with observations collected daily from December 1964 through February 1965 at 40 sites in the St. Louis area. Uncertainties in locating several large point sources precluded the use of results at 5 sites. Model estimates at 34 of the 35 remaining sites were within a factor of 2, with 14 within 30%. A reanalysis of the same data was performed by Calder (1971) using the Climatological Dispersion (CDM) model, and using a revised

²² Reported factor of over or under estimation and correlation coefficient (r^2) was deduced through a linear regression with the intercept forced to be at the origin.

characterization of the area source emissions by Turner and Edmisten (1968). A major enhancement within the CDM over the model employed by Martin was to include an area source algorithm based on the narrow plume hypothesis (Calder, 1977). In spite of the attempts to improve the characterization of area source emissions and the dispersion from these low-level sources, the comparison results were similar to those achieved by Martin. Calder speculated that possible factors contributing to the tendency to overestimate the observed concentration values were: an inherently crude emissions inventory, no day versus night variation in emission rates, and the crude estimates of mixing height employed.

Turner et al. (1971) summarized the results obtained in applying the CDM model to estimate the annual average particulate and Sulfur dioxide concentration values for the New York area for 1969. Sulfur dioxide observations were available for comparison at 75 locations, and total suspended particulate matter observations were available for comparison at 113 locations. This version of the CDM employed the Briggs (1969) plume rise algorithms (in contrast to use of the Holland (1953) algorithms used by Martin and Calder in the St. Louis comparisons). For sulfur dioxide, it appears the CDM tended to slightly overpredict² concentration values by a factor of 1.11. Seventy-one of the 75 values were within a factor of 2, with 47 values within 30%. For particulates, it appears the CDM tended to slightly underpredict² concentration values by a factor of 0.93. 111 of the 113 values were within a factor of 2, with 94 within 30%.

Irwin and Brown (1985) applied the CDM model to estimate 1976 annual average sulfur dioxide concentration values for the St. Louis area. There were 13 sites, but omission of a lead smelter from the emission inventory precluded use of data at two sites for model performance comparisons. The emission inventory and monitoring results were obtained as part of the St. Louis Regional Air Pollution Study (Strothmann and Schiermeier, 1979). These simulations differ with those computed by Turner et al. in that urban dispersion parameters were used, based on tracer studies conducted in St. Louis (McElroy and Pooler, 1968; Gifford, 1976). It was determined that although the area source emissions constituted only 3.5% of the total area and point source emissions, estimated concentrations from area sources ranged from 14 to 67% of the total concentration estimated at the monitoring sites. For the 11 sites, it was found that CDM slightly over-predicted concentration values by a factor of 1.10 with a correlation coefficient (r^2) equal to 0.96. Nine of the 11 sites have estimates within a factor of 2, with 3 values within 30% of those observed.

The version of CDM applied by Irwin and Brown is similar to the Industrial Source Complex Long-Term (ISCLT) model (U.S. Environmental Protection Agency, 1995). The ISCLT area source algorithm nearly approximates what is obtained when one computes area source impacts using an hour-by-hour simulation (which employs a double integral over the area and hence is currently our best expression of dispersion from an area). The emphasis on improving the treatment of area source impacts reflects the recognition that area source emissions (if present) often

account for a major portion of the simulated impacts. The primary focus of Irwin and Brown was to investigate the sensitivity of the annual concentration estimates to the resolution employed in defining the area source emissions. Within the central part of St. Louis, 0.5 by 0.5 km grids had been used to define the emissions, whereas in the suburbs, the emissions were defined using grids as large as 10 to 20 km on a side. It was found that any reduction in the resolution, say by redefining the emissions into grids of 1 km on a side, significantly reduced the concentration estimates, and caused CDM to underestimate the annual average concentration values (especially in the central portion of the city).

In the studies summarized, it is important to remember that the long-term models have evolved from first generation to second generation models, with the adoption of improved characterizations for plume rise, plume dispersion, and treatment of area sources. Except for the simulations for Nashville by Pooler and for St. Louis by Martin and Calder, the average bias has been slight, with typically 80 to 90% of the estimates being within a factor of two of those observed. This model performance was achieved with research grade emission inventories that had little to no bias. The lesson to be learned from modeling studies of annual or seasonal concentration values is that the skill in the modeling results is typically at the mercy of the diligence employed in specifying the diffuse low-level emissions, as they can dominate the analysis.

The results by Gifford and Hanna (1973), Hanna et al. (1982) and Irwin and Brown (1985) confirmed the importance of specifying these diffuse low-level emissions (typically characterized using area sources) with as much care and resolution as feasible. Interestingly, this lesson is rarely considered when emission inventories are developed. The tradition in inventory development is to estimate the total mass of emissions. This means that the low-level diffuse emissions, which may represent less than 10% of the total mass of emissions, receive the least attention and quality control, even though they may account for as much as 60% of the observed impacts on nearby receptors. This becomes of particular concern when attempting to characterize impacts from species directly emitted into the atmosphere. The uncertainty in distributing (in time and space) the low-level emissions ultimately defines the lowest resolution possible in the modeling assessment.

The long-term urban-scale models provided the first demonstrations of how air quality modeling could be used in the development of emission control strategies for state implementation plans. They also provided an important lesson on properly estimating the spatial distribution and temporal behavior of low-level diffuse emissions, especially for estimation of human exposures from these low-level emissions.

5 Development of Tropospheric Chemistry Models

From a review of the historical record, we see that sulfur was recognized or suspected as the basis of many disastrous episodes that focused attention on air pollution as a health problem: December 1930 in Meuse Valley, Belgium; October 1948 in Donora, Pennsylvania; 1952 and 1956 in London, England; and November 1953 in New York, New York (Stern, 1977). The local and urban-scale plume dispersion models discussed in sections 3 and 4, either ignored chemical transformations or treated their effects as a first-order linear decay. These models were primarily developed for use in control programs to reduce sulfur emissions. By the 1960s, ozone was becoming to be recognized as the basis of the smog events first made famous in Los Angeles, which are now seen not only in California but also from Texas through Georgia, and in all the states along the eastern shore of the United States. In the late 1960s, Europe began a concerted attack on resolving the transport and chemistry of sulfur emissions; whereas, the United States began a concerted attack on resolving the transport and chemistry of ozone. Interestingly, as these investigations matured, each became aware that regional transport and fate could not be ignored, and in many instances was the dominant scale to be modeled. By the mid-1970s, concerns began to be raised that the EPA's program to control Total Suspended Particulate was not sufficiently reducing health risks from particulates. The true problem was perceived to be the very fine particles that could be easily trapped within the lungs.

The development of air pollution models that account for atmospheric chemistry and the formation of secondary products adds several complicating factors to the modeling process, which must be addressed in some manner, or the model simulations are stymied. One must have a model for the chemical kinetics. The reaction rates are determined not only by the availability of the proper chemical constituents, but are also typically functions of air temperature, humidity, and incoming solar radiation. As a further complication, the chemistry is rarely of the elementary variety, but involves a system of coupled reactions that in theory might involve hundreds of relationships, but in practice must be simplified and parameterized to a smaller resolved set based on computational resources. Air pollution chemistry often involves characterizing the time and space variations of the emissions of several chemical species over a broad area from many sources, whose individual contributions are incrementally small compared to the total (from all sources). This is a massive job fraught with uncertainties, that even today have yet to be well addressed. As the computation domain increases in size, simple terrain and land use characterizations must be replaced with more comprehensive characterization of the variations in terrain elevation and land cover, and the effects such variations induce on the local meteorology and emissions. The combination of these factors results in simulation models that are computationally more demanding, which adds a further complication of attempting to simplify the problem without losing some sought after quality. Finally, the nonlinear pathways for the formation and destruction of chemical species make the assessment of model performance through a direct comparison of final products, say ozone

observed versus ozone predicted, problematic. The model has many ways to provide a seemingly correct answer for all the wrong reasons and, if this were happening, it would negate the usefulness of the model to determine control strategies.

The following historical review of EPA's development of tropospheric air pollution models is divided along regulatory and legislative programs. Section 5.1 provides a review of the development of models for EPA for characterization of tropospheric ozone²³. The idea of controlling tropospheric ozone using local controls of precursor emissions is eventually seen to be insufficient. Section 5.2 provides a review of the development of models for the characterization of acid deposition. Here, the lessons learned in Europe and in the ozone model development program immediately focus on regional transport. The next three sections focus on the 10-year period of 1990-2000. Section 5.3 reviews the development of a model to characterize the transport and fate of fine-particulates (aerosols). Section 5.4 reviews the development of models for characterization of toxic impacts to Great Waters as required by the CAAA of 1990. Section 5.5 reviews the renovation of computer modeling, stimulated by the High Performance Computing Act of 1991, which assisted the EPA in laying the basis for development of a one atmosphere air quality model.

5.1 Ozone

Los Angeles suffered smog events as early as 1903, when the industrial smoke and fumes were so thick that residents mistakenly believed an eclipse of the sun was happening. The smog on July 26, 1943 is often reported as the first recorded episode. After 1943, the frequency of these smog events increased, but the causes were unknown. On June 10, 1947, California signed into law an Air Pollution Control Act²⁴, authorizing the creation of county-level Air Pollution Control Districts (Los Angeles County was first to create a county-level Air Pollution Control District). These events have bearing on the development of tropospheric chemistry models of air pollution, because it was field data collected in Los Angeles over a series of years that provided a basis for Haagen-Smit (1950) to be able to show that photochemical reactions were the source of the Los Angeles smog. Then Haagen-Smit (1952) was able to show that a mixture of nitrogen dioxide and certain hydrocarbons in air yields ozone in the presence of sunlight. The chemistry kinetics of the reactions were not yet well known, but experiments by Haagen-Smit and Fox (1955) seemed to show that for Los Angeles, the number of ozone molecules seemed to be proportional to the product of the number of

²³ See <http://www.ksg.harvard.edu/gea/pubs.htm> for a review of the legislative and model development for assessment of tropospheric ozone in both the US and Europe by T.J. Keating and A. Farrell (1998). "Problem Framing and Model Formulation: The Regionality of Tropospheric Ozone in the United States and Europe". Belfer Center for Science and International Affairs (BCSIA) Discussion Paper E-98-11, Cambridge, MA: Environment and Natural Resources Program, Kennedy School of Government, Harvard University.

²⁴ See <http://www.arb.ca.gov/html/brochure/history.htm>.

molecules of nitrogen dioxide and hydrocarbons. We know now that this characterization is a gross simplification, but interestingly enough, Frenkeil (1957) used this model of ozone production to show that the contribution of each pollution source to the ozone concentration is not directly additive. The sum of the individual contributions was less than the ozone produced when all sources were simulated simultaneously. It appears that F.N. Frenkiel's simulations may be the first air pollution computer simulation, and his results may be the first to comprehensively demonstrate the complexity that chemistry introduces into assessing the effect of different control strategies.

For the 20-year period from Haagen-Smits' early papers on ozone formation to the mid-1970s, the conventional wisdom was that tropospheric ozone formation could only take place in atmospheric environments that were heavily polluted with automobile exhausts and strongly illuminated with sunlight. Leighton (1961) provided a comprehensive analysis of the known principal reactions in smog formation during this period. The next advance was to realize the importance of the role of hydroxyl radical (Levy, 1971, 1972), and the interplay with methane and carbon monoxide (Crutzen, 1973, 1974). The chain of reactions and list of products were expanding rapidly. Several attempts were made by California consulting firms and universities to develop partial photochemical air quality models during the early 1970s, for example: a three-dimensional Eulerian model was developed by Roth et al. (1971) and Reynolds et al. (1973) of Systems Applications, Inc.; a single-moving cell model by Weisburd et al. (1971) and Wayne et al. (1973) of Systems Development Corporation; a Lagrangian column-of-cells model by Eschenroeder and Martinez (1971) and Eschenroeder et al. (1972) of General Research Corporation; and a particle-in-cell model by Sklarew et al. (1971) of Systems, Science and Software, Inc. Each of these were attempts to grapple with the dilemma of sacrificing some aspect of the problem, in order to have reasonable run times and confine the numerical computations to be within the memory limits of the available computers.

EPA was funding the early photochemical model investigations, but the resulting models found only limited use by regulatory agencies. A statistical relationship had been derived - between the 6:00 to 9:00 AM ambient total and non-methane hydrocarbon concentrations, and the corresponding daily maximum ambient ozone concentration - using data from the Continuous Air Monitoring Project (CAMP stations) and Los Angeles during the late 1960s (Schuck et al., 1970; U.S. Environmental Protection Agency, 1971). This was summarized in the 1971 Appendix J to Title 40, Part 51 of the *Code of Federal Regulations*, and was used to estimate the degree of reduction in hydrocarbon emissions (total and non-methane) needed to achieve the primary NAAQS for photochemical ozone (1-hour average of 0.08 ppm, not to be exceeded more than once per year at any one location). One of many shortcomings of the approach was its inability to address transport effects, such as entrainment of unscavenged ozone, which can result from transport from other regions or from ozone trapped aloft overnight.

The first reports on photochemical smog in London and Western Europe were presented by Derwent and Stewart (1973) and Guicherit and van Dop (1977). By 1977, EPA had completed its efforts to find a replacement for the 1971 Appendix J procedure. Based on smog chamber studies, a chemical kinetics model was derived for the formation of ozone from a mixture of propylene, n-butane and nitrogen oxides. This kinetics model formed the basis of the EPA Empirical Kinetic Modeling Approach (EKMA), which utilized a set of empirical ozone isopleths depicting the maximum afternoon ozone concentration downwind of a city as a function of initial morning concentrations of precursor emissions (non-methane hydrocarbons and nitrogen oxides), precursor emissions occurring later in the day, meteorological conditions, reactivity of the precursor mix, and concentrations of ozone and precursors transported from upwind areas. EKMA was a single-column box model that could be envisioned as following a trajectory. As the column of air is advected with the winds, emissions that enter are assumed to be instantly mixed uniformly within the column. From early morning to mid-afternoon, the column height increases to simulate the growth of the mixing height during the day and effects of entrainment of pollutants trapped aloft (Dodge, 1977). This model contained a detailed characterization of ozone formation and fate, and retained computational efficiency. For the next 10 years, EKMA found widespread use to predict the relative changes needed in the precursor emissions necessary to reduce observed maximum ozone concentration for an area to be below the new 1-hour maximum ozone NAAQS of 0.12 ppm.

EPA had recommended two approaches for formulating State Implementation Plans to achieve the NAAQS for ozone. The first was EKMA that allowed development of city-specific plans. The second approach allowed the use of a grid-based photochemical air quality model, which by necessity used a reduced (or lumped) chemical model. From 1977 to 1987, the EPA sponsored research resulted in two reduced mechanisms: the lumped molecule (surrogate species) approach (Carter et al., 1986; Lurmann et al., 1987) and the lumped structure (Carbon Bond I through IV) approach (Whitten et al., 1980; Gery et al., 1988). The critical review by Seinfeld (1988) described the evolution of the first-generation grid models towards becoming second-generation models, and also summarized several of the practical implementation problems of the grid models, which primarily resided in the considerable database needed for their use. He also noted that rigorous, universally-accepted performance criteria for grid-based photochemical air quality models do not exist, a statement that is still true in 2005.

For regulatory applications, EPA released version 2 of the Urban Airshed Model (UAM-II) in 1980 (U.S. EPA, 1980) and later recommended it as the preferred model for ozone planning in urban environments (U.S. EPA, 1986). In 1988, improvements were made to the chemical mechanism and a system of preprocessors for preparing emissions and meteorological inputs were added to create a second-generation modeling system, UAM-IV (Gery et al., 1988). As the limitations of EKMA became recognized, UAM-IV began to emerge as the dominant tool for urban-scale ozone planning.

As described by Strothmann and Schiermeier (1979), a White House initiative in late 1971 called for development and validation of improved air quality simulation models upon which cost-effective pollutant control strategies could be based. This provided the basis for EPA's St. Louis Regional Air Pollution Study (RAPS). Planning for this study began in August 1971, and field investigations were conducted approximately between 1973 and 1978. One of the primary objectives of RAPS was to create a comprehensive and accurate database for all criteria pollutants and selected non-criteria pollutants, for use in developing and evaluating air quality simulation models, with particular emphasis on photochemical models. For this purpose, the Regional Air Monitoring System (RAMS) was designed and operated, which consisted of 25 remotely operated, automated monitoring stations controlled and polled via telemetry by a central data acquisition system. Station locations were chosen with care to avoid being unduly affected by emissions from some local nearby source. Comprehensive point and area source emission inventories were developed including emissions of sulfur oxides, carbon monoxide, oxides of nitrogen, hydrocarbons and particulates. Seventeen stations had 30-m meteorological masts while the other sites had 10-m masts. The meteorological instrumentation was comprehensive, including wind sensors, temperature, dew point, pressure, and solar radiation. In addition, the 30-m masts had a 5 to 30 m temperature difference measurement, and a UVW Gill anemometer for turbulence measurements. An upper air-sounding network was established to provide a definition of the winds and temperature structure aloft. A review of the many publications spawned by this study reveals that they fall into two basic categories: studies of urban air quality and meteorology (e.g., Ching and Doll, 1981; Clarke et al., 1981; Godowitch et al., 1979, 1981; Karl, 1980; Shreffler, 1978) and studies of air quality model performance (e.g., Schere and Shreffler, 1983; Turner and Irwin, 1983, 1985; Turner et al., 1985).

EPA-sponsored field studies (e.g., U.S. Environmental Protection Agency, 1976) revealed the regional nature of the ozone problem. It was becoming increasingly clear that local reductions in ozone precursor emissions were an insufficient abatement strategy for many areas of the U.S. Crafting an effective ozone reduction program would require following the fate of air masses for several days, or in other words, a regional abatement strategy. In 1977, EPA began the development of the Regional Oxidant Model (ROM) (Lamb, 1983, 1984) which found extensive use in the examination of the effects of alternative emission reductions on ozone concentration for the eastern United States. The chemistry kinetic mechanism used in ROM was the lumped structure approach (Carbon Bond I through IV). To conserve computer memory, the atmosphere was vertically divided into three layers: layer 1, the surface-layer and lower boundary layer; layer 2, a layer whose top followed the diurnal extent of the mixed layer; and layer 3, an upper layer capping inversion layer. The wind fields were determined by interpolation on an hour-by-hour basis from observations at surface and upper air stations. The strength of this model was its ability to follow the chemistry of 28 species, and cover almost one-fourth of the United States in one run. The

limitations were the complexity of model setup, and use of boundary conditions²⁵ tuned to particular locales through extensive testing, which precluded recommending unassisted use of the model for compliance modeling (Schere and Wayland, 1989).

In 1991 the U.S. National Research Council, with funding support from the EPA, completed its scientific assessment of the state of knowledge of the physical and chemical sciences relevant to the characterization of tropospheric ozone (National Research Council, 1991a). They concluded that despite a major regulatory effort, the ozone control programs for the 1970 to 1990 period had failed. The State Implementation Plans were fundamentally sound as planning instruments, but seriously flawed due to the lack of a verification program. Emission inventories were seen to be highly uncertain, with anthropogenic volatile organics significantly underestimated, and they saw a need to recognize the important role of biogenic volatile organic emissions in simulating tropospheric ozone. The National Research Council review also noted that despite over a decade of experience in ozone modeling, there had yet to be a consistent set of evaluation procedures, notwithstanding the widely recognized need for such methodology. At this point in time, the UAM model with Carbon Bond II was in wide use. There had been some testing in several models with Carbon Bond IV kinetics (CBM-IV). The software package that allowed EKMA control strategies to be estimated using optional chemical kinetics models was upgraded for a fourth time to include CBM-IV and a feature that allowed a user-defined mechanism, OZIPM-4 (U.S. Environmental Protection Agency, 1988a). Recognizing the importance of regional transport, U.S. Environmental Protection Agency (1988b) issued guidance that suggested that UAM might be used to provide the regional boundary conditions for use in the OZIPM analyses.

In 1991, the results and conclusion of a 3-year study called the Regional Ozone Modeling for Northeast Transport (ROMNET) program were published (Possiel et al., 1991). This investigation used ROM version 2.1, employing meteorological scenarios from episodic periods in 1980, 1983, 1985 and 1988, with emissions for each episode and five control strategy projected emission inventories for each episode for 1995 and 2005. A major conclusion was that the areas outside of the corridor of cities along the east coast of the United States may have to add controls beyond those necessary to solve their local problems in order to reduce transport of air pollutants and precursors into these areas. For most of the domain, the production of ozone was seen to be limited by the oxides of nitrogen, with ozone production limited by the availability of volatile organic compounds in areas with large oxides of nitrogen emissions. Meteorology played a major role in the buildup and limitation of regional ozone. These results confirmed the important regional nature of the ozone formation and the need for development of regional air

²⁵ Generally, ROM was run with tropospheric clean boundary conditions, and EPA's Aerometric Information Retrieval System (AIRS) ozone measurements could be used for continental side boundaries (<http://www.epa.gov/airs/airsaqs/>).

pollution control programs. These ROMNET results were confirmed in a later investigation that employed ROM version 2.2 (Roselle and Schere, 1995). In this later investigation, a 9-day period in July 1988 was simulated for the eastern US, with 17 simulations of various control strategies. The improvements made in going from ROM version 2.1 to version 2.2 included a well-mixed convective boundary layer model, improved characterization of wind flow during nighttime inversion conditions, upgraded characterization of turbulence over urban areas, and upgraded parameterizations of the vertical cumulus cloud flux. There were other studies as well, and it was seen that advances in scientific understanding were not altering our growing awareness of both the regional nature of ozone formation and the general conclusions found in ROMNET. All of the studies highlighted need an operational regional ozone model for routine use. In 1996, the decision was made that all subsequent oxidant model development would be conducted within the one atmosphere paradigm, which at the time was called Models-3/Community Multi-Scale Air Quality (CMAQ) modeling system.

There was a sense, left by the 1991 National Research Council review, that the ozone models in routine use were need of revamping. The modeling tools under development were admittedly pushing the limits of the computers of this time. Expanding the scope to include regional transport would only exacerbate the problems imposed by the computer limitations. The ozone standard and the effectiveness of the control programs were in question. We close this section of the discussion with the recognition that the 1990 decade is the advent of third generation models, which will require redesign of the numerical framework, the chemistry mechanism, fuller characterization of mesoscale meteorological effects, and consideration of the possibility of feedbacks between the chemistry, meteorology, and surface heat and moisture balance.

5.2 Acid Deposition

Even though our emphasis is regulatory model development for EPA, it is worthwhile to examine Europe's interest in air quality modeling of sulfates for two reasons. First, a comparison of Europe's early models for sulfate reveals that they are conceptually similar to the designs used in the US for early ozone models. Second, when the US finally began to focus on modeling sulfates, they borrowed heavily from the experiences of Europe. The period from the mid-1950s through the mid-1970s can be viewed as the development of a conceptual model for the acidification of precipitation in Europe. The acidification of precipitation in Europe was first noticed in samples collected from the European Air Chemistry Network, established in the mid-1950s (Ottar, 1978). Analyses of these data showed that in Europe, the central area with highly acid precipitation was expanding. The main acid component was sulfuric acid, and was seen to be related to the increasing use of sulfur-containing fossil fuels in Europe. The Organization for Economic Co-operation and Development (OECD) recommended a full investigation. With the approval in 1972 by the OECD, the first measurement program was launched. A second measurement program was completed in 1975.

By 1977 it was becoming clear that even though the countries with the largest emissions also received the largest depositions of acidic rain, those regions with low emissions received more pollution from other countries than from their own sources.

Development of mathematical simulation models in Europe had a decided focus on long range transport effects during the period from 1970 to 1980. The early Lagrangian models followed moving air parcels along trajectories (Eliassen, 1978), and the transformation and deposition were approximated using an assumed rate of transformation of sulfur dioxide to sulfate, and assumed wet and dry deposition velocities for sulfur dioxide and sulfate. The early Eulerian grid models had similar characterizations for the transformation and deposition, and suffered (as all early grid models) from undesired computational dispersion (Nordo et al., 1974). These models could achieve high correlations with annual average concentration values, but were incapable of correlating well with 24-hour averages (or less). Statistical models were developed that were able to describe the broad features of the annual average patterns (Rodhe, 1972; Fisher, 1983). The purpose of these statistical modeling efforts was to confirm the conceptual model that had been constructed from analysis of precipitation records that the developed industrial regions of central Europe were responsible for most of the acidification of the precipitation seen in Norway and Sweden.

A change occurred in the direction of model development and air pollution policy in the United States around 1976. Control of sulfur dioxide had decreased urban levels of sulfur dioxide, but these decreases did not seem to be accompanied by a proportional decrease in urban sulfate, which was popularly called acid rain. Of the existing explanations for the lack of decrease in sulfate levels, the results from European investigations seemed to provide the most plausible theory, that is, the long range transport of sulfur emissions was responsible for the observed urban sulfate levels.

There were significant scientific uncertainties in the health effects and in the available characterizations for long range transformation-transport of sulfate. To provide a scientifically sound assessment of the extent of the acid rain problem, Congress passed and President Carter signed the Acid Precipitation Act of 1980 (Public Law 96-294). The Act directed the United States Government to conduct a ten-year assessment to determine the causes and consequences of acid precipitation, and to develop options for reducing known effects. The National Acid Precipitation Assessment Program (NAPAP) was created in response to this congressional charge. NAPAP formally involved twelve Federal agencies, and informally several states and provinces of Canada, EPRI, the National Association of the Paper Industry for Air and Stream Improvement, the Mellon-Foundation, and the Natural Resources Defense Council. NAPAP was reauthorized for an indefinite period through Title IX of the CAA Amendments of 1990, Cowling (1992). Thus, in the late 1970s and throughout the 1980s, funding for model development for abatement of sulfur dioxide and urban ozone was reduced to

support an aggressive program for development of regional-scale acid precipitation air quality models.

The first of a series of plume mapping and sampling field studies was the Midwest Interstate Sulfur Transformation and Transport (MISTT) from 1973 to 1976 (Wilson, 1978). The electric power utilities sponsored the Sulfate Regional Experiment in Northeastern United States (SURE), which began in 1976 with a network of 54 hi-vol, and sequential samplers stations distributed somewhat randomly throughout the northeastern United States to provide measurements of particle mass, sulfate, sulfite, nitrate, chlorate, ammonium and water-soluble organics (Perhac, 1978). EPA initiated the Sulfur Transport and Transformation in the Environment (STATE) field studies, of which the first was the 1978 Tennessee Plume Study (TPS) (Schiermeier et al., 1979). Using aircraft sampling, the TPS attempted to quantify changes in plume characteristics and composition out to distances of 500 km. The NOAA Air Resources Laboratory coordinated the 1983 Cross-Appalachian Tracer Experiment (CAPTEX), which involved over eighty sequential ground-level tracer samplers of perfluorocarbon at distances of 300 to 1100 km from release sites (Ferber et al., 1986). The upper-air soundings were increased to four per day, and seven aircraft provided vertical distributions of the tracer. This rich database has found frequent use to test a variety of advancements in regional-scale modeling techniques, including: Four Dimensional Data Assimilation (FDDA) (Kao and Yamada, 1988); particle dispersion modeling (Lee, 1987); and delayed shear enhancement (Moran and Pielke, 1996).

In 1982, EPA asked the National Center for Atmospheric Research (NCAR) to assess the state of the sciences that would be involved in developing comprehensive acid deposition modeling systems. This assessment (National Center for Atmospheric Research, 1983a, 1983b) and other independent assessments (MOI, Work Group II, 1982; Electric Power Research Institute, 1984) concluded that it was feasible to develop a comprehensive wet and dry acid deposition model. In 1983, the Acid Deposition Modeling Project was established at NCAR to develop a model suitable for use by NAPAP. The project was funded by the EPA and the National Science Foundation (NSF), and it was based at NCAR until 1987. With the shift in 1987 towards model testing and application, the project was moved to the Atmospheric Sciences Research Center (ASRC) of the State University of New York (SUNY) in Albany, NY. Several versions and enhancements were made to the Regional Acid Deposition Model (RADM) as a consequence of this work. RADM was a numerical grid model that subdivided the northeastern United States into a 35 by 38 horizontal grid with six to fifteen vertical levels. Aqueous-phase reactions in clouds are a major contributor to atmospheric acidification; therefore, it was important to employ a chemistry kinetic mechanism that could correctly predict the concentration, solubility, and rate of mass transfer of oxidizing agents such as hydrogen peroxide, ozone, methyl hydrogen peroxide, peroxy acetic acid, and hydroxyl and hydroperoxy radicals. With these concerns in mind, the RADM organic chemistry mechanism was developed using a reactivity lumped molecule approach. By 1990, the gas-phase chemical reaction mechanism

contained over 100 reactions and followed over 50 species. New methods were found to limit numerical solver uncertainties; enhancements were made to better address aqueous-phase in-cloud chemistry and dry deposition fluxes were computed for 13 species (Chang et al. [1990], 4-113).

The abundance of naturally occurring hydrocarbons in the atmosphere had been recognized for some time (Arnts and Meeks, 1981; Peterson and Tinge, 1980; Rasmussen, 1972). Even before modeling studies by Chameides et al., 1988 and Trainer et al., 1987 were suggesting the need to consider biogenic hydrocarbon emissions for estimating the production of photochemical oxidant, EPA reported on the development of a computer algorithm for estimating biogenic emissions (Novak and Reagen, 1986). This system, called the Biogenic Emissions Software System (BESS), was designed to produce hourly gridded hydrocarbon emissions for an early version of the ROM. In parallel with this effort, researchers at Washington State University devised a method for estimating seasonal, county-wide hydrocarbon emissions across the US (Lamb et al., 1987). These estimates were used for early parts of the NAPAP. These two methods for estimating biogenic emissions were combined by Young et al. (1989), which became a generalized scheme called the Biogenic Emissions Inventory System (BEIS) that could service either ROM or RADM (Pierce et al., 1990).

The meteorological model for RADM was the Pennsylvania State University/National Center for Atmospheric Research (PSU/NCAR) Mesoscale Model, Version 4 (MM4). EPA initiated work towards development of this model in the early 1970s with a research grant to the Pennsylvania State University (Anthes et al., 1974; Anthes and Warner, 1978; Anthes et al., 1987). This research involved converting a mesoscale meteorological model that simulated hurricane dynamics where atmospheric processes are strongly forced, into an air quality meteorological model, which often must deal with weakly forced or stagnant conditions. This model was the first to employ Newtonian Relaxation, or nudging, in which the model state was relaxed toward the observed state by adding to one or more of the prognostic equations, artificial tendency terms that were based on the difference between the two states. In making the conversion for air quality modeling, the nudging was extended to include surface boundary layer variables (Stauffer and Seaman, 1990; Stauffer et al., 1991).

The 1980 charge to perform a comprehensive scientific assessment of the fate of sulfate and the aggressive response by NAPAP to form a comprehensive regional-scale acid precipitation model accelerated the advancement of chemical solvers, the characterization of meteorological transport and atmospheric processes. The demands for more complete characterizations of the chemistry placed increasing demands for detailed comprehensive emission inventories. For instance, the 1990 version of RADM 2.0 required hourly emissions of sulfur dioxide, sulfate, nitric oxide, nitrogen dioxide, ammonia, carbon monoxide, and 15 classes of volatile organic compounds (VOCs) (Chang et al. [1990], 4-27). The Acid Precipitation Act of 1980 and the resulting creation of the NAPAP caused an

intersection between the critique of what science can affirm and the development of policy. One of the many lessons learned was that science cannot answer policy questions, which are value-based; whereas science can provide an assessment of the consequences of alternative strategies. This was not an easy intersection as witnessed by the comments and reflections of those involved (Cowling, 1992; Kingdon, 1995, Lackey and Blair, 1997; Alm, 2000).

The RADM NAPAP assessment was completed in 1990 with significant participation by many ARL NOAA scientists (Hicks et al., 1990; Binkowski et al., 1990; Chang et al., 1990; Dennis et al., 1990a, b). Of the many advances made in developing and applying RADM, of significance are: 1) a dynamic mesoscale meteorological model (MM4) was successfully tailored for use in air quality simulations by extending FDDA to include nudging of winds and moisture within the planetary boundary layer; 2) MM4 was successfully coupled to a dynamic air quality model (RADM) with a comprehensive characterization of oxidant and sulfate chemistry, and fate; 3) the importance on air quality modeling results of the simulation of cloud fields, cloud processes, and heterogeneous and aqueous chemistry was successfully demonstrated; 4) an aggregation methodology was successfully developed that allowed long-term concentration averages to be estimated using a combination of short-term episodic results (Samson et al., 1990); and 5) a series of engineering versions of RADM were successfully developed that allowed rapid and accurate investigation of sulfur control strategies without the need to make additional runs of the resource and computationally demanding RADM.

In the years following the completion of the RADM evaluation and its use in the NAPAP assessment, there were several important advances that were tested and evaluated. A simple non-local closure model for characterizing vertical mixing within a convective boundary layer (CBL) (Pleim and Chang, 1992) addressed the findings of the convective tank experiments by Willis and Deardorff (1976, 1978, 1981) within the context of an Eulerian grid model. The model, named the Asymmetrical Convective Model (ACM), allows mixing from the lowest model layer directly to all other layers in the CBL, but restricts downward transport to proceed only to the next lower layer, in order to emulate the rapid upward mixing of convective eddies, and the much slower downward mixing typical of convective boundary layers. They installed ACM within RADM and saw that the rapid transport of surface emissions of nitrogen oxide and nitrogen dioxide into layers aloft coupled with the slower downward mixing resulted in lower ozone concentrations throughout the mixed layer than would be obtained using conventional vertical mixing models. In 1993 and 1994 (Poole-Kober and Viebrock, 1993, 1994), ARL staff performed several in-house investigations to better understand how grid resolution in the vertical and horizontal affected RADM model performance. It was concluded that increasing the vertical resolution from 6 to 15, and then to 30 layers improved the simulation of nocturnal surface concentration values of ozone, because the oxides of nitrogen emissions emitted into a thinner lowest layer were less diluted, and this enhanced the titration of

ozone at night. In a 1994 investigation, ARL staff conducted in-house sensitivity analyses using RADM to test the potential of two heterogeneous reactions on oxidant photochemistry. One was a heterogeneous reaction of N_2O_5 with water to produce nitric acid, and hence, the termination of photochemical active oxides of nitrogen. The other was the conversion of hydroperoxy radical to hydrogen peroxide. There was evidence that this reaction occurs on wetted aerosols when aqueous copper concentration is sufficiently high to act as a catalyst. Investigations concluded that the first reaction could be included in an operational RADM, but the second reaction relied on copper content estimates of aerosols, which was considered to be too uncertain for operational use.

In 1993, a one-dimensional prototype program was developed that consisted of a simple surface energy and moisture parameterization including explicit representation of soil moisture (Noillian and Planton, 1989) with the ACM model. The coupled surface and planetary boundary layer (PBL) model performs integrated simulations of soil temperature and soil moisture in two layers as well as PBL evolution, and vertical transport of heat, moisture, and momentum within the PBL. Comparisons of modeling results with observations taken during a two-day period of the Wangara field study and several days from the First ISLSCP Field Experiment (FIFE) in 1987 and FIFE in 1989 illustrated the model's ability to simulate ground temperature, surface fluxes, and boundary layer development accurately (Pleim and Xiu, 1993). This model was then incorporated into MM4, essentially replacing the existing high resolution PBL model, and work was initiated to develop an advanced FDDA technique for indirect nudging of soil moisture. By 1996, the model had been installed within the newly released MM5 (Grell et al., 1994) and was denoted as MM5PX. There were several improvements provided in MM5, the main one being that it contained both the hydrostatic and non-hydrostatic equations of motion. Indirect nudging of soil moisture was seen to explain errors in simulated air temperature, humidity and PBL heights (Pleim and Xiu, 1995). Collaborative research with NCAR converted this surface model for inclusion in MM5 version 3, which was released in July 2000.

It is 1996 at this point in the discussion, and the decision is made that all subsequent acid deposition model development would be conducted within the one atmosphere paradigm, which at the time was called Models-3.

5.3 Aerosols

In 1987, early models of the three general approaches available for the characterization of the aerosol distribution were being investigated (Hudischewskyj et al., 1987). The three approaches involved a continuous representation (Suck and Brock, 1979; Tsang and Brock, 1982, 1983), a sectional representation (Gelbard and Seinfeld, 1980; Seigneur, 1982, Gelbard, 1984; Warren and Seinfeld, 1985), and a modal representation (Whitby, 1978, 1981, 1985; Saxena et al., 1986). The modal model represents the entire fine aerosol distribution as the summation of two log-normal distributions. The processes that

affect the aerosol distribution are simulated by altering the zero-th, third and sixth moments of these two distributions. The modal representation was determined to be on average 400 times faster with average errors for nitrate, ammonium, total mass, and the light scattering coefficient (b_{scat}) all well within 10 percent in comparison with the other two representations. With the completion of the Modal Aerosol Dynamics (MAD) model, (Whitby, 1990; Whitby et al., 1991), developmental work was initiated to install the MAD model into RADM. A technique for estimating dry deposition fluxes for particulate matter was developed that accounted for the particle size-dependent effects of Brownian motion, inertial impaction, and gravitational settling (Bullock, 1990). Comparisons with measured field data (Wesely et al., 1985) provided a basis for selecting a deposition velocity characterization by Pleim et al., 1984. By 1994 the focus was on improving the characterization of cloud interactions on aerosol size dependence and on the characterization of wet deposition (Binkowski and Shankar, 1994; Shankar and Binkowski, 1994). In 1995, the number of chemical aerosol species was increased by adding nitrate and organic carbon to the existing list of sulfate, ammonium, and water.

The first generation Regional Particulate Model (RPM) was formed in 1989 by adding an aerosol chemical and kinetic mechanism to RADM/EM to characterize the development and fate of aerosols. This model was then capable of simulating sulfate aerosols in seven size ranges (a sectional approach), and considered the effects of nucleation, condensation, evaporation, coagulation, and aqueous aerosol chemistry. This model was developed to assist in policy development and promulgation of air quality standards for fine particles, visibility, and acid aerosols (Bullock et al., 1989). Preliminary review of predicted sulfate concentration values for August 3-6, 1979 of the Northeast Regional Oxidant Study (NEROS), and for April 22-24, 1981 of the Oxidation and Scavenging Characteristics of April Rains (OSCAR) tended to be highest where observed visibility was lowest. Aerosol concentration values near the source regions tended to be low, with higher aerosol concentration values further downwind of the source regions.

In 1995, a new method for modeling dry deposition of gaseous chemical species was developed to take advantage of the more sophisticated surface model implemented in MM5PX (Pleim et al., 1996, 1997), and was tested against field data observations for ozone deposition. Since MM5PX had a parameterization for evapotranspiration, the same stomatal and canopy conductances could be used to compute dry deposition velocities of gaseous species. While developing the model, it was seen that it could be easily extended for use to compute dry deposition velocities directly from field measurements (Pleim et al., 1999). The scheme potentially provides a means for accurately estimating the dry deposition velocity of ozone, and perhaps other gaseous species such as sulfur dioxide and carbon monoxide, from relatively inexpensive field networks and without the need for direct chemical eddy correlation measurements.

By 1996, the RPM had become a complete aerosol and visibility modeling system (Binkowski and Shankar, 1995; Binkowski and Ching, 1996), and the decision was made that RPM would be incorporated into the Models-3/CMAQ framework.

5.4 Toxics

Title III of the CAAA of 1990 required an assessment of the annual atmospheric deposition of toxic substances to the Great Waters that consist of the Great Lakes, the Chesapeake Bay, Lake Champlain, and the coastal waters of the US. This included the identification of the sources and assessment of their relative contributions. To provide an interim assessment using off-the-shelf technology, it was decided to adapt an existing model, called RELMAP (Eder et al., 1986), to simulate atmospheric deposition of toxic substances (Clark et al., 1992; Clark, 1992). It was assumed that the substances are chemically inert and deposit at rates based on published physical attributes (i.e., Henry's law coefficients, liquid-phase vapor pressures, and phase partitioning ratios). Using existing emission inventories, it was possible to simulate 22 toxic substances, and the preliminary results confirmed that the transport scales of the substances deposited to Lake Michigan varied significantly. In 1993, this effort focused 1) on the characterization of mercury emissions from all major anthropogenic sources, and 2) on mercury emissions and other designated toxic pollutant (arsenic, cadmium, lead, and 17 separate dioxin/furan congeners) only from coal-fired utilities. The latter effort culminated in a final mercury study report to the U.S. Congress (U.S. Environmental Protection Agency, 1997) and in a final report to the U.S. Congress on the hazardous air pollutant study for the electric utility steam generating units (U.S. Environmental Protection Agency, 1998a). Recent laboratory studies of chemical reactions of mercury and its compounds in air and in water (Lin and Pehkonen, 1999) suggest that the chemistry mechanism of RELMAP mercury may not accurately reflect the complex nature of mercury chemistry, especially in cloud water. In response to this, work has begun to modify CMAQ (discussed in section 5.5) to include mercury and various mercury mechanisms as modeled species. One of the serious uncertainties to be addressed in this work will be estimating the concentration of chloride ions in cloud water from marine to continental locations.

It was realized, at the inception of the work effort just described, that there were limitations inherent in the RELMAP modeling system for the treatment of chemistry and cloud processes. Hence in 1991, the EPA Office of Research and Development and the Air, Radiation and Toxics Division of EPA Region III created the Chesapeake Bay Evaluation and Deposition (CBED) Committee. This second effort was to have a research focus, but also serve a practical regulatory goal of investigating what reductions might be expected in nitrate deposition to the Chesapeake watershed and to the tidal Bay, resulting from control programs brought about by the CAAA of 1990 to reduce ozone. In particular, the Chesapeake Bay Program jurisdictions had a goal of reducing nitrogen and phosphorus pollution by 40 percent (from 1985 levels) by the year 2000. In the course of this work, it was decided to provide the RADM deposition results to the

Chesapeake Bay Watershed Model (Donigian et al., 1991; Linker et al., 1993). This provided a means for estimating the nitrogen loadings to be expected in the tidal waters of the Bay, based on estimated reductions in atmospheric nitrogen loadings to the Bay waters. By 1996, the focus was on defining scenarios to be simulated by RADM, which would be run with a 20 km grid resolution covering the Chesapeake Bay watershed, and to link these results to the watershed model. These analyses were directed towards assessing the reductions that might be anticipated in nitrogen deposition, resulting from the implementation of three scenarios: 1) the expected 1990 CAAA oxidant-related emission reductions when mandatory control programs are applied; 2) scenario 1, plus a low emission vehicle program and emission limits applied to large fuel combustors in the Northeast Ozone Transport Region, and 3) scenario 2 applied to all states in the Chesapeake Bay watershed. From these results, it appears that scenarios 1 and 2 would reduce nitrogen loadings by about 10 to 15 percent, whereas scenario 3 would reduce nitrogen loadings perhaps as much as 30 percent (U.S. Environmental Protection Agency, 1996; Dennis, 1997). A significant finding in these investigations was the importance of considering the transport of deposited nitrogen by feeder streams that drain into the tidal Bay, which might account for as much as 20 percent of the total nitrogen loading to the tidal Bay, and thus, the benefits of considering control programs that affect the entire watershed system. In 2000, plans were made to use an extended RADM that incorporates the full dynamics of secondary inorganic fine particle formation in order to study ammonia deposition, and to produce revised estimates of the deposition of oxidized nitrogen to the Chesapeake Bay and its environs.

The Chesapeake Bay study provided ample demonstration of the benefits of linking environmental models (air, soil, and aquatic) in assessing pollution impacts. During these investigations it became increasingly apparent that there were many scientific issues and uncertainties in linking together process-oriented models from different media (air, soil, water) that simulate the transport and fate of pollutants. Thus, a long-term research and development project was started in 2000, called the Multimedia Integrated Modeling System (MIMS), whose goal was the development of a modeling system with predictive capability for transport and fate of nutrients and chemical stressors over multiple scales, to allow assessment of air quality and watershed management practices on stream and estuary conditions. The system would involve characterization of chemicals through the hydrologic cycle, or the response of ecological systems to land-use change. Currently, MIMS is not anticipated to couple Models-3/CMAQ within MIMS, but use results from Models-3/CMAQ as input to the MIMS simulations.

There is a class of local-scale modeling that up until this point has not been addressed in this review, and it has to do with what is traditionally referred to as human exposure modeling. Human exposure modeling assessments have had a role in the regulatory assessments leading up to establishing or revising the NAAQS. The goal of such modeling assessments is to characterize the distribution of exposures that the population will experience due to ambient levels of pollutant

concentration. Studies of human time-activity patterns show that people move from various indoor environments to outdoor environments, and the movement involves commuting from one location to another. The term microenvironments is used to denote different places (car, home, office, construction site, restaurant, sports arena, parks, etc.) one might describe as their location during a daily activity record. The time one spends in each of these microenvironments is a function of age and occupation. Modeling exposures of populations (age-sex-occupation subgroups or cohorts) then becomes combining the microenvironmental concentration with time-activity patterns specific to each cohort, and extrapolating these results to include the entire population (Duan, 1981, 1989). An early successful model of this form for simulating personal exposures, called SHAPE (Ott et al., 1988), was evaluated for carbon monoxide exposures using personal exposure data collected in Denver, CO (Johnson, 1983). These investigators have since extended these modeling concepts to allow the investigation of how much of PM₁₀ personal exposures can be attributed to ambient emissions versus indoor emissions (Ott et al., 2000).

Data on human activity patterns were combined with measurements of ambient concentrations using the NAAQS exposure model (NEM) (Biller et al., 1981) to estimate population exposures, and to assess the effectiveness of proposed rulemaking involving particulate matter (Johnson and Paul, 1981), carbon monoxide (Johnson and Paul, 1983) and nitrogen dioxide (Johnson and Paul, 1984). To improve the characterization of variability possible in the population exposures, the NEM modeling assumptions regarding air exchange rates between microenvironments, generation of time-activity patterns, and certain other empirical parameterizations were converted from being average characterizations to probability distributions. This second-generation NEM (pNEM) was then used to assess carbon monoxide exposures to Denver residents (Johnson, 1992) and ozone exposures in the Chicago urban area (McCurdy, 1994). In accordance with a peer review recommendation that pNEM be evaluated against actual personal exposure data, an evaluation was conducted in which pNEM estimates of carbon monoxide were compared with carbon monoxide observations (Law et al., 1997) available from a personal exposure monitoring study conducted in Denver (Johnson, 1983). The evaluation results suggested that pNEM was underestimating the highest personal exposures and overestimating the lowest personal exposures.

Using concepts from the probabilistic NEM model, a Hazardous Air Pollutant Exposure Model (HAPEM) was streamlined and specialized for use in simulating exposures from mobile source emissions (Johnson et al., 1992), and the model came to be called HAPEM-MS. Of significance was the fact that the model and its required databases were revised so that the model could be run on a desktop computer rather than a mainframe computer. HAPEM-MS was then used to estimate carbon monoxide exposures for Denver (Glen and Zelenka, 1994). In 1998, HAPEM-MS was used to produce the exposure estimates for the National Air Toxics Assessment for the base year of 1996. This assessment produced results that are useful in understanding the quality of air and its possible effect on human

health nationwide. Specifically, it provided estimates of 1) the release of 33 toxic atmospheric compounds into the air from various sources; 2) the concentration of these compounds in air; 3) the exposure of populations to this air; and 4) the risk of both cancer and non-cancer health effects resulting from this exposure. Work has continued on this through 2000, and it is expected that additional years will eventually be simulated²⁶.

The preceding discussion of pNEM and HAPEM-MS described population exposure models that assume that either monitoring data or model estimates are available for characterizing the ambient concentration values. In 2000, a new project was initiated with a goal of developing algorithms for linking Eulerian grid-based air quality models to human exposure models to provide a means for understanding, quantifying and assessing the health impacts and risks of airborne particles and air toxics. In designing these algorithms, it is anticipated that details of the concentration variation will require algorithms that directly or indirectly estimate the subgrid neighborhood-scale variation in the concentration values. To initiate this project, an Eulerian grid model (CMAQ, discussed in section 5.5) was run for the Philadelphia Metropolitan Area for three grid resolutions (12, 4 and 1.33 km) to investigate the sensitivity of the simulated surface layer ozone and PM_{2.5} concentrations to grid resolution. Future investigations are needed to develop methods not only for assessing the practical limits of grid modeling, but also for addressing urban canopy effects, exchanges between microenvironments, and methods for extrapolation of episodic results for longer-term exposure time-scales. Along these lines, research was initiated in 1998 to acquire and apply Computational Fluid Dynamics (CFD) models, with the goal to simulate the pathway from the source of emissions to human exposures.

5.5 One Atmosphere

Bringing knowledge together (as a junction of streams, for the purpose of understanding) to form what is now commonly called one atmosphere modeling is an apt characterization of the period from 1990 to present. In truth, bringing knowledge together is how model development has always occurred. The decade, 1990 to 2000, was special because of the advancement in computer memory capacities and computational speed. This advancement allowed the blending together of more detailed and comprehensive descriptions of atmospheric physics and chemistry that heretofore had been forced by numerical capabilities to be treated either simplistically or separately. In anticipation of new computing capabilities and the possible consequences, Congress passed the High Performance Computing Act in 1991 (Public Law 102-194), which authorized a 5-year program with initial focus on high-speed parallel computing and networking. The additional funds, resulting from participating in this initiative, made it possible for the EPA to blend together research results from oxidant modeling with ROM and acid precipitation modeling with RADM, and also to develop and incorporate a

²⁶ For status of these activities, consult: <http://www.epa.gov/ttn/atw/nata/>.

pragmatic and innovative simulation of aerosol dynamics and chemistry all under one modeling framework. This allowed assessment of pollutant impacts as a complex mixture, rather than treating each pollutants effect independently.

The High Performance Computing and Communication Program (HPCC) is part of a larger Federal program sanctioned under the High Performance Computing Act of 1991 (Public Law 102-194) and coordinated through the Committee on Information and Communications of the National Science and Technology Council. The major program goals are: 1) build advanced capabilities to address multi-pollutant and multimedia issues; 2) adapt environmental management to high performance computing and communications environments; and 3) provide a modeling and decision support environment that is easy to use and responsive to environmental problem solving needs of key State, Federal and Industrial users.

There was nearly a 5-year lag from 1991 before shifts can be seen that directly related to High Performance Computing Act funds. The design of the Models-3 Framework and CMAQ modeling system was drafted in 1993 and 1994, and workshops were held in August and September of 1994 to assist in finalizing the concept designs. From these deliberations, the minimum acceptable functionality and the targeted capabilities were formalized for the Initial Operating Version of Models-3/CMAQ (Byun et al., 1995a; Dennis et al., 1996). The Models-3 Framework paradigm was designed to have multiple processing layers, which would allow rapid updates and development without having to redesign the entire framework (Byun et al., 1995b).

The Models-3 Framework was designed to be the interface that assists the user in operating the modeling systems. It included various components (e.g., to define the pathways to files; to manage updates and modifications to the source code; to define the domain, coordinate system, and science assumptions of an application; to manage the emissions processing).

The Community Multi-scale Air Quality (CMAQ) modeling system was designed to be a third-generation model that could simultaneously simulate multiple air quality issues, including tropospheric ozone, fine particles, toxics, acid and nutrient deposition, and visibility degradation. The initial science capabilities of CMAQ were derived from ROM, RADM and RPM. Unique to CMAQ is its multi-scale capabilities so that separate models are not needed for urban and regional scale air quality modeling. To implement multi-scale capabilities in CMAQ, several issues had to be addressed, such as scalable atmospheric dynamics and generalized coordinates that depend on the desired model resolution. The meteorological model had to be capable of simulating either hydrostatic conditions for large regional scales, where the atmosphere is assumed to have a balance of vertical pressure and gravitational forces with no net vertical acceleration on larger scales, or non-hydrostatic conditions for smaller scales such as urban environs where hydrostatic balance cannot be assumed. Because CMAQ is designed to handle scale-dependent meteorological formulations, CMAQ's governing equations are

expressed in a generalized coordinate system. This approach ensures consistency between CMAQ and the meteorological modeling system. The generalized coordinate system determines the necessary grid and coordinate transformations, and it can accommodate various vertical coordinates and map projections. By making CMAQ a modeling system that addresses multiple pollutants and different spatial scales, CMAQ has a "one atmosphere" perspective.

One of the project goal was to deliver for public testing a beta-test version of the Initial Operating Version (IOV) by the summer of 1997. To accomplish this goal, a variety of modules had to be tested and incorporated into Models-3/CMAQ. The Aerosol and Visibility Module was developed from the RPM and the deciview was added as a visibility metric (Pitchford and Malm, 1994). An advanced module was developed for specifying the photodissociation rates (Roselle et al., 1996) with the rates computed hourly for a gridded domain using clear-sky radiation rates, modeled temperatures, pressure, cloud fields, albedo and total ozone column data. A plume-in-grid module was developed to provide a more realistic treatment of the subgrid-scale physical and chemical processes affecting emissions from major elevated point sources (Godowitch et al., 1995). Further investigations were completed that demonstrated that the aggregation method, developed for the NAPAP RADM assessment, was capable of estimating long-term impacts from a sample of shorter episodes (Eder and LeDuc, 1996a, b; Cohn et al., 1999), and thus, solidifying the basis for incorporating the method into the Models-3 Framework. Initially, the Geocoded Emission Modeling and Projection (GEMAP) system was used as a basis for developing a flexible emissions processing system (Wilkinson et al., 1994). GEMAP was enhanced to include BEIS2 (Geron et al., 1994, 1995) for estimation of biogenic emissions, the RADM chemical speciation mechanism, the Carbon Bond IV mechanism, and the University of California's State Air Pollution Research Center (SAPRC) mechanisms (Lurmann, 1991). When further enhancements were made to GEMAP in 1997, to include the EPA Mobile 5a mobile-source emission processor, and to include links to the MM5 meteorological model, the new emissions processing system came to be called the Models-3 Emission Processing and Projection System (MEPPS).

In 1998, work began to replace MEPPS with the Sparse Matrix Operator Kernel Emissions (SMOKE[®], developed by MCNC-North Carolina Supercomputing Center), which employs a matrix approach to complete the repetitive computations involved in producing very large emission databases. It is anticipated that SMOKE[®] will be at least an order of magnitude faster than MEPPS. In June 1998, Models-3/CMAQ version 2 was made available. To save expenses, the initial design of the Framework involved managing and sharing of information between several third-party programs. It became a resource intensive activity to adapt the Framework to various workstation environments, and to revise the Framework to be compatible with format changes resulting from upgrades in the third-party software. Since resources were never allocated to convert the Framework to one operating system, the Framework operations were reduced and simplified in each of the successive releases of the new versions of Model-3/CMAQ. The release of

Models-3/CMAQ version 3 in June of 1999 included Y2K updates to the support software, except for MM5. The release of Models-3/CMAQ version 4, in June 2000, simplified the installation procedures, and improvements were made to provide support for software updates and user help via the Models-3 web site²⁷.

6 Current Issues and Trends in Model Development

The purpose of the preceding discussions was to provide a historical review of the development of regulatory air quality models within the United States as viewed from the EPA, with a focus on the NOAA ARL scientists who provided EPA meteorological and air quality modeling support.

The Atomic Energy Act of 1954 established the requirement for Weather Bureau Field Offices to provide technical services in environmental impact assessment to Federal agencies. President Nixon's Reorganization Plan Number 4 in 1970 established the NOAA, and established a basis for NOAA to provide EPA support in the development of air quality models. In the late 1960s and early 1970s, the urban-scale long-term air quality models provided a proof of concept that air quality models could be used by the states to develop state implementation plans (SIPs) to relate the control of emissions with estimated air quality impacts, and thereby provide a rationale for how the States could achieve the NAAQS set by the EPA. The early models evolved from the Gaussian plume model that was developed in England during the period of 1916 to the early 1930s to investigate the effects of gas warfare. The special needs of characterizing air quality impacts from industrial stack emissions stimulated research into buoyant plume rise and convective dispersion processes. Wind tunnel investigations provided a basis for investigating building wake effects on atmospheric dispersion. As these investigations evolved, Gaussian plume models were provided with new capabilities that allowed their use to satisfy the Clean Air Act Amendments of 1977, accepting usage of air quality models as a means for demonstrating compliance for the development of State Implementation Plans and for permits required by the New Source Review program. By the late 1970s, Gaussian plume models had gained widespread use in regulatory assessments, and during the late 1990s, efforts were underway to extend the usefulness of these models for more complex transport situations through the use of puff dispersion models. During the early 1970s, tropospheric photochemical ozone models were being developed to characterize ozone impacts within a city. These early grid models, struggling with poorly understood chemical kinetics and uncertain emission inventories, were severely limited by the memory capabilities and computation speed of computer technology. As field and laboratory studies began to resolve the uncertainties in the physical processes, it became increasingly clear that the scale of the problem was much larger than the domain of a city or even a state. The Clean Air Act Amendments of 1990 required the use tropospheric chemistry air quality models

²⁷ For current status of Models-3/CMAQ consult: <http://www.epa.gov/asmdnerl/CMAQ/index.html>.

for demonstrating a plan for attainment of the ozone NAAQS. By the 1990s, advances in scientific understanding of ozone formation, acid deposition and aerosols coupled with advances in computer science provided a basis for the development of second and third generation (one atmosphere) regional-scale chemistry-aerosol grid models for use in regulatory assessments. It is seen that the Clean Air Act Amendments of 1977 and 1990 formalized the acceptance and use of air quality models in regulatory assessments. In the 1990s, EPA placed increased emphasis towards characterizing human exposures to toxics, which may in some instances require simulation of air chemistry. Human exposure models couple the time history of pollutant species within microenvironments with human activity patterns. Such models have increased interest in the development of air quality models that can address neighborhood scale impacts within comprehensive grid models.

In developing this review, three issues seem to resurface more than once, and appear to deserve special comment, namely: 1) a trend to require a complete documentation of the assumptions made (transparency) and a formal exploration of the consequences of these assumptions in air quality assessments, 2) a need for the use of standardized methods in development of emission inventories, and 3) a need for development and use of science-based model performance standards.

6.1 Transparency and Consequences of Assumptions

The recommendations by the National Academy of Sciences Committee on the Institutional Means for Assessment of Risks to Public Health (National Research Council, 1983) planted a seed within the U.S. Congress and within the EPA regulatory culture that formalized uncertainty assessments to promote acceptance of regulatory policy decisions. Prompted by the significant scientific uncertainties in the health effects and in the available characterizations for long range transformation-transport of sulfate, Congress passed the Acid Precipitation Act of 1980 (Public Law 96-294). This directed the United States Government to conduct a ten-year assessment to determine the causes and consequences of acid precipitation, and to develop options for reducing known effects. The National Acid Precipitation Assessment Program (NAPAP) was created in response to this congressional charge. The NAPAP assessment of 1990 validated the effort that went into the development of the Regional Acid Deposition Model (RADM).

One of the recommendations, resulting from the National Research Council's (1991) review of the state of knowledge of the physical and chemical sciences relevant to the characterization of tropospheric ozone, was that periodic reviews of this kind were needed. In response to this recommendation, the North American Research Strategy for Tropospheric Ozone (NARSTO)²⁸ was formed with over 70

²⁸ http://eosweb.larc.nasa.gov/GUIDE/campaign_documents/base_narsto_project.html.

participating organizations from Canada, Mexico and the United States. During their deliberations, it was decided to broaden the purview to include fine particles. Twenty-four critical reviews of the science disciplines involved in characterizing tropospheric ozone were prepared as part of the NARSTO assessment, of which seventeen were published in Volume 34 of *Atmospheric Environment*. The focus of the assessment was on the state of science knowledge and possible regulatory implications. It was concluded that the main science advances from 1990 to 2000 mostly confirmed hypotheses and results reported earlier. With each assessment, there can be seen an increased attention to attempt to make transparent the assumptions, not only of the science being reviewed, but of the assessment process itself, to critically review each assumption, and to attempt to assess the known uncertainties on conclusions reached.

The goals, to state the scientific assumptions and to explore the consequent uncertainties on conclusions reached, have been expressed in the guidelines for exposure assessment (U.S. Environmental Protection Agency, 1992, <http://www.epa.gov/ncea/exposure.htm>, and 1998, <http://www.epa.gov/ncea/ecorsk.htm>), which describe the general concepts of human and ecological exposure assessments, including recommendations on the presentation of results and the characterization of uncertainty. These guidelines recommend that assumptions be explicitly stated, and the uncertainties associated with these assumptions be discussed as well as the possible implications on conclusions reached. In this context, it is worth noting that the 1990 CAAA called for residual risk assessments to be conducted to assess whether further reductions are needed in order to mitigate exposures to toxic emissions. The large NRC and NARSTO assessments, the EPA guidelines and the 1990 CAAA all support a trend for creation and use of large science committees to provide independent assessments of the science progress with a focus on the implications for regulatory decisions. It is reasonable to anticipate that future pollution mitigation programs will increasingly require public acceptance, and to gain this support the regulatory community will increasingly call upon formal assessments to make transparent the assumptions made and consequent uncertainties. The strength of these assessments is that they are considered to be unrehearsed, unbiased, and have no hidden agenda. To date, the integrity of these assessments has successfully relied on the integrity of the individuals involved. As the climate surrounding the decision making process becomes more contentious, there may be a call to define formal assessment procedures. Developing standardized procedures that foster making the science assumptions and decision assumptions transparent, and for characterizing the consequences of these assumptions will be a trend to look for in the future.

6.2 Emission Inventories

Assembling and checking the quality of air quality models' emission inventory has always been recognized as a most difficult task. Seinfeld (1988) described the emission inventories for then typical urban-scale ozone air quality model applications as being immense databases that might contain on the order of 500 to several thousand individual point sources and up to several hundred area source categories. Biogenic and vegetative emissions of volatile organics have historically been largely neglected. He characterized the techniques used to quantify uncertainties relying upon the judgment of the inventory specialist. The National Research Council's (1991a) review of ozone modeling expressed concerns because of the underestimation of anthropogenic VOC emissions that 1) mandated emission controls in past years were a smaller fraction of the total than originally anticipated, and thus, limited the effectiveness of these controls, and 2) planned control strategies for future years will likely require fundamental revisions. The critical review by Placet et al. (2000) concluded that the standard emissions factors (U.S. Environmental Protection Agency, 1985b) were representative of older industries constructed prior to 1970. The three main steps (speciation, temporal scaling, spatial allocation), needed to convert the emission inventories for use by air quality models, were seen to be crude and uncertain. Projecting the consequences of these uncertainties on conclusions reached in emission control strategies was seen as problematic and difficult. The investigations by Hanna et al. (1998, 2001) estimated the uncertainty distribution for the domain-wide maximum ozone concentration was close to log-normal, with 95% of the values within a factor of ± 1.6 from the median, with uncertainties in anthropogenic VOC emissions from area sources having the most influence.

Although one might call for extensive programs to assess and reduce emission inventory uncertainties, the reality of the situation is that most of the problems are well identified and progress is being made within the limits imposed by available resources. The uncertainties in those sources characterized as area sources (mobile, small businesses, biogenics) are recognized and efforts are underway to develop improvements. Results from the Southern Oxidant Study (SOS) (Chameides and Cowling, 1995) indicate that oxides of nitrogen emissions from Tennessee, for example may be comparable with those of the coal-fired power plants in the state (Williams et al., 1992; Valente and Thornton, 1993). The 1992 SOS tunnel studies suggest that improvements have been made in our ability to characterize mobile emissions (Pierson et al., 1996). Problems in the characterization of biogenic emissions are being traced to uncertainties in characterizing land use, so efforts are underway to develop improved land use maps. Thus, of all the actions that have been suggested, one of the more pragmatic and cost effective suggestion appears to be the proposal to promote the use of EPA's Emission Inventory Improvement Program (EIIP, 1996). This is a set of standard procedures that provide preferred and alternative methods for emissions estimation; if employed, it would promote consistency. Improvements would still be needed in the estimates of emission factors, and assumptions used (e.g.,

effectiveness of control, activity levels, growth rates). However, promoting use of standardized procedures that foster consistency in emission inventory development will be a trend to look for in the future.

6.3 Model Performance Standards

One of the luxuries of developing new characterizations of dispersion of a relatively inert pollutant from an isolated source is that tracer field data studies can be used to evaluate the model performance. This is not the case for tropospheric models that characterize chemical processes and aerosol processes, which means that uncertainties in emission characterization becomes a part of the problem in evaluating the performance of these models. In spite of these differences and many attempts that have been made²¹, consensus standards have yet to be devised for assessing air quality model performance. Turner (1979) noted that there were no recognized model performance standards (metersticks). Dennis and Downton (1984), Seinfeld (1988), and Russell and Dennis (2000) all have noted that evaluations conducted have not tested the suitability of tropospheric air chemistry models to simulate changes in air quality that involve substantial changes in emissions. Russell and Dennis (2000) further note that simple comparisons of observed and simulated ozone values are insufficient to determine whether the chemical processes were properly characterized.

In 1996, an effort was initiated within the American Society for Testing and Materials (ASTM, <http://www.astm.org>) to foster the development of standard methods for evaluating the performance of air quality models. The first product of this effort was a Standard Guide for the Statistical Evaluation of Atmospheric Dispersion Model Performance (D 6589). Within the annex of this guide, an example procedure was defined that would allow testing of dispersion models in their ability to characterize the average maximum concentration as a function of distance downwind from an isolated source whose emissions can be treated as being relatively inert. This procedure also provides an objective statistical test to define when differences in performance are significant. The plans are to create a series of formal ASTM Test Methods (“metersticks” as called by Turner in 1979) that can be cited by regulatory agencies as approved methods for characterizing model performance. The initial work will focus on dispersion models, and then as experience is gained, expand the purview to include models that characterize atmospheric chemistry and aerosol formation processes. Developing standard “metersticks” of model performance within ASTM has the potential for having far reaching effects, as it would provide an international basis for comparing model development efforts and establishing international acceptance standards for air quality models for use in legal proceedings and regulatory decision making.

Acknowledgments

This work was funded in part by the United States Environmental Protection Agency through an Interagency Agreement (139-384-83) with the National Oceanic and Atmospheric Administration.

It has been subjected to Agency review and approved for publication. Mention of trade names or commercial products does not constitute endorsement or recommendation for use.

References

Alm, L.R., 2000. *Crossing Borders, Crossing Boundaries: the Role of Scientists in the U.S. Acid Rain Debate*. Praeger Publishers, 147 pages.

Anthes, R.A., Seaman, N., Sobel, J., and Warner, T., 1974. *The development of mesoscale models suitable for air pollution studies*. Select Research Group in Air Pollution Meteorology, 2nd Annual Report: Vol. I, U.S. Environmental Protection Agency, Research Triangle Park, NC 27711, pp. 6-233.

Anthes, R.A., and Warner, T., 1978. Development of hydrodynamic models suitable for air pollution and other mesometeorological studies. *Monthly Weather Review*. 106:1045-1078.

Anthes, R.A., Hsle, E.Y., and Kuo, Y.H., 1987. *Description of the Penn State/NCAR Mesoscale Model version 4 (MM4)*, NCAR Technical Note, NCAR/TN-282+STR, National Center for Atmospheric Research, Boulder, CO, 66 pages.

Arnts, A., and Meeks, S., 1981. Biogenic hydrocarbon contribution to the ambient air of selected areas. *Atmosphere Environment*, 15(9):1643-1651.

Barad, M.L., and Haugen, D.A., 1959. A preliminary evaluation of Sutton's hypothesis for diffusion from a continuous point source. *Journal of Meteorology*. Vol. 16(1):12-20.

Benkley, C.W., and Bass, A., 1979. *User's guide to MESOPUFF (Mesoscale Puff) Model*. Environmental Research and Technology, Inc., Concord, MA.

Bennet, M., and Hunter, G.C., 1997. some comparisons of lidar estimates of peak ground-level concentrations with the predictions of UK-ADMS. *Atmospheric Environment*. 31(3):429-439.

Biller, W.R., Feagans, T.B., Johnson, T.R., Duggan, G.M., Paul, R.A., McCurdy, T., and Thomas, H.C., 1981. A general model for estimating exposure associated with alternative NAAQS. Paper No. 81-18.4. In *Proceedings of the 74th Annual Meeting of the Air Pollution Control Association*, June 21-26, 1981, Philadelphia, PA, 25 pages.

Binkowski, F.S., and Ching, J.K.S., 1996. Modeling the particulate mass and visibility using the EPA Regional Particulate Model. Preprints of the *9th Joint Conference on Applications of Air Pollution Meteorology with A&WMA*, January 28-February 2, 1996, Atlanta, GE, American Meteorological Society, Boston, MA, pages 565-569.

Binkowski, F.S., and Shankar, U., 1994. Development of an algorithm for the interaction of a distribution of aerosol particles with cloud water for use in a three-dimensional Eulerian air quality model. *Abstracts, 4th International Aerosol Conference*, August 29-September 2, 1994, Los Angeles, CA, Richard C. Flagan (Ed.), American Association for Aerosol Research, Cincinnati, OH, page 220.

Binkowski, F.S., and Shankar, U., 1995. The Regional Particulate Matter Model, 1. Model description and preliminary results. *Journal of Geophysical Research*. 100(D12):26,191-26,209.

Binkowski, F.S., Chang, J.S., Dennis, R.L., Reynolds, S.J., Samson, P.J., and Shannon, J.D., 1990. Regional acid deposition modeling. Acidic Deposition. State of Science and Technology Report 3. Volume 1, Emissions, Atmospheric Processes and Deposition, National Acid Precipitation Assessment Program, 722 Jackson Place, NW, Washington DC.

Briggs, G., 1965. *A Plume Model Compared With Observations*. Paper 65-44 presented at Annual Meeting of the Air Pollution Control Association, June 20-24, 1965, Toronto, Ontario, 23 pages.

Briggs, G.A., 1969. *Plume Rise*. TID-25075. U.S. Atomic Energy Commission, Available from the National Technical Information Service, U.S. Department of commerce, Springfield, VA 22151, 85 pages.

Briggs, G.A., 1975. Plume Rise Predictions. *Lectures on Air Pollution and Environmental Impact Analyses*, D. A. Haugen, Ed., American Meteorological Society, Boston, pages 59-111.

Briggs, G.A., 1989. Field measurement of vertical diffusion in convective conditions. Preprints, 6th Joint Conference on Applications of Air Pollution Meteorology, January 30-February 3, 1989. Anaheim, CA, American Meteorological Society, Boston, MA, pages 167-170.

Briggs, G.A., 1993a. Final results of the CONDORS convective diffusion experiment. *Boundary Layer Meteorology*, Dordrecht, The Netherlands, 62(1-4):315-328.

Briggs, G.A., 1993b. Plume dispersion in the convective boundary layer, Part II, Analyses of CONDORS field experiment data. *Journal of Applied Meteorology*, American Meteorological Society, Boston, MA, 32(8):1388-1425.

Bullock, O.R. Jr., 1990. The effect of size-dependent dry deposition velocities in an Eulerian regional-scale particulate model. Preprints, 18th International Technical Meeting of NATO/CCMS on Air Pollution Modeling and its Application, Volume 1, May 13-17, 1990, University of British Columbia, Vancouver, BC, Canada. NATO/CCMS, Brussels, Belgium, pages 145-152.

Bullock, O.R. Jr., Roselle, S.J., and Heilman, W.E., 1989. *Development and preliminary testing of a first-generation regional aerosol model*. Status report, Atmospheric Research and Exposure Assessment Laboratory, Research Triangle Park, NC 109 pages.

Byun, D.W., Hanna, A., Coats, C., and Hwang, D., 1995b. Models-3 air quality model prototype science and computational concept development. In Regional Photochemical Measurement and Modeling Studies. TR-24. *Transactions of an International Specialty Conference*, San Diego, CA, November 8-12, 1993. Air & Waste Management Association, Pittsburgh, pages 197-212.

Byun, D.W., Coats, C.J., Hwang, D., Fine, S., Odman, T., Hanna, A., and Galluppi, K.J., 1995a. Prototyping and implementation of the multi-scale air quality models for high performance computing. In High Performance Computing Symposium 1995; Grand Challenges in Computer Simulation. Proceedings of the 1995 Simulation Multiconference, Phoenix, AZ, April 9-12, 1995. Adrian M., Tentner (Ed.), The Society for Computer Simulation, San Diego, CA, pages 527-532.

Calder, K.L., 1969. *A Narrow Plume Simplification For Multiple Urban Source Models*. (Unpublished note from K.L. Calder to F.A. Gifford), 11 pages.

Calder, K.L., 1971. A climatological model for multiple source urban air pollution. Paper presented at First Meeting of the NATO/CCMS Panel on Modeling. Paper published in Appendix D of *User's Guide for the Climatological Dispersion Model*. EPA-R4-73-024. Office of Research and Development, U.S. Environmental Protection Agency, Research Triangle Park, NC 27711, pages 73-105.

Calder, K.L., 1977. Multiple-source plume models of urban air pollution - their general structure. *Atmospheric Environment*. Vol. 11, pages 403-414.

Carruthers, D.J., Holroyd, R.J., Hunt, J.C.R., Weng, W.S., Robins, A.G., Apsley, D.D., Thomson, D.J., and Smith, F.B., 1994. UK-ADMS: a new approach to modelling dispersion in the earth's atmospheric boundary layer. *Journal of Wind Engineering*. (52):139-153.

Carter, W.P.L., Lurmann, F.W., Atkinson, R., and Lloyd, A.C., 1986. Development and testing of a surrogate species chemical reaction mechanism, Volumes I and II. EPA-600/3-86-031, U.S. Environmental Protection Agency, Research Triangle Park, NC 27711.

Chameides, W.L., and Cowling, E.B., 1995. The state of the Southern Oxidants Study. Policy Relevant Findings in Ozone Pollution Research, 1988-1994. North Carolina State University, Raleigh, NC.

Chameides, W., Lindsay, R., Richardson, J., and Klang, C., 1988. The role of biogenic hydrocarbons in urban photochemical smog. Atlanta as a case study. *Science*, 241:1473-1475.

Chang, J.S., Middleton, P.B., Stockwell, W.R., Walcek, C.J., Pleim, J.E., Lansford, H.H., Binkowski, F.S., Seaman, N.L., McHenry, J.N., Madronich, S., Samson, P.J., and Hass, H., 1990. The regional acid deposition model and engineering model. Acidic Deposition. State of Science and Technology Report 4. Volume 1, Emissions, Atmospheric Processes and Deposition, National Acid Precipitation Assessment Program, 722 Jackson Place, NW, Washington DC.

Ching, J.K.S., and Doll, D.C., 1981. Temporal variation of ground heat flux for soil and concrete using net radiation data. *Proceedings of the 5th Symposium on Turbulence, Diffusion and Air Pollution*, March 9-13, Atlanta, GA., American Meteorological Society, Boston, MA, pages 171-172.

Clark, T.L., 1992. Atmospheric deposition of toxic metals to Lake Michigan: Preliminary annual model calculations. Proceedings of the 1992 U.S. EPA/A&WMA International Symposium on Measurement of Toxic Air Pollutants. Durham, NC, May 1992. U.S. Environmental Protection Agency, Research Triangle Park, NC, and Air & Waste Management Association, Pittsburgh, PA, pages 681-686.

Clark, T.L., Blakley, P., and Mapp, G., 1992. Model calculations of the annual atmospheric deposition of toxic metals to Lake Michigan. Abstracts Book from the Air & Waste Management Association 86th Annual Meeting, Kansas City, Missouri, June 21-26, 1992. Air & Waste Management Association, Pittsburgh, PA, 92-84.17.

Clarke, J.R., Ching, J.K.S., and Godowitch, J.M., 1981. Spatial characteristics of surface boundary layer turbulence in an urban area. *Proceedings of the 5th Symposium on Turbulence, Diffusion and Air Pollution*, March 9-13, Atlanta, GA., American Meteorological Society, Boston, MA, pages 167-168.

Cohn, R., Eder, B.K., and LeDuc, S.K., 1999. An aggregation and episode selection scheme designed to support Models-3 CMAQ. In *Science Algorithms of the EPA Models-3 Community Multiscale Air Quality (CMAQ) modeling system*. Chapter 17, D.W. Byun, and J.K.S. Ching (Eds.). EPA/600/R/99/030. National Exposure Research Laboratory, U.S. Environmental Protection Agency, Research Triangle Park, NC, pages 1-66.

Cowling, E.B., 1992. The performance and legacy of NAPA. *Ecological Applications*, 2(2):111-116.

- Cramer, H.E., 1957. A practical method for estimating the dispersal of atmospheric contaminants. *Proceeding of 1st National Conference on Applied Meteorology*. American Meteorological Society, Hartford, CT. pages C-33 through C-55.
- Crutzen, P.J., 1973. A discussion of the chemistry of some minor constituents in the stratosphere and troposphere, *Pure Appl. Geophys.*, 106-108:1385-1399.
- Crutzen, P.J., 1974. Photochemical reactions initiated by and influencing ozone in unpolluted tropospheric air. *Tellus*, 26:47-57.
- DeMarrais, G.A., 1974. *A History of Air Pollution Meteorology Through 1969*. NOAA Technical Memorandum ERL ARL-74. Air Resource Laboratory, Silver Spring, MD. 78 pages.
- Dennis, R.G., 1997. Using the Regional Acid Deposition Model to determine the nitrogen deposition airshed of the Chesapeake Bay watershed. In *Atmospheric Deposition of Contaminants to the Great Lakes and Coastal Waters*. J.E. Baker (Ed.). STAC Press, Pensacola, FL, pages 393-413.
- Dennis, R.,L., and Downton, M.W., 1984. Evaluation of urban photochemical models for regulatory use. *Atmospheric Environment*. 18:2055-2069.
- Dennis, R.L., Byun, D.W., Novak, J.H., Galluppi, K.J., Coats, C.J., and Vouk, M.A., 1996. The next generation of integrated air quality modeling: EPA's Models-3. *Atmospheric Environment*. 30:1925-1938.
- Dennis, R.G., Barchet, W.R., Clark, T.L, McHenry, J.N, and Reynolds, S.D. , 1990a. Evaluation of regional acidic deposition models. Acidic Deposition. State of Science and Technology Report 5. *Volume 1, Emissions, Atmospheric Processes and Deposition, National Acid Precipitation Assessment Program*, 722 Jackson Place, NW, Washington, DC.
- Dennis, R.G., Binkowski, F., Clark, T., McHenry, J., Reynolds, S., and Seilkop, S., 1990b. Selected application of the Regional Acid Deposition Model and Engineering Model. Acidic Deposition. State of Science and Technology Appendix 5F. *Volume 1, Emissions, Atmospheric Processes and Deposition, National Acid Precipitation Assessment Program*, 722 Jackson Place, NW, Washington, DC.
- Dewert, R.G., and Stewart, H.N.M., 1973. Elevated ozone levels in the air of Central London, *Nature*. (241):342-343.
- Dodge, M.C., 1977. Combined use of modeling techniques and smog chamber data to derive ozone - precursor relationships. Proceedings of the *International Conference on Photochemical Oxidant Pollution and Its Control*, EPA-600/3-77-001b. U.S. Environmental Protection Agency, Research Triangle Park, NC 27711. pages 881-889.
- Donigian, A.S., Jr., Bicknell, B.R., Patwardhan, A.S., Linker, L.C., Alegre, D.Y., Chang, C.H., and Reynolds, R., 1991. *Watershed Model Application to Calculate Bay Nutrient Loads: Phase II Findings and Recommendation*. U.S. Environmental Protection Agency, Chesapeake Bay Program, Annapolis, MD.
- Duan, N., 1981. Micro-Environmental Types: A Model for Human Exposure to Air Pollution. *SIMS Technical Report No. 47*, Stanford California Department of Statistics, Stanford University, 24 pages.

Duan, N., 1989. Estimation of microenvironmental concentration distributions using integrated exposure measurements. Proceedings of the *Research Planning Conference on Human Activity Patterns*. T.H. Stars (Ed.). EPA/600/4-89/004. Office of Research and Development, U.S. Environmental Protection Agency, Las Vegas, NV, pages 15-1 to 15-14.

Eberhard, W.L., Moninger, W.R., Briggs, G.A., 1988. Plume dispersion in the convective boundary layer, Part I, CONDORS field experiment and example measurements. *Journal of Applied Meteorology*, American Meteorological Society, Boston, MA, 27(5):599-616.

Eder, B.K., and LeDuc, S.K., 1996a. Aggregation of selected RADM simulations to estimate annual ambient air concentrations of fine particulate matter. Preprints, *9th Joint Conference on the Applications of Air Pollution Meteorology with A&WMA*. January 28-February 2, 1996, Atlanta, Georgia. American Meteorological Society, Boston, MA, pages 390-392.

Eder, B.K., and LeDuc, S.K., 1996b. Can selected RADM simulations be aggregated to estimate annual concentrations of fine particulate matter? In *Measurement of Toxic and Related Air Pollutants. VIP-64. Proceedings of an International Specialty Conference*, Research Triangle Park, NC, May 7-10, 1996, U.S. Environmental Protection Agency, RTP, NC and Air & Waste Management Association, Pittsburgh, PA, pages 732-739.

Eder, B.K., Coventry, D.H., Clark, T.L., and Bollinger, C.E., 1986. *RELMAP: A Regional Lagrangian Model of Air Pollution user's guide*. EPA/600/8-86/013. Atmospheric Sciences Research Laboratory, Research Triangle Park, NC, 137 pages.

Electric Power Research Institute 1984. *Regional air quality model assessment and evaluation*. EA-36-71, Research Project 1630-21, Electric Power Research Institute, Palo Alto, CA.

Eliassen, A., 1978. The OECD study on long range transport of air pollutants, long range transport modelling. *Atmospheric Environment*. Vol. 12:479-487.

Eliassen, A., 1980. A review of long-range transport modeling. *Journal of Applied Meteorology*. Vol. 19(3):231-240.

Eliassen, A., Hov, Ø., Isaksen, I.S.A., Saltbones, J., and Stordal, F., 1982. A Lagrangian long-range transport model with atmospheric boundary layer chemistry. *Journal of Applied Meteorology*. Vol. 21:1645-1661.

Emissions Inventory Improvement Program, 1997. EIPP Technical Report Series, Volumes I through X, available from: <http://www.epa.gov/ttn/chief/eiip/techreport/index.html>.

Eschenroeder, A.Q., and Martinez, J.R., 1971. *Concepts and application of photochemical smog models*. Technical Memo 151B. General Research Corporation, Santa Barbara, CA.

Eschenroeder, A.Q., Martinez, J.R., and Nordsieck, R.A., 1972. *Evaluation of a diffusion model for photochemical smog simulation*. CR-1-273. General Research Corporation, Santa Barbara, CA.

Federal Register, 1980. Reconsideration of the use of Pasquill-Gifford dispersion coefficients for stability class A in setting emission limitations for four Ohio power plants; petitions for reconsideration. *45 FR 74041*, pages 74041-74047.

Ferber, G.J., Heffter, J.L., Draxler, R.R., Lagomarsino, R.J., Thomas, F.L., Dietz, R.N., Benkovitz, C.M., 1986. Cross-Appalachian Tracer Experiment (CAPTEX 83) Final Report. *NOAA Technical Memorandum ERL ARL-142*, Air Resources Laboratory, Silver Spring, MD, 60 pages.

- Fisher, B.E.A., 1983. A review of the processes and models of long-range transport of air pollutants. *Atmospheric Environment*. Vol. 17(10):1865-1880.
- Fox, D.G., 1981): Judging air quality model performance. *Bulletin of the American Meteorological Society*. (62):599-609.
- Fox, D.G., 1984. Uncertainty in air quality modeling. *Bulletin of the American Meteorological Society*. (65):27-36.
- Frenkiel, F.N., 1957. Atmospheric pollution in growing communities. *Publication 4276. Smithsonian Report for 1956*, Smithsonian Institution, Washington, DC, pages 269-299.
- Friedlander, S.K., and Seinfeld, J.H., 1969. A dynamic model of photochemical smog. *Environmental Science & Technology*. 3(11):1175-1181.
- Gelbard, F., 1984. MAEROS. *Aerosol Science and Technology*. 3:117-118.
- Gelbard, F., and Seinfeld, J.R., 1980. Simulation of multicomponent aerosol dynamics. *Journal Colloid Interface Science*. 78:485-501.
- Geron, C.D., Guenther, A.B., and Pierce, T.E., 1994. An improved model for estimating emission of volatile organic compounds from forests in the eastern United States. *Journal of Geophysical Research*. 99(D6):12,773-12,791.
- Geron, C.D., Pierce, T.E., and Guenther, A.B., 1995. Reassessment of biogenic volatile organic compound emissions in the Atlanta area. *Atmospheric Environment*. 29:1569-1578.
- Gery, M.W., Whitten, G.Z., and Killus, J.P., 1988. *Development and Testing of the CBM-IV for urban and regional modeling*. EPA/600/3-88/012, Office of Air Quality Planning and Standards, U.S. Environmental Protection Agency, Research Triangle Park, NC 27711.
- Gifford, F.A., Jr. 1961. Uses of routine meteorological observations for estimating atmospheric dispersion. *Nuclear Safety*. Vol. 2(4):47-51.
- Gifford, F.A., 1976. Turbulent diffusion-typing schemes: a review. *Nuclear Safety*. Vol 17(1):68-86.
- Gifford, F.A. and Hanna, S.R., 1970. Urban air pollution modelling. *Proceedings of the Second International Clean Air Congress*. Paper ME-320. Washington, D.C., pages 1146-1151.
- Gifford, F.A. and Hanna, S.R., 1973. Modeling urban air pollution. *Atmospheric Environment*. (7):131-136.
- Glen, W.G., and Zelenka, P.J., 1994. Trends in CO exposure for Denver using population based exposure model. Abstracts Book, 4th Conference of the International Society for Exposure Analysis, Research Triangle Park, North Carolina, September 18-21, 1994. International Society for Exposure Analysis, Host, School of Public Health, University of North Carolina at Chapel Hill, Chapel Hill, NC, page 146.
- Godowitch, J.M., Ching, J.K.S., and Clarke, J.F., 1979. Dissipation of the nocturnal inversion layer at an urban and rural site in St. Louis, MO. *Proceedings of the 4th Symposium on Turbulence, Diffusion and Air Pollution*. January 15-18, Reno, NV, American Meteorological Society, Boston, MA, pages 416-420.

Godowitch, J.M., Ching, J.K.S., and Clarke, J.F., 1981. Urban/rural and temporal variations in PBL turbulence parameters and length scales over St. Louis, MO. *Proceedings of the 5th Symposium on Turbulence, Diffusion and Air Pollution*. Atlanta, GA, American Meteorological Society, Boston, MA, pages 171-172.

Godowitch, J.M., Ching, J.K.S., and Gillani, N.V., 1995. A treatment for Lagrangian transport and diffusion of subgrid scale plumes in an Eulerian grid framework. Preprints, *11th Symposium on Boundary Layers and Turbulence*. March 27-31, 1995, Charlotte, NC. American Meteorological Society, Boston, pages 86-89.

Grell, G.A., Dudhia, J., and Stauffer, D.R., 1994. A Description of the Fifth-Generation Penn State/NCAR Mesoscale Model (MM5). *NCAR Technical Note, NCAR/TN-398+STR*, National Center for Atmospheric Research, Boulder, CO, 138 pages.

Gryning, S.E., Holtslag, A.A.M., Irwin, J.S, Sivertsen, B., 1987. Applied dispersion modelling based on meteorological scaling parameters. *Atmospheric Environment*. Vol. 21(1):79-89.

Guicheri, R., and van Dop, H., 1977. Photochemical production of ozone in Western Europe (1971-1975) and its relation to meteorology. *Atmospheric Environment*. (11):145-155.

Haagen-Smit, A.J., 1950. The air pollution problem in Los Angeles. *Engineering Science*. Vol. 14:7-14.

Haagen-Smit, A.J., 1952. Chemistry and physiology of Los Angeles smog. *Industrial Engineering Chemistry*. Vol. 44:1342

Haagen-Smit, A.J. and Fox, M.M., 1955. *SAE Transactions*, Vol. 63:575.

Hamming, W.J., MacPhee, R.D., and Taylor, J.R., (1960): Contaminant concentrations in the atmosphere of Los Angeles County. *Journal of Air Pollution Control Association*. Vol. 10(1):7-16.

Hanna, S.R., and Chang, J.C., 1991. Revision of the hybrid plume dispersion (HPDM) for application to urban areas. H. van Dop and D.G. Steyn (Editors), *Air Pollution Modeling and its Application VIII*, Plenum Press, New York, NY, pages 751-758.

Hanna, S.R., and Paine, R.J., 1989. Hybrid plume dispersion model (HPDM) development and evaluation. *Journal of Applied Meteorology*. American Meteorological Society, Boston, MA, 28(3):206-224.

Hanna, S.R., Briggs, G.A., and Hosker, R.P., 1982. *Handbook on Atmospheric Diffusion*. Available as DE82002045 (DOE/TIC-11223) from the National Technical Information Service, U.S. Department of Commerce, Springfield, VA 22161, 108 pages.

Hanna, S.R.; Chang, J.C., and Fernau, M.E., 1998. Monte Carlo Estimates of Uncertainties in Predictions by a Photochemical Grid Model (UAM-IV) Due to Uncertainties in Input Variables, *Atmospheric Environment*, Vol. 32, pages 3617-3628.

Hanna, S.R., Zhitang, L., Christopher, F., Wheeler, N., Vukovich, J., Arunachalam, S., Fernau, M., and Hanse, D.A., 2001. Uncertainties in predicted ozone concentrations due to input uncertainties for the UAM-V photochemical grid model applied to the July 1995 OTAG domain. *Atmospheric Environment*. (35):891-903.

Hicks, B.B., Draxler, R.R., Albritton, D.L., Fehsenfeld, F.C., Dodge, M., Schwartz, S.E., Tanner, R.L., Hales, J.M., Meyers, T.P., and Vong, R.J., 1990. Atmospheric processes research and process model development. Acidic Deposition. State of Science and Technology Report 2. *Volume 1, Emissions, Atmospheric Processes and Deposition*, National Acid Precipitation Assessment Program, 722 Jackson Place, NW, Washington, DC.

Holland, J.Z., 1953. *A Meteorological Survey of the Oak Ridge Area: Final Report Covering the Period 1948-1952*. ORO-99, Technical Information Service, Atomic Energy Commission, Oak Ridge, TN, 584 pages.

Holzworth, G.C., 1964. Estimates of mean maximum mixing depths in the contiguous United States. *Monthly Weather Review*. Vol. 92(5):235-242.

Huber, A.H., and Snyder, W.H., 1976. Building wake effects on short stack effluents. Preprints of *Third Symposium on Atmospheric Diffusion and Air Quality*, American Meteorological Society, Boston, MA, pages 235-242.

Hudischewskyj, A.B., Saxena, P., and Seigneur, C., 1987. *Development of Computer Modules of Particulate Processes for Regional Particulate Model*. Contract No. 68-02-4076. Atmospheric Sciences Research Laboratory, U.S. Environmental Protection Agency, Research Triangle Park, NC 27711, 284 pages.

Hunt, J.C.R., and Snyder 1980. Experiments on stably and neutrally stratified flow over a model three-dimensional hill. *Journal of Fluid Mech.* (98):671-704.

Hyde, W.L., 1952. *Atmospheric Radioactivity Following Nuclear Explosions*. Office of Naval Research, Technical Report ONRL-66-52, London, England.

Irwin, J.S. and Brown, T.M., 1985. A sensitivity analysis of the treatment of area sources by the Climatological Dispersion Model. *Journal of the Air Pollution Control Association*. Vol. 35(4):39-364.

Irwin, J.S., and Smith, M.E., 1984. Potentially useful additions to the rural model performance evaluation. *Bulletin of the American Meteorological Society*. (65):559-568.

Jasanoff, S., 1990. *The Fifth Branch, Science Adviser as Policymakers*. Harvard University Press, Cambridge, MA, 302 pages.

Johnson, T.R., 1983. *A Study of Personal Exposure to Carbon Monoxide in Denver, Colorado*. EPA 600/4-84-014. Office of Research and Development, Environmental Monitoring Systems Laboratory, U.S. Environmental Protection Agency, Research Triangle Park, NC, 272 pages.

Johnson, T.R., 1992. *Estimation of Carbon Monoxide Exposures and Associated Carboxyhemoglobin Levels in Denver Residents Using a Probabilistic Version of NEM*. Report prepared by International Technology Air Quality Services, Contract 68-DO-0062, Work Assignment no. 1-4, Office of Air Quality Planning and Standards, U.S. Environmental Protection Agency, Research Triangle Park, NC.

Johnson, T.R., and Paul, R.A., 1981. *The NAAQS Model (NEM) and Its Application to Particulate Matter*. Draft report prepared by PEDCo Environmental, Inc., Durham, NC., Office of Air Quality Planning and Standards, U.S. Environmental Protection Agency, Research Triangle Park, NC.

Johnson, T.R., and Paul, R.A., 1983. *The NAAQS Model (NEM) and Its Application to Carbon Monoxide*. EPA-450/5-83-003. Report prepared by PEDCo Environmental, Inc., Durham, NC., Contract 68-02-3390, Office of Air Quality Planning and Standards, U.S. Environmental Protection Agency, Research Triangle Park, NC., 197 pages

Johnson, T.R., and Paul, R.A., 1984. *The NAAQS Model (NEM) and Its Application to Nitrogen Dioxide*. Draft report prepared by PEDCo Environmental, Inc., Durham, NC., Office of Air Quality Planning and Standards, U.S. Environmental Protection Agency, Research Triangle Park, NC. 71 pages.

Johnson, T.R., McCoy, M., and Capel, J.E., 1992. *Enhancements to the Hazardous Air Pollutant Exposure Model (HAPEM) as Applied to Mobile Source Pollutants*. Report prepared by IT Air Quality Services, Office of Air Quality Planning and Standards, Office of Air Quality Planning and Standards, U.S. Environmental Protection Agency, Research Triangle Park, NC.

Kao, C.-Y. J., and Yamada, T., 1988. Use of the CAPTEX data for evaluations of a long-range transport numerical model with a four-dimensional assimilation technique. *Monthly Weather Review*, Vol. 116:293-306.

Karl, T.R., 1980. Study of the spatial variability of ozone and other pollutants at St. Louis, Missouri. *Atmospheric Environment*. 14(6):681-694.

Kingdon, J.W., 1995. *Agenda, Alternatives and Public Policies*. 2nd edition, Harper Collins College Publishers, 254 pages.

Lackey, R.T., and Blair, R.L., 1997. Science, policy, and acid rain. *Renewable Resources Journal*. Vol. 15(1):9-13.

Lamb, B., Fuenther, A., Gay, D., and Westbery, H., 1987. A national inventory of biogenic hydrocarbon emissions. *Atmospheric Environment*, 21(8):1695-1705.

Lamb, R.G., 1983. *Regional Scale (1000km) Model of Photochemical Air Pollution, Part 1, Theoretical Formulation*. EPA/600/3-83-035. U.S. Environmental Protection Agency, Environmental Sciences Research Laboratory, Research Triangle Park, NC 27711.

Lamb, R.G., 1984. *Regional Scale (1000km) Model of Photochemical Air Pollution, Part 2, Input Processor Network Design*. EPA/600/3-84-085. U.S. Environmental Protection Agency, Environmental Sciences Research Laboratory, Research Triangle Park, NC 27711.

Law, P.L., Liroy, P.J., Zelenka, M.P., Huber, A.H., and McCurdy, T.R., 1997. Evaluation of a probabilistic exposure model applied to carbon monoxide (pNEM/CO) using Denver personal exposure monitoring data. *Journal of Air & Waste Management Association*. (47):491-500.

Lawson, R., and Snyder, W.H., 1983. *Determination of Good-Engineering-Practice Stack Height: a Fluid Model Demonstration Study for a Power Plant*, EPA/600/3-83-024. U.S. Environmental Protection Agency, Research Triangle Park, NC 27711. 70 pages.

Lee, I.Y., 1987. Numerical simulations of cross-application transport and diffusion. *Boundary-Layer Meteorology*, (39):53-66.

Lee, R.F., Perry, S.G., Cimorelli, A.J., Paine, R.J., Venkatram, A., Weil, J.C., and Wilson, R.B., 1996. AERMOD: The developmental evaluation. (Gryning and Schiermeier, Eds.) *Air Pollution and Its Application XI*, Plenum Press, NY, pages 623-630.

- Leighton, P.A., 1961. *Photochemistry of Air Pollution*. Academic Press, New York and London, 279 pages.
- Levy, A., 1971. Normal atmosphere: large radical and formaldehyde concentrations predicted. *Science*, 173:141-143.
- Levy A., 1972. Photochemistry of the lower troposphere. *Planet, Space Science*, 20:919-935.
- Lin, C.J., and Pehkonen, S.O., 1999. The chemistry of atmospheric mercury: A review. *Atmospheric Environment*. 33(13):2067-2079.
- Linker, L.C., Stigall, G.E., Chang, C.H., and Donigian, A.S., 1996. Aquatic Accounting : Chesapeake Bay Watershed Model Quantifies Nutrient Loads. *Water Environment and Technology*. 8(1):48-52.
- List, R.J., 1954. On the transport of atomic debris in the atmosphere. *Bulletin of American Meteorological Society*. Vol. 35(7):315-325.
- List, R.J., 1971. *Smithsonian Meteorological Tables*. Volume 114, Smithsonian Institution Press, City of Washington DC.
- Lucas, D.H., 1958. The atmospheric pollution of cities. *International Journal of Air and Water Pollution*. (1):71-86.
- Lurmann, F.W., 1991. *Implementation of the 1990 SAPRAC Chemical Mechanism in the Urban Airshed Model*. Prepared for the South Coast Air Quality Management District by Sonoma Technology, Inc., Santa Rosa, CA. 169 pages.
- Lurnamm, F.W., Carter, W.P.L., and Coyner, L.A., 1987. *A Surrogate Species Chemical Reaction Mechanism for Urban-Scale Air Quality Simulation Models*. EPA-600/3-87-014, U.S. Environmental Protection Agency, Research Triangle Park, NC 27711.
- Machta, L., and Harris, D.L., 1955. Effects of atomic explosions on weather. *Science*. Vol. 131(3134):75-81.
- Martin, D.O., 1971. An urban diffusion model for estimating long term average values of air quality. *J. of the Air Pollution Control Association*. Vol 21(1):16-19.
- McCurdy, T., 1994. *Estimating Ozone Exposures in the Chicago Urban Area Using a Second-Generation Probabilistic Version of NEM*. U.S. Environmental Protection Agency, Office of Air Quality Planning and Standards, Research Triangle Park, NC.
- McElroy, J.L. and Pooler, F., 1968. *St. Louis Dispersion Study Volume II-Analysis*. National Air Pollution Control Administration. Publication Number AP-53. U.S. Department of Health Education and Welfare, Arlington, VA. 51 pages.
- Meade, P.J., and Pasquill, F., 1958. A study of the average distribution of pollution around Stayhorpe. *International Journal of Air Pollution*. Pergamon Press. Vol. 1, pages 60-70.
- MOI, Work Group II 1982. *Atmospheric Sciences and Analysis, Regional Modeling Subgroup Report*. Report No. 2F-M, Oct. 15.
- Moran, M.D., and Pielke, R.A., 1996. Delayed shear enhancement in mesoscale atmospheric dispersion. *8th Joint Conference on the Applications of Air Pollution Meteorology with A&WMA*, American Meteorological Society, Boston, MA, pages 96-103.

National Center for Atmospheric Research, 1983a. *Regional Acid Deposition: Design and Management Plan for a Comprehensive Modeling System*. NCAR/TN-215+PPR, National Center for Atmospheric Research, Boulder, CO, 33 pages.

National Center for Atmospheric Research, 1983b. *Regional Acid Deposition: Models and Physical Process*, NCAR/TN-214+STR, National Center for Atmospheric Research, Boulder, CO, 386 pages.

National Research Council 1983. *Risk Assessment in the Federal Government, Managing the Process*. Washington, D.C., National Academy Press, 191 pages.

National Research Council 1991a. *Rethinking the Ozone Problem in Urban and Regional Air Pollution*. Washington, D.C., National Academy Press, 489 pages.

National Research Council 1991b. *Human Exposure Assessment for Airborne Pollutants: Advances and Opportunities*. Washington, D.C., National Academy Press, 344 pages.

National Research Council 1994. *Science and Judgment in Risk Assessment*. Washington DC, National Academy Press, 651 pages.

Netterville, D.D.J., 1990. Plume rise, entrainment and dispersion in turbulent winds. *Atmospheric Environment*. 24A:1061-1081.

Nohebel, G., 1965. Chimney emissions and immissions: standardization of formulae for estimation of plume rise and ground level concentrations. *International Journal of Air and Water Pollution*. Vol. 9(11):763-766.

Noilhan, J., and Planton, S., 1989. A simple *parameterization of land surface processes for meteorological models*. *Monthly Weather Review*. 117(3):536-549.

Nordo, J., Eliassen, A., and Saltbones, J., 1974. Large-scale transport of air pollutants. *Advances in Geophysics*. Vol. 18B, Academic Press, pages 137-150.

Novak, J.H., and Reagan, J.A., 1986. A comparison of natural and man-made hydrocarbon emission inventories necessary for regional acid deposition and oxidant modeling. Paper No. 86-30. In: *Proceedings of the 70th Annual APCA Meeting*, Air Pollution Control Association, Pittsburgh, PA, June 1986.

Ottar, B., 1978. An assessment of the OECD study on long range transport of air pollutants (LRTAP). *Atmospheric Environment*. Vol. 12:445-454.

Ott, W., Thomas, J., Mage, D., and Wallace, L. 1988. Validation of the Simulation of Human Activity and Pollutant Exposures (SHAPE) model using paired days from the Denver, CP, carbon monoxide field study. *Atmospheric Environment*. (22):249-287.

Ott, W., Wallace, L., and Mage, D., 2000. Predicting particulate (PM10) personal exposure distributions using a random component superposition statistical model. *Journal of Air & Waste Management Association*. 50:1390-1406.

Owen, B., Edmunds, H.A., Carruthers, D.J., and Singles, R.J., 2000. Prediction of total oxides of nitrogen and nitrogen dioxide concentrations in a large urban area using a new generation urban scale dispersion model with integral chemistry model. *Atmospheric Environment*. 14:397-406.

Pasquill, F., 1961. The estimation of the dispersion of windborne material. *Meteorology Magazine*. Vol. 90(1063):33-49.

- Perhac, R.M., 1978. Sulfate regional experiment in northeastern United States: the SURE program. *Atmospheric Environment*. Vol. 12:641-647.
- Perry, S.G., 1992a. CTDMPLUS: a dispersion model for sources near complex topography. Part I: technical formulations. *Journal of Applied Meteorology*. American Meteorological Society, Boston, MA, 31(7):633-645.
- Perry, S.G., 1992b. CTDMPLUS: a dispersion model for sources near complex topography. Part II: performance characteristics. *Journal of Applied Meteorology*. American Meteorological Society, Boston, MA, 31(7):646-660.
- Perry, S.G., Cimarella, A.J., Lee, R.F., Paine, R.J., Venkatram, A., and Weil, J.C., 1994. AERMOD: a dispersion model for industrial source applications. *Proceedings of the 87th Annual Meeting of the AW&MA*, 94-TA23.04, AW&MA, Pittsburgh, PA.
- Peters, L.K., Berkowitz, C.M., Garmichail, G.R., Easter, R.C., Fairweather, G., Ghan, S.J., Hales, J.M., Leung, L.R., Pennell, W.R., Potra, R.A., Saylor, R.D., and Tsang, T.T., 1995. The current state and future direction of Eulerian models in simulating the tropospheric chemistry and transport of trace species: a review. *Atmospheric Environment*. Vol. 29(2):189-222.
- Petersen, W.B., 1982. *Estimating Concentration Downwind from an Instantaneous Puff Release*. EPA 600/3-82-078. Environmental Science Research Laboratory, U.S. Environmental Protection Agency, Research Triangle Park, NC 27711. 73 pages.
- Petersen, W.B., and Lavdas, L.G., 1986. *INPUFF 2.0 - A Multiple Source Gaussian Puff Dispersion Algorithm User's Guide*. EPA 600/8-86-024. Atmospheric Sciences Research Laboratory, U.S. Environmental Protection Agency, Research Triangle Park, NC 27711. 104 pages.
- Peterson, E., and Tingey, D., 1980. An estimate of the possible contribution of biogenic sources to airborne hydrocarbon concentrations. *Atmospheric Environment*, 14(1):79-81.
- Pierce, T.E, Lamb, B., and Van Meter, A., 1990. Development of a biogenic emissions inventory system for regional scale air pollution models. Paper No. 90-94.3. In: *Proceedings of the 83rd Annual AWMA (formerly APCA) Meeting*, June 24-29, 1990. Air and Waste Management Association, Pittsburgh, PA. 16 pages.
- Pierson, W.R., Gertler, A.W., Robinson, N.R., Sagebiel, J.C., Zielinske, B., Bishop, G.A., Siedman, D.H., Zweidinger, R.B., and Ray, W.D., 1996. Real-world automotive emissions - summary of studies in the Fort McHenry and Tuscarora Mountain tunnels. *Atmospheric Environment*. 30:2233-2256.
- Pitchford, M.L., and Malm, W.C., 1994. Development and application of a standard visual index. *Atmospheric Environment*. 20:1049-1054.
- Placet, M., Mann, C.O., Gilbert, R.O., and Niefer, M.J., 2000. emissions of ozone precursors from stationary sources: a critical review. *Atmospheric Environment*. 34:2183-2204.
- Pleim, J.E., and Chang, J.S., 1992. A non-local closure model for vertical mixing in the convective boundary layer. *Atmospheric Environment*. 26A:965-981.
- Pleim, J.E., and Xiu, A., 1993. Development and testing of a land-surface and PBL model with explicit soil moisture parameterization. Preprints, *Conference on Hydroclimatology*, January 17-22, 1993, Anaheim, CA, American Meteorological Society, Boston, pages 45-51.

Pleim, J.E., and Xiu, A., 1995. Development and testing of a surface flux and planetary boundary layer model for application in mesoscale models. *Journal of Applied Meteorology*. 34:19-32.

Pleim, J.E., Xiu, A., Finkelstein, P.L., and Clarke, J.F., 1997. Evaluation of a coupled land-surface and dry deposition model through comparison to field measurements of surface heat, moisture and ozone fluxes. Preprints, *12th Symposium and Boundary Layers and Turbulence*, July 28-August 1, 1997, Vancouver, British Columbia, Canada. American Meteorological Society, Boston, MA, pages 4787-479.

Pleim, J.E., Finkelstein, P.L., Clarke, J.R., and Ellestard, T.G., 1999. A technique for estimating dry deposition velocities based on similarity with latent heat flux. *Atmospheric Environment*. 33:2257-2268.

Pleim, J.E., Venkatram, A., and Yarmartino, R., 1984. ADOM/TADAR model development program. *Volume 4, Dry Deposition* ERT Document No. P-8980-520, Concord, MA.

Pleim, J.E., Clarke, J.F., Finkelstein, P.L., Cooter, E.J., Ellestad, T.G., Xiu, A., and Angevine, W.M., 1996. Comparison of measured and modeled surface fluxes of heat, moisture and chemical dry deposition. In *Air Pollution Modeling and Its Application XXI*. Volume 21. S.-E. Gryning and F.A. Schiermeier (Eds.). Plenum Press, New York, NY, pages 613-621.

Poole-Kober, E.M., and Viebrock, H.J., 1993. Fiscal Year 1992 Summary Report of NOAA Atmospheric Sciences Modeling Division Support to the U.S. Environmental Protection Agency. *NOAA Technical Memorandum ERL ARL-203*, Air Resources Laboratory, Silver Spring, MD, June 1993, 85 pages.

Poole-Kober, E.M., and Viebrock, H.J., 1994. Fiscal Year 1993 Summary Report of NOAA Atmospheric Sciences Modeling Division Support to the U.S. Environmental Protection Agency. *NOAA Technical Memorandum ERL ARL-206*, Air Resources Laboratory, Silver Spring, MD, June 1994, 103 pages.

Pooler, F., 1961. A prediction model of mean urban pollution for use with standard wind roses. *International Journal of Air and Water Pollution*. Vol. 4(3/4):199-211.

Possiel, N.C., Milich, L.R., and Goodrich, B.R., (Eds.), 1991. *Regional Ozone Modeling for Northeast Transport (ROMNET) Project Final Report*. EPA-450/4-91-002a. Office of Air Quality Planning and Standards, Research Triangle Park, NC.

Randerson, D., 1979. Review panel on sigma computations. *Bulletin of the American Meteorological Society*. 60:682-683.

Randerson, D. (Editor) 1984. *Atmospheric Science and Power Production*. DE84005177 (DOE/TIC-27601), National Technical Information Service, U.S. Department of Commerce. Springfield, VA 22161. 850 pages.

Rasmussen, R., 1972. What do the hydrocarbons from trees contribute to air pollution? *Journal of the Air Pollution Control Association*, 22(7):537.

Reynolds, S.D., Seinfeld, J.H., and Roth, P.M., 1973. Mathematical modeling of photochemical air pollution -- I. Formulation of the model. *Atmospheric Environment*. (7):1033-1062.

Rodhe, H., 1972. A study of the sulfur budget for the atmosphere over Northern Europe. *Tellus*. Vol. 24:128-138.

Roselle, S.J., and Schere, K.L., 1995. Modeled response of photochemical oxidants to systematic reductions in anthropogenic volatile organic compound and NO_x emissions. *Journal of Geophysical Research*. 100(D11):22,929-22,941.

Roselle, S.J., Hanna, A.F., Lu, V., Jang, J-C.C., Schere, K.L., and Pleim, J.E., 1996. Refined photolysis rates for advanced air quality modeling systems., Preprints, *9th Joint Conference on the Applications of Air Pollution Meteorology with A&WMA*, January 28-February 2, 1996, Atlanta, Georgia. American Meteorological Society, Boston, pages 213-216.

Roth, P.M., Reynolds, S.D., Roberts, P.J.W., and Seinfeld, J.H., 1971. *Development of a Simulation Model for Estimating Ground Level Concentrations of Photochemical Pollutants*. Report 71-8AI-21. Systems Applications, Inc., Beverly Hills, CA.

Russell, A., and Dennis, R., 2000. NARSTO critical review of photochemical models and modeling. *Atmospheric Environment*. Vol. 34:2283-2324.

Samson, P.J., Brook, R., and Stillman, S., 1990. *Estimation of Seasonal and Annual Acid Deposition through Aggregation of Three-Day Episodic Periods*. EPA/600/3-90/059, Atmospheric Research and Exposure Assessment Laboratory, Research Triangle Park, NC,. 146 pages.

Saxena, P., Hudischewskuyj, A.G., Seigneur, C., and Seinfeld, J.H., 1986. A comparative study of equilibrium approaches to the chemical characterization of secondary aerosols. *Atmospheric Environment*. 20:1471-1483.

Schere, K.L., and Shreffler, J.H., 1983. *Final Evaluation of Urban-scale Photochemical Air Quality Simulation Models*. EPA-600/3-82-094. Environmental Sciences Research Laboratory, Research Triangle Park, NC 27711. 259 pages.

Schere, K.L., and Wayland, E., 1989. *EPA Regional Oxidant Model (ROM 2.0), Evaluation on 1980 NEROS Data Bases*. EPA-600/S3-89/057. U.S. Environmental Protection Agency, Research Triangle Park, NC 27711. 351 pages.

Schiermeier, F.A., Wilson, W.E., Pooler, F., Ching J.K.S., and Clarke, J.F., 1979. Sulfur transport and transformation in the environment (STATE): a major EPA research program. *Bulletin of American Meteorological Society*. Vol. 60(11):1303-1312.

Schock, M.R., and Weber, S.F., 1984. *MSPUFF Mesoscale Air Quality Computer Modeling System*. Division of Environmental Waste Management and Research. North Dakota State Department of Health. Bismarck, ND.

Schrenk, H.H., Heimann, H., Clayton, G.D., Gafafer, W.M., and Wexler, H., 1949. *Air Pollution in Donora, PA*. Public Health Bulletin No. 306. U.S. Public Health Service, Washington DC, 173 pages.

Schuck, E.A., Altshuller, A.P., Barth, D.S., and Morgan, G.B., 1970. Relationship of hydrocarbons to oxidants in ambient atmospheres. *Journal of Air Pollution Control Association*. Volume 20, No. 5:297-302.

Scire, J.S., Yamartino, R.J., and Fernau, M.E., 2000a. *A User's Guide for the CALMET Meteorological Model*. Earth Tech, Concord, MA, <http://www.src.com> (accessed March 2000).

Scire, J.S., Strimaitis, and Yamartino, R.J., 2000b. *A User's Guide for the CALPUFF Dispersion Model*. Earth Tech, Concord, MA, <http://www.src.com> (accessed March 2000).

Scire, J.S., Lurmann, F.W., Bass, A., and Hanna, S.R., 1984. *Users Guide to MESOPUFF II Model and Related Processor Programs*. Environmental Research and Technology, Inc., Concord, MA, Prepared for Office of Research and Development, U.S. Environmental Protection Agency, Research Triangle Park, NC.

Scorer, R.S., 1959. The behavior of chimney plumes. *International Journal of Air Pollution*. (1):198-220.

Seibert, P., Beyrich, F., Gryning, S-E., Joffre, S., Rasmussen, A., Tercier, P., 2000. Review and intercomparison of operational methods for the determination of the mixing height. *Atmospheric Environment*. Vol. 34:1001-1027.

Seigneur, C., 1982. A model of sulfate aerosol dynamics in atmospheric plumes. *Atmospheric Environment*. 16:2207-2228.

Seigneur, C., Praised, P., Hope, PK, Grosjean, D., 1999. Modeling atmospheric particulate matter. *Environmental Science & Technology*. Vol. 3:80A-86A.

Seinfeld, J.H., 1988. Ozone air quality models: a critical review. *Journal of the Air Pollution Control Association*. 14:616-645.

Shankar, W.H., and Binkowski, F.S., 1994. Sulfate aerosol wet deposition in a three-dimensional Eulerian air quality modeling framework. Abstracts, *4th International Aerosol Conference*, August 29-September 2, 1994, Los Angeles, CA, Richard C. Flagan (Ed.), American Association for Aerosol Research, Cincinnati, OH, page 417.

Shreffler, J.H., 1978. Detection of centripetal heat-island circulations from tower data in St. Louis. *Boundary-Layer Meteorology*, (15):229-242.

Skalew, R.C., Fabrick, A.J., and Prager, J.E., 1971. *A Particle-In-Cell method for Numerical Solution of the Atmospheric Diffusion Equation and Application to Air Pollution Problems*. Final Report (NTIS PB-299-290). Systems, Science and Software, Inc., La Jolla, CA.

Smith, M.E., 1984. Review of the attributes and performance of 10 rural diffusion models. *Bulletin of the American Meteorological Society*. (65):554-558.

Snyder, W.H., 1972. Similarity criteria for the application of fluid models to the study of air pollution meteorology. *Boundary-Layer Meteorology*. (3):113-134.

Snyder, W.H. and Lawson, R.E., jr., 1976. Determination of a necessary height for a stack close to a building - a wind tunnel study. *Atmospheric Environment*. (10):683-691

Snyder, W.H., Thompson, R.S., Eskridge, R.E., Lawson, R.R., Castro, I.P., Lee, J.T., Hunt, J.C.R, Ogawa, Y., 1985. The structure of strongly stratified flow over hills: dividing-streamline concept. *Journal of Fluid Mech.*, (152):249-288.

Stauffer, D.R., and Seaman, N.L., 1990. Use of four-dimensional data assimilation in a limited-area mesoscale model. Part I: Experiments with synoptic-scale data. *Monthly Weather Review*, Vol. 118:1250-1277.

Stauffer, D.R., Seaman, N.L., and Binkowski, F.S., 1991. Use of four-dimensional data assimilation in a limited-area mesoscale model. Part II: Effects of data assimilation within the planetary boundary layer. *Monthly Weather Review*, Vol. 119:734-754.

Stern, A.C., 1976, 1977. *Air Pollution. Volume 1. Air Pollutants, Their Transformation and Transport; Volume 2. The Effect of Air Pollution; Volume 3. Measuring, Monitoring, and Surveillance of Air Pollution; Volume 4. Engineering Control of Air Pollution; Volume 5. Air Quality Management.* Academic Press, New York.

Strothmann, J.A., and Schiermeier, F.A., 1979. *Documentation of the Regional Air Pollution Study (RAPS) and Related Investigations in the St. Louis Air Quality Control Region.* EPA-600/4-79-076. Environmental Science Research Laboratory, Office of Research and Development, U.S. Environmental Protection Agency, Research Triangle Park, NC. 715 pages.

Suck, S.H., and Brock, J.R., 1979. Evolution of atmospheric aerosol particle size distributions via Brownian coagulation: Numerical simulation. *Journal of Aerosol Science.* 10:581-590.

Sutton, O.G., 1947. The theoretical distribution of airborne pollution from factory chimneys. *Quarterly Journal of the Royal Meteorology Society.* (73):426-436.

Taylor, G.I., 1945. Dynamics of a Mass of Hot Gas Rising in the Air, *USAEC Report MDDC-919 (LADC-276)*, Los Alamos Scientific Laboratory.

Trainer, M., Williams, E., Parrish, E., Buhr, M., Allwind, E., Westberg, H., Fahsenfeld, R., and Liu, S., 1987. Models and observations of the impact of natural hydrocarbons on rural ozone. *Nature,* 329:705.

Tsang, T.H., and Brock, J.R., 1982. Aerosol coagulation in the plume from a cross-wind line source. *Atmospheric Environment.* 16:2229-2235.

Tsang, T.H., and Brock, J.R., 1983. Simulation of condensation aerosol growth by condensation and evaporation. *Aerosol Science and Technology.* 2:311-320.

Turner, D.B., 1961. Relationships between 24-hour mean air quality measurements and meteorological factors in Nashville, Tennessee. *Journal of Air Pollution Control Association.* (11):483-489.

Turner, D.B., 1964. A diffusion model for an urban area. *Journal of Applied Meteorology.* Vol. 3(2):83-91.

Turner, D.B., 1967. *Workbook of Atmospheric Dispersion Estimates.* Public Health Service Publication No. 999-AP-26. U.S. Public Health Service, Cincinnati, OH. 84 pages.

Turner, D.B., 1979. Atmospheric dispersion modeling. a critical review. *Journal of Air Pollution Control Association.* Volume 29(5):502-519.

Turner, D.B. and Edmisten, N.G., 1968. *St. Louis SO₂ Dispersion Model Study - Description of Basic Data.* (Unpublished report, Division of Meteorology, NAPCA). Atmospheric Sciences Modeling Division, U.S. Environmental Protection Agency, Research Triangle Park, NC 27711.

Turner, D.B. and Irwin, J.S., 1983. Comparison of sulfur dioxide estimates from the model RAM with St. Louis measurements. *Air Pollution Modeling and Its Application II*, (Edited by C. De Wispelaere), Plenum Press, pages 695-707.

Turner, D.B., and Irwin, J.S., 1985. The relation of urban model performance to stability. *Air Pollution Modeling and Its Application IV*, (Edited by C. De Wispelaere), Plenum Press, pages 721-732.

Turner, D.B. and Novak, J.H., 1978. *User's Guide for RAM, Volume 1, Algorithm Description and Use*. EPA-600/8-78-016a. Office of Research and Development, U.S. Environmental Protection Agency, Research Triangle Park, NC 27711, 70 pages.

Turner, D.B., Chico, T., and Catalano, J.A., 1986. *TUPOS - A Multiple Source Gaussian Dispersion Algorithm Using On-Site Turbulence Data*. EPA-600/8-86-010 [NTIS PB 86-181 310/AS]. U.S. Environmental Protection Agency, Research Triangle Park, NC 27711, 171 pages.

Turner, D.B., Irwin, J.S., and Busse, A.D., 1985. Comparison of RAM model estimates with 1976 St. Louis RAPS measurements of sulfur dioxide. *Atmospheric Environment*. (19):247-253.

Turner, D.B., Zimmerman, J.R., and Busse, A.D., 1971. An evaluation of some climatological models. Paper presented at Third Meeting of the NATO/CCMS Panel on Modeling. Paper published in Appendix E of *User's Guide for the Climatological Dispersion Model*. EPA-R4-73-024. Office of Research and Development, U.S. Environmental Protection Agency, Research Triangle Park, NC 27711, pages 107-131.

Turner, D.B., Bender, L.W., Pierce, T.E., and Petersen, W.B., 1989. Air quality simulation models from EPA. *Environmental Software*. Vol. 4(2):52-61.

U.S. Environmental Protection Agency 1971. *Air Quality Criteria for Nitrogen Oxides*. AP-84. U.S. Environmental Protection Agency, Office of Air Quality Planning and Standards, Research Triangle Park, NC 27711.

U.S. Environmental Protection Agency, 1976. *Formation and Transport of Oxidants Along Gulf Coast and in Northern U.S.* EPA-450/3-76-033. U.S. Environmental Protection Agency, Office of Air Quality Planning and Standards, Research Triangle Park, NC 27711, 481 pages.

U.S. Environmental Protection Agency 1977. *User's Manual for Single-Source (CRSTER) Model*. EPA-450/2-77-013, U.S. Environmental Protection Agency, Office of Air Quality Planning and Standards. Research Triangle Park, NC 27711, 303 pages.

U.S. Environmental Protection Agency 1978a. *User's Guide for RAM*. EPA-600/8-78-016a, Environmental Sciences Research Laboratory, U.S. Environmental Protection Agency, Research Triangle Park, NC 27711.

U.S. Environmental Protection Agency 1978b, 1986, 1987, 1995. *Guideline on Air Quality Models*. EPA-450/2-78-027, [This Guideline has been updated several time: 1986 as EPA-450/2-78-027R; 1987 as EPA/450/2-78/027R-SUPPL-A; 1993 as EPA-450/2-78-027R-B, and 1995 it was updated and incorporated into Appendix W to 40 CFR Part 51], U.S. Environmental Protection Agency, Office of Air Quality Planning and Standards. Research Triangle Park, NC 27711.

U.S. Environmental Protection Agency 1979. *Industrial Source Complex (ISC) Dispersion Model User's Guide*. Volume I EPA-450/4-79-030 and Volume II EPA-450/4-79-031, U.S. Environmental Protection Agency, Research Triangle Park, NC 27711.

U.S. Environmental Protection Agency 1980. *Guideline for Applying the Airshed Model to Urban Areas*. EPA-450/4-80-020, U.S. Environmental Protection Agency, Office of Air Quality Planning and Standards Research, Triangle Park, NC 27711.

U.S. Environmental Protection Agency 1985a. *Fluid Modeling Demonstration of Good-Engineering-Practice Stack Height in Complex Terrain*. EPA/600/3-85-022, U.S. Environmental Protection Agency, Research Triangle Park, NC 27711, 89 pages.

U.S. Environmental Protection Agency, 1985b. *Compilation of Air Pollutant Emission Factors, Vol. 1: Stationary Point and Area Sources*, AP-42, 4th Edition, GPO No. 055-000-00251-7, U.S. Environmental Protection Agency, Research Triangle Park, NC.

U.S. Environmental Protection Agency 1988a. *User's Guide for Executing OZIPM-4 (Ozone Isopleth Plotting with Optional Mechanisms, Version 4) with CMB-IV (Carbon-bond Mechanisms-IV) or Optional Mechanisms*. Volume I, description of the ozone isopleth plotting package, version 4. EPA/600/8-88-073a, Atmospheric Sciences Research Laboratory, U.S. Environmental Protection Agency, Research Triangle Park, NC 27711, 240 pages.

U.S. Environmental Protection Agency, 1988b. *Development and Testing of the CBM-IV (Carbon-Bond Mechanism) for Urban and Regional Modeling*. EPA/600/3-88/012, Atmospheric Sciences Research Laboratory, U.S. Environmental Protection Agency, Research Triangle Park, NC 27711, 431 pages.

U.S. Environmental Protection Agency, 1992. *Guidelines for Exposure Assessment*. EPA/600Z-92/001. Federal Register 57: 22888 - 22938, 169 pages.

U.S. Environmental Protection Agency 1995. *Users Guide for the Industrial Source Complex (ISC3) Dispersion Models, Volume I - User Instructions*. EPA-454/B-95-003a. Office of Air Quality Planning and Standards, U.S. Environmental Protection Agency, Research Triangle Park, NC 27711, 320 pages.

U.S. Environmental Protection Agency 1996. *EPA At Research Triangle Park. Twenty Five Years of Environmental Protection*. Office of Administration and Resources Management, Research Triangle Park, NC 27711, 50 pages.

U.S. Environmental Protection Agency 1997. *Mercury Study Report to Congress. Volume I: Executive Summary*. EPA-452/R-97-003. Office of Air Quality Planning and Standards and Office of Research and Development, Research Triangle Park, NC.

U.S. Environmental Protection Agency 1998a. *Study of Hazardous Air Pollutant Emissions from Electric Utility Steam Generating Units - Final Report to Congress*. Volume 1. EPA-453/R-98-004a. Office of Air Quality Planning and Standards, Research Triangle Park, NC.

U.S. Environmental Protection Agency, 1998b. *Guidelines for Ecological Risk Assessment*, Federal Register 63(93): 26846-26924, 188 pages.

U.S. Weather Bureau 1955. *Meteorology and Atomic Energy*. AECU 3066, U.S. Atomic Energy Commission, Washington DC, 169 pages.

Valente, R., J., and Thornton, F.C., 1993. Emissions of NO from soil at a rural site in central Tennessee. *Journal of Geophysical Research*. 98:16745-16753.

Warren, D.R., and Seinfeld, J.R., 1985. Simulation of aerosol size distribution evolution in systems with simultaneous nucleation, condensation, and coagulation. *Aerosol Science and Technology*. 4:31-43.

Wayne, G., Kokin, A., and Wiesburd, M.I., 1973. *Controlled Evaluation of the Reactive Environmental Simulation Model (REM)*, EPA-R4-73-013, U.S. Environmental Protection Agency, Research Triangle Park, NC.

Weil, J.C., 1988. Plume Rise. In: *Lectures on Air Pollution Modeling* (A. Venkatram and J.C. Wyngaard (Eds.)). American Meteorological Society, Boston, MA, pages 119-166.

Weil, J.C., 1992. Updating the ISC model through AERMIC. *Proceedings of the 85th Annual Meeting of the AW&MA*, 92-100.11, AW&MA, Pittsburgh, PA.

Weil, J.C., and Brower, R.P., 1984. An updated Gaussian plume model for tall stacks. *Journal of Air Pollution Control and Association*. (34):818-827.

Weil, J.C., and Corio, L.A., 1988. *A Modification of the PPSP Dispersion Model for Highly Buoyant Plumes*. PPRP-MP-60, Maryland Power Plant Research Program, 46 pages.

Weisburd, M., Wayne, G., Danchick, R., Kokin, A., and Stein, A., 1971. *Development of a Simulation Model for Estimating Ground Level Concentrations of Photochemical Pollutants*. Final Report. TM-(L), 4673/000/00. System Development Corp., Santa Monica, CA.

Wesely, M.L., Cook, D.R., and Hart, R.L., 1985. Measurement and parameterization of particulate sulfur dry deposition over grass. *Journal of Geophysical Research*. 90(D1):2131-2143.

Whitby, K.T., 1978. The physical characteristics of sulfur aerosols. *Atmospheric Environment*. 12:135-159.

Whitby, K.T., 1981. Determination of aerosol growth rates in the atmosphere using lumped aerosol dynamics. *Journal of Aerosol Science*. 12:174-178.

Whitby, E.R., 1985. *The Modal Aerosol Dynamics Model. Part I. Solution of the Internal Terms of the General Dynamic Equation of Aerosols*. Report to the U.S. Environmental Protection Agency. Department of Mechanical Engineering. University of Minnesota, Minneapolis, MN.

Whitby, E.R., 1990. *Modal Aerosol Dynamics Modeling*. Ph.D. thesis, University of Minnesota, Minneapolis, MN.

Whitby, E.R., McMurray, P.H., Shankar, U., and Binkowski, F.S., 1991. *Modal Aerosol Dynamics Modeling*. EPA/600/3-91-030. [NTIS PB 91-161-729]. Atmospheric Research and Exposure Assessment Laboratory, Research Triangle Park, NC 27711.

Whitten, G.Z., Hogo, H., and Killus, J.P., 1980. The carbon-bond mechanism: a condensed kinetic mechanism for photochemical smog. *Environmental Science & Technology*. 14:690-700.

Wilkins, E.T., 1953. *Air Pollution and the London Fog of December 1952*. The Royal Sanitary Institute. Vol. 74(1):1-15.

Wilkinson, J.G., Loomis, G.F., McNally, D.E., Emigh, R.A., and Tesche, T.W., 1994. *Technical Formulation Document: SARMAP/LMOS Emissions Modeling System (EMS-95)*, AG90/TS26, prepared by Alpine Geophysics, Pittsburgh, PA. For the Lake Michigan Air Directors Consortium and California Air Resources Board.

Williams, E.J., Guenther, A., Fehsenfeld, F.C., 1992. An inventory of nitrate oxide emissions from soils in the United States. *Journal of Geophysical Research*. 97(D7):7511-7519.

Willis, G.E., and Deardorff, J.W., 1976. A laboratory model of diffusion in to the convective planetary boundary layer. *Quarterly Journal of the Royal Meteorological Society*. (102):427-445.

Willis, G.E., and Deardorff, J.W., 1978. A laboratory study of dispersion from an elevated source within a modeled convective planetary boundary layer. *Atmospheric Environment*. 12(6-7):1305-1312.

Willis, G.E., and Deardorff, J.W., 1981. A laboratory study of dispersion from a source in the middle of the convectively mixed layer. *Atmospheric Environment*. 15(2):109-117.

Wilson, W.E., 1978. Sulfates in the atmosphere: a progress report on project MISTT. *Atmospheric Environment*. Vol. 12:537-547.

Young, J.O., Alssa, M., Boehm, T.L., Coats, C.J., Elchinger, J.R., Roselle, S.J., Van Meter, A.R., Wayland, R.A., and Pierce, T.E., 1989. *Development of the Regional Oxidant Model, Version 2.1*. EPA/600/3-89/044. (NTIS PB89-194252). EPA, Office of Research and Development, Atmospheric Research and Exposure Assessment laboratory, Research Triangle Park, NC.

Chapter 19

Case Studies – Air Pollution Modeling at Local, Regional, Continental, and Global Scales

A chapter dedicated to the topic “Case Studies – Air Pollution Modeling at Local, Regional, Continental, and Global Scales” was presented in Volume I of this book series.

This topic will be further expanded in Volume III.

BRANK P 2009

Chapter 20

The Future of Air Pollution Modeling

A chapter dedicated to the topic “The Future of Air Pollution Modeling” was presented in Volume I of this book series.

This topic will be further expanded in Volume III.

BRANK P 2000

Chapter 21

Active Groups in Air Pollution Modeling

A chapter dedicated to the topic “Active Groups in Air Pollution Modeling” was presented in Volume I of this book series.

This topic will be further expanded in Volume III.

BRAND
PAPER

Chapter 22

Available Software

A chapter dedicated to the topic “Available Software” was presented in Volume I of this book series.

This topic will be further expanded in Volume III.

BRANK P 2000

Chapter 23

Available Databases

A chapter dedicated to the topic “Available Databases” was presented in Volume I of this book series.

This topic will be further expanded in Volume III.

BRANK P 2009

Chapter 24

Physical Modeling of Air Pollution

A chapter dedicated to the topic “Physical Modeling of Air Pollution” is expected to be included in Volume III of this book series and will cover Wind Tunnels, Water Channels, and Aerosol and Cloud Chamber facilities.

BRAND
PAPER

Table of Contents – Volume I¹

	Preface	xi
	About the Editor	xiii
	About the Publishers	xv
	About the Chapter Authors	xvii
1	The Problem – Air Pollution	1
	1 Our Natural Environment	1
	2 Air Pollution, Some Definitions	3
	3 Primary and Secondary Pollutants	4
	4 A Short History of Air Pollution Modeling	5
	5 Air Pollution Regulations	8
2	The Tool – Mathematical Modeling	13
	1 Why Air Quality Modeling	13
	2 Modeling Categorized	14
	3 Modeling the Atmosphere	19
	4 Modeling Alternatives	20
	5 Spatial and Temporal Scales	22
	6 Spatial and Temporal Resolution	23
	7 Uncertainty: Bias, Imprecision, and Variability	24
	8 Evaluation of Model Performance	25
	9 Data Needs	27
	10 Uses of Models	29
3	<i>Emission Modeling</i>	33
4	Air Pollution Meteorology	37
	1 Synoptic Meteorology	38
	2 Boundary-Layer Meteorology	61
5	<i>Meteorological Modeling</i>	101
6	Plume Rise	103
	1 Introduction	108
	2 Semi-Empirical Formulations	112
	3 Advanced Plume Rise Models	131
	4 Particle Models for Plume Rise	137
	5 Special Cases	157
7	<i>Gaussian Plume Models</i>	183

¹ Chapters in italics will be provided in subsequent volumes.

7A	Introduction to Gaussian Plume Models	185
1	Introduction	186
2	The Point Source in the Atmospheric Boundary Layer	186
3	The Atmospheric Boundary Layer	190
4	Dispersion in the Atmospheric Boundary Layer	193
5	Building Downwash	197
6	Terrain Treatment	199
7	Modifications to the Gaussian Framework	202
8	Concluding Remarks	206
8	<i>Gaussian Puff Models</i>	209
9	<i>Special Applications of Gaussian Models</i>	211
10	Eulerian Dispersion Models	213
1	Air Quality Modeling Methods	214
2	Eulerian Formulations	218
3	Analytical Solutions for Ideal Atmospheric Conditions	232
4	Numerical Solution Methods	237
5	Numerical Algorithms for Advection	244
6	Horizontal Diffusion Algorithm	251
7	Vertical Diffusion Algorithm	258
8	Simplified Eulerian Models	268
	Appendix A	272
	Appendix B	276
	Appendix C	279
11	<i>Lagrangian Particle Models</i>	293
12	<i>Atmospheric Transformations</i>	297
13	<i>Deposition Phenomena</i>	301
14	<i>Indoor Air Pollution Modeling</i>	303
15	<i>Modeling of Adverse Effects</i>	305
16	<i>Statistical Modeling</i>	307
17	<i>Evaluation of Air Pollution Models</i>	309
18	<i>Regulatory Air Quality Models</i>	311
19	Case Studies – Air Pollution Modeling at Local, Regional, Continental, and Global Scales	313
1	List of Case Studies	314
2	Additional Information on Case Studies Relevant to Air Pollution Modeling/Simulation	323

20	The Future of Air Pollution Modeling	325
1	Processor Technology and Air Pollution Modeling	325
2	Comprehensive Modeling Systems (CMS)	330
21	Active Groups in Air Pollution Modeling	355
1	List of Active Groups	356
2	Additional Information on Groups Working on Air Pollution Modeling Issues	360
22	Available Software	363
1	Short-Range Models	366
2	Urban and Regional Photochemical Models	380
3	Long-Range Transport Models for Acid Deposition, Visibility Impairment and Complex Terrain	387
4	Emergency Release and Dense Gas Models	394
5	Meteorological Models	406
23	Available Databases	409
1	Overview	409
2	The Challenges	411
3	Characteristics of Weather Data Sets	413
4	NCEP Gridded Data Products	414
5	Data Archival	416
6	Reanalysis Techniques	418
7	Mesoscale Prognostic Models	421
8	Future Developments	423
	Authors' Index	427
	Subject Index	429

Blank Page

In Memoriam: Philip M. Roth (1939-2004)



On April 5, 2004, Philip (Phil) Roth passed away after a long illness. Phil was the lead author of *The Tool – Mathematical Modeling*, which appears in Chapter 2 of *AIR QUALITY MODELING – Theories, Methodologies, Computational Techniques, and Available Databases and Software, Vol. 1 – Fundamentals* (P. Zannetti, Editor), published by The EnviroComp Institute and the Air & Waste Management Association.

After receiving his PhD in chemical engineering from Princeton University in 1966, Phil Roth joined Shell Development Company in Emeryville, CA. In 1969, Phil left Shell to establish the Environmental Studies Group at Systems Applications, Inc. Phil collaborated with John Seinfeld and Steve Reynolds at Caltech to develop a three-dimensional model of photochemical smog, which was eventually to become known as the Urban Airshed Model (UAM). Phil's early involvement in modeling focused on applications to the Los Angeles basin. The three papers Phil co-authored with Steve Reynolds and John Seinfeld in 1973 and 1974 published in *Atmospheric Environment* are generally considered to have launched the field of photochemical air pollution modeling. Based on these initial modeling experiences, Phil became a strong advocate for continued research to better understand key physical and chemical processes associated with smog formation, for the conduct of a stressful model evaluation process, and for the sound interpretation and usage of photochemical modeling results.

The first major application of the UAM in a regulatory situation was undertaken in the early 1980s with an analysis of the potential impacts of NO_x reductions from Los Angeles petroleum refineries. The rulemaking process that followed the completion of this study convinced Phil that industry and agencies should develop cooperative programs to address ozone modeling in a technically sound manner. This concept was put into play with the South Central Coast Cooperative Aerometric Monitoring Program (SCCAMP), which was initiated in early 1983.

That same year, Phil left Systems Applications, Inc. to continue his professional practice as a private consultant.

In the mid-1980s, Phil recognized that an approach similar to that adopted for SCCCAMP was needed in the southern San Joaquin Valley to understand and address continuing ozone problems. Phil played key roles in a series of field measurement, data analysis, and modeling studies conducted in central California, including the San Joaquin Valley Air Quality Study and the California Regional PM10/PM2.5 Air Quality Study. The success of the initial studies in the San Joaquin Valley spawned additional integrated monitoring/modeling studies in other parts of the country. In the early 1990s, Phil was involved in planning activities for the Lake Michigan Ozone Study.

In 1990, Phil founded Envair, an association of private consultants providing research and consulting services in the environmental and earth sciences. Phil was a tireless advocate for the careful and systematic applications of photochemical models at the regulatory level. He was the principal author of a major report on the status of photochemical air quality modeling, which was part of the NARSTO state-of-science assessment for ozone. Recognizing the limitations of grid-based modeling, he initiated the development of an observation-based methodology for determining whether ozone formation at a particular site is VOC or NO_x limited.

Phil's wisdom, dedication to excellence, and friendship will be especially missed by those of us who had the privilege of working closely with him.

Authors'/Contributors' Index¹ for Volumes I and II

Anfossi, Domenico	I – p 103 II – p 93
Builtjes, Peter J.H.	I – p 1
Byun, Daewon W.	I – p 213
Canepa, Elisa	I – p 103 II – p 503
Carrington, David B.	II – p 267
Chow, Judith C.	II – p 455
Degrazia, Gervásio	II – p 93
Eastman, Joseph L.	I – p 409
Ferrero, Enrico	II – p 93
Finzi, Giovanna	II – p 397
González Barras, Rosa M.	II – p 233
Hibberd, Mark	II – p 93
Hurley, Peter	II – p 93
Irwin, John S.	II – p 503 , 557
Keen, Cecil S.	I – p 409
Lacser, Avraham	I – p 213
Lee, Russell	I – p 363
Luhar, Ashok	II – p 93
Lyons, Walter A.	I – p 409
Michelsen, Hope	II – p 163
Moon, Dennis A.	I – p 409
Moussiopoulos, Nicolas	I – p 313, 355
Nelson, Thomas E.	I – p 409
Nunnari, Giuseppe	II – p 397

¹ Readers are encouraged to use the CD-ROM version of the book for text searching.

Oettl, Dietmar	I – p 325
Pepper, Darrell W.	II – p 267
Pérez, Juan L.	II – p 233
Physick, William	II – p 93
Pun, Betty K.	II – p 163
Reynolds, Steven D.	I – p 13
Richter, Richard O.	II – p 351
Roth, Philip M.	I – p 13
San José, Roberto	I – p 325 II – p 233
Seigneur, Christian	II – p 163
Sheehan, Patrick J.	II – p 351
Sorbjan, Zbigniew	I – p 37 II – p 11
Thé, Jesse	I – p 185, 363
Tourlou, Paraskevi-Maria.....	I – p 313, 355
Trini Castelli, Silvia	II – p 93
van Dop, Han.....	I – p 103 II – p 93
Venkatram, Akula	I – p 185
Watson, John G.	II – p 455
Yamartino, Robert J.	I – p 213
Zannetti, Paolo	I – p 213

Subject Index¹ for Volumes I and II

Abatement	I – p 313, 355
Acid deposition	I – p 363
Advection	I – p 213
AERMOD.....	I – p 185, 409
Aerodynamic resistance.....	II – p 233
Air-conditioning	II – p 267
Air dispersion models.....	I – p 363
Air pollution	I – p 1, 185, 313, 355
Air pollution episode	I – p 313, 355
Air pollution model(s).....	I – p 185, 409
Air pollution modeling	I – p 1, 325
Air pollution regulations	I – p 1
Air quality	I – p 185
	II – p 557
Air quality forecasting.....	I – p 313, 355
	II – p 397
Air quality modeling	I – p 13, 213
	II – p 233
Air quality models	I – p 363
Ambient measurement.....	II – p 455
Ambient turbulence	I – p 103
Aqueous reactions	II – p 164
Atmospheric boundary layer	I – p 37, 185
	II – p 11
Atmospheric chemistry.....	II – p 164
Atmospheric motions	I – p 37
Building contamination	II – p 267
Building effects	I – p 185
Building safety	II – p 267
Bulk resistance	II – p 233
Buoyant plumes.....	I – p 103
Canopy resistance.....	II – p 233
CALMET	I – p 409
CALPUFF	I – p 409
Chemical mass balance (CMB).....	II – p 455
Chemical mechanisms	II – p 164
Chemical transformation	I – p 13
Chemical transport models	II – p 164
Clean Air Act	II – p 557
Clean Air Act Amendments	II – p 557
Cloud-free boundary layer.....	II – p 11
Cloud-topped boundary layer.....	II – p 11
Combustion facilities.....	II – p 351
Compensation point.....	II – p 233
Complex terrain.....	I – p 363
Complex terrain dispersion	I – p 185
Constant flux layer	II – p 233
Convection	I – p 37
	II – p 11
Convective boundary layer.....	I – p 185

¹ Readers are encouraged to use the CD-ROM version of the book for text searching.

Data needs	I	- p 13
Decision support system.....	II	- p 397
Dense gas models	I	- p 363
Deposition	II	- p 233
Deposition of air pollutants	I	- p 313, 355
Diagnostic models	I	- p 363
Diffusion.....	I	- p 37, 213
Direct chemical exposures.....	II	- p 351
Dispersion.....	I	- p 185, 313, 355
Dispersion modeling.....	I	- p 13, 103
Eddy diffusivity.....	I	- p 213
Effective plume heights.....	I	- p 103
Emergency releases	I	- p 363
Emissions modeling	I	- p 13
Eulerian modeling	I	- p 213
Fate modeling	II	- p 351
Fluid dynamics	II	- p 267
Footprint analysis	II	- p 94
Four-dimensional data assimilation.....	I	- p 363
Future modeling	I	- p 325
Gaussian dispersion model.....	I	- p 185
Gaussian model(s).....	I	- p 13, 363
Grid-based models.....	I	- p 13
Hazardous air pollutants.....	II	- p 164
Hazardous waste incinerators	II	- p 351
Heterogeneous reactions.....	II	- p 164
Human health	II	- p 351
Indirect chemical exposures	II	- p 351
Indoor air quality	II	- p 267
Internet	I	- p 325
ISC.....	I	- p 185
Jet plumes	I	- p 103
Kinetics.....	II	- p 164
Lagrangian air pollution modeling	II	- p 94
Langevin equation	II	- p 94
Lagrangian models	I	- p 363
Large-eddy simulations	II	- p 11
Local and non-local closure	I	- p 213
Long-range transport	I	- p 363
	II	- p 94
Mesoscale dispersion.....	II	- p 94
Meteorological data.....	I	- p 363, 409
Mixed layers.....	I	- p 37
	II	- p 11
Mixing	I	- p 37
	II	- p 11
Model development.....	II	- p 557
Model evaluation.....	II	- p 503
Model performance evaluation.....	I	- p 13
Model quality assurance	II	- p 503
Modeling	I	- p 313, 355
Monin-Obukhov theory.....	II	- p 233
Numerical algorithms	I	- p 213
Numerical modeling	II	- p 267
Ozone formation.....	I	- p 313, 355
Particle models	I	- p 363

Particulate matter (PM)	II – p	164 , 455
Particulate transport.....	II – p	267
Performance measures.....	II – p	503
Photochemical models.....	I – p	13, 363
Plume-in-grid	II – p	164
Plume models	I – p	363
Pollution control.....	I – p	313, 355
Prognostic models	I – p	363
Puff models	I – p	363
Radicals	II – p	164
Receptor model.....	II – p	455
Regional models.....	I – p	363
Regulatory application	I – p	13
Regulatory model	I – p	185
Resolution.....	I – p	13
Resuspension.....	II – p	267
Risk assessment.....	II – p	351
RUC2.....	I – p	409
Secondary air pollutants	II – p	164
Second-hand smoke.....	II – p	267
Self-induced turbulence.....	I – p	103
Short-range models.....	I – p	363
Similarity theories	I – p	37
Simulation	I – p	313, 355
Simulation models	I – p	13
Source apportionment.....	II – p	455
Source profile	II – p	455
Stability conditions.....	I – p	103
Stable boundary layer.....	I – p	185
Statistical indices	II – p	503
Statistical model evaluation.....	II – p	503
Stochastic models	II – p	94 , 397
Stratospheric ozone	II – p	164
Street canyon	I – p	313, 355
Surface fluxes.....	II – p	233
Terrain data	I – p	363
Thermodynamics	II – p	164
Transport	I – p	313, 355
Transport modeling	II – p	351
Tropospheric ozone.....	II – p	397
Turbulence.....	I – p	37
	II – p	11
Turbulence modeling.....	II – p	267
Uncertainty	I – p	13
Uncertainty analysis	II – p	503
Urban models	I – p	363
Urban ozone	II – p	164
Urban plume.....	I – p	313, 355
Ventilation.....	II – p	267
Visibility	I – p	363
Volatile organic compound (VOC)	II – p	455
Weather systems.....	I – p	37

Blank Page

Additional Information About the Chapter Authors/ Contributors for Volumes I and II

Anfossi, Domenico

- [CV](#)
- [Picture](#)

Builtjes, Peter J.H.

- [Picture](#)

Byun, Daewon W.

- [Bio](#)
- [Picture](#)

Canepa, Elisa

- [CV](#)
- [CV-short](#)
- [Picture](#)

Carrington, David B.

- [CV](#)
- [Picture](#)

Chow, Judith C.

- [CV](#)
- [Picture](#)

Degrazia, Gervásio

- [CV](#)
- [Picture](#)

Ferrero, Enrico

- [Bio](#)
- [Picture](#)

Finzi, Giovanna

- [CV](#)
- [Picture](#)

González Barras, Rosa M.

- [CV](#)

Hibberd, Mark

- [Bio](#)
- [Picture](#)

Hurley, Peter

-  [Bio](#)
-  [Picture](#)

Irwin, John S.

-  [CV](#)

Lacser, Avraham

-  [CV](#)

Lee, Russell

-  [CV](#)

Luhar, Ashok

-  [Bio](#)
-  [Picture](#)

Lyons, Walter A.

-  [CV](#)
-  [Bio](#)
-  [Picture](#)

Michelsen, Hope

-  [CV](#)
-  [Picture](#)

Moussiopoulos, Nicolas

-  [Picture](#)

Nunnari, Giuseppe

-  [CV](#)
-  [Picture](#)

Öetl, Dietmar

-  [CV](#)
-  [Picture](#)

Pepper, Darrell W.

-  [CV](#)
-  [Picture](#)

Pérez, Juan L.

-  [CV](#)
-  [Picture](#)

Physick, William

- [📁 Bio](#)
- [📁 Picture](#)

Pun, Betty K.

- [📁 CV](#)
- [📁 Picture](#)

Richter, Richard O.

- [📁 CV](#)
- [📁 Picture](#)

Roth, Philip M.

- [📁 In Memoriam](#)

San José, Roberto

- [📁 CV](#)
- [📁 Picture](#)

Seigneur, Christian

- [📁 CV](#)
- [📁 Picture](#)

Sheehan, Patrick J.

- [📁 CV](#)
- [📁 Picture](#)

Sorbjan, Zbigniew

- [📁 CV](#)
- [📁 Picture](#)

Trini Castelli, Silvia

- [📁 CV](#)
- [📁 Picture](#)

van Dop, Han

- [📁 CV](#)
- [📁 Picture](#)

Venkatram, Akula

- [📁 Picture](#)

Watson, John G.

- [📁 CV](#)
- [📁 Picture](#)

Yamartino, Robert J.

-  [CV](#)
-  [Picture](#)

Zannetti, Paolo

-  [CV](#)
-  [Picture](#)